VOLUME II - ACCOMPLISHMENTS

FACILITATING NEW DISCOVERIES IN SEISMOLOGY AND EXPLORING THE EARTH

THE NEXT DECADE

IRIS

PROPOSAL TO NSF
JULY 1, 2011 –
SEPTEMBER 30, 2013

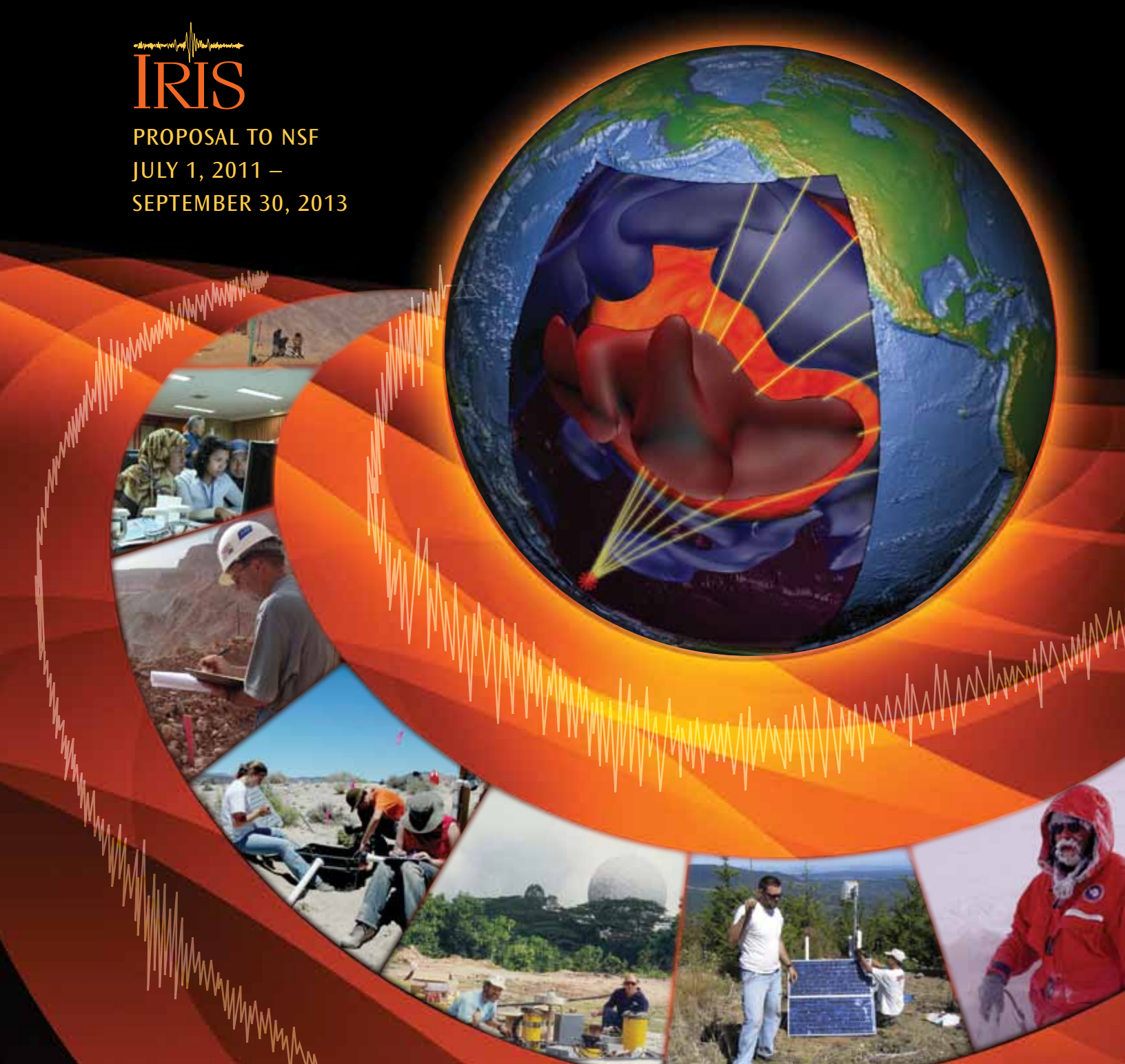

This proposal is submitted by IRIS on behalf of the Board of Directors, which represents the full membership of the Consortium, and thus the collective scientific interests of those 114 U.S. research institutions. The proposal includes contributions from IRIS Program Standing Committees and other governing and advisory bodies of the Consortium, which collectively include more than 60 faculty members who are actively engaged in research projects that are funded by the National Science Foundation.

The proposal and supporting materials are bound in two volumes. Volume I includes the Project Summary, Description, and Budget, as well as descriptions of the individual programs into which IRIS organizes its activities. Volume II is an overview of scientific accomplishments that are based on use of IRIS facilities.

The Project Description begins with an introduction to the IRIS Consortium and facilities, followed by a précis of research facilitated by IRIS. The Project Description also includes a description of activities required to sustain facilities that support state-of-the-art research, a vision for transitioning all IRIS activities into an integrated suite of services, and a brief outline of our funding request.

The Budget is an explication of our estimates of costs to carry out the activities that are summarized in the Project Description and detailed in the Program Descriptions.

The Program Descriptions are synopses of the infrastructure and operation of IRIS core facilities and several related programs. Each synopsis includes an overview of the program's development and its activities under the current Cooperative Agreement, and a detailed description of plans and resources requested to continue meeting the current needs of the research community and support investigators pursuing new opportunities.

The Review of Accomplishments is comprised principally of nearly 250 one-page vignettes, contributed by the research community, and based on research that has been enabled by IRIS, in most cases through use of one or more of the core IRIS facilities or USArray.

FACILITATING NEW DISCOVERIES IN SEISMOLOGY AND EXPLORING THE EARTH

THE NEXT DECADE

IRIS

PROPOSAL TO NSF
JULY 1, 2011 –
SEPTEMBER 30, 2013

Submitted to
National Science Foundation
Division of Earth Sciences
Instrumentation and Facilities Program

By
Incorporated Research Institutions for Seismology
1200 New York Avenue, NW, Suite 800
Washington, D.C. 20005

On behalf of
Board of Directors
and 114 Member Research Institutions
of the IRIS Consortium

September 2010

BOARD OF DIRECTORS

Susan Beck, Susan (Chair)..... University of Arizona
Jim Gaherty (Vice Chair) ..... Columbia University
Don Forsyth (Secretary)..... Brown University
Susan Bilek ..... New Mexico Institute of Mining and Technology
Ed Garnero..... Arizona State University
Steve Grand..... University of Texas at Austin
John Hole..... Virginia Polytechnic Institute and State University
Steven Roecker..... Rensselaer Polytechnic Institute
Doug Wiens..... Washington University in St. Louis

COMMITTEE CHAIRPEOPLE

Xiaodong Song ..... GSN Standing Committee..... University of Illinois at Urbana-Champaign
Richard Allen ..... PASSCAL Standing Committee ..... University of California, Berkeley
Keith Koper..... DMS Standing Committee ..... Saint Louis University
Glenn Kroeger..... E&O Standing Committee ..... Trinity University
Thorne Lay..... Planning Committee..... University of California, Santa Cruz
Matt Fouch..... USArray Advisory Committee ..... Arizona State University
John Collins..... Instrumentation Committee ..... Woods Hole Oceanographic Institution
Anne Meltzer..... International Development Seismology Committee ..... Lehigh University

SENIOR STAFF

Timothy Ahern..... DMS Program Manager and Director of Data Services
Kent Anderson ..... GSN Operations Manager and Acting GSN Program Manager
Robert Busby ..... Transportable Array Manager
Olga Cabello..... Director of International Development Seismology
James Fowler ..... Senior Advisor for Engineering and Instrumentation
James Gridley..... PASSCAL Program Manager
Candy Shin ..... Chief Financial Officer and Director Financial Services
David Simpson ..... President
John Taber ..... E&O Program Manager and Director of Education and Public Outreach
Raymond Willemann ..... Director of Planning and Community Activities
Robert Woolly ..... Director of Program Support and Special Projects
Robert Woodward ..... USArray Director and Director of Instrumentation Services

CONTENTS

EARTHQUAKE SOURCE STUDIES

EPISODIC TREMOR AND SLIP, TRIGGERED EARTHQUAKES

NON-EARTHQUAKE SOURCES

FAULT STRUCTURE

CRUSTAL STRUCTURE

LITHOSPHERE, LITHOSPHERE/ASTHENOSPHERE BOUNDARY

UPPER MANTLE STRUCTURE AND DYNAMICS

LOWER MANTLE, CORE-MANTLE BOUNDARY

WHOLE MANTLE STRUCTURE

OUTER AND INNER CORE STRUCTURE

Introduction: Five Years of Innovation, Discovery, and Transformation

Edward J. Garnero *(Arizona State University)*

The combination of investment in efficient community facilities such as IRIS, a deeper embrace of open data practices exemplified by IRIS, and rapid and cross development in complementary fields embraced by IRIS, has resulted in explosive progress in the geosciences over the last five years. Material presented in this Accomplishments Section clearly demonstrates such progress in numerous aspects of the Earth sciences and in related disciplines of the oceanic, atmospheric, and polar sciences. Much of the research presented here is facilitated directly by the IRIS core programs; some is facilitated by USArray and other components of the EarthScope project, which is in part based on the principals and expertise of the IRIS core programs. Some research requires use of multiple facilities, including those operated by IRIS. The material in this volume exemplifies progress in the Geosciences that would have been slower, more difficult, or in some cases impossible without shared facilities to collect, manage, distribute, and process data.

Scientists at large and small institutions across the U.S. and around the world now regularly contribute to scientific progress in joint and complementary projects that are tractable in part because of ready access to key data and products provided by IRIS facilities. Thus, it is unsurprising that the project descriptions come from authors based at institutions all across the U.S., with nearly one-third of contributer institutions in other countries. This network of investigators contributes to understanding both in areas traditionally studied through seismology—earthquake source and fault processes and structure, and Earth structure from crust to core—and in emerging areas of research—such as climate science, environmental monitoring, natural resource mapping, national security, and planetary science. Especially in these new applications of seismology, collaborations are often multi-disciplinary and transformative, which presents both new opportunities for individual scientists and new challenges for facilities to meet their needs.

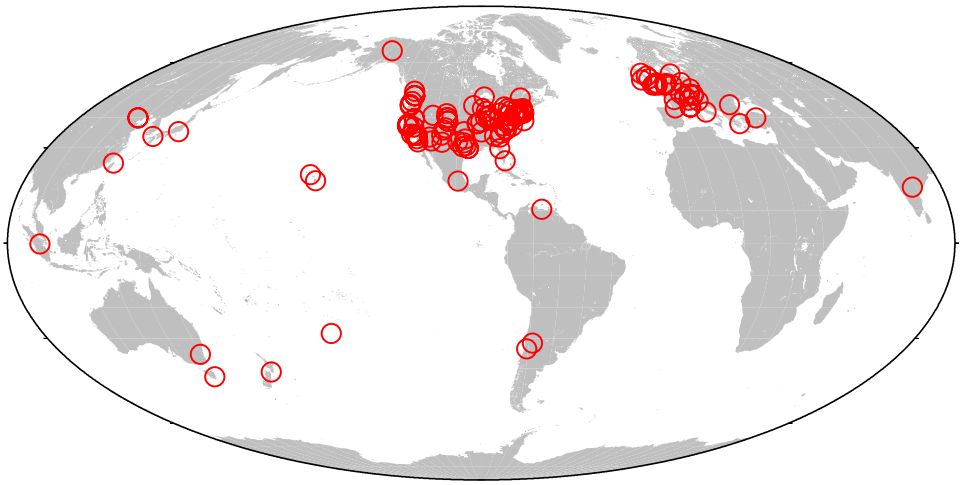

IRIS was founded as a consortium of 34 U.S. research institutions. Today, projects that utilize IRIS-managed facilities are led by investigators at hundreds of institutions world-wide. Red symbols indicate institution of researchers that contributed to this volume.

Nearly 250 community-submitted "one-pagers" have been collected and organized into eleven categories. The Earth is a continuum, with mineralogical and dynamical phenomena spanning large regions or depths; this, combined with the fact that many investigations cross traditional boundaries, results in an organizational challenge: the ordering of research projects is somewhat subjective and some projects might fit naturally into more than one category. For example, studies of the uppermost mantle—perhaps as revealed by seismic shear wave anisotropy—both describe lithospheric fabric and mineralogical structure and offer insight about deeper dynamical phenomena in the upper mantle associated with subduction. Classification challenges aside, the breadth of discoveries remains readily apparent. Following the topic of Education and Outreach, the one-pagers are grouped into four categories about seismic sources and faults, and then six categories linked to structure and dynamics generally in progressively deeper layers of the Earth:

- Education and Outreach
- Earthquake Source Studies
- Episodic Tremor and Slip, and Triggered Earthquakes

- Non-Earthquake Seismic Sources
- Fault Structure
- Crustal Structure
- Lithosphere and Asthenosphere Structure
- Upper Mantle Structure
- Lower Mantle Structure
- Whole Mantle Structure
- Outer and Inner Core Structure

The one-pagers are preceded by topical summaries that frame IRIS-enabled science in traditional and emerging areas of research. The summaries emphasize a number of areas that were central to Seismological Grand Challenges in Understanding Earth's Dynamics Systems, a community written document resulting from the Long-Range Science Plan for Seismology Workshop (September 18-19, 2008, Denver CO). The summaries were not intended to exhaustively survey the science of all of the contributed one-pagers; rather, they provide clear examples of exciting areas of research that are core to understanding how Earth works, from the outer veneer of Earth upon which we live, to the planet's center. The summaries also include scientific pursuit of understanding resources and hazards, including coupling of the solid Earth with the oceans and atmosphere. The following summaries are included:

- Why Do Faults Slip?
- How Do Plates Evolve?
- The Lithosphere-Asthenosphere Boundary
- The Global Stress Field: Constraints from Seismology and Geodesy
- How are Earth's Internal Boundaries Affected by Dynamics, Temperature, and Composition?
- Near-Surface Environments - Hazards and Resources
- Interdisciplinary Study of the Solid Earth, Oceans and Atmosphere

A number of fields not in the traditional scope of seismology have grown immensely over the last five years, including ambient noise tomography, documentation and characterization of episodic tremor and slip, the triggering of earthquakes, mapping of the lithosphere-asthenosphere boundary, mapping of the mantle's dynamical motions (e.g., slabs and plumes), especially as they relate to surface observables (e.g., plate tectonics), and coupling between Earth's outermost shells (hydrosphere, atmosphere, and solid Earth). While the successes are readily apparent, many of the discoveries introduce new unknowns and exciting future directions, some of which are framed in the topical summaries. Thus, the first 25 years of IRIS powerfully exemplify a community coming together to build and sustain services that both accelerate progress and stimulate unanticipated and serendipitous development and discovery by freely providing data and resources to the whole globe. The data quality and quantity have enabled a far clearer picture into earthquake processes and Earth circulation science (from plates to whole mantle and core convection), and at the same time raised important new questions. It is important to note that E&O has been defined by similar innovation and progress over the last 5 years. The E&O one-pagers demonstrate IRIS-facilitated science, tools, and products not only are entering the classroom, but also living room and libraries, and beyond.

The topical summaries and project descriptions frame the emergence of IRIS into a new era, one in which traditional boundaries are being crossed as scientists and educators from a wide swath of disciplines are coming together to answer scientific questions well beyond the traditional scope of seismology. The pages that follow demonstrate the remarkably broad (and broadening) scope of research enabled by the IRIS facilities. In an era where other disciplines have also progressed rapidly over the last decade—active tectonics, geomorphology, mineral physics, glaciology, and geodynamics, to name a few—these pages demonstrate how readily researchers from those disciplines can form productive collaborations with seismologists, in part from strong support by responsive services. As high quality data continue to be collected, archived, and widely disseminated, the scientific scope of seismologically related research will continue to grow; we anticipate new research directions will be motivated by the discoveries described here.

Interdisciplinary Study of the Solid Earth, Oceans and Atmosphere

Michael Hedlin, Kris Walker and Catherine de Groot-Hedlin *(University of California, San Diego)*

In many respects the geophysical study of the Earth's atmosphere and oceans is akin to our study of the Earth's solid interior. Geophysical phenomena radiate energy in all three media providing signals that can be used to study the source characteristics as well as illuminate the structure of the media the signals probe. The three media are interconnected not only by similar intellectual challenges and opportunities but also by physics. Boundaries between the media are not rigid; signals that originate at a source in one medium often transmit into the adjacent medium. Alternatively, some sources (e.g. volcanoes, shallow earth or ice quakes, ocean swell) are located at a boundary between media and may inject energy into both media simultaneously. Considering this interconnectedness, and given that today we have unprecedented coverage of the three media with global and dense regional networks of sensors, there are unprecedented opportunities for groundbreaking interdisciplinary research [*Arrowsmith et al.*, 2010]. In this brief summary we outline a few key research areas and sketch out potential avenues for interdisciplinary research.

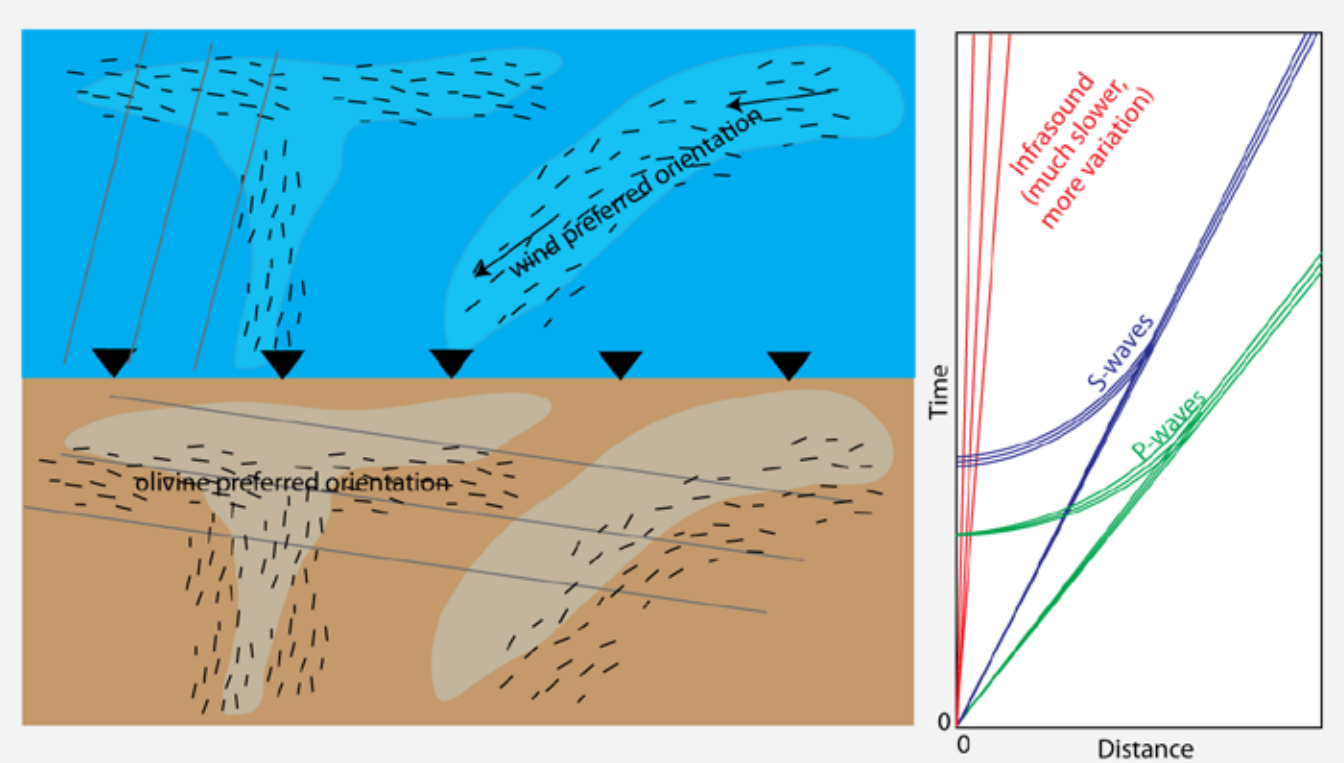

This cartoon shows typical wavefront geometries observed at the Earth's surface for atmospheric infrasound (left-top) and solid earth seismic P and S waves (left-bottom) for telesonic and teleseismic events, respectively. This cartoon also illustrates atmospheric acoustic velocity anisotropy due to the wind (left-top) and mantle seismic velocity anisotropy due to the alignment of olivine crystals (left-bottom). Both seismic energy and acoustic energy can be detected by seismometers (triangles) at the solid earth/atmosphere interface because of seismic-acoustic coupling. The panel on the right shows the move-out of relatively slow infrasound waves and relatively fast P and S seismic waves in the solid earth. Although not illustrated here, similar coupling occurs at the atmosphere-ocean interface and at the seafloor.

Constraining atmospheric structure

Much progress has been made drawing on data from ground-based sensors and meteorological satellites to model the structure of the atmosphere. One plainly evident and key difference between the structure of the atmosphere and the solid earth is that the atmosphere varies constantly at all time scales. A key difference in constraining this structure is that direct measurements of acoustic travel times are not incorporated into atmospheric models. Models of atmospheric wind speed are less certain above 35 km altitude as there are no direct routine global measurements at these altitudes. Winds above 35 km are inferred from temperature and pressure fields. Improving the accuracy of atmospheric models would not only benefit the atmospheric

acoustics community by permitting a better understanding of infrasound waveforms but many other communities in atmospheric science that rely on accurate models of the atmosphere.

Another related key issue in atmospheric acoustics is that the global network is very sparse. There are currently ~ 45 globally spaced infrasound arrays that sample infrasound signals that traverse structure of the atmosphere, which varies at all length scales, as well as time scales. This structure is grossly under-sampled by these infrasound stations, impeding great progress in our understanding of certain aspects of infrasound propagation. For example, the sparse global network impedes progress in testing and refining atmospheric velocity models using acoustic travel times.

The fact that infrasound signals readily couple to the Earth's surface and generate seismic waves is proving to be very helpful in infrasound science. The USArray seismic network records several hundred large atmospheric acoustic sources each year at a density that is considerably greater than what is offered by the infrasound network. Although the infrasound community has known that acoustic energy from any source may take one of several paths to the ground, and have inferred the existence of acoustic wave travel time branches, it has not been possible to view and study these branches in any detail using infrasound data. The USArray is shedding light on acoustic branches that are akin to seismic branches that exist in the solid Earth, paving the way for progress in probing the structure of the atmosphere and testing, and eventually improving, our models of atmospheric structure [*Hedlin et al.*, 2010].

Interdisciplinary study of "dual" geophysical phenomena

Much of the activity in the solid Earth, atmosphere and oceans occurs near a boundary between these media. Although we have long known that various sources that are located at a boundary between media and inject energy into both, we have historically more often studied such sources using one type of sensor.

Volcanoes: A common example is volcanoes, which can be intense acoustic sources, but have long been monitored and studied seismically. Although much progress has been made on the physics of volcano processes using seismic data, our understanding of the seismo-acoustic volcano source is likely to remain incomplete without also considering the information carried up into the atmosphere by acoustic energy that these sources emit.

Shallow earthquakes: Thrusting earthquakes readily couple to infrasound above the hypocenter due to piston-like vertical ground motion, and at greater distances due to surface waves. It is now well documented that rugged topography set in motion by a distant earthquake also radiates acoustically into the atmosphere [*e.g. Le Pichon*, 2002]. Infrasound arrays are shedding light on these extended earthquake sources by providing the data needed to accurately track the progression of the seismic wavefield across entire mountain chains.

Ice quakes: Ice quakes are readily detected seismically however locating them with these instruments is complicated by inherently complex, and inaccurate, ice velocity models. These events are also readily detected, and accurately located, by infrasound arrays. Understanding processes that lead to ice-edge loss has major implications in a changing climate, as coastal currents are impacted by fresh-water discharge.

Joint studies and inversions using microbaroms and microseisms

"Microbaroms" are acoustic oscillations with a period of 3 to 10 s and are typically recorded with amplitudes in the tenths of Pascals. The seismic counterpart, "microseisms," have periods of 3 to 20 s. It has been known for a long time that the occurrence of microbaroms and microseisms are correlated to ocean wave activity, either in the deep ocean or along the coastlines. These two signals are often studied individually, with relatively small infrasound arrays or seismic networks. Recent studies seek to use variations of microseism generation over the long-term (decades) to study changes in ocean wave energy that may be related to climate variations. Hypotheses to explain microseisms have existed for a long time, but rigorous testing of these have proven to be difficult due to limited data availability. Hypotheses for microbarom source generation have more recently been advanced. When the USArray transportable array will be upgraded with infrasound sensors, as described below, this network will be

extremely well suited for not only studying the source physics associated with microseisms and microbaroms in unprecedented spatial and temporal detail, but also imaging the structure of the solid Earth and atmosphere probed by this "song of the sea."

The seismo-acoustic USArray

Although seismic and acoustic sensors have been deployed together (e.g. seismo-acoustic arrays deployed by Southern Methodist University in Texas, Nevada and South Korea, some stations in the Global Seismographic Network) it is not common to combine the two. The 400 station USArray transportable array is currently being enhanced with the addition of infrasound microphones and long-period (DC to tens of seconds) air pressure sensors at each element. The recording of acoustic energy will accelerate the study of acoustic branches by yielding direct recordings of atmospheric acoustic signals, rather than acoustic-to-seismic coupled signals. Simultaneous and continuous observations of atmospheric and seismic noise should facilitate adaptive seismometry – a process analogous to adaptive optics in which the effects of atmospheric loading at the Earth's surface are accounted for on seismic channels to reduce noise at long periods.

The unprecedented semi-continental seismo-acoustic network should also benefit atmospheric science. The surface air pressure is one of the key observables in atmospheric dynamics. The structure and evolution of the surface pressure field characterizes and to some extent drives atmospheric processes on planetary scales (climate, general circulation, atmospheric tides), synoptic scales ("weather"), mesoscales (gravity waves, jet streams, inertial oscillations) and microscales (convection, turbulence, Kelvin-Helmholtz instabilities, nocturnal drainage flows). Therefore, monitoring, predicting and understanding climate, weather and air quality are impossible without accurate and precise observations of the surface pressure over a wide range of time and length scales.

Looking to the future: interdisciplinary research

The solid earth, oceans and atmosphere are interconnected and it seems clear that interdisciplinary studies can provide new insights into the workings of a wide range of geophysical phenomena. It should be possible to use the well-developed seismic recording, archiving, and data distribution approach of IRIS to effectively study not only the earth's solid interior structure and geophysical phenomena, but to provide a deeper understanding of atmospheric structure and atmospheric and oceanic activity. Perhaps as this interconnectedness between fields becomes clearer it will become more common to collect multiple types of data (e.g. add infrasound sensors to a seismic deployment, and vice versa) and increase the scientific return from our investment in infrastructure.

References

Arrowsmith, S.J., Johnson, J.B., Drob, D. and Hedlin, M.A.H., 2010, The seismo-acoustic wavefield: A new paradigm in studying geophysical phenomena, *Rev. Geophys.* (in press).

Hedlin, M.A.H., Drob, D., Walker, K. and de Groot-Hedlin, C., 2010, A study of acoustic propagation from a large bolide in the atmosphere with a dense seismic network, *J. Geophys. Res.*– Solid Earth (in press).

Le Pichon, A., J. Guilbert, A. Vega, M. Garces, and N. Brachet (2002b), Ground-coupled air waves and diffracted infrasound from the Arequipa earthquake of June 23, 2001, *Geophys. Res. Lett., 29*(18), 1886, doi:10.1029/2002GL015052.

Near-Surface Environments – Hazards and Resources

M. Beatrice Magnani *(CERI, University of Memphis)*

As worldwide population grows, so do societal demands on our planet. In the last few decades, human activity has expanded to areas never previously colonized, sometimes at the cost of extensive environmental degradation and resource depletion. Communities have developed in areas prone to geohazards and have become vulnerable to seismic, volcanic and landslides threats. Even renewable resources, such as groundwater, have become increasingly scarce and fragile. Within the scientific community there is wide recognition of the challenges scientists and policymakers face in effectively forecasting natural events, preparing communities to survive hazards, and sustainably managing available resources.

In this context, near surface geophysics, intended as the study of the shallow layers of the Earth from the surface to a depth of ~3 km, plays a critical role. Crucial information for hazard assessment is locked within the upper crust and most human activities rely on vital resources that are within the first 5 km of our solid planet. The mechanical properties of the shallow materials are critical both for engineering purposes and for seismic hazard assessment and mitigation policies, as they control ground motion and amplification effects during large earthquakes. Imaging of deformation (faulting and folding) of shallow layers is important in predicting future ground rupture and associated hazards. The youngest sediments deposited at/near the surface have recorded with great detail past climate changes and therefore can provide us with a key to decipher the present climate variability.

From a historical point of view, virtually every shallow investigation technique can be traced back to petroleum exploration, and even earlier, as electrical methods applied to mining date as far back as the 1860s. The growth and success in the last 75 years has been guided by advances in instruments and computer-processing techniques. Thanks to technological progress, today's near surface equipment is financially affordable, easily deployable and user-friendly. This versatility has made near surface investigation approachable to a large number of investigators, so that the community of scientists/users has grown both in number and diversity and, over the last three decades, sections and focus groups have emerged within every major professional organization. Today, near surface geophysics applications are as numerous and multidisciplinary as societal needs, and span from groundwater and mining exploration to engineering, from archeology to seismic hazard, from remediation planning at contaminated sites to glacial and paleo-climatology studies.

Examples

The adaptability of the near surface high-resolution method makes it one of the best tools to deploy in the field for rapid response missions in case of catastrophic natural events such as large magnitude earthquakes, landslides and volcanic eruptions. Immediately after the January 12, 2010 Haiti M7.9 earthquake, an NSF-funded rapid response expedition was able to image the underwater effect of the earthquake by mapping the shifted sediments on the seafloor and by imaging the Enriquillo-Plantain Garden Fault beneath the seafloor using CHIRP, multibeam and sidescan sonar (Fig. 1). Rapid response and high resolution imaging tools in these situations are critical for assessing the risk of large earthquakes in the same area in the weeks and months after a large earthquake.

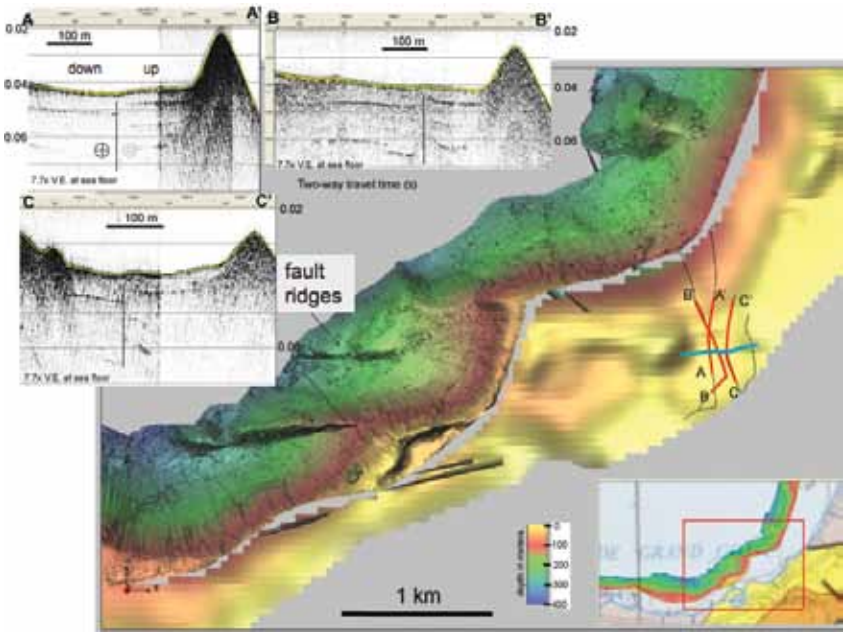

Figure 1: High resolution seismic and bathymetry data collected using a Kundson pole mounted 3.5 KHz CHIRP and by a Reson SeaBat 8101 gridded at 8 m merged with the seafloor picked on the "mini-chirp" gridded at 50 m over the area of the January 12, 2010 M7.9 Haiti earthquake. Two strands of the Enriquillo-Plantain Garden Fault are visible as seafloor scarps on the slope and in the shallow subsurface (Hornbach et al., submitted to Nature Geosciences).

The application of near surface geophysics (especially seismology) has been particularly successful in seismic hazard assessment and neotectonic studies. Locations, magnitudes and dates of earthquakes are critical information for probabilistic seismic hazard assessments, which in turn dictate modern hazard zoning, emergency response and risk mitigation strategies. Near surface seismic imaging often bridges the gap existing between deeper, more conventional basin-scale data and the surface (Fig. 2), allowing the integration of information derived from other disciplines (e.g. geology, paleoseismology).

Last, but not less important, near surface geophysical methods are an excellent tool to use for education. Thanks to the availability of equipment, teachers and researchers routinely include field courses in the existing curriculum where students learn hands-on to plan, deploy, acquire, process and interpret geophysical data. Field courses provide dynamic and challenging environment where students learn the fundamentals of this discipline and its practical application from beginning (planning) to end (interpretation).

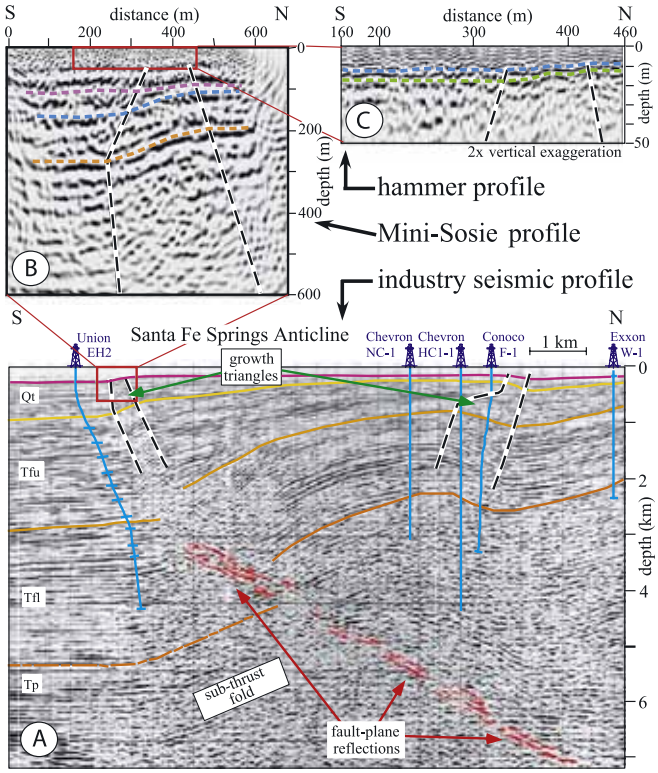

Figure 2: Multiscale seismic reflection images of the forelimb fold structure of the Puente Hill Thrust (PHT) near the Los Angeles (CA) metropolitan area, showing upward narrowing zone of active folding (growth triangle) delimited by sharply defined axial surfaces. A) Industry profile; B) MiniSosie profile; C) Hammer profile. These overlapping profiles provide a complete image of forelimb folding above the segment of the Puente Hills thrust fault that ruptured during the 1987 M6.0 Whittier Narrows earthquake. (After Leon et al., 2007).

The way forward

In spite of its accessibility, imaging the shallow subsurface poses a formidable challenge, because of the heterogeneity of the near surface Earth structure. The most reliable solutions of near surface problems are achieved by using a combination of shallow exploration methods (e.g. seismic, electrical, electromagnetic, gravity and radar). Integration of different datasets (through joint inversion, for example) is producing promising results in extracting mechanical properties of materials (e.g. permeability, porosity) and their variation through time. This is vital information for monitoring water (or contaminant) transport through aquifers and to plan a sustainable management of this precious resource.

Virtually every field can benefit from an expansion from 2D to 3D methods. Due to the daunting heterogeneity of the shallow Earth, the third dimension is critical in several applications of near surface geophysics. For example, site amplification and non-linear response of shallow materials associated with strong shaking can only be effectively evaluated by mapping the subsurface seismic properties in 3D over large areas.

Without doubt the strength of near surface geophysics lies in the high resolution it provides, which is second only to drilling, trenching and other direct investigation methods. Improving resolution and bandwidth can and should be pursued, as well as achieving faster and more reliable data processing methods capable of abating the noise that plagues near surface data. This progress will naturally unfold as the user base continues to expand and new practical applications of this method emerge.

References

Hornbach, M.J., Braudy, N., Briggs, R.W., Cormier, M.-H., Davis, M.B., Diebold, J.B.,Dieudonne, N., Douilly, R., Frohlich, C., Gulick, S.P.S., Johnson, H., Mann, P., McHugh, C., Mishkin, K., Prentice, C.S., Seeber, L., Sorlien, C., Steckler, M.S., Smythe, S.J., Taylor, F.W., Templeton, J., Uplift and sliding and tsunamigenesis along a strike-slip fault, *Nature Geosciences*, in review, 2010.

Leon, L.A., Christofferson, S.A., Dolan, J.F., Shaw, J.H. And Pratt, T., Earthquake-by-earthquake fold growth above the Puente Hills blind thrust fault, Los Angeles, California: Implications for fold kinematics and seismic hazard, *J. Geophys. Res., Vol. 112*, B03S03, doi:10.1029/2006JB004461, 2007.

Why Do Faults Slip?

Emily Brodsky *(University of California, Santa Cruz)*

One of the most fundamental goals of seismology is to define the forces and processes initiating and propagating earthquake fault rupture. Generating such a mechanistic understanding requires probing the variety of slip events on faults with the full seismological arsenal.

Determining the physics of fault slip first requires the identification of the earthquake locations, the kinematics of the slip, and the relationship of both to long-term tectonic processes. IRIS's GSN combined with temporary deployments and the extensive shared data from other networks available at the DMC has enabled new connections between slip and plate motions to be made, from the Pacific rim to Southern Africa. Identifying the rupture kinematics correctly is a prerequisite to using geological constraints to identify the physical conditions necessary for rapid slip. For instance, *Bilek et al.* (2009) show that there are systematic along-strike variations in rupture velocity in the Aleutians, suggesting distinct geological features that affect rupture propagation can be identified. Having a global database of rupture properties for all moderate to large earthquakes is now within reach. New methodologies that capitalize on the expanded continuous waveform archive promise vastly more precise locations in the near future [*Barmin et al.*, 2010].

Earthquake locations can also generate surprises. As USArray marches across the country, new populations of intraplate earthquakes are being discovered throughout the continent [*e.g., Lockridge et al.*, this volume]. The high quality seismograms being recorded by both the TA and FA deployments allow seismologists to measure the stress changes, rupture properties and kinematics of these intraplate events to determine whether or not they are systematically different in any way from interplate earthquakes. Such comparisons can elucidate the role of fault maturity in determining rupture properties.

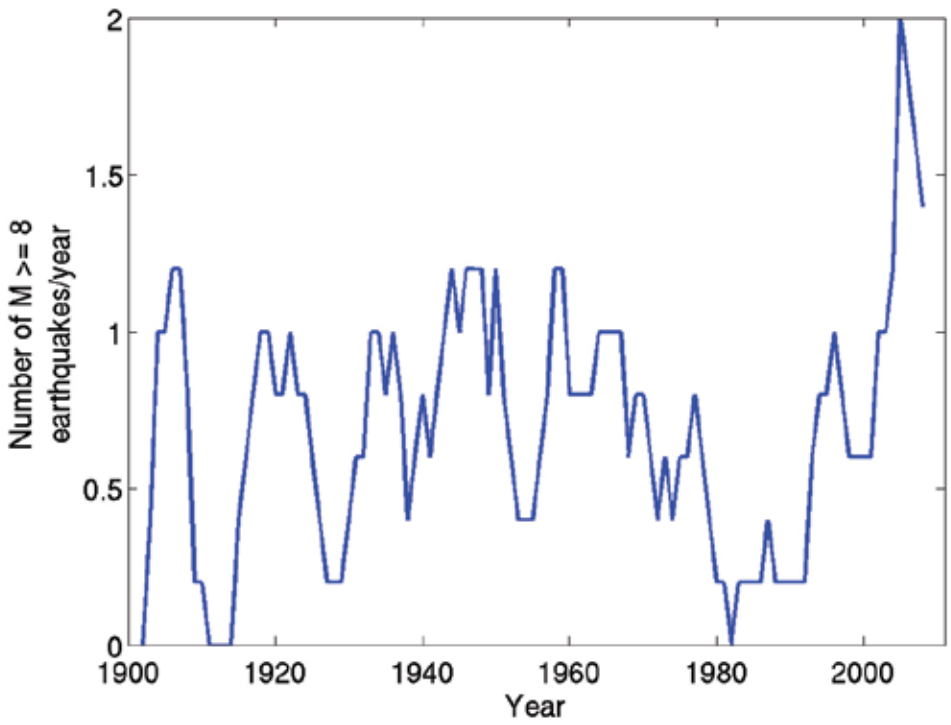

Fig. 1. Number of shallow (depth ≤ 60 km) earthquakes per year with M ≥ 8.0 for the composite PAGER Catalog10, with M being the preferred magnitude as reported by the catalog. Data are smoothed with a five-year running average. The average rate prior to 2004 is 0.63 ± 0.34 earthquakes/year. The rate peaks at 2 earthquakes/yr after the 2004 Sumatra-Andaman event, which is over 60% higher than any prior peak rate, and more than 3 times the average rate over the previous century. The average rate over the 5.5 years following the 2004 Sumatra-Andaman earthquake is 1.64 earthquakes/yr, which is 2.5 times the long-term average.

One of the most exciting new avenues for probing fault rupture has arisen out of the discovery of episodic tremor and slip. This novel set of seismological phenomena provides information about the array of fault failure processes. No longer is it thought that faults are limited to either stick-slip (seismic slip) or long-term creep. The observations in Cascadia, California, Japan, Chile, Mexico, Costa Rica and New Zealand, all demonstrate that the spectrum of fault slip is much richer than anticipated. Like earthquakes, the episodic creep events occur over a range of sizes; but unlike earthquakes, the largest creep events tend to be fairly regular and predictable. These regular changes in the stress state of major subduction zones could make large earthquakes more likely during these predictable periods. At least one observation finds that a creep event triggered a large (M7) earthquake [*Prichard et al.*, this volume].

Measurements thus far indicate that episodic tremor and slip occurs in distinct zones from seismic rupture or steady creep. These observations lend strong evidence to the hypothesis that rupture characteristics are controlled by the frictional properties of the fault at well-bounded pressure and temperature conditions. This evidence is particularly interesting in light of the recent work on the velocity dependence of rock friction. A series of laboratory experiments and theoretical studies in the last decade have shown that high-speed fault friction is expected to be dramatically lower (coefficient of friction μ=0.1-0.2) than the static failure values normally used in Byerlee's Law (μ=0.6-0.85) [*e.g. Brodsky and Kanamori*, 2001; *Andrews*, 2002; *Di Toro et al.*, 2004; *Rice* 2006; *Yuan and Prakash*, 2008; *Tanikawa and Shimamoto*, 2009]. These inferences are currently supported by the relative low heat flow measured over faults after earthquakes [*Kano et al.*, 2006] and geological evidence for unusual products formed in seismogenic zones [*e.g., Boullier et al.*, 2009]. Therefore, the fault traction during the relative slow slip of the creep events should be governed by a distinct set of processes from those governing slip during earthquakes. Comparing the seismologically derived source histories of creep events and earthquakes provides an opportunity to test these predictions.

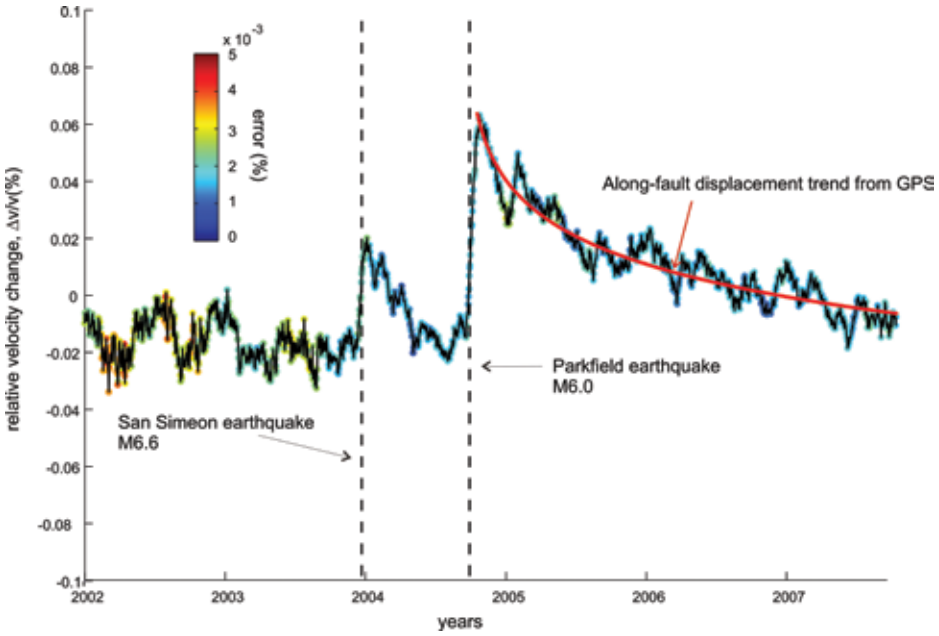

Figure 2: Temporal evolution of the velocity in the region of Parkfield for the period 2002-2008 (see *Brenguier et al.* 2008 for details).

Any further understanding of the control fault properties have on rupture requires an understanding of the role of heterogeneity in determining nucleation sites and controlling the extent and vigor of rupture. Interestingly, some of the clearest insight into this problem in recent years has come from seismological observation on non-tectonic slip processes. A suite of observations on landslides, icebergs and glaciers with PASSCAL portable instruments show that the non-tectonic systems can have repeating, regular earthquakes and distinctive regions (asperities) of initiation. Such regular behavior is occasionally also seen on tectonic fault systems, such as the repeating multiplets at Parkfield [*Nadeau and Johnson*, 1998]. The comparison suggests that some of these novel non-tectonic systems behave surprisingly like a simple slider-block. The applicability of a simple fault model to several novel classes of failure provides new physical models for those phenomena while also illuminating the important role of interaction in tectonic systems. For simple isolated regions with some degree of creep, a slider block framework works well. The analogy may run even deeper. For instance, non-tectonic asperities can have radiated energy just like tectonic ones [*Moyer et al.*, this volume; *Dreger et al.*, this volume]. The juxtaposition of these behaviors suggests that some of the complexity of tectonic systems may be a result of the strongly coupled nature of fault systems.

The interactions among fault strands is a hallmark of most tectonic systems. The mutual triggering also provides opportunities to directly measure the stresses required for earthquake or tremor initiation. This strategy is yielding insight into the role of afterslip in generating nearfield earthquakes [*Peng and Zhao*, this volume]. At a larger scale, *Brodsky et al.* [this volume] suggest that the measured triggering thresholds combined with the strong global shaking of the M9.2 Sumatra earthquakes can explain the recent spurt of magnitude 8 earthquakes. These triggering studies are beginning to directly address earthquake prediction by probing the conditions necessary for earthquake initiation and providing a methodology to track whether the failure stress changes in time. New technologies, like distributed MEMS sensors, promise to provide more information about earthquake interactions during the hard-to-capture critical moments of an early aftershock sequences [*Lawrence and Cochran*, this volume].

Another probe of fault evolution is provided by measuring the seismic velocity (and by inference the stress) changes during an earthquake cycle. This method has only recently become feasible on a large scale as a direct result of the now continuous recording at high resolution of stations archived at the IRIS DMC. *Xu et al.* [this volume] used an ambient noise strategy to capture strength changes in the Southwest Pacific after the 2004 Sumatra earthquake and *Brenguiller et al.* (2008) showed spectacular tracking of the fault zone velocity evolution and aftershock rates following the 2004 M6 Parkfield. As this measurement was made near the SAFOD drill site, the study illustrates the potential of combining modern geodetic, seismic, rheologic and geologic information to ultimately determine why faults slip.

References

Andrews, D.J., 2002. A fault constitutive relation accounting for thermal pressurization of pore fluid. *J. Geophys. Res., 107*(B12), 2363, doi:10.1029/2002JB001942.

Barmin, M.P., A.L. Levshin, Y. Yang, and M.H. Ritzwoller, 2010. Epicentral Location Based on Rayleigh Wave Empirical Green's Functions from Ambient Seismic Noise. Submitted to *Geophys. J. Int*.

Bilek, S.L., H.R. DeShon, and E.R. Engdahl, 2009, Along-Strike Variations in Shallow Earthquake Distribution and Source Parameters Along the Kurile-Kamchatka Arc, EOS Trans AGU, 90(52), Fall Meet. Suppl., Abstract T23B-1908.

Boullier, A.M., Yeh, E.-C., Boutareaud, S., Song, S.-R., and Tsai, C.-H. 2009. Microscale anatomy of the 1999 Chi-Chi earthquake fault zone. *Geochem. Geophys. Geosyst., 10*, Q03016,doi:10.1029/2008GC002252.

Brenguier F., M. Campillo,C. Hadziioannou, N.M. Shapiro, R.M. Nadeau, E. Larose, 2008, Postseismic Relaxation Along the San Andreas Fault at Parkfield from Continuous Seismological Observations, *Science, 321*, 1478 – 1481.

Brodsky, E.E., and H. Kanamori, 2001. Elastohydrodynamic lubrication of faults. *Journal of Geophysical Research, 106*(B8), 16357–16374.

Kano, Y., J. Mori, R. Fujio, H. Ito, T. Yanagidani, S. Nakao, and K.-F. Ma, 2006, Heat signature on the Chelungpu fault associated with the 1999 Chi-Chi, Taiwan earthquake, *Geophys. Res. Lett., 33*, L14306, doi:10.1029/2006GL026733.

Nadeau, R. M., and L. R. Johnson, Seismological studies at Parkfield VI: Moment release rates and estimates of source parameters for small repeating earthquakes, B*ull. Seismol. Soc. Am., 88*, 790–814, 1998.

Rice, J.R., 2006. Heating and Weakening of fault during earthquake slip. *J. Geophys. Res., 111*, B05311, doi: 10.1029/2005JB0040006.

Tanikawa, W., and T. Shimamoto, 2009, Frictional and transport properties of the Chelungpu fault from shallow borehole data and their correlation with seismic behavior during the 1999 Chi-Chi earthquake, *J. Geophys. Res. 114*, B01402, doi:10.1029/2008JB005750.

Yuan, F. and V. Prakash, 2008. Slip weakening in rocks and analog materials at co-seismic slip rates, *J. Mech. and Phys. Solids, 56*, 542-560.

The Global Stress Field: Constraints from Seismology and Geodesy

William E. Holt *(Stony Brook University)*

Seismology has played a fundamental role in advancing our understanding of the dynamics of the Earth's lithosphere. Quantitative dynamic models of the lithosphere rely on accurate structural constraints of the crust and mantle. Other constraints are provided by earthquake source mechanisms, seismic anisotropy measurements, and attenuation studies. IRIS has provided a major infrastructure that has facilitated more than two decades of progress in understanding Earth structure and earthquake source mechanisms. These structural and kinematic constraints form the observational basis upon which dynamic models can be built that address the driving forces of plate tectonics and the role of lateral and vertical variations in rheology.

For example, the global model of *Ghosh et al.* [2008, 2009] relies heavily on constraints from seismic observations. They address the dynamic problem by solving the vertically integrated force balance equations for a self-consistent solution of the depth-integrated deviatoric stress field within the Earth's lithosphere. The driving forces that feed into this model are observationally constrained values. The first driving force is associated with differences in gravitational potential energy (GPE) of the lithosphere. GPE is the depth integrated vertical stress, and thus depends on topography (including dynamic topography) and density values of layers from surface to base of lithosphere. Therefore, constraints for GPE values are constrained, in part, by surface wave and receiver function analyses [e.g., *Xu et al.*, 2007; *Yang et al.*, 2009]. A second major driving force is associated with coupling of lithosphere with mantle flow, which yields both radial and horizontal tractions at the base of the lithosphere. This coupling gives rise to lithospheric stresses. *Ghosh et al.* [2008] determined these tractions using an instantaneous global 3-D convection model that had both lateral and radial mantle viscosity structure; mantle seismic tomography models helped to define the mantle density variations. Because tomographic models often reveal the complexity in geometry and depth extent of foundered (subducted) lithosphere [e.g., *Pesicek et al.*, 2010], calculations used in *Ghosh et al.* [2008] include a model 3-D flow field that mimics subduction on a global scale.

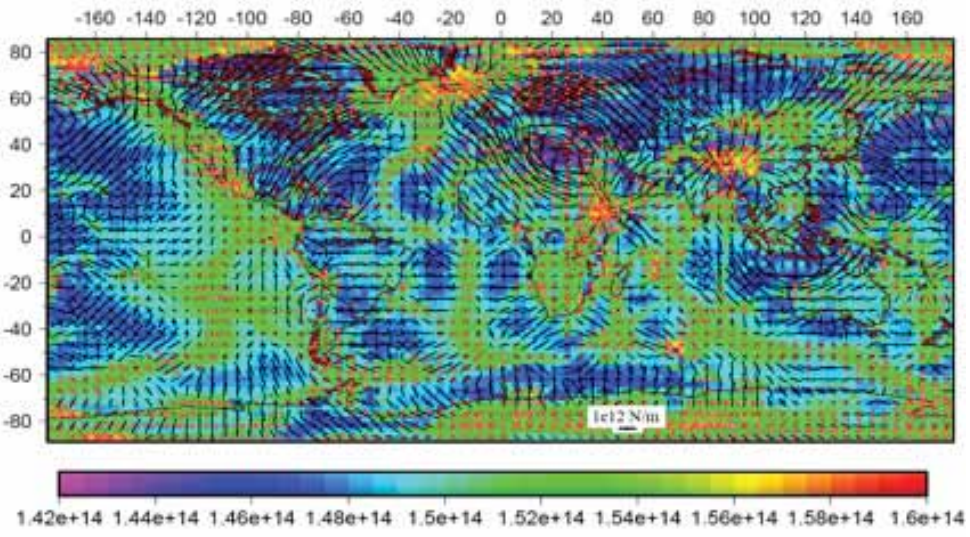

Figure 1. Depth integrated deviatoric stress field solution [Ghosh et al., 2009] (lines), plotted on top of gravitational potential energy (GPE, colored map). The GPE values are defined by seismically constrained crustal thickness values as well as ocean plate cooling models. Red arrows are deviatoric extension directions; bold arrows are deviatoric compression directions.

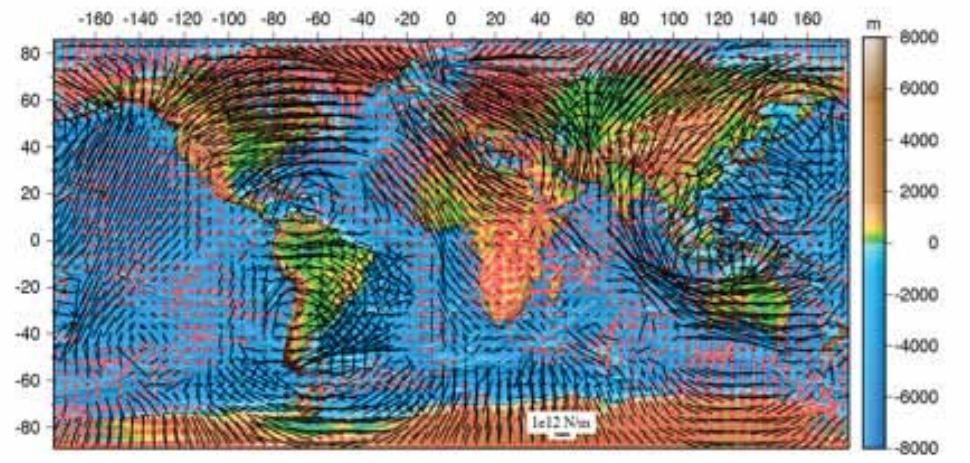

Figure 2. Best fit total deviatoric stress field that is associated with global GPE differences (Figure 1) and applied tractions from a mantle circulation model that includes effects of subduction and upwelling regions [Ghosh et al., 2008]. Red arrows are deviatoric extension directions; bold arrows are deviatoric compression directions.

The global dynamic model described here was then tuned

to provide a best match with the Global Strain Rate Model [*Kreemer et al.*, 2003], which is defined by over 5000 GPS observations, with additional constraints from the Global Centroid Moment Tensor Catolog [*Ekström et al.*, 2005; *Hjorleifsdottir and Ekström*, 2010]. Modeling reveals that a best fit to plates and deforming plate boundary zones is achieved if driving forces are partitioned equally between stresses arising from GPE differences and stresses associated with coupling between lithosphere and mantle convection. Other factors required are (A) a strong viscosity contrast (2-3 order magnitude) between lithosphere and asthenosphere (asthenosphere viscosity is of order 1x1019 Pa-s), (B) mantle flow that leads plate motion beneath major orogens such as the Andes and Central Asia, and (C) a long wavelength counterflow beneath western North America. Depth integrated stress magnitudes within the lithosphere are 1-4x1012 N/m. This level of stress energy in the plate tectonic system implies that weakening mechanisms (weak faults, presence of water in upper mantle, etc.) are important for enabling strain accommodation within the plate boundary zones on Earth. Many of these findings, such as the mantle flow field that yields a best match to stress indicators, can be further tested in a variety of tectonic regions with additional seismic observations.

Although the dynamic model of *Ghosh et al.* [2008, 2009] includes the influence of 3-D subduction related flow, it nevertheless lacks the effects of stress guide connectivity between deep slabs and surface plates, and it also lacks the effects of slab bending at the trenches. Therefore, further refinements in our understanding of the driving forces responsible for earthquakes, plate motions, and tectonic processes of mountain building and basin formation in general, will require high resolution, full 3-D dynamic models of the entire planet from core to surface. Constraints for such high-resolution models will come, in part, by continuing to take advantage of advances in seismology [e.g., *Spasojevic et al.*, 2009]. These future advances will be made possible through improved future station coverage of continents and oceans, and the strong PI-driven science that IRIS enables.

References

Ekstrom, G, Dziewonski, AM, Maternovskaya, NN, Nettles, M (2005), Global seismicity of 2003: centroid-moment-tensor solutions for 1087 earthquakes, *Phys. Earth Planet. Inter., 148*.

Ghosh, A., W. E. Holt, L. Wen, A. J. Haines, and L. M. Flesch (2008), Joint modeling of lithosphere and mantle dynamics elucidating lithosphere-mantle coupling, *Geophys. Res. Lett., 35*, L16309, doi:10.1029/2008GL034365.

Ghosh, A., W. E. Holt, and L. M. Flesch (2009), Contribution of Gravitational Potential Energy Differences to the Global Stress Field, *Geophys. Jour. Int.*, doi: 10.1111/j.1365-246X.2009.04326.x

Hjorleifsdottir, V., Ekstrom, G (2010), Effects of three-dimensional Earth structure on CMT earthquake parameters, *Phys. Earth Planet. Inter, 179*.

Kreemer, C., W.E. Holt, and A. J. Haines (2003), An integrated global model of present-day plate motions and plate boundary zones, *Geophys, J. Int., 154*(1), 8-34.

Pesicek, JD, Thurber, CH, Widiyantoro, S Zhang, H DeShon, HR Engdahl, ER (2010), Sharpening the tomographic image of the subducting slab below Sumatra,the Andaman Islands and Burma, *Geophys. J. Int., 182*.

Spasojevic, Sonja, Liu, Lijun, Gurnis, M. (2009), Adjoint models of mantle convection with seismic, plate motion, and stratigraphic constraints: North America since the Late Cretaceous, *Geochem. Geophys. Geosyst, 10*.

Xu, LL, Rondenay, S., van der Hilst, RD (2007), Structure of the crust beneath the southeastern Tibetan Plateau from teleseismic receiver functions, *Phys. Earth Planet. Inter., 165*.

Yang, YJ, Ritzwoller, MH, Levshin, AL, Shapiro, NM (2009), Ambient noise rayleigh wave tomography across Europe, *Geophys. J. Int., 168*.

How Do Plates Evolve?

Gene Humphreys *(University of Oregon)*

Understanding the nature, creation, and evolution of plates has progressed rapidly in the ~40 years since the plate tectonics scientific revolution recognized their existence and dominant role in Earth behavior and evolution. This remarkable progress is a result of advanced observations in many disciplines, often focused with concepts provided by consensus models, but also by accidental discoveries. The following represents a consensus framework of this complex subject; further integration, model development, and fundamental observations will surely lead to refinements of these views.

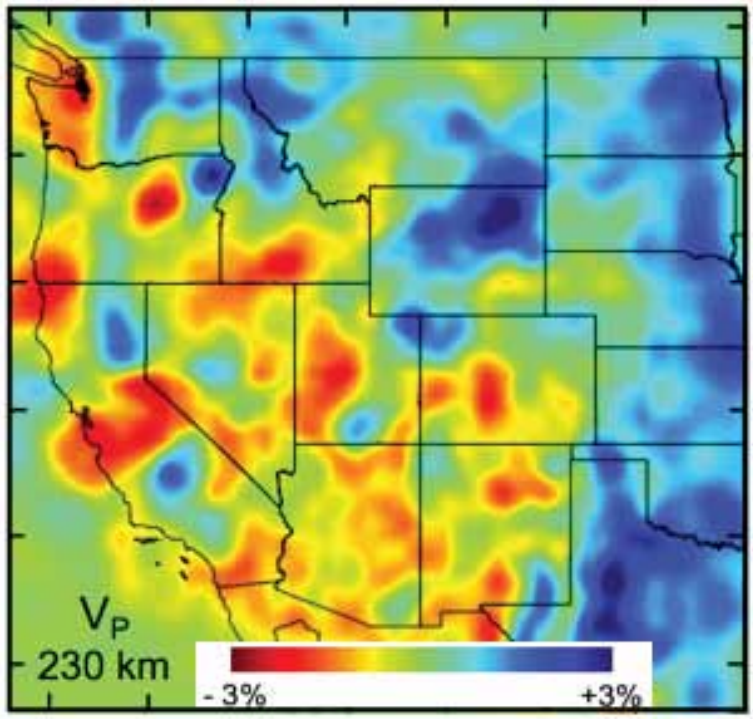

P-wave velocity structure near the base of the western U.S., from Schmandt and Humphreys (2010). Velocity variations this great reflect temperature variations. Such structure indicates that vertical flow velocities create temperature variations at rates greater than are healed by conduction, i.e., the region is experiencing vigorous small-scale convection. High-resolution imaging at this scale has only been possible since the deployment of EarthScope's USArray.

Oceanic Lithosphere.

The relatively short life, rigid behavior and regular cycling of ocean lithosphere from ridge to subduction zone results in plates that appear simple compared to continents; this simplistic view arises in part from oceanic plates being under water and hence difficult to observe and study in detail. It is well understood that oceanic lithosphere is created at mid-ocean spreading centers, cools as it moves away, and sinks into the Earth at subduction zones. Important processes include decompression melting beneath the spreading center; seismic imaging finds magma chambers are small or absent, suggesting they are transient and magma residence time is short. Off-axis magmatism and asymmetric spreading reflect interactions between the lithosphere and underlying asthenosphere that, at scales larger than the mid-ocean ridge, are not completely passive. Anomalously low seismic velocities beneath spreading centers at depths of 100 km or more may indicate small amounts of vapor-induced partial melting, dehydrating the asthenosphere at these depths. Much higher degrees of partial melting occur above ~70 km, depleting the asthenosphere of basaltic components, thereby increasing both buoyancy and solidus temperature. As the ocean lithosphere moves away from the spreading center and cools, it incorporates this compositionally stratified structure. Further cooling thermally accretes asthenosphere into the growing thermal boundary layer. Cooling, dehydration, depletion and relatively mafic compositions are responsible for making an ocean lithosphere that resists deformation. Ocean floor flattening (relative to predictions of thermal cooling) is taken as evidence for significant rates of convective loss of lower lithosphere, and as the plates age, the occurrence of off-axis magmatic events (e.g., hotspot construction of plateaus and aseismic ridges) locally builds thick crust, further depleting the upper mantle, and creates compositional and density heterogeneity within the plate. Seawater circulation through the upper ocean lithosphere, occurring primarily near the spreading center and where the plate flexes near a subduction zone, creates hydrous minerals in the upper plate, and it is this fairly complicated lithosphere that subducts.

Continental Lithosphere.

Compared to oceanic lithosphere, continents are more complex and less understood. It is clear that compositional differentiation through magmatism creates relatively felsic rocks that are more buoyant, radiogenic, hydrous, and easier to melt than their parent rocks, and sufficient accumulation of such rocks creates a mass that resists subduction. The magmatic compliment to the felsic rocks, typically depleted mantle, is also strong and compositionally buoyant compared to parent rocks, thus collecting beneath the relatively felsic accumulation. Subduction at the margins of proto-continents leads to further differentiation,

tectonic disruption and mass accumulation (through arc magmatism and accretion), resulting in the creation of complex and relatively stable continents. Magmatic segregation was more complete early in Earth's history, and the resulting depleted mantle lithosphere formed especially stable cratons. Knowledge of this process is informed by xenolith, seismic, and isostatic studies. But to more thoroughly understand continental evolution, knowledge of mass balance, the rates and processes by which mass moves, and how these have changed through time is necessary. Processes of growth tend to be preserved, whereas processes of consumption are inferred indirectly.

A theme in the last decade is a growing awareness of the diversity and significance of processes that remove and cycle continent back into the Earth's interior. Beyond mass budgets, processes of segregation and the creation of internal structure are basic to continental evolution. Nearly all of these facets are not well understood on very long time scales (or even in the recent past or present). But this is changing rapidly, and important new insights are coming from mantle studies, such as seismic identification of: a lithosphere-asthenosphere boundary, continental lithosphere that apparently convectively falls or drips downwards (possibly by delamination processes), and larger scale mantle circulation as revealed by tomography (in some cases from crust to core). Western U.S. studies have been central to many of these findings, with EarthScope providing many of the key data.

As a community we are trying to understand how present day observed and imaged structures and processes relate to long-term plate evolution. The concept of a simple thermal boundary layer continental lithosphere is being fundamentally revised into one with an important compositional (depleted) origin and a lithosphere-asthenosphere boundary layer, requiring revision of thermal boundary layer and cooling models. A number of exciting findings are emerging, which relate to plate history in varying degrees, and may manifest in seismic structures. For example, there appears to be relatively rapid lithospheric removal beneath volcanic arcs, currently most prominently beneath the Andes but also beneath western U.S. [e.g., *DeCelles et al.*, 2009]; if correct, how is this mantle lithosphere rebuilt? Much of the presumed downwelling beneath the western U.S. involves depleted Precambrian mantle, apparently eclogite loaded and destabilized by magmatic infiltration. Furthermore, xenolith studies suggest that basal North American lithosphere was removed during the Laramide orogeny, most compellingly in and around Wyoming [e.g., *Carlson et al.*, 1999]. Mantle tomography images a high-velocity feature extending to ~250 km beneath most of Wyoming, a depth from which the post-Laramide xenoliths argue for a lithosphere not of North America origin, suggesting a lithospheric growth process of unknown character. Another example involves the accretion of ocean lithosphere (and its presumed "continentalization") and magmatic growth away from subduction zones, most recently related to the Yellowstone hotspot and, in the recent past, by regional heating and widespread volcanism in what now is the Basin and Range, related to the removal of the Laramide-age flat slab.

The western U.S. continues to provide an opportunity to study important continental evolution processes. With EarthScope and IRIS data, a truly unique and unprecedented opportunity exists to image and examine active plate processes like never before. In looking forward, we wish to better understand continental evolution in a global context, especially through geologic time, informed by findings in the western U.S. As more data become available, new processes, some complicated and complex, will continue to be discovered and replace simpler old paradigms. By all appearances, much of the character of continents appears active and far from equilibrium.

References

Carlson, R.W., A.J. Irving, and B.C. Hearn Jr., in Gurney, J.J., J.L. Gurney, M.D. Pascoe, and S.H. Richardson, eds., Proceedings of the 7th International Kimberlite Conference, Vol. 1: Cape Town, Red Roof Design, p. 90-98, 1999.

DeCelles, P.G., M.N. Ducea, P. Kapp and G. Zandt, Cyclicity in cordilleran orogenic systems, *Nature Geoscience, v. 2*, doi:10.1038/ngeo469, 2009.

Schmandt, B., and E. Humphreys, Complex subduction and small-scale convection revealed by body-wave tomography of the western United States upper mantle, *Earth Planet. Sci. Lett.*, doi:10.1016/j.epsl.2010.06.047, 2010.

The Lithosphere-Asthenosphere Boundary

James Gaherty *(Lamont-Doherty Earth Observatory)*

The lithosphere-asthenosphere boundary (LAB) represents one of the most dynamically important boundaries in the Earth. Essentially all surface deformation– earthquakes, volcanic activity, slow tectonic deformation – results from forces associated with mantle convection in the asthenosphere; the transmittal of these forces (and related melting products) through the nearly rigid lithosphere depends on the nature of the LAB. In particular, the viscosity contrast across the LAB is a key but largely unknown element of plate tectonics. This contrast almost certainly has a thermal component related to the cooling of the lithosphere, but investigators have long speculated that layering of composition and/or melt content may strongly modulate or control the rheological transition across the LAB.

Over the last decade, the nature of the LAB has crystallized into a "grand challenge" within the seismological community, fuelled by advances in laboratory observations of deformation mechanisms and the elastic properties of mantle rocks combined with improved seismological imaging techniques for shallow mantle structure. The new laboratory data provide the means to accurately account for the effect of temperature, volatiles, and grain size on seismic wavespeed, and these studies suggest that the seismic velocity transition observed across the LAB in both continental and ocean regions is too sharp, and too large, to be purely thermal [e.g., *Faul and Jackson*, 2006]. The question of whether this discrepancy implies a wet and/or partially molten asthenosphere, a change in grain size, or something else entirely, remains unanswered.

The IRIS community is rallying to address this question. The past five years have seen a surge of activity utilizing IRIS data to provide better seismological constraints on the LAB, as documented in the accompanying research accomplishments. A number of groups are utilizing P-to-S and S-to-P conversions to explore the discontinuity structure of the shallow mantle. Historically these analyses have exploited single-station P-to-S conversions that are relatively insensitive to structure within the upper 200 km of the mantle due to noise associated with crustal reverberations. Advanced P-to-S imaging techniques, and adaption of the analysis to S-to-P conversions, are providing relatively robust images of discontinuities within this depth interval (Figure 1). Regional surface-wave analyses, in particular using large-aperture (e.g., PASSCAL) arrays, are yielding high-resolution estimates of absolute velocity and attenuation across the lithosphere-asthenosphere transition that can be directly compared to the laboratory-based predictions. Finally, estimates of variations in the layering of seismic anisotropy provide an alternative means to map the LAB.

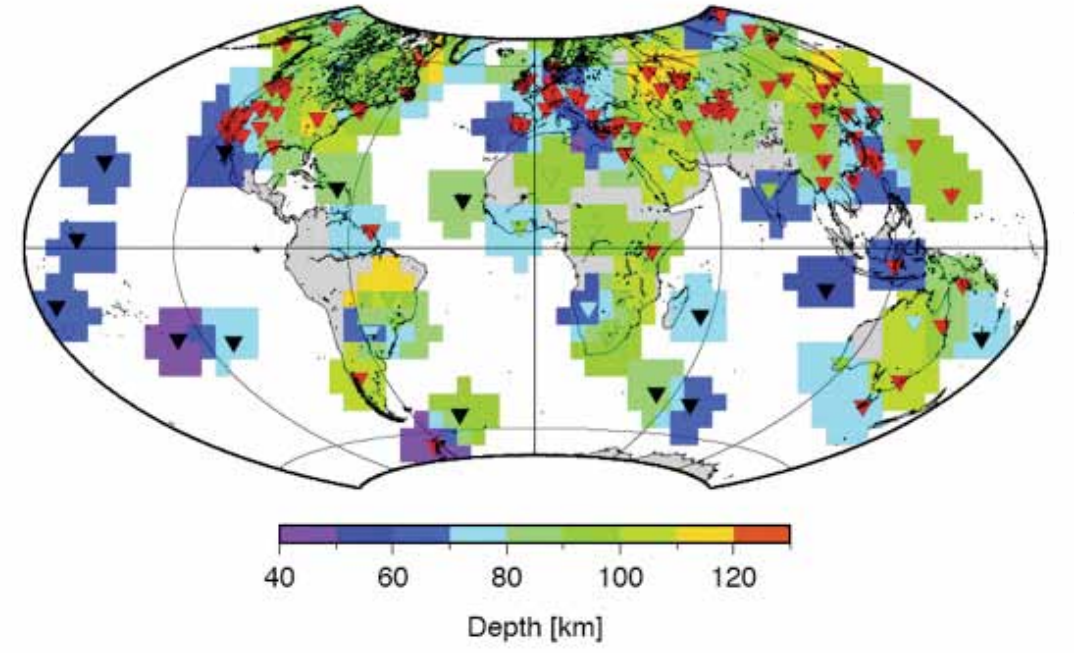

Global map of the depth to the lithosphere-asthenosphere boundary imaged using Ps receiver functions (Rychert and Shearer, 2009). Color indicates depth. Triangles show the 169 stations used in this study. Station color corresponds to tectonic regionalization: Oceanic – black, Phanerozoicorogenic zones and magmatic belts – red, Phanerozoic platforms – cyan, Precambrian shields and platforms – green. Average LAB depth varies from 95 ± 4 km beneath Precambrian shields and platforms to 81 ± 2 km beneath tectonically altered regions and 70 ± 4 km at oceanic island stations.

A number of intriguing results are emerging from these analyses. They confirm that the seismically observed LAB does not correspond to the base of a thermally controlled lithosphere – the seismic boundary is much too sharp, and generally too shallow, to be dictated by temperature. On a global scale, the depth to the seismic LAB generally correlates with expected tectonic variations in lithospheric thickness: shallowest beneath oceans and regions of young tectonism, deeper beneath older cratonic interiors (Figure 1). However, in detail, the depth to the LAB from converted body-wave phases is not always consistent with lithospheric thickness inferred from surface waves; in particular, it is much too shallow in cratonic regions, where surface-wave velocities imply high-wavespeed lithosphere extending to 200 km or deeper. One interpretation of this discrepancy is that the LAB observed in the body-wave studies does not represent the base of the lithosphere at all; alternatives include layering in mantle fabric associated with continental assembly, as suggested by some of the new anisotropy results (Figure 2), and/or compositional layering within the continental lithosphere. Continued advances in imaging of the lithosphere-asthenosphere system will help to resolve these issues, which will be directly facilitated through continuation of the IRIS facilities that provide important data to the seismological community.

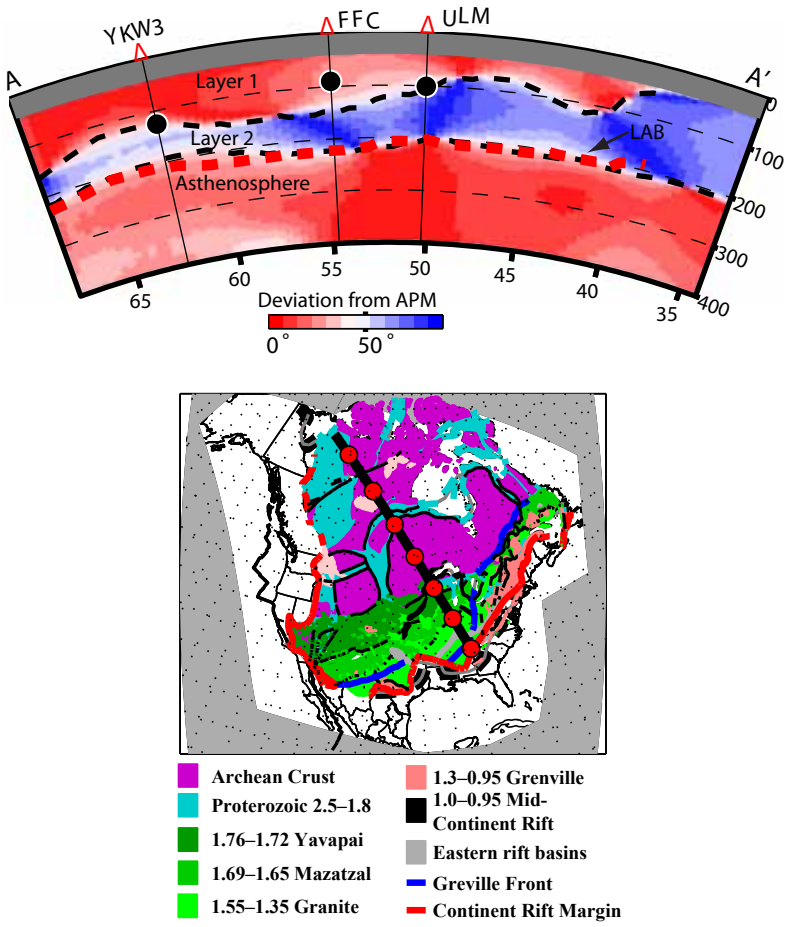

Figure 2. Upper mantle layering defined by changes in the direction of fast axis of azimuthal anisotropy. Change in anisotropy would produce Ps conversions, and is within the depth range of the Ps observations from global studies. Upper panel displays fast axis direction relative to the NA absolute plate motion direction, as a function of depth along a depth cross-section shown in the lower panel. Figure from H. Yuan and B. Romanowicz [this volume].

References

Faul, U. H., and I. Jackson, The seismological signature of temperature and grain size variations in the upper mantle, *Earth. Planet. Sci. Lett., 234*, 119-134, 2005.

Rychert, C. A., and P. M. Shearer, A global view of the lithosphere-asthenosphere boundary, *Science, 324*, doi: 10.1126/science.1169754, 2009.

How are Earth's Internal Boundaries Affected by Dynamics, Temperature, and Composition?

Maureen D. Long *(Yale University)*

The nature of dynamic processes that operate in Earth's interior - and the thermal and chemical structures that result from these processes - remain fundamental questions for solid earth geophysics. The tools of observational seismology, facilitated by the increasing availability of broadband seismic data from around the world, yield the tightest constraints available on deep Earth structure, and in combination with geodynamical models and mineral physics experiments yield powerful insights into processes operating in the Earth. Dynamic processes affect the Earth's internal boundaries, including the asthenospheric upper boundary layer of the mantle convective system, the seismic discontinuities associated with the mantle transition zone, and the core-mantle boundary (CMB) region, including both the CMB itself and the D" layer. Understanding the detailed structure in the vicinity of these internal boundaries can help us to distinguish the (often competing) effects of dynamic processes and variations in temperature and composition on seismological observations. Key observables include velocity and attenuation structure (both isotropic and anisotropic) and the location and character of seismic discontinuities. For example, observations of seismic anisotropy, which is particularly important in the boundary layers of the mantle's convective system, can yield direct constraints on mantle flow patterns and on the processes that control these patterns (Figure 1). Rapid progress has been made over the past several years in the seismological characterization of the Earth's internal boundaries, much of it enabled by IRIS facilities, and in using these observations to arrive at insights into deep Earth dynamics.

The Earth's upper mantle encompasses the upper boundary layer of the mantle convective system and includes both the rigid lithospheric mantle (including plates) and the weak asthenosphere, which manifests itself in low seismic velocities and which concentrates deformation that results in anisotropy (Figure 1). The nature of the lithosphere-asthenosphere boundary has been probed in detail using receiver function analysis and other methods, which has in turn yielded insight into the thermal and rheological nature of the asthenosphere. Information about the three-dimensional seismic structure of the upper mantle is available from global tomographic models, which have improved rapidly over the past several years due to increasingly dense seismic networks and theoretical improvements such as the use of full waveform tomography. On a regional scale, data from the EarthScope initiative and other projects have yielded spectacular images of seismic velocities beneath the western United States, which are still being interrogated for insight into upper mantle dynamics, as well as the evolution of plates and plate boundaries. Upper mantle velocity and attenuation structure contain information about temperature and composition (and therefore about the dynamic processes that cause lateral variations in these properties), but separating

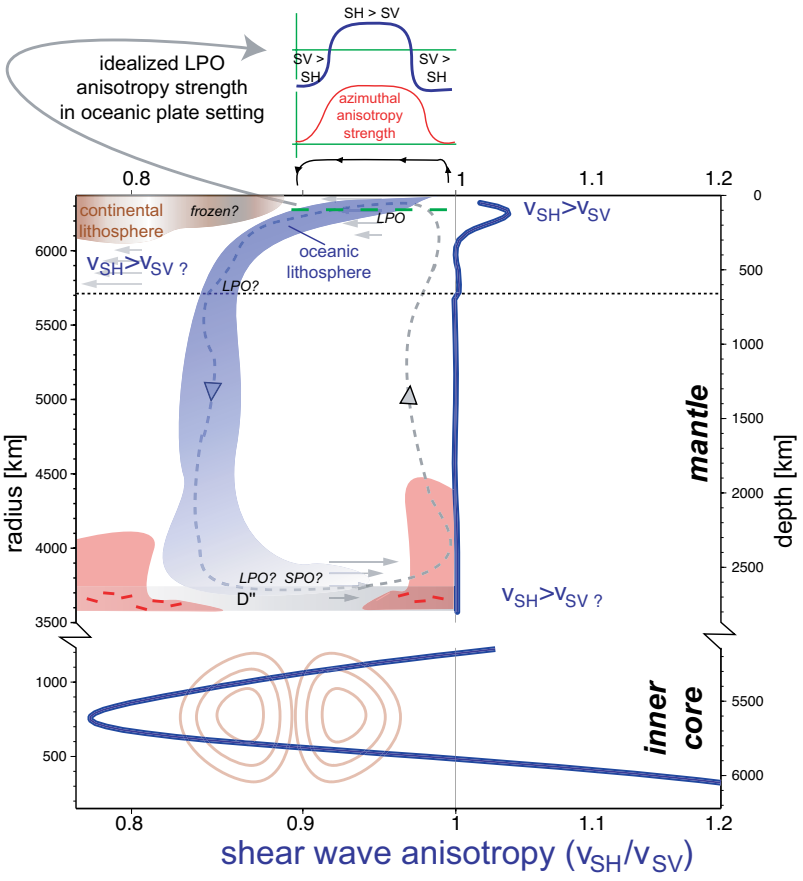

Figure 1. Simplified illustration of the first-order anisotropic structure of the Earth, from Long and Becker (2010). The heavy blue lines in the center show average radial anisotropy in the mantle and core, with a possible mantle flow trajectory for a downwelling slab (blue) displacing a thermo-chemical pile (red) at the CMB shown as a dashed line. Anisotropic structure is most pronounced in the upper and lower boundary layers of the mantle, as well as the inner core. In the upper mantle, flow is primarily horizontal, except beneath upwellings and downwellings, which are associated with primarily vertical flow. At the base of the mantle, possible horizontal flow due to slab material impinging upon the CMB is shown, which may lead to anisotropy.

thermal and compositional effects remains a significant challenge. Observations of upper mantle seismic anisotropy, including shear wave splitting measurements and surface wave observations, yield relatively direct constraints on the pattern of mantle flow in the upper mantle boundary layer, which can in turn be related to the larger-scale mantle convective system. First-order comparisons of seismic anisotropy observations beneath ocean basins to the predictions made by global convection models have been successful, but the patterns of anisotropy observed in more complex tectonic settings such as subduction zones remain to be completely understood.

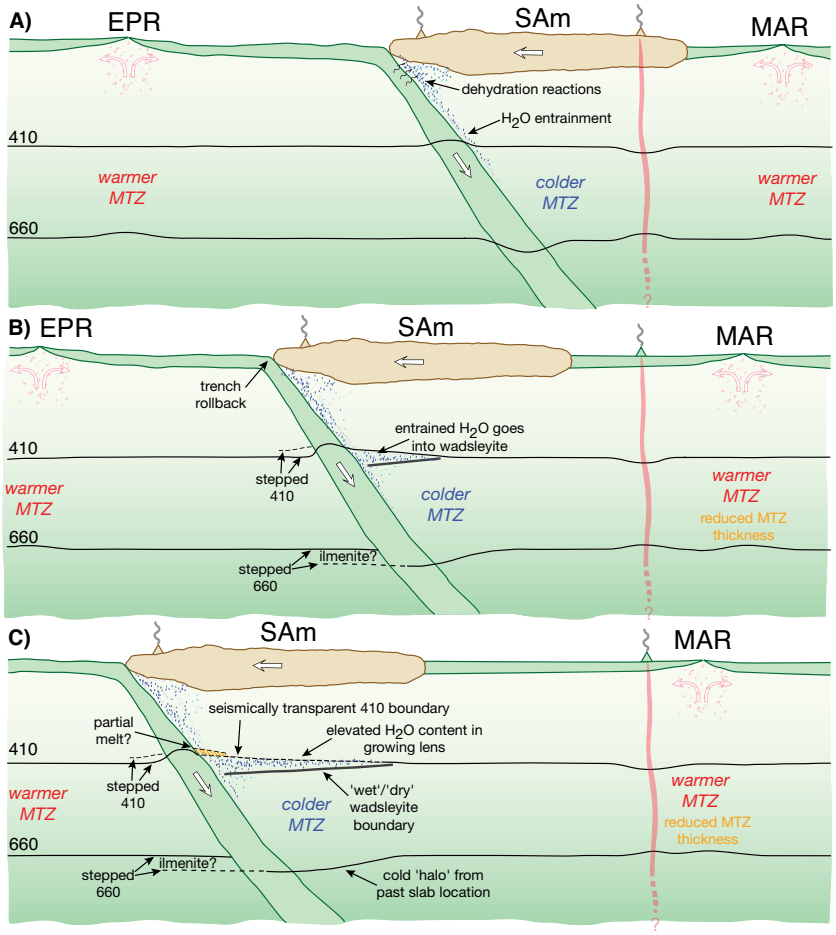

Figure 2. Illustration of possible effects of subduction and slab rollback on transition zone structure beneath South America, from Schmerr and Garnero (2007). In (a), water is brought into the transition zone by entrainment of hydrated upper mantle materials and/or transported within the slab. The cold downgoing slab initially results in an elevated 410-km discontinuity and a depressed 660-km discontinuity. As the continent moves westward due to trench rollback (b), buoyant hydrated wadsleyite collects at the top of the transition zone and elevates the 410-km discontinuity. The final geometry of the hydrated lens and the relatively colder and warmer regions of the transition zone are shown in (c).

The mantle transition zone, which encompasses the region between 410 and 660 km depth, plays host to a variety of phase transitions in mantle minerals, including the transitions from olivine to wadsleyite and from ringwoodite to perovskite and ferropericlase. Each of these phase transitions is associated with a sharp change in seismic velocities that manifests itself as a discontinuity; the precise depth and character of each transition is affected by temperature, composition, and volatile content. Therefore, knowledge about the depth, sharpness, and velocity gradient of transition zone discontinuities yields insight into physical conditions in the transition zone and into the dynamic processes that produce these conditions. While the first-order, one-dimensional structure of the transition zone has been known for decades, the recent explosion in the availability of broadband seismic data has enabled detailed transition zone discontinuity imaging on both a global scale and in the context of more regional problems. A regional example is shown in Figure 2, where the transition zone structure beneath South America is interpreted in terms of mantle dynamics and chemistry. In addition to the study of discontinuities, insight into the thermochemical structure and dynamics of the transition zone can be gleaned from global tomographic models, which have recently been interpreted in terms of lateral variations in temperature and water content which can be related to the locations of mantle upwellings and subducting slabs.

In one-dimensional seismic velocity models, the lower mantle (from the base of the transition zone to the top of the D" layer) is relatively simple, but recent work has demonstrated that there are, in fact, several features evident from the seismic wavefield that are associated with sharp "boundaries" in the lower mantle. For example, large-scale low shear velocity features have been identified in the lower mantle beneath the Pacific and Africa; sometimes referred to as "superplumes" (while their exact dynamical context is not presently constrained), these low shear velocity regions have been shown to have sharp lateral boundaries that are thought to reflect chemical, as well as thermal, variations. Seismic discontinuities at mid- to lower-mantle depths have also been identified, particularly beneath the western Pacific subduction zones, although these discontinuities do not appear to be global features. Their cause remains enigmatic, but their intermittent appearance likely reflects variations in thermal and/or chemical structure in the mid-mantle. The boundary at the base of the transition zone between the upper and lower parts of the mantle may itself constitute an important control on whole mantle dynamics; observations of inferred stagnant slabs at the base

of the transition zone and a difference in the spectrum of lateral heterogeneity between the upper and lower mantle in global tomographic models have been interpreted as evidence that mantle convection may be partially layered.

The D" region at the base of the mantle, located just above the CMB, represents one of the most exciting frontiers for exploiting seismological observations to gain insight into deep Earth dynamics. The existence of a seismic discontinuity at the top of the D" layer has been known for several decades, but its cause remained enigmatic until the discovery of the post-perovskite phase transition provided a natural hypothesis for its origin. Parallel developments in experimental and theoretical mineral physics and observational seismology, enabled particularly by dense broadband array data, has led to rapid strides in our understanding of the D" discontinuity and its dynamical implications. Detailed imaging of lowermost mantle structure has led to a suggestion of an intermittently observed double discontinuity indicative of regional "lenses" of post-perovskite above the CMB. In turn, these observations have been used to estimate CMB temperatures and heat flux values, yielding insight into first-order questions about the evolution of the Earth's interior. The D" layer is also associated with an increase in lateral heterogeneity in seismic velocity structure in tomographic models, which has recently been interpreted in terms of variations in both thermal and chemical structure, as well as the presence of ultra-low velocity zones (ULVZs) which are hypothesized to be due to the presence of partial melt and which have been characterized in increasing detail in recent years. Finally, the delineation and interpretation of seismic anisotropy at the base of the mantle has the potential to allow for the characterization of lowermost mantle flow patterns, with important implications for our understanding of mantle dynamics. In contrast to the bulk of the lower mantle, which is generally isotropic, D" exhibits anisotropy in many regions, with a variety of anisotropic geometries proposed. Much work remains to be done to characterize D" anisotropy in enough detail to understand the causative mechanism and to relate it reliably to mantle flow patterns, but this represents a promising avenue for understanding the dynamics of the lowermost mantle.

The deepest of the Earth's internal boundaries are associated with the core, and the vertical gradient in density between the silicate mantle and the liquid outer core is the most dramatic in the Earth's interior. The structure of the CMB itself, the lowermost outer core, the inner core boundary, and the solid inner core have been probed with increasing detail in recent years; as with much of the ongoing research on Earth's interior boundaries, this work has been enabled by both the long-running stations of the IRIS GSN and by dense broadband arrays that are often associated with the PASSCAL program. Spatial and temporal variations in the structure of both the inner core boundary and the inner core as a whole have been suggested, with implications for possible inner core super-rotation, the nature of outer core convection, the growth history of the inner core, and the driving forces of the geodynamo. Seismic anisotropy has been observed in the solid inner core using both normal mode and body wave observations, and it appears that the inner core encompasses several distinct anisotropic domains, although consensus on the nature and causes of inner core anisotropy has not yet been reached.

Progress in the characterization of thermochemical structure and dynamic processes associated with the Earth's internal boundaries over the past several years has been exciting and rapid. The continuing expansion of the availability of global broadband seismic data and the increasing use of analysis techniques that exploit more fully the information contained in the full seismic wavefield provide exciting avenues for future progress. Seismological observations, in combination with insights from complementary fields such as geodynamics and mineral physics, remain the most powerful tools available for probing the structure and dynamics of the Earth's interior, and discoveries such as those described here continue to be made possible by the IRIS facilities that allow for the collection and dissemination of data from both long-running global networks and from dense temporary experiments. The continued expansion of data availability from IRIS facilities will continue to enable advances in the study of the Earth's interior dynamics.

References

Long, M. D., Becker, T. W., 2010. Mantle dynamics and seismic anisotropy. *Earth Planet. Sci. Lett.*, in press.

Schmerr, N., and E. Garnero, 2007. Topography on Earth's upper mantle discontinuities from dynamically induced thermal and chemical heterogeneity, *Science, 318*, 623-626.

Towards a Global School Seismic Network

Paul Denton *(British Geological Survey)*

Scientists often work in a virtual global laboratory, collaborating with partners in countries overseas who they might never meet. Seismologists have been doing this for over a century ever since John Milne set up the first global seismic network from his garden shed in Shide on the Isle of Wight in 1910. He used the irregular mail-ships of the day to exchange seismograms with far flung outposts. Today school students and teachers in high schools across the world can experience what it is like to do science on a global scale and use the internet to exchange data in near real time with colleagues on any continent. Schools are using very simple mechanical seismometers in their own classrooms coupled to simple digitisers and PC's used for datalogging to detect and analyse seismic signals from across the world.

In 2009 the school seismology projects of the UK, Ireland and the USA merged their online databases to create a seamless and integrated environment where teachers from any country can automatically view and download data files submitted by teachers in any other country. UK and Ireland schools are using a simple horizontal pendulum seismometer which shows up S and surface waves well. US schools use a vertical sensor with a Lacoste type suspension which gives a stronger P wave signal.

The devastating earthquakes in Haiti and Chile during early 2010 highlighted the effectiveness of global monitoring in schools, and within days of the M8.8 event in Chile 45 schools had posted their seismograms online for all to see. In 2010 and beyond we are working hard to try and widen the reach of the global school seismology network and support seismologists in Africa and elswhere to set up their own local school seismology networks.

Acknowledgements: I would like to thank Matt Toigo from IRIS and Tom Blake from DIAS for their assistance with linking our projects together. See project websites at www.bgs.ac.uk/ssp, www.iris.edu/hq/sis, and www.dias.ie/sis

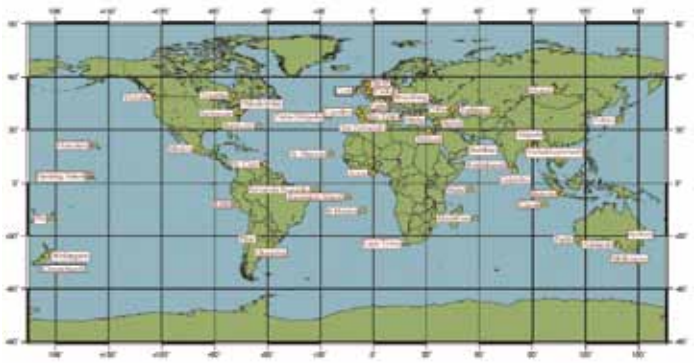

Milne network 1910

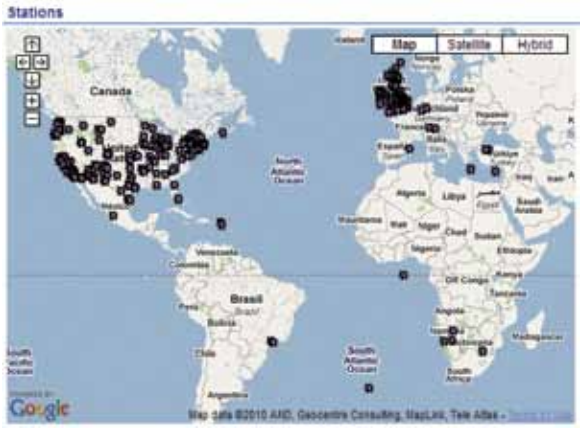

Schools network 2010

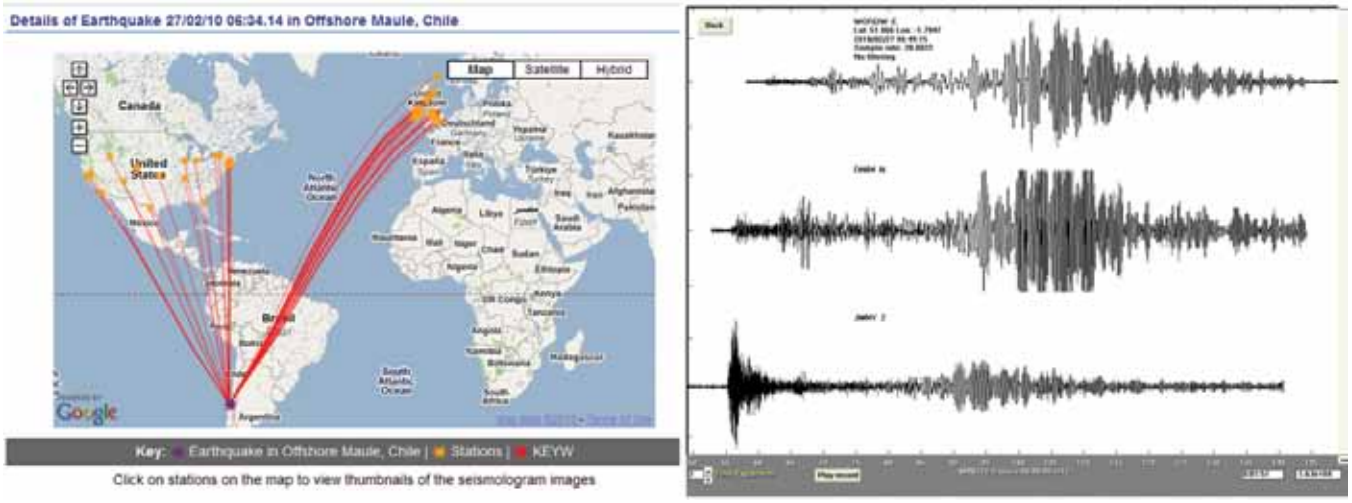

Data from the M8.8 Chile earthquake was recorded by schools right across the world. Seismograms recorded by schools in the UK (top), Ireland (middle) and the US (bottom).

The Quake-Catcher Network: Bringing Seismology to Homes and Schools

Elizabeth S. Cochran *(University of California, Riverside),* **Jesse F. Lawrence** *(Stanford University),* **Jennifer Saltzman** *(Stanford University),* **Carl M. Christensen** *(Stanford University),* **Michael Hubenthal** *(Incoroporated Research Institutions for Seismology),* **John Taber** *(Incoroporated Research Institutions for Seismology)*

The Quake-Catcher Network (QCN) is a collaborative initiative for developing the world's largest, low-cost strong-motion seismic network by utilizing sensors in and attached to volunteer internet-connected computers [*Cochran et al., 2009a,b*]. QCN is not only a research tool, but provides an educational tool for teaching earthquake science in formal and informal environments. A central mission of the Quake-Catcher Network is to provide software and hardware so that K-12 teachers, students, and the general public can better understand earthquakes while participating in the collection and analysis of seismic data. The primary educational outreach goals are 1) to present earthquake science and earthquake hazards in a modern and exciting way, and 2) to provide teachers and educators with seismic sensors, interactive software, and educational modules to assist in earthquake education. QCNLive (our interactive educational computer software) displays recent and historic earthquake locations and 3-axis real-time acceleration measurements. This tool is useful for demonstrations and active engagement for all ages, from K-college. QCN provides subsidized sensors at $49 for the general public and $5 for K-12 teachers. Teachers and academics are taking QCN into classrooms across the United States and around the world. With greater understanding, teachers and interested individuals can share their new knowledge, resulting in continued participation in the project, and better preparation for earthquakes in their homes, businesses, and communities.

References

Cochran, E.S., J.F. Lawrence, C. Christensen, and R. Jakka, The Quake-Catcher Network: Citizen science expanding seismic horizons, Seismol. Res. Lett., 80, 26-30, 2009.

Cochran E., Lawrence J., Christensen C., Chung A., A novel strong-motion seismic network for community participation in earthquake monitoring, IEEE Inst & Meas, 12, 6, 8-15, 2009.

Acknowledgements: This work was performed with support from NSF-GEO0753435, NSF-GEO0753290, NSF-EAR0952376 and an IRIS subaward. We thank the thousands of volunteer participants who make the Quake-Catcher Network possible.

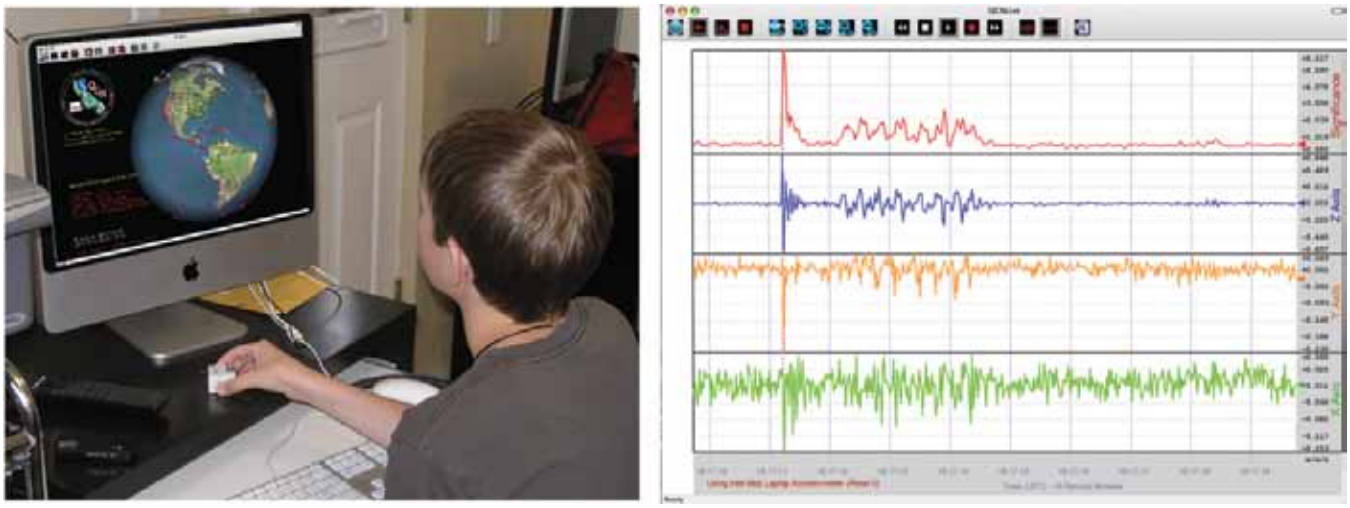

Left: Student using the QCNLive software to explore earthquakes around the world. Right: Display of the real-time output from a MEMS sensor in the QCNLive software.

On-Line Seismology Curriculum for Use with Educational Seismographs

Alan Kafka *(Weston Observatory, Department of Geology and Geophysics, Boston College),* **Anastasia Macherides Moulis** *(Weston Observatory, Department of Geology and Geophysics, Boston College),* **Leslie Campbell** *(Weston Observatory, Department of Geology and Geophysics, Boston College),* **Michael Barnett** *(Weston Observatory, Department of Geology and Geophysics, Boston College),* **Camelia Rosca** *(Weston Observatory, Department of Geology and Geophysics, Boston College),* **John Ebel** *(Weston Observatory, Department of Geology and Geophysics, Boston College)*

We developed a user-friendly, on-line seismology curriculum for teachers, students, and anyone else who operates an educational seismograph. The goal of this endeavor is to provide a resource on the web for people who are looking for some guidance regarding what they can do with their AS1 (or EQ1) seismograph once they have successfully installed it and have it up and running. The curriculum exercises are linked together with a unifying theme that helps guide students to engage in their own inquiry regarding what is recorded by their seismograph. A very common question that we hear from students and teachers, is: "The news reported that there was a _____ magnitude earthquake in _____. Did we record it on our seismograph?" Using this question as a "hook", we encourage scientific inquiry by designing our curriculum around asking students to look at their own seismograms and figure out the answer to this question by themselves. The philosophy behind this approach is that, in the process of learning how to go about answering this specific question, students will become more comfortable with scientific inquiry in general. The figure shows the structure of the on-line curriculum, which can be found at http://bcespcurriculum.wordpress.com.

The blue boxes in the figure represent exercises that are part of the curriculum, and the words in italics, such as Inquire, Explore, Investigate, Learn, etc. depict the aspect of the scientific method that is highlighted in a particular exercise. During any exercise, many of these aspects of scientific investigation will, of course, be expected to be happening, but the words in italics indicate what part of the process is highlighted in that exercise.

This curriculum was assessed by way of a pre-post test administered to classes using this curriculum as part of the Boston College Educational Seismology Project (BC-ESP). We investigated how well the test assesses content and comprehension of the topics we cover, as well as readability and appropriate grade level of the test questions. Based on an analysis of how the pre-test results compare with the post-test results, we found that: (1) the test is suitable for the population it was used for, and (2) the students made significant gains between the pre-test and the post-pest, providing evidence that the curriculum is effective.

Acknowledgements: This work was performed with support from an IRIS subaward to Weston Observatory, Department of Geology and Geophysics, Boston College.

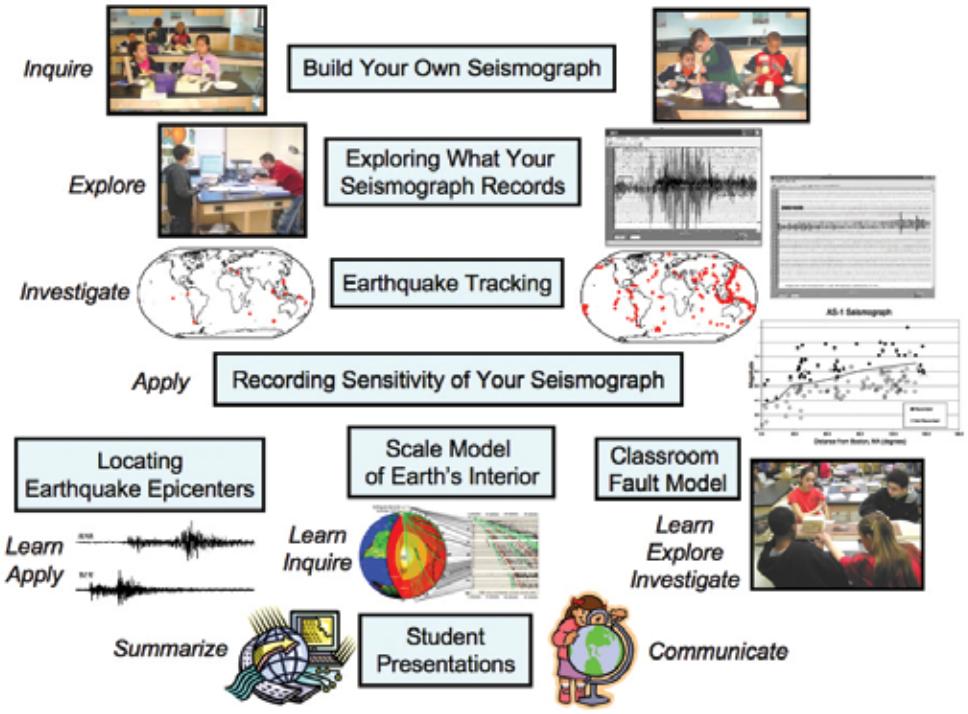

Structure of the BC-ESP on-line curriculum. Blue boxes represent specific exercises that are part of the curriculum. Words in italics, such as Inquire, Explore, Investigate, Learn, etc. depict the aspects of the scientific process that are highlighted in a particular exercise.

Seismology in Schools (seismeolaíocht sa Scoil) Pilot Programme, Dublin Ireland

Thomas Blake *(Dublin Institute for Advanced Studies)*

An Outreach pilot programme called Seismology in Schools (Seismeolaíocht sa Scoil) was introduced by the Dublin Institute for Advanced studies to 50 primary and secondary schools throughout Ireland. This programme has been enthusiastically received by both teachers, students and parents alike. Using the seismometer and associated software distributed in this programme, students are able to record earthquakes from the other side of the world in real-time. The implementation of the pilot programme has been very a successful joint venture between DIAS, (Dublin Institute for Advanced Studies), ATECI, (Association of Teachers Educations Centers in Ireland), BGS (British Geological Survey) and IRIS (Incorporated Research Institutions for Seismology). A major contribution to the success of the programme is the teaching materials available to the teachers and students from the E&O Section of IRIS. Teacher training days organized by DIAS ensured that the teachers went back into the classroom fully conversant with the hardware, software and animated teaching software necessary to teach the programme. Significant success has been achieved in the pilot already as students from Scoil Chonglais, Co Wicklow, won 1st Prize in the Senior Chemical, Physical and Mathematical Sciences Category at the BT 2009 Young Scientist Competition for their research into seismic waves using the school's seismometer. The next phase of the programme for 2010 is to consolidate the learning and data collection techniques in the participating schools outlined in the training days and practiced by the students for the last year. Ultimately students will be in a position to share their earthquake data with other schools initially in Ireland, the UK, and USA. The international makeup of our partners reflects the fact that seismology is an international subject that transcends national boundaries. Recognising this internationality, the next phase of the programme starts to explore the possibilities of the twining schools of a similar educational level with a view to students exchanging earthquake data, firstly with another Irish school and in subsequent years with schools in the UK, USA and Africa via the internet. The experience of the seismology in schools pilot programme for students reinforces the idea that when science is relevant, learners become more engaged and see how science is reflected in the reality of their own lives and what they read in the newspaper.

Acknowledgements: DIAS would like to acknowledge the contribution in time, expertise, funding and material by ATECI, (Association of Teachers Educations Centers in Ireland), BGS (British Geological Survey) Edinburgh, Scotland and IRIS (Incorporated Research Institutions for Seismology) in the USA.

Programme presenters and teachers at the 1st Teachers Workshop for Seismology in Schools (Seismeolaíocht sa Scoil) Programme, held in Dublin in April, 2009

Presentation by Mr Matt Toigo, IRIS at the 1st Teachers Workshop for Seismology in Schools (Seismeolaíocht sa Scoil) Programme, held in Dublin in April, 2009

Teachers on the Leading Edge: Earth Science Teacher Professional Development Featuring Pacific Northwest Earthquake and Tsunami Hazards

Bob Butler *(University of Portland)*

Exploring Mt Hood volcanic history and hazards.

Teachers on the Leading Edge (TOTLE) is a professional development program for K-12 Earth Science teachers in the Pacific Northwest. TOTLE offered five-day summer workshops in 2008 – 2010 for Earth Science teachers from Oregon and Washington states. Through a problem-solving approach to active continental margin geology, teachers learn how geoscientists developed our understanding of Pacific Northwest plate tectonics, earthquakes, and volcanoes and how EarthScope research is advancing frontiers of knowledge. This cutting-edge science content learning is blended with pedagogical sessions led by award-winning TOTLE Master Teachers. Three days of classroom and computer-based studies of active continental margin geology and EarthScope science are reinforced by two field days investigating Cascadia great earthquakes and tsunamis and Cascade volcanic hazards. Participants in TOTLE workshops receive maps, posters, and experimental apparatus that greatly facilitate transfer of workshop learning to Earth Science classroom teaching.

Examining the ghost forest produced by the 1700 great Cascadia earthquake.

Educational software, video lectures, animations, and K-12 Earth Science lesson plans are prominently featured in TOTLE teacher workshops. Robert Butler worked extensively with Jenda Johnson (IRIS E&O) and John Lahr (USGS Emeritus Seismologist, now deceased) on compilation and organization of educational seismology resources currently published by IRIS and EarthScope as the DVD Middle School Teachers' Guide to Earthquakes and Seismology. Michael Hubenthal (IRIS E & O) and Shelley Olds (UNAVCO E&O) attended the 2008 TOTLE – EarthScope workshop and provided insightful feedback on workshop design that led to program improvements between 2008 and 2009. Butler currently works with Tammy Bravo, Jenda Johnson, and John Taber to produce teaching resources for all magnitude 7 or larger earthquakes worldwide and for smaller earthquakes of regional interest in the Pacific Northwest. All of these teaching resources are tailored for middle-school Earth Science and are posted on the IRIS Recent Earthquakes Teachable Moments web site (http://www.iris.edu/hq/retm) within four to 16 hours after a notable earthquake. These teaching resources have received high acclaim from and wide use by K-12 Earth Science teachers across the US. Teachers on the Leading Edge personnel look forward to many years of fruitful collaborations with IRIS Education and Outreach.

Brian Atwater (USGS Seattle) explaining Cascadia tsunami geology along the banks of the Copalis River near the central Washington coast.

Acknowledgements: Teachers on the Leading Edge is supported by a grant from the NSF EarthScope Program. Collaborations with IRIS Education and Outreach, the US Geological Survey, and the Oregon Department of Geology and Mineral Industries have been essential to the development of TOTLE.

The Earth Science Literacy Initiative

Michael Wysession *(Washington University),* **John Taber** *(IRIS)*

In 2009, the Earth Science Literacy Initiative (ESLI), which was led by Michael Wysession (Chair, IRIS E&O Committee) and John Taber (Manager, IRIS E&O Program), created a document entitled the Earth Science Literacy Principles (ESLPs) that contains a framework of the essential information that all citizens should know about Earth Science. The program was run by an outstanding Organizing Committee that also included David A. Budd (University of Colorado), Karen Campbell (University of Minnesota), Martha Conklin (UC Merced), Ellen Kappel (Geo Prose), Nicole LaDue (Michigan State), Gary Lewis (GSA), Robert Raynolds (Denver Museum of Science and Nature), Robert W. Ridky (USGS), Robert M. Ross (Paleontological Research Institute), Barbara Tewksbury (Hamilton College), and Peter Tuddenham (College of Exploration).

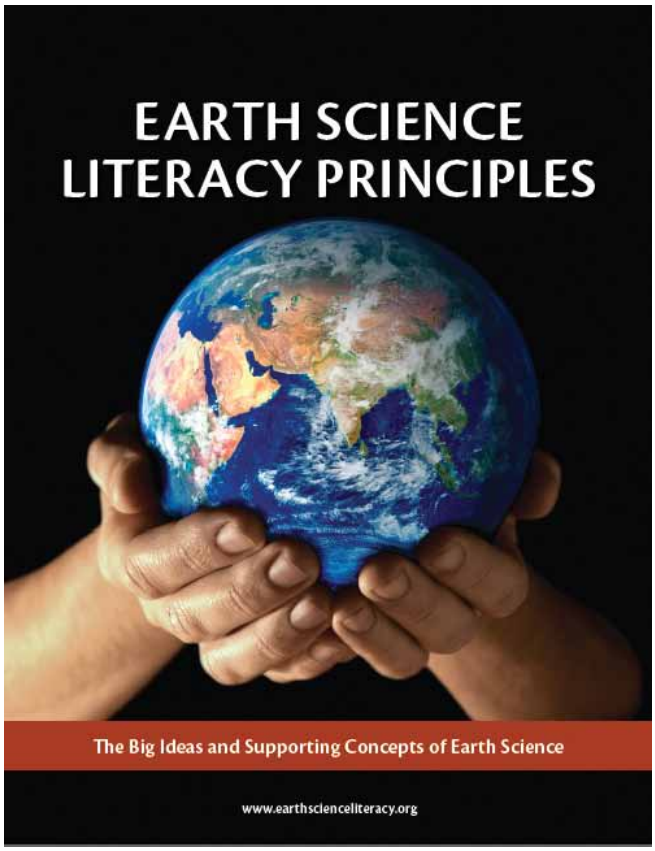

The Earth Science Literacy Principles, presented as a published brochure and available on line at www.earthscienceliteracy.org, contains 9 "big ideas" and 75 supporting Concepts that outline the essential understandings that all citizens should know about Earth science. Its creating was led by members of the IRIS E&O program.

Understanding Earth science concepts is critical for humanity to successfully respond to these challenges and thrive in the decades to come. The twenty-first century will be defined by challenges such as understanding and preparing for climate change and ensuring the availability of resources such as water and energy, issues that are deeply rooted in the Earth sciences. To address this need, ESLI was formed in 2008 with the task to create a succinct document outlining what all citizens should know about Earth science. This document followed vigorous discussions at several workshops and multiple reviews. The resulting (ESLPs) consisted of 9 "Big Ideas" and 75 "Supporting Concepts" that highlighted the fundamental understandings of Earth science. Combined with similar efforts from the Ocean, Atmosphere, and Climate communities, it forms a foundation of essential information in the geosciences that has had a tremendous impact in many ways.

The ESLPs have already had broad-reaching applications in both public and private arenas. It is helping to guide future decisions involving governmental legislation and educational science standards. For example, the ESLPs were used to guide the formation of a new K–8 national science program developed in 2009 by Pearson. The ESLPs were also the basis for the Earth science part of the "Conceptual Framework for Science Education Standards" by the National Research Council, which will be used as the foundation for future national science education standards within the US. For more information, see www.earthscienceliteracy.org

References

Wysession, M., *et al.*, The Earth Science Literacy Principles, NSF, 2009.

Acknowledgements: Funding was provided by NSF: EAR-0832415 (Wysession) and NSF: EAR-0832418 (Taber).

USArray Education and Outreach in Southwest Indian Country

Steven Semken *(Arizona State University, School of Earth and Space Exploration)*

The EarthScope project has benefited greatly from permission to deploy USArray and Plate Boundary Observatory geophysical instruments on American Indian lands. Some instruments were sited near K-14 schools with expectations that (1) in the short term, students and teachers would be able to monitor "their" station online, and (2) long after deployment, the school would benefit from a continuing outreach association with the EarthScope project and the greater geoscience research community.

A cross-cultural workshop (NAPP-ES) held at ASU in 2005 yielded a number of specific recommendations for follow-up education and outreach activities [*Semken et al., 2007*]. As USArray moves out of tribal lands in the intermountain West and traverses Indian country in the Rockies and Great Plains, it is important to remain constructively engaged with Native schools and communities.

A follow-up E&O workshop, Exploring Southwest Geology and Geophysics through the EarthScope program, was held in Flagstaff, Arizona on 26-27 September 2009 and served 20 K-12 and college teachers from schools located on or near Native American nations across Arizona, many of which hosted seismic stations during the USArray deployment in Arizona in 2007-2009. The workshop was co-led by geoscience educators from ASU, UNAVCO, and IRIS, with visiting speakers from NAU, USGS, and the National Park Service. Educational materials produced for and used at the workshop can be accessed at http://cws.unavco.org:8080/cws/learn/2009/earthscopeArizona/.

Further education and outreach activities among Southwest Native nations are planned.

References

Semken, S., Fouch, M., Garnero, E., Zah, P., & Lippert, D. (2007). Meshing American Indian concerns with goals of EarthScope's USArray. Eos, Transactions, American Geophysical Union, 88(31), 309-310.

Acknowledgements: The NAPP-ES workshop and follow-up meetings were supported by award EAR-0454502 from the EarthScope Science Program of the National Science Foundation. Siting-related outreach work was supported by a grant from the USArray Siting Outreach Program. The Flagstaff E&O workshop was supported by IRIS, UNAVCO, and ASU.

Teachers participating in the September 2009 workshop in Flagstaff.

Implementing Inquiry-Based Approaches in Geoscience Education and Research

Michael Brudzinski *(Miami University of Ohio)*

One of the most important issues in geoscience is the growing disparity between workforce needs and our ability to produce well trained students. This project is examining whether inquiry-based approaches to education and research can aid in this challenge by partnering with the successful IRIS Undergraduate Internship Program and building on a university-wide course revision project converting introductory courses from lecture-based to inquiry-based. The inquiry-based approach is also a natural one to investigate an exciting new observation that plate boundary faults produce episodic tremor and slip (ETS). This project has 3 integrated research and teaching initiatives:

1. Expand the inquiry-based approach to other courses by i) developing a workshop to train high school instructors how to use this approach in an AP environmental science class and by ii) constructing a new second-course at the college level that focuses on how physical processes associated with plate tectonics relate to geologic hazards. These efforts ensure that students are practicing the scientific method not just memorizing the outcomes;
2. Expand the investigations of ETS behavior by i) searching for ETS in a global context using newly developed detection algorithms and by ii) investigating the spatial and temporal relationships between tremor, slow slip, earthquakes, and geologic structures. These efforts cultivate physical understanding of how faults move and generate hazards;
3. Expand the student research experience by i) offering undergraduate research to a larger set of students including an investigation into what makes a successful research project and by ii) experimenting with online research discussion both in classes and with collaborating research groups. These efforts identify key areas for improvement in the integration of teaching and research.

Collectively, the integrated teaching and research plan targets 3 broader impact outcomes that address the key issue of preparing a scientifically trained workforce:

1. Encourage students to consider a career in geoscience through earlier exposure to experiences with intrinsic motivation (i.e., AP credit or personal interest in hazards);
2. Retain majors and graduate students through work on newly developed areas of research (i.e., ETS) that address problems of high societal importance (i.e., what causes earthquakes);
3. Improve students' scientific training through more regular use of the scientific method.

Acknowledgements: NSF EAR-0847688

From an IRIS Lecture Tour to a General Audience Book About Midwest Earthquakes

Seth Stein *(Northwestern University)*

Following earthquakes of public interest, seismologists are effective at explaining to the media about the earthquake's location, magnitude, and tectonic setting. However, the underlying research questions are typically not discussed, in part owing to the challenge of explaining ongoing and unresolved scientific questions. As a result, we often do not show the public the challenges and complexities of earthquake research. An exception is IRIS/SSA Distinguished Lectures, which give the speaker the motivation and time to explain earthquake research in some depth. In 2006 I gave IRIS/SSA lectures on "Giant earthquakes: Why, Where, When, and What We Can Do" at a number of science museums. Although the focus was on the largest earthquakes, the lecture also explained general concepts of plate tectonics, earthquakes, seismology, and earthquake hazards. Giving the lectures was interesting and satisfying, and indicated that the material could be presented using an approach that focused on the key ideas and unresolved issues. Based on this experience, I have incorporated much of this material in a new book written for a non-technical audience: "Disaster Deferred: How new science is changing our view of earthquake hazards in the Midwest" that will be published in fall 2010 by Columbia University Press.

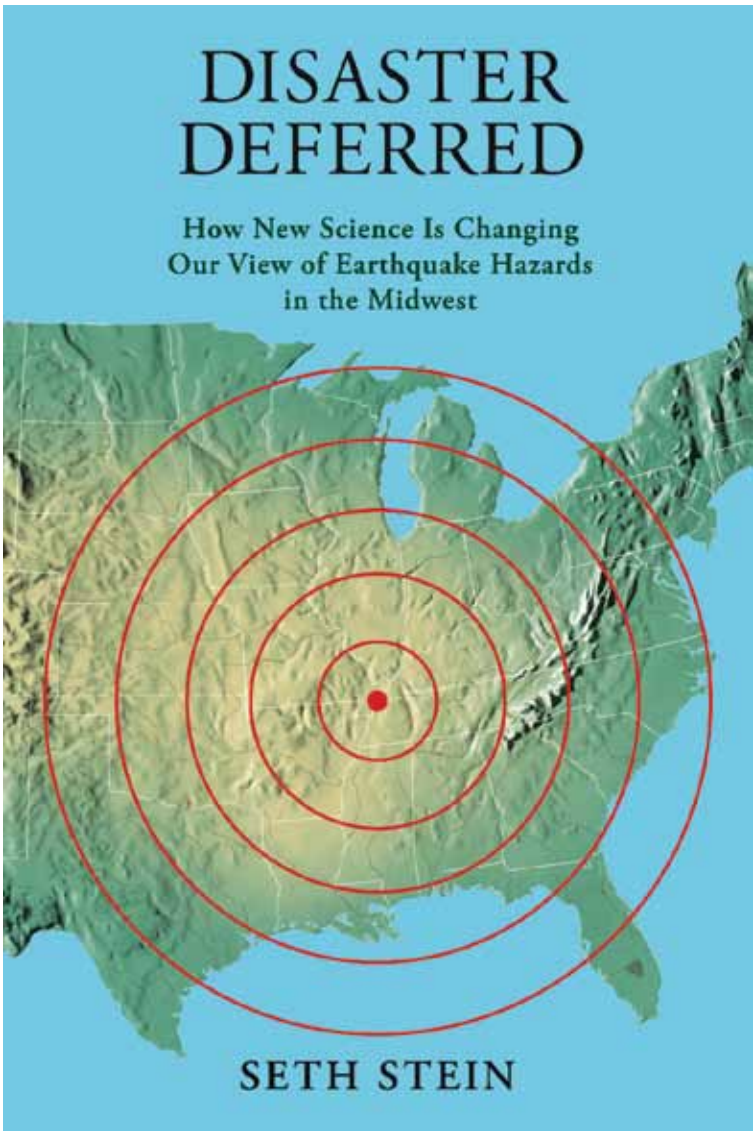

"Disaster Deferred: How new science is changing our view of earthquake hazards in the Midwest" will be published in fall 2010 by Columbia University Press.

Active Earth Display Kiosk Education and Outreach Missouri Department of Natural Resources

Hylan Beydler *(Missouri Department of Natural Resources, Division of Geology and Land Survey),* **Ed Clark** *(Museum of Missouri Geology – Rolla)*

The Active Earth Display kiosk provides an exciting educational opportunity for teaching earthquake science in the informal environment of the Ed Clark Museum of Missouri Geology. The museum is located at the Division of Geology of Land Survey, Missouri Department of Natural Resources, 111 Fairgrounds Road, Rolla, Mo. The virtual tools, animations and interactive, real-time presentation of seismic data and the science behind it has drawn visitors from all walks of life and all age groups including students, scouts, geology and other nature club members, families, scientists, community and state leaders, and those traveling along Interstate 44 and historic U.S. Route 66.

Visitors are welcome to tour the museum at their own pace, while others request a tour led by a staff geologist who enhances the experience by sharing additional geologic information. EarthScope literature provided by IRIS is also available.

Especially exciting is that the AED has afforded greater information dissemination about earthquake potential in the New Madrid Seismic Zone; the most seismically active area east of the Rockies, which lies in southeastern Missouri and neighboring states. A series of webpages about the NMSZ developed by MoDNR staff are integrated in the AED. Visitors also learn about the large earthquakes that occurred in the NMSZ in the winter of 1811-12, and about the fast approaching 200th anniversary of the historic events. Staff members also educate visitors about the department's responsibility for activating the Post-Technical Earthquake Clearinghouse, which is a clearinghouse for scientists wishing to enter the affected area in the event of a large, damaging earthquake in the NMSZ.

In August 2010 and 2011, the AED will relocate to Sedalia, where more than 25,000 people are expected to visit it at the Historic Womans Building during the Missouri State Fair. Sedalia is 90 miles east of Kansas City. EarthScope Transportable Array Stations have arrived in that region, and continue to be placed in Missouri throughout 2010, with full state coverage in 2011. The AED also debuts on the state Capitol grounds in Jefferson City where more than 2,000 fifth graders and others will have an opportunity to learn about earthquakes during MoDNR's Earth Day celebration April 22, 2011.

The AED has greatly enhanced the learning experience for young people and life-long learners interested in earthquakes.

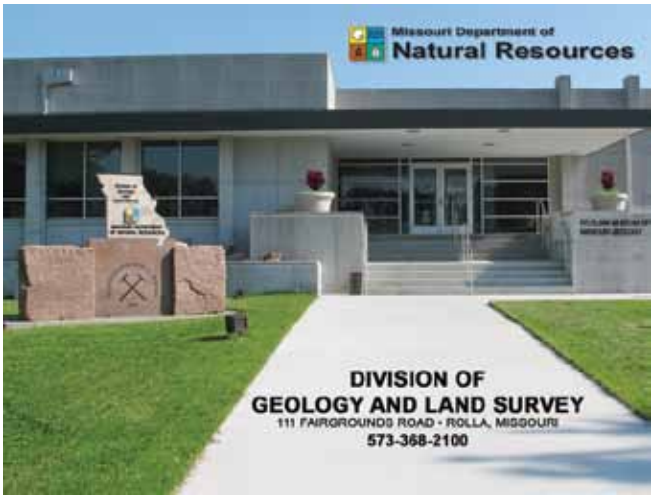

The Ed Clark Museum of Missouri Geology is located at the Missouri Department of Natural Resources' Division of Geology and Land Survey, 111 Fairgrounds Road in Rolla, Missouri. The museum provides a background for staff to share the importance of the state's natural resources and highlights rocks, minerals and fossils found in our state. The museum also identifies the role the division plays in the management and protection of these resources.

The Active Earth Display kiosk is popular stop for visitors to the Ed Clark Museum of Missouri Geology.

The Active Earth Display kiosk will debut at the Missouri State Fair, in Sedalia, August 12-22 and will return in 2011.

Explorer Series

Robert Bartolotta *(Cleveland Museum of Natural History)*

The Cleveland Museum of Natural History has offered a public lecture series nearly since the museum was founded in 1920. In 1997 the museum developed a seismology program with leftover parts from the defunct John Carroll University Seismic Observatory. Mostly a monitoring program initially eventually developed into a Seismic Observatory of our own and participation in the The Ohio Seismic Network OhioSeis under the direction of Dr. Michael C. Hansen within the Ohio Department of Natural Resources, Division of Geological Survey. Thanks to IRIS, SSA and the Distinguished Lecture Series, the museum has hosted six speakers since 2003. It has been an honor for the museum to host Dr. Susan Hough, Dr. Anne Sheehan, Dr. David Wald, Dr. Uri ten Brink, Dr. Seth Stein and Dr. Roger Bilham. All of these IRIS/SSA sponsored speakers have brought a world of knowledge to our Explorer Series. The tradition of hosting an IRIS speaker in conjunction with Earth Science Week will continue in 2010 with a program by Dr. Brian Stump speaking about forensic seismology.

The IRIS Workshop as Outreach

Wayne D Pennington *(Michigan Technological University)*

The IRIS Workshop is not usually considered to be an element of outreach, but it is. And here is why:

No seismologist is an expert in all aspects of the field. Some, such as myself, were experts in some areas years ago, but my own career has drifted into a few niche specialties, only peripherally related to mainstream solid-earth seismology as currently practiced. Yet, I need to teach classes and advise graduate students, and serve on student committees. I can do that from a position of ignorance, or I can do it from a position of knowledge, and IRIS Workshops help me obtain that knowlege.

I have long appreciated the IRIS Workshop for two major reasons: (1) it is always attractive to attend, being inexpensive for IRIS member representatives and in a nice location; and (2) it provides, in a couple of relatively painless days, an in-depth introduction to some of the most advanced and current topics of research. In one half-day session, I can learn about a topic of which I had been vaguely aware, and learn from the masters: speakers who had been invited based on their expertise and on their ability to present the topic well. In the course of one Workshop, I can learn enough about three or so different topics to go back to my home institution and teach the topic at the undergraduate or beginning-graduate level; I can speak intelligently with people on these topics; and I can point graduate students whose research may benefit, to the experts and/or top papers on the topic, and help those students understand it all.

True, the main reason for the Workshop is (probably) for the researchers to communicate with each other. But, to me, the main advantage of the Workshop is that it provides an opportunity to master subjects that would have taken tedious days of hard mental labor with published papers otherwise (assuming I would know where to start). It is outreach to people like me.

Image of Plenary Session in 2010. (From IRIS website.)

Workshop "Earth System Science for Educators" at North Carolina A&t State University

Solomon Bililign *(North Carolina A&T State University)*

Over the past five years, AfricaArray (AA) program has established a multifaceted geosciences education and research program in Africa with a US component to enhance diversity in the geosciences. The Incorporated Research Institutions for Seismology (IRIS) has played a pivotal role in AA by providing refurbished data loggers for the seismic network, by archiving and distributing seismic data, and by supporting a summer workshop for high school science teachers at NCAT.

The participants of the 2009 teachers workshop at North carolina. Workshop instructors included John Taber (E&O Program Manager, IRIS Consortium), Lev Horodyskyi (Pennsylvania State University), Angela Reusch (Pennsylvania State University), Michael Hubenthal (Education Specialist, IRIS).

A workshop"Earth System Science for Educators" has been run for 5 years with assistance from the IRIS Education and Outreach Program. The workshop was run fully by IRIS in the first year, and since 2007, with the establishment of the National Oceanic and Atmospheric Administration (NOAA) Interdisciplinary Scientific Environmental Technology Cooperative Science Center (ISETCSC) Center at North Carolina A&T State University the workshop has expanded the content to include atmospheric sciences with instructors from NOAA. The goals of ISETCSC are consistent with the goals of Africa Array: to increase the number of educated, trained, and graduated students from underrepresented communities. The workshop has become so successful that in the summer of 2008 there were 150 applications for the 25 available slots. The participants are eligible to receive up to 4 continuing education units (CEU) credits. With additional support from NSF the number of participants was increased to 50 in 2009. The workshop was filled to capacity with 50 teachers with a lot more on the waiting list.

Earth science has become a required course in North Carolina School systems, and most teachers lacked the necessary training and background to be effective teachers. The AA workshops have been instrumental in increasing the skills and knowledge of a number of teachers in North Carolina, and teachers were able to develop curriculum material and teaching aid for their classes as a result of their participation in the workshops.

Acknowledgements: The workshops were made possible by support from NSF-PIRE program and NOAA Cooperative Agreement No: NA06OAR4810187

IRIS Undergraduate Intern Research: Colorado Seismicity

Christina Viviano *(University of Colorado at Boulder),* **Gaspar Monsalve** *(University of Colorado at Boulder),* **Anne Sheehan** *(University of Colorado at Boulder)*

The IRIS undergraduate intern program pairs promising undergraduate students with research mentors from IRIS member institutions for a summer of seismological research. The student research culminates in a technical presentation at the national AGU meeting, and often leads to published research or contributions to publications. Undergraduate intern Christina Viviano participated in the project described here as part of the IRIS Undergraduate Internship Program, and the work resulted in a paper published in Seismological Research Letters. Viviano's project involved analysis of data from the Rocky Mountain Front IRIS PASSCAL seismic experiment (RMF). The RMF experiment consisted of the installation of 33 broadband seismic stations spread throughout Colorado with a few additional stations in Kansas and Utah. The use of this relatively dense seismic network, with an average seismometer separation of 75 km, allowed for the detection and location of Colorado earthquakes on a regional scale.The Rocky Mountain Front experiment was one of the first PASSCAL experiments, occurring in 1992. The data are archived at the IRIS DMC and analysis such as this many years after the original experiment is still possible. The analysis resulted in a six-month catalog of regional seismicity, which combined with additional temporary deployments contributes to improved understanding of Colorado seismicity. Though the majority of the events detected during the six-month deployment were classified as mining blasts (about 80%), the remaining remaining events reveal a six-month snapshot of seismicity in the state. Twenty-four events characterized as earthquakes were recorded during the six-month deployment. Extrapolation of our small sample of seismicity to higher magnitudes indicates that, at the most, two earthquakes of magnitude 6 are expected to occur every 1,000 years. However, the validity of the extrapolation of results based on a small data set is tenuous. A long-term uniform seismic network would give a better representation of the seismicity of Colorado, and further analysis will be advanced through the EarthScope USArray deployment.

References

Monsalve, G., C. Viviano, and A. Sheehan, An assessment of Colorado seismicity from a statewide temporary seismic station network, *Seismol. Res. Lett.*, v. 79, n. 5, p. 645-652, 2008.

Acknowledgements: We thank Frederick Blume and Gregory Bensen for their hard work in archiving the continuous RMF seismic data at the IRIS DMC many years after the original experiment, Art Lerner-Lam for running the RMF experiment, and IRIS for providing seismometers and assistance. Christina Viviano participated in this project as part of the IRIS Undergraduate Internship Program, funded by the National Science Foundation (NSF– EAR-0453427). The archiving of the continuous RMF data at the IRIS DMC 10 years after the original experiment and the seismicity analysis presented here were supported by NEHRP Grant No. 03HQGR0091.

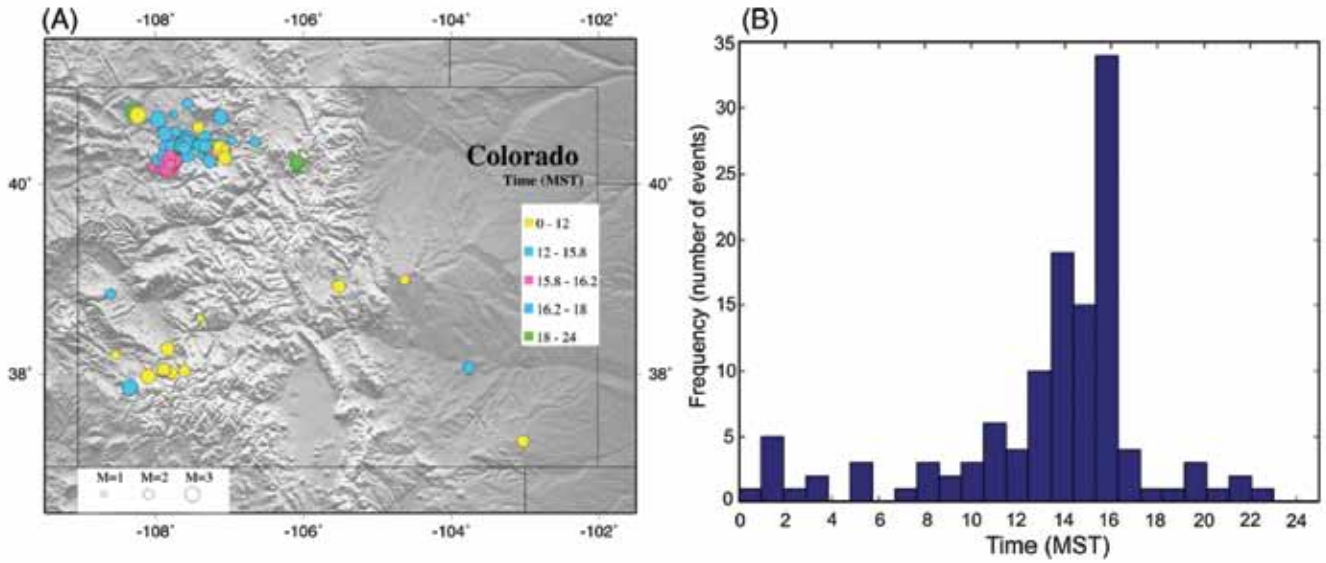

Seismic events (including suspected mine blasts) recorded by the RMF network between May and December 1992. (A) Seismicity map with symbol size scaled by event magnitude and colored by event origin time of day. Note the predominance of afternoon events (hours 12–18 MST). (B) Time-of-day histogram of events. Note the peaks at afternoon hours (hours 12–18 MST).

The IRIS Internship Cycle: From Intern to Graduate Student to Intern Mentor

Andy Frassetto *(University of Copenhagen)*

Serving as an overture to seismological theory and application, computing methods, and fieldwork; IRIS internships have introduced undergraduate students to the rigors of graduate school and eventual careers in geophysics. During my internship in 2003 the program resembled a summer job away from home, where students worked on a research project at their host institute and then convened at AGU to meet and present their results. Now the program has become an institution unto itself, starting with a week-long orientation that creates a peer group which can engage and support itself throughout the summer when spread across the U.S. [*Hubenthal et al., 2009*]. The satisfaction of participating in the development of this program and witnessing its impact firsthand is trumped by hosting an intern. In many respects this experience is a natural sequel to doing an internship. When supervising an intern, the formative experiences during the internship program and graduate school helped me to recognize what enables a successful summer project.

Like many IRIS interns, I matriculated to the school of my internship for graduate study in seismology. When an appropriate summer project arose, my advisor and I proposed to host a student during the summer of 2008. That intern, Jamie Ryan, participated in the last orientation that I helped oversee and worked on a study of earthquake focal mechanisms using data from the Sierra Nevada EarthScope Project [*Ryan et al., 2008*]. Working with Jamie was a pleasure, and his work will be featured prominently in a future publication on the fundamentally important seismicity occurring beneath the Sierra Nevada. Jamie will be starting graduate study in seismology at Arizona in the fall of 2010.

There are many skills involved in research that become engrained and thus may be hard to articulate when steering an intern's summer project. These include developing set goals and timetables, focusing literature searches, resolving code and program errors, recognizing data issues, integrating an interpretation with other constraints, *et al*. Experiencing this process via a previous internship allows a host greater finesse as a mentor. The transition of former interns to intern hosts has been unfolding over the last few years within the classes of IRIS alumni. This lineage of researchers with a specific familiarity and appreciation for the scope and goals of the internship program should continue to fortify a new generation of seismologists.

References

Ryan, J.C., A. Frassetto, O. Hurd, G. Zandt, H. Gilbert, T. Owens, C. Jones (2008), Focal Mechanisms for Deep Crustal Earthquakes in the Central Foothills and Near Yosemite National Park in the Sierra Nevada, California, Eos Trans. AGU, 89(53), Fall Meet. Suppl., Abstract S33B-1957.

Hubenthal, M., Wysession, M., Aster, R. (2009), Virtual cohorts and face-to-face recruitment: Strategies for cultivating the next generation of the IRIS Community, Eos Trans. AGU, 90(52), Fall Meet. Suppl., Abstract ED23B-02.

Acknowledgements: Thanks to Jamie Ryan for his dedicated work during the summer internship and while finishing his undergraduate degree and to George Zandt and Susan Beck for introducing me to the IRIS program.

IRIS Membership and E&O Program Team up for Intern Orientation Week

Richard Aster *(New Mexico Tech),* **Michael Hubenthal** *(IRIS Consortium)*

"Technology alone is not enough to create a strong social cohesion and sense of community among online members... It is essential to apply some techniques that help members in online communities enthusiastically and willingly work together" [*Ubon and Kimble, 2003*]. Students accepted into the IRIS Internship Program, prior to heading to their sponsoring institutions, attend a 5-day orientation to develop a strong sense of community among the interns and to provide an introduction to some of the most exciting aspects of modern seismology. Extensive experience with Earth science "field camps" shows that, for example, discussing earthquakes and faulting at the base of a dramatic fault scarp, provides a vastly richer learning experience than the normal classroom setting. Because of its excellent location for field experiences along Rio Grande Rift, a wide-ranging Earth Science department, its teaching, research, and computational facilities, and state-of-the art field equipment and expertise at the IRIS PASSCAL Instrument Center, New Mexico Tech (NMT) has successfully hosted the orientation since 2006. Instructors lead a variety of field excursions to collect and analyze active and passive seismic data and explore the relationship to regional and local scale geologic structures, and cutting-edge science questions [*e.g., Hubenthal et al., 2007*]. Orientation Week also highlights in-depth laboratory exercises and special lectures/discussion sessions by faculty and staff. Formative observations of instruction by the internship facilitator, who is trained in instructional supervision, help tailor instruction to the group and ensure quality delivery. Classroom sessions introduce interns to a variety of topics including: history and theory of seismology, earthquakes and earth structure, geophysical inverse theory, general reflection and refraction theory, and seismological data collection and seismic processing. Lab sessions introduce interns to the basics of UNIX and to computer programs that students are likely to encounter (e.g., Matlab, GMT and ProMax), and research-grade field equipment used by NSF and other researchers. Participants during 2010 included: Seth Stein (Northwestern University), M. Beatrice Magnani (University of Memphis), Catherine Snelson, Gary Axen, William McIntosh, Pnina Miller, Rick Aster, and Hunter Knox (NMT), Darren Hart (Sandia National Laboratories), Michael Hubenthal and John Taber (IRIS), and Robert Porritt (U.C. Berkeley).

IRIS Interns installing a broadband seismic station in 2010. Students installed three stations and analyzed teleseismic seismograms recorded over a three-day period.

References

Hubenthal, M., Taber, J., Aster, R., IRIS Undergraduate Internship Program and Orientation Enters its Second Year, Proc. EarthScope National Meeting, Monterey, CA, 2007.

Ubon, A., Kimble, C., Supporting the creation of social presence in online learning communities using asynchronous text-based CMC, Proceedings of the The 3rd International Conference on Technology in Teaching and Learning in Higher Education, 295-300, 2003.

Community-Outreach Efforts in Data Collection and Analysis for the 2008 Mogul Earthquake Sequence

Annie Kell-Hills *(University of Nevada, Reno),* **Mahesh S. Dhar** *(University of Nevada, Reno),* **Mayo Thompson** *(University of Nevada, Reno),* **John N. Louie** *(University of Nevada, Reno),* **Kenneth D. Smith** *(University of Nevada, Reno)*

Beginning Feburary 28, 2008 the residents of west Reno and Sparks, Nevada experienced continuous earthquakes ranging in magnitude from M1.0 to M5.0, centered in the west Reno neighborhoods of Mogul and Somersett. The occurrence of these earthquakes within residential areas stimulated the attention of the public and the media, providing an opportunity for the Nevada Seismological Laboratory (NSL) to involve the public in earthquake research. The NSL invited the public to host single-channel USArray Flexible Array RefTek RT-125A (Texan) recorders in their homes during May and June of 2008. Reno and Sparks residents volunteered to attend training sessions on installing and hosting recorders at their residences, filling the many gaps in NSL's permanent and RAMP station arrays. The use of instruments from the IRIS PASSCAL center allowed us to accommodate the unprecedented volume of public interest in local aftershock response. During the deployments, the 90 instruments covered a dense area of the Reno area with 106 different deployed locations (see figure). Evaluation of recorded seismograms for a M3.1 event display atypical responses for areas of bedrock and basin fill, in that bedrock seismograms in the north of Reno displayed higher than expected amplitudes and long durations, and that some regions of basin fill showed lower than expected amplitudes. Comparing these seismograms allows us to better interpret basin depths and bedrock locations for the Reno basin, and allows us to develop better models for local earthquake hazards. Analyses of the recorded data include time delay calculations and straight-ray tomography. A back-projection of pick delays indicates positive delays in the volcanic hills north of Reno, atypical of bedrock settings. Curve fitting on a time-distance plot for the M3.1 event estimated a hypocentral depth greater than the depth derived from NSL's permanent stations, motivating a study relocating the event depths. Data were then used to relocate the 97 recorded events by integrating event arrival times recorded with the PASSCAL instruments with the NSL network database for the permanent, strong-motion, and RAMP stations. Results from simple hypoinverse runs show that the dense station dataset drastically improves event locations, providing a better understanding of this swarm under urbanized Reno.

Acknowledgements: Research partially supported by the U.S. Geological Survey (USGS), Department of the Interior, under USGS award number 08HQGR0046. The views and conclusions contained in this document are those of the authors and should not be interpreted as necessarily representing the official policies, either expressed or implied, of the U.S. Government. Instruments used in the field program were provided by the PASSCAL facility of the Incorporated Research Institutions for Seismology (IRIS) through the PASSCAL Instrument Center at New Mexico Tech. Data collected during this experiment are available through the IRIS Data Management Center. The facilities of the IRIS Consortium are supported by the National Science Foundation under Cooperative Agreement EAR-0552316 and by the Department of Energy National Nuclear Security Administration.

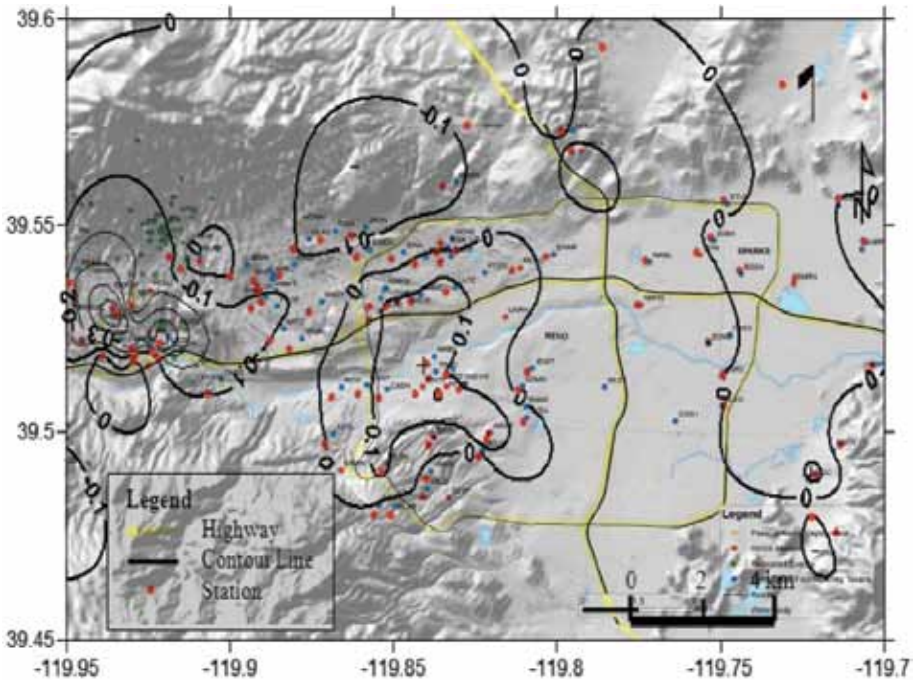

Location of deployed USArray Flexible Array Texan seismographs (red and blue) along with station time-delay contours calculated using both the permanent and portable stations.

USArray Student Siting Program Has a Big Impact in Oklahoma

Randy Keller *(University of Oklahoma)*

The Student Siting Program had a number of positive outcomes for the students from the University of Oklahoma who were involved. These impacts began with our trip to the training workshop where they had a chance to meet fellow students from around the southwest and visit another university. The summer support provided them a positive professional experience and saved 3 out of the 4 from menial summer jobs. They all enjoyed seeing parts of our state they had never seen before and meeting landowners who where mostly very helpful. However, they did come back with some interesting stories about some of their encounters. Catherine Cox was a new MS student and had a particularly positive experience that led toward her being very effective in helping layout and plan logistics for a large NSF project, the High Lava Plains project, after her siting work was finished. She is currently finishing her MS and is continuing her education in our PhD program. She was also asked to help with a subsequent Student Siting Program training workshop. Jonathan Green, Julianna Gay, and Matt Hamilton all went on to finish their BS degrees with excellent academic records and are now pursuing their MS degrees. They all remember their siting experience fondly. Their interest in EarthScope certainly spread across our student body and made them more aware of the project. An example of how good relations with landowners were in most cases is an event that occurred when a large group of students, faculty and media attended the equipment installation at a site near our university this spring. The landowner was very helpful and even cooked hamburgers for the crowd. We had two young visiting scientists from China attended this event and also became very interested in EarthScope. Pictures of this event are included in this report.

Acknowledgements: This research was supported by a sub-award from IRIS.

Figure 1: Catherine Cox at a TA station installation.

Figure 2: Seismologist Austin Holland speaking to the media during a TA station installation.

Site Reconnaissance for Earthscope USArray: A Vehicle for Integrating Geophysics and GIS Education with Outreach to the Community While Saving Money

Anne Trehu *(Oregon State University),* **Perle Dorr** *(IRIS)*

Identification and permitting of sites for seismic stations of EarthScope's USArray Transportable Array is a very ambitious undertaking. Initial site reconnaissance requires integration of information from a variety of geographic databases as well as an understanding of the regional geology and tectonics, the objectives of the EarthScope and USArray programs, and the technical requirements for a seismically quiet site. It thus provides rich opportunities for students in Earth sciences and geography to apply and enhance their knowledge. During summer 2005, Oregon State University (OSU) and IRIS initiated the USArray student-driven site reconnaissance program that continues today with participation by universities in the regions where stations will be installed in the following year or two.

The program began with a 3-day workshop for 11 students (8 from OSU; 3 from Arizona State University) organized by Anne Trehu (OSU geophysics), Mark Myers (OSU geography) and Bob Busby (USArray). The workshop included lectures about the scientific objectives of EarthScope, training on procedures to identify sites that meet the requirements of USArray, and a field trip to find a few local sites. Prior to going into the field, GIS tools using databases assembled by OSU, IRIS, and the Institute for the Application of Geospatial Technology were used to identify locations that met as many requirements as possible: 1) appropriate topography and geology; 2) adequate distance from cultural noise sources; 3) private ownership; and 4) digital cell phone coverage.

GIS lab work was followed by field visits to make contact with landowners and identify specific sites. In rural areas, University extension agents provided a valuable introduction to the local community. The "products" of this project were formal "Reconnaissance Reports" that included contact information, special site considerations and detailed instructions for finding the sites. Site locations were finalized by professional USArray staff.

Since this initial pilot program, the Transportable Array has conducted six additional siting workshops that have trained nearly 100 students who have identified locations for about 900 seismic stations. Based on feedback from the participants, the program has evolved, and continues to incorporate new techniques and technologies. The more recent workshops have placed more emphasis on determining and assessing site communications and the application of customized GIS products for initial site reconnaissance. But one thing that has not changed is the fact that the Transportable Array site reconnaissance program is popular among students and PIs alike. It has also proven to be an efficient and cost-effective way to locate a large number of sites while simultaneously providing an exciting practical training opportunity for students and transmitting the excitement of USArray to the public.

Students and instructors who participated in the 2005 Transportable Array Site Reconnaissance Program.

Educational and Outreach Experience from EarthScope/USArray 2010 Summer Siting Program

Jer-Ming Chiu *(CERI, The University of Memphis)*

The IRIS siting program has provided a very exciting educational and learning opportunity for two summer interns, William Jackson and Brian Young, as well to many landowners who we deal with in northern Mississippi, western Tennessee, western Kentucky, and southern Illinois. Summary of comments from the two interns are included below.

Brian Young (left) and William Jackson (right) are listening to a brief instruction of regional geology and oil field operation status in southern Illinois by Michael D. Podolsky (second from the right), a petroleum geologist, before heading to field to find a nearby site (R45A) near Fairfield, Illinois.

Will Jackson: During my internship with Earthscope and USArray, through the University of Memphis, I feel that I have gained valuable experiences and learned numerous lessons that will help me in my future career as a graduate student and professional. Several of the most significant things learned this summer include: 1) Communication Skills - whether it be face to face, on the phone, or in a professional setting, I gained a new found confidence that allowed me to communicate my idea to the person that I was engaging. 2) Successful Planning – creating and implementing a plan that included many different facets that had to be organized and carried out from start to finish. 3) Teamwork – whether it be with the professionals from Earthscope or with my team leader and partner, this internship gave me an opportunity to experience teamwork with professionals from the Earth Sciences that allowed me to gain knowledge of many other aspects beyond just the USArray project. I feel that the skills that I have obtained over the summer interning with Earthscope will help me throughout the rest of my graduate studies along with my professional career. In summary this summer internship has been an invaluable experience that I will never forget and always be indebted to the people who allowed me the opportunity.

Brian Young: Being a Physics undergraduate, prior to my participation in the Earthscope project I had never had any field experience outside of a laboratory, at all. Through my siting endeavors with my partner, we explored rural areas and farmland from northern Mississippi to western Kentucky, all the way up to St. Louis, Missouri. Not only did we drive around for days looking for suitable places for next year's seismic stations to be installed, experiencing the local landscapes and culture, but by speaking with landowners about the project and asking for their permission to install a seismic station on their land, we learned effective methods for presenting scientific projects to people who may not even know what a "seismic station" is. During the first few weeks of our siting experience, we could only find about one suitable site a day, and many landowners declined to host a seismic station on their land, having no interest in the project. Though frustrating, we eventually gained experience in explaining this exciting and ground-breaking project to local landowners, and many became enthusiastic to hosting a site for Earthscope and USArray – scientific endeavors of unprecedented scale. Into July and nearing the completion of our siting job, we were able to find two, or even three landowners in as many as three different states to agree to host a seismic station, all in a single day of siting.

Acknowlegements: This project is sponsored by the IRIS siting program at ISIS 1310 BP10. Landowners in the northern Mississippi, western Tennessee, western Kentucky, and southern Illinois help to make this siting project possible.

jAmaseis: Seismology Software Meeting the Needs of Educators

Ben Coleman *(Moravian College)*

jAmaseis is a piece of educational software that replaces and updates Amaseis, the current standard program IRIS supports through "Seismographs in Schools." jAmaseis allows users to send and receive seismic data in realtime, filter data, fit a seismogram to travel time curves, triangulate event epicenters on a globe, estimate event magnitudes, and generate images showing seismograms and corresponding calculations. Users accomplish these tasks through an interface specifically designed to enhance education.

Beyond providing educators with an improved version of AmaSeis with new features, jAmaseis offers a number of benefits. Most importantly, the scope of the educational seismology program is significantly larger because jAmaseis allows an educator to use the wealth of resources already developed for AmaSeis without actually possessing a seismometer. In addition, new classroom pedagogies are possible. With jAmaseis, a user can view and manipulate multiple streams of data simultaneously and produce visual representations of the results. Using these capabilities, an educator can instruct students to compare or combine the analysis of various seismic records, providing a deeper learning experience. Finally, because jAmaseis untethers the seismometer from the viewing computer, new applications are possible. For example, jAmaseis can be used to create engaging displays in public spaces simply by mounting a computer monitor.

Work on jAmaseis is a productive collaboration between IRIS and Moravian College. At Moravian, a large percentage of the computer science students are involved in the design and implementation of jAmaseis as either a project within a computer science course or as a summer research experience. These students interact with members of the IRIS Education and Outreach group and see the complete development process from design through implementation. This type of hands-on experience is rarely found in undergraduate computer science programs, and consequently the students have the opportunity to publish at peer-reviewed conferences, have stronger resumes upon graduation, and can draw on their experience during interviews for perspective jobs.

jAmaseis is currently under active development, with plans for release to beta testers in August 2010 and release to the general public during the summer of 2011.

Acknowledgements: This work is supported by an NSF sub-award from the IRIS E&O program and through the Student Opportunities for Academic Research (SOAR) program at Moravian College.

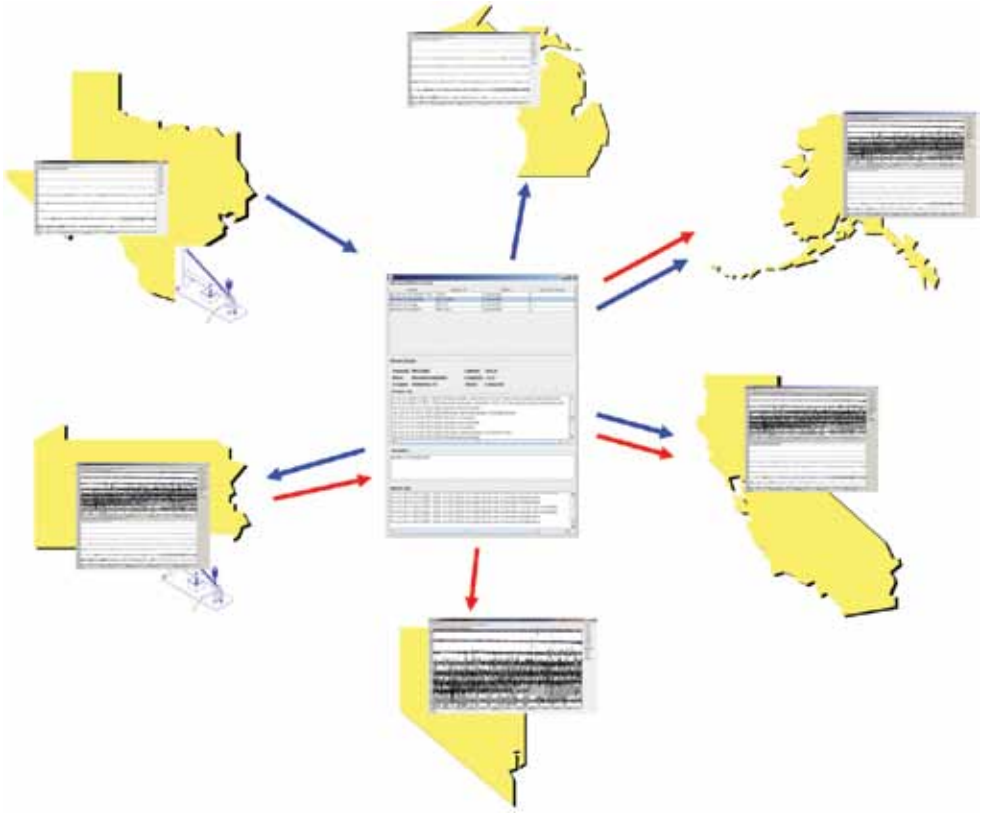

The scope of educational seismology is expanded because users have access to realtime data over the Internet. The users in Texas and Pennsylvania send data to the data server. Users in Michigan, Alaska, California, and Pennsylvania receive the data from Texas from the server. Similarly, users in Alaska, California, and Nevada receive the data sent from Pennsylvania.

Visualizing the Ground Motions of Earthquakes: the USArray Ground Motion Visualization (GMV)

DMC Products Group *(IRIS DMC)*

When an earthquake occurs, the seismic waves radiate away from the source and travel in different directions and produce ground shakings that last from a few seconds to minutes. Amplitude, duration and nature of shaking at each point on the Earth's surface depend on the size of the earthquake, distance from the source and type of seismic waves. Seismic stations record these ground motions at the station site while seismic arrays that deploy several stations within an area, sample the ground motion over an area. Deployment of dense arrays, in which array sites are closely spaced, provide an opportunity to visualize earthquake ground motions by looking at a series of snapshots that depict ground motion at individual array sites over time.

The Transportable Array component of the USArray/EarthScope project is a rolling array of 400 broadband stations deployed on a uniform 70-km grid. This very large aperture array, along with other stations from USArray, is well suited to visualize seismic waves crossing the contiguous United States. The USArray GMV is an IRIS DMS product that illustrates how seismic waves travel away from an earthquake by depicting the recorded wave amplitudes at each seismometer location using colored circles. The color of each circle represents the amplitude of the ground motion as detected by the station's seismometer and it changes as waves of differing amplitude travel past the seismometer. Blue circles represent downward ground motion while the red circles represent upward ground motions with the darker colors indicating larger amplitudes.

Acknowledgements: Product development within the IRIS DMS is supported by the NSF grants #EAR-0552316 and EAR-0733069.

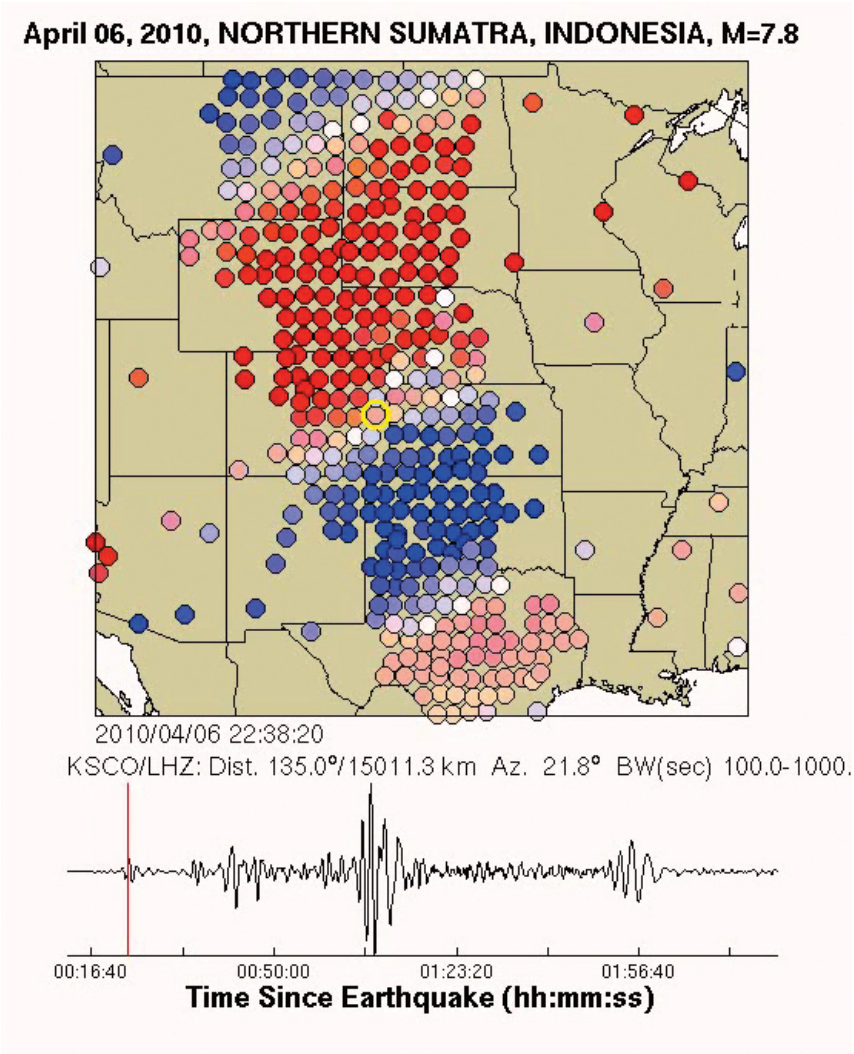

Ground Motion Visualization (GMV) of the April 6, 2009 earthquake of Northern Sumatra, Indonesia.

Near Real-Time Simulations of Global CMT Earthquakes

Jeroen Tromp *(Princeton University),* **Dimitri Komatitsch** *(University de Pau, CNRS & INRIA),* **Vala Hjörleifsdottir** *(Lamont-Doherty Earth Observatory),* **Qinya Liu** *(University of Toronto),* **Hejun Zhu** *(Princeton University),* **Daniel Peter** *(Princeton University),* **Ebru Bozdag** *(Princeton University)*

We have developed a near real-time system for the simulation of global earthquakes. Prompted by a trigger from the Global Centroid Moment Tensor (CMT) Project, the system automatically calculates normal-mode synthetic seismograms for the Preliminary Reference Earth Model, and spectral-element synthetic seismograms (Komatitsch & Tromp 2002) for 3D mantle model S362ANI (Kustowski et al. 2008) in combination with crustal model Crust2.0 (Bassin et al. 2000). The 1D and 3D synthetics for more than 1800 seismographic stations operated by members of the international Federation of Digital Seismograph Networks are made available via the internet and the Incorporated Research Institutions for Seismology Data Management Center (IRIS; iris.edu). The record length of the synthetics is 100 minutes for CMT events with magnitudes less than 7.5, capturing R1 and G1 at all epicentral distances, and 200 minutes for CMT events with magnitudes equal to or greater than 7.5, capturing R2 and G2. The mode simulations are accurate at periods of 8 s and longer, whereas the spectral-element simulations are accurate between periods from 17 s to 500 s. The spectral-element software incorporates a number of recent improvements, e.g., the mesh honors the Moho as a first-order discontinuity underneath the oceans and continents, and the performance of the solver is enhanced by reducing processor cache misses and optimizing matrix-matrix multiplication. In addition to synthetic seismograms, the system produces a number of earthquake animations, as well as various record sections comparing simulated and observed seismograms.

References

Bassin, C., Laske, G., and G. Masters, 2000. The current limits of resolution for surface wave tomography in North America, in EOS Trans. Am. Geophys. Union, vol. F897, p. 81.

Kustowski, B., Ekström, G., and A.M. Dziewonski, 2008. Anisotropic shear-wave velocity structure of the Earth's mantle: A global model, J. Geophys. Res., 113, B06306, doi:10.1029/2007JB005169.

Komatitsch, D. and J. Tromp, 2002. Spectral-element simulations of global seismic wave propagation—I. Validation, Geophys. J. Int., 149, 390–412.

Acknowledgements: This research was supported by the National Science Foundation under grant EAR-0711177.

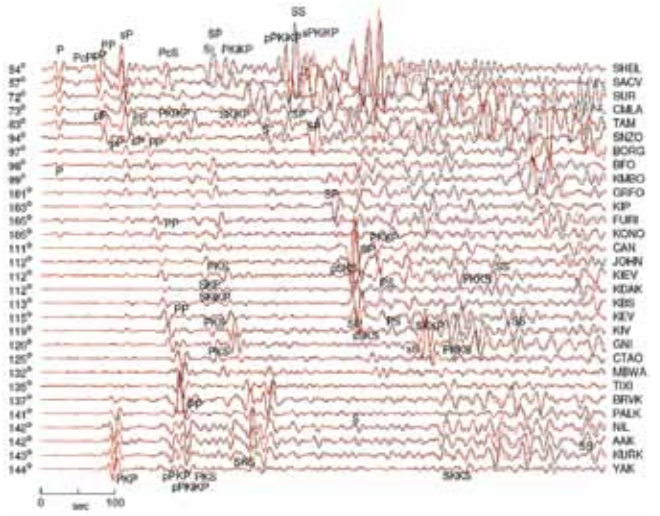

Vertical component record section comparing data (black) and SEM synthetics (red) for the September 3, 2008, Mw = 6.3 Santiago del Estero, Argentina earthquake, which occurred at a depth of 571 km. The records are aligned on the P wave, plotted as a function of epicentral distance, and bandpass filtered between 17 s and 60 s. Major seismological body wave arrivals are labeled. Epicentral distance is plotted to the left of each set of traces, and FDSN station identification codes are plotted to the right.

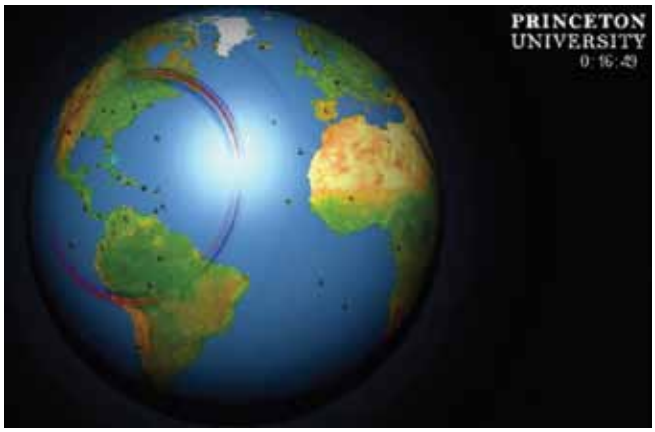

Snapshot of a spectral-element simulation of the January 12, 2010, Mw = 7.1 Haiti earthquake. The near real-time system produces animations of all earthquakes reported by the Global CMT Project. The animations show the velocity wavefield on Earth's surface as a function of time. Red: upward motion; Blue: downward motion. The prominent waves are the Rayleigh surface waves, and one can vaguely see SS waves crossing, e.g., Greenland.

New DMC Data Product: Standardized Event Information Plots Generated in Near Real Time for All M>5.5 Earthquakes

DMC Products Group *(IRIS DMC)*

As part of the extended product development effort at the IRIS DMC, we have begun to produce a suite of plots automatically generated in near real-time following all M>5.5 earthquakes. Plots will include record sections, vespagrams, time-distance envelope stacks, time-azimuth envelope stacks, station maps with signal-to-noise ratio and peak amplitudes indicated, phase centered record sections and various source-time function estimates. Depending on the plot type, plots will be generated using various data sets (all IRIS broadband data, USArray, southern California, Pacic Northwest Seismic Network...) in different frequency bands and for vertical, radial and transverse components. The plots will be available by plot type through our searchable product archive as well as on event-based webpages. These standardized plots will allow users to quickly scan data quality for seismic phases of interest or analyze many various features of earthquakes such as rupture duration and direction, coda duration, and complexity (impulsive vs emergent or single event vs doublet).

Acknowledgements: Product development within the IRIS DMS is supported by the NSF grants #EAR-0552316 and EAR-0733069.

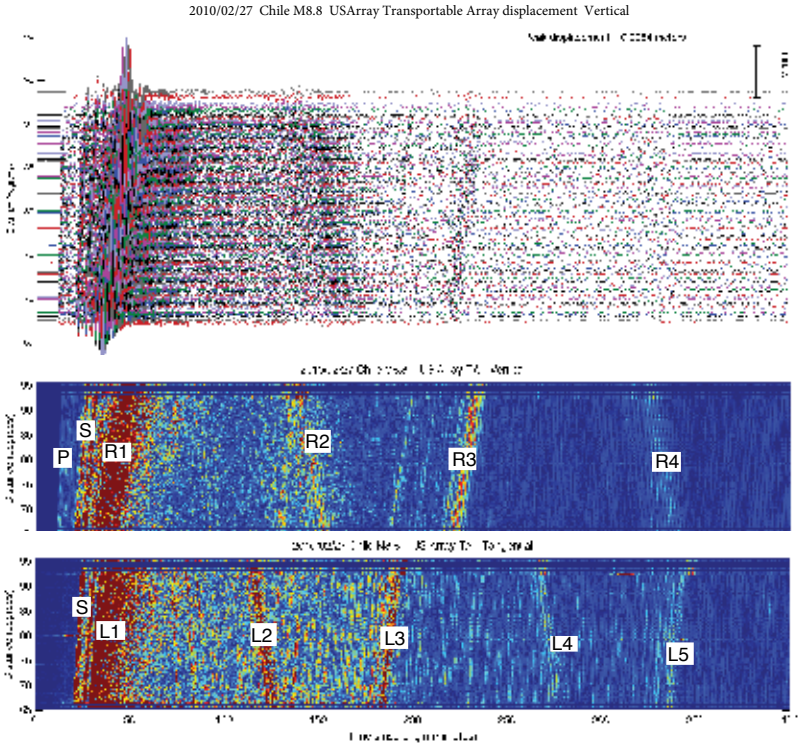

The long aperture and station densit of USArray allow for spectacular record sections such as these from the Feb, 2010 M8.8 Chile earthquake. Long period record sections are routinely generated for all large earthquakes (top) as well as nonlinear versions (bottom), which enhance the coherence of later major and weak arrivals. The bottom panels show clear Rayleigh and Love wave multiples.

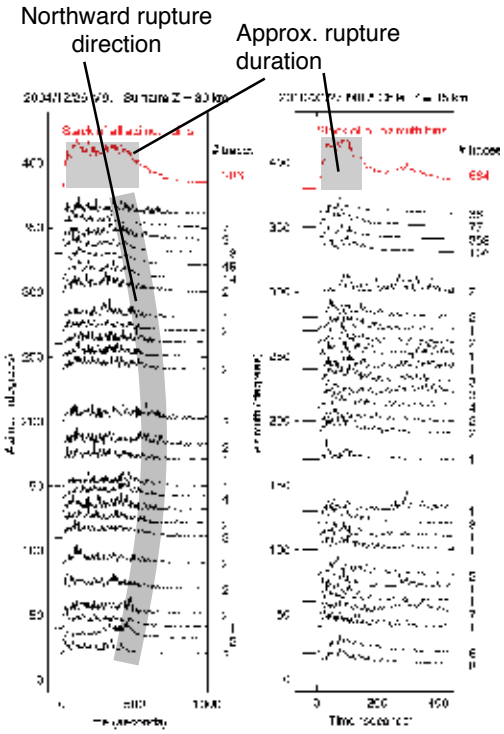

Short period envelopes of data between 30-95 degrees ditance are stacked in azimuthal bins. Quick looks at these plots can identify source features such as rupture duration, direction and complexity.

FuncLab: A MATLAB Interactive Toolbox for Handling Receiver Function Datasets

Kevin C. Eagar *(School of Earth and Space Exploration, Arizona State University),* **Matthew J. Fouch** *(School of Earth and Space Exploration, Arizona State University)*

We developed FuncLab, a new MATLAB graphical user interface (GUI) toolbox, for the management and analysis of teleseismic receiver functions. The ability to import and manage potentially large receiver function datasets within the MATLAB environment independent of the method of receiver function computation is the foundation of FuncLab. Additional modules for commonly employed processing and analysis methods, such as common conversion point and Hκ stacking, are built around the FuncLab management system. We also provide a framework for the development of future modules that implement alternative analysis methods. Users start by importing data in SAC format and creating an independent project with a formal directory structure, setup by FuncLab. Metadata, such as station and event information, for each record are stored in arrays housed within a MAT-file in the project directory. To handle large datasets and allow faster processing, FuncLab does not store receiver function or seismogram time series data in MAT-files, but rather selectively reads this data only during analysis or visualization processes. Through user-friendly GUIs, information and visualizations of each record are easily accessible. One of the key strengths of FuncLab is its ability to facilitate the always time-consuming pre-processing step of data selection, or trace editing, through visualization of many records at a time. Other processing, preference setting, and data export are also handled by GUIs, providing a combination of customization for experienced researchers and intuitive guidance for beginners. The IRIS Data Management Center is currently developing a conduit to provide receiver functions generated from the EarthScope Automated Receiver Survey (EARS) into a format that can be directly imported into FuncLab. FuncLab will be released to the community in late summer 2010.

References

Eagar, K.C. and M.J. Fouch, FuncLab: A MATLAB interactive toolbox for handling receiver function datasets, to be submitted to Computers and Geosciences, August 2010.

Acknowledgements: We would like to thank Rick Aster and Gary Pavlis for organizing extremely helpful MATLAB tutorials on receiver functions for the IRIS/Earthscope Imaging Science Workshop at Washington University in 2006 that first inspired KCE to deal with this problem in MATLAB. We would also like to thank Mike Thorne for his original SACLAB codes (http://web.utah.edu/thorne/software.html) for importing SAC files into MATLAB, much of which was modified for use with FuncLab. Thanks also to Manoch Bahavar and Chad Trabant of the IRIS Data Management Center and Philip Crotwell for extensive work in providing data products from the EARS project to be directly compatible with the new FuncLab MATLAB toolbox. This research was supported by National Science Foundation award EAR-0548288 (MJF EarthScope CAREER grant).

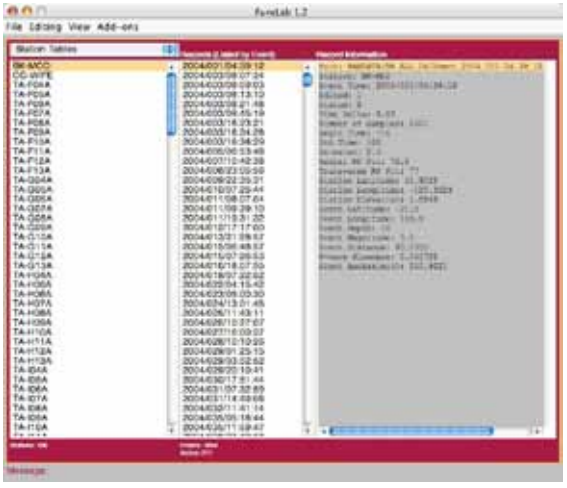

Screenshot of main FuncLab GUI. Items under the File, Editing, View, and Add-ons menus may be accessed from this screen. Top-left drop-down box lists the types of "tables" used to organize receiver function records. Tables are listed in the left panel. Records in the selected table (highlighted in left panel) are listed in the center panel. Metadata for the selected record (highlighted in center panel) are shown in the right panel. Information about number of tables, records, and active records are listed below the left and center panels, respectively. Text displayed at the bottom is used to convey short messages to the user about ongoing or finished processes.

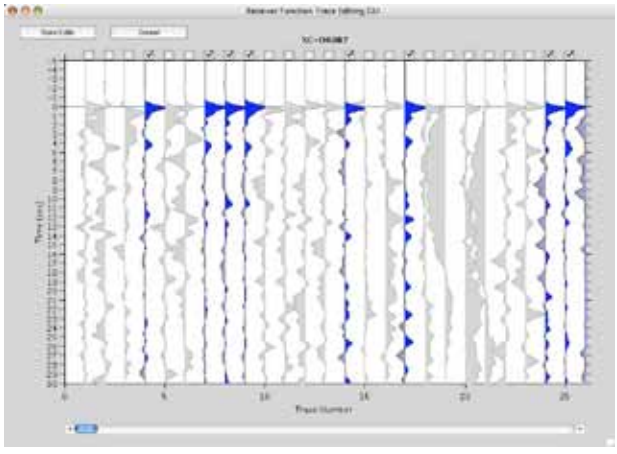

Screenshot of receiver function Trace Editing GUI. Wiggle traces of records in a selected table are displayed with blue (or red, not shown) fill denoting positive amplitudes and dark gray fill denoting negative amplitudes. Check boxes above waveforms allow the user to change the record status to "on" (checked) or "off" (unchecked). Unchecked records also shaded light gray. Scrollbar at the bottom allows the user to scan through all records listed in the table.

SEIZMO: a Matlab and GNU Octave Seismology Toolbox

Garrett Euler *(Washington University in St. Louis),* **Michael Wysession** *(Washington University in St. Louis)*

SEIZMO is a Matlab and GNU Octave based toolbox encompassing a collection of nearly 400 seismology related functions that provide a framework for seismic data preparation, quality control, and analysis akin to that of Seismic Analysis Code [*Goldstein and Snoke, 2005*]. There are numerous functions for reading/writing standard seismic data formats, displaying and editing metadata, plotting seismograms, creating animations, data processing, and interactive analysis. Data processing capabilities include correlation, convolution, deconvolution, detrending, differentiation, integration, interpolation, resampling, filtering, merging, response transferring, rotation, stacking, spectral analysis, tapering, and windowing. The toolbox contains collections of functions for arrival time determination and quality control with cross correlation and cluster analysis, Rayleigh wave two plane-wave analysis, seismic ambient noise processing, and frequency-wavenumber analysis. SEIZMO utilizes direct access to the TauP toolkit [*Crotwell et al., 1999*] to administer predicted arrival times, raypaths, pierce points, and travel time curves for several widely recognized 1D seismic earth models. Mapping in SEIZMO draws on the numerous projections available in the M_Map toolbox. The seismology toolbox also incorporates several 3D mantle models, a catalog of moment tensors from the Global CMT project, and a database of instrument responses available through IRIS. There are functions to aid in rapid prototyping and customization for new functions and documentation for every function is accessible through the inline help system.

The project is currently in the development stages with stable releases expected in late 2010. More information and prereleases can be found at the project's webpage, http://epsc.wustl.edu/~ggeuler/codes/m/seizmo

References

Goldstein, P., A. Snoke, (2005), SAC Availability for the IRIS Community, IRIS Data Management Center Electronic Newsletter.

Crotwell, H. P., T. J. Owens, and J. Ritsema (1999). The TauP Toolkit: Flexible seismic travel-time and ray-path utilities, *Seismol. Res. Lett., 70*, 154

Acknowledgements: This research is supported by NSF grant EAR-0544731.

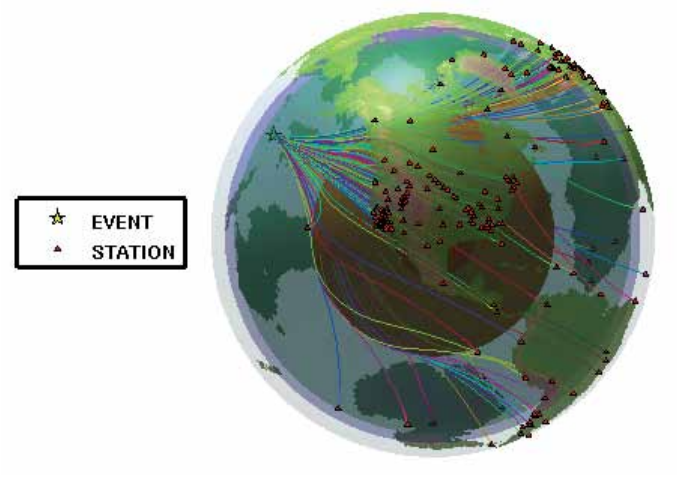

Snapshot of a rotatable and zoomable 3D plot of grazing and core-diffracted P-wave ray paths for numerous stations recording a Mw 7.5 earthquake in the Philippine Islands region on March 5, 2002. The translucent shells correspond to the major discontinuity depths of the Earth.

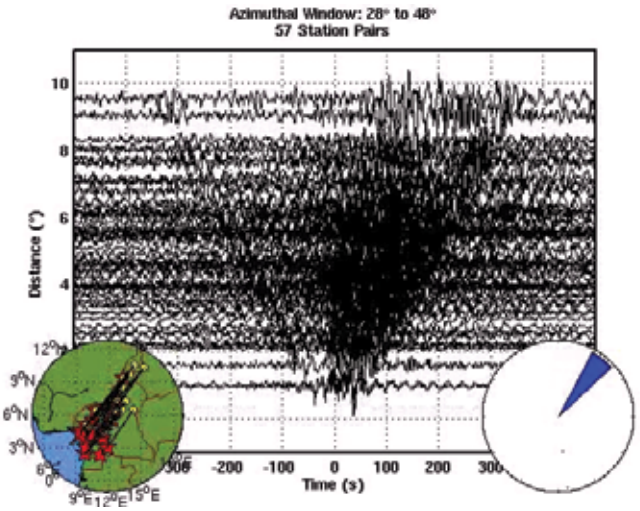

One frame from an animation produced with SEIZMO that portrays the azimuthal variations in Green's function recovery from the cross correlation of ambient noise recorded by a PASSCAL deployment in Cameroon between 2005 and 2007 (yellow circles). Traces in the main window are sorted by interstation distance for the pairings in the map on the lower-left. The strong asymmetric arrivals in the positive time range are Rayleigh waves from a persistent source of microseismic energy off the station pair great circle paths.

Five Years of Distributing the Seismic Analysis Code (SAC) Software

Brian Savage *(University of Rhode Island),* **Arthur Snoke** *(Virginia Tech),* **Tim Knight** *(IRIS DMC)*

SAC (Seismic Analysis Code) is a general purpose interactive program designed for the study of sequential signals, especially time-series data. SAC was developed by the Lawrence-Livermore National Lab (LLNL) in the mid-80s, and it was maintained and distributed by them until 2005. At that time, in collaboration with LLNL, IRIS began distributing SAC to IRIS members and took over SAC development. [*Goldstein & Snoke, 2005*]. In late 2006, IRIS enhanced SAC's capabilities and created a "derivative product," thus expanding the licensing agreement and allowing the distribution of SAC software to collaborators including the USGS, members of FDSN and other non-U.S. seismological institutes. The new license agreement led to a large increase in the number of SAC requests each year. Between 2006 and 2007, there was a 237% increase in SAC distributions (see chart and figure below).

Between 2005 and June 2010, there have been four major updates of the SAC package. (See the 2009 newsletter article referenced below that accompanied the release of SAC v101.3b.) Further information about the package, including instructions for requesting the software, can be found at the IRIS SAC software page: .

There have been over 4,000 SAC Software requests by scientists and programmers from Feb 2005 to June 2010. (Because the program has been updated four times, many scientists who had downloaded an earlier version, request an updated version.) SAC is available for Linux, Mac, Solaris and Cygwin/Windows computer platforms.

The majority of users request the Linux binary (58%), followed by Mac (29%) and Solaris (13%). In 2008, IRIS began distributing the SAC source code for Cygwin/Windows (429 requests). The SAC source code is requested by 69% of the users. SAC users include students, professors, scientists, engineers and programmers. For further details on the statistics of the SAC distribution by IRIS, see the 2010 newsletter article referenced below.

References

Goldstein, P. & Snoke, A, SAC Availability for the IRIS Community, RIS DMS Newsletter Vol7 no1 http://www.iris.edu/news/newsletter/vol7no1/page1.htm

Knight, T. (2010), SAC Software Statistics, IRIS DMS Newsletter Vol12 no1 http://www.iris.edu/news/newsletter/vol12no1/sac_stats.htm

Sac Development Team, Sac v101.3 – New version of SAC Software released in August 2009. IRIS DMS Newsletter Vol11 no2 http://www.iris.edu/news/newsletter/vol11no2/sac.htm

Acknowledgements: The distribution of SAC software was supported by an NSF grant.

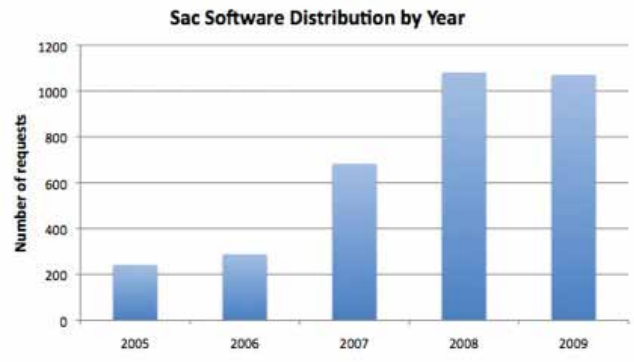

International demand for the SAC software increased following a new license agreement in 2006. The number of SAC requests started to level off in 2009. (Knight, 2010)

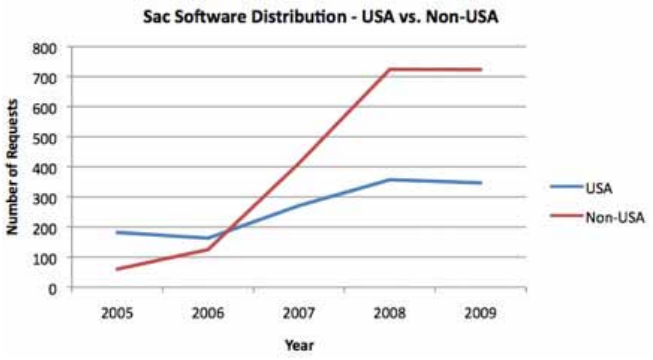

Seismologists worldwide use the SAC software distributed by the IRIS DMC. 38% of SAC requests come from the USA, while 62% of the requests are international. (Knight, 2010)

The NSF IRIS EarthScope USArray Array Network Facility (ANF): Metadata, Dataflow, Phase Picks, and State of Health Monitoring

J. A. Eakins *(Univ. of California, San Diego),* **F. L. Vernon** *(Univ. of California, San Diego),* **R. L. Newman** *(Univ. of California, San Diego),* **L. Astiz** *(Univ. of California, San Diego),* **V. Martynov** *(Univ. of California, San Diego),* **J. Tytell** *(Univ. of California, San Diego)*

Since 2004, the EarthScope USArray Array Network Facility has been responsible for: metadata distribution; data delivery of all currently operational Transportable Array (TA) stations; data delivery for all post-deployment recovered baler data; station command and control with the goal of improving data quality, data availability, and data completeness; providing useful interfaces for personnel at the Array Operations Facility including access to both current and historic state of health information; distribution of station end-of-life reports; and quality control checks for all data. The Transportable Array is a challenging project due to the dynamic nature of the network. Stations are in place for 18 months to two years, leading to ~18 installations and 18 removals per month. Various tools using the Antelope software package have been developed to deal with the constant influx of data, changes to the metadata, remote retrieval to fill data gaps, and alarm generation and reactionary scripts when state of health parameters exceed given thresholds.

As of June 2010, we maintain data for 893 TA stations (1049 total stations with contributing networks): approximately 400 TA stations are operational at any point in time. Analysts have reviewed over 48,000 events with nearly three million reviewed arrivals available. Phase pick files for reviewed events are available from both the DMC and the ANF website. Round Robin Database (RRD) plots of state-of-health values, maps of the current deployment status, movies of the deployment history, the state of data return, as well as many additional monitoring tools are available from http://anf.ucsd.edu.

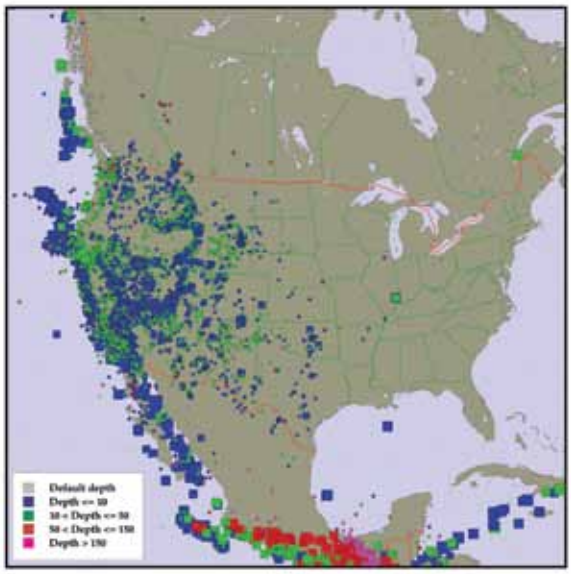

Seismic events recorded by the NSF supported Earthscope USArray Transportable Array. Analysts review events in near real-time with over 48,000 events reviewed since 2004. All seismic sources are included.

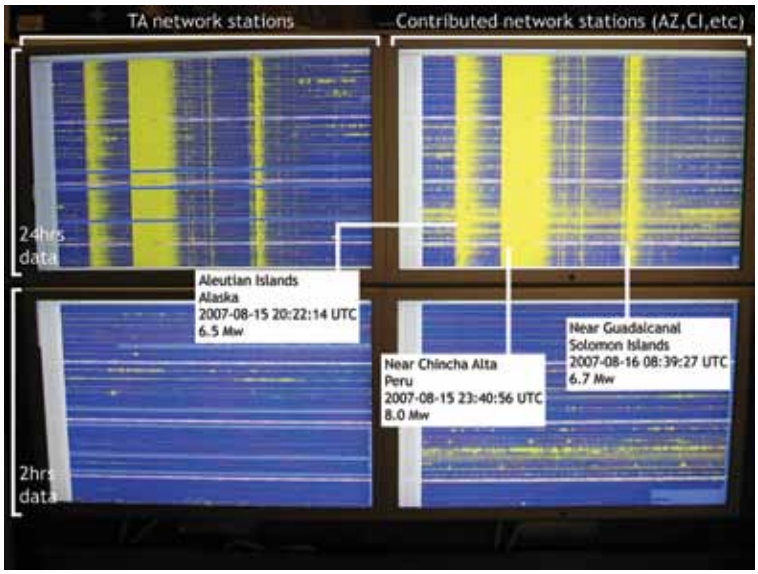

A busy day at the ANF office. Three teleseismic events (6.5Mw+) were recorded within 18 hours. Photo taken: 11:45AM PDT Thursday 16 August 2007. Local media often visit the ANF office when newsworthy events occur.

IRIS DMS Data Products, Beyond Raw Data at the IRIS DMC

DMC Products Group *(IRIS DMC)*

The IRIS DMC has begun an increased eort to create, archive and distribute products derived from raw data that serve as the basis for research needs or end-use education and outreach material. ese products expand the DMC's oerings beyond the raw data traditionally accessed at the DMC. Data products are being produced both by the scientic community and the IRIS DMC. In most cases these new products, particularly the ones produced at the DMC, will be routinely generated and serve as consistent data sets. To ensure that useful and appropriate products are created and managed at the DMC, a Data Products Working Group (DPWG) representing the research community was formed to evaluate and propose product ideas.

Products released or near realease include USArray Ground Motion Visualizations (GMVs), the EarthScope Automated Receiver Survey (EARS) developed at the University of South Carolina, suites of event plots, Princeton 1D & 3D synthetic seismograms and the Earth Model Collaboration (EMC) for exchange, preview and download of tomography models. Many more product ideas are in consideration and will be evaluated and developed in the near future.

See http://www.iris.edu/dms/products/ for more information.

Acknowledgements: Product development within the IRIS DMS is supported by the NSF grants #EAR-0552316 and EAR-0733069.

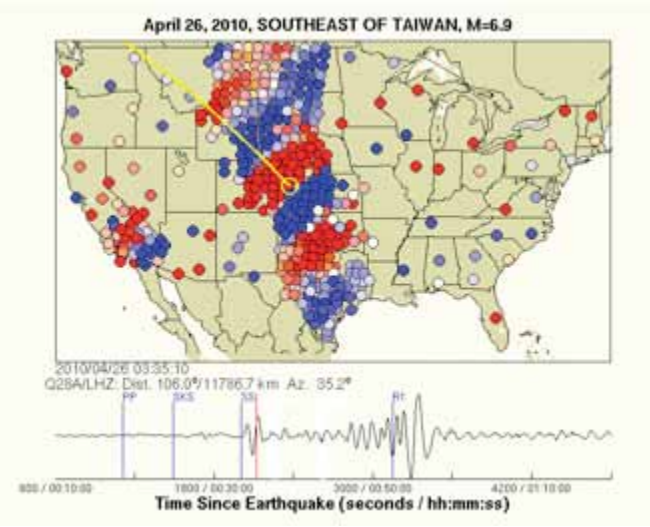

USArray Ground Motion Visualizations (GMVs): a visualization of seismic waves crossing the contiguous United States, see www.iris.edu/dms/products/usarraygmv/

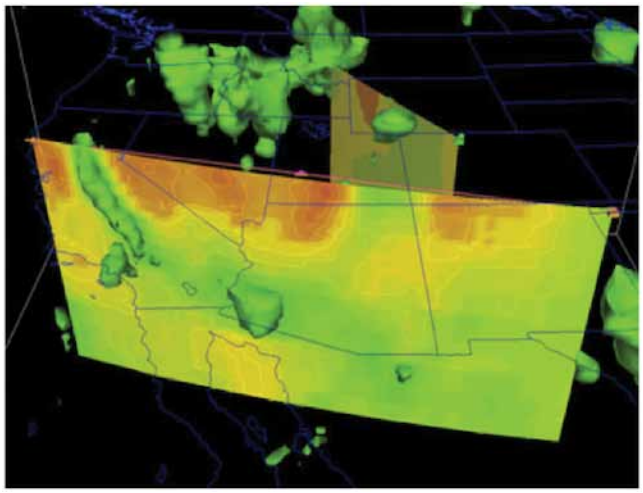

Earth Model Collaboration (EMC): a web site dedicated to the preview and distribution of tomography models.

Seismicity and Faulting in the Southern Gulf of California

Danielle F. Sumy *(Lamont-Doherty Earth Observatory),* **James B. Gaherty** *(Lamont-Doherty Earth Observatory),* **Tobias Diehl** *(Lamont-Doherty Earth Observatory),* **Won-Young Kim** *(Lamont-Doherty Earth Observatory),* **John Collins** *(Woods-Hole Oceanographic Institution)*

The Sea of Cortez Ocean-Bottom Array (SCOOBA) seismic experiment consists of a 4-component broadband ocean-bottom seismic (OBS) array that recorded earthquakes and other natural seismic signals for nearly 12 months between October 2005 and October 2006. The 14-station array was designed to complement the onshore NARS-Baja experiment run by Utrecht University, Cal Tech, and CICESE. Two subarrays were centered within the Alarcon and Guaymas basins, coinciding with previous refraction and MCS lines [*Lizarralde et al., 2007*], with ~20 km spacing. Four additional instruments were deployed at ~100 km spacing. Over 650 earthquakes (depths < 35 km) were recorded by the array, with ~320 M>3.5 earthquakes and seven M>5 strike-slip events within the southern gulf that are accompanied by several foreshocks and aftershocks. Most of these events are located on the major NW-SE strike slip faults that delineate the plate boundary, but a few appear to be located on faults well away from the nominal plate boundary. For sufficiently well-recorded and paired events, we are in the process of applying the hypoDD double-difference algorithm to obtain high-precision relative relocations. Additionally, we are working towards modeling the Rayleigh waves of ~30 events to determine the mechanisms of on- and off-axis activity. These locations and mechanisms of earthquake activity will improve our understanding of the distribution of seismic deformation within the greater extensional zone in the southern GoC. These data have been archived at the IRIS DMC, and are openly available to the community.

References

Lizarralde, D., G. J. Axen, H. E. Brown, J. M. Fletcher, A. Gonzalez-Fernandez, A. J. Harding, W. S. Holbrook, G. M. Kent, P. Paramo, F. Sutherland and P. J. Umhoefe, Variation in the styles of rifting in the Gulf of California, *Nature, 448*, 466-469, 2007.

Acknowledgements: Funding is from the NSF MARGINS program, award number OCE 0436411 for James Gaherty at LDEO, and OCE 0305140 for John Collins at WHOI.

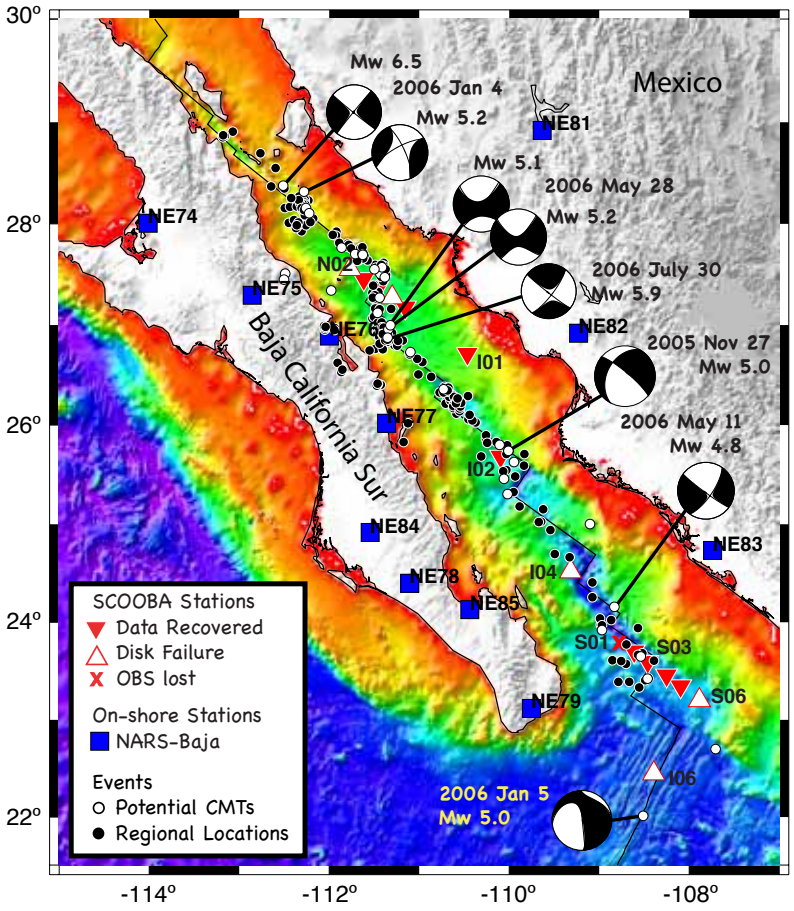

Figure 1. Location of the SCOOBA OBS stations (triangles), as well as complementary on-shore broadband NARS-Baja stations (blue squares). Also shown are Global CMT mechanisms for seven large events recorded by the array, our modeled mechanism for the 27 November 2005 event, and the locations for ~300 of our best-located events (black circles).

Local Earthquakes in the Dallas-Ft. Worth Region

Brian Stump *(Southern Methodist University),* **Cliff Frohlich** *(University of Texas at Austin),* **Chris Hayward** *(Southern Methodist University),* **Eric Potter** *(University of Texas at Austin)*

Injection or removal of fluids in the shallow crust can trigger earthquakes. In October 2008 and May 2009, small earthquakes occurred which were felt by numerous Dallas-Fort Worth (DFW) residents. PASSCAL provided six, three-component broad-band seismographs that were operated for two months following the October 2008 earthquakes. Preliminary analysis of these data and regional seismic data [*Frohlich et al., 2010*] demonstrates that: (1) Between 30 October 2008 and 31 December 2009, approximately 180 earthquakes occurred with probable hypocenters on or near DFW airport property; (2) Eleven of these were locatable by the local network and had hypocenters with focal depths of ~4.4 km situated along a 1.1 km SW-NE line near the south boundary of the DFW airport (Figure); (3) These hypocenters were situated approximately 500 m from a 4.2 km deep saltwater disposal (SWD) well where injection began on 12 September 2008, seven weeks before the first earthquake; (4) The hypocenters and the SWD well were situated near a mapped NE-SW trending subsurface fault, oriented such that slip along this fault was consistent with regional tectonic stresses; and (5) No evidence was found that drilling, hydrofracture, or natural gas production caused the earthquakes. The timing and proximity to the SWD well suggests that fluid injection at the SWD well may have induced the earthquakes. In June 2009, residents of Cleburne, TX, felt a second series of small earthquakes 60 miles south of DFW. Ten seismograph stations were deployed. Preliminary analysis of these data indicates that small earthquakes continued near Cleburne until at least November 2009, and that they also occurred near a SWD well. Following the felt earthquakes local and national news media called attention to the possible relationship between the earthquakes and the ongoing development of natural gas in the Fort Worth Basin. Even though the largest of the earthquakes had a magnitude of only M3.3, and they seemed unrelated to hydraulic fracturing, groups opposed to the development of tight gas shales considered them as evidence supporting their position. As noted in the Wall Street Journal, "the quake concerns come at a sensitive time for the industry, which is battling proposed legislation in Congress that would more heavily regulate hydraulic fracturing."

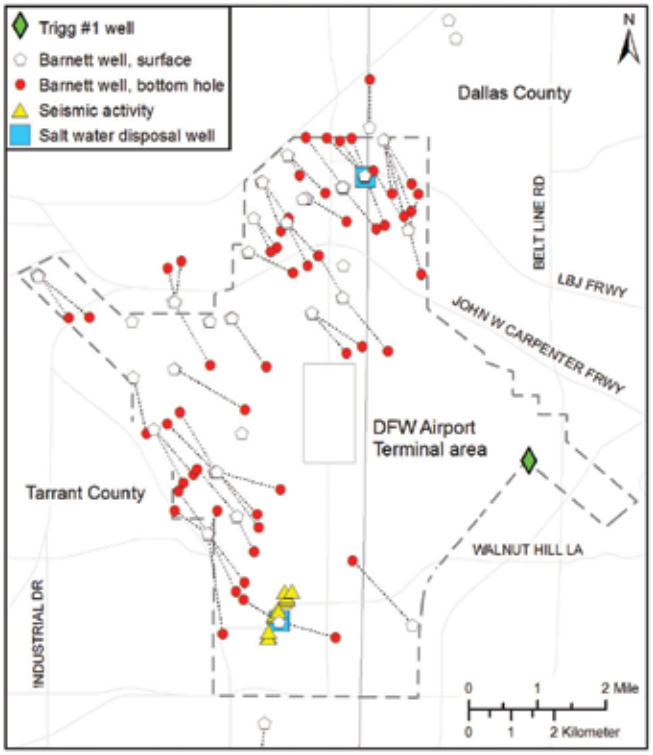

Map of DFW airport, showing location of earthquakes located by the temporary network (yellow triangles), tops and bottom of producing gas wells (white and red circles), and SWD wells (blue squares). The mean of the DFW earthquake location estimates using a linear velocity model is less than a kilometer from the bottom of the south SWD well.

References

Frohlich, C., E. Potter, C. Hayward, and B. Stump, Dallas-Fort Worth earthquakes coincident with activity associated with natural gas production, *Leading Edge, 29*, 270-275, 2010.

Use of ANSS Strong-Motion Data to Analyze Small Local Earthquakes

Kristine Pankow *(University of Utah Seismograph Stations),* **James Pechmann** *(University of Utah Seismograph Stations),* **Walter Arabasz** *(University of Utah Seismograph Stations)*

Traditionally, accelerometers have been used for recording triggered strong-ground motions from earthquakes with M > 4. The data from these instruments have been primarily used by engineers for building design and by seismologists modeling fault rupture histories. Although older generation strong-motion instruments were "incapable of recording small or distant earthquakes" (USGS, 1999, p. 12), advances in accelerometer and digital recording technology have greatly reduced this limitation. Following the 2002 Denali Fault earthquake we learned that modern continuously telemetered strong-motion instruments provide valuable recordings of some teleseismic earthquakes [Pankow et al., 2004]. Since then, we have learned that these instruments also provide valuable recordings of small (0.5 < M < 4) local earthquakes. Hundreds of modern strong-motion instruments have been deployed during the last decade as part of the U.S. Geological Survey Advanced National Seismic System (ANSS). Using the archive of continuous data from University-of-Utah-operated ANSS stations stored at the IRIS DMC, we determined the magnitude and distance ranges over which first arrivals could be successfully picked from accelerometers located on both rock and soil in northern Utah (see figure). The earthquake dataset consisted of 31 earthquakes (M 0.5 to M 3.2) located in the Salt Lake Valley. Somewhat surprisingly, earthquakes as small as M 2 are well-recorded on accelerometers to epicentral distances of 35 to 45 km at soil sites and 70 km at rock sites. ANSS accelerometers are collecting a rich new dataset, much of which is being archived at the IRIS DMC. This dataset is important not just for recording "the big one" and for strong-motion seismology, but also for studies of teleseisms, structure, and local seismicity.

References

Pankow, K.L., W.J. Arabasz , S.J. Nava, and J. C. Pechmann, Triggered seismicity in Utah from the 3 November 2002 Denali fault earthquake, *Bull. Seismol. Soc. Amer., 94*, S332-S347, 2004.

Pankow, K.L., J. C. Pechmann, and W.J. Arabasz , Use of ANSS strong-motion data to analyze small local earthquakes, *Seismol. Res. Lett., 78*, 369-374,2007.

USGS, An assessment of seismic monitoring in the United States: Requirement for an Advanced National Seismic System: U.S. Geological Survey Circular 1188, 55 p., 1999.

Acknowledgements: This project was supported by the U.S. Geological Survey, Department of the Interior, under USGS award number 04HQAG0014, and by the State of Utah under a line-item appropriation to the University of Utah Seismograph Stations.

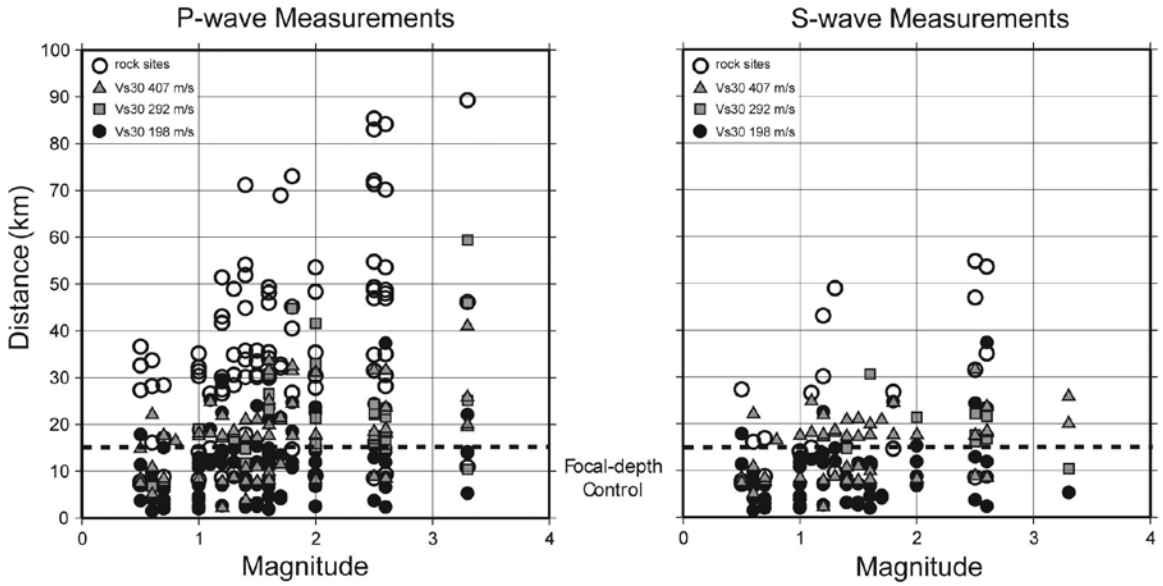

Plots (from Pankow et al., 2007) showing the distribution, as a function of distance, magnitude, and site response unit (see key) of all measurable arrival times for P-waves (left) and S-waves (right) recorded by accelerometers from 31 earthquakes in the western Salt Lake Valley. The dashed line at 15 km distance envelops those picks (< 15 km) that could improve focal-depth control.

Epicentral Location Based on Rayleigh Wave Empirical Green's Functions from Ambient Seismic Noise

Anatoli Levshin *(University of Colorado at Boulder),* **Michail Barmin** *(University of Colorado at Boulder),* **Michael Ritzwoller** *(University of Colorado at Boulder)*

A new method to locate the epicenter of regional seismic events is developed with strengths and limitations complementary to existing location methods. This new technique is based on applying Empirical Green's Functions (EGFs) for Rayleigh waves between 7 and 15 sec period that are determined by cross-correlation of ambient noise time-series recorded at pairs of seismic receivers. The important advantage of this method, in comparison with standard procedures based on use of body wave travel times, is that it does not employ an earth model. Rather it is based on interpolating the EGFs to arbitrary hypothetical event locations. The method is tested by locating well known "Ground Truth" crustal events in the western US as well as locating seismic stations using the principal of reciprocity. Data from the EarthScope/ USArray Transportable Array as well as regional networks were used for location. In these applications, location errors average less than 1 km, but are expected to vary with event mechanism and depth.

References

Barmin, M.P., A.L. Levshin, Y. Yang, and M.H. Ritzwoller, 2010. Epicentral Location Based on Rayleigh Wave Empirical Green's Functions from Ambient Seismic Noise. Submitted to *Geophys. J. Int.*

Acknowledgements: This research was supported by DoE/NNSA contract DE-AC52-09NA29326

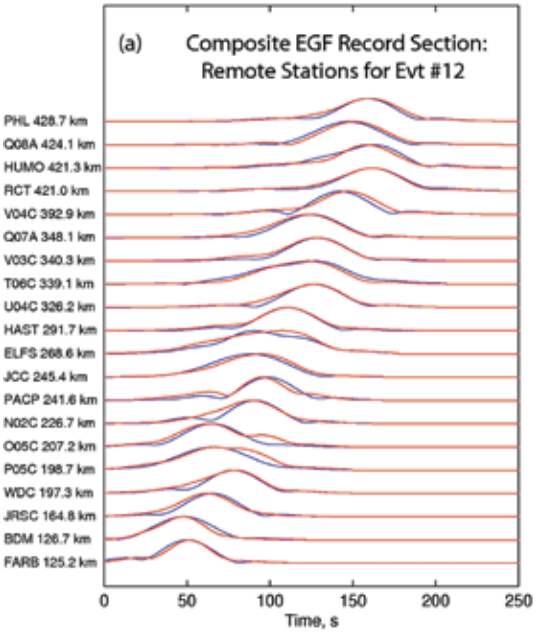

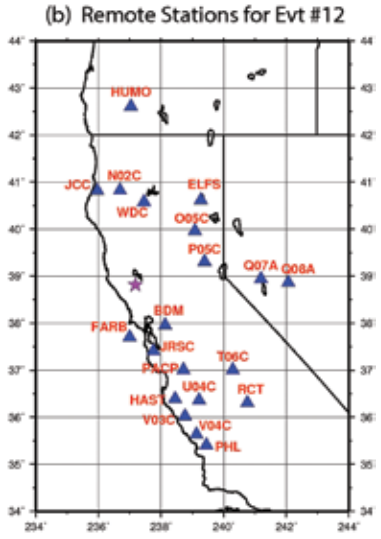

Record section of the Composite Empirical Green's Functions compared with the earthquake records at 20 remote stations for Event on in Northern California. (a) Envelope functions of the earthquake observed at the remote stations (red lines) are compared with envelopes of the Composite EGFs (blue lines). Band-pass: 7-15 sec period. Epicentral distances and station names are indicated at left. (b) Locations of the remote stations (blue triangles) and the earthquake (red star).

Schema of the Crandall Canyon mine. Our location of the event (green star) and corresponding 90% confidence ellipse. The left yellow push-pin marks the USGS event location, and the right push-pin is the approximate location of the mine collapse and trapped miners.

Rupture Fault Determination of the 2008 Mt. Carmel, Illinois, Earthquake in Wabash Valley Seismic Zone

Hongfeng Yang *(Saint Louis University),* **Lupei Zhu** *(Saint Louis University),* **Risheng Chu** *(Caltech)*

The April 18, 2008 Mt. Carmel Earthquake (magnitude 5.2) in southeastern Illinois underscores potential earthquake hazards in the Wabash Valley seismic zone. Since there was no surface rupture, the causal fault of the earthquake was not clear. In this study, we first developed a sliding-window cross-correlation (SCC) detection technique and detected more than 120 aftershocks in the two-week time window following the mainshock by applying the technique to continuous waveforms. We then precisely relocated 28 aftershocks out of all detected events by the double-difference relocation algorithm using accurate P- and S-wave differential arrival times between events obtained by waveform cross correlation. After relocation, we used the L1 norm to fit all located events by a plane to determine the mainshock fault plane. The best-fit plane has a strike of 292° and dips 81° to the northeast. By combining the aftershocks locations and focal mechanism solutions, we conclude that the April 18 earthquake occurred on a nearly vertical left-lateral strike-slip fault orienting in the WNW-ESE direction. The fault coincides with the proposed left-stepping Divide accommodation zone in the La Salle deformation belt and indicates reactivation of old deformation zone by contemporary stresses in the Midcontinent.

References

Yang, H., L. Zhu, and R. Chu, Fault-plane determination of the 18 April 2008 Mt. Carmel, Illinois, earthquake by detecting and relocating aftershocks, *Bull. Seismol. Soc. Amer., 99*(6), 3413-3420, 2009

Acknowledgements: This work is supported by NSF grant EAR-0609969. Waveform data are from the IRIS DMC.

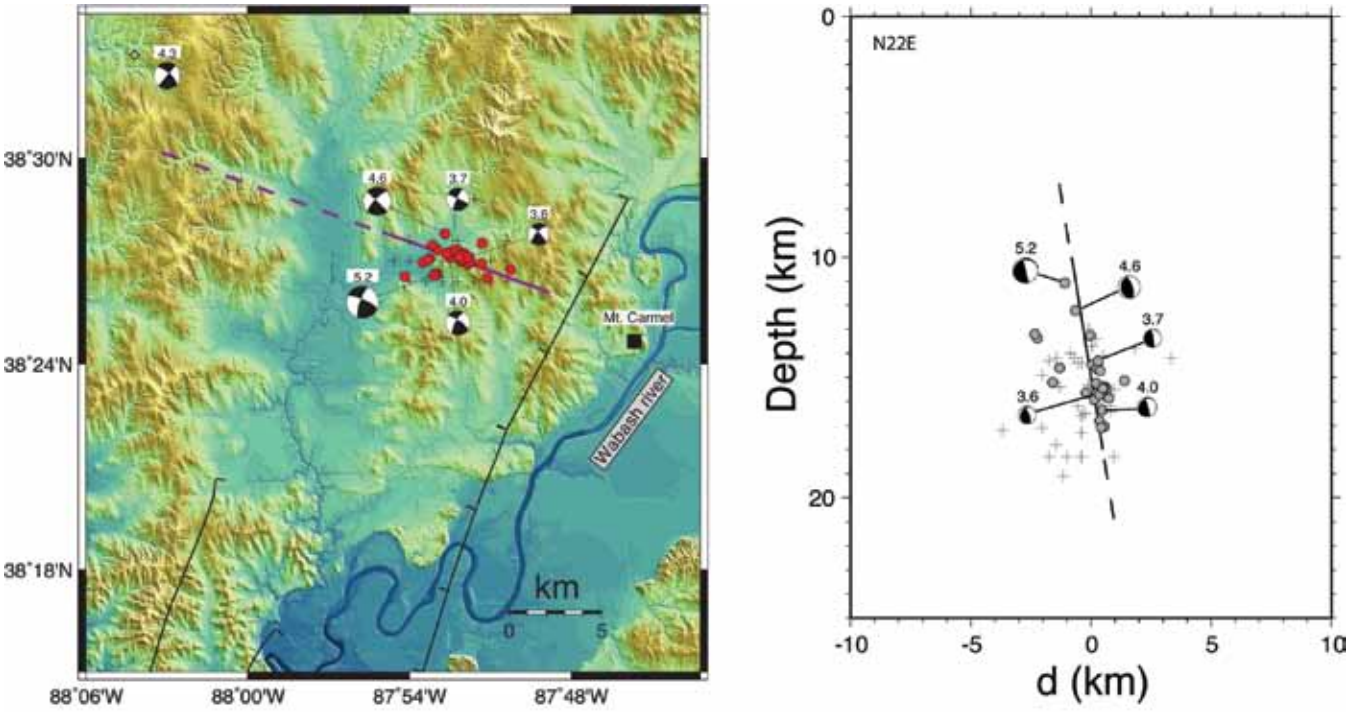

Map view (left) and vertical cross-section (right) of located aftershocks (red dots) of the 2008 Mt Carmel Earthquake. Their locations and earthquake focal mechanisms (beach balls) of the main-shock and four largest aftershocks suggest that the main-shock occurred on a nearly vertical fault orienting WNW-ENE (represented by the straight line).

Analysis of Spatial and Temporal Seismicity Patterns within Arizona During the Deployment of the EarthScope USArray Transportable Array (March 2006 - April 2009)

Jeffrey Lockridge *(Arizona State University),* **Matthew Fouch** *(Arizona State University),* **J. Ramon Arrowsmith** *(Arizona State University)*

Monitoring earthquake activity across the state of Arizona has historically been restricted by a paucity of regional seismic stations. Prior to 2006, earthquakes within Arizona were located at a rate of less than 30 events per year, presenting significant challenges for studies linking seismic activity and lithospheric strain accommodation. In this study, we utilize broadband seismic data recorded within Arizona by the EarthScope USArray Transportable Array (TA) (http://earthscope.org) to improve the characterization of the sources of tectonic strain accumulation and the mechanisms by which it is released. We built a Google Earth KMZ of global event data using EarthScope ANF monthly event archives to examine the spatial and temporal distribution of seismicity within Arizona during the deployment of the USArray TA. To date, we have identified 12 areas of seismicity within Arizona that exhibit event swarms with clear spatial and temporal correlations. We analyzed waveform data using the Antelope Environmental Data Collection Software package. We examined data from 8 TA stations nearest to each of 3 case studies and hand-picked P and S arrivals to generate a catalog of events for each swarm. We used a 1-5 Hz bandpass filter to detect events and a 0.3 Hz high-pass filter or no filter to pick arrivals. We present preliminary swarm characterization for these three case studies, which were chosen due to their distinctly different tectonic settings. (1) The linear-trending (NNE-SSW) Roosevelt Swarm is located within the Arizona Transition Zone and is adjacent to Roosevelt Lake, a ~35 km long reservoir on the Salt River with a maximum depth of ~100 m. (2) The spatially clustered Uinkaret Swarm is geologically located beneath the Uinkaret Volcanic Field on the north rim of the Grand Canyon (last known eruption ~1,100 years ago). The swarm is juxtaposed between 2 notable Quaternary faults (Hurricane and Toroweap) and is located within the Northern Arizona Seismic Belt along the western tectonic boundary of the Colorado Plateau. (3) The spatially clustered Shonto Swarm is geologically located within the Colorado Plateau. The nearest volcanic field is located ~47 km to the NE, and no known faults have been identified in the vicinity of this swarm.

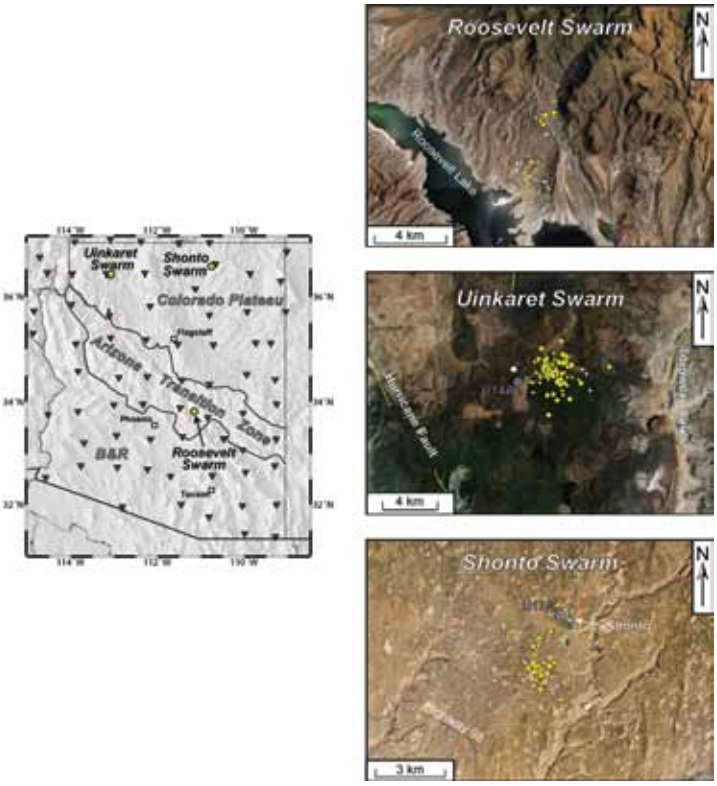

Figure Captions: Left: Locations of three earthquake swarms investigated as part of this study (yellow circles), USArray Transportable Array stations (red triangles), and the geologic/physiographic provinces of Arizona. Right Column: Google Earth screen captures of events from USArray ANF monthly archives (white circles), new events located as part of this study (yellow circles), and USArray TA stations (blue circles). Top Right: Roosevelt Swarm - 62 detections from 6/21/2007 to 6/28/2007 with 20 located events (3+ stations). Mag = 1.6 to 2.5 ml; Avg Depth = 3.8 km; Peak Activity = 10 events/hour. Middle Right: Uinkaret Swarm: 345 detections from 12/4/2007 to 12/17/2007 with 20 located events (3+ stations). Mag = 0.7 to 3.2 ml; Avg Depth = 13.5 km; Peak Activity = 18 events/hour. Bottom Right: Shonto Swarm: 172 detections from 8/29/2008 to 9/29/2008 with 34 located events (3+ stations). Mag = 0.8 to 2.8 ml; Avg Depth = 5.8 km; Peak Activity = 6 events/hour.

Acknowledgements: Acknowledgements: Financial support for this project came from U.S. National Science Foundation grant EAR-0548288 and the Federal Emergency Management Agency (FEMA). A huge thanks to the USArray Transportable Array team for installing and maintaining the stations used for this study. Waveform and Antelope database data were provided by Frank Vernon (USArray Array Network Facility) and the IRIS Data Management Center. Thanks also to the USArray Array Network Facility for a preliminary USArray event catalog. Historical Arizona earthquake database was provided by the Arizona Earthquake Information Center and the Arizona Integrated Seismic Network. Aerial photographs and Google Earth interface provided by Google.

Mozambique Earthquake Sequence of 2006: High-Angle Normal Faulting in Southern Africa

Z Yang *(Univ. of Colorado, Boulder),* **W.-P. Chen** *(Univ. of Illinois, Urbana)*

We report source mechanisms for the six largest shocks of the Mozambique earthquake sequence of 22 February 2006. The main shock of this sequence is one of the largest (Mw ~ 7.0) to occur in Africa over the past 100 years and its P waveforms alone are sufficient to show that north-south trending normal faulting near the surface continues to depths of more than 15 km along an exceptionally steep dip of 76° ± 4°. This new result shows that globally seismogenic normal faulting spans a wide range of dips, from about 30° to 75°. S waveforms, when combined with a minor component of left-lateral slip observed in the field, indicate the rake to be between −80° and −89° which, in turn, places a new constraint on relative plate motions: Complications from a nonspecific Rovuma microplate notwithstanding, our results favor the Euler pole between the Somalia and Nubia plates to lie southward of the epicenters.

Acknowledgements: We thank E. Calais, C. Collettini, C. Hartnady, R. Sibson, S. Stein, and Y. D. Zheng, for helpful discussions. In particular, S. Marshak suggested antithetic faulting in a listric master system. The data management centers of IRIS and GEOSCOPE kindly provided seismograms to us, and D. Doser, C.J. Ebinger, and B.W. Stump made careful reviews of the manuscript. This work is supported by the U.S. National Science Foundation grant EAR9909362 (Project Hi-CLIMB: An Integrated Study of the Himalayan-Tibetan Continental Lithosphere during Mountain Building, contribution I06). Any opinions, findings, and conclusions or recommendations expressed in this material are those of the authors and do not necessarily reflect those of the NSF.

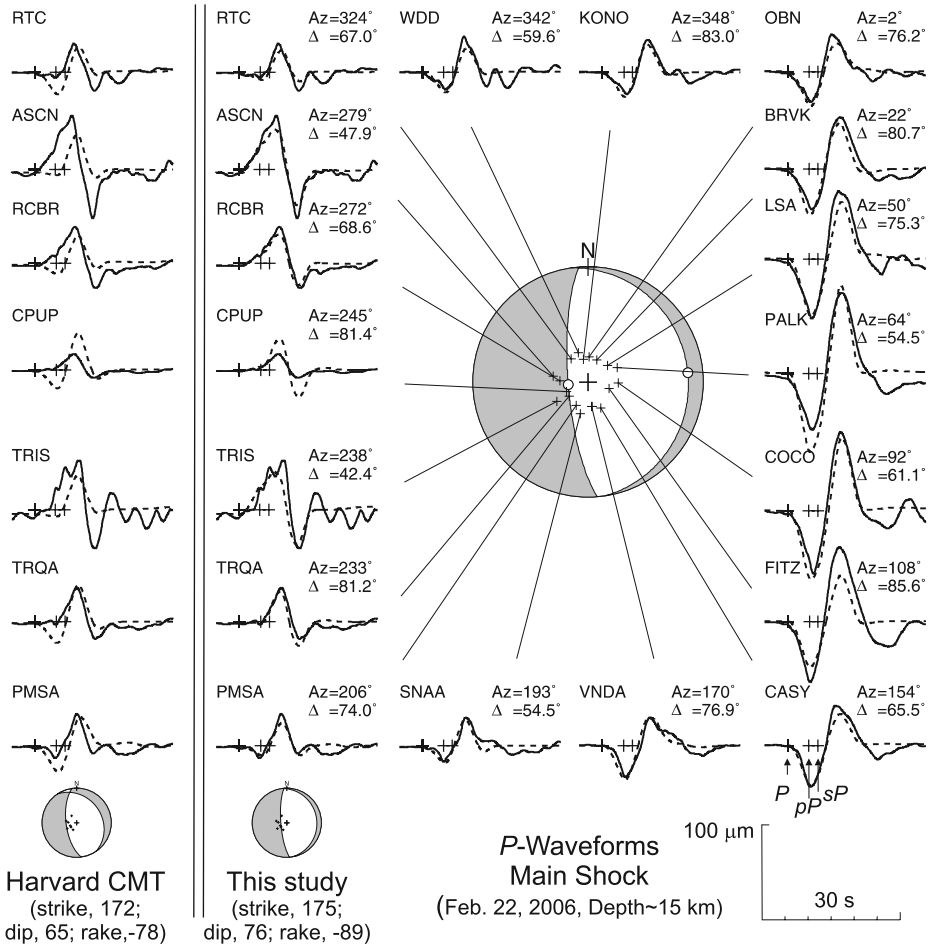

(right) Comparison between observed (solid traces) and synthetic P waveforms (dashed traces) of the main shock. The synthetic seismograms are calculated with a rupture history (source time function) represented by a symmetric triangle of 7.5 s in duration. Notice excellent azimuthal distribution of observations which are well matched by synthetic seismograms. (left) Comparison of synthetic seismograms based on the Harvard CMT solution with selected observations whose polarities of first motions are violated in several cases because a dip angle of 65° is too low. Open circles in the plot of fault plane solution are poles of nodal planes.

Exceptional Ground Motions from the April 26, 2008 Mogul Nevada Mw 5.0 Earthquake Recorded by PASSCAL Rapid Array Mobilization Program (RAMP) Stations

Glenn Biasi *(University of Nevada Reno),* **John G. Anderson** *(University of Nevada Reno),* **Kenneth D. Smith** *(University of Nevada Reno),* **Ileana Tibuleac** *(University of Nevada Reno),* **Rasool Anooshehpoor** *(University of Nevada Reno),* **David von Seggern** *(University of Nevada Reno)*

An unusually shallow swarm of earthquakes began 28 February 2008 beneath Mogul, Nevada, a small suburb a few km west of Reno. Earthquake depths of as shallow as 2 km were confirmed on instrumentation immediately over the hypocentral area, and residents routinely reported feeling events as small as Ml 1.5 or smaller. The swarm also exhibited an accelerating moment release over a period of several weeks. The slow build-up of the swarm allowed UNR to deploy four PASSCAL RAMP instruments in the epicentral area in early April 2008 to improve location control and map swarm evolution. Importantly, the RAMP stations included strong-motion sensors to ensure that any larger earthquakes would be recorded on scale.

Seismic activity accelerated throughout April, culminating in an Mw 5.0 mainshock at 06:40 UTC 26 April 2008 [*Anderson et al., 2009*]. Two stations immediately above the mainshock recorded component accelerations over 800 cm/s^2. Mean horizontal accelerations exceed 0.6 g at three of the four stations. The strongest peak acceleration was 1,164 cm/s^2, or about 1.19 g, at station MOGL, about 0.4 km from the epicenter. The peak vector velocity at MOGL was 54 cm/s, at a frequency of about 3 Hz. These accelerations far exceed design ground motions for the residential construction of the community, but nevertheless, damage to wood-frame buildings there was minimal. Ground motions also far exceeded predictions from the major ground motion regression equations, apparently because of the shallow hypocentral depth of about 3 km. At the same time, attenuation of peak ground motions was greater than predictions, suggesting that source-side attenuation was greater than for earthquakes with a more typical depth of 5-10 km. Peak accelerations and velocities from this earthquake would place it in the top 25 strongest ground motions ever recorded [*Anderson, 2010*]. These amazing recordings and new insights into shallow earthquake swarms would have remained unknown without timely access to PASSCAL RAMP instruments.

References

Anderson, J. G., I. Tibuleac, A. Anooshehpoor, G. Biasi, K. Smith, and D. von Seggern (2009). Exceptional ground motions recorded during the April 26, 2008 Mw 5.0 earthquake in Mogul, Nevada, *Bull. Seismol. Soc. Amer., 99*, 3475-3486.

Anderson, J. G. (2010). Source and site characteristics of earthquakes that have caused exceptional ground accelerations and velocities, *Bull. Seismol. Soc. Amer., 100*, 1-36.

Acknowledgements: The permanent network in western Nevada and easternmost California was supported by the United States Geological Survey under Cooperative Agreement 07HQAG0015.

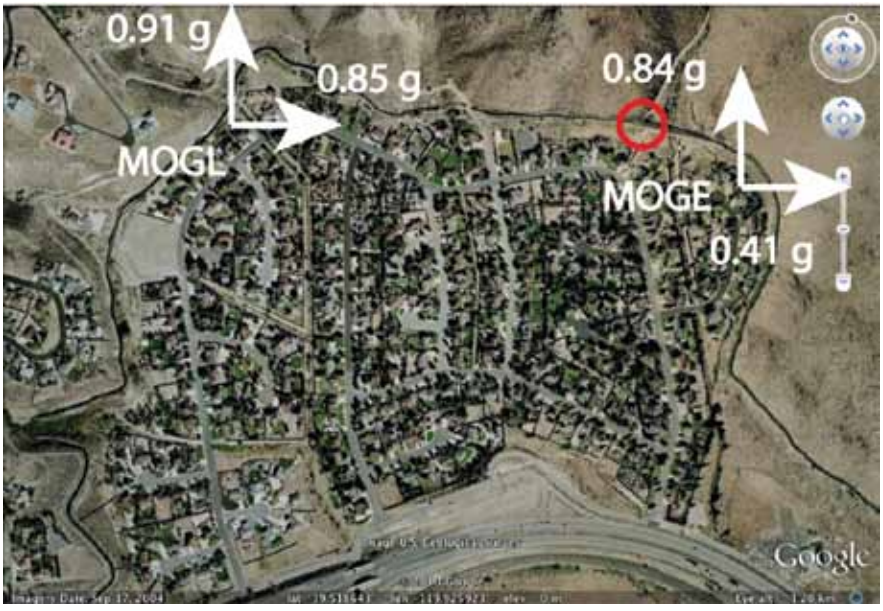

Mogul, Nevada community (Google Earth; center 39.5186, -119.9262; ~1.5 km N-S photo extent), with component ground accelerations measured from PASSCAL RAMP stations MOGL and MOGE. April 26, 2008 Mw 5.0 mainshock epicenter is indicated by the red circle.

Detailing a Shallow Crustal Earthquake Swarm beneath the Mogul, Nevada with PASSCAL RAMP Instrumentation

Glenn Biasi, Kenneth D. Smith, John G. Anderson *(University of Nevada, Reno)*

An anomalous swarm of shallow earthquakes began on 28 February 2008 beneath the suburban communities of Mogul and Somersett, Nevada, about 12 km west of downtown Reno. Initially the swarm consisted of a few earthquakes per week, but accelerated during March 2008 to include several felt events per day. Residents routinely reported feeling earthquakes of Ml 1.5 or smaller. Earthquake depths as shallow as 2 km were confirmed by a short-period station in the epicentral region. The relatively slow onset and sustained activity of the swarm provided time to request seismic instruments from the PASSCAL Rapid Array Mobilization Program (RAMP) pool. Four RAMP stations with broadband and strong-motion sensors were deployed in the epicentral area by 9 April 2008. The swarm began to accelerate in earnest in early April, with four Ml 3 or greater earthquakes on 15 April, two Ml 4 events on 24 April, and what proved to be the mainshock, an Mw 5.0 earthquake at 06:40 on 26 April 2008. This earthquake produced component ground accelerations in excess of 0.8 g at two stations, and horizontal vector accelerations in excess of 1.1 g at one station [*Anderson et al., 2009*]. These ground motions caused widespread non-structural and content damage to residences in the area.

Because of the social impact of the swarm and its potential to continue or even grow, six RAMP instruments deployed in central Nevada were relocated in early May to the epicentral area. An innovation in this deployment is that the RAMP stations were integrated by IP radio telemetry, beginning in late April 2008 into the permanent seismic monitoring network of the region operated by the University of Nevada Reno (UNR) (Figure 1). Antelope processing software at UNR allowed RAMP stations to be integrated seamlessly into the main network. This provided UNR personnel with highest-quality real-time information as the swarm evolved.

The Mogul swarm continued at a high level of daily activity through June 2008, and did not return to an activity rate similar to its first week until mid-August. Double-difference hypocentral relocations (Figure 2) identify a NW-trending vertical structure, consistent with the mainshock and focal mechanisms, with a smaller NE-trending spur toward the north end of the rupture zone. The Mogul swarm did not occur on any known or suspected fault and geologic investigation has not identified any surface expression or structure. Continuous GPS data gathered with the event resolved motions up to 2.5 cm at the surface, but indicate a geodetic moment release approximately twice as large as would be expected from the seismicity.

The Mogul sequence was the subject of a one-hour documentary by the National Geographic organization Naked Science series and aired by national cable-TV providers. Information is available at http://channel.nationalgeographic.com/series/naked-science/4232/Videos#tab-Overview.

References

Anderson, J. G., I. Tibuleac, A. Anooshehpoor, G. Biasi, K. Smith, and D. von Seggern (2009). Exceptional ground motions recorded during the April 26, 2008 Mw 5.0 earthquake in Mogul, Nevada, *Bull. Seismol. Soc. Amer., 99*, 3475-3486.

Acknowledgements: The permanent network in western Nevada and easternmost California was supported by the United States Geological Survey under Cooperative Agreement 07HQAG0015.

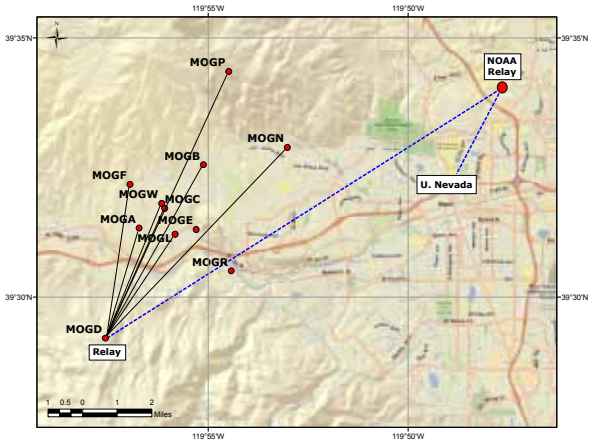

igure 1. PASSCAL RAMP stations and telemetry paths for the Mogul, Nevada earthquake swarm of 2008. Station MOGE used a cell modem, and station MOGR could not be telemetered by radio or cell because of line-of-sight issues. Seismic data was relayed to UNR and integrated into regional seismic network operations in real time.

Figure 2. Double-difference relocated earthquakes of the Mogul, Nevada earthquake swarm. The mainshock had an Mw of 5.0, but a local magnitude Ml 4.7. The mainshock hypocenter was approximately 3 km depth. Hypocenters do not coincide with any known fault or geologic structure. Downtown Reno, Nevada is near the east edge of the image.

The 2010 Mw7.2 El Mayor-Cucapah Earthquake Sequence, Baja California, Mexico and Southernmost California, USA: Active Seismotectonics along the Mexican Pacific Margin

Egill Hauksson *(Caltech, Seismological Laboratory),* **Joann Stock** *(Caltech, Seismological Laboratory),* **Kate Hutton** *(Caltech, Seismological Laboratory),* **Wenzheng Yang** *(Caltech, Seismological Laboratory),* **Antonio Vidal** *(CICESE, Mexico),* **Hiroo Kanamori** *(Caltech, Seismological Laboratory)*

The El Mayor-Cucapah earthquake sequence started with preshocks in March 2010, and a sequence of 15 foreshocks of M>2 (up to M4.4) that occurred during the 24 hours preceding the mainshock. The foreshocks occurred along a north-south trend near the mainshock epicenter. The Mw7.2 mainshock that occurred on the 4th of April exhibited complex faulting, possibly starting with a ~M6 normal faulting event, followed ~15 sec later by the main event, which included simultaneous normal and right-lateral strike-slip faulting. The aftershock zone extends for 120 km from the south end of the Elsinore fault zone at the US-Mexico border almost to the northern tip of the Gulf of California. The waveform-relocated aftershocks form two abutting clusters, of about equal length of 50 km each, as well as a 10 km north-south aftershock zone just north of the epicenter of the mainshock. Even though the Baja California data are included, the magnitude of completeness and the hypocentral errors increase gradually with distance to the south of the international border. The spatial distribution of large aftershocks is asymmetric with five M5+ aftershocks located to the south of the mainshock, and only one M5.7 aftershock but numerous smaller aftershocks to the north. Further, the northwest aftershock cluster exhibits complex faulting on both northwest and northeast planes. Thus the aftershocks also express a complex pattern of stress release along strike. The overall rate of decay of the aftershocks is similar to the rate of decay of a generic California aftershock sequence. In addition, some triggered seismicity was recorded along the Elsinore and San Jacinto faults to the north but significant northward migration of aftershocks has not occurred. The synthesis of the El Mayor-Cucapah sequence reveals transtensional regional tectonics, including the westward growth of the Mexicali Valley as well as how Pacific North America plate motion is transferred from the Gulf of California in the south into the southernmost San Andreas fault system to the north.

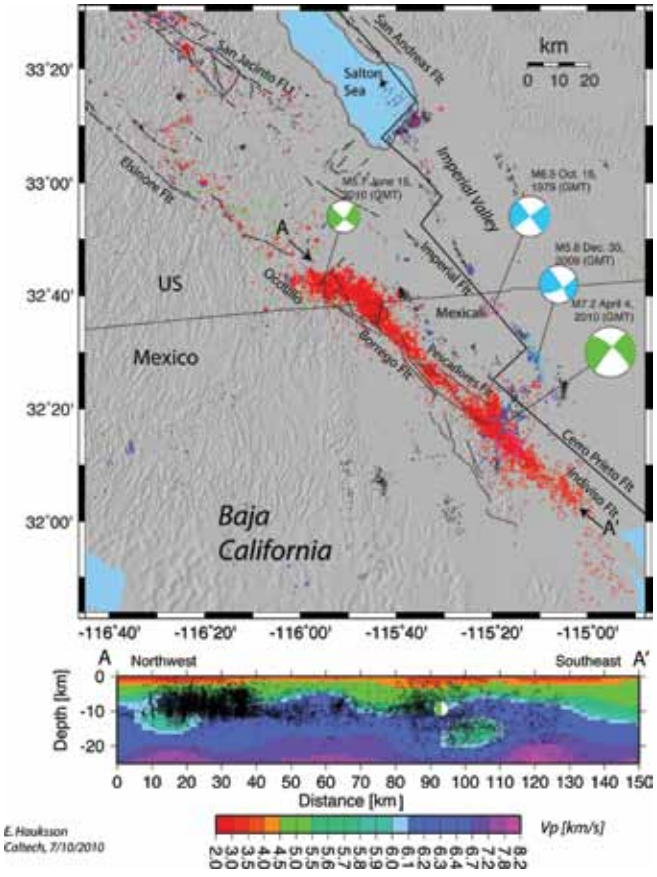

Map of the relocated hypocenters of foreshocks, mainshock, and aftershocks and 2009 background seismicity. The mainshock epicenter is indicated by a star. Foreshocks are shown as blue open circles beneath the mainshock star. The locations of the Vp cross section are indicated by the A-A' (includes focal mechanism of mainshock).

References

Hauksson, E., J. Stock, K. Hutton, W. Yang, A. Vidal, and H. Kanamori, The 2010 Mw7.2 El Mayor-Cucapah Earthquake Sequence, Baja California, Mexico and Southernmost California, USA: Active Seismotectonics Along the Mexican Pacific Margin, Submitted to *Pure Appl. Geophys.* Topical Issue: Geodynamics of the Mexican Pacific Margin, 10 July 2010

Acknowledgements: This research was supported by the USGS, SCEC, and CICESE.

Along-strike Variations in Shallow Earthquake Distribution and Source Parameters along the Kurile-Kamchatka Arc

Susan L. Bilek *(Earth and Environ. Science Dept., New Mexico Tech),* **Heather R. DeShon** *(CERI, University of Memphis),* **E. Robert Engdahl** *(Dept. of Physics, Univ. of Colorado)*

Observations in the last decade suggest a spectrum of slip durations for subduction zone earthquakes arising from rupture velocities that range from typical ~3 km/s, to 1 km/s for tsunami earthquakes, and even slower for other slip events. In order to understand conditions required to produce these slow rupture velocities, it is useful to clearly define areas where slow earthquakes occur. Our project addresses this goal by a) determining source parameters for large catalogs of subduction zone earthquakes, with an initial focus in expanding catalogs near documented tsunami earthquakes, and b) improving locations of these earthquakes to define regions of the interface that produce slow slip events through a new methodology that improves on the relocation technique of Engdahl, van der Hilst, and Buland (EHB). We show here results for 119 thrust mechanism earthquakes near the plate interface in the Kurile-Kamchatka subduction zone, an area with 2 documented tsunami events in 1963 and 1975 and afterslip following large coseismic slip. We determine a variety of earthquake source parameters using IRIS waveform data in multi-station body wave deconvolution methods and finite fault waveform inversion. Using the revised locations and their moment-normalized source durations, we find patches of events with long rupture durations around the 1963 tsunami event, along central Kuriles, and in southern Kamchatka, south of observed afterslip in 1997 (Figure 1).

References

Bilek, S.L., H.R. DeShon, and E.R. Engdahl, 2009, Along-Strike Variations in Shallow Earthquake Distribution and Source Parameters Along the Kurile-Kamchatka Arc, EOS Trans AGU, 90(52), Fall Meet. Suppl., Abstract T23B-1908

Acknowledgements: We gratefully acknowledge NSF-OCE support for this project (OCE-0840908 to SLB, OCE-0841022 to HRD, and OCE-0841040 to ERE.

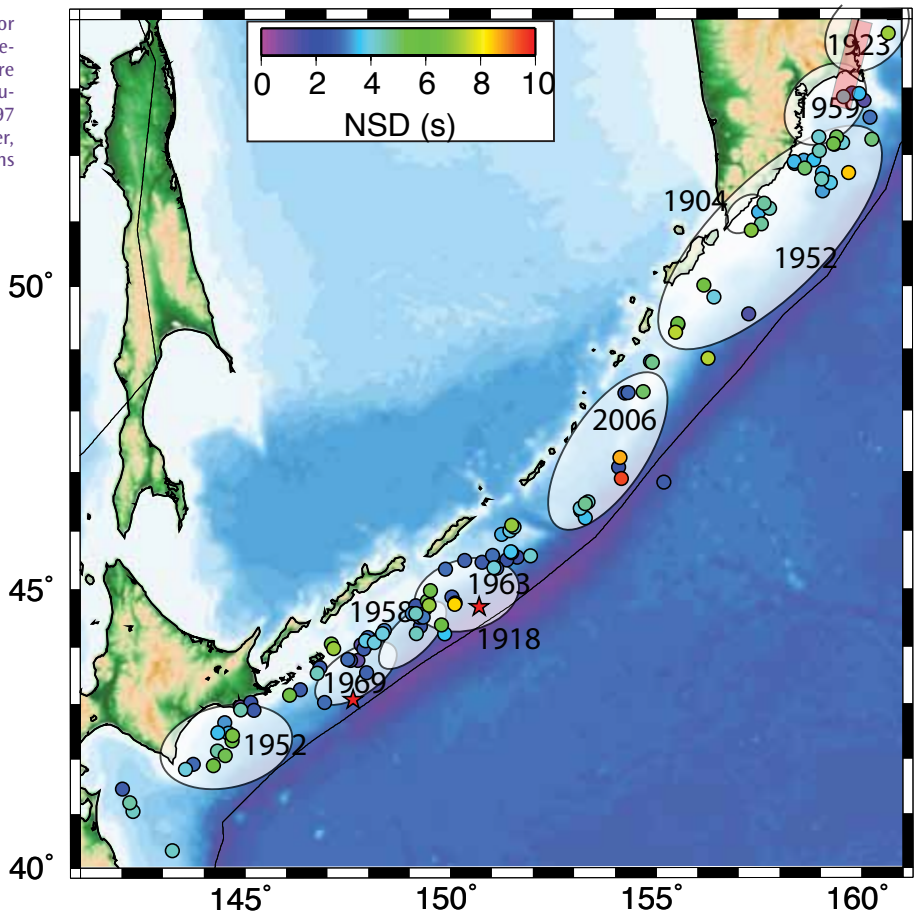

Moment normalized rupture duration (NSD) for earthquakes with revised locations along the Kurile-Kamchatka subduction zone. Our results suggest more recent earthquakes that occurred near the 1963 tsunami earthquake (red star) and south of the 1997 afterslip (red rectangle) have long duration character, suggesting the possibility of similar fault conditions leading to both slip processes.

Effects of Kinematic Constraints on Teleseismic Finite-Source Rupture Inversions: Great Peruvian Earthquakes of 23 June 2001 and 15 August 2007

Thorne Lay *(Univ. California, Santa Cruz),* **Charles J. Ammon** *(The Pennsylvania State University),* **Alexander R. Hutko** *(US Geological Survey),* **Hiroo Kanamori** *(California Institute of Technology)*

The rupture processes of two great under-thrusting earthquakes along the coast of Peru in 2001 and 2007 involve slip distributions that are distinctive from the predominantly unilateral or bilateral rupture expansion of many great events. Commonly used finite-source rupture model inversion parameterizations, with specified rupture velocity and/or short duration of slip at each grid point, applied to the seismic recordings for these two events lead to incorrect slip-distributions or inaccurate estimation of rupture velocities as a result of intrinsic kinematic constraints imposed on the model slip distributions. Guided by large aperture array back-projections of teleseismic broadband P-wave signals that image slip locations without imposing a priori kinematic constraints on the rupture process, we exploit the availability of large global broadband body and surface wave data sets to consider the effects of varying the kinematic constraints in teleseismic finite-source waveform inversions. By allowing longer than usual rupture durations at each point on the fault using a flexible subfault source time function parameterization, we find that the anomalous attributes of the 2001 and 2007 Peru earthquake ruptures are readily recognized and accounted for by compound rupture models. The great 23 June 2001 (Mw = 8.4) earthquake involved an initial modest-size event that appears to have triggered a much larger secondary event about 120 km away that developed an overall slip distribution with significant slip located back along the megathrust in the vicinity of the initial rupture. The great 15 August 2007 (Mw = 8.0) earthquake was also a composite event, with a modest size initial rupture followed by a 60 sec delayed larger rupture that initiated ~50-60 km away and spread up-dip and bilaterally. When back-projections indicate greater rupture complexity than captured in simple slip-pulse-type rupture model, one should allow for possible long-subfault-slip-duration or composite triggered sequences, and not overly constrain the earthquake slip distribution.

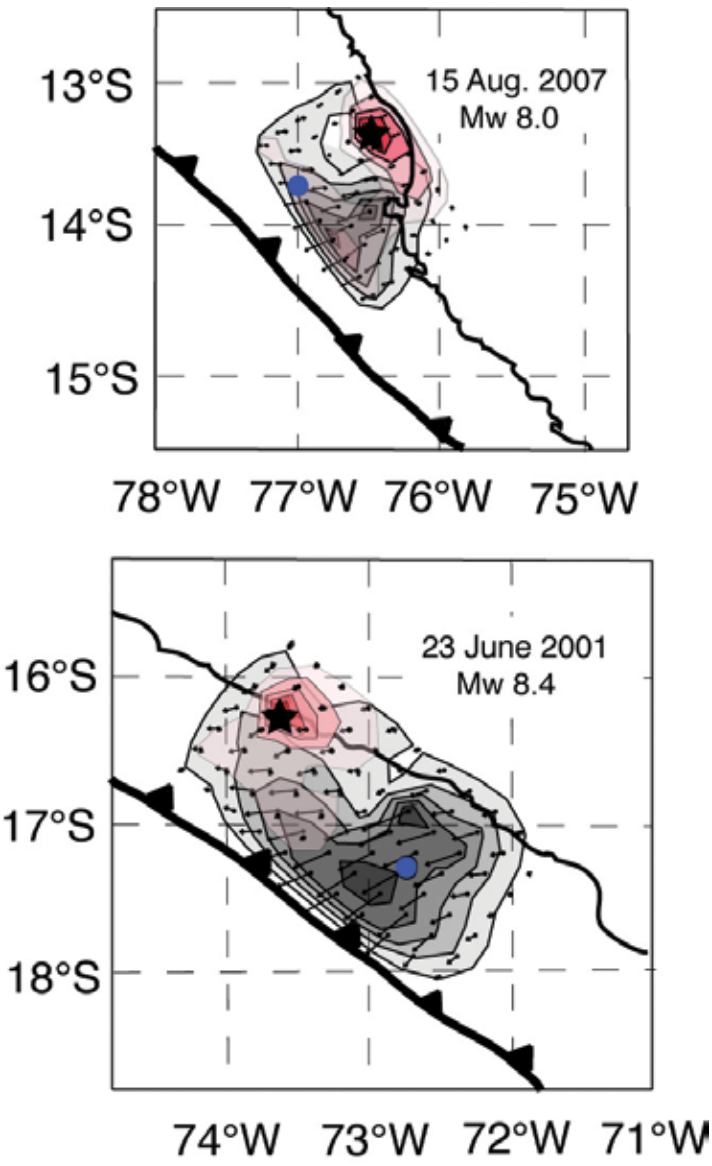

Maps showing the slip distribution for the preferred doublet event models for the 2007 (top) and 2001 (bottom) Peru earthquakes. The slip region for the first event in each pair is indicated by the orange tones. The stars indicate the USGS epicenters and the blue circles indicate the CMT centroid.

Acknowledgements: Supported by NSF grants EAR0453884 and EAR0635570 (TL) and USGS Award Number 05HQGR0174 (CJA).

The 2006-2007 Kuril Islands Great Earthquake Sequence

Thorne Lay *(Department of Earth and Planetary Sciences, Univ. California Santa Cruz),* **Hiroo Kanamori** *(Seismological Laboratory, California Institute of Technology),* **Charles J. Ammon** *(Department of Geosciences, The Pennsylvania State University),* **Alexander R. Hutko** *(U.S. Geological Survey),* **Kevin Furlong** *(Department of Geosciences, The Pennsylvania State University),* **Luis Rivera** *(Institut de Physique du Globe de Strasbourg)*

The southwestern half of a ~500-km-long seismic gap in the central Kuril Island arc subduction zone experienced two great earthquakes with extensive pre-shock and aftershock sequences in late 2006 to early 2007. The nature of seismic coupling in the gap had been uncertain due to the limited historical record of prior large events and the presence of distinctive upper plate, trench and outer-rise structures relative to adjacent regions along the arc that have experienced repeated great interplate earthquakes in the last few centuries. The intraplate region seaward of the seismic gap had several shallow compressional events during the preceding decades (notably an Ms 7.2 event on 16 March 1963), leading to speculation that the interplate fault was seismically coupled. This issue was partly resolved by failure of the shallow portion of the interplate megathrust in an Mw = 8.3 thrust event on 15 November 2006. This event ruptured ~250 km along the seismic gap, just northeast of the great 1963 Kuril Island (Mw = 8.5) earthquake rupture zone. Within minutes of the thrust event, intense earthquake activity commenced beneath the outer wall of the trench seaward of the interplate rupture, with the larger events having normal-faulting mechanisms. An unusual double band of interplate and intraplate aftershocks developed. On 13 January 2007, an Mw = 8.1 extensional earthquake ruptured within the Pacific plate beneath the seaward edge of the Kuril trench. This event is the third largest normal-faulting earthquake seaward of a subduction zone on record, and its rupture zone extended to at least 33 km depth and paralleled most of the length of the 2006 rupture. The great event aftershock sequences were dominated by thrust faulting for the 2006 rupture zone, and normal faulting for the 2007 rupture zone. A large intraplate compressional event occurred on 15 January 2009 (Mw = 7.4) near 45 km depth, below the rupture zone of the 2007 event and in the vicinity of the 16 March 1963 compressional event. The fault geometry, rupture process and slip distributions of the two great events are estimated using very broadband teleseismic body and surface wave observations. This great earthquake doublet demonstrates the heightened seismic hazard posed by induced intraplate faulting following large interplate thrust events. Future seismic failure of the northeastern region that has also experienced compressional activity seaward of the megathrust warrants particular attention.

References

Lay, T., H. Kanamori, C. J. Ammon, A. R. Hutko, K. Furlong, and L. Rivera (2009). The 2006-2007 Kuril Islands great earthquake sequence, *J. Geophys. Res., 114*, B113208, doi:10.1029/2008JB006280.

Acknowledgements: Supported by NSF grants EAR0453884 and EAR0635570 (TL) and USGS Award Number 05HQGR0174 (CJA).

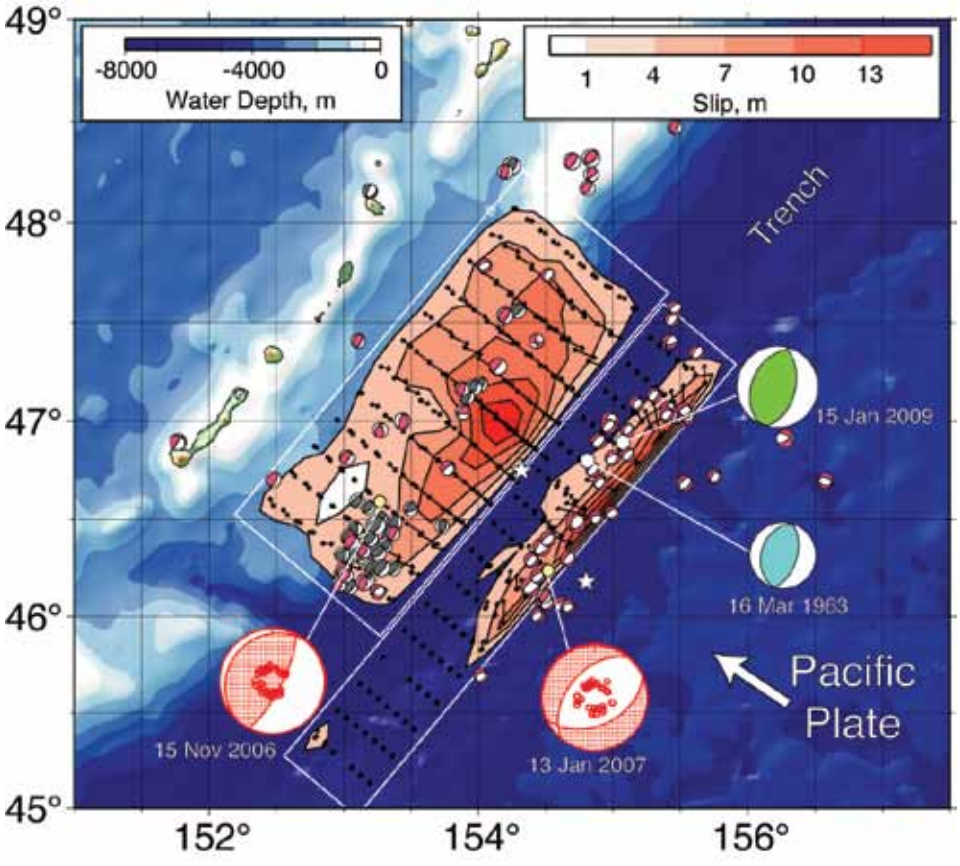

Surface map projection of coseismic slip for the 15 November 2006 (average slip 7.0 m) and the northwest dipping plane for 13 January 2007 (average slip 6.7 m at depths less than 25 km) events (NEIC epicenters: yellow circles, CMT centroid epicenters: stars).

Imaging of the Source Properties of the February 27, 2010, Maule, Chile Earthquake Using Data from the Transportable Array

Eric Kiser *(Harvard University),* **Miaki Ishii** *(Harvard University)*

The availability of high-quality data from a large, dense network of seismic stations achieved by the Transportable Array component of the USArray project has proven fruitful in studies of the subsurface structure. These data also provide vital information for imaging some of the rupture properties of giant earthquakes. The coherent arrivals throughout the array, combined with time-reversal to potential source locations, converts rich information of the waveform of a particular seismic phase to rupture propagation and relative energy release. This back-projection approach requires minimal a priori knowledge of the event, and with near real-time data, such as those from the Transportable Array, the analysis can be performed within the time window relevant for hazard mitigation, especially for tsunami assessment. The figure below shows an example of the application of the technique to the Maule, Chile earthquake that occurred on February 27, 2010 (Mw8.8). The Transportable Array was at a teleseismic distance for an effective P-wave back-projection. The large size of the array provided the necessary range in distance and azimuth for high resolution of the rupture process, and some details of the event are imaged with little artifacts. The rupture propagates primarily to the north from the epicentre for a length of 360 km and lasts about 120 seconds, corresponding to a rupture velocity of about 3.0 km/s. There is also a lower amplitude (relative to northern rupture) signal imaged to the south of the epicentre which reaches its maximum level at about 80 seconds after the event initiation. The images suggest a bilateral nature of the earthquake, and that the potential slip distribution is far from uniform, with main energy release located north of the epicentre occurring in the later part of the 120-second duration.

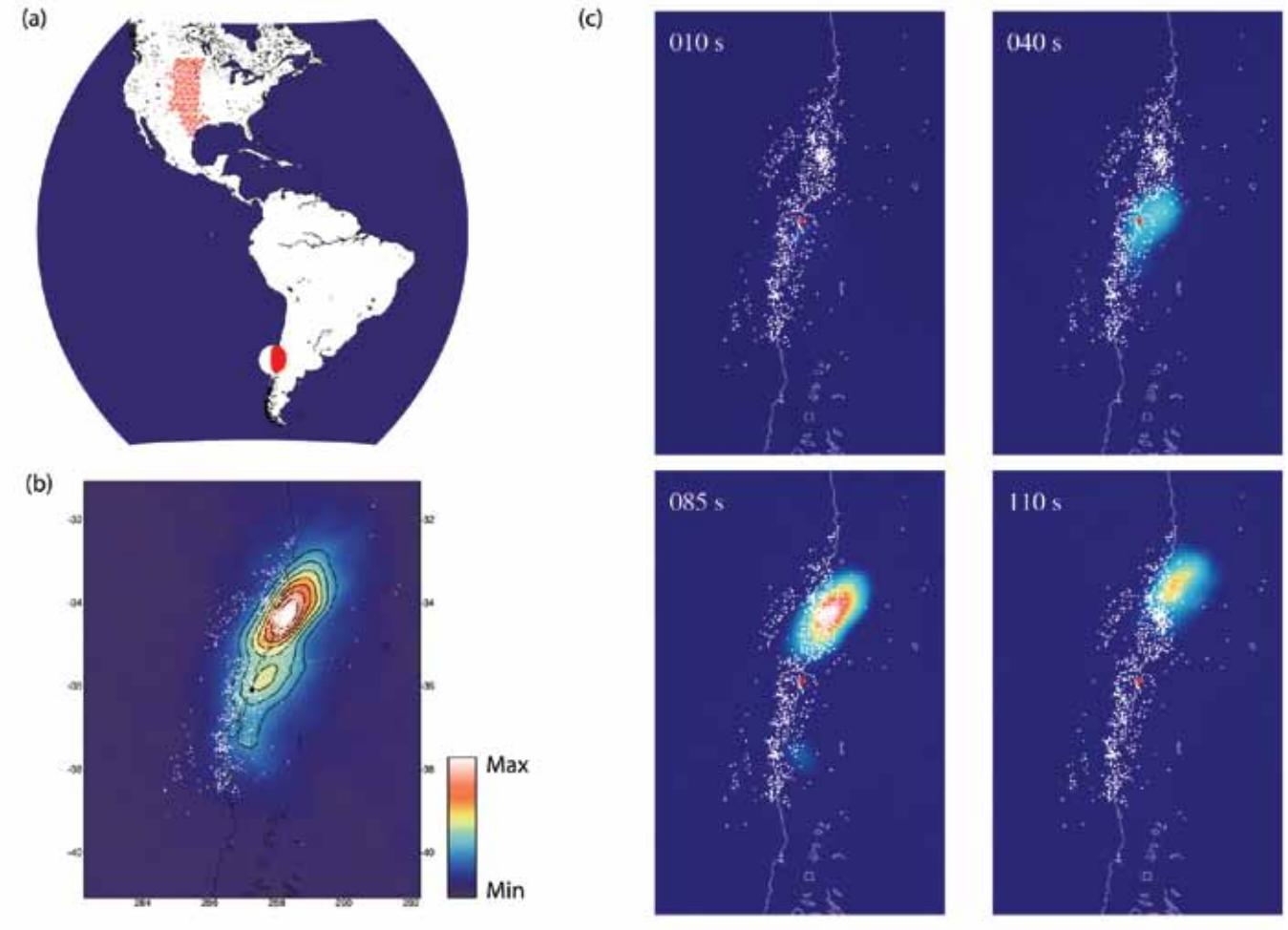

Back-projection results from the February 27, 2010, Mw8.8, Maule, Chile earthquake. (a) The distribution of TA stations (red triangles). (b) Relative energy release of the entire earthquake. The white dots are aftershocks. (c) Relative energy release at different times of the rupture.

Using MEMS Sensors and Distributed Sensing For a Rapid Array Mobilization Program (RAMP) Following the M8.8 Maule, Chile Earthquake

Jesse F. Lawrence *(Stanford University),* **Elizabeth S. Cochran** *(University of California, Riverside)*

The Quake-Catcher Network (QCN) exploits recent advances in sensing technologies and distributed sensing techniques. Micro-Electro-Mechanical Systems (MEMS) triaxial accelerometers are very low cost and interface to any desktop computer via USB cable enabling dense strong motion observations. Shake table tests show the MEMS accelerometers record high-fidelity seismic data and provide linear phase and amplitude response over a wide frequency range. Volunteer sensing using distributed computing techniques provides a mechanism to expand strong-motion seismology with minimal infrastructure costs, while promoting community participation in science. QCN has approximately 2000 participants worldwide that collect seismic data using a variety of MEMS sensors internal and external to computers. Distributed sensing allows for rapid transfer of metadata from participating stations, including data used to rapidly determine the magnitude and location of an earthquake. Trigger metadata are received with average data latencies between 3-7 seconds; the larger data latencies are correlated with greater server-station distances. Trigger times, wave amplitude, and station information are currently uploaded to the server for each trigger.

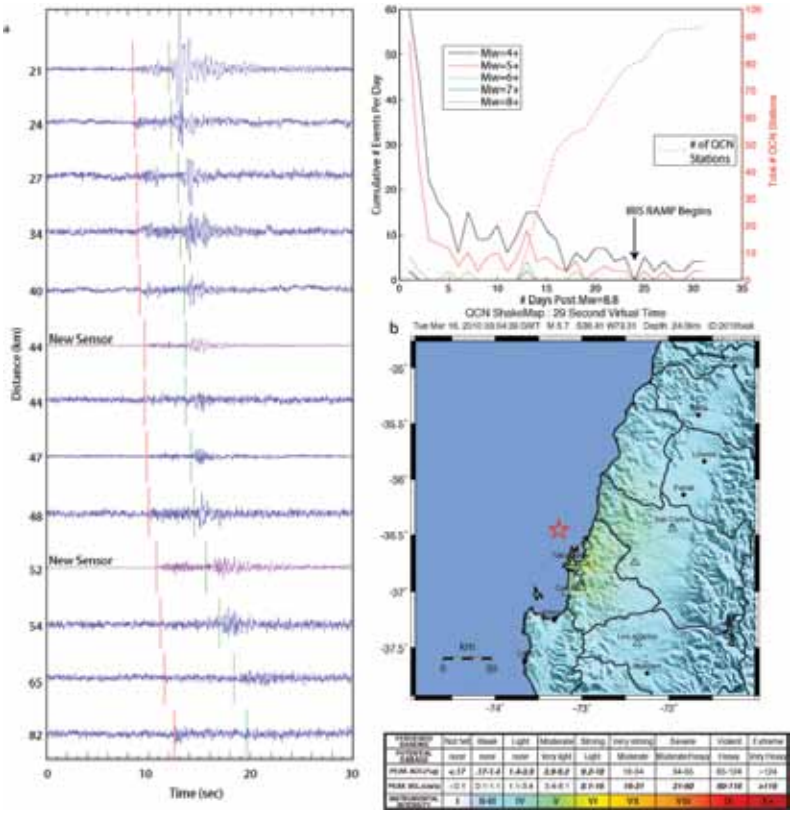

Figure 1: Left: Accelerograms from a M5.1 aftershock of the 27 February 2010 M8.8 Maule, Chile earthquake recorded on QCN stations in the Bio Bio region. Top right: Number of earthquakes and cumulative number of QCN stations installed versus days after the mainshock. Bottom right: Shake map produced using QCN records to locate and estimate the magnitude of the aftershock.

Following the 27 February 2010 M8.8 earthquake in Maule, Chile we initiated a QCN Rapid Aftershock Mobilization Program (RAMP) and installed 100 USB sensors to record aftershocks. The USB accelerators were deployed mainly in regions directly affected by the mainshock and were densely concentrated around ConcepciÃ³n. Using this data, we refined our triggering and event detection algorithms and tested, retrospectively, whether the network can rapidly and accurately identify the location and magnitude of the moderate to large aftershocks (M>4). Figure 1 illustrates QCNâ€™s ability to grow rapidly, record large aftershocks, and produce useful results such as earthquake locations and ShakeMaps. These results suggest that MEMS sensors installed in homes, schools, and offices provide a way to dramatically increase the density of strong motion observations for use in earthquake early warning. With QCNâ€™s low-latency real-time data collection strategy, future investigations with next-generation sensors will yield data pertinent to ground shaking, earthquake location, and rupture mechanics in near real-time.

References

Cochran, E.S., J.F. Lawrence, C. Christensen, and R. Jakka, The Quake-Catcher Network: Citizen science expanding seismic horizons, *Seismol. Res. Lett., 80*, 26-30,2009.

Cochran E., Lawrence J., Christensen C., Chung A., A novel strong-motion seismic network for community participation in earthquake monitoring, IEEE Inst & Meas, 12, 6, 8-15, 2009.

Acknowledgements: This work was preformed with support from NSF-EAR1035919, NSF-GEO0753435, and an IRIS subaward. We thank the thousands of volunteer participants who make the Quake-Catcher Network possible.

Teleseismic Inversion for Rupture Process of the 27 February 2010 Chile (Mw 8.8) Earthquake

Thorne Lay *(University of California Santa Cruz),* **Charles J. Ammon** *(The Pennsylvania State University),* **Hiroo Kanamori** *(California Institute of Technology),* **Keith D. Koper** *(Saint Louis University),* **Oner Sufri** *(Saint Louis University),* **Alexander R. Hutko** *(Incorporated Research Institutions for Seismology)*

The 27 February 2010 Chile (Mw 8.8) earthquake is the fifth largest earthquake to strike during the age of seismological instrumentation. The faulting geometry, slip distribution, seismic moment, and moment-rate function are estimated from broadband teleseismic P, SH, and Rayleigh wave signals obtained from Global Seismic Network and FDSN stations. We explore some of the trade-offs in the rupture-process estimation due to model parameterizations, limited teleseismic sampling of seismic phase velocities, and uncertainty in fault geometry. The average slip over the ~81,500 km2 rupture area is about 5 m, with slip concentrations down-dip, up-dip and southwest, and up-dip and north of the hypocenter. Relatively little slip occurred up-dip/offshore of the hypocenter. The average rupture velocity is ~2.0-2.5 km/s.

References

Lay, T., C. J. Ammon, H. Kanamori, K. D. Koper, O. Sufri, and A. R. Hutko (2010). Teleseismic inversion for rupture process of the 27 February 2010 Chile (Mw 8.8) earthquake, *Geophys. Res. Lett.*, in press.

Acknowledgements: This work was supported by NSF grant EAR0635570 and USGS Award Number 05HQGR0174.

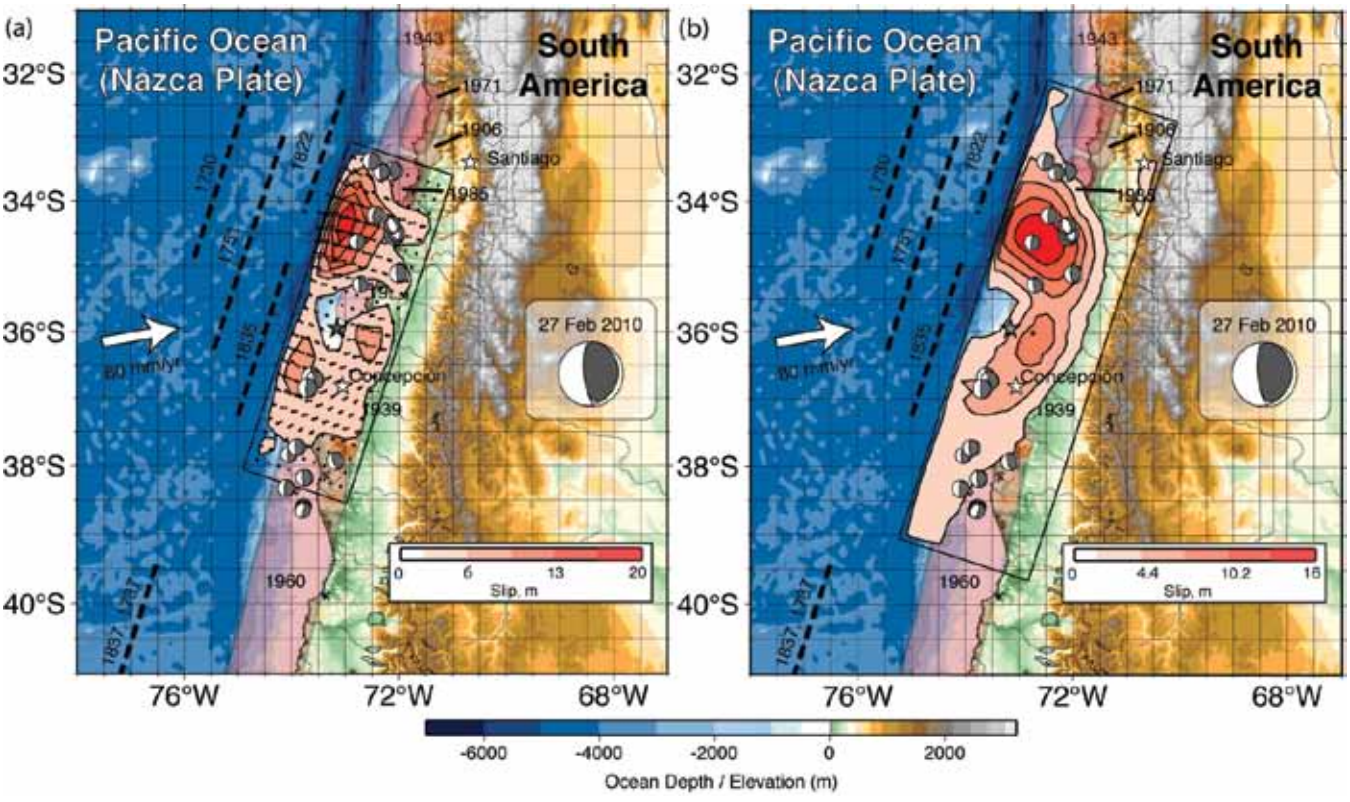

Maps of the finite-fault slip distributions obtained by inversion of (a) teleseismic P and SH waves and (b) teleseismic P waves, SH waves, and R1 STFs. The background map is the same as Figure 1, with the GCMT focal mechanism shown in the insets. The P and SH inversion allows for variable rake at each grid position, with the slip vectors for the hanging wall being shown, and their relative amplitudes contoured. The rupture velocity used for the P and SH inversion was 2.5 km/s and it was 2.25 km/s for the P, SH and R1 STF inversion.

The 2009 Samoa-Tonga Great Earthquake Triggered Doublet

Thorne Lay *(University of California Santa Cruz),* **Charles J. Ammon** *(The Pennsylvania State University),* **Hiroo Kanamori** *(California Institute of Technology),* **Luis Rivera** *(Institut de Physique du Globe de Strasbourg),* **Keith D. Koper** *(Saint Louis University),* **Alexander R. Hutko** *(U.S. Geological Survey, NEIC)*

Great earthquakes (having seismic magnitudes ≥ 8) usually involve abrupt sliding of rock masses at a boundary between tectonic plates. Such interplate ruptures produce dynamic and static stress changes that can activate nearby intraplate aftershocks, as is commonly observed in the trench-slope region seaward of a great subduction zone thrust event1-4. The earthquake sequence addressed here involves a rare instance in which a great trench-slope intraplate earthquake triggered extensive interplate faulting, reversing the typical pattern and broadly expanding the seismic and tsunami hazard. On 29 September 2009, within two minutes of the initiation of a moment magnitude 8.1 normal faulting event in the outer trench-slope at the northern end of the Tonga subduction zone, two major interplate underthrusting subevents (moment magnitudes = 7.8, 7.8), with total moment equal to a second great moment magnitude 8.0 earthquake, ruptured the nearby subduction zone megathrust. The collective faulting produced tsunami waves with localized regions of ~12 m run-up that claimed 192 lives in Samoa, American Samoa and Tonga. Overlap of the seismic signals obscured the fact that distinct faults separated by more than 50 km had ruptured with different geometries, with the triggered thrust faulting only being revealed by detailed seismic wave analyses. Extensive interplate and intraplate aftershock activity was activated over a large region of the northern Tonga subduction zone.

References

Lay, T., C. J. Ammon, H. Kanamori, L. Rivera, K. Koper, and A. R. Hutko (2010). The 29 September 2009 Great Samoa earthquake, *Nature*, in press.

Acknowledgements: This work was supported by NSF grant EAR0635570 and USGS Award Number 05HQGR0174.

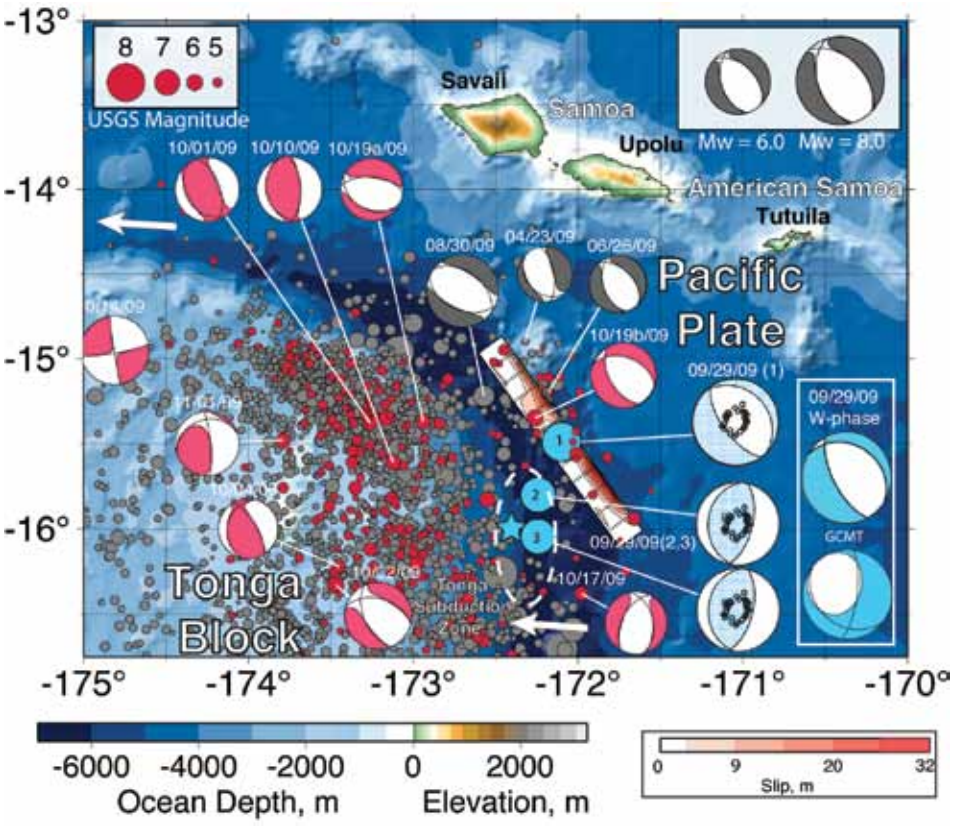

The great (Mw 8.1) 29 September 2009 Samoa earthquake ruptured an outer trench-slope normal fault (#1 blue mechanism and numbered blue circle) with the indicated fault plane and slip distribution and co-seismically triggered two initially unrecognized major (Mw 7.8, 7.8) thrust fault subevents (#2,3 blue mechanisms and circles) on the megathrust. The star indicates the centroid location estimated for event 3 from regional surface wave modeling. Gray circles indicate the locations and magnitudes of shallow (depth < 100 km) earthquakes from 01 January 1973 up to the 2009 great earthquake sequence, including three moderate-size (MW = 5 to 6.6) trench-wall/outer-rise extensional events between April and August 2009 for which global centroid-moment tensor17 solutions (gray coloring) are indicated (the Mw scaling of all GCMT solutions is indicated in the top right inset). Red circles indicate earthquake epicenters and magnitudes (top left inset gives the scaling) for the mainshock and aftershocks.

The Global Aftershocks of the 2004 Sumatra-Andaman Earthquake

Emily E. Brodsky *(UC Santa Cruz),* **Thorne Lay** *(UC Santa Cruz),* **Nicholas van der Elst** *(UC Santa Cruz)*

The 26 December 2004 Sumatra-Andaman Mw 9.15 earthquake was the largest earthquake to occur since the 1964 Alaska earthquake. In the subsequent 5.5 years, 9 great shallow earthquakes (M>= 8) have struck around the world giving a rate of 1.64 per year, whereas the prior century averaged 0.63 ± 0.34 per year.

Dynamic wave triggering effects combined with highly productive seismicity cascades could explain the rate increase. Seismic waves can trigger earthquakes to great distances. The resultant seismicity rate increase is observed to be proportional to the peak amplitude of the waves for a specific region (Fig. 1a). Over a broad swath of the globe, the 2004 Sumatra-Andaman earthquake generated ground velocities of over 0.01 cm/s (Fig. 1b), which are sufficient to trigger sizable rate changes (greater than a few percent) in susceptible regions (Fig 1a).

Once propagating seismic waves trigger a region, the remote sequences decay following Omori's Law [*Brodsky, 2006*]. Most of the triggered earthquakes are small, but each earthquake spawns further earthquakes, which occasionally can be larger than the initial events. These large events can in turn trigger other remote sequences.

References

Brodsky, E.E., *Geophys. Res. Lett., 33*, L15313, doi:10.1029/2006BL026605, (2006).

Jiang, C. and Z. Wu, H. Ma, L. Zhou, *Acta Seismologica Sinica, 3*, 189-200, (2009).

Van der Elst, N. J. and E. E. Brodsky, *J. Geophys. Res.*, doi:10.1029/2009JB006681, in press.

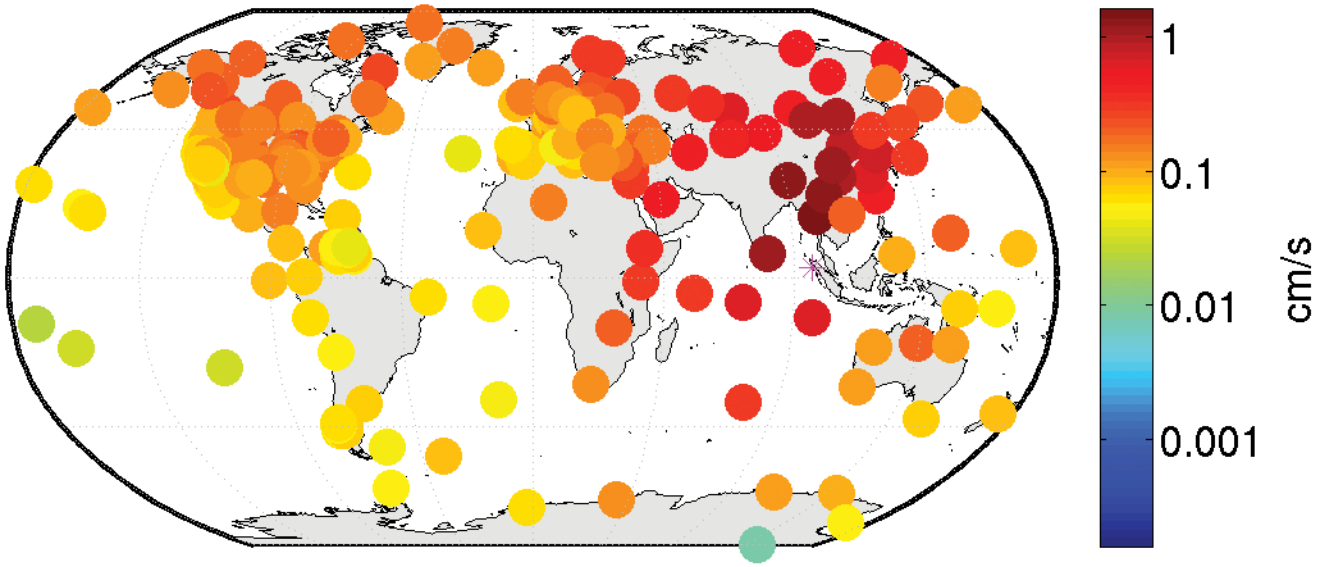

(a) Fractional earthquake rate increase as a function of peak dynamic strain from seismic waves [Van der Elst and Brodsky, in press]. The empirical relationship indicates that seismicity rates should increase significantly if ground shaking exceeds 0.01 cm/s. (b) Global map of recorded peak vertical ground velocities for the 2004 Sumatra-Andaman earthquake (epicenter at magenta star) indicating the widespread occurrence of strong shaking.

Temporal Changes of Surface Wave Velocity Associated with Major Sumatra Earthquakes from Ambient Noise Correlation

Zhen J. Xu *(Department of Geology, University of Illinois at Urbana-Champaign),* **Xiaodong Song** *(Department of Geology, University of Illinois at Urbana-Champaign)*

Detecting temporal changes of medium associated with major earthquakes has major implications for understanding earthquake genesis. The recent development of passive imaging through cross correlation of diffusive wavefield provides great opportunity in monitoring such changes because of the complete repeatability of the data processing procedures. We acquired 54 months of long period continuous data from Jan. 2004 to Jun. 2008 for stations in the Southeast Asia region from IRIS DMC. The stations are operated by GSN, Malaysia, Japan, and China. We retrieved empirical Green's functions (EGFs) of surface wave between stations through cross correlation of continuous ambient noise data [*Bensen et al., 2007*]. We compared EGFs at different time periods before and after earthquake with a reference EGF. We observed clear temporal changes up to 1.44 s in Rayleigh wave after three major earthquakes in Sumatra region in Dec. 2004, Mar. 2005, and Sep. 2007 and a plausible precursor signal before Dec. 2004 event. However such changes were absent in Love waves. The temporal changes in Rayleigh wave appeared over a broad area near the source for a few months after the earthquakes and are frequency dependent. The observations are interpreted as stress changes and subsequent relaxation in upper-mid crust in the immediate vicinity of the rupture and the broad area near the fault zone.

References

Bensen, G. D., et al. (2007) Processing seismic ambient noise data to obtain reliable broad-band surface wave dispersion measurements. *Geophys. J. Int. 169*: 1239-1260

Acknowledgements: All data were downloaded from IRIS DMC. This work was supported by NSF (EAR8038188) and AFRL (FA8718-07-C-0006)

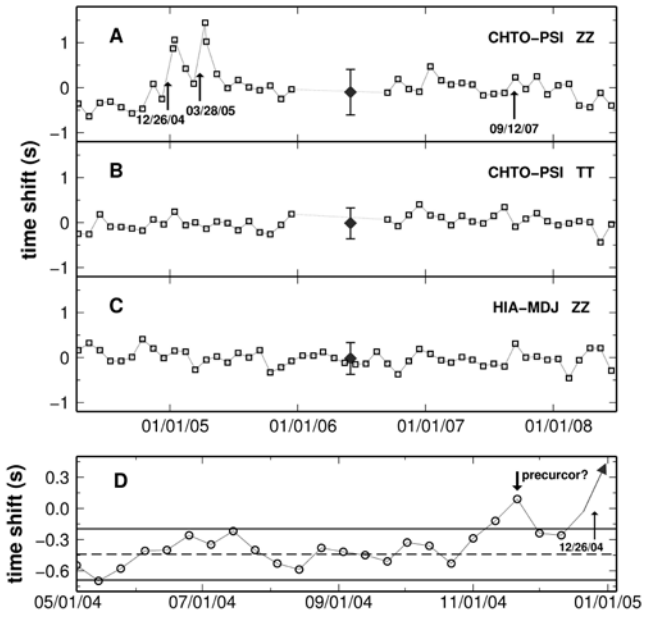

Time shifts of various station pairs, relative to reference stack of all time periods. (A-C) Rayleigh wave for CHTO-PSI from vertical (Z) component correlation (A), Love wave for CHTO-PSI from tangential (T) component correlation (B), and a stable reference pair HIA-MDJ outside Sumatra region in northeast China (C). (D) Enlarged view of time shifts of CHTO-PSI Rayleigh wave before Dec. 2004 event.

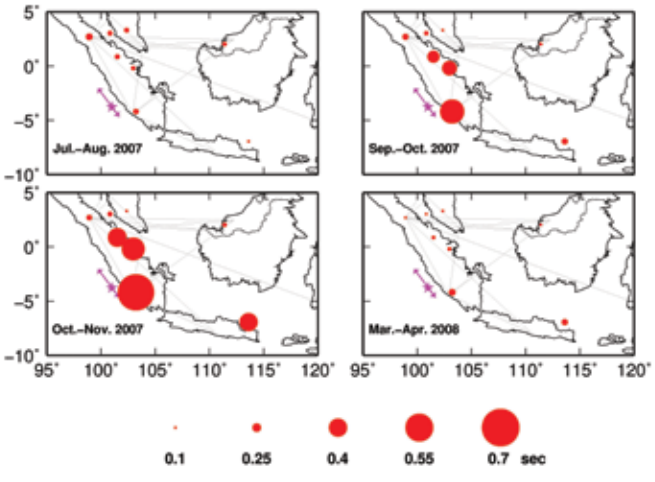

Snapshots of time-shift maps before (upper left), during (Upper Right), and after (Lower, left and Right) the 2007 event.

The 17 July 2006 Java Tsunami Earthquake (Mw = 7.8)

Charles J. Ammon *(Department of Geosciences, The Pennsylvania State University),* **Hiroo Kanamori** *(Seismological Laboratory, California Institute of Technology),* **Thorne Lay** *(Department of Earth and Planetary Sciences, Univ. California Santa Cruz),* **Aaron A. Velasco** *(Department of Geological Sciences, Univ. Texas El Paso)*

The 17 July 2006 Java earthquake involved thrust faulting in the Java trench and excited a deadly tsunami (~ 5-8 m) that inundated the southern coast of Java. The earthquake's size estimates vary significantly with seismic wave period: very long-period signals (300-500+ s) indicate a seismic moment of 6.7 x 10**20 Nm (Mw = 7.8), Ms (~20 s) = 7.2, mb (~1 s) = 6.2, while shaking intensities (3-10 Hz) were ≤ MMIV. The large tsunami relative to Ms characterizes this event as a tsunami earthquake. Like previous tsunami earthquakes, the Java event had an unusually low rupture speed of 1.0-1.5 km/s, and occurred near the up-dip edge of the subduction zone thrust fault. Most large aftershocks involved normal faulting. The rupture propagated ~200 km along the trench, with several pulses of shorter period seismic radiation superimposed on a smooth background rupture with an overall duration of ~185 s. The rupture process was analyzed using finite fault inversion of P, SH, and Rayleigh wave source time functions, with the excellent quality of the data providing good resolution of the rupture velocity (Ammon et al., 2006). This is the best recorded tsunami earthquake since the 1992 Nicaragua rupture, and the great expansion of broadband data since that time enables much more robust characterization of the anomalous source process.

References

Ammon, C. J., H. Kanamori, T. Lay, and A. A. Velasco (2006), The 17 July 2006 Java tsunami earthquake, *Geophys. Res. Lett.*, 233, L234308, doi:10.10239/2006GL028005.

Acknowledgements: The facilities of the IRIS Data Management System were used to access the data used in this study.

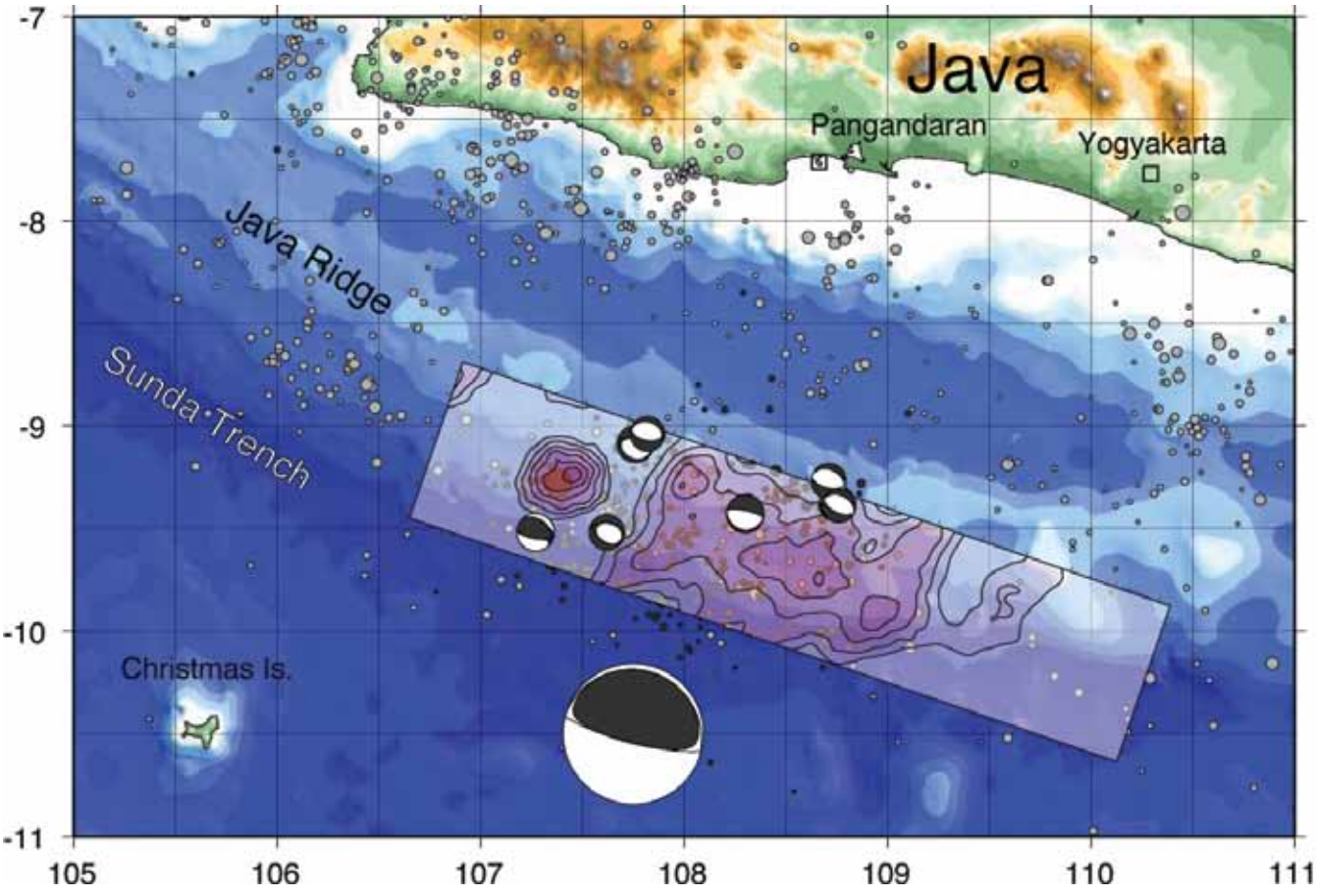

Map showing the Global CMT solutions for the 17 July 2006 Java tsunami earthquake and regional aftershocks and NEIC epicenters of mainshock (star), aftershocks (dark circles), and prior activity (gray circles).

Tsunami Early Warning Using Earthquake Rupture Duration and P-Wave Dominant-Period: The Importance of Length and Depth of Faulting

Anthony Lomax *(ALomax Scientific, Mouans-Sartoux, France),* **Alberto Michelini** *(Istituto Nazionale di Geofisica e Vulcanologia, Rome)*

After an earthquake, rapid, real-time assessment of hazards such as ground shaking and tsunami potential is important for early warning and emergency response. Tsunami potential depends on sea floor displacement, which is related to the length, L, width, W, mean slip, D, and depth, z, of earthquake rupture. Currently, the primary discriminant for tsunami potential is the centroid-moment tensor magnitude, MwCMT, representing the product LWD, and estimated through an indirect, inversion procedure. The obtained MwCMT and the implied LWD value vary with the depth of faulting, assumed earth model and other factors, and is only available 30 min or more after an earthquake. The use of more direct procedures for hazard assessment, when available, could avoid these problems and aid in effective early warning. Here we present a direct procedure for rapid assessment of earthquake tsunami potential using two, simple measures on P-wave seismograms – the dominant period on the velocity records, Td, and the likelihood that the high-frequency, apparent rupture-duration, T0, exceeds 50-55 sec. Td and T0 can be related to the critical parameters L, W, D and z. For a set of recent, large earthquakes, we show that the period-duration product TdT0 gives more information on tsunami impact, It, and size, At, than MwCMT and other currently used discriminants. All discriminants have difficulty in assessing the tsunami potential for oceanic strike-slip and back-arc, intraplate earthquake types. Our analysis and results suggest that tsunami potential is not directly related to the product LWD from the "seismic" faulting model, as is assumed with the use of the MwCMT discriminant. Instead, knowledge of rupture length, L, and depth, z, alone can constrain well the tsunami potential of an earthquake, with explicit determination of fault width, W, and slip, D, being of secondary importance. With available real-time seismogram data, rapid calculation of the direct, period-duration discriminant can be completed within 6-10 min after an earthquake occurs and thus can aid in effective and reliable tsunami early warning.

References

Lomax, A., and A. Michelini (2009), Tsunami early warning using earthquake rupture duration, *Geophys. Res. Lett., 36,* L09306.

This work Submitted to *Geophys. J. Int.,* 2 Apr 2010.

Acknowledgements: This work is supported by the 2007-2009 Dipartimento della Protezione Civile S3 project. The IRIS DMC (http://www.iris.edu) provided access to waveforms used in this study; we thank all those who install, operate and maintain seismic stations worldwide.

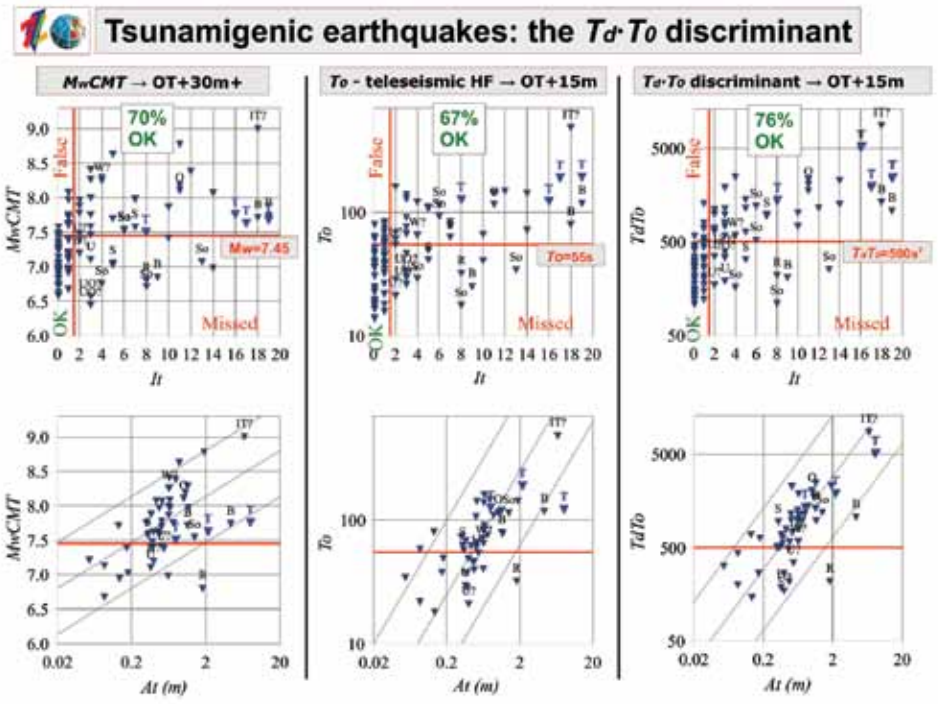

Comparison of centroid-moment tensor magnitude, M_w^{CMT}, (left column), apparent source duration, T_0, (centre column) and teleseismic, period-duration, T_dT_0, (right column) with tsunami importance, I_t, (upper row) and representative tsunami amplitude at 100km, A_t, (lower row). Vertical red lines show the target $I_t \geq 2$ threshold; horizontal red lines show the optimal cutoff values for the M_{wp}, M_w^{CMT}, T_0 and T_dT_0 discriminants; quadrants containing correctly identified tsunamigenic and non-tsunamigenic events are labelled "OK"; quadrants containing incorrectly identified events are labelled "Missed" and "False". The A_t and T_0 axes use logarithmic scaling. Diagonal lines show possible linear relationships between A_t and M_0 (lower left), T_0 (lower centre) and T_dT_0 (lower right). Event labels show earthquakes type for non interplate-thrust events with $I_t \geq 2$ (I–interplate-thrust; T–tsunami earthquake (blue); O–outer-rise intraplate; B–back-arc or upper-plate intraplate; So–strike-slip oceanic, S–strike-slip continental, R–reverse-faulting).

Seismic Cycles on Oceanic Transform Faults

Jeff McGuire *(WHOI),* **Margaret Boettcher** *(University of New Hampshire),* **John Collins** *(WHOI)*

The long-standing hypothesis that the timing of the largest earthquakes is primarily controlled by quasi-periodic seismic cycles, where stress builds up for an extended period of time and then is released suddenly in a large earthquake, has been difficult to verify due to the long repeat times (50-1000 years) of the largest earthquakes on most faults. By contrast, repeat times of the largest oceanic transform fault earthquakes are remarkably short and regular. Thermal processes appear to have a strong control on oceanic transform seismicity including the magnitude of the largest earthquake on a particular fault [Boettcher and Jordan, 2004]. Using datasets from the Global Seismic Network that span 20+ years of recording at the same sites, we determined that the largest earthquakes on warm EPR transform faults repeat every ~5 years on a relatively regular cycle [McGuire, 2008]. Moreover, the duration of the seismic cycle increases for colder faults according to a simple scaling relation [Boettcher and McGuire, 2009]. The quasi-periodic nature of oceanic transforms seismic cycles allowed us to successfully position an array of ocean bottom seismometers on the Gofar Transform Fault to capture a Mw 6.0 earthquake in 2008. Our successful experiment on the Gofar Fault has further demonstrated that oceanic transform faults have predictable seismic characteristics including relatively regular seismic cycles.

References

Boettcher, M. S., and T. H. Jordan (2004), Earthquake Scaling Relations for Mid-Ocean Ridge Transform Faults, *J. Geophys. Res.*, B12302, doi:1029/2004JB003110.

Boettcher, M. S., and J. J. McGuire (2009), Scaling relations for seismic cycles on mid-ocean ridge transform faults, *Geophys. Res. Lett., 36*, L21301, doi:21310.21029/22009GL040115.

McGuire, J. J. (2008), Seismic Cycles and Earthquake Predictability on East Pacific Rise Transform Faults, *Bull. Seismol. Soc. Amer., 98*, 1067-1084, doi: 1010.1785/0120070154.

Acknowledgements: We thank the Global Seismic Network program for collecting the datasets over the last 20+ years that were necessary for us to conduct this research.

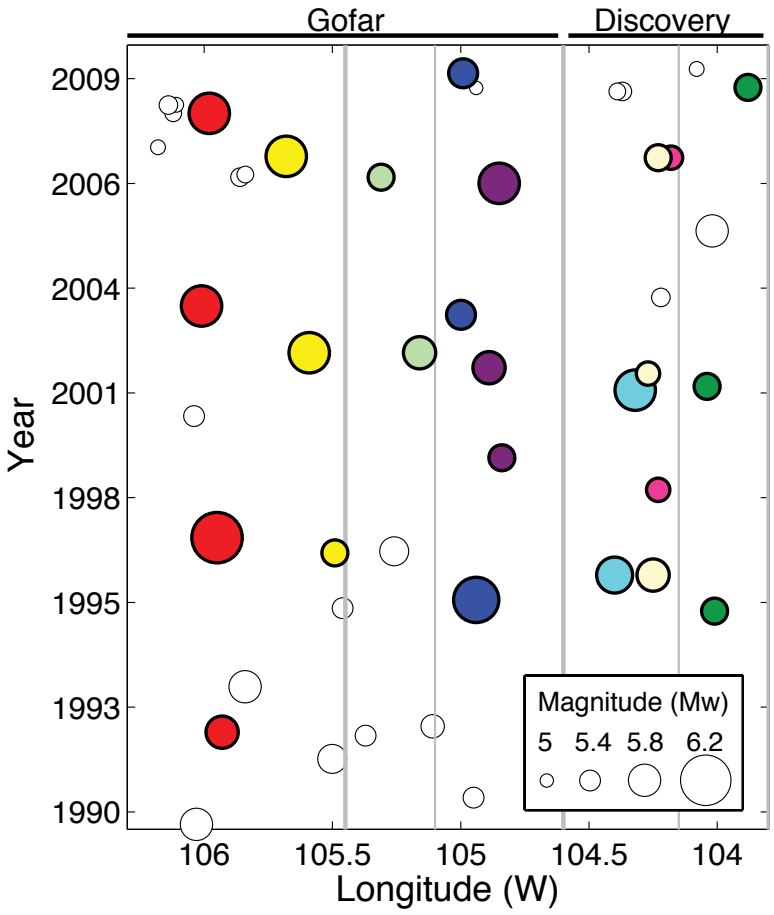

Figure 1. Updated after McGuire [2008]. Earthquakes in the Global CMT catalogs for the Gofar and Discovery transform faults for the time period from 1990–2010. Pairs of MW ≥ 5.5 mainshocks that have been determined to have overlapping rupture areas are shown with matching colors and are not at exactly the same longitude due to errors in the CMT location estimates. Major and minor spreading centers are shown by thick and thin gray lines, respectively.

Split Normal Modes and Beachfront Hotels

Seth Stein *(Northwestern University)*

On December 26, 2004 a giant earthquake beneath the Indonesian island of Sumatra generated a massive tsunami that crossed the Indian Ocean in a few hours, wreaking destruction along seacoasts and causing at least 250,000 deaths. Initial seismological studies suggested that only part of the 1200-km long fault zone had broken, so an even larger earthquake could be forthcoming. However, analysis of the splitting pattern of earth's longest period (> 20 minute) normal modes using IRIS broadband data showed that the entire fault zone had ruptured. This result explained the perplexing pattern of the tsunami damage. Combining these data with the motions of the plates involved measured by combining seafloor magnetic data and high-precision GPS then implied that such earthquakes should occur about 500 years apart, as later confirmed by paleotsunami studies. Hence contrary to initial fears, rebuilding the crucial tourist facilities at their previous locations made sense.

The December earthquake also give insight into the long-standing question of which trenches can have such giant earthquakes. The earthquake was much larger than expected from a previously proposed relation, based on the idea of seismic coupling, in which such earthquakes occur only when young lithosphere subducts rapidly. Moreover, a global reanalysis finds little support for this correlation. Hence it appears that much of the apparent differences between subduction zones, such as some trench segments but not others being prone Mw> 8.5 events and hence oceanwide tsunamis, may reflect the short earthquake history sampled. This possibility is supported by the variability in rupture mode at individual trench segments.

References

Stein, S., and E. A. Okal, Speed and size of the Sumatra earthquake, *Nature, 434*, 581-582, 2005.

Stein, S. and E. Okal, Ultralong period seismic study of the December 2004 Indian Ocean earthquake and implications for regional tectonics and the subduction process, B*ull. Seismol. Soc. Amer., 97*, S279-S295, 2007.

Stein, S. and E. Okal, Observations of ultralong period normal modes from the December 2004 Sumatra-Andaman earthquake, *Phys. Earth Planet. Int., 175* 53-62, 2009.

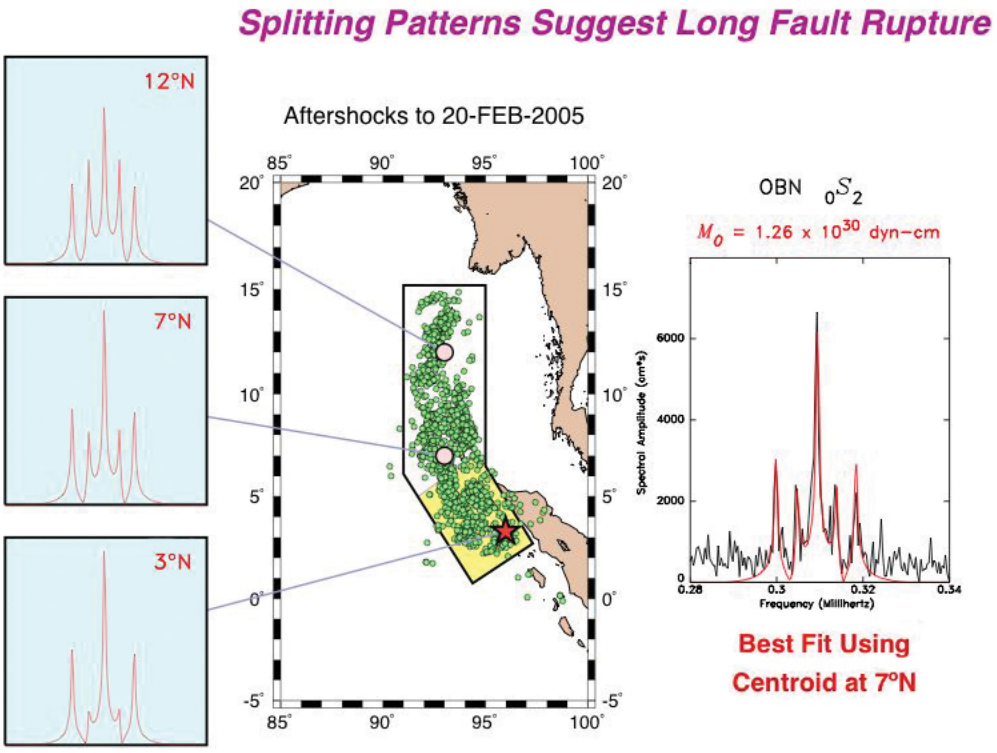

Split singlet pattern for 0S2 normal mode multiplet showing dependence on source latitude. Map at center illustrates the two possible models of source rupture: the short fault initially inferred from body wave inversion and the long fault suggested by the distributions of aftershocks (small circles). The diagrams at left show theoretical splitting patterns at Obninsk, Russia (OBN) for sources located at the original USGS epicenter (3°N; star), at 7°N, and towards the northern end of the long fault (12°N). The right panel shows that the best fit occurs for a centroid of moment release at 7°N, at the center of the aftershock zone but outside the rupture zone of the short fault model. (Stein and Okal, 2007)

Migration of Early Aftershocks Following the Mw6.0 2004 Parkfield Earthquake

Zhigang Peng *(Georgia Institute of Technology),* **Peng Zhao** *(Georgia Institute of Technology)*

A large shallow earthquake is immediately followed by numerous aftershocks with a significant portion missing in existing earthquake catalogs, mainly due to masking of the mainshock coda and overlapping arrivals [e.g., Peng et al., 2006]. Recovering these missing early aftershocks is important for understanding the physical mechanisms of earthquake triggering, and tracking post-seismic deformation around the mainshock rupture zone. We use waveforms of relocated events along the Parkfield section of the San Andreas Fault (SAF) as templates, and scan through continuous waveforms for 3 days around the 2004 Mw6.0 Parkfield earthquake to detect missing aftershocks [Peng and Zhao, 2009]. We identify 11 times more aftershocks than reported in the standard Northern California Seismic Network (NCSN) catalog. The newly detected aftershocks show clear migration in both along-strike and down-dip directions with logarithmic time since the mainshock, consistent with the numerical simulations on expansions of aftershocks caused by propagating afterslip. The cumulative number of early aftershocks increases linearly with postseismic deformation in the first 2 days, supporting the view that aftershocks are driven primarily by afterslip.

References

Peng, Z., J. E. Vidale, and H. Houston (2006), Anomalous early aftershock decay rates of the 2004 M6 Parkfield earthquake, *Geophys. Res. Lett.*, *33*, L17307, doi:10.1029/2006GL026744.

Peng, Z., and P. Zhao (2009), Migration of early aftershocks following the 2004 Parkfield earthquake, *Nature Geosci.*, 2, 877-881, doi:10.1038/ngeo697.

Acknowledgements: This work was supported by the USGS NEHRP program G09AP00114.

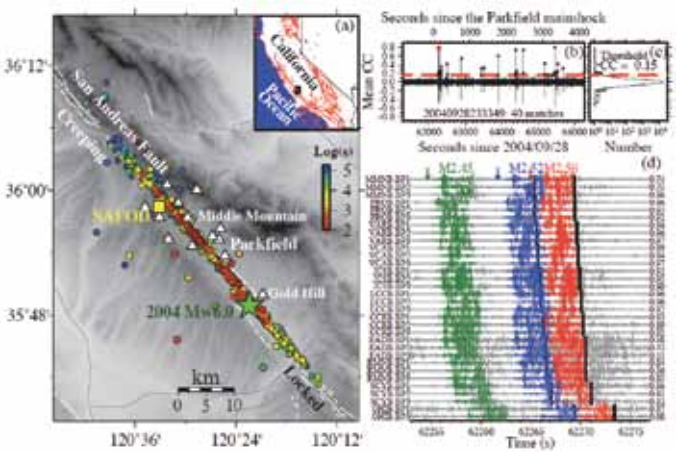

Newly detected aftershocks showing migrations after the 2004 Mw6.0 Parkfield earthquake. (a) Map of the Parkfield section of the San Andreas Fault (SAF; white lines). The newly detected aftershocks are color-coded by their occurrence times (in logarithmic scales) since the Parkfield mainshock (green star). (b) Mean cross-correlation (CC) functions for the template event 20040928233349. The black dots are positive detections above the threshold (red dashed line) and the red dot corresponds to the detected M2.56 event at ~140 s after the mainshock. (c) The histogram of the mean CC functions. (d) A comparison of the template waveforms (red) and the continuous waveforms (gray) for each component of 11 stations. Waveforms shown in green and blue colors correspond to other two events that occurred nearby. The arrows mark the origin times of the three events.

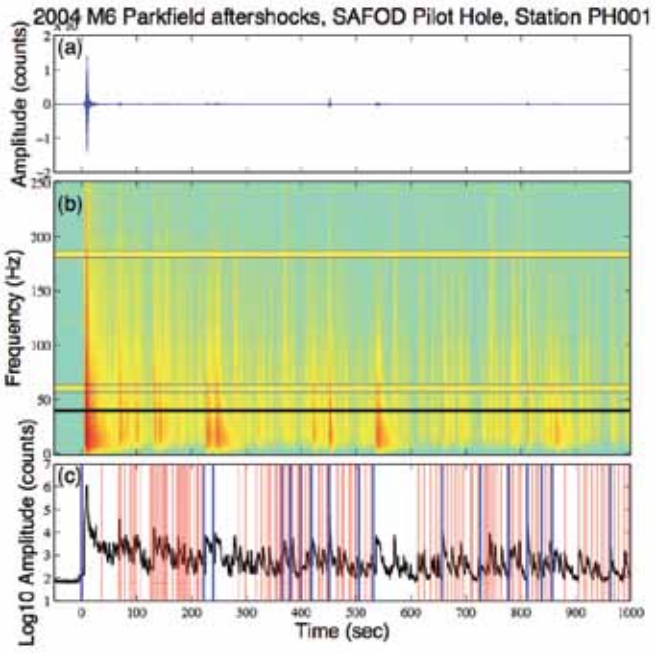

Early aftershocks of the 2004 Parkfield earthquake recorded by the SAFOD Pilot Hole station. (a) The raw vertical-component seismogram recorded at the SAFOD Pilot Hole station PH001 within the first 1000 s after the 2004 Mw6.0 Parkfield earthquake. (b) The corresponding spectrogram of (a) showing the mainshock and numerous early aftershocks. The think horizontal line at 40 Hz marks the corner of the high-pass filter, and the thin bands around 60 and 184 Hz mark the continuous electronic noise. (c) The envelope functions of the median-averaged spectrogram above 40 Hz. The vertical blue and red lines mark the origin times of 16 and 130 aftershocks listed in the NCSN catalog and detected by our technique, respectively.

Mapping Subduction Zone Fault Slip with Teleseismic and Geodetic Data

Matthew E. Pritchard *(Cornell University),* **Chen Ji** *(University of California, Santa Barbara),* **Eric Fielding** *(Jet Propulsion Lab),* **Jack Loveless** (*Harvard University),* **Mark Simons** *(Caltech), Tim Dixon (University of Miami)*

In an effort to understand the behavior of the megathrust fault in the Peru-Chile subduction zone, we have used seismic and geodetic observations to determine the location of fault slip during different parts of the earthquake cycle (co-seismic, post-seismic, and inter-seismic). During the co-seismic time period, we can invert teleseismic waveforms from the GSN and geodetic data (InSAR and GPS) both jointly and separately to constrain the rupture process. We have combined the seismic and geodetic data to study 8 earthquakes (6.7 < Mw < 8.4) in southern Peru and northern Chile that occurred between 1993 and 2007 (Fig. 1), providing one of the most detailed space-time rupture histories available in a subduction zone and yielding new discoveries about the generation of large earthquakes in this area [Pritchard et al., 2006; Pritchard et al., 2007; Pritchard & Fielding, 2008; Loveless et al., 2010]. In northern Chile, because of the spatially and temporally dense geodetic data and constraints on earthquake locations and slip from the GSN, we can clearly separate co-seismic and post-seismic deformation. We document a complex mosaic of phenomena including large earthquakes, post-seismic after-slip with a spatial distribution that appears to be tied to variations in coastal morphology, and the first observations with sufficient resolution in both time and space to infer triggering of a large (Mw > 7) earthquake by a so-called ``silent earthquake" [Pritchard & Simons, 2006]. Using the teleseismic and geodetic data together, we have shown that in order to make reliable two-dimensional models of earthquake slip for subduction zone earthquakes larger than magnitude 7.5 (necessary for hazard and other types of studies), we cannot use standard techniques. We must either combine teleseismic data with the geodetic data [Pritchard et al., 2007; Pritchard & Fielding, 2008] or use new analysis methods recently developed by others [Lay et al., 2010]. We used our detailed models of the 6 largest earthquakes to study potential relationships between the rupture areas and other observables in an effort to better forecast the location of large earthquakes. We find no obvious or simple relationship between various other proposed physical processes and the earthquake slip in these earthquakes. However, analysis of the forearc gravity field and its gradients shows correlation with many of the observed slip patterns, as suggested by previous studies [Loveless et al., 2010].

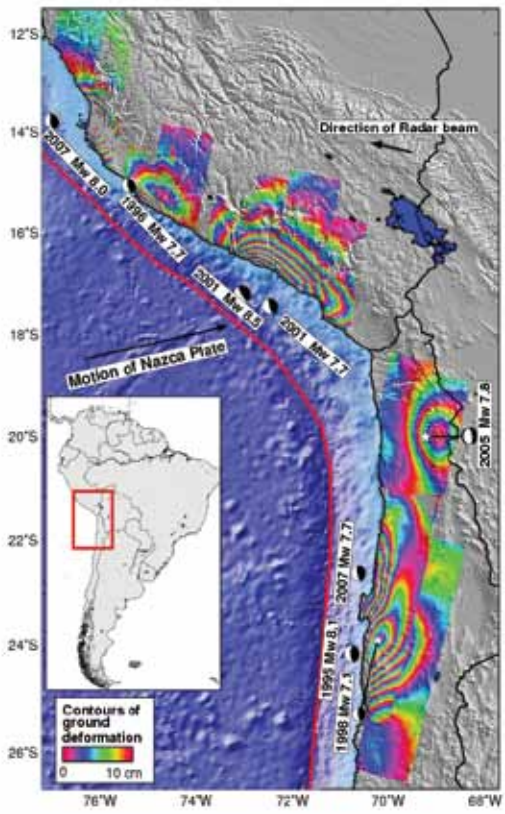

Contours of ground deformation (10 cm interval) from some large subduction zone earthquakes in the central Andes as measured by the ERS-1, ERS-2 and Envisat satellites of the European Space Agency. Deformation is in the line-of-sight of the radar beam, which is about 23 degrees from vertical and projected onto the map as a black arrow. The largest magnitude of ground deformation during the earthquakes is off-shore, but these dense on-land images of ground displacement provide new information about the details of the fault motion during the earthquake.

References

J. P. Loveless, M. E. Pritchard, and N. Kukowski, Testing mechanisms of subduction zone segmentation and seismogenesis with slip distributions from recent Andean earthquakes, *Tectonophysics, 2009*, in press.

M. E. Pritchard, and E. J. Fielding, A study of the 2006 and 2007 earthquake sequence of Pisco, Peru, with InSAR and teleseismic data, *Geophys. Res. Lett., 35*, 10.1029/2008GL033374, 2008.

M. E. Pritchard, E. Norabuena, C. Ji, R. Boroschek, D. Comte, M. Simons, T. Dixon, and P. A. Rosen, Teleseismic, geodetic, and strong motion constraints on slip from recent southern Peru subduction zone earthquakes, *J. Geophys. Res., 112*, 10.1029/2006JB004294, 2007.

M. E. Pritchard, and M. Simons, An aseismic fault slip pulse in northern Chile and along-strike variations in seismogenic behavior, *J. Geophys. Res., 111*, 10.1029/2006JB004258, 2006.

M. E. Pritchard, C. Ji, and M. Simons, Distribution of slip from 11 Mw > 6 earthquakes in the northern Chile subduction zone, *J. Geophys. Res., 111,* 10.1029/2005JB004013, 2006.

Apparent Stress Variations at the Osa Peninsula, Costa Rica, Influenced by Subducted Bathymetric Features

Pamela A. Moyer *(Earth and Environ. Science Dept., New Mexico Tech),* **Susan L. Bilek** *(Earth and Environ. Science Dept., New Mexico Tech),* **W. Scott Phillips** *(Earth and Environ. Sciences Div., Los Alamos Natl. Lab.)*

Subducted bathymetric features such as seamounts have been modeled as areas of strong frictional behavior between the subducting and overriding plates. These models describe subducted features as "sticking" to the overriding plate, thereby increasing stress at the feature until slip occurs. On the Pacific Coast of Costa Rica, a number of bathymetric features enter the Middle America Trench near the Osa Peninsula (Figure 1). Using data collected and processed through a PASSCAL experiment from six land seismometers and data from twelve ocean bottom seismometers, aftershocks of the 1999 6.9 Mw Quepos thrust-faulting event were analyzed to investigate the influence subducted features have on earthquake rupture near the Osa Peninsula. Apparent stress values between 0.1 MPa and 2.5 MPa were found for 114 aftershocks using seismic coda techniques. An average apparent stress value two times higher than the global average apparent stress value for thrust-faulting events at oceanic subduction zones was found for the analyzed events. The range of apparent stress values observed near the Osa Peninsula, and high average value, suggests areas of stress concentration along the subduction interface as a result of strong frictional behavior due to bathymetric features at depth.

References

Moyer, P.A., S.L. Bilek, and W.S. Phillips (2009), Apparent stress variations at the Osa Peninsula, Costa Rica, and the role of subducting topography, EOS Trans AGU, 90(52), Fall Meet. Suppl., Abstract T23B-1892.

Acknowledgements: We gratefully acknowledge NSF funding for this project NSF-OCE 0751610 to SLB.

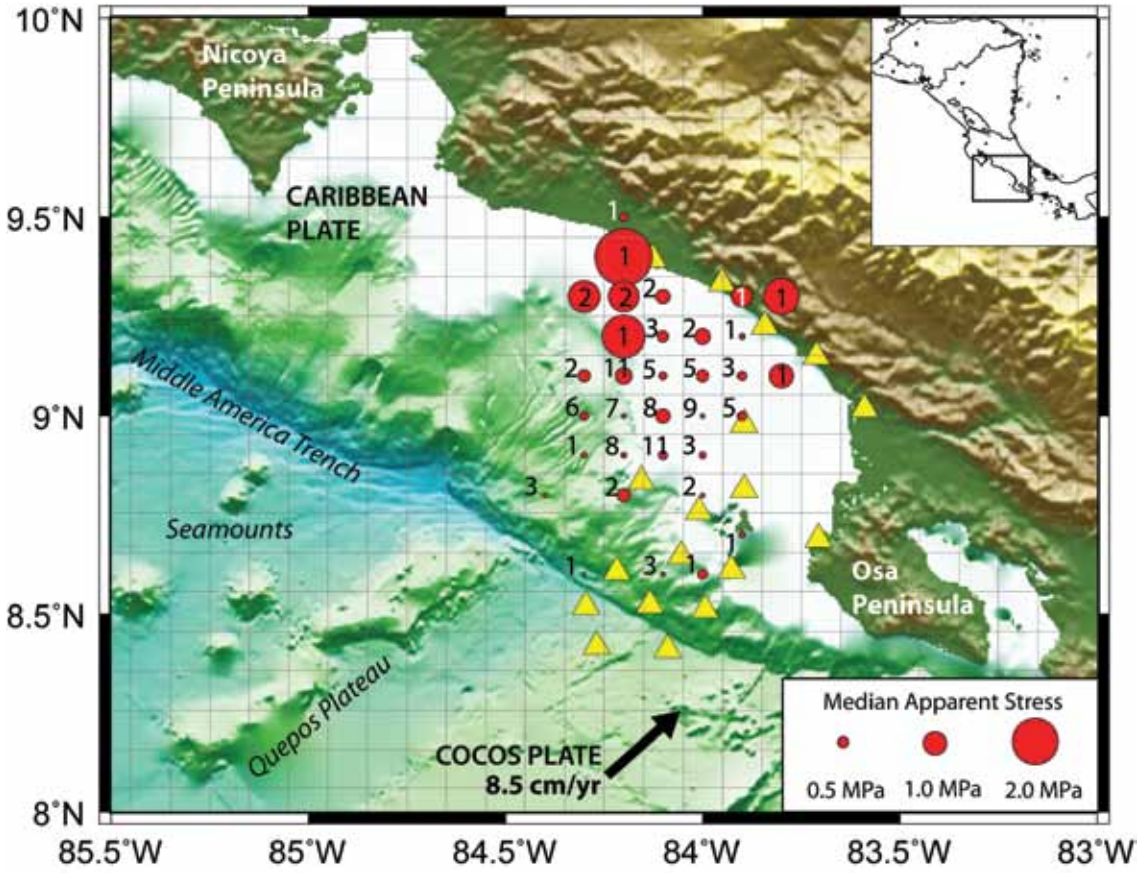

Median apparent stress values for events near the Osa Peninsula, Costa Rica in 0.1 x 0.1 degree grids. The size of the red circle indicates the median value of apparent stress for events within that grid. Numbers of events used to compute the median within each grid are noted. Yellow triangles are land and ocean bottom seismometers used in this study. A range of apparent stress values was observed near the Osa Peninsula with concentrations of high apparent stress indicative of strong frictional behavior along the subduction interface due to bathymetric features at depth.

Deep Earthquake Mechanics, Slab Deformation, and Subduction Forces

Linda M. Warren (*Saint Louis University*)

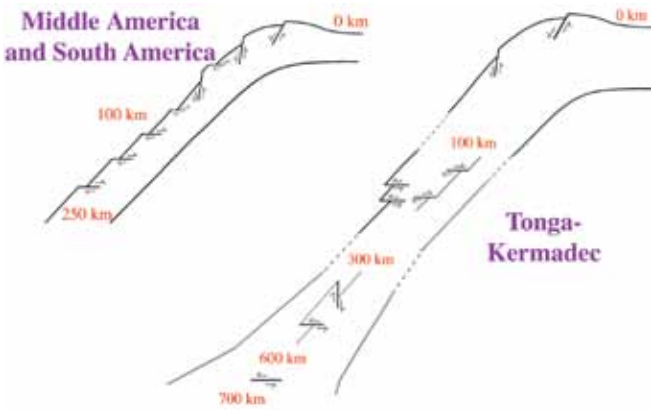

Schematic cross-section showing fault orientations in subducting slabs.

Deeper than ~50 km depth in the Earth, the confining pressure is so high that it should prevent earthquakes from occurring. However, subduction zone earthquakes occur down to ~700 km depth. Based of the stability of minerals in the subducting lithosphere, mechanisms such as dehydration embrittlement and transformational faulting have been proposed for generating the earthquakes. These mechanisms have different implications for the orientation of earthquake fault planes, so they can be tested by identifying fault planes. Applying a method developed by Warren and Silver [*2006*] to data from all available seismic networks, we analyze the directivity of 200 large deep earthquakes in the Tonga [*Warren et al, 2007a*], Middle America [*Warren et al, 2008*], and central South America [*Warren et al, 2007b*] subduction zones to identify the fault planes for ~1/4 of the earthquakes. Despite large differences in temperature and lithospheric thickness, we observe similar fault-plane orientations with depth in all three subduction zones. The dominant steep, trenchward-dipping faults of the outer rise may be reactivated down to 100 km depth, while subhorizontal faults also slip from 40-100 km depth. From 100-300 km depth, all identified faults are subhorizontal. While inconsistent with the reactivation of the dominant outer-rise fault orientation, this orientation could be consistent with the reactivation of the seaward-dipping faults, and recent numerical experiments [*Faccenda et al, 2009*] suggest that the less prominent faults may be preferentially reactivated because of the stress field in the bending slab. The similarity in the onset depth of horizontal faulting in the three subduction zones suggests that it is controlled by pressure rather than temperature or other tectonic parameters. In Tonga, which has a double seismic zone with opposite stress orientations in each plane of seismicity, deformation along these subhorizontal faults causes the slab to thin, indicating that slab pull is the primary force controlling slab seismicity at intermediate depths. While seismicity in our Middle and South America study areas stops by 250 km depth, Tonga earthquakes occur down to nearly 700 km depth. The fault-plane orientations of earthquakes >300 km depth match the patterns expected for the creation of a new system of faults: we observe both subhorizontal and subvertical fault planes consistent with a down-dip-compressional stress field. Slip along the two fault orientations causes the slab to thicken as it subducts and encounters resistance to lower mantle penetration. This resistance also results in an increase in the frequency of subhorizontal fault planes >600 km depth.

References

Warren, L.M., A.N. Hughes, and P.G. Silver (2007a), Earthquake mechanics and deformation in the Tonga-Kermadec subduction zone from fault-plane orientations of intermediate- and deep-focus earthquakes, *J. Geophys. Res., 112*.

Warren, L.M., M.A. Langstaff, and P.G. Silver (2008), Fault-plane orientations of intermediate-depth earthquakes in the Middle America trench, *J. Geophys. Res., 113*, B01304.

Warren, L.M., and P.G. Silver (2006), Measurement of differential rupture durations as constraints on the source finiteness of deep-focus earthquakes, *J. Geophys. Res., 111*.

Acknowledgements: This work was supported by the National Science Foundation through grant EAR-0733170 and through Independent Research and Development time while the author worked at the Foundation, and by the Carnegie Institution of Washington through a Harry Oscar Wood Postdoctoral Fellowship.

Automated Identification of Teleseismically Recorded Depth Phases with Application to Improving Subduction Zone Earthquake Locations

Heather R. DeShon *(CERI, Univ. of Memphis),* **E. Robert Engdahl** *(Univ. of Colorado-Boulder),* **Shishay Bisrat** *(CERI, Univ. of Memphis),* **Susan L. Bilek** *(New Mexico Institute of Technology),* **Jeremy Pesicek** *(Univ. of Wisconsin-Madison),* **Clifford H. Thurber** *(Univ. of Wisconsin-Madison)*

A large portion of the seismogenic megathrust of most subduction zones lies beneath the ocean, which ultimately limits the amount of local seismic data available for high precision earthquake location studies. Standard single-event teleseismic earthquake locations are limited in their ability to provide the level of precision necessary to properly evaluate spatio-temporal aftershock variability, to constrain subducting plate geometry, or to investigate temporal strain release. Earthquake locations in global catalogs can be in error by 10's of kilometers in location and depth due to the use of imprecise arrival time picks, phase misidentification, poor station coverage, etc. Improvements to teleseismic event location, especially in depth, can be accomplished using more accurate depth phase arrival times. We have developed a new method to identify depth phases (pP, pwP, sP) and improve P onset times that takes advantage of the high quality IRIS Global Seismic Network waveforms available through the IRIS Data Management Center. The picker uses abrupt amplitude changes of the power spectral density (PSD) function calculated at optimized frequencies for each waveform. The technique identifies depth phases not reported in the standard catalogs and works over a wide-range of depths. The additional depth phases are incorporated with the ISS, ISC, and NEIC phase catalogs and relocated using the EHB teleseismic location approach [Engdahl et al., 1998]. The automatically identified depth phases and revised EHB catalogs are being used for two subduction zone studies: 1) Teleseismic double-difference relocation and tomography along the Andaman-Sunda subduction zone, which takes advantage of the extensive global recordings of the 2004, 2005, and 2007 great (M>8) Sumatra earthquakes [i.e. Pesicek et al., 2010]; 2) A global study characterizing earthquake source durations in subduction zones, with a focus on identifying unusually slow source processes such as those associated with tsunami earthquakes [i.e. Bisrat et al., 2009]. To date, we have provided nearly 29,000 new phases to the EHB catalog for ~1250 earthquakes in the Sumatra, Java, Kurile, Japan, Peru, and Alaska subduction zones. Epicentral changes following relocation using additional depth phases are generally small (<5 km). Changes in depth may be on the order of 5-20 km for some events, while the standard deviation of depth changes within each subduction zone is ~5 km.

References

Bisrat, S.T., H.R. DeShon, E.R. Engdahl, S.L. Bilek (2009), Improved Teleseismic Locations of Shallow Subduction Zone Earthquakes, Eos Trans. AGU, 90(52), Fall Meet. Suppl., Abstract T23B-1913.

Engdahl, R.E, R. Hilst and R. Buland (1998), Global teleseismic earthquake relocation with improved travel times and procedures for depth determination. *Bull. Seismol. Soc. Amer., 88*, 722-743.

Pesicek, J.D., C.H. Thurber, H. Zhang, H.R. DeShon, and E.R. Engdahl (2010), Teleseismic Double-difference Relocation of Earthquakes along the Sumatra-Andaman Subduction Zone using a Three-Dimensional Model, *J. Geophys. Res.*, (in press).

Acknowledgements: We gratefully acknowledge NSF EAR and OCE support (EAR0608988, OCE0841022 to HRD; EAR0609613, OCE0841040 to ERE; OCE0941077 to SLB; EAR0608988 to CT).

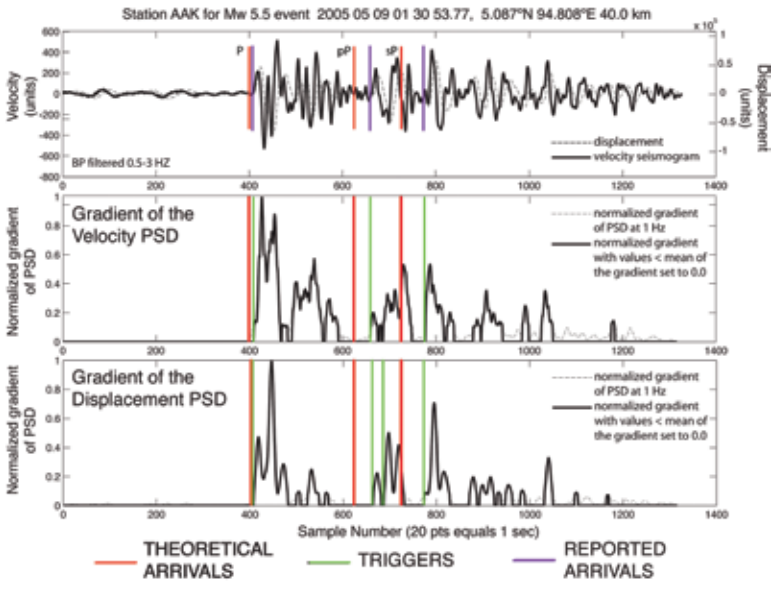

Figure 1: Example of the automated depth phase identification procedure applied to a Mw 5.5 earthquake occurring at 40 km depth in the Sunda subduction zone. (top) Velocity and displacement waveforms recorded at GSN station AAK. The theoretical arrival times for P, pP and sP (red) and the new reported arrivals (purple) following the automated procedure are shown. (middle, bottom) The automated method uses abrupt changes the gradient of the power spectral density function (PSD) of both the velocity and displacement time series, termed triggers (green), and associates triggers with likely phases. The initial identifications may be dynamically reidentified during the EHB relocation process.

The Puzzle of the Bardarbunga, Iceland Earthquake: No Volumetric Component in the Source Mechanism

Hrvoje Tkalčić *(The Australian National University),* **Douglas S. Dreger** *(University of California at Berkeley),* **Gillian R. Foulger** *(Durham University),* **Bruce R. Julian** *(United States Geological Survey)*

A volcanic earthquake with Mw=5.6 occurred beneath the Bárdarbunga caldera in Iceland on September 29, 1996. This earthquake is one of a decade-long sequence of M5+ events at Bárdarbunga with non-double-couple mechanisms in the global CMT catalogue. Fortunately, it was recorded well by the regional-scale Iceland Hotspot Project seismic experiment. We investigated the event with a complete moment tensor inversion method [*Tkalčić et al., 2009*] using regional long-period seismic waveforms and a composite structural one-dimensional model from receiver function and surface wave constraints. The moment tensor inversion using data from stations of the Iceland Hotspot Project yields a non-double-couple solution with a 67% vertically oriented compensated linear vector dipole component, a 32% double-couple component and a statistically insignificant (2%) volumetric (isotropic) contraction. This indicates the absence of a net volumetric component, which is puzzling in the case of a large volcanic earthquake that apparently is not explained by shear slip on a planar fault. A possible volcanic mechanism that can produce an earthquake without a volumetric component involves two offset sources with similar but opposite volume changes. We show that although such a model cannot be ruled out, the circumstances under which it could happen are rare.

References

Tkalčić H., D. S. Dreger, G. R. Foulger, and B. R. Julian (2009). The puzzle of the Bardarbunga, Iceland earthquake: No volumetric component in the source mechanism, *Bull. Seismol. Soc. Amer., 99*: 3077-3085.

Acknowledgements: We are grateful to IRIS DMC center for efficiently archiving and distributing continuous waveform data.

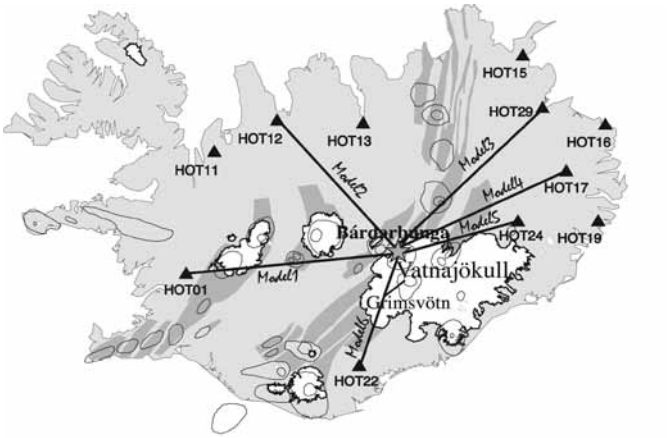

Figure 1

Map showing the main tectonic and volcanic features in Iceland. Glaciers are shown in white and spreading segments in dark gray. Volcanoes are shown with thin lines. The Bárdarbunga earthquake is shown with the white star. Triangles are locations of the eleven Iceland Hotspot Project broadband stations used in the moment tensor inversion. Lines indicate the locations of the six different one-dimensional models used between the source and stations.

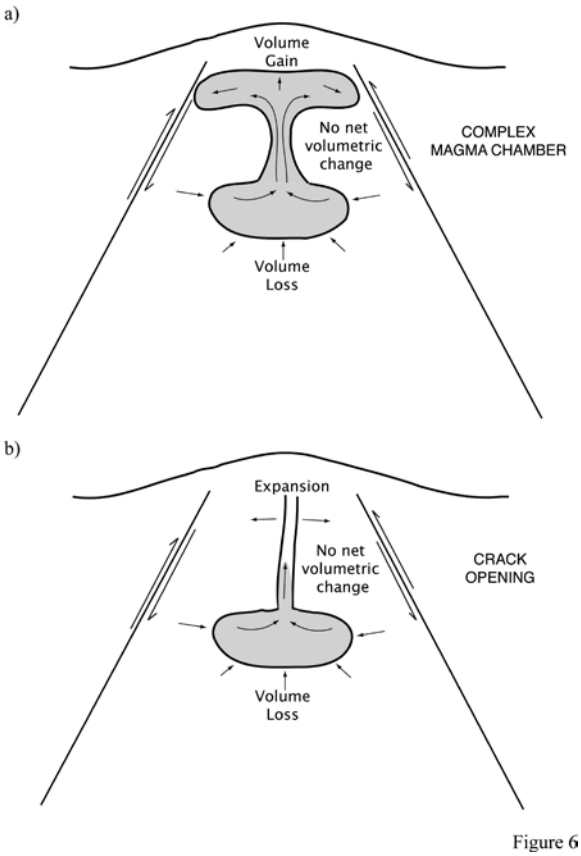

Figure 6

Sketch of tested models with two compensating sources reproducing a vertically oriented CLVD in dilatation (where volumetric exchange is equal and opposite in sign): (a) a complex magma chamber; (b) an implosive source and a vertical, horizontally opening crack above.

Evaluating Ground Motion Predictions of Usgs 3d Seismic Model of the San Francisco Bay Area with Broadband Seismograms

Arthur Rodgers *(Lawrence Livermore National Laboratory),* **Anders Petersson** *(Lawrence Livermore National Laboratory)*

The USGS (Menlo Park) developed a three-dimensional (3D) geologic and seismic model of the greater San Francisco Bay Area for the purposes of computing earthquake ground motions. This model was used to compute scenario ground motions for the 1906 San Francisco [Aagaard et al., 2008b], 1989 Loma Prieta [Aagaard et al., 2008a] and a suite of Hayward Fault earthquakes [Aagaard et al., in press]. While scenario ground motion calculations are important for investigating the amplitude, duration and variability of motions from large damaging earthquakes, the accuracy of such predictions depends on the accuracy of the 3D model. We evaluated the USGS 3D model of the Bay Area by computing predictions of broadband waveforms for 12 moderate (Mw 4-5) earthquakes and comparing them to the observed waveforms [Rodgers et al., 2008]. Calculations were performed using WPP (an elastic finite difference code developed at LLNL) on massively parallel computers. Data were obtained from IRIS for Berkeley Digital Seismic Network (BDSN) and USArray broadband stations. The figure below shows a snapshot of the vertical component displacements for an earthquake near Glen Ellen (Sonoma County). Also shown is the comparison of the observed (blue) and computed (red) three-component seismograms at two stations: BKS (Berkeley) and JRSC (Stanford). Note that the motions at BKS are more complex and longer duration due to basin propagation effects from the San Pablo Bay, however the 3D model predicts this energy quite well. The motions at JRSC are simpler and the 3D model predicts the weaker late arriving energy on the transverse (T) component. This analysis found that the USGS 3D model could predict the amplitude, duration and waveform shapes of moderate earthquake ground motions quite well however we did find that phase delays reveal that shear velocities in the model were too fast. This information was used to revise the model for subsequent ground motion modeling.

References

Aagaard, B., T. Brocher, D. Dreger, A. Frankel, R. Graves, S. Harmsen, S. Larsen, K. McCandless, S. Nilsson, N. A. Petersson, A. Rodgers, B. Sjogreen and M. L. Zoback, (2008b). Ground motion modeling of the 1906 San Francisco earthquake II: Ground motion estimates for the 1906 earthquake and scenario events, *Bull. Seismol. Soc. Amer., 98*, 1012-1046

Rodgers, A., A. Petersson, S. Nilsson, B. Sjogreen and K. McCandless (2008). Broadband Waveform Modeling of Moderate Earthquakes in the San Francisco Bay Area To Evaluate the USGS 3D Seismic Velocity Model, *Bull. Seismol. Soc. Amer., 98*, 969-988

Acknowledgements: This work performed under the auspices of the U.S. Department of Energy by Lawrence Livermore Nation

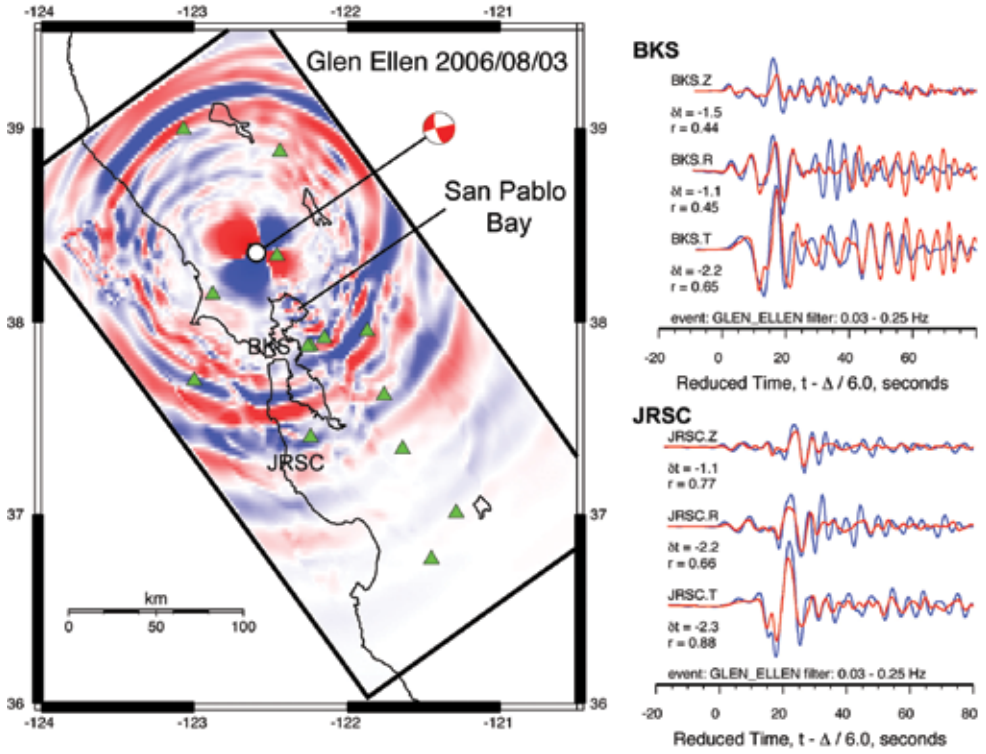

(left) Snapshot of vertical component displacement for an earthquake near Glen Ellen with BDSN and USArray broadband stations (green triangles). (right) Comparison of observed (blue) and computed (red) three-component seismograms at stations BKS (Berkeley, top) and JRSC (Stanford, bottom).

Physics-Based Shake Map Simulation for the 2008 Wells, Nevada Earthquake

John N. Louie *(University of Nevada, Reno)*

The standard USGS ShakeMap for the Feb. 21, 2008 M6.0 Wells, Nevada earthquake shows many "bulls-eye" anomalies. The simple ShakeMap algorithm tried to average between high shaking in the populated basins reported by citizens to the USGS Community Internet Intensity Map (CIIM), and low shaking measured at several USArray Transportable Array (TA) stations on bedrock. Starting with the complex basin-thickness map of Saltus and Jachens [1995], we built a 3d seismic-velocity model that also included a projection of shallow geotechnical velocities. Various models for the directivity of rupture of 15x15-km normal-fault planes fed into computations predicting shaking across the region, employing the physics-based E3D code of Larsen et al. [2001]. The simulated peak-ground-velocity (PGV) maps show a high degree of channeling along the many basins in the region, with adjacent basin and bedrock areas only 2 km apart predicted to experience levels of shaking differing by a factor of ten. There is also evidence that strong basin shaking "tunnels" across narrow parts of bedrock ranges separating basins. The physics-based shake map is highly heterogeneous in this Basin and Range region (see figure) and contains prominent features that a standard, statistical USGS ShakeMap cannot predict. The physics-based simulation produces a good match against PGV values recorded at nearby TA stations, when an eastward rupture directivity is used at the source. The match is highly sensitive to the rupture directivity.

References

Larsen, S., Wiley, R., Roberts, P., and House, L., 2001, Next-generation numerical modeling: incorporating elasticity, anisotropy and attenuation: Society of Exploration Geophysicists Annual International Meeting, Expanded Abstracts, 1218-1221.

Saltus, R. W., and Jachens, R. C., 1995, Gravity and basin-depth maps of the Basin and Range Province, Western United States: U.S. Geological Survey, Geophysical Investigations Map, Report: GP-1012, 1 sheet.

Acknowledgements: Research partially supported by the U.S. Geological Survey (USGS), Department of the Interior, under USGS award numbers 08HQGR0046 and 08HQGR0015. The views and conclusions contained in this document are those of the authors and should not be interpreted as necessarily representing the official policies, either expressed or implied, of the U.S. Government.

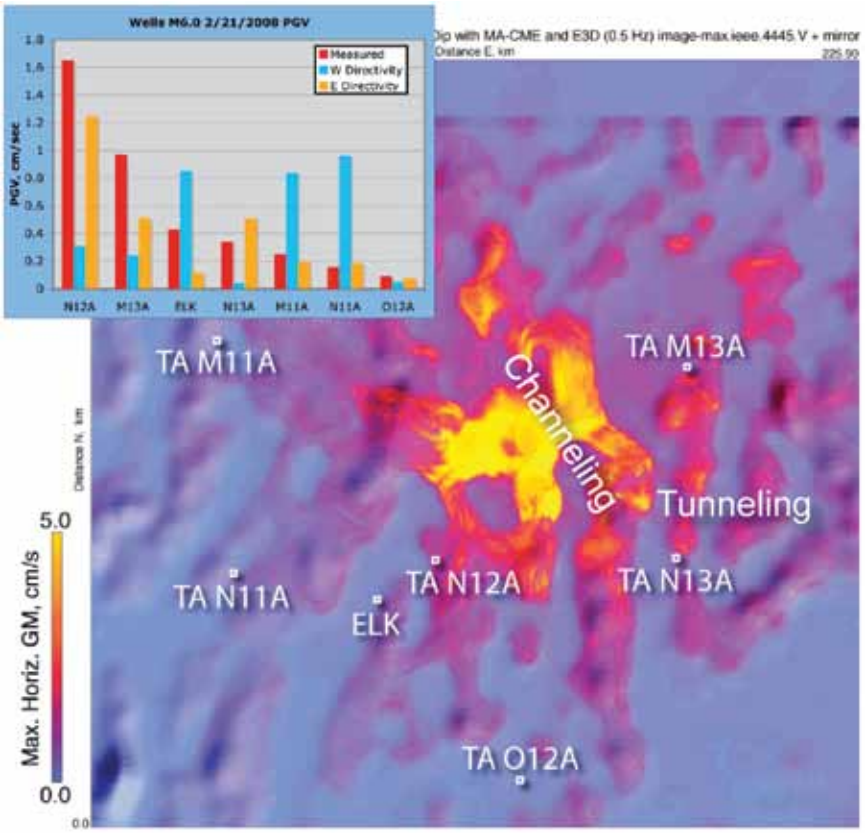

Shaded-relief map of basin-floor topography in northeastern Nevada (Saltus and Jachens, 1995) surrounding the Feb. 21, 2008 Wells earthquake, 225 km on a side (the basin dataset used ends artificially at 42°N). Locations of USArray Transportable Array (TA) stations recording the event are indicated. Warmer colors correspond to greater shaking computed for the event by the E3D code of Larsen et al. (2001), including the effects of geologic basins and predicted geotechnical velocities. Solid yellow indicates peak ground velocities (PGV) above 5 cm/s. This computation assumes an eastward directivity of the earthquake rupture. Shaking is high along the many basins, and high levels of shaking channel along the basins and can tunnel across ranges between basins, with examples indicated. In the inset graph this shaking prediction (orange bars) matches the recorded PGV (red) well, while other directions of directivity (blue) do not match.

Tremor Monitoring

Aaron Wech *(University of Washington)*

Since their discovery nearly a decade ago, advances in both instrumentation and methodology in subduction zones around the world have brought the causal connection between seismically observed tectonic tremor and geodetically observed slow slip into sharper focus—with it becoming increasingly clear that tremor serves as a proxy for slow slip. Considering geodesy's lower limits in spatio-temporal resolution together with the abundance of low-level, ageodetic tremor, this connection makes tremor a key component in monitoring when, where, and how much slip is occurring. Because slow slip transfers stress to the updip seismogenic portion of the plate interface, monitoring transient events may serve in forecasting the threat of a megathrust earthquake by inferring the temporal and spatial variations in the loading of the seismogenic zone. We use waveform envelope correlation & clustering [*Wech and Creager, 2008*] methodology to automatically detect and locate tremor. Applying this technique to TA, PASSCAL, PBO, and regional network data, we map tremor epicenters from northern California to mid- Vancouver Island and present a system that monitors and reports tremor activity in near-realtime on an interactive webpage [*Wech, 2010*]. Collectively the resulting product is an automatic margin-wide tremor catalog and a website disseminating this information in a way that is accessible and engaging to the general population yet remains valuable as a tool for scientific synergy across institutions and disciplines: www.pnsn.org/tremor

References

Wech, A.G., and K.C. Creager (2008), Automatic detection and location of Cascadia tremor, *Geophys. Res. Lett., 35*, L20302.

Wech, A.G. (2010), Interactive Tremor Monitoring, *Seismol. Res. Lett., 81*:4, July/August 2010.

Audet, P., et al. (2010), Slab morphology in the Cascadia fore arc and its relation to episodic tremor and slip, *J. Geophys. Res., 115.*

Acknowledgements: This work was funded by USGS grant #'s 08HQGR0034, G09AP00024, & G10AP00033. Realtime data are provided by the Pacific Northwest Seismic Network, Pacific Geoscience Center, Plate Boundary Observatory, and Northern California Regional Network.

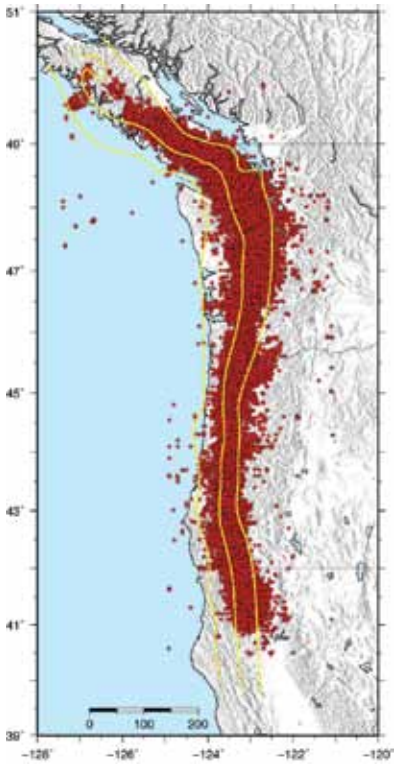

Tremor map. Margin-wide epicenters from 2006-2009 using TA, PASSCAL, PBO, and regional network data. Yellow lines are 20, 30, and 40 km isodepths from Audet et al. [2010].

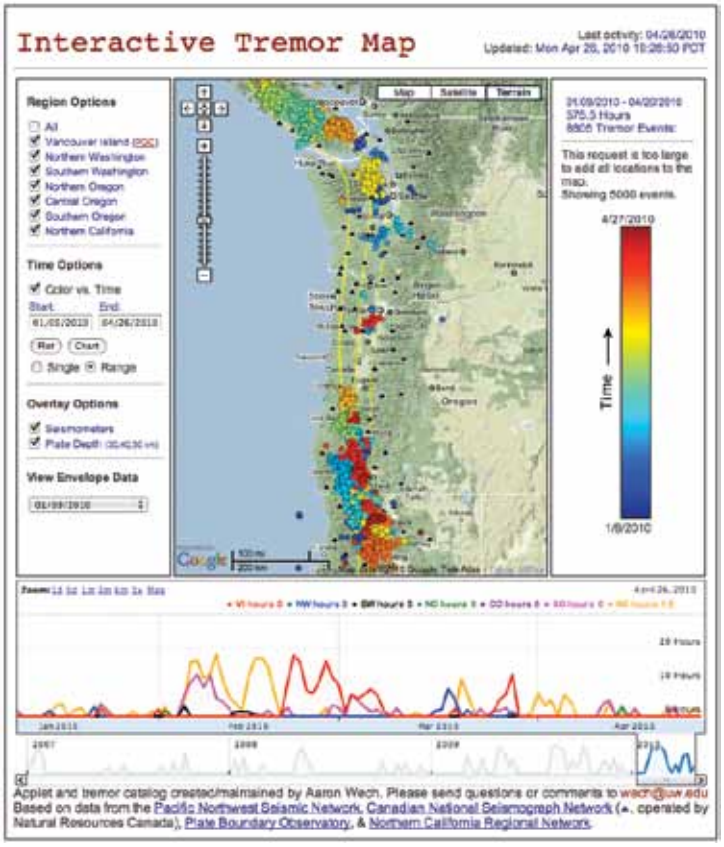

A screenshot of the web product resulting from this near-realtime system.

Non-Volcanic Tremor along the Oaxaca Segment of the Middle America Subduction Zone

Michael Brudzinski *(Department of Geology, Miami University of Ohio),* **Héctor Hinojosa-Prieto** *(Department of Geology, Miami University of Ohio),* **Kristen Schlanser** *(Department of Geology, Miami University of Ohio),* **Enrique Cabral-Cano** *(Departamento de Geomagnetismo y Exploración, Instituto de Geofísica, Universidad Nacional Autónoma de México),* **Alejandra Arciniega-Ceballos** *(Departamento de Vulcanología, Instituto de Geofísica, Universidad Nacional Autónoma de México),* **Oscar Diaz-Molina** *(Departamento de Geomagnetismo y Exploración, Instituto de Geofísica, Universidad Nacional Autónoma de México),* **Charles DeMets** *(Department of Geology and Geophysics, University of Wisconsin-Madison)*

The Oaxaca subduction zone is an ideal area for detailed studies of plate boundary deformation as rapid convergent rates, shallow subduction, and short trench-to-coast distances bring the thermally defined seismogenic and transition zones of the plate interface over 100 km inland. Previous analysis of slow slip events in southern Mexico suggests they may represent motion in the transition zone, defining the downdip edge of future megathrust earthquakes. A new deployment consisting of broadband seismometers distributed inland along the Oaxaca segment provide the means to examine whether non-volcanic tremor (NVT) signals can also be used to characterize the boundary between the seismogenic and transition zones. In this study, we established that NVT exists in the Oaxaca region based on waxing and waning of seismic energy on filtered day-long seismograms that were correlated across neighboring stations, and further supported by appropriate relative time moveouts in record sections, and spectrograms with narrow frequency bands. 18 prominent NVT episodes that lasted upwards of a week were identified during the 15 months analyzed (June 2006 to September 2007), recurring as frequently as every 2-3 months in a given region. We analyze NVT envelope waveforms with a semi-automated process for identifying prominent energy bursts, and analyst-refined relative arrival times are inverted for source locations. NVT burst epicenters primarily occur between the 40-50 km contours for depth of the plate interface, except in eastern Oaxaca where they shift towards the 30 km contour as the slab steepens. NVT hypocenters correlate well with a high conductivity zone that is interpreted to be due to slab fluids. NVT is more frequent, shorter in duration, and located further inland than GPS-detected slow slip, while the latter is associated with a zone of ultra-slow velocity interpreted to represent high pore fluid pressure. This zone of slow slip corresponds to approximately 350–450°C, with megathrust earthquakes, microseismicity, and strong long-term coupling occurring immediately updip from it. This leaves NVT primarily in a region further inland from the thermally defined transition zone, suggesting that transition from locking to free slip may occur in more than one phase.

Acknowledgements: NSF EAR-510812

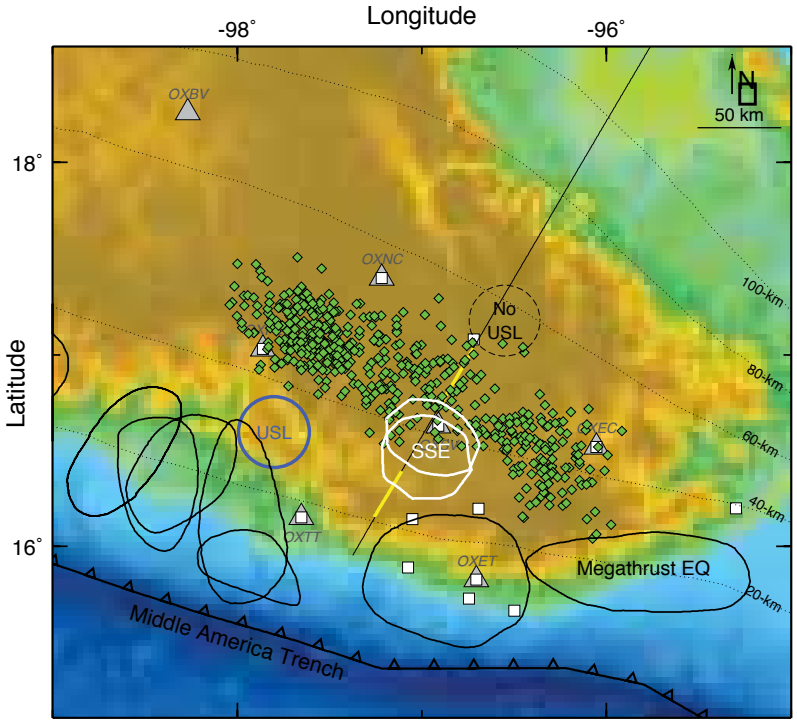

Map of the study region focused along the Oaxaca segment of the Middle American Subduction Zone. Grey triangles (seismic) and white squares (GPS) show the state of the joint network in 2006-2007 that is used to determine the extent of non-volcanic tremor in July 2006 (green line, this study) and the 100 mm slip contour for slow slip events in early 2006 and early 2007 (white ovals) [Correa-Mora et al., 2008; 2009]. Black ovals are approximate rupture zones of large subduction thrust earthquakes over the past 50 years as estimated from locations of rupture aftershocks. Straight line is a profile of magnetotelluric measurements with areas of high conductivity near the subduction interface highlighted in yellow [Jödicke et al., 2006]. Dotted lines are isodepths of the subducting plate from analysis of seismicity [Pardo and Suarez, 1995]. Blue circle indicates where an ultra-slow velocity layer has been detected, and dashed circle indicates where it is absent.

Slow Slip and Tremor in the Northern Costa Rica Seismogenic Zone

S.Y. Schwartz *(University of California, Santa Cruz),* **J.I. Walter** *(UC Santa Cruz),* **T.H. Dixon** *(Univ. of Miami),* **K. Outerbridge** *(Univ. of Miami),* **J.M. Protti** *(OVSICORI-UNA),* **V. Gonzalez** *(OVSICORI-UNA)*

Several episodes of slow slip and tremor are believed to have occurred at the plate boundary of northern Costa Rica between 2000 and 2008. The evidence for these events varies and consists of: 1) correlated fluid flow excursions and seismic tremor recorded on ocean bottom instruments in 2000 [*Brown et al., 2005*]; 2) offsets in continuous GPS data in September 2003; 3) offsets in GPS data accompanied by seismic tremor in May 2007 [Outerbridge et al., 2010]; and 4) strong prolonged seismic tremor in August 2008. Modeling of the 2000 event suggested that slip occurred at shallow depth, between the surface and ~15 kilometers. The much better constrained slip distribution of the 2007 event consisted of 2 patches, the stronger centered at ~30 km depth, near the down dip transition from stick-slip to stable sliding, and the weaker patch located at ~6 km depth at the up dip edge of the shallow frictional transition. Tremor locations for the 2008 episode locate offshore at depths of between 6-10 km . The 2003 event was recorded on too few instruments to be modeled. These results are significant in that they are the first to suggest that slow slip occurs at the up dip transition from stick-slip to stable sliding; locations of slow slip in other environments have been limited to the down dip frictional transition.

Due to the relatively small surface displacements (1-2 cm) associated with Costa Rica slow slip events, the coincident occurrence of seismic tremor is important for their detection and study. Similar to tremor observations in southwest Japan, Costa Rica tremor consists of swarms of low-frequency earthquakes that occur as repetitive stick-slip motion on the plate interface [*Brown et al., 2009*], contains very low frequency earthquakes, with dominant energy between 20-50 s, and appears to be tidally modulated.

References

Brown, J. R., G. C. Beroza, S. Ide, K. Ohta, D. R. Shelly, S. Y. Schwartz, W. Rabbel, M. Thorwart, and H. Kao (2009), Deep low-frequency earthquakes in tremor localize to the plate interface in multiple subduction zones, *Geophys. Res. Lett., 36*, L19306.

Brown, K. M., M. D. Tryona, H. R. DeShon, L. M. Dorman, and S. Y. Schwartz, (2005), Transient fluid pulsing and seismic tremor: Evidence of episodic creep at the updip edge of the seismogenic zone, Costa Rica, *Earth Planet. Sci. Lett., 238*, 189-203.

Outerbridge, K. C., T. H. Dixon, S. Y. Schwartz, J. I. Walter, M. Protti, V. Gonzalez, J. Biggs, M.M. Thorwart, and W. Rabbel (2010), A tremor and slip event on the Cocos-Caribbean Subduction zone as measured by a GPS and seismic network on the Nicoya Peninsula, Costa Rica, *J. Geophys. Res.*, in press.

Acknowledgements: This research was supported by several grants from NSF's MARGINS and Instrumentation and Facilities programs including OCE- 0841061 and OCE-0841091 along with EAR-0842338, EAR-0506463, EAR-0502488, EAR-0842137, EAR-0502221 and EAR-0506382.

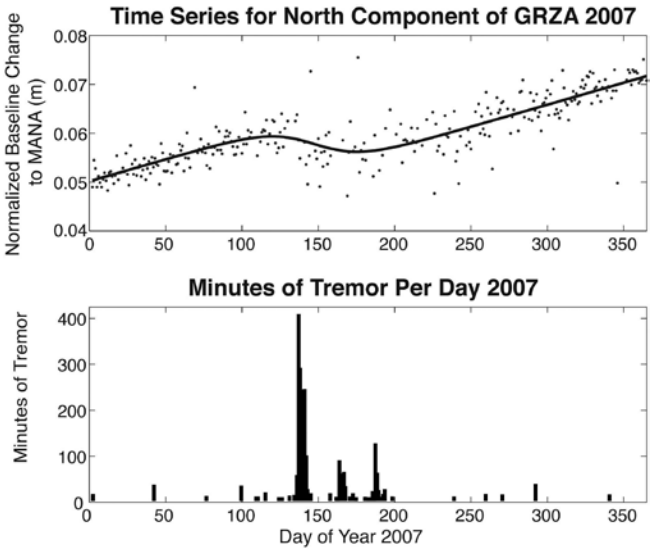

North component of displacement at station GRZA compared to a histogram of cumulative tremor duration per day for the entire year of 2007. The onset and duration of the geodetically determined slow slip correlates well with the peaks in the tremor time series.

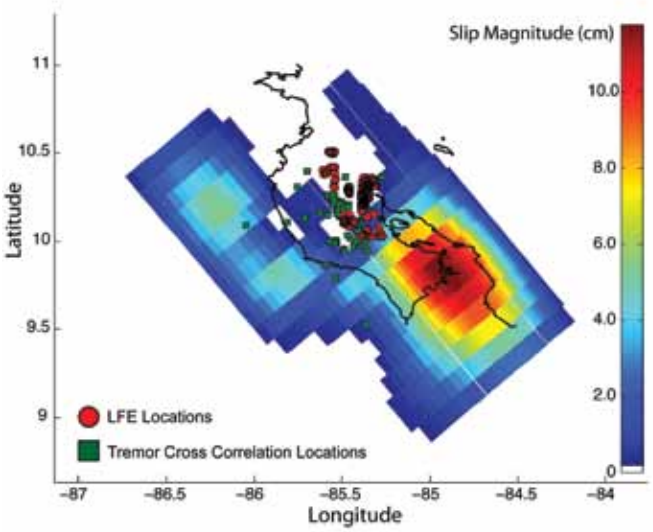

Locations of tremor episodes and Low Frequency Earthquakes (LFEs) compared with the 2007 slow slip distribution.

An Earthquake-Like Magnitude-Frequency Distribution of Tectonic Tremor in Northern Cascadia

Kenneth Creager *(University of Washington),* **Aaron Wech** *(University of Washington),* **Heidi Houston** *(University of Washington),* **John Vidale** *(University of Washington)*

Major episodic tremor and slip (ETS) events with Mw 6.4 to 6.7 repeat every 15 ± 2 months within the Cascadia subduction zone under the Olympic Peninsula. Although these major ETS events are observed to release strain, smaller "tremor swarms" without detectable geodetic deformation are more frequent. We employ a Waveform Envelope Cross-Correlation and Clustering (WECC) [Wech and Creager, 2008] algorithm to search every 50%-overlapping 5-minute window for tremor. The resulting 20,000 tremor epicenters from 2006 through 2009 in northern Washington naturally cluster in space and time into the 91 tremor swarms analyzed here. We find that 88 inter-ETS tremor swarms account for 45% of the total duration of tremor detection during the last three ETS cycles. Considering duration as proportional to moment release, the swarms follow a standard Gutenberg-Richter frequency-magnitude relation, with the major ETS events lying on the trend defined by inter-ETS swarms. This relationship implies that 1) inter-ETS swarms are fundamentally similar to the major events, just smaller and more frequent; and 2) despite fundamental differences in moment-duration scaling, the tremor magnitude-frequency distribution has the same power law trend of normal earthquakes with a b-value of 1.

References

Aguiar, A. C., et al. (2009), Moment release rate of Cascadia tremor constrained by GPS, *J. Geophys. Res., 114*, 1-11.

Wech, A. G., and K. C. Creager (2008), Automated detection and location of Cascadia tremor, *Geophys. Res. Lett., 35*, 1-5.

Acknowledgements: This study was supported by the National Science Foundation/EarthScope (EAR-0545441) and the USGS (08HQGR0034, G09AP00024, G10AP00033). Primary data were supplied by PNSN, EarthScope, PBO and PGC seismometers.

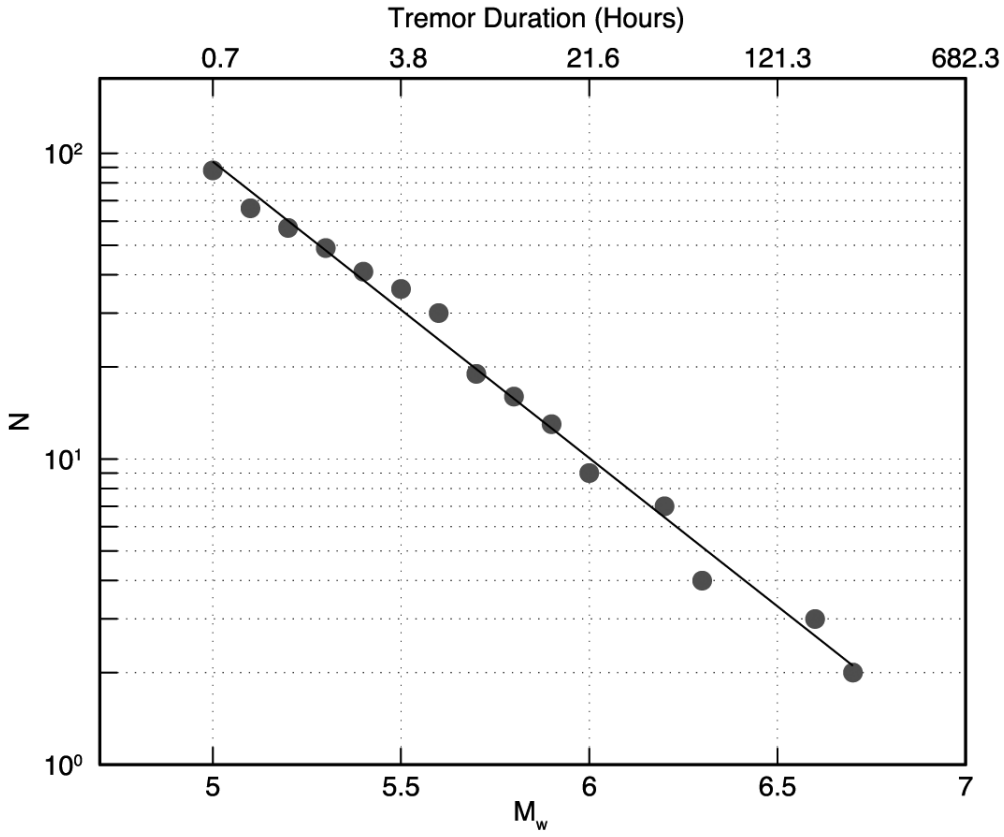

Figure 1. Log of number (N) of tremor swarms exceeding durations given on upper axis can be fit with a straight line indicating that N is proportional to τ ^-0.65 where τ is the duration of a tremor swarm. We assume that the seismic moment is proportional to tremor duration scaled by Mo (N-m) = 5.2x10^16 τ (hrs) [Aguiar et al., 2009] to equate duration (upper axis) to moment magnitude (lower axis). This allows a standard Gutenburg-Richter style analysis and produces a b-value of 1.0 (logN = a − bMw), which is within the range commonly seen for regular earthquakes.

The Slumgullion Natural Laboratory

Joan Gomberg *(US Geological Survey),* **Paul Bodin** *(University of Washington),* **Bill Schulz** *(US Geological Survey),* **Jason Kean** *(US Geological Survey)*

Observational advances continue to reveal diversity in the seismic signals associated with fault slip. A particularly rich example are episodes of slow fault slip near major plate boundaries that manifest as geodetically observed aseismic deformation abetted by a new family of seismic signals (named 'episodic tremor and slip' or ETS). While the driving forces and scales differ, there are striking parallels between some observations and models of ETS and of landslide behaviors. To explore common features and the underlying processes we are studying the Slumgullion landslide in southwest Colorado, and an ideal natural laboratory for observing fault slip and associated phenomena. Unlike crustal- or plate-scale studies significant deformation can be measured within a single field season, because the Slumgullion moves at average rates of up to 2 cm/day. We completed a field experiment on the Slumgullion to test several hypotheses, particularly that slip along the basal surface and side-bounding faults occurs with comparable richness of aseismic and seismic modes as crustal- and plate-scale boundaries. From August 18-26, 2009 we monitored the seismic radiation with 88 short-period vertical seismometers recorded on "Texan" seismographs from the IRIS PASSCAL facility. The seismographs, with interstation spacings of 25-50 m, recorded continuously at 250 samples per second. In addition, we recorded deformation on several extensometers that continuously measure slip across one of the two lateral faults bounding the landslide, and tracked displacements of 29 sites on and off the slide with an automated total-station and differential GPS. More observations came from 2 borehole-mounted piezometers and a meteorological station.

The seismic data contain an abundance of network-wide coherent signals with an amazing variety of characteristics. We observed impulsive earthquakes with clear P,S, and surface wave phases. There are also "repeaters", or multiplets of slidequakes with very similar waveforms. There are episodes of tremor-like radiation coherent across our network. Noteably, a diurnal variation in the slide velocity tracks atmospheric pressure fluctuations, which correlates with the rates of repeating harmonic seismic signals. This correlation and our analyses of the wavefield associated with these events leads us to suggest that the signals are trapped waves generated at a 'sticky spot' within the side-bounding strike-slip fault.

Acknowledgements: This work was funded through the US Geological Venture Capital Program.

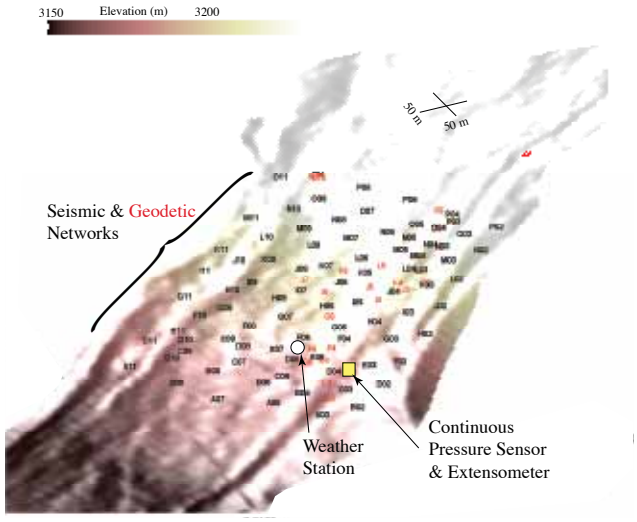

Topographic map of the narrowest and fastest section of the Slumgullion landslide, showing the locations of the seismographs (labeled), weather station, and pressure sensor, all of which recorded continuously. The outer-most lines of seismic stations lie outside the active slide, which is bounded by strike slip faults nearest the seismic stations numbered 03 and 02. R00 is a few meters from the nearest road. 'Geodetic' stations correspond to prisms that serve as targets for the robotic total station and 3 extensometers (2 not shown are located above and below the networks).

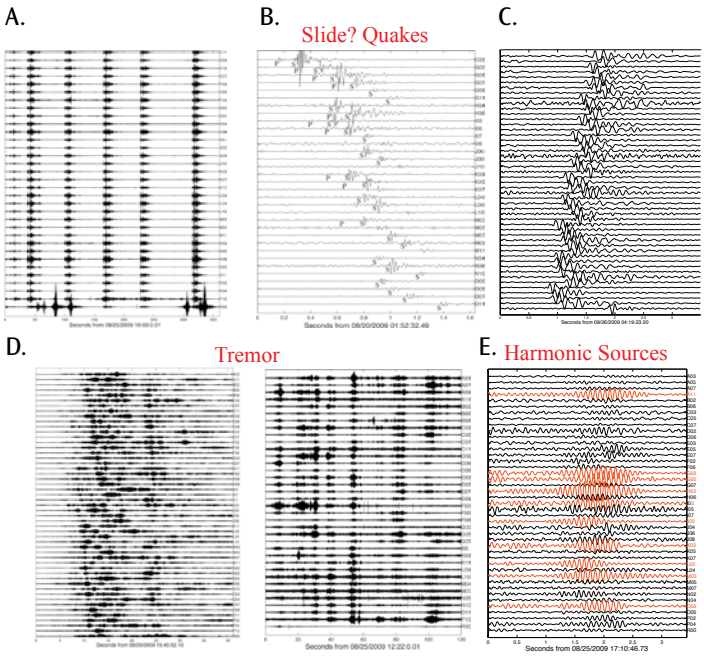

A. The relatively long duration waveforms of events in this vigorous sequence, which lasted several tens of minutes, suggest the sources are similar but not identical in location, mechanism, and size. B. Waveforms from a single, tiny quake show clear P and S arrivals & suggest an impulsive shear source a few hundred meters from station C03. This quake is part of a sequence containing tens of events within a few minutes. C. Example of probable Rayleigh wave packets from similar sources that occurred throughtout the experiment. D. Record of many signals with the same characteristics as tremor observed in plate-scale systems. Their durations last from several seconds to minutes. Although preliminary examination of envelope functions appears to show promise (e.g. envelopes correlate visually at multiple stations), we have yet to quantitatively analyze the tremor signals. E. Record of hundreds of events with waveforms similar to these transient harmonic signals. The largest amplitude signals are shown in orange and are recorded at stations near the side-bounding fault.

Distribution and Triggering Threshold of Non-Volcanic Tremor Near Anza, Southern California

Elizabeth S. Cochran *(University of California, Riverside),* **Tien-Huei Wang** *(University of California, Riverside)*

To study the distribution and characteristics of non-volcanic tremor in Southern California, we use broadband data collected by the Southern California Seismic Network (SCSN) surface stations near Anza, California and five Plate Boundary Observatory (PBO) borehole stations. To determine the stress amplitude and orientation needed to trigger tremor, we examined 41 teleseismic earthquakes chosen with epicentral distances greater than 1900 km, from diverse azimuths and Mw over 7.0 from 2001 to 2008. We found that only the 2002 Mw7.8 Denali earthquake, with the largest surface wave amplitudes of all of the teleseismic events, triggered detectable tremor. We are currently determining more precise locations of individual tremor bursts in the of Denali-triggered NVT using a template-matching method [*Shelly et al., 2009*]. The templates will be used to precisely locate the tremor and to examine the spatial and temporal evolution of triggered tremor. Once the tremor are located, we will determine the precise stress pertubation caused by the Denali earthquake at the tremor hypocenter.We will then compare the triggering threshold for tremor to the stress perturbation from teleseisms that trigger local earthquakes on the San Jacinto Fault. From this study we hope to illuminate differences in the response of earthquakes and tremor to stress pertubations.

References

Shelly, D. R., Ellsworth, W. L., Ryberg, T., Haberland, C., Fuis, G. S., Murphy, J., Nadeau, R. M., and Burgmann, R. (2009), Precise location of San Andreas Fault tremors near Cholame, California using seismometer clusters: Slip on the deep extension of the fault, *Geophys. Res. Lett., 36*, L01303.

Acknowledgements: This work is supported by NSF (EAR0943892) and SCEC (09054).

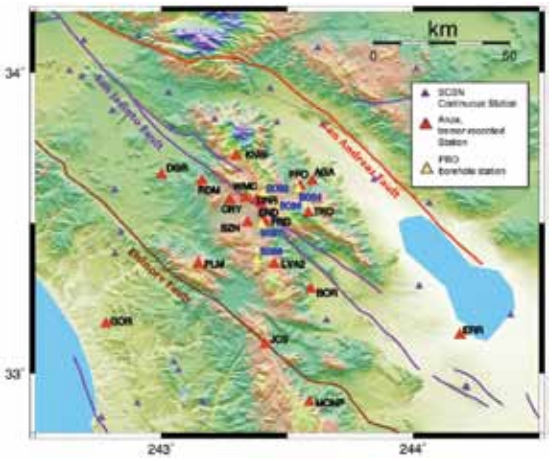

Map of seismic stations using the analysis. SCSN stations that detected tremor are shown by red triangles, borehole stations that detected tremor are shown by yellow triangles, and other SCSN stations are shown by blue triangles.

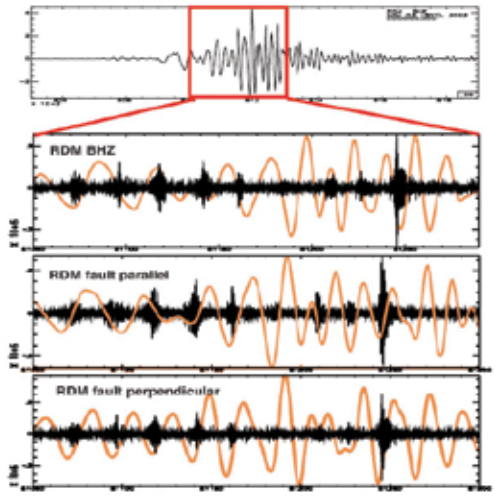

Waveform examples of Denali tremor on station RDM that is triggered by the passing surface waves of the Denali earthquake. The upper panel shows the Denali earthquake recorded on the vertical component of RDM. The region that is expanded in the lower panels is highlighted in red. The lower panels span 250 seconds and show all three components (vertical, fault parallel, and fault perpendicular). The orange curves show the surface waves of the earthquake in nm/sec and the black curves show the data filtered between 2-8 Hz (amplitude is exaggerated by 20,000).

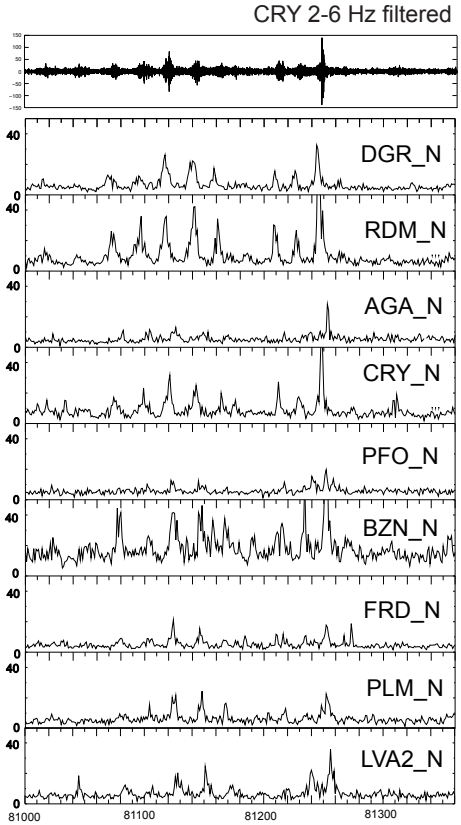

Filtered seismogram (top) and envelope functions of all surface stations that recorded the tremor triggered by the Denali surface waves. Large amplitude bursts are well-correlated in time. Borehole station records are not included in this analysis since most PBO stations were installed after 2006.

Intimate Details of Tremor Observed by a Dense Seismic Array

Abhijit Ghosh *(University of Washington),* **John E. Vidale** *(University of Washington),* **Justin R. Sweet** *(University of Washington),* **Kenneth C. Creager** *(University of Washington),* **Aaron G. Wech** *(University of Washington),* **Heidi Houston** *(University of Washington),* **Emily E. Brodsky** *(University of California Santa Cruz)*

We installed a dense small aperture seismic array in Cascadia, and captured the episodic tremor and slip event in May 2008. We developed a new beam-backprojection (BBP) method to detect and locate non-volcanic tremor [Ghosh et al., 2009]. BBP method detects up to 4 times more duration of tremor during a weak episode, and gives unprecedented resolution in relative tremor location, compared to a conventional envelope cross-correlation method. We track tremor minute-by-minute using BBP method, and map spatiotemporal tremor distribution over different time scales. Over short time scale (several minutes), tremor shows rapid, continuous, slip-parallel migration with a velocity of ~50 km/hr [Ghosh et al., 2010a]. Over the time scale of several hours, slip-parallel tremor bands sweep Cascadia along-strike with a velocity of ~10 km/day [Ghosh et al., 2010b]. Finally, over the time scale of several days, tremor develops distinct moment patches that overlap with geodetic slip patch on the interface [Ghosh et al., 2009]. While heterogeneity on the plate interface may cause tremor moment patches, along-strike stress transfer can explain slow along-strike marching of tremor bands. These varied and intriguing observations lead toward a unified view of tremor distribution in space and time.

References

Ghosh, A., J. E. Vidale, J. R. Sweet, K. C. Creager, A. G. Wech, and H. Houston (2010a), Toward a unified view of tremor distribution in space and time, *Seismol. Res. Lett., 81*(2), pp. 297 (SSA Annual Meeting 2010)

Ghosh, A., J. E. Vidale, J. R. Sweet, K. C. Creager, A. G. Wech, and H. Houston (2010b), Tremor bands sweep Cascadia, *Geophys. Res. Lett., 37*, L08301.

Ghosh, A., J. E. Vidale, J. R. Sweet, K. C. Creager, and A. G. Wech (2009), Tremor patches in Cascadia revealed by seismic array analysis, *Geophys. Res. Lett., 36*, L17316.

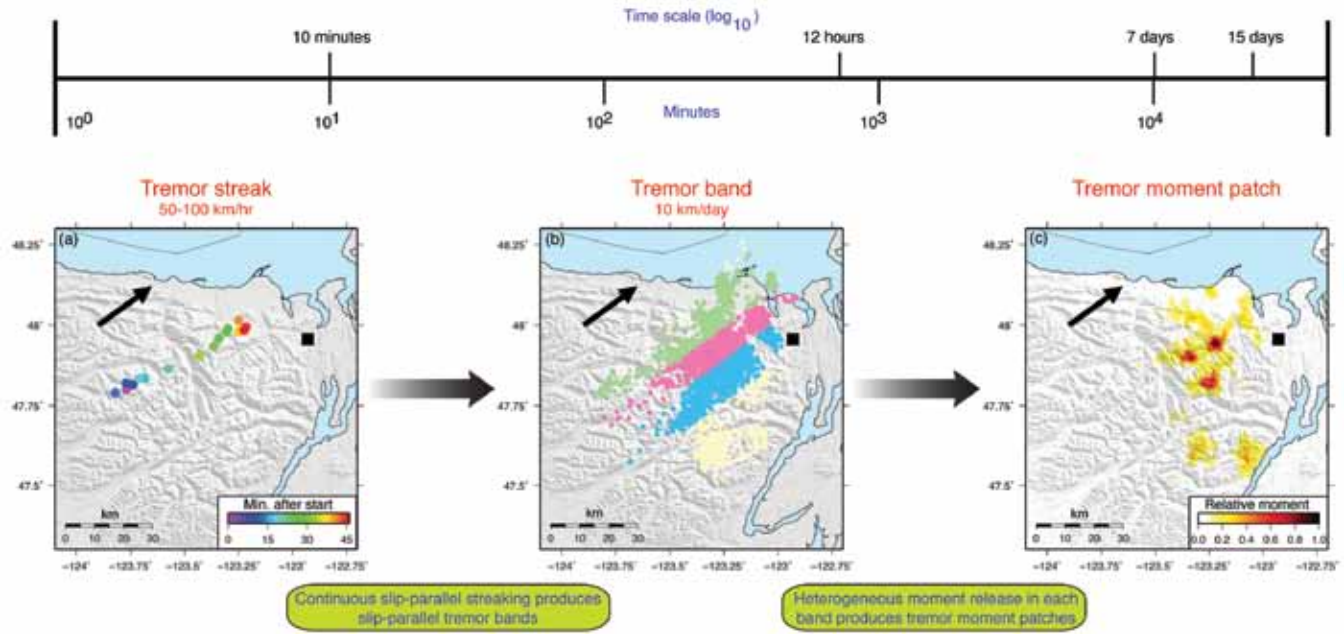

A unified view of tremor distribution in time and space: a time scale (log10) is shown at the top. The maps show different elements of spatiotemporal tremor distribution observed over different time scales. Positions of the maps along the time scale approximately correspond to the time scales over which these elements are typically observed. Arrow in each map indicates slip direction of CSZ. Black solid square marks the Big Skidder array. (a) Slip-parallel tremor streak. Colored circles represent tremor locations. Time is color-coded to show rapid tremor migration over short time scale. (b) Slip-parallel tremor bands defining the long-term slower along-strike tremor migration over time-scales of hours to a day. Solid colored circles are tremor locations. Blue, pink, and green locations define the tremor bands. Faint yellow locations fall outside the tremor bands. (c) Relative band-limited tremor moment patches that release much of the seismic moment during an ETS event.

Tidal Triggering of LFEs Near Parkfield, CA

Amanda Thomas *(University of California - Berkeley),* **Roland Burgmann** *(University of California - Berkeley),* **David Shelly** *(United States Geological Survey)*

Studies of nonvolcanic tremor (NVT) in Japan, Cascadia, and Parkfield, CA have established the significant impact of small stress perturbations, such as the solid earth and ocean tides, on NVT generation [*Thomas et al., 2009 and references therein*]. Similar results irrespective of tectonic environment suggest that extremely high pore fluid pressures are required to produce NVT. We analyzed the influence of the solid earth and ocean tides on a catalog of ~500,000 low frequency earthquakes (LFEs) constituting 88 event families distributed along a 150-km-long section of the San Andreas Fault centered at Parkfield [*Shelly, D. R. and J. L. Hardebeck, 2010*]. LFEs comprising the tremor signal are grouped into families based on waveform similarity and precisely located using waveform cross-correlation. Analogous to repeating earthquakes, LFE families are thought to represent deformation on the same patch of fault. While the locations of repeating earthquakes are assumed to be coincident with the location of asperities in the otherwise aseismically creeping fault zone, NVT occur below the seismogenic zone, where fault zones behave ductilely. We explored the sensitivity of each of these LFE families to the tidally induced shear (RLSS) and normal (FNS), and stresses on the SAF [*Thomas et al., 2010*]. Nearly all of the 88 LFE families are triggered by positive RLSS and in general correlation increases as a function of depth. Some LFE families experience enhanced triggering during times of extensional normal stress while others preferentially respond to compression. The level of correlation appears to be spatially continuous along the fault but exhibits no depth dependence. Future research efforts will focus on using the LFE response to tidal influence to place constraints on the mechanical properties of the deep San Andreas fault.

References

Thomas, A.M., R. M. Nadeau, and R. Burgmann (2009) Tremor-tide correlations and near-lithostatic pore pressure on the deep San Andreas fault. *Nature. 462*, 1048-1051, doi:10.1038/nature08654.

Shelly, D. R., and J. L. Hardebeck (2010), Precise tremor source locations and amplitude variations along the lower-crustal central San Andreas Fault, *Geophys. Res. Lett.*, doi:10.1029/2010GL043672, in press.

Thomas, A.M., Burgmann, R. and D. Shelly (2010) Tidal triggering of LFEs near Parkfield, CA. SSA annual meeting. Poster presentation.

Acknowledgements: This work was supported by the NSF and the USGS.

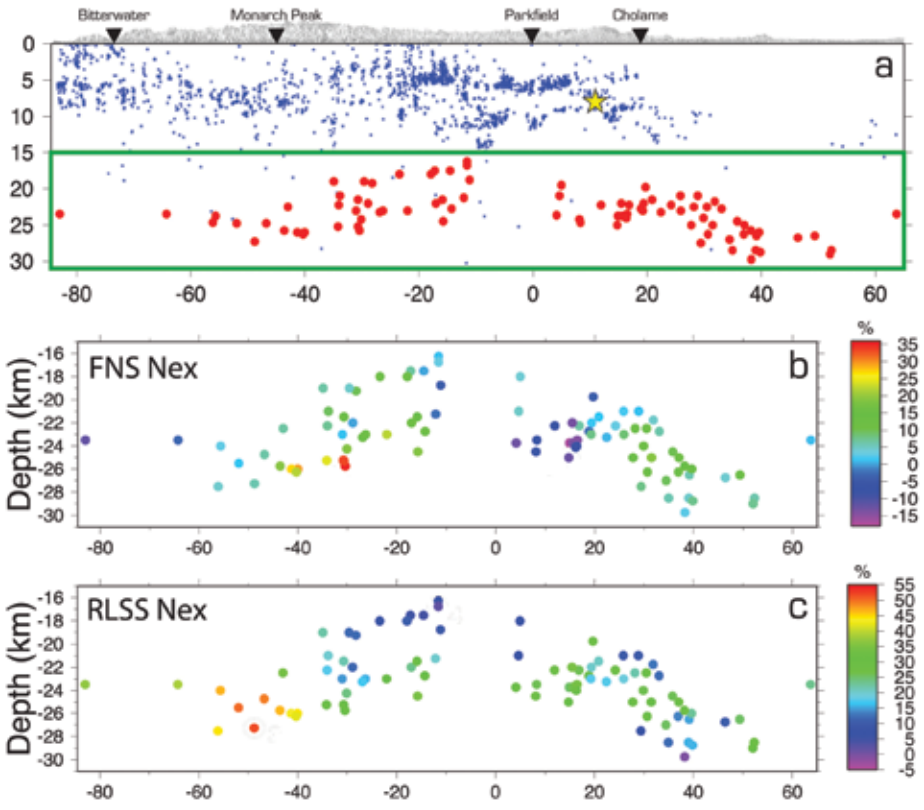

Figure 1: (a) Along-fault cross section of the SAF viewed from the south-west. Vertically exaggerated topography is shown in grey. Local towns are marked by inverted triangles. Hypocenters of SAF seismicity, the 2004 Parkfield earthquake, and LFE locations are shown as blue dots, yellow star, and red circles respectively. Panels (b) and (c) are delineated by the green box. (b) LFE locations color coded by their FNS Nex (percent excess = [actual number of LFEs during times of positive FNS – expected number of LFEs during times of positive FNS]/expected number of LFEs during times of positive FNS). (c) LFE locations color coded by the RLSS Nex values.

Global Search of Triggered Tremor and Low-Frequency Earthquakes

Zhigang Peng *(Georgia Institute of Technology)*

Deep "non-volcanic" tremor and episodic slow-slip events are among the most interesting discoveries in earthquake seismology in the last decade. These events have much longer source durations than regular earthquakes, and are generally located near or below the seismogenic zone where regular earthquakes occur. Tremor and slow-slip events appear to be extremely stress sensitive, and could be instantaneously triggered by distant earthquakes and solid earth tides. We have conducted a global search of triggered tremor and low-frequency earthquakes (LFEs) associated with large regional and teleseismic earthquakes. These include the Parkfield-Cholame section of the San Andreas Fault [Gomberg et al., 2008; Peng et al., 2009], the Calaveras fault in northern California and the San Jacinto Fault in southern California [*Gomberg et al., 2008*], and beneath the Central Range in Taiwan [Peng and Chao, 2008]. In several places, we found that tremor is often initiated by the Love waves, and continues to be modulated during the subsequent Rayleigh waves. Many LFEs were identified during the triggered tremor episode, and triggered LFEs sometimes showed fast migrations along the fault strike, similar to ambient LFEs/tremor and possibly reflecting triggered micro-slow-slip events. Long-period and large-amplitude surface waves from both regional and teleseismic events have a greater potential of triggering tremor, and inferred triggering threshold is on the order of ~1kPa, suggesting that the deep faults are critically stressed, most likely due to near-lithostatic fluid pressures.

References

Gomberg, J., J. L. Rubinstein, Z. Peng, K. C. Creager, and J. E. Vidale (2008), Widespread triggering of non-volcanic tremor in California, S*cience, 319*, 173.

Peng, Z., and K. Chao (2008), Non-volcanic tremor beneath the Central Range in Taiwan triggered by the 2001 Mw7.8 Kunlun earthquake, *Geophys. J. Int.* (Fast track), 825, 829.

Peng, Z., J. E. Vidale, A. Wech, R. M. Nadeau and K. C. Creager (2009), Remote triggering of tremor along the San Andreas fault in central California, *J. Geophys. Res., 114*, B00A06.

Acknowledgements: This work was supported by the National Science Foundation (EAR-0809834, EAR-0956051).

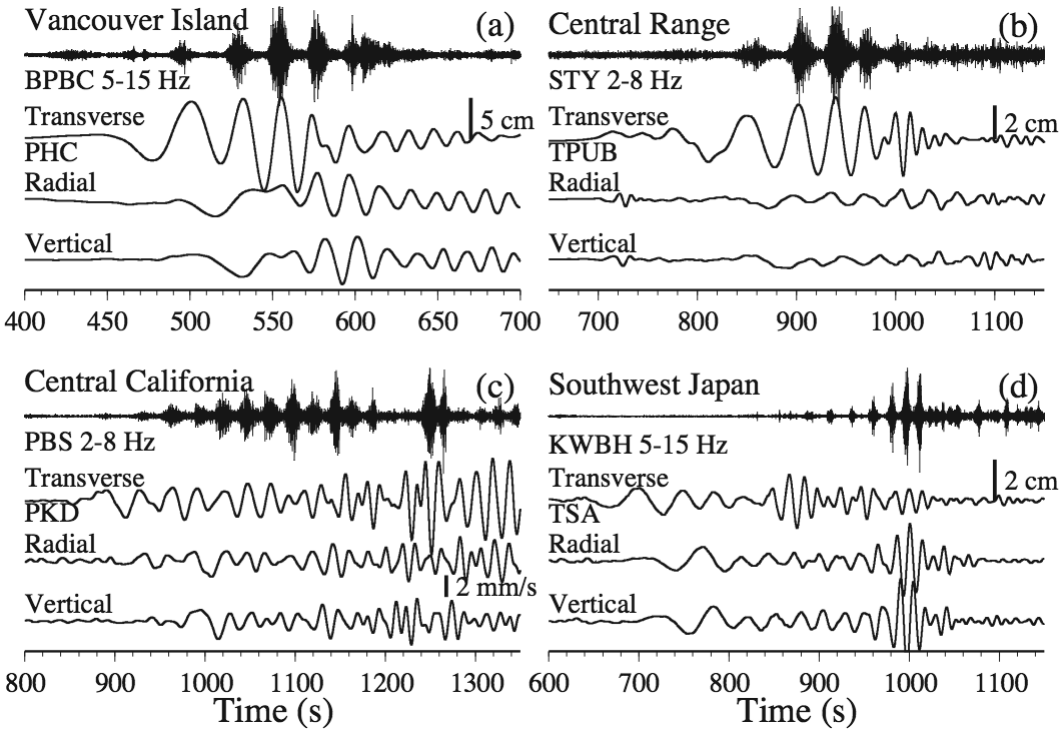

A comparison of surface waves of large teleseismic earthquakes and triggered tremor beneath (a) Vancouver Island in British Columbia [Rubinstein et al., 2007], (b) the Central Range in Taiwan [Peng and Chao, 2008], (c) the San Andreas Fault in Central California [Peng et al., 2009], and (d) the subduction zone is Southwest Japan [Miyazawa et al., 2008]. The traces have been time-shifted to reflect the relationship between the surface waves and tremor at the source region.

Cascadia Transition Zone: Tremor as a Fault Strength Indicator

Aaron Wech *(University of Washington),* **Ken Creager** *(University of Washington)*

As oceanic lithosphere descends beneath continents in subduction zones worldwide, the contact between the two plates undergoes a transformation in response to a variety of physical parameters that vary with increasing depth. The result of this transformation is a transition in fault coupling from fully locked on the shallow, updip side to stable sliding downdip where the oceanic plate descends into the mantle. But how this transition zone works is not entirely understood. Updip of tremor, the fault yields no displacement for hundreds of years, constantly accumulating stress before breaking in the form of a megathrust earthquake. On the downdip side, the plates are thought to stably slide past each other at a constant rate without increasing stress. By accumulating stress for months to years between discrete episodes of stable moment release, episodic tremor and slip (ETS) provides an intermediate mechanism for accommodating plate convergence between the locked and stable sliding end members in relatively young, warm subduction zones. We use automatically detected tectonic tremor as a slow slip indicator in northern Cascadia to observe updip migration and a depth-dependent transition in slip size and periodicity. Our observations fill in the transition zone spectrum with a continuum of slow slip behavior that reflects the fault strength. This behavior is explained by a fractal-like stress transfer model controlled by friction, which provides a new and intuitive understanding of subduction zone dynamics.

References

Wech, A.G., and K.C. Creager (2010) Cascadia transition zone: tremor as a fault strength indicator, IRIS Meeting.

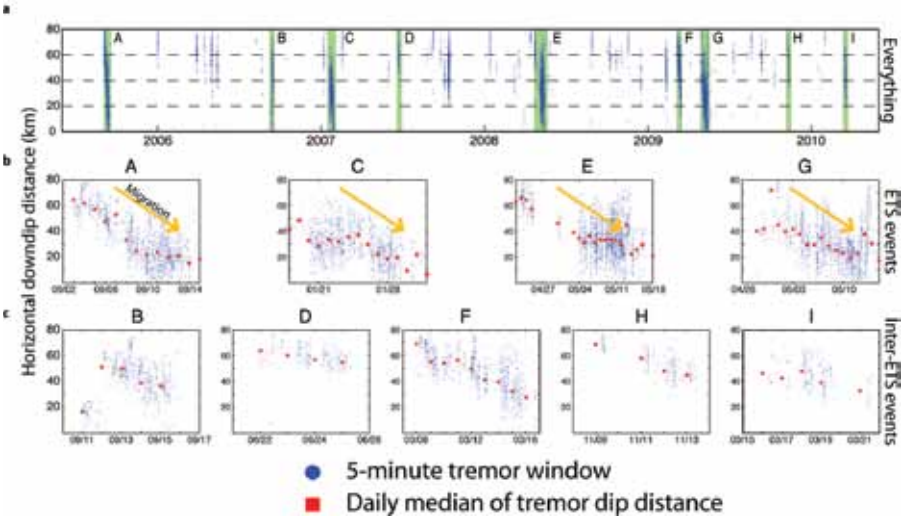

Updip tremor migration. (a) Horizontal downdip tremor distance versus time of northern Washington catalog showing many small swarms downdip and larger swarms initiating deep and migrating updip. (b) Migration for the past 4 ETS episodes. Blue dots represent tremor epicenters and red squares show median daily downdip distance. (c) Example migration of 5 small and large inter-ETS tremor swarms.

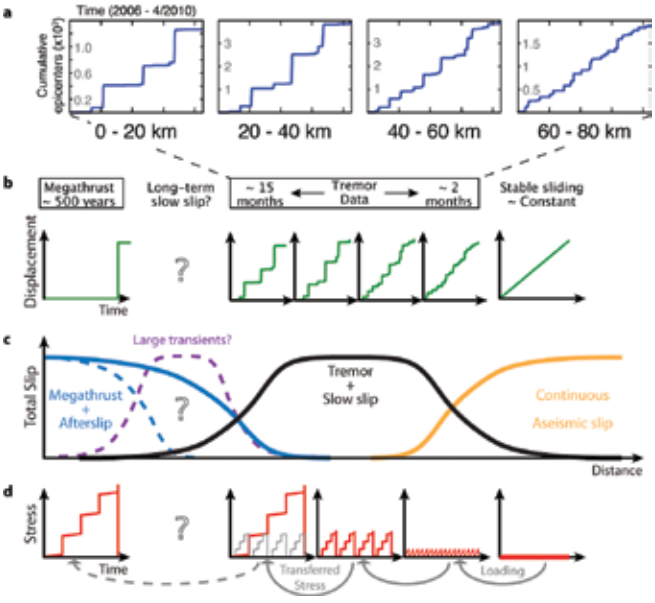

Displacement history profiles and transition zone model. (a) Cumulative tremor profiles in each strike-perpendicular bin showing a transition from small, frequent slip downdip to larger, less frequent slip updip. (b) Profiles of displacement timelines from the locked zone to stable sliding with results from a inserted in the transition zone. (c) Profile schematic showing how the different regions accommodate plate convergence. Our results may predict long-term slow slip updip (purple dashed line), which would shift the downdip limit of the megathrust (blue dashed line) updip. (d) Schematic profile of stress timelines illustrating our stress transfer model. Stable sliding loads the downdip tremor region, which is weakly coupled and slips easily. Each slip relieves stress locally and transfers stress updip to a stronger portion of the fault with a higher stress threshold. This is a fractal-like process where the local stress is the integrated effect of downdip slip.

Slab Morphology in the Cascadia Fore Arc and Its Relation to Episodic Tremor and Slip

Pascal Audet *(University of California Berkeley),* **Michael Bostock** *(University of British Columbia),* **Devin Boyarko** *(Miami University),* **Mike Brudzinski** *(Miami University),* **Richard Allen** *(University of California Berkeley)*

Episodic tremor and slip (ETS) events in subduction zones occur in the general vicinity of the plate boundary, downdip of the locked zone. In developing an understanding of the ETS phenomenon it is important to relate the spatial occurrence of nonvolcanic tremor to the principal structural elements within the subduction complex. In Cascadia, active and passive source seismic data image a highly reflective, dipping, low-velocity zone (LVZ) beneath the fore-arc crust; however, its continuity along the margin is not established with certainty, and its interpretation is debated. In this work we have assembled a large teleseismic body wave data set comprising stations from northern California to northern Vancouver Island. Using stacked receiver functions we demonstrate that the LVZ is well developed along the entire margin from the coast eastward to the fore-arc basins (Georgia Strait, Puget Sound, and Willamette Valley). Combined with observations and predictions of intraslab seismicity, seismic velocity structure, and tremor hypocenters, our results support the thesis that the LVZ represents the signature of subducted oceanic crust, consistent with thermal-petrological modeling of subduction zone metamorphism. The location of tremor epicenters along the revised slab contours indicates their occurrence close to but seaward of the wedge corner. Based on evidence for high pore fluid pressure within the oceanic crust and a downdip transition in permeability of the plate interface, we propose a conceptual model for the generation of ETS where the occurrence and recurrence of propagating slow slip and low-frequency tremor are explained by episodic pore fluid pressure buildup and fluid release into or across the plate boundary.

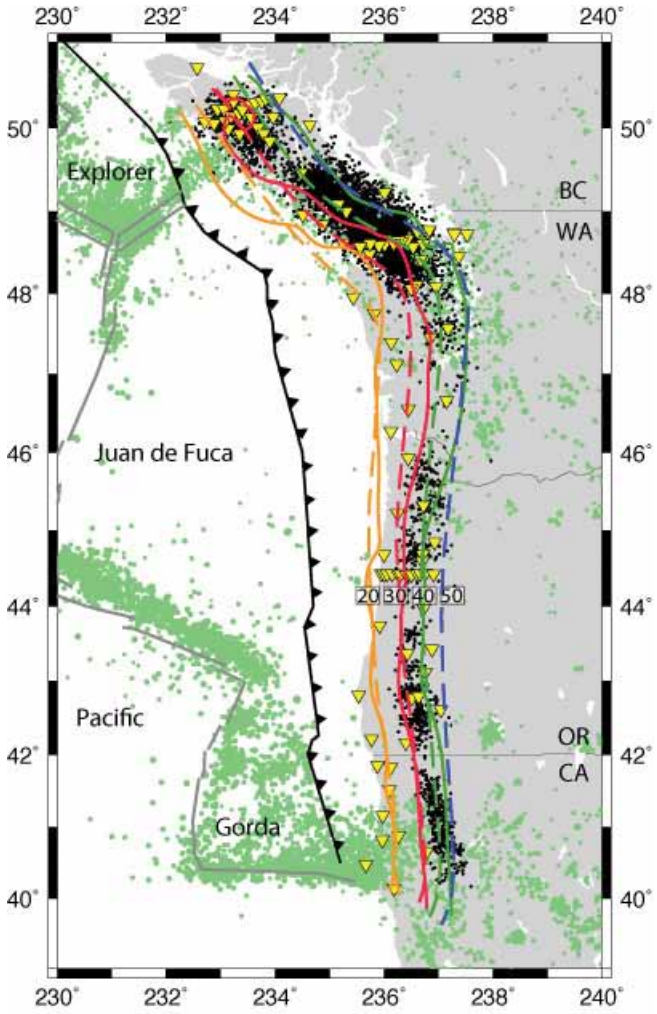

Depths contours of the top of the plate interface from receiver functions (this study, solid lines) and a compilation of various studies (dashed lines, McCrory et al., 2006) along the Cascadia margin. Earthquake epicenters from the GSC and USGS catalogues for M > 2 are shown as green dots; tremor epicenters appear as black dots. Broadband stations used in the analysis are displayed as inverted yellow triangles. Numbers indicate depth (in km) to each contour. Solid black line with arrowheads indicates the location of the trench offshore.

References

Audet, P., M. G. Bostock, D. C. Boyarko, M. R. Brudzinski, and R. M. Allen (2010), Slab morphology in the Cascadia fore arc and its relation to episodic tremor and slip, *J. Geophys. Res., 115*, B00A16

McCrory, P. A., J. L. Blair, and D. H. Oppenheimer (2006), Depth to the Juan de Fuca slab beneath the Cascadia subduction margin—A 3-D model for sorting earthquakes, U.S. Geol. Surv. Data Ser., 91, U.S. Geol. Surv., Reston, Va. (Available at http://pubs.usgs.gov/ds/91/)

Acknowledgements: This work was partially funded by the Miller Institute for Basic Research in Science (UC Berkeley) through a Fellowship to P.A., the Natural Science and Engineering Research Council (Canada), and the National Science Foundation. Data are made available by the Canadian National Data Center (CNDC) and the IRIS consortium.

Regional Moment Tensor Solutions for Source-Type Identification: The Crandall Canyon Mine Collapse

Douglas Dreger *(Berkeley Seismological Laboratory),* **Sean Ford** *(Lawrence Livermore National Laboratory),* **William Walter** *(Lawrence Livermore National Laboratory)*

Seismic moment tensor methods are now routinely applied at many scales from the study of micro-earthquakes to the characterization of damaging great earthquakes, and applied at regional distances they are proving to be a reliable tool for distinguishing between earthquakes and events associated with volcanic processes [*e.g. Dreger et al., 2000*], and other man-made sources of seismic radiation such as from explosions, or mining activity [*e.g. Ford et al., 2009*]. On August 6, 2007 a magnitude 3.9 seismic event was associated with the tragic collapse of a Utah coal mine. The event was well recorded by UUSS, USGS, and Earthscope USAarray stations (Fig. 1) The moment tensor inversion of complete, three-component, low-frequency (0.02 to 0.10 Hz) displacement records recovers a mechanism that is most consistent with the gravity driven vertical collapse of a horizontally oriented underground cavity (Fig. 1a). The seismic moment tensor of the event, is comprised 78% from a closing horizontal crack and a secondary 22% non-crack component, which results from the fitting of the large amplitude Love waves that were observed on the tangential component (Fig. 1c). Plausible interpretations of the secondary source include sympathetic vertical dip-slip faulting, non-uniform crack closure, and elastic relaxation in response to the mine collapse [*Ford et al., 2008*]. The moment tensor solution produces a pure dilatational P-wave first-motion mechanism consistent with the P-wave polarity observations [Pechman et al., 2008]. The source-type diagram [*Hudson et al., 1989*] in Fig. 1a illustrates the deviation from a pure earthquake double-couple (DC) source at the center in terms of a volumetric component (explosion or implosion) on the ordinate, and deviatoric component in terms of a volume compensated linear vector dipole (CLVD) on the abscissa. The mine-collapse event plots in the region of a negative or closing crack similar to solutions obtained for other mine and Nevada Test Site (NTS) cavity collapses [*Ford et al., 2009*]. The application of seismic moment tensor analysis to non-tectonic seismic events such as buried explosions or underground collapses as illustrated here, demonstrates the feasibility of continuous monitoring of regional distance seismic wavefields for source-type identification useful for nuclear explosion monitoring and possible emergency response.

References

Dreger, D. S., H. Tkalcic, and M. Johnston (2000). Dilational processes accompanying earthquakes in the Long Valley Caldera, *Science, 288,* 122-125.

Ford, S., D. Dreger and W. Walter (2008). Source Characterization of the August 6, 2007 Crandall Canyon Mine Seismic Event in Central Utah, *Seismol. Res. Lett., 79,* 637-644.

Ford, S. R., D. S. Dreger, and W. R. Walter (2009), Identifying isotropic events using a regional moment tensor inversion, *J. Geophys. Res., 114,* B01306.

Acknowledgements: We acknowledge DOE BAA contract DE-FC52-06NA27324 (BSL) and Contract W-7405-Eng-48 (LLNL) for support of this work.

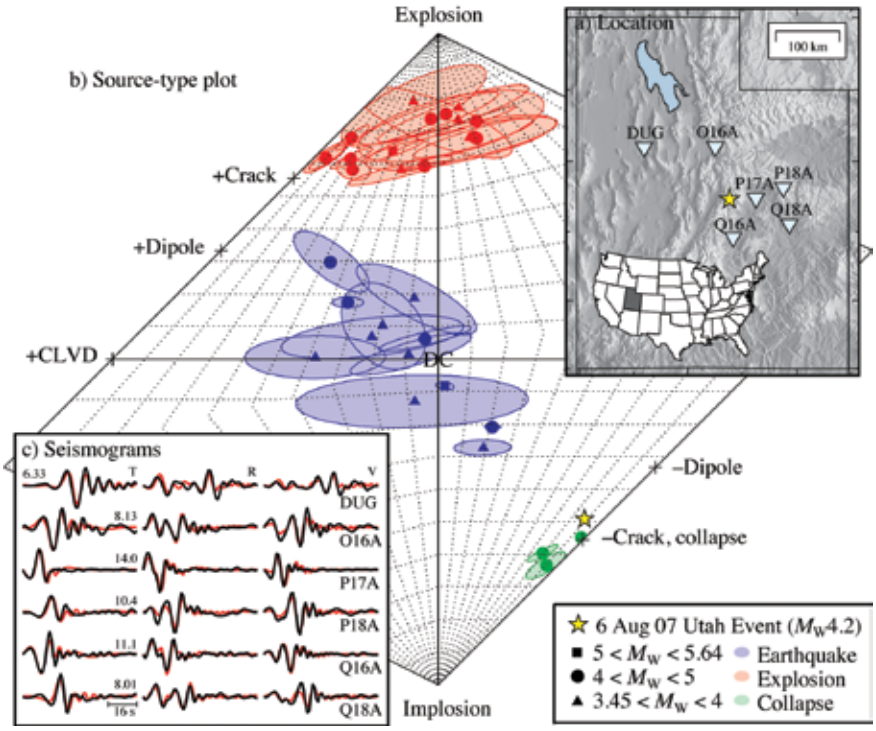

Fig 1. A) Source type plot showing separation of earthquake, explosion and collapse (yellow star shows the 08/06/2007 mine-collapse event). B) Location of the 08/06/2007 mine-collapse event and the 6 closest stations. C) Observed (black) and predicted (red) displacement waveforms (0.02 to 0.1 Hz).

Source Analysis of the Memorial Day Explosion, Kimchaek, North Korea

Sean R. Ford *(Lawrence Livermore National Laboratory),* **William R. Walter** *(Lawrence Livermore National Laboratory),* **Douglas S. Dreger** *(Berkeley Seismological Laboratoy)*

We perform a series of source inversions for the 25 May 2009 (Memorial Day) North Korean seismic event using intermediate period (10-50s) complete waveform modeling using data housed at IRIS. An earthquake source is inconsistent with the data and the best-fit full seismic moment tensor is dominantly explosive (~60%) with a moment magnitude (Mw) of 4.5. A pure explosion solution yields a scalar seismic moment of 1.8e22 dyne-cm (Mw4.1) and fits the data almost as well as the full solution. The difference between the full and explosion solutions is the predicted fit to observed tangential displacement, which requires some type of non-isotropic (non-explosive) radiation. Possible causes of the tangential displacement are additional tectonic sources, tensile failure at depth, and anisotropic wave propagation. Similar displacements may be hidden in the noise of the 2006 event. Future analyses of this type could be used to identify and characterize non-earthquake events such as explosions and mine collapses.

References

Ford, S.R., D. Dreger, and W. R. Walter, Source analysis of the Memorial Day explosion, Kimchaek, North Korea, *Geophys. Res. Lett., 36* (L21304), 2009

Acknowledgements: We acknowledge DOE BAA contract DE-FC52-06NA27324 (BSL) and Contract W-7405-Eng-48 (LLNL) for suppor

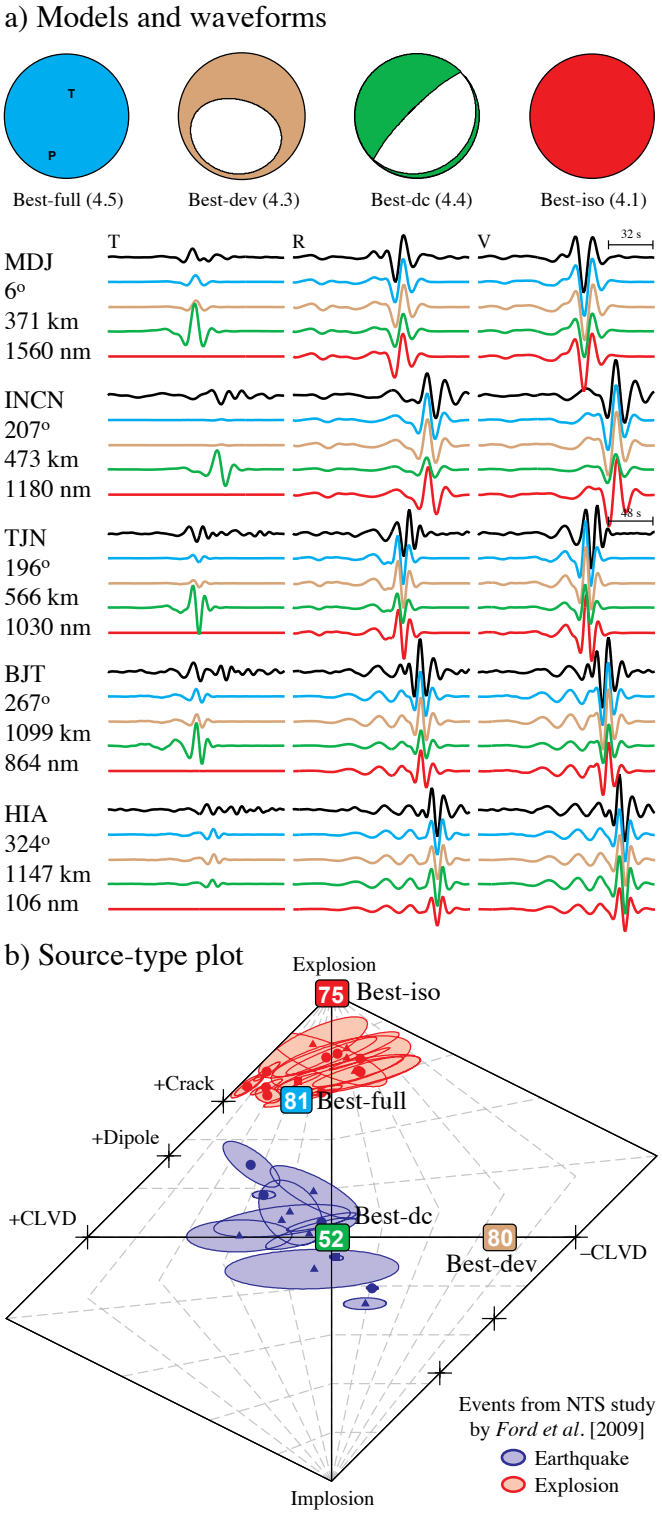

a) Models and their respective forward-predicted waveforms as a function of color compared with the actual waveforms (black line) all filtered between 10-50 sec period. b) Source-type plot with various solutions corresponding to the models given in a) and their associated fit percent.

Studying Earth's Wave Climate Using the Global Microseism

Richard Aster *(New Mexico Institute of Mining and Technology),* **Daniel McNamara** *(US Geological Survey, Golden, CO),* **Peter Bromirski** *(Integrative Oceanography Division, Scripps Institution of Oceanography, UC San Diego)*

Globally ubiquitous seismic background noise peaks, visible as broad peaks in seismic spectra with modes near 7 and 14 s period, are generated via two distinct mechanisms that transfer storm-generated gravity wave energy to the seismic wave field. Continuous digital ground motion data recorded by the Global Seismographic Network and precursor networks provide a unique integrative record of ocean wave to seismic coupling at regional to global scales [Aster et al., 2008] that can be applied to chronicle microseism power extreme events over hourly to decadal time periods. Because most land-observed microseism surface wave energy is generated at or near coasts [e.g. Bromirski et al., 1999], microseism metrics are particularly relevant to assessing changes in coastal ocean wave energy. For example, extreme microseism winter storm season event counts quantify the widespread wave influence of the El Nino Southern Oscillation (ENSO). The double-frequency (near 7 s) microseism is generated by interacting (standing wave) components of the ocean wave field, and is observed to be particularly volatile, likely both because of its quadratic dependence on wave height and because of its sensitivity to both incident wave angle and to coastal conditions that control ocean swell reflectivity. This suggests that the weaker single-frequency (near 14 s) microseism directly generated by ocean swell at coasts is a more representative seismic proxy for broad-scale ocean wave energy estimation. Metrics of extreme microseism events since the 1970s suggest slight positive trends in the northern hemisphere, and slightly declining trends in the Southern Hemisphere [Aster et al., 2010]. Microseism metrics are extendable to the pre-digital era through the digitization of analogue seismograms from long-running observatories, and thus offer the opportunity to quantify and characterize the wave influence of ENSO and other climate variations through to the early 20th century.

References

Aster, R., D.E. McNamara, and P. Bromirski (2008), Multi-decadal climate-induced variability in microseisms, *Seismol. Res. Lett., 79*, 194-202, doi:10.1785/gssrl.79.2.194.

Aster, R., D.E. McNamara, and P. Bromirski (2010), Global Trends in Extremal Microseism Intensity, *Geophys. Res. Lett*. in press.

Bromirski, P. D., R. E. Flick, and N. Graham (1999), Ocean wave height determined from inland seismometer data: Implications for investigating wave climate changes in the Northeast Pacific, *J. Geophys. Res.*, 104, 20,753-20,766.

Acknowledgements: The Global Seismographic Network is a cooperative scientific facility operated jointly by the Incorporated Research Institutions for Seismology, the United States Geological Survey (USGS), and the National Science Foundation. P. Bromirski has been supported in this research by the California Department of Boating and Waterways. Richard Boaz contributed significantly to database programming.

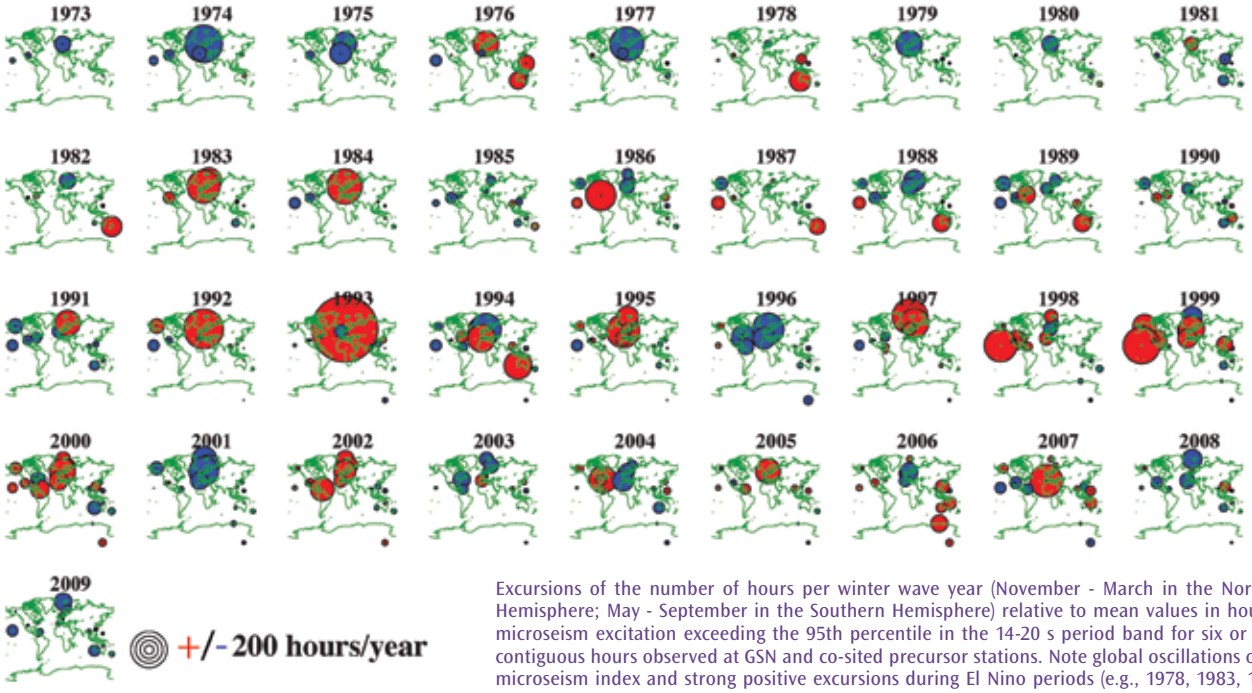

Excursions of the number of hours per winter wave year (November - March in the Northern Hemisphere; May - September in the Southern Hemisphere) relative to mean values in hours of microseism excitation exceeding the 95th percentile in the 14-20 s period band for six or more contiguous hours observed at GSN and co-sited precursor stations. Note global oscillations of this microseism index and strong positive excursions during El Nino periods (e.g., 1978, 1983, 1998). After Aster et al. (2010).

Iceberg Tremor and Ocean Signals Observed with Floating Seismographs

Richard Aster *(New Mexico Institute of Mining and Technology),* **Douglas MacAyeal** *(University of Chicago),* **Peter Bromirski** *(Integrative Oceanography Division, Scripps Institution of Oceanography, UC San Diego),* **Emile Okal** *(Northwestern University)*

Recent deployments of broadband seismometers atop Earth's largest floating ice bodies, the ice shelves and tabular icebergs of Antarctica have spurred the study of seismic and inertial phenomena associated with the dynamic (ocean tide- and ocean-wave-driven forcing) interaction of these bodies with the oceans, with the seafloor, and with each other. Harmonic and chaotic tremor-like signals generated by floating ice undergoing dynamic processes (collision and breakup) have been studied using both floating ice-deployed seismometry [*MacAyeal et al., 2008; Martin et al., 2010*] and by far-flung instruments at out to teleseismic/transoceanic distances. While much remains to be learned about the phenomenology and processes of these tremor sources and their impact on ice-body integrity, PASSCAL deployments in the Ross Sea region have shown that highly harmonic episodes of iceberg tremor are generated by extraordinarily sequences of repetitive stick-slip icequakes occurring at ice-ice contacts [*MacAyeal et al., 2008*], and that more chaotic signals, with some harmonic components, are generated during the grounding, during both breakup and nondestructive collisions [*Martin et al., 2010*]. Seismometers deployed atop floating ice further function as exquisitely sensitive buoys that can detect and characterize transoceanic swell, infragravity waves [*Cathles et al., 2009; Bromirski et al., 2010*], tsunamis [*Okal et al., 2006*], and regional ocean wave trains arising from calving icebergs [*MacAyeal et al., 2009*]. Recent work suggests that networks of seismometers on floating ice shelves can also uniquely measure repetitive ocean-driven strain fields that are projected to increase in frequency under climate change scenarios, and may contribute to the breakup of ice shelves [*Bromirski et al., 2010*].

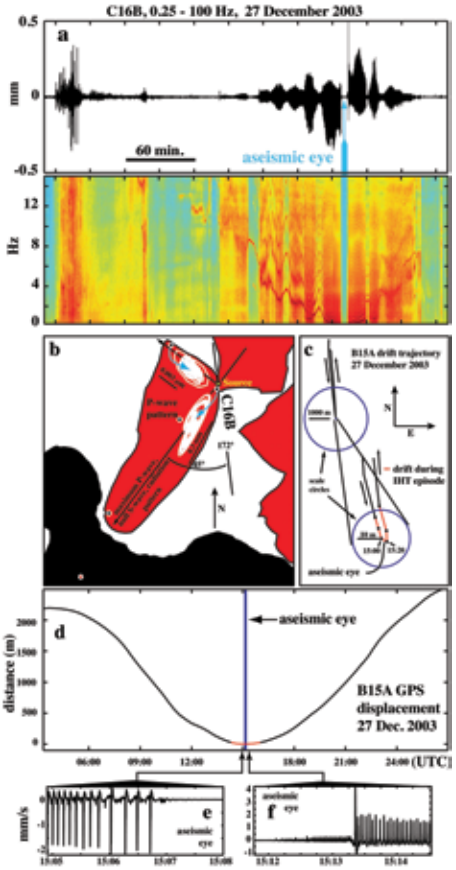

Iceberg tremor recorded by PASSCAL seismographs on iceberg C16 near Ross Island, Antarctica. a) Iceberg harmonic tremor (IHT) recorded bat C16B displayed as a vertical displacement seismogram and spectrogram; note the aseismic "eye". b) Map of station deployment, outline of Ross Island (black); icebergs (red); locations of C16 seismographs (white dots). White traces show particle motion at two stations (B and C) during IHT excitation; note quasi-P particle motion consistent with horizontal stick-slip motion between C16 and the moving B15A to the northwest. c) B15A GPS tidally-driven position relative to (the fixed) C16; lower graph shows a blowup showing reversing motion during IHT excitation (red). d) B15A GPS position showing the timing of the eye (a) and IHT tremor period (red). e and f) expanded view of seismogram showing repeating reversing stick-slip events due to the relative iceberg motions shown in (c) and (d); note polarity reversal as B15 motion reverses. After MacAyeal et al. [2008]

References

Bromirski, P., Sergienko, O., MacAyeal, D. (2010). Transoceanic infragravity waves impacting Antarctic ice shelves, Geophys. *Res. Lett., 37*, L02502, doi:10.1029/2009GL041488.

Cathles, L.M., Okal, E., MacAyeal, D. (2009). Seismic observations of sea swell on the floating Ross Ice Shelf, Antarctica, *J. Geophys. Res., 114*, F02015, doi:10.1029/2007JF000934.

MacAyeal, D. R., Okal, E., Aster, R., Bassis, J. (2008). Seismic and hydroacoustic tremor generated by colliding icebergs, J. *Geophys. Res., 113*, F03011, doi:10.1029/2008JF001005.

MacAyeal, D., Okal, E., Aster, R., Bassis, J. (2009). Seismic observations of glaciogenic ocean waves (micro-tsunamis) on icebergs and ice shelves, *J. Glaciology, 55*, 193-206, doi:10.3189/002214309788608679.

Martin, S., et al. (2010). Kinematic and seismic analysis of giant tabular iceberg breakup at Cape Adare, Antarctica, *J. Geophys. Res., 115*, B06311, doi:10.1029/2009JB006700.

Okal, E., MacAyeal, D. (2006). Seismic recording on drifting icebergs: Catching seismic waves, tsunamis and storms from sumatra and elsewhere, *Seismol. Res. Lett., 77*, 659-671, doi:10.1785/gssrl.77.6.659.

Acknowledgements: Instruments were provided by IRIS through the PASSCAL Instrument Center at New Mexico Tech. The Global Seismographic Network (GSN) is a cooperative scientific facility operated jointly by the Incorporated Research Institutions for Seismology, the USGS, and the National Science Foundation. All seismic data in this paper are available from the IRIS Data Management Center. Financial and logistical support was generously provided by the National Science Foundation under grants OPP-0229546, OPP-0229492, OPP- 0230028, OPP-0229305, and ANT-0538414.

Observations of Seismic and Acoustic Signals Produced by Calving, Bering Glacier, Alaska

Joshua P. Richardson *(Michigan Technological University),* **Gregory P. Waite** *(Michigan Technological University),*
Katelyn A. FitzGerald *(Michigan Technological University),* **Wayne D. Pennington** *(Michigan Technological University)*

Using short-period seismometers and small-aperture arrays of infrasound sensors, we recorded 126 calving and iceberg breakup events from the terminus of the Bering Glacier during five days in August 2008. The seismic signals were typically emergent, narrow-band, and lower-frequency (1-5 Hz), similar to seismic records from other glaciers, observed on a local scale [e.g. Qamar, 1988; O'Neel et al., 2007]. The acoustic records were characterized by shorter-duration, higher-frequency signals with more impulsive onsets. We demonstrate that triangular infrasound arrays permit improved locations of calving events over seismic arrivals that rely on a relatively complicated, poorly known, velocity model. We also discovered that a large percentage of events located away from the active calving face of the glacier and within Vitus Lake. The use of infrasound sensors proved extremely important in the differentiation of different parts of the source mechanism with one part propagating waves through the air and another propagating waves through the ground. Understanding the processes relating to ice-edge loss has serious implications in a changing climate, as fresh-water discharge has a significant impact on coastal currents within the Gulf of Alaska. [Richardson et al., 2010]

References

O'Neel, S., and W. T. Pfeffer (2007), Source mechanics for monochromatic icequakes produced during iceberg calving at Columbia Glacier, AK, *Geophys. Res. Lett., 34,* L22502.

Qamar, A. (1988), Calving icebergs: A source of low-frequency seismic signals from Columbia Glacier, Alaska, *J. Geophys. Res., 93*, 6615–6623.

Richardson, J. P., G. P. Waite, K. A. FitzGerald, and W. D. Pennington (2010), Characteristics of seismic and acoustic signals produced by calving, Bering Glacier, Alaska, *Geophys. Res. Lett., 37*, L03503.

Acknowledgements: The seismic instruments were provided by the Incorporated Research Institutions for Seismology (IRIS) through the PASSCAL Instrument Center at New Mexico Tech. Data collected will be available through the IRIS Data Management Center. The facilities of the IRIS Consortium are supported by the National Science Foundation under Cooperative Agreement EAR-0552316, the NSF Office of Polar Programs, and the DOE National Nuclear Security Administration. We would also like to thank the Michigan Tech Remote Sensing Institute, the Michigan Tech Office of the Vice President for Research, and the Michigan Tech Fund for their financial support.

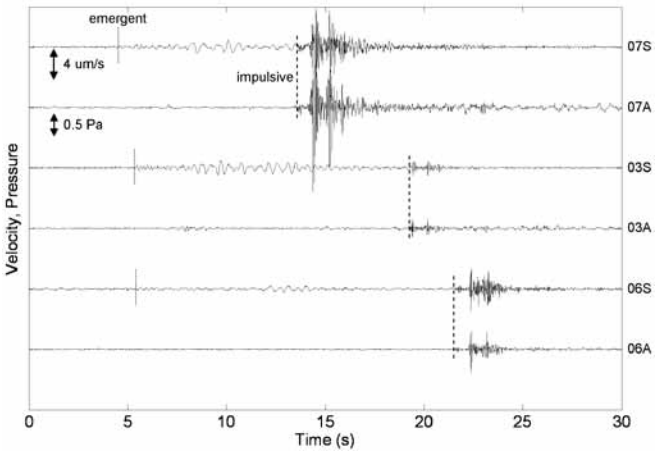

Vertical seismic (S) and coincident acoustic (A) traces recorded at each site from a single calving event on 07 August 2008 at 08:06 UTC. [Richardson et al., 2010]

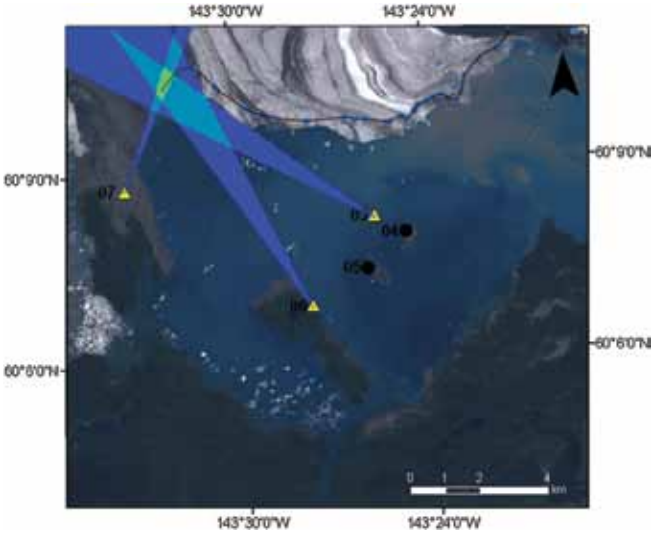

An example of the resulting solution produced by the intersection of three 99.7% confidence wedges at each array. [Richardson et al., 2010]

Elucidating the Stick-Slip Nature of the Whillans Ice Plain

Jacob Walter *(University of California, Santa Cruz),* **Emily E. Brodsky** *(University of California, Santa Cruz),* **Slawek Tulaczyk** *(University of California, Santa Cruz),* **Susan Y. Schwartz** *(University of California, Santa Cruz)*

The Whillans Ice Plain (WIP) is an approximately 200 km x 100 km x 600 m portion of the West Antarctic Ice Sheet that slips up to 0.5 m over a duration of 30 minutes, twice daily. Such bi-daily, tidally modulated stick-slip speed-ups provide insight into glacier dynamics and may be a unique analogue to tectonic earthquake/slow slip rupture. We deployed a network of continuously-operating GPS receivers in 2007 and operated on-ice broadband seismometers (partially provided by PASSCAL) during the austral summer of 2008 on WIP. Previous work during the 2004 field season suggested that these speed-ups initiate as failure of an asperity on or near "Ice Raft A" that triggers rupture across the entire WIP [*Wiens et al., 2008*]. Our results for the 2008 field season locate the slip initiation farther to the south of this feature, closer to the grounding line and the southernmost extent of the Ross Ice Shelf. A strong correlation between the amplitude of seismic waves generated at the rupture front and the total slip achieved over the duration of the slip event (~ 30 min) suggests slip-predictable behavior [Walter et al., submitted] or the ability to forecast the eventual slip based on the first minute of seismic radiation. Arrival time information compiled from stations QSPA and VNDA (continuous seismic data archived and provided by the IRIS DMC) show that successive slip events propagate with different rupture speeds (100-300 m/s) that strongly correlate (R-squared = 0.73, p-value = 0.0012) with the recurrence interval. In addition, the amount of slip achieved during each event appears to be correlated with the rupture speed. Our work suggests that the far-field transmission of seismic waves from glacier action is not dependent upon bulk ice movement, but rapid basal stress changes [*Walter et al., submitted*]. The availability of on-ice broadband seismometers and data at stations QSPA and VNDA yield important information regarding mechanics and dynamics of ice stream beds at the scale of 10s to 100s of km. Subglacial processes are notoriously difficult to constrain on these large scales, which are relevant to the understanding of regional and continental ice motion.

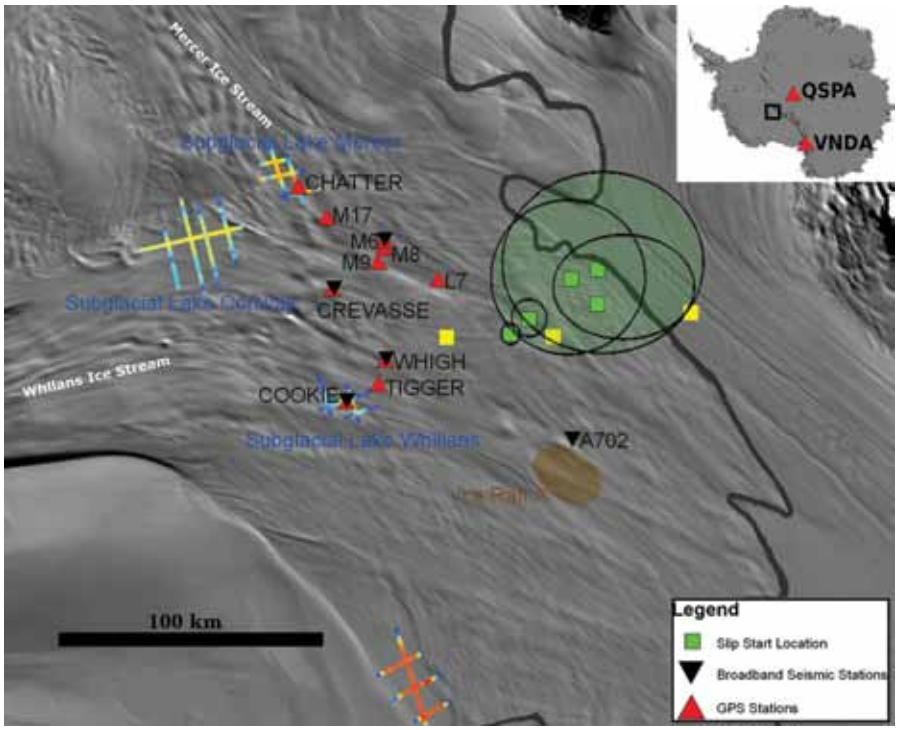

Station location map depicting continuous GPS network and broadband station names for the 2008 field season. Subglacial lake geometry is shown as IceSAT tracks, adapted from Fricker et al. [2007]. The green shaded circles 95% confidence level error ellipses encircling slip-start locations, shown as green squares. Yellow squares indicate slip-start locations with only three station observations.

References

Fricker, H. A., T. Scambos, R. Bindschadler (2007), An active subglacial water system in West Antarctica mapped from space, ***Science, 315***(5818): 1544-1548.

Walter, J. I., Brodsky, E. Tulaczyk, S., Schwartz, S., and R. Pettersson, submitted, Slip- predictability and dynamically fluctuating rupture speeds on a glacier-fault, Whillans Ice Plain, West Antarctica, ***J. Geophys. Res***. Earth Surface.

Wiens, D. A., S. Anandakrishnan, J. P. Winberry, and M. A. King (2008), Simultaneous teleseismic and geodetic observations of the stick-slip motion of an Antarctic ice stream, ***Nature, 453***: 770774.

Acknowledgements: This work was funded primarily by NSF Antarctic Sciences Division Grant number 0636970. Support for JW is provided by a NASA Earth and Space Science Fellowship. Some broadband seismic equipment was provided by PASSCAL. The IRIS DMC manages and archives data from stations QSPA and VNDA.

Infrasonic Imaging with the USArray

Kris Walker *(Laboratory for Atmospheric Acoustics, IGPP, SIO, Univ. of California, San Diego),* **Michael Hedlin** *(Laboratory for Atmospheric Acoustics, IGPP, SIO, Univ. of California, San Diego),* **Catherine de Groot-Hedlin** *(Laboratory for Atmospheric Acoustics, IGPP, SIO, Univ. of California, San Diego)*

The USArray directly measures ground motion, which can mostly be attributed to ocean waves, earthquakes, volcanoes, and weather systems that load the Earth's surface. Another source of ground motion is the transfer of atmospheric acoustic energy into seismic energy at the Earth's surface. Infrasound (low frequency sound below ~20 Hz) can travel great distances unattenuated in atmospheric ducts created by layers of slow sound speed. The infrasound wave field is rich due to a variety of anthropogenic and geophysical phenomena including earthquakes, volcanoes, landslides, meteors, lightning and sprites, auroras, and oceanic and atmospheric processes. Globally spaced microbarometer arrays with apertures of 100 m to 2 km are typically used to study these sources. However, these arrays are separated by thousands of kilometers, which places considerable limits on what they can teach us about infrasound source physics. The USArray is in a position to study infrasound sources in unprecedented detail. Array processing methods, such as reverse-time migration (RTM), may work well in automated detection and location of infrasound sources registered by the USArray (see also Hedlin et al. contribution). Hundreds of sources have been detected thus far using this technique. For example, below is a USArray "infrasonic image" of a Vandenberg Air Force Base rocket launch.

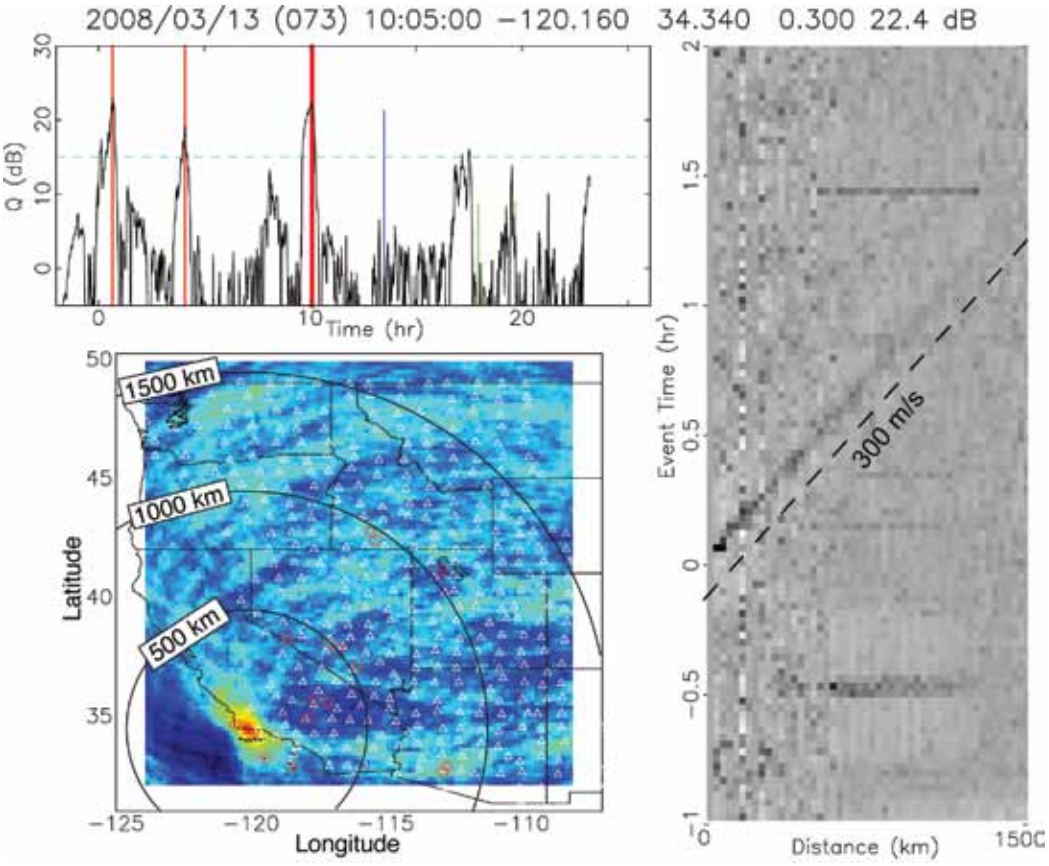

The detector function (upper left) images the source in time; there is a peak at the launch time (thick red line) with a signal-to-noise ratio of 22 dB. Other colored lines indicate known regional and teleseismic earthquake times. The map shows the seismic energy migrated back to the source, where it constructively interferes, imaging the source in space at the source time. The record section to the right shows that the migrated energy moves out at ~300 m/s, indicating that rocket infrasound is observed out to ~1500 km. Horizontally aligned signals are earthquakes.

Probing the Atmosphere and Atmospheric Sources with the USArray

Michael Hedlin *(Laboratory for Atmospheric Acoustics, U.C. San Diego),* **Kris Walker** *(Laboratory for Atmospheric Acoustics, U.C. San Diego),* **Catherine de Groot-Hedlin** *(Laboratory for Atmospheric Acoustics, U.C. San Diego),* **Doug Drob** *(Naval Research Laboratory)*

The USArray is designed to image the subsurface structure of the United States with exceptional resolution at a continental scale and for studies of regional and teleseismic earthquakes. Although the sensors of this network directly measure ground motion, they indirectly measure other phenomena that affect ground motion. It has been known for a long time that infrasound can be detected by seismometers through acoustic-to-seismic conversion at the ground/atmosphere interface. The USArray data archive contains recordings of several hundred large atmospheric events. One example is a bolide that burst above Oregon State on February 19, 2008 and was recorded by several hundred seismic stations and four infrasound arrays. The bolide source parameters were precisely determined by the seismic data, and the time-offset records show several phase branches corresponding to multiple arrivals. Such branches have never before been observed in such spectacular detail because infrasound arrays separated by thousands of kilometers are typically used for infrasound studies. The branches from such a large number of events occurring through the year are proving to be very useful for study of infrasound propagation and atmospheric structure.

Acknowledgements: We would like to acknowledge Earthscope and IRIS for data from the USArray without which this study would not have been possible. We would like to thank Matt Fouch at the University of Arizona and David James at the Carnegie Institution of Washington for giving us access to data from their High Lava Plains Seismic Experiment. We would also like to thank Gene Humphries at the University of Oregon for giving us access to data from the Wallowa Flexible Array Experiment. This article was made possible through support provided by US Army Space and Missile Defense Command. The opinions expressed herein are those of the authors and do not necessarily reflect the views of the US Army Space and Missile Defense Command.

USArray stations and regional infrasound arrays at the time of the bolide event.

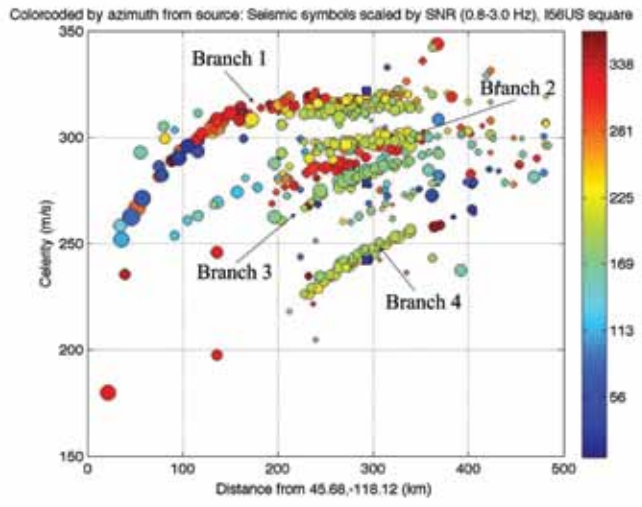

All branches from this event recorded by seismic stations and the infrasound array I56US. Symbols are scaled by SNR and colored by azimuth from the source. Signals from the lone infrasound array near the source are represented by the blue squares at 300 km.

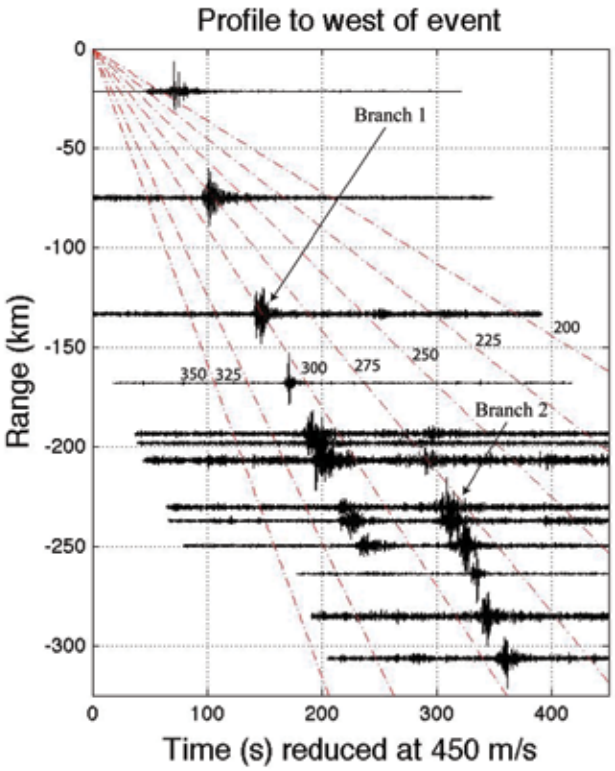

A record section to the west of the event. We see two acoustic branches (at celerities from 225 to 312 m/s) to a range of over 300 km in this direction.

Harmonic Tremor on Active Volcanoes: Seismo-Acoustic Wavefields

Jonathan Lees *(University of North Carolina, Chapel Hill),* **Jeffrey Johnson** *(New Mexico Institute of Technology)*

Harmonic tremor is often observed on active volcanoes where seismo-acoustic arrays are deployed. In this presentation we review characteristic observational phenomena and discuss the continuum from monochromatic, oscillatory behavior through periodic acoustic pulses (i.e. chugging) to spasmodic drumming on numerous volcanoes world wide. Harmonic tremor can provide detailed constraints on physical parameters controlling activity in active vents through physical modeling. These include physical constraints on the vent geometry, composition and density of the multiphase fluids, and visco-elastic parameters of choked flow in the conduits. Examples will show seismic tremor with and without an associated acoustic emission, an indicator of dynamic processes occurring at the top of the active vent. While explosive activity can range widely between volcanoes, harmonic tremor often exhibits remarkably similar behavior on vents as diverse as Karymsky, Tungurahua, Reventador, and Santiaguito Volcanoes. For example, chugging activity typically has a consistent 0.7-2 Hz signal on many volcanoes world wide. Commonly observed gliding, where frequency modulates over time, suggests that conditions in the conduit are non-stationary, and must be treated with specialized time series analysis tools. We explore these phenomena and highlight possible models explaining these near surface vent emissions.

References

Lees, J.M., Johnson, J.B., Ruiz, M., Troncoso, L. and Welsh, M., (2008). Reventador Volcano 2005: Eruptive Activity Inferred from Seismo-Acoustic Observation. *J. Volcanol. Geotherm. Res., 176*(1): 179-190, doi:10.1016/j.jvolgeores.2007.10.006.

Lees, J.M. and Ruiz, M., (2008). Non-linear Explosion Tremor at Sangay, Volcano, Ecuador. *J. Volcanol. Geotherm. Res., 176*(1): 170-178 doi:10.1016/j.jvolgeores.2007.08.012

Johnson, J. B., and J. M. Lees (2000), Plugs and Chugs – Strombolian activity at Karymsky, Russia, and Sangay, Ecuador, *J. Volcanol. Geotherm. Res., 101*, 67-82.

Acknowledgements: NSF: EAR-9614639 , "Side Edge of Kamchatka Slab", June 1, 1997-July 31, 2000. NSF Proposal No: EAR-0738768 Title: Co

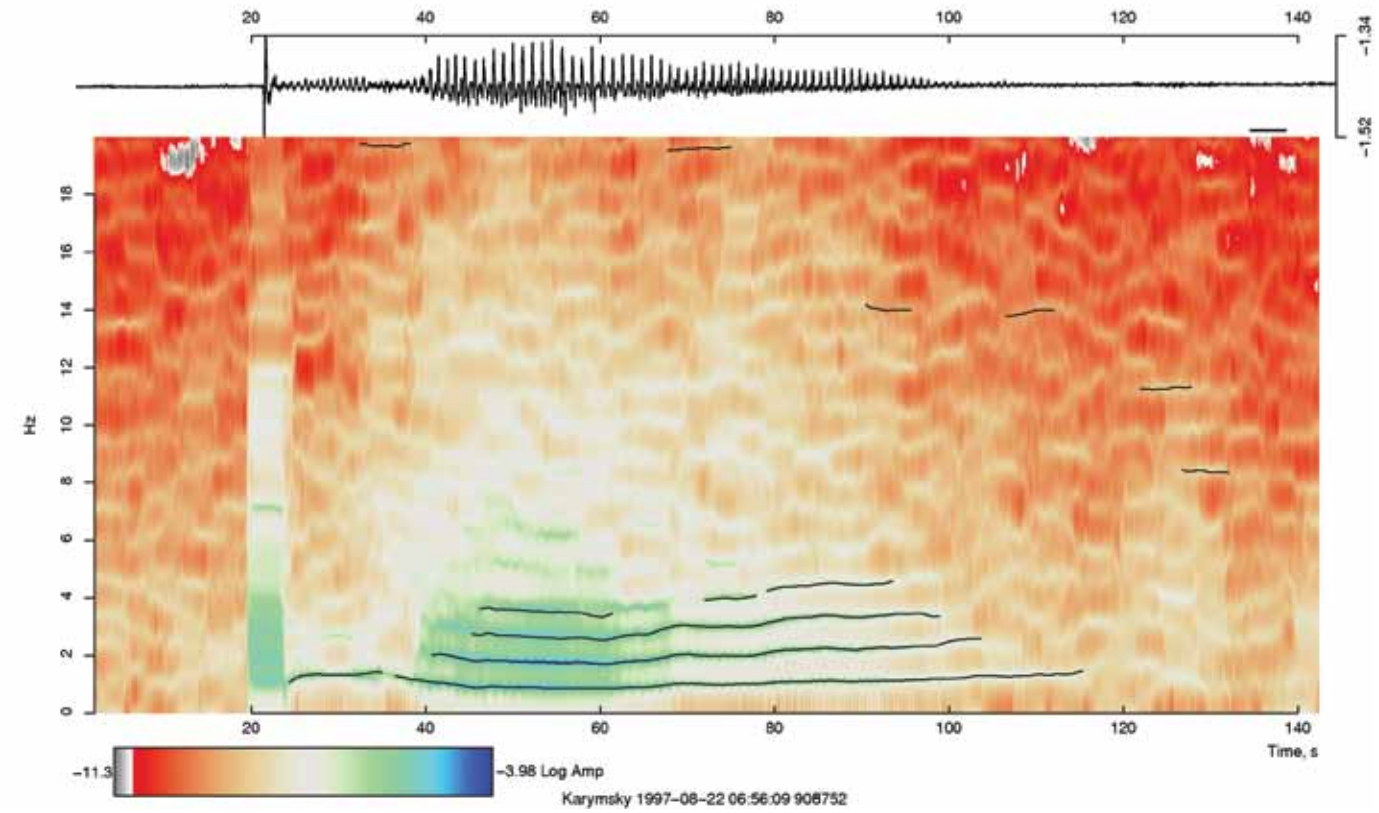

Spectrogram of Karymsky Volcano chugging, 1997. Lines represent the fundamental and possible integer harmonics of the chugging sequence.

Volcanic Plume Height Measured by Seismic Waves Based on a Mechanical Model

Stephanie Prejean *(Alaska Volcano Observatory, USGS),* **Emily Brodsky** *(UC Santa Cruz)*

In August 2008 an unmonitored, largely unstudied Aleutian volcano, Kasatochi, erupted catastrophically. Here we use seismic data to infer the height of large eruptive columns, like those of Kasatochi, based on a combination of existing fluid and solid mechanical models. In so doing, we propose a connection between common observable, short-period seismic wave amplitude, to the physics of an eruptive column. To construct a combined model, we estimate the mass ejection rate of material from the vent based on the plume height, assuming that the height is controlled by thermal buoyancy for a continuous plume. Using the calculated mass ejection rate, we then derive the equivalent vertical force on the Earth through a momentum balance. Finally, we calculate the far-field surface waves resulting from the vertical force. Physically, this single force reflects the counter force of the eruption as material is discharged into the atmosphere. We explore the applicability of the combined model to relatively high frequency seismic waves recorded at ~ 1 s. The model performs well for the 2008 eruption of Kasatochi volcano and the 2006 eruption of Augustine volcano. The consistency between the seismically inferred and measured plume heights indicates that in these cases the far-field 1 s seismic energy radiated by fluctuating flow in the volcanic jet during eruption is a useful indicator of overall mass ejection rates. Use of the model holds promise for characterizing eruptions and evaluating ash hazards to aircraft in real time based on far-field short-period seismic data.

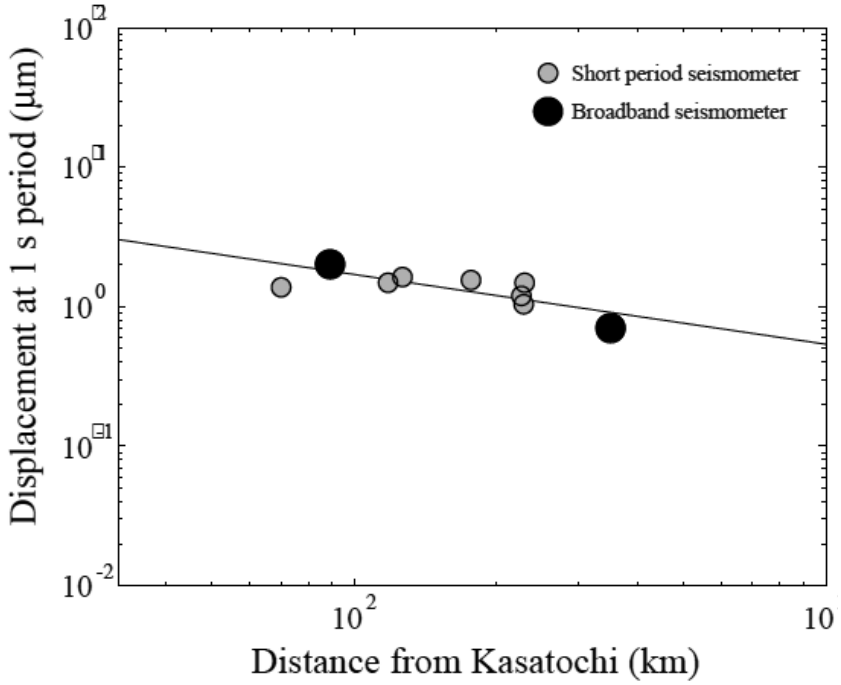

Ground displacement at 1 s period of co-eruptive seismicity with distance from Kasatochi volcano for the large ash producing explosion at 2008. Large dots are broadband stations ATKA and AMKA. Small dots are short-period stations. Preferred forward model fit shown with solid line.

Anomalous Earthquakes Generated by Collapse of Magma Chambers

Ashley Shuler, Göran Ekström *(Department of Earth and Environmental Sciences, Columbia University, Lamont-Doherty Earth Observatory)*

Recent advances in earthquake detection using intermediate period surface waves have resulted in the discovery of hundreds of earthquakes (Mw>4.5) that previously went unrecorded in global seismicity catalogs [Ekström, 2006]. Many of these events are located in areas with good station coverage, and may have escaped detection due to unusual source properties. A series of five such earthquakes were detected near Nyiragongo Volcano in the Democratic Republic of the Congo between 2002 and 2005. The first three events occurred several days after the massive fissure eruption of Nyiragongo in January 2002. The final two events occurred in 2003 and 2005, and are not linked to a major eruption in the region, but did occur as the level of Nyiragongo's summit lava lake was rising. This set of earthquakes is anomalous in two regards. First, these earthquakes are depleted in high-frequency energy over approximately 0.1 Hz, and can be considered slow earthquakes. Second, centroid-moment-tensor solutions indicate that these earthquakes are highly non-double-couple, each having a large compensated-linear-vector-dipole component of the moment tensor. This indicates that the double couple model for shear failure on a planar fault cannot explain the radiation pattern of these earthquakes. Drawing on models based on similar observations from other active volcanoes [Nettles and Ekström, 1998; Ekström and Nettles, 2002], we propose that the earthquakes are caused by slip on pre-existing, non-planar faults located beneath the edifice of the volcano. We suggest a mechanism in which these newly detected earthquakes are generated by the collapse of the roof of a shallow magma chamber along an inward-dipping cone-shaped ring fault [Shuler and Ekström, 2009]. As one might expect, these events can occur in association with an ongoing volcanic eruption. In the case of the first three earthquakes, diking events during the 2002 eruption reduced the pressure in a shallow magma chamber, leading it to collapse along the pre-existing ring fault. However, a similar mechanism can also explain the occurrence of these earthquakes due to the transport of magma from deeper to more shallow magma chambers. The earthquakes in 2003 and 2005 occurred during a period of lava lake level rise, and so are associated with magma ascent processes. The detection of this type of earthquake at other active volcanoes may be useful for inferring magma transport and determining the likelihood of future eruptions.

References

Ekström, G. (2006), Global Detection and Location of Seismic Sources by Using Surface Waves, *Bull. Seismol. Soc. Amer., 96*(4A), 1201-1212.

Shuler, A., and G. Ekström (2009), Anomalous earthquakes associated with Nyiragongo Volcano: Observations and potential mechanisms, *J. Volcanol. Geoth. Res., 181*(3-4), 219-230.

Nettles, M., and G. Ekström (1998), Faulting mechanism of anomalous earthquakes near Bárdarbunga Volcano, Iceland, *J. Geophys. Res., 103*(B8), 17,973-17,983.

Ekström, G. and M. Nettles (2002), Detection and location of slow seismic sources using surface waves, Eos Trans. AGU, 83(47), Fall Meet. Suppl., Abstract S72E-06.

Acknowledgements: The seismic waveforms used in this study were obtained from the GSN, GEOSCOPE, GEOFON, and MEDNET. Additional data from the Ethiopia and Kenya Broadband Experiments were also utilized (PI Andy Nyblade). The facilities of the IRIS Data Management System, and specifically the IRIS Data Management Center, were used for access to waveforms and metadata required in this study. The schematic diagram in Figure 1 was rendered by Liz Starin. This work was funded by National Science Foundation Award EAR-0639963. Ashley Shuler was also supported by an NSF Graduate Research Fellowship.

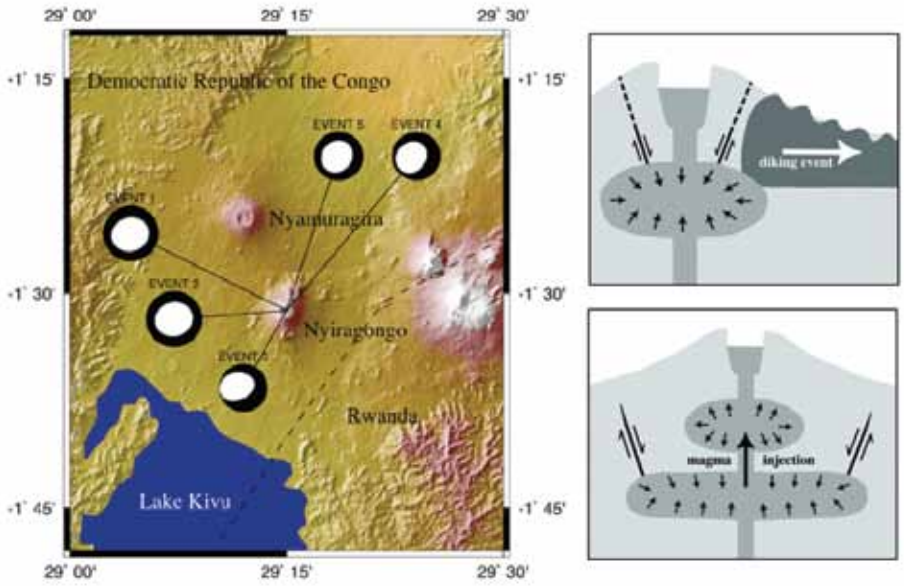

Focal mechanisms for newly detected earthquakes at Nyiragongo. Schematic diagram on right shows the physical mechanism for these events. Earthquakes are generated by slip on inward-dipping ring faults due to deflation of shallow magma chambers. This can be caused either by diking events during volcanic eruptions (top), or by the transport of magma from deeper to more shallow magma chambers (bottom).

Eruption Dynamics at Mount St. Helens Imaged from Broadband Seismic Waveforms: Interaction of the Shallow Magmatic and Hydrothermal Systems

Gregory Waite *(Michigan Technological University)*

The 2004-2008 eruption at Mount St. Helens was characterized by dome building and shallow, repetitive, long-period (LP) earthquakes. We analyzed the seismicity using a temporary array of 19 intermediate band PASSCAL seismometers deployed during the second half of 2005 from ~1 to 6 km from the active vent. Waveform cross-correlation of the LP events shows they were remarkable similarity for a majority of the earthquakes over periods of several weeks, indicating a repetitive source mechanism. Stacked spectra of these events display multiple peaks between 0.5 and 2 Hz that are common to most stations; this suggests the low-frequency waveforms are due to a source process, rather than path affects. When the first motions were discernible, they were dilatational on stations at all distances and azimuths. In addition to the LP events, lower-amplitude very-long-period (VLP) events commonly accompany the LP events. We modeled the source mechanisms of LP and VLP events in the 0.5 - 4 s and 8 - 40 s bands, respectively by full waveform inversion. The source mechanism of the LP events includes: 1) a volumetric component modeled as resonance of a gently NNW-dipping, steam-filled crack located directly beneath the actively-extruding part of the new dome and within 100 m of the crater floor and 2) a vertical single force attributed to movement of the overlying dome. The VLP source, which also includes volumetric and single-force components, is 250 m deeper and NNW of the LP source, at the SW edge of the 1980s lava dome. The volumetric component points to the compression and expansion of a shallow, magma-filled sill, which is subparallel to the hydrothermal crack imaged at the LP source, coupled with a smaller component of expansion and compression of a dike. The single-force components are due to changes in the velocity of magma moving through the conduit. The location, geometry and timing of the sources suggest the VLP and LP events are caused by perturbations of a common crack system.

References

Waite, G. P., B. A. Chouet, and P. B. Dawson (2008), Eruption dynamics at Mount St. Helens imaged from broadband seismic waveforms: Interaction of the shallow magmatic and hydrothermal systems, *J. Geophys. Res., 113*(B2), B02305.

Acknowledgements: Funding was provided primarily by the USGS Mendenhall Postdoctoral Fellowship. The IRIS-PASSCAL Instrument Center provided instruments and support for the temporary network. Data collected are available through the IRIS Data Management Center. The facilities of the IRIS Consortium are supported by the National Science Foundation under Cooperative Agreement EAR-0552316, the NSF Office of Polar Programs and the DOE National Nuclear Security Administration

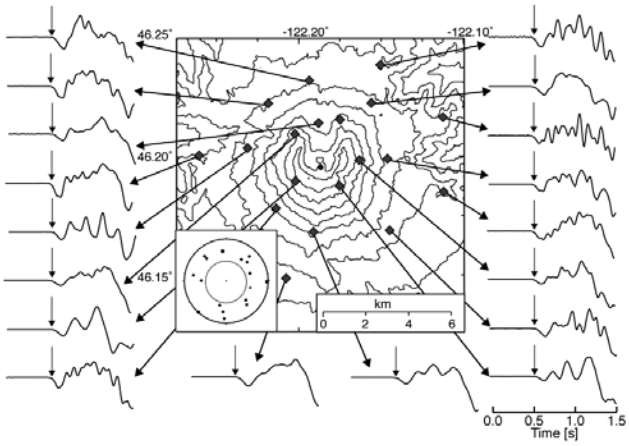

Figure 1. Dilatational first motions are clear at all of the broadband stations for a sample event from 31 July 2005, plotted as a circle in the crater. The focal sphere in the inset shows distribution of the first motion recordings for the broadband stations, with a dashed line in the middle outlining the region where there are no broadband stations.

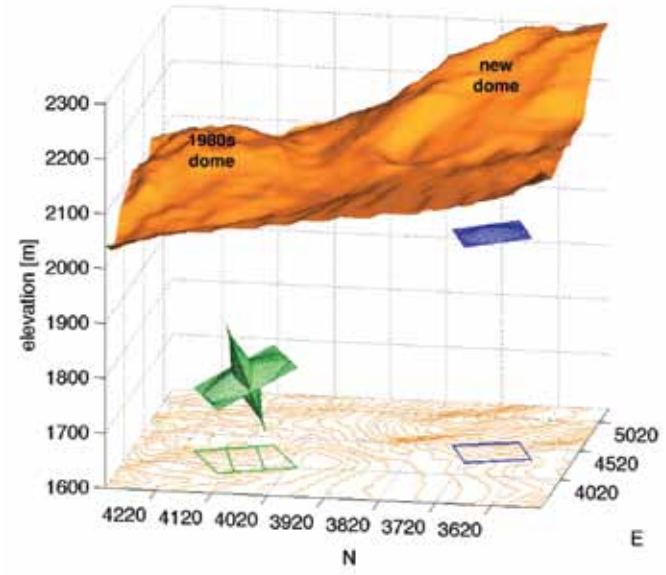

Figure 2. East-northeast, three-dimensional, perspective view of the LP crack (blue) and VLP sill-dike (green) sources. Topography is shown as a surface and is contoured on the bottom at 20 m. Distances are in m and are relative to the origin of the 20-m-grid model used to calculate Green functions.

The Seismic Story of the Nile Valley Landslide - Foreshocks, Mainshock and Aftershocks

Kate Allstadt, John Vidale, Weston Thelen, Paul Bodin *(Univ. of Washington)*

The Nile Valley landslide, in Washington State, 11 October 2009, was a translational slide involving a volume of material on the order of 10^7 cubic meters. It damaged a highway and several houses and diverted a river, causing flooding. Fortunately no one was injured because the landslide gave warning "foreshocks," - rumbling sounds, rocks raveling, and a smaller precursory landslide in the days and hours beforehand.

The "mainshock" was a complex ground failure sequence occurring over the course of about 24 hours. The more energetic events generated seismic signals that were captured by two Pacific Northwest Seismic Network (PNSN) short-period regional stations 12 and 29km away. This precise seismic timeline, in combination with detailed eyewitness reports and studies of the geology of the landslide resulted in a detailed account of the unfolding of a landslide unlike any other. This timeline is shown on Figure 1.

After the landslide occurred, we installed 16 temporary seismic stations. Despite a lack of significant continued movements, our instruments detected more than 60 small events, or "aftershocks." We were able to locate some of the larger events using beamforming techniques. The events were at the headscarp north of the slide, most likely slope failures due to instability of the newly created cliff-face.

References:

Anderson, D. and G. Taylor (2010), Nile Landslide Timeline Narrative Report, Washington State Dept of Transportation, Unpublished Report.

Acknowledgements: Thanks to the Washington State DNR and DOT, in particular to Doug Anderson and Gabe Taylor. Also to IRIS PASSCAL for lending us equipment and Agnes Helmstetter for sharing her event location methods.

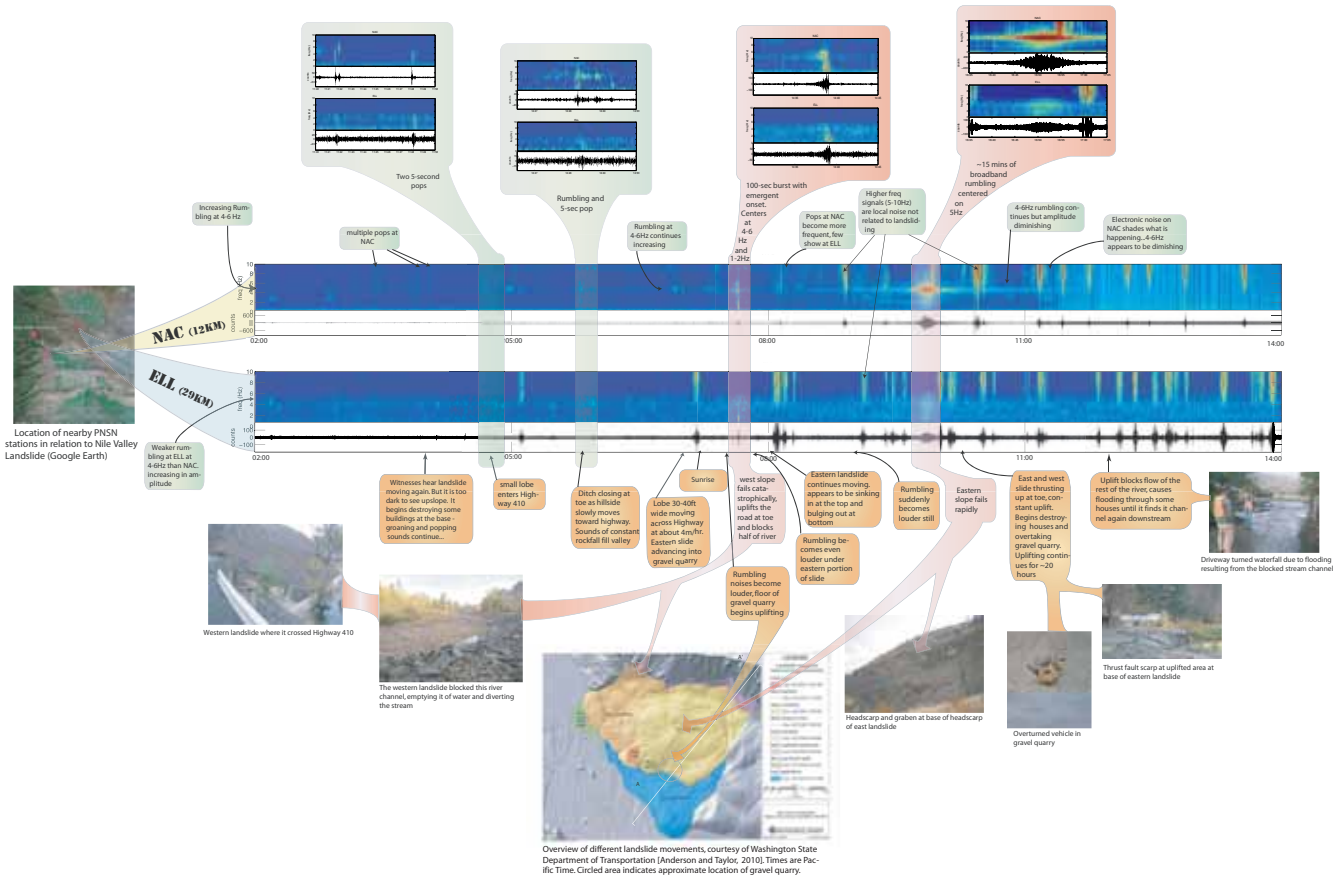

Seismic Timeline of the Nile Valley Landslide showing the main sliding sequence as detected at the two closest PNSN regional stations, both short period, vertical instruments. Station locations in relation to the slide are shown on the map at left. The spectrogram showing 12 hours of the landslide is shown on top and the traces filtered from 1 to 7Hz are shown below for each station. The seismic timeline is narrated in green at the top and the corresponding eyewitness timeline is narrated in orange at bottom. Times are Pacific Time.

A Search for the Lunar Core Using Array Seismology

Peiying Patty Lin *(Arizona State University),* **Renee Weber** *(U.S. Geological Survey),* **Edward Garnero** *(Arizona State University)*

Apollo Passive Seismic Experiment (Apollo PSE) seismometers were deployed on the nearside of the Moon between 1969 and 1972, and continuously recorded 3 components of ground motion until late 1977. These data provide a unique opportunity for investigating a planetary interior other than the Earth. PSE data potentially provide the most direct information about the structure of the lunar interior, including the thermal and compositional evolution of the Moon. The size and the state of the Moon¡¦s core remain primary questions regarding the deep lunar interior. Past seismic models of the lunar interior report significantly diminished resolution in the deepest Moon, and frequently don't cite model solutions in the deepest 500 km of the interior.

In this study, we investigate the PSE data for the presence of seismic energy that may have been reflected (or converted) from the presence of a material property contrast associated with the lunar core-mantle boundary (CMB). Borrowing from the successes of CMB imaging on Earth, we use array-stacking techniques in effort to reveal relatively low amplitude but coherent seismic signals that would otherwise be below the background noise level (noting that for the Moon, seismic coda and noise levels have been shown to be significant [*Jarosch, 1977*]. We systematically search for either P or S wave down-going energy that reflects from the CMB, with the possibility of mode conversion. The four main possibilities are PcP, ScS, ScP and PcS.

Deep moonquakes have been shown to occur and repeat in specific locations; about 65 unique clusters of deep moonquakes were identified and located by Nakamura [*2005*]. Our first processing step involved a stacking of data in each cluster [Bulow et al., 2005]. However, even in the cluster stacks, data display emergent arrivals. We thus apply a polarization filter, which is based on a product between orthogonal components of motion that enhances signals which partition onto each component, as opposed to noise. The polarized cluster stacks are then stacked a second time after time-shifting traces according to theoretical predictions of core-reflection times. This experiment, commonly referred to as double array stacking, is done for a large range of possible core radii. Preliminary analyses indicate PcP gives the most stable results, with strong evidence for a reflector at 200 km radius. ScP, while less certain, suggests an additional reflector at 330 km radius. We explore the possibility of a solid inner and fluid outer core explaining these results, a structure advocated by other methods, e.g. from laser ranging data [*Williams et al., 2006*].

References

Jarosch, H. (1977), *Bull. Seismol. Soc. Amer., 67*, 1647-1659.

Nakamura, Y. (2005), *J. Geophys. Res., 110*, doi:10.1029/2004JE002332

Bulow R.C. et al. (2005), *J. Geophys. Res., 110*, doi:10.1029/2005JE002414

Williams J. G. et al (2006), Advances in Space Research, 37, 67-71.

Acknowledgements: This research was supported by NSF grant.

Shallow Low-Velocity Zone of the San Jacinto Fault from Local Earthquake Waveform Modeling

Hongfeng Yang *(Saint Louis University),* **Lupei Zhu** *(Saint Louis University)*

The damaged zone associated with a fault zone (FZ) can amplify the ground motion and may control the earthquake rupture process and slip localization during earthquakes. It may hold the key for us to understand the earthquake physics. Therefore, it is important to image the structure of the FZ. We developed a method to determine the depth extent of low-velocity zone (LVZ) associated with a FZ using S-wave precursors from local earthquakes. The precursors are diffracted S waves around the edges of LVZ and their relative amplitudes to the direct S waves are sensitive to the LVZ depth. We applied the method to data recorded by three temporary arrays across three branches of the San Jacinto fault zone. The FZ dip was constrained by differential travel times of P waves between stations at two side of the FZ. Other FZ parameters (width and velocity contrast) were determined by modeling waveforms of direct and FZ-reflected P and S waves [*Li et al, 2007*]. We found that the LVZ of the Buck Ridge fault branch has a width of ~150 m with a 30-40% reduction in Vp and a 50-60% reduction in Vs. The fault dips 70 to southwest and its LVZ extends to 2 km in depth. The LVZ of the Buck Ridge fault is not centered at the surface fault trace but is located to its northeast, indicating asymmetric damage during earthquakes.

References

Li, H., L. Zhu, and H. Yang, High-resolution structures of the Landers fault zone inferred from aftershock waveform data, *Geophys. J. Int., 17*, 2007.

Yang, H., and L. Zhu, Shallow low-velocity zone of the San Jacinto fault from local earthquake waveform modeling, *Geophys. J. Int.*, in revision, 2010

Acknowledgements: This work is supported by NSF grant EAR-0609969. The field work was assisted by IRIS and PASSCAL.

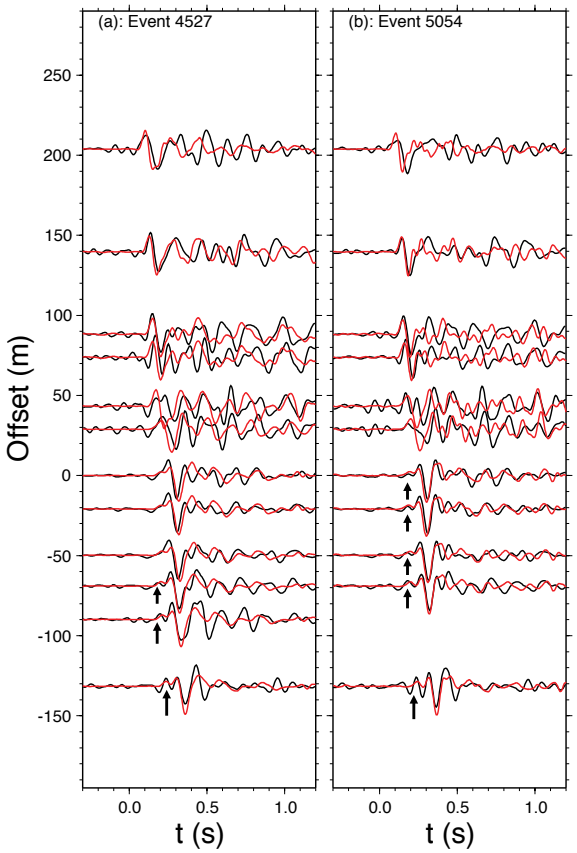

Figure 1: S and Sdiff wave data (black) and synthetic waveforms (red). From left to right, two events, (a) 4527, (b) 5054, recorded by the BRF array. Event locations are shown in Fig. 2.Black arrows point to the Sdiff phase.

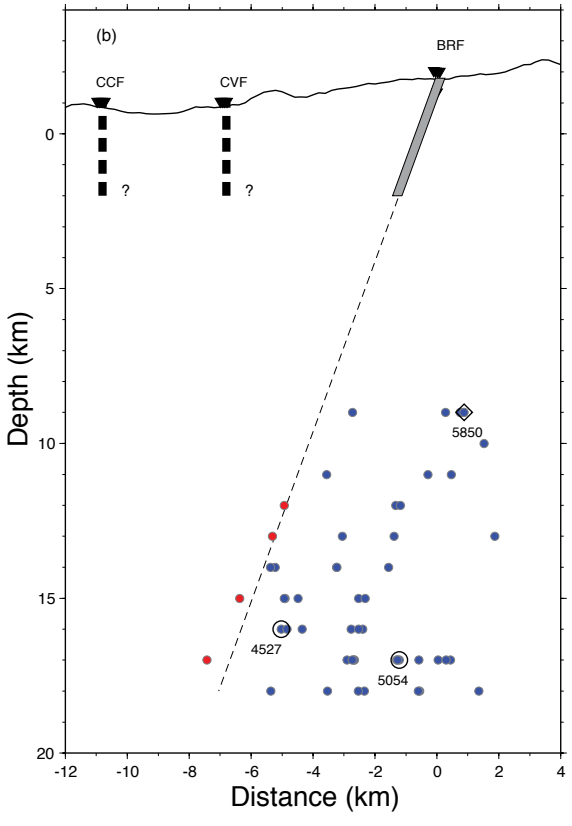

Figure 2: Cross-section of locations of events recorded by the BRF array. Blue and red colors represent positive and negative P-wave travel time differences between the northeastern-most and southwestern-most stations of the array, respectively. For those events whose waveforms are shown,event numbers are marked on their locations. The grey bar represents the extent of LVZ of BRF. Thick dashed lines stand for LVZs of the Coyote Creek fault and the Clark Valley fault.

Seismic Imaging of the Mt. Rose Fault, Reno, Nevada: A Landslide Block Cut by Faulting

Annie Kell-Hills *(University of Nevada, Reno),* **John N. Louie** *(University of Nevada, Reno),* **Satish Pullammanappallil** *(Optim, Inc.)*

The Reno-area basin, sited at the western limit of the Basin and Range province within the Walker Lane, borders the Carson Range of the Sierra Nevada Mountains on the east. Triangular facets observed along an abrupt range front of the Carson Range indicate active faulting, motivating research in this rapidly urbanized area. Within the Mt. Rose fan complex, we trace a continuous ~1.4 mile long, north-northeasterly striking scarp offsetting both pediment surfaces and young alluvium at fan heads. A paleoseismic trench excavated across the scarp north of Thomas Creek at ~39.4° N latitude by A. Sarmiento and S. Wesnousky reveals a sharp, planar, low angle contact presumed to be a low angle normal fault (LANF). The trench study alone does not allow for conclusive evidence for a LANF, suggesting the collection of a high-resolution shallow seismic reflection profile in November 2009. The application of advanced seismic processing revealed a low-angle structure as prominent as the alluvium-to-granite interface of the 1954 Dixie Valley rupture, a LANF [*Abbott et al.*, 2001]. Commercial SeisOpt®@2D™ software and P-wave arrival times provided an optimized velocity model. The velocity section and survey shot gathers provided input for the Kirchhoff pre-stack depth migration (PSDM) in the figure, revealing the complex structure in full detail to 50 m depths. Layers of Tertiary sandstone are disrupted by an ancient landslide slip surface, which is cut more recently by offset of the Mt. Rose fault trace. Truncations of layers of underlying Tertiary andesite help locate the fault and constrain its dip to less than 30°. This advanced seismic exploration below a paleoseismic trench confirms fault structure and details the earthquake hazard within the populated urban basin.

References

Abbott, R. E., J. N. Louie, S. J. Caskey, and S. Pullammanappallil, 2001, Geophysical confirmation of low-angle normal slip on the historically active Dixie Valley fault, Nevada: *J. Geophys. Res., 106*, 4169-4181.

Acknowledgements: Research partially supported by the U.S. Geological Survey (USGS), Department of the Interior, under USGS award number G09AP00051. The views and conclusions contained in this document are those of the authors and should not be interpreted as necessarily representing the official policies, either expressed or implied, of the U.S. Government.

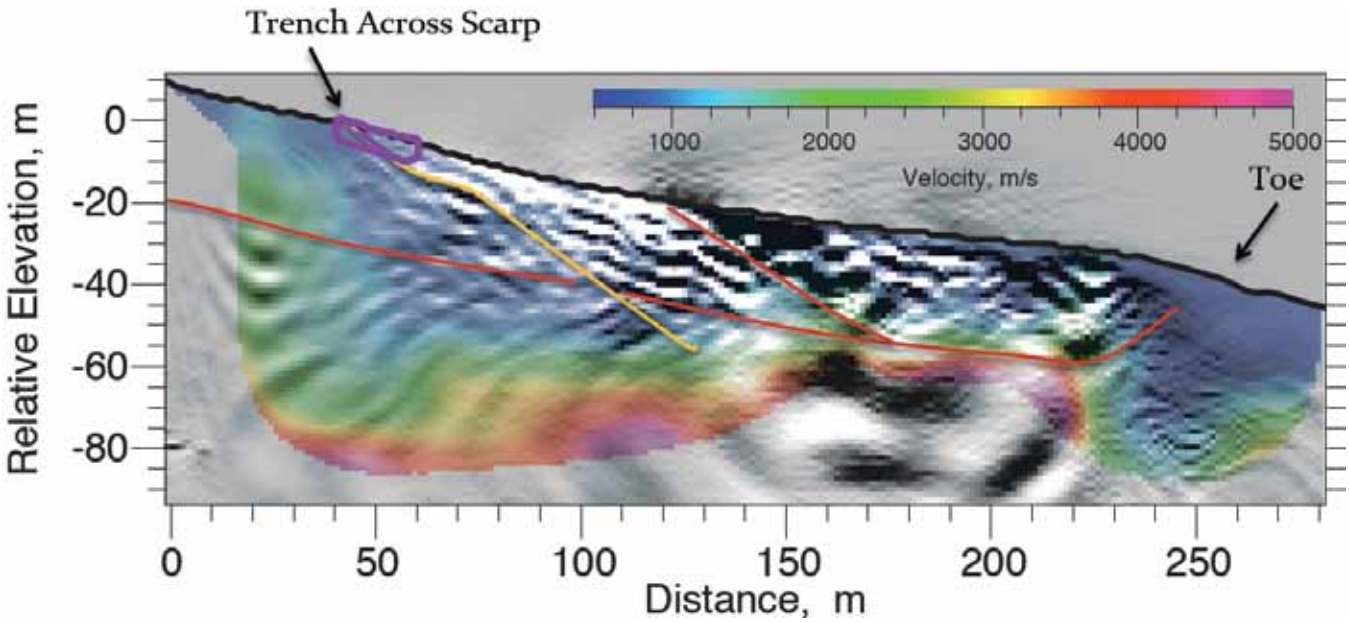

Interpreted depth section running approximately west (left) to east (right) across the Mt. Rose fault scarp at Sarmiento's trench. No vertical exaggeration. Colors indicate velocities optimized from 1st-arrival picks, with unsaturated, fractured, slow Quaternary alluvium and Tertiary sands (blue at Vp=800-900 m/s) overlying Tertiary andesites (green and red). The interpreted Mt. Rose normal fault (yellow line) cuts an ancient landslide slip surface (red line) at low angle.

Faulting Processes During Early-Stage Rifting: RAMP Response to the 2009-2010 Northern Malawi Earthquake Sequence

James Gaherty *(Lamont-Doherty Earth Observatory of Columbia University),* **Donna Shillington** *(Lamont-Doherty Earth Observatory of Columbia University),* **Scott Nooner** *(Lamont-Doherty Earth Observatory of Columbia University),* **Cindy Ebinger** *(University of Rochester),* **Andy Nyblade** *(Pennsylvania State University)*

On December 6, 2009, an unusual sequence of earthquakes began in the Karonga region in northern Malawi (Fig. 1). The sequence initiated with an Mw 5.8 event, which was followed 32 hours later by an Mw 5.9 event, and then nearly 12 days later by an Mw 6.0 event. Within this time span there were an additional six Mw > 5 events, with many more events that were at or below the threshold of the NEIC location system. Such events are very rare in the Malawi portion of the East African rift (EAR); prior to this sequence, the NEIC catalog [which dates to, 1973] contains only three events of M > 5 within the rift valley between 9-12°S latitude. This contrasts with both the Western and Eastern branches of the EAR through Kenya and Tanzania, which between them have experienced 115 M > 5 events in the same time period. Nearly all other moderate-size earthquakes within the Western Rift appear to be on major border faults, but the locations, mechanisms and event depths of the Karonga events imply that they occurred due to slip on normal faults within the hanging wall block. They offer a rare opportunity to evaluate how early-stage rifting is accommodated within the hanging wall of the system.

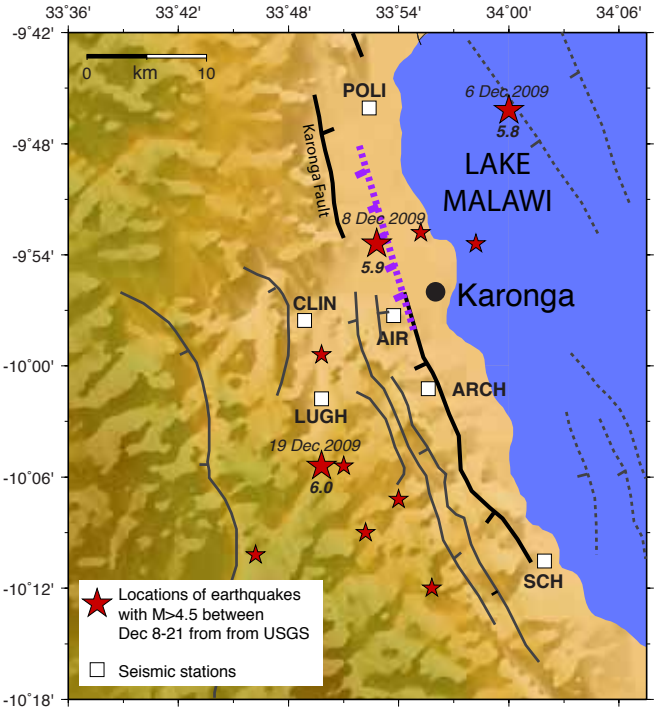

Figure 1. Locations of main events from NEIC catalogue (red stars), seismic stations in RAMP deployment (white squares and text) and a subset of faults onshore (black and grey lines) and offshore (grey dotted lines). Purple dotted line indicates interpreted fault of Biggs et al. (2010) based on InSAR data.

The December 2009 earthquake sequence resulted in four casualties, 300 injuries and thousands of displaced people. Malawi currently has very limited capacity to monitor and locate such earthquakes; they have no permanent national network. With the support of IRIS PASSCAL, we undertook a Rapid Array Mobilization Program (RAMP) deployment at the request of the Director of the Malawi Geological Survey Department (MGSD). We deployed six broadband stations for a four-month period to monitoring aftershock activity. We recorded several thousand local events, and analysis is ongoing. This technical response complimented the post-event aid that was being provided by NGO's and government agencies. Through our field activities, we explained the earthquakes to teachers, police officers and villagers. We provided television and radio interviews about earthquakes and the necessity of seismic monitoring, and blogged about our undertaking (http://blogs.ei.columbia.edu/blog/tag/east-africa-rift/). We trained personnel from the MGSD in seismic equipment and field methods. This effort directly resulted in the purchase of equipment by the MGSD for 9 stations to begin a seismic network in Malawi; they purchased the same equipment employed in our RAMP deployment.

References

Biggs, J., E. Nissen, T. Craig, J. Jackson, and D. P. Robinson (2010), Breaking up the hanging wall of a rift-border fault: the 2009 Karonga Earthquakes, Malawi, *Geophys. Res. Lett., 37,* doi:10.1029/2010GL043179.

Acknowledgements: Funding for the RAMP deployment was provided by Columbia University through the Lamont-Doherty Earth Observatory and the Earth Institute. The IRIS PASSCAL program provided the instruments, as well as financial support for shipping. Data collection and instrument recovery supported by the NSF RAPID grant EAR-1019379.

Structure of the California Coast Ranges and San Andreas Fault at Safod from Seismic Waveform Inversion and Reflection Imaging

Florian Bleibinhaus *(Virginia Tech; now at Salzburg Univ.),* **John A. Hole** *(Virginia Tech),* **Trond Ryberg** *(GeoForschungsZentrum, Potsdam),* **Gary S. Fuis** *(U. S. Geological Survey, Menlo Park)*

A seismic reflection and refraction survey across the San Andreas Fault (SAF) near Parkfield provides a detailed characterization of crustal structure across the location of the San Andreas Fault Observatory at Depth (SAFOD). Steep-dip prestack migration and frequency domain acoustic waveform tomography were applied to obtain highly resolved images of the upper 5 km of the crust for 15 km on either side of the SAF. The resulting velocity model constrains the top of the Salinian granite with great detail. Steep-dip reflection seismic images show several strong-amplitude vertical reflectors in the uppermost crust near SAFOD that define a 2-km-wide zone comprising the main SAF and two or more local faults. Another prominent subvertical reflector at 2–4 km depth 9 km to the northeast of the SAF marks the boundary between the Franciscan terrane and the Great Valley Sequence. A deep seismic section of low resolution shows several reflectors in the Salinian crust west of the SAF. Two horizontal reflectors around 10 km depth correlate with strains of seismicity observed along-strike of the SAF. They represent midcrustal shear zones partially decoupling the ductile lower crust from the brittle upper crust. The deepest reflections from 25 km depth are interpreted as the crust-mantle boundary.

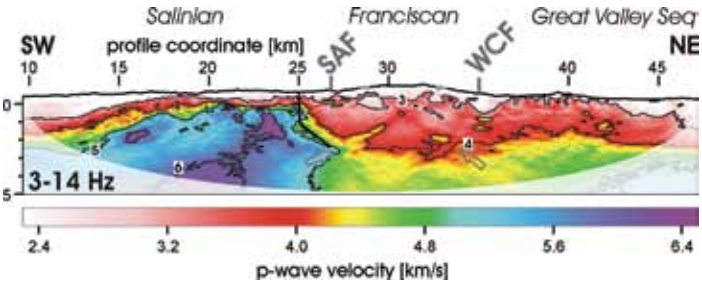

Waveform inversion velocity model using 3.2 to 14.4 Hz data. A thick black line marks the SAFOD main hole. Contour lines are annotated in kilometers per second.

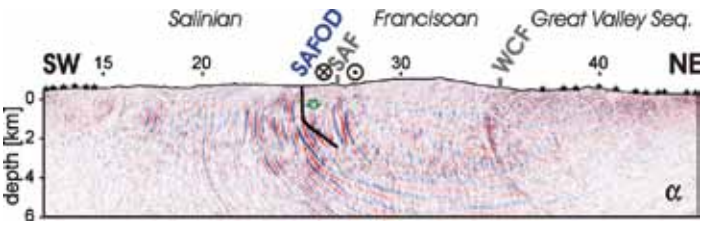

Steep-dip prestack depth migrated image. The shots used to produce the image are indicated on top. The section was normalized for subsurface coverage.

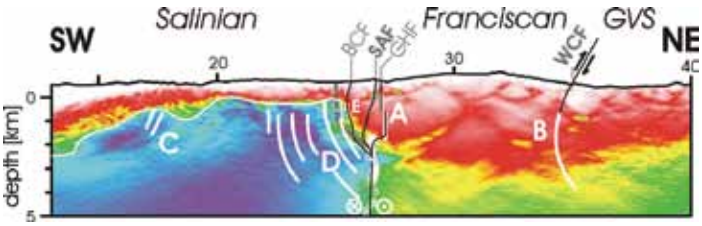

Manual line drawing of the major reflectors from the steep-dip migration (thick white lines) overlaid onto the final waveform tomography velocity model. The top of the Salinian granite, as inferred from the 5 km/s contour, is marked by a thin white line. Local earthquake hypocenters (white circles) constrain the position of the SAF at depth. Solid black lines are interpretation. The surface positions of faults are: BCF, Buzzard Canyon; SAF, San Andreas; GHF, Gold Hill; WCF, Waltham Canyon.

References

Bleibinhaus, F., J. A. Hole, T. Ryberg, and G. S. Fuis (2007), Structure of the California Coast Ranges and San Andreas Fault at SAFOD from seismic waveform inversion and reflection imaging, *J. Geophys. Res., 112*, B06315.

Acknowledgements: This work was funded by U.S. National Science Foundation grant EAR-0106534. The data collection was supported by NSF, the Deutsche Forschungsgemeinschaft, the GeoForschungsZentrum Potsdam, and the U.S. Geological Survey.

Characterizing the Calico Fault Damage Zone Using Seismic and Geodetic Data

Elizabeth S. Cochran *(University of California, Riverside),* **Yong-Gang Li** *(University of Southern California),* **Peter M. Shearer** *(Scripps Institution of Oceanography),* **Sylvain Barbot (Scripps Institution of Oceanography), Yuri Fialko** *(Scripps Institution of Oceanography),* **John E. Vidale** *(University of Washington)*

During earthquakes slip is often localized on preexisting faults, but it is not well understood how the structure of crustal faults may contribute to slip localization and energetics. Growing evidence suggests that the crust along active faults suffers anomalous strain and damage during large quakes. Seismic and geodetic data from the Calico fault in the eastern California shear zone reveal a wide zone of reduced seismic velocities and effective elastic moduli. Using seismic travel times, trapped waves, and interferometric Synthetic Aperture Radar observations, we document seismic velocities reduced by 40 - 50% and shear moduli reduced by 65% compared to wallrock in a 1.5-km-wide zone along the Calico fault [*Cochran et al., 2009*]. Observed velocity reductions likely represent the cumulative mechanical damage from past earthquake ruptures. No large earthquake has broken the Calico fault in historic time, implying that fault damage persists for hundreds or perhaps thousands of years. These findings indicate that faults can affect rock properties at substantial distances from primary fault slip surfaces, and throughout much of the seismogenic zone, a result with implications for the portion of energy expended during rupture to drive cracking and yielding of rock and development of fault systems.

References

Cochran, E.S., Li, Y.-G., Shearer, P.M., Barbot, S., Fialko, Y., and Vidale, J.E., Seismic and Geodetic Evidence for Extensive, Long-Lived, Fault Damage Zones, *Geology, 37*(4), 315-318, 2009.

Acknowledgements: This research was supported by NSF (EAR-0439947) and SCEC (contribution number 1185).

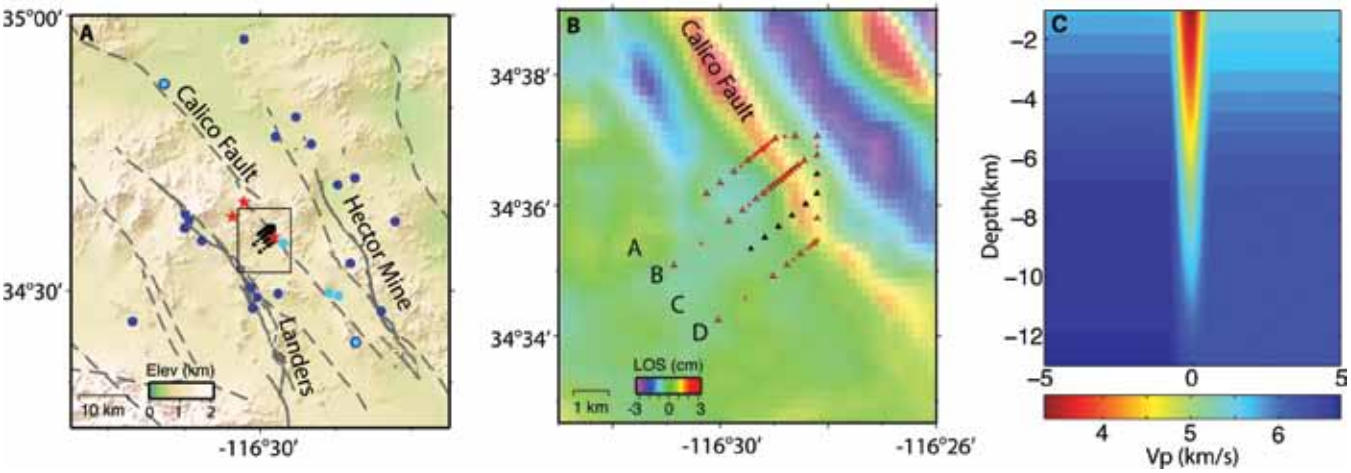

Figure 1. (A) A shaded relief map of the Mojave Desert region. Regional faults are shown by dashed gray lines and the Landers and Hector Mine ruptures are shown by solid gray lines. Light and dark blue circles indicate local earthquakes used in the fault zone trapped wave and travel-time analyses, respectively. Light blue circles with a dark blue outline were used in both analyses. Red stars denote shots. Black triangles and circles show seismic stations. The gray square outlines the region in Figure 1B. (B) High-pass-filtered coseismic interferogram from the 16 October 1999 Hector Mine earthquake that spans the time period from 13 January 1999 – 20 October 1999 (after Fialko et al., 2002). Colors denote variations in the line of sight (LOS) displacements. Black triangles and red circles are intermediate-period and short-period seismic stations. (C) Best fit model of P-wave low velocity zone with a 40% reduction in velocity estimated from seismic and geodetic data.

Temporal Variations in Crustal Scattering Structure Near Parkfield, California, Using Receiver Functions

Pascal Audet *(University of California Berkeley)*

We investigate temporal variations in teleseismic receiver functions using 11 yrs of data at station PKD near Parkfield, California, by stacking power spectral density (PSD) functions within 12-month windows. We find that PSD levels for both radial and transverse components drop by ~5 dB following the 2003 San Simeon (M 6.5) earthquake, with a persistent reduction in background levels of ~2 dB, relative to the pre-2003 levels, after the 2004 Parkfield (M 6) earthquake, corresponding to an estimated decrease in shear-wave velocity of ~0:12 and ~0:06 km/sec, respectively, or equivalent negative changes in Poisson's ratio of ~0:02 and ~0:01. Our results suggest that the perturbation originates at middle to lower crustal levels, possibly caused by the redistribution of crustal pore fluids, consistent with increased and sustained tremor activity near Parkfield following both earthquakes. This study shows that we can resolve temporal variations in crustal scattering structure near a major seismogenic fault using the receiver function method.

References

Audet, P., 2010. Temporal variations in crustal velocity structure near Parkfield, California, using receiver functions, *Bull. Seismol. Soc. Amer., 100.*

Ozacar, A. A., and G. Zandt (2009). Crustal structure and seismic anisotropy near the San Andreas fault at Parkfield, California, *Geophys. J. Int., 178*, 1098–1104

Acknowledgements: This work was supported by the Miller Institute for Basic Research in Science (UC Berkeley). Data was made available by the Northern California Earthquake Data Center (NCEDC).

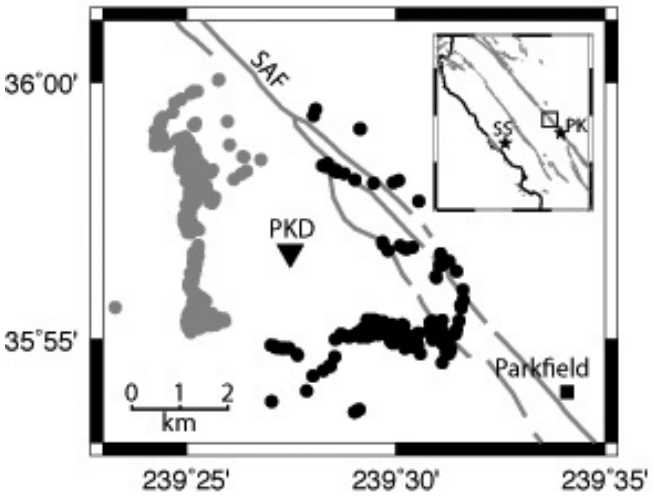

Moho piercing points of receiver functions grouped in two back-azimuth ranges of incoming wave fields (black, 0–200°; gray, 225–360°) at station PKD near Parkfield, California, with respect to study region (inset, major faults in gray). This grouping also corresponds to sampled volumes exhibiting different contrasts in VP/VS of the upper to middle crust with lower values in the west (Ozacar and Zandt, 2009) . San Andreas Fault is indicated by the gray lines near Parkfield. Stars in inset indicate the location of the 2003 San Simeon (SS) and 2004 Parkfield (PK) earthquakes.

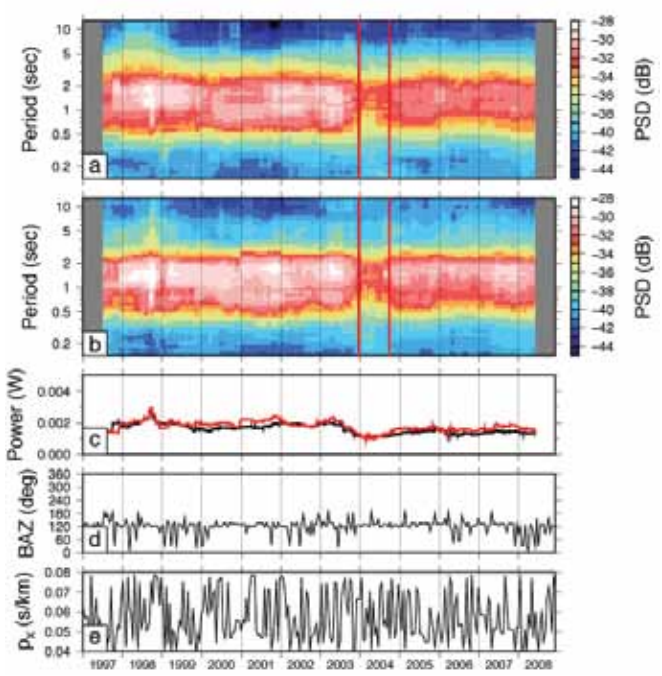

Temporal variations in receiver functions at station PKD for back azimuths 0–200°. Top panels show power spectral density of receiver functions binned within 95% overlapping, 12-month windows for (a) radial and (b) transverse components. (c) Corresponding variations in total power (black line, radial; gray line, transverse). Distribution of the 284 events with respect to (d) back azimuth and (e) slowness of incoming wavefields is presented in bottom panels. The thick vertical lines in (a) and (b) indicate times of the San Simeon (2003) and Parkfield (2004) earthquakes.

Preseismic Velocity Changes Observed from Active Source Monitoring at the Parkfield SAFOD Drill Site

Fenglin Niu *(Department of Earth Science, Rice University),* **Paul G. Silver** *(Department of Terrestrial Magnetism, Carnegie Institution of Washington),* **Thomas M. Daley** *(Earth Sciences Division, Lawrence Berkeley National Laboratory),* **Xin Cheng** *(Department of Earth Science, Rice University),* **Ernest L. Majer** *(Earth Sciences Division, Lawrence Berkeley National Laboratory)*

It is well known from laboratory experiments that seismic velocities vary with the level of applied stress [*e.g., Birch, 1960; Nur and Simmons, 1969*]. Such dependence is attributed to the opening and closing of microcracks due to changes in the stress normal to the crack surface [*e.g., O'Connell & Budiansky, 1974*]. In principle, this dependence constitutes a stress meter, provided that the induced velocity changes can be measured precisely and continuously. Indeed, there were several attempts in the 1970s to accomplish this goal using either explosive or non-explosive surface sources [*e.g., Leary et al., 1979*]. However, source repeatability and the precision of travel-time measurements only recently became adequate to observe the effect of tidal and barometric stress changes on seismic velocities in the field [*Yamamura et al., , 2003; Silver et al., 2007*]. The SAFOD pilot and main holes provided an unprecedented opportunity for a continuous active-source cross-well experiment to measure velocity changes at seismogenic depth. A specially designed 18-element piezoelectric source and a three-component accelerometer were deployed inside the pilot and main holes, respectively, at ~1 km depth. Over a two months period, we found a 0.3% change in the average S-wave velocity along the ~10 m baseline between the pilot and main holes. The velocity change showed an excellent anti-correlation with the barometric pressure. We attributed this anti-correlation to stress sensitivity of seismic velocity and the stress sensitivity is estimated to be 2.4x10-7 /Pa. Our results thus indicate that substantial cracks and/or pore spaces exist even at seismogenic depths and may thus be used to monitor the subsurface stress field. We also observed two large excursions in the travel-time data that are coincident with two earthquakes that are among those predicted to produce the largest coseismic stress changes at SAFOD (Figure 1) [*Niu et al, 2008*]. The two excursions started approximately 10 and 2 hours before the events, respectively, suggesting that they may be related to pre-rupture stress induced changes in crack properties, as observed in early laboratory studies [*e.g., Scholz, 1968*].

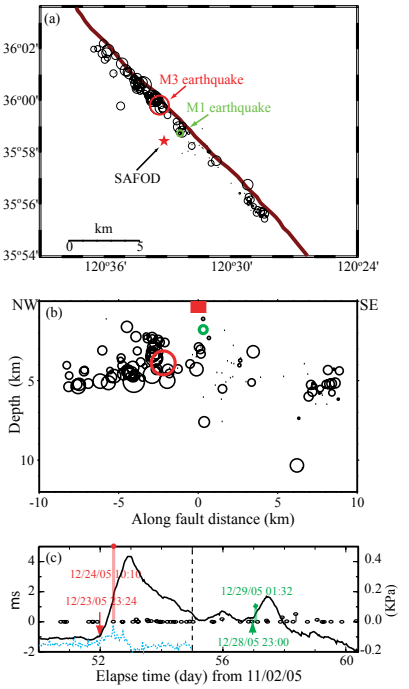

Figure 1 (a) Map of the experiment site showing the SAFOD drill site and the seismicity (circles). (b) Depth distribution of earthquakes that occurred in the experimental period. Red square, red and green circles indicate the SAFOD experiment site, the M3 and M1 earthquake, respectively. (c) Predicted coseismic stress changes at SAFOD for earthquakes occurring between December 22 of 2005 (day 50) and January 1 of 2006 (day 60). Note velocity changes (arrows) started a few hours before the two earthquakes (solid lines).

References

Birch, F. (1960), The velocity of compressional waves in rocks to 10 kilobars, part 1, *J. Geophys. Res., 65*, 1083–1102.

Leary, P.C., P.E. Malin, R.A. Phinny, T. Brocher, and R. Voncolln (1979), Systematic monitoring of millisecond travel time variations near Palmdale, California, *J. Geophys. Res., 84*, 659-666.

F. Niu, P. Silver, T. Daley, X. Cheng, E. Majer, 2008, Preseismic velocity changes observed from active source monitoring at the Parkfield SAFOD drill site, *Nature, 454*, doi:10.1038/nature07111.

Nur, A., and G. Simmons (1969), The effect of saturation on velocity in low porosity rocks, *Earth Planet. Sci. Lett., 7*, 183-193.

Scholz, C.H. (1968), Microfracturing and the inelastic deformation of rock I: compression, *J. Geophys. Res., 73*, 1417-1432.

Silver, P.G., T.M. Daley, F. Niu, and E.L. Majer

(2007), Active Source Monitoring of Cross-Well Seismic Travel Time for Stress-Induced Changes, . *Bull. Seismol. Soc., 97*, 281 - 293.

Yamamura, K., O. Sano, H. Utada, Y. Takei, S. Nakao, and Y. Fukao (2003), Long-term observation of in situ seismic velocity and attenuation, *J. Geophys. Res., 108*, 10.1029/2002JB002005.

Acknowledgements: We would like to thank the NSF funded SAFOD program and all the people involved for providing the experiment site, Rob Trautz of LBNL for supplying the barometric pressure logger, Dr. Mark Zumberge of University of California San Diego for providing the SAFOD strainmeter data, Don Lippert and Ramsey Haught of LBNL for helping the field work.

High-Resolution Locations of Triggered Earthquakes and Tomographic Imaging of Kilauea Volcano's South Flank

E. M. Syracuse *(University of Wisconsin-Madison),* **C. H. Thurber** *(University of Wisconsin-Madison),* **C. J. Wolfe** *(University of Hawaii at Manoa),* **P. G. Okubo** *(Hawaii Volcano Observatory),* **J. H. Foster** *(University of Hawaii at Manoa),* **B. A. Brooks** *(University of Hawaii at Manoa)*

Kilauea's south flank is the source of historic tsunamigenic earthquakes and is unusual in that it is one of the few non-subduction zone settings in which slow slip events (SSEs) have been observed to date. These SSEs have been observed every one to two years since 1997 and trigger earthquakes island-ward of the slip area. However, the exact locations of the triggered seismicity and the slow slip relative to the decollement fault underlying the south flank have been uncertain.

A temporary network of 20 seismometers, termed the SEQ network, was deployed on Kilauea's south flank to record the SSE that was predicted to occur in March 2007. Although the SSE did not occur until June 17 2007, the temporary SEQ network recorded over 3000 earthquakes, including those triggered by the SSE. We relocate hypocenters of volcano-tectonic earthquakes and invert simultaneously for P- and S-wave velocity structure using waveform cross-correlation and double-difference tomography using data from the SEQ network, as well as data from the permanent Hawaii Volcano Network (HVO) network, with additional data from other previous temporary arrays. The best-constrained hypocenters are those recorded by both the SEQ and HVO networks, which show the decollement as a subhorizontal layer of seismicity at 8 km depth that is several hundred meters (or less) thick in most areas. The eastern portion of the decollement shows little topography, while the western portion is gently dipping to the southeast, possibly due to a buried seamount. The seismicity triggered by the June 2007 SSE includes over 400 earthquakes overlapping with the southern edge of the decollement seismicity, indicating that both the slow slip and the triggered seismicity occur on the decollement.

A shallower swarm of earthquakes also occurred at 2 to 7 km depth in April 2007 near Apua Point, and may have been indirectly triggered by the Mw 8.1 Solomon Islands earthquake at ~6000 km distance, which occurred 48 hours prior to the beginning of the swarm. The locations and focal mechanisms of these earthquakes indicate that they likely occurred on the Hilina Pali fault along a dip angle of 30°.

Acknowledgements: This work was supported by NSF grant EAR-0910352, with instruments supplied by PASSCAL and AVO.

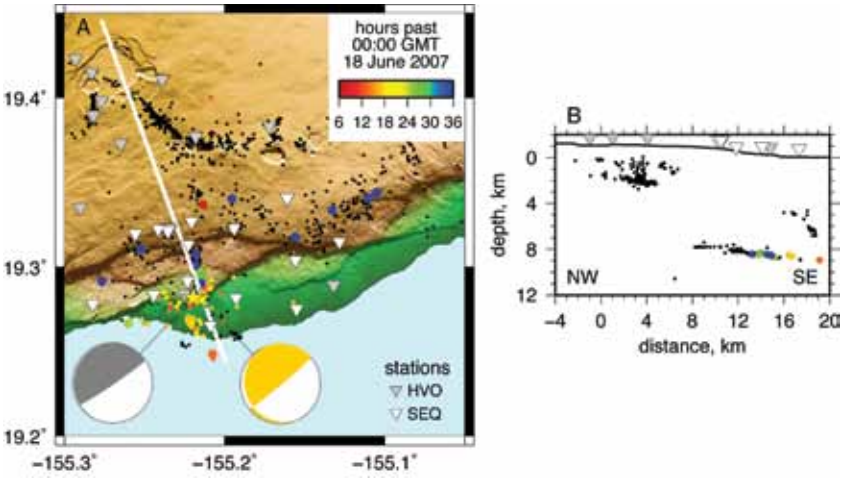

A) Seismicity recorded by SEQ & HVO stations. Earthquakes recorded just by SEQ stations during SSE are smaller colored circles. The focal mechanism of a triggered earthquake (orange) is the same as that of typical decollement seismicity (gray). B) Cross section along the white line in A.

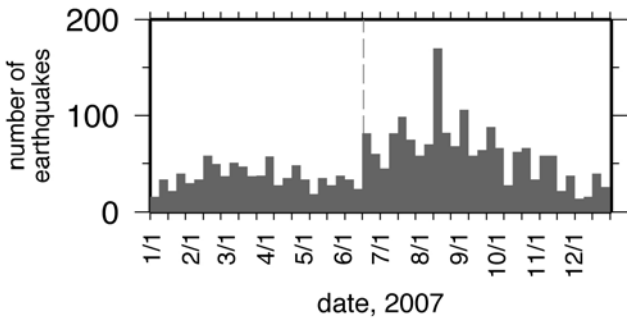

Histogram of seismicity deeper than 6 km from the HVO catalog, showing the increase in seismicity following the SSE.

Crustal Seismic Anisotropy in Southern California

Ryan Porter *(University of Arizona),* **George Zandt** *(University of Arizona),* **Nadine McQuarrie** *(Princeton University)*

Understanding lower crustal deformational processes and the related features that can be imaged by seismic waves is an important goal in active tectonics and seismology. Using data from publicly available stations, we calculated teleseismic receiver functions to measure crustal anisotropy at 38 broadband seismic stations in southern California. Results reveal a signature of pervasive seismic anisotropy located in the lower crust that is consistent with the presence of schists emplaced during Laramide flat slab subduction. Anisotropy is identified in receiver functions by the large amplitudes and small move-out of the diagnostic converted phases. Within southern California, receiver functions from numerous stations reveal patterns indicative of a basal crustal layer of hexagonal anisotropy with a dipping symmetry axis. Neighborhood algorithm searches [Frederiksen et al., 2003] for depth and thickness of the anisotropic layer and the trend and plunge of the anisotropy symmetry (slow) axis have been completed for the stations. The searches produced a wide range of results but a dominant SW-NE trend of the anisotropy symmetry axes emerged among the measurements. When the measurements were assigned to crustal blocks and restored to their pre-36 Ma locations and orientations using the reconstruction of *McQuarrie and Wernicke* [2005], the regional scale SW-NE trend became even more consistent (Fig. 1). This suggests that anisotropy predates Pacific-North American plate strike slip motion, though a small subset of the results can be attributed to NW-SE shearing that may be related to San Andreas transform motion (Fig 1). We interpret this dominant trend as a fossilized fabric within schists, created from a top-to-the-southwest sense of shear that existed along the length of coastal California during pre-transform, early Tertiary subduction. Comparison of receiver function common conversion point stacks to seismic models from the active LARSE experiment shows a strong correlation between the location of anisotropic layers and "bright" reflectors from *Fuis et al.* [2007], further affirming these results (Fig. 2).

References

Frederiksen, A. W., H. Folsom, and G. Zandt (2003), Neighbourhood inversion of teleseismic Ps conversions for anisotropy and layer dip, *Geophys. J. Int., 155*(1), 200-212.

Fuis, G. S., M. D. Kohler, M. Scherwath, U. ten Brink, H. J. A. Van Avendonk, and J. M. Murphy (2007), A comparison between the transpressional plate boundaries of the South Island, New Zealand, and southern California, USA: the Alpine and San Andreas Fault systems, in A Continental Plate Boundary: Tectonics at South Island, New Zealand, edited by D. Okaya, T. Stern and F. Davey, pp. 307-327, American Geophysical Union.

McQuarrie, N., and B. P. Wernicke (2005), An animated tectonic reconstruction of southwestern North America since 36 Ma *Geosphere, 1*(3), 147–172.

Acknowledgements: This work was funded by a grant from Southern California Earthquake Center and NSF EAR Earthscope Program award #0745588.

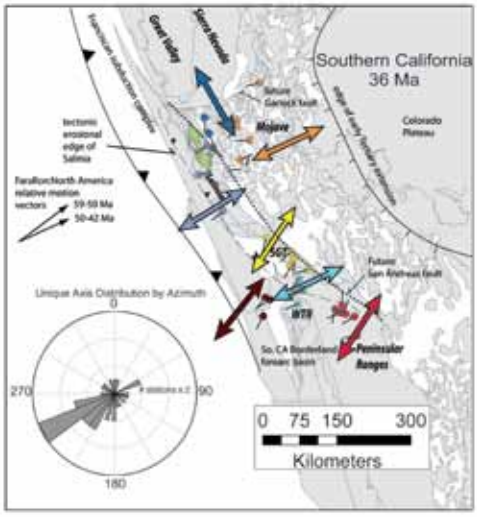

Figure 1. Map of station locations and unique anisotropy axis orientations at 36 Ma based on the reconstruction of McQuarrie and Wernicke (2005). Station color-coding corresponds to the crustal blocks. The large arrows show the best fitting block trend-lines rotated back to their orientation at 36 Ma. The rose diagram shows the number of stations with anisotropy trends within each 10° bin when rotated back to their 36 Ma orientations. Vectors show Early Tertiary Farallon-North America relative motion vectors.

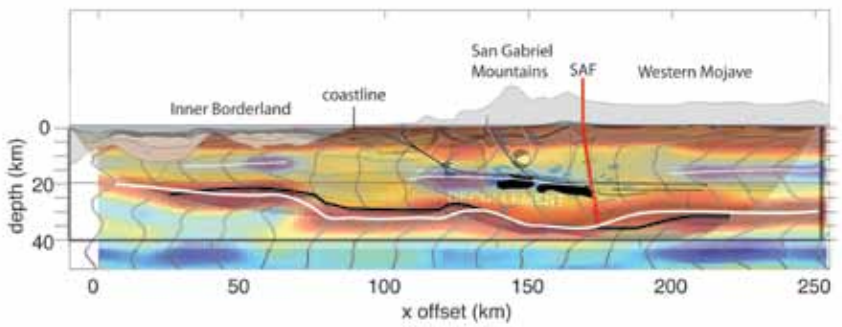

Figure 2. Common Conversion Point (CCP) cross-section for southern California, overlain with results from the LARSE project (Fuis et al., 2007) to illustrate similarities. In the RF stack, red shading corresponds to positive polarity arrivals and blue to negative. The thick white line represents the RF Moho, while the thick black line represents the LARSE Moho. Thin white lines represent structures (i.e., top of potential shear zones) seen in RFs. The thin black lines represent reflectors interpreted as a decollement in the LARSE cross-section and the thick black bodies represent the LARSE bright reflectors (Fuis et al., 2007). The thick vertical red line is the projection of the San Andreas fault.

Adjoint Tomography of the Southern California Crust

Carl Tape *(Harvard University),* **Qinya Liu** *(University of Toronto),* **Alessia Maggi** *(University of Strasbourg),* **Jeroen Tromp** *(Princeton University)*

We iteratively improve a 3D tomographic model of the southern California crust using numerical simulations of seismicwave propagation based on a spectral-element method (SEM) in combination with an adjoint method. The initial 3D model is provided by the Southern California Earthquake Center. The data set comprises three-component seismicwaveforms (i.e. both body and surface waves), filtered over the period range 2-30 s, from 143 local earthquakes recorded by a network of 203 stations. Time windows for measurements are automatically selected by the FLEXWIN algorithm. The misfit function in the tomographic inversion is based on frequency-dependent multitaper traveltime differences. The gradient of the misfit function and related finite-frequency sensitivity kernels for each earthquake are computed using an adjoint technique. The kernels are combined using a source subspace projection method to compute a model update at each iteration of a gradient-based minimization algorithm. The inversion involved 16 iterations, which required 6800 wavefield simulations. The new crustal model, m16, is described in terms of independent shear (Vs) and bulk-sound (Vb) wave speed variations. It exhibits strong heterogeneity, including local changes of +/- 30 percent with respect to the initial 3D model. The model reveals several features that relate to geological observations, such as sedimentary basins, exhumed batholiths, and contrasting lithologies across faults. The quality of the new model is validated by quantifying waveform misfits of full-length seismograms from 91 earthquakes that were not used in the tomographic inversion. The new model provides more accurate synthetic seismograms that will benefit seismic hazard assessment.

References

Tape, C., Liu, Q., Maggi, A., Tromp, J., 2009, Adjoint tomography of the southern California crust, *Science, 325*, 988–992.

Tape, C., Liu, Q., Maggi, A., Tromp, J., 2010, Seismic tomography of the southern California crust based on spectral-element and adjoint methods, *Geophys. J. Int., 180*, 433-462.

Maggi, A., Tape, C., Chen, M., Chao, D., Tromp, J., 2009, An automated time-window selection algorithm for seismic tomography, *Geophys. J. Int., 178*, 257–281.

Acknowledgements: Seismic waveforms were provided by the data centers listed in Table 2 (IRIS, SCEDC, NCEDC). All earthquake simulations were performed on the CITerra Dell cluster at the Division of Geological & Planetary Sciences (GPS) of the California Institute of Technology. We acknowledge support by the National Science Foundation under grant EAR-0711177. This research was supported by the Southern California Earthquake Center. SCEC is funded by NSF Cooperative Agreement EAR-0106924 and USGS Cooperative Agreement 02HQAG0008.

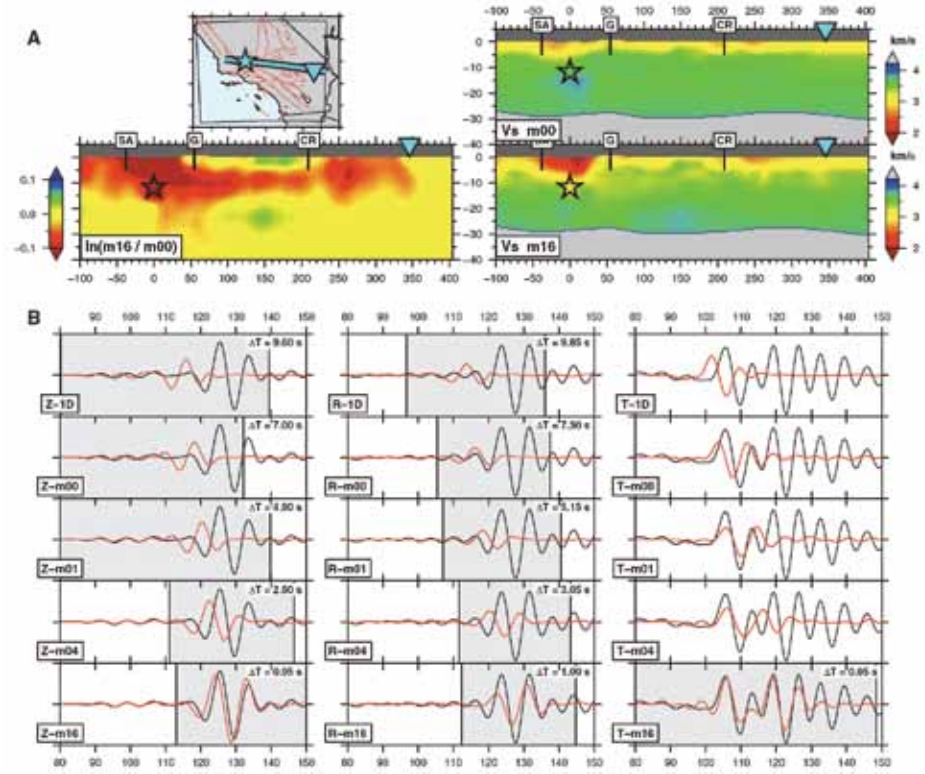

Iterative improvement of a three-component seismogram. (A) Cross section of the Vs tomographic models for a path from a Mw 4.5 earthquake (star) on the White Wolf fault to station DAN (triangle) in the eastern Mojave Desert. Upper right is the initial 3D model, m00; lower right is the final 3D model, m16; and lower left is the difference between the two, ln(m16/m00). Faults labeled for reference are San Andreas (SA), Garlock (G), and Camp Rock (CR). (B) Iterative three-component seismogram fits to data for models m00, m01, m04, and m16. Also shown are synthetic seismograms computed for a standard 1D model. Synthetic seismograms (red) and recorded seismograms (black), filtered over the period range 6 to 30 s. Left column, vertical component (Z); center column, radial component (R); right column, transverse component (T). Inset "DT" label indicates the time shift between the two windowed records that provides the maximum cross-correlation.

Nature of Crustal Terranes and the Moho in Northern Costa Rica from Receiver Function Analysis

Lepolt Linkimer *(Department of Geosciences, University of Arizona),* **Susan L. Beck** *(Department of Geosciences, University of Arizona),* **Susan Y. Schwartz** *(Department of Earth and Planetary Sciences, University of California),* **George Zandt** *(Department of Geosciences, University of Arizona),* **Vadim Levin** *(Department of Earth and Planetary Sciences, Rutgers University)*

The Central American subduction zone in northern Costa Rica shows along-strike variations in both the incoming and overriding plates. By analyzing the subducting oceanic Moho (M1) and the upper plate Moho (M2) with receiver functions, we investigate the variability in the hydration state of the subducting Cocos Plate and the nature of crustal terranes within the overriding Caribbean Plate. We calculate high-quality P- and PP- wave receiver functions using broadband data of the Global Seismology Network, Geoscope Project, and the CRSEIZE, Pocosol, and Corisubmod experiments. In addition, we estimate the depth (H) and vertically averaged Vp/Vs (k) to Moho and present a sensitivity study to explore the effects of a dipping interface on receiver functions and the H and k estimates. Our results are consistent with a drier oceanic mantle subducting beneath the southernmost part of the Nicoya Peninsula, as compared to a serpentinized oceanic mantle subducting beneath the northern part. In the Caribbean Plate, we describe the nature of the Mesquito, Nicoya, and Chorotega terranes by integrating new and published Vp/Vs estimates. Both the Nicoya and Chorotega terranes display high Vp/Vs (1.80-1.92) consistent with their oceanic character. In contrast, the oceanic Mesquito Terrane mostly displays lower Vp/Vs (1.62-1.80) more compatible with continental crust, which may indicate that subduction zone magmatism is modifying the crust to display continental character (see Figure). Our estimates show that the deepest M2 (~42 km) is observed in the volcanic arc region whereas the shallowest M2 (~27-33 km) is observed in parts of the fore-arc and back-arc regions.

References

DeShon, H. R., and S. Y. Schwartz (2004), Evidence for serpentinization of the forearc mantle wedge along the Nicoya Peninsula, Costa Rica, *Geophys. Res. Lett., 31*, L21611.

MacKenzie, L., G. A. Abers, K. M. Fischer, E. M. Syracuse, J. M. Protti, V. Gonzalez, and W. Strauch (2008), Crustal structure along the southern Central American volcanic front, *Geochem. Geophys. Geosyst., 9*, Q08S09.

Sallarès, V., J. J. Dañobeitia, and E. R. Flueh (2001), Lithospheric structure of the Costa Rican Isthmus: Effects of subduction zone magmatism on an oceanic plateau, *J. Geophys. Res., 106*(B1), 621-643.

Acknowledgements: Data from stations JTS, HDC, and CRSEIZE (in part) were obtained from the Data Management Center via IRIS. Thanks to S. Husen and V. Maurer for making the CORISUBMOD data available. Partial funding was provided by NSF grants EAR0510966 (S. Beck and G. Zandt) and EAR0506463 (S. Schwartz).

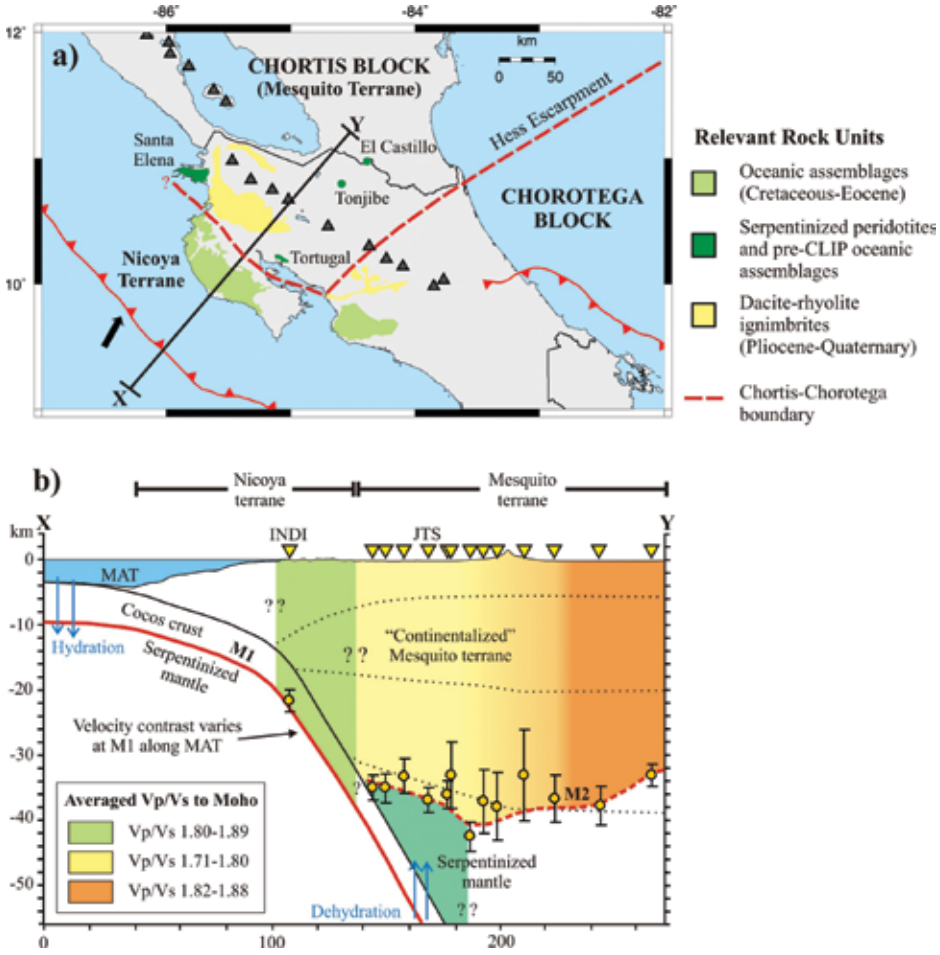

Generalized interpretation of terrane boundaries at surface (a) and along the X-Y cross-section (b) integrating results from this study, DeShon and Schwartz [2004], MacKenzie et al. [2008], and SallarÃ¨s et al. [2001].

Crustal Structure of the High Lava Plains of Oregon: A Large Controlled-Source Experiment

Catherine Cox *(University of Oklahoma),* **Randy Keller** *(University of Oklahoma)*

The High Lava Plains (HLP) of eastern Oregon and adjacent parts of Idaho and Nevada were the target of a very large controlled-source seismic experiment in early September 2008. This survey was designed to image the crust and upper mantle with the purpose of understanding the tectonics and mechanisms that drive the intraplate volcanism of the High Lava Plains and how this volcanism is related to the Cascade subduction zone and the Basin and Range province. This was survey proved successful thanks to the 67 scientists, students, and volunteers deployed 2612 Texan short-period seismic recorders and 120 RT-130 recorders from the PASSCAL and EarthScope instrument pools, and fired 15 seismic sources spaced across the High Lava Plains (HLP) region. This was the largest number of instruments deployed in an on-land controlled-source seismic experiment on a crustal scale. This army of helpers included 42 students from 12 different universities, mainly the University of Oklahoma, Stanford, Oregon State, Arizona State, MIT, Miami-Ohio, University of Texas at Dallas, and Rhode Island, as well as a team from the Carnegie Institution of Washington. These deployers were ably assisted by 6 staff members from the PASSCAL/EarthScope Instrument Center. This deployment also took advantage of the >100 seismometers in the HLP broadband array whose deployment over the three years was led by Carnegie Institution of Washington and Arizona State University. The University of Oregon, Michigan Tech, and the U. S. Geological Survey also deployed an array in the Newberry volcano area to record earthquakes and the seismic sources. Together, these efforts are providing a deep and three-dimensional image of the structure of this region.

New instrumentation built by the PASSCAL Instrument Center staff made it possible to carry out 3C recording using three Texan single-channel instruments at a site to study detailed crustal structure and anisotropy across the towering Steens Mountain region. The seismometers were located to provide high-resolution images of the mantle and crust directly beneath the path of volcanism that dotted the High Lava Plains during the past 16 Ma. In addition to the seismic component, the overarching project, funded by the National Science Foundation's Continental Dynamics program, includes field geologists, petrologists, and geodynamicists interested in resolving the origin of the sudden massive outpouring of basalt volcanism 16 million years ago and the puzzling trend of age-progressive rhyolite domes that reaches west toward Newberry volcano, the youngest complex in the trend. Our results show that: 1) the crust thicken east of Steens Mountain near the 0.706 Sr isotope line; 2) Basin and Range structures extend well north of their physiographic expression; and 3) HLP lower crust has relatively high velocity suggesting underplating.

Acknowledgements: This study was supported by the Continental Dynamics Program of the National Foundation (Award EAR-0641515)

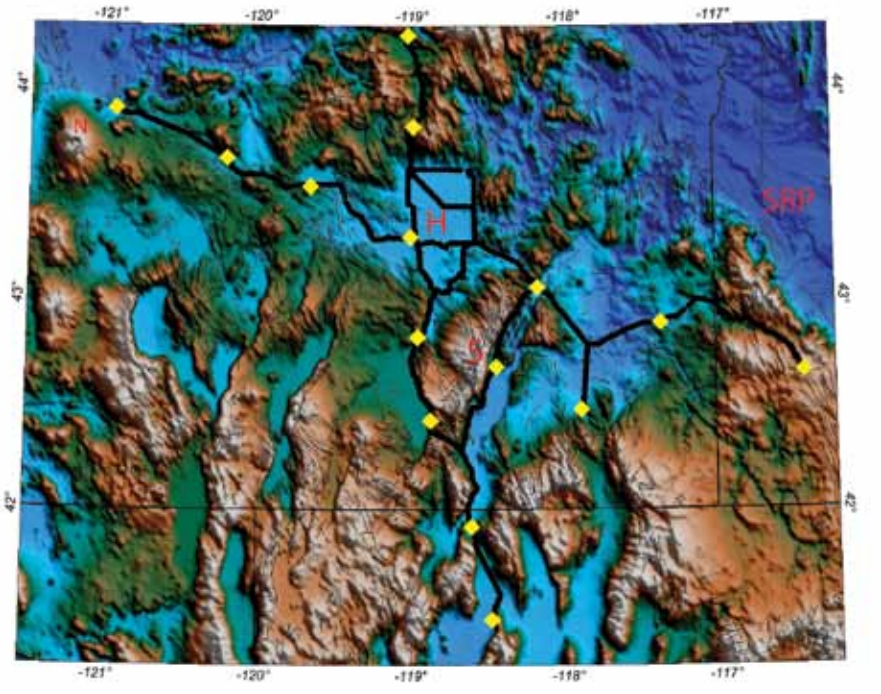

Index map of the High Lava Plains controlled-source experiment. Yellow diamonds indicate shot points; black lines indicate the main instrument deployment. N-Newberry Volcano. H-Harney Basin. S-Steens Mountain. SRP-Snake River Plain.

Shear Velocity Images of the Cascadia ETS Source Region

Josh A. Calkins *(Lamont-Doherty Earth Observatory),* **Geoffrey A. Abers** *(Lamont-Doherty Earth Observatory),* **Göran Ekström** *(Lamont-Doherty Earth Observatory),* **Kenneth C. Creager** *(University of Washington),* **Stéphane Rondenay** *(Massachusetts Institute of Technology)*

High-resolution 3D shear velocity (Vs) images of the western Washington lithosphere reveal structural segmentation above and below the plate interface correlating with transient deformation patterns. Using a spectral technique [Ekström et al, 2009], we extracted phase velocities from cross-correlated ambient noise recorded by the densely spaced "CAFE" Earthscope FlexArray. The spectral approach resolves shear velocities at station offsets less than 1 wavelength, significantly shorter than typically obtained by standard group-velocity approaches, increasing the number of useable paths and resolution. Tomographic images clearly illuminate the high Vs (>4.5 km/sec) subducting slab mantle. The most prominent anomaly is a zone of low Vs (3.0-3.3 km/sec) in the mid to lower continental crust, directly above the portion of the slab expected to be undergoing dehydration reactions. This low velocity zone (LVZ), which is most pronounced beneath the Olympic Peninsula, covers an area both spatially coincident with and updip of the region of most intense episodic tremor and slip (ETS). The low Vs and comparison with published P-wave velocity models indicate that Vp/Vs ratios in this region are greater than 1.9, suggesting a fluid rich lower crust. The LVZ disappears southward, near 47° N, coincident with sharp decreases in intraslab seismicity and ETS activity as well as structural changes in the slab. The spatial coincidence of these features suggests that long-term fluid-fluxing of the overriding plate via dewatering of a persistently hydrated patch of the Juan de Fuca slab may partially control slip on the plate interface and impact the rheology of the overriding continental crust.

References

Abers G.A., L.S. Mackenzie, S.Rondenay, Z. Zhang, A.G. Wech, and K.C. Creager, 2009. Imaging the source region of Cascadia tremor and intermediated-depth earthquakes. *Geology, 37*, 1119-1122.

Calkins, J.A., G.A. Abers, G. Ekstrom, K.C. Creager, and S. Rondenay. Shallow structure of the Cascadia subduction zone beneath western Washington from spectral ambient noise correlation. Submitted to *J. Geophys. Res.*, 2010.

Ekström, G., G. A. Abers, and S. C. Webb, 2009. Determination of surface-wave phase velocities across USArray from noise and Aki's spectral formulation. *Geophys. Res. Lett., 36*, L18301.

Acknowledgements: This work was funded by the National Science Foundation grant EAR-0544847.

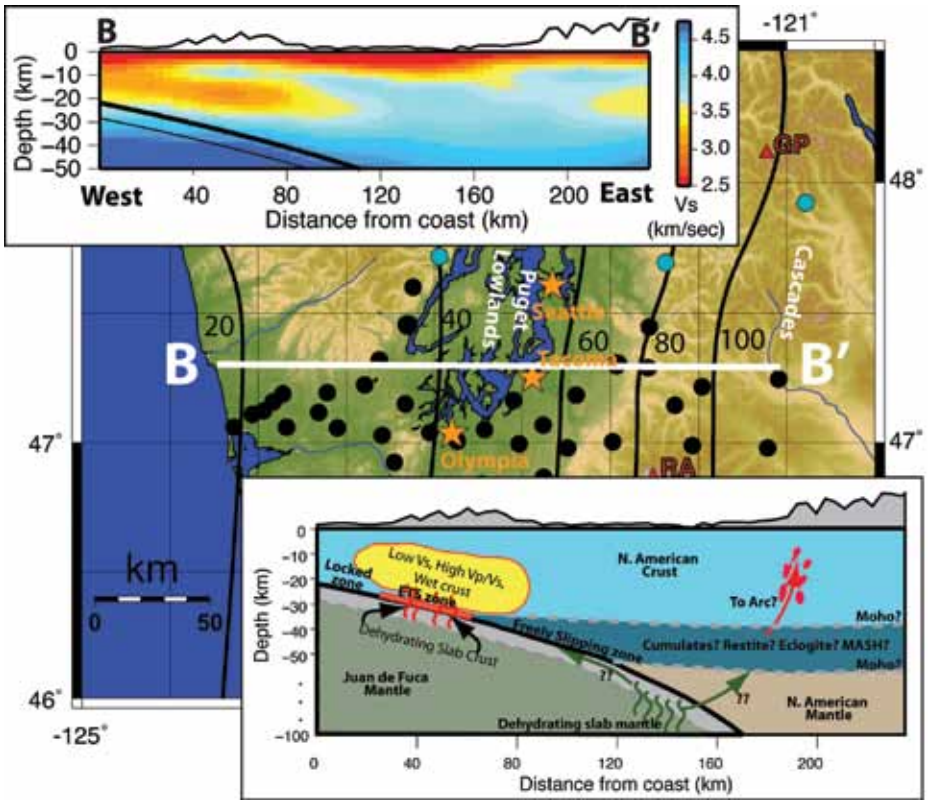

Results and interpretation of shear velocity imaging of Western Washington from spectral ambient noise analysis. Shaded relief map in the background shows PASSCAL stations (black circles), locations of major cities and topographic features, and the depth to the subducting slab in km (black lines and numbers, from McCrory et al, 2004). Upper panel shows shear velocity profile along line B-B', highlighting the low Vs zone in the North American plate directly above the portion of the subducting Juan de Fuca slab (thick black line, after Abers et al, 2009) expected to be undergoing dehydration reactions. Lower right panel is a cartoon illustrating the main features of the Vs model near the center of the CAFE array and possible interpretations.

Controlled Source Seismic Experiments in Northern China

Randy Keller *(University of Oklahoma),* **Gao Rui** *(Chinese Academy of Geological Sciences)*

SinoProbe is China's ambitious national joint earth science research project that was established to develop a comprehensive understanding of the deep interior beneath the Chinese continent. As one of the eight major programs within SinoProbe, SinoProbe-02 initiated a large-scale controlled-source seismic experiment in North China under the leadership of the Chinese Academy of Geological Sciences (CAGS) of the Ministry of Land and Resources (MLR) in cooperation with the University of Oklahoma and University of Missouri-Columbia. This experiment was conducted in December of 2009, and consisted of three coordinated seismic recording efforts along a profile that extended from near Beijing northwestward to the Mongolian border. The profile began near the eastern edge of the Western Block of the North China Precambrian craton, crossed this feature to the Solonker suture zone, and ended in the Central Asian orogenic belt (CAOB) (Fig.1).

The CAOB is one of the world's most prominent sites of formation juvenile Phanerozoic crust. In the southern segment of the CAOB, the Solonker suture zone was involved in the final closure of the paleo–Asian Ocean and amalgamation of the North China craton and Mongolian arc terranes. South of the Solonker suture zone, the zone of seismicity around the city of Zhangbei is most seismically active region in north China and includes the 19 January 1998 Zhangbei earthquake that claimed ~50 lives and caused severe damage.

The experiment employed a combination of 2-D seismic reflection imaging and refraction/wide-angle reflection methods. The seismic reflection profile used explosive sources each recorded at 600-1200 locations for 30 seconds to create a common-midpoint (CMP) stacked image. For the refraction/wide-angle reflection portion of the experiment, 8 large shots were fired and recorded in several cases to distances of 200 km. The main seismic monitoring system employed was the single-channel RefTek 125 ("Texan") recorder from the PASSCAL/UTEP instrument pool. Along the profile, 4 deployments of 300 Texan instruments were placed a ~1 km intervals (index map, sky-blue line). In addition, 120 supplementary, 3-component recording systems were deployed as part of the reflection data recording system (index map, yellow line).

Acknowledgements: The authors acknowledge China NSF grants 40830316 and the support of Sinoprobe-02. We also thank the following participants from USA: Galen Kaip, Stephen Holloway, Steven Harder, Jefferson Chang, Catherine Cox who were funded by a US NSF PIRE grant (0730154).

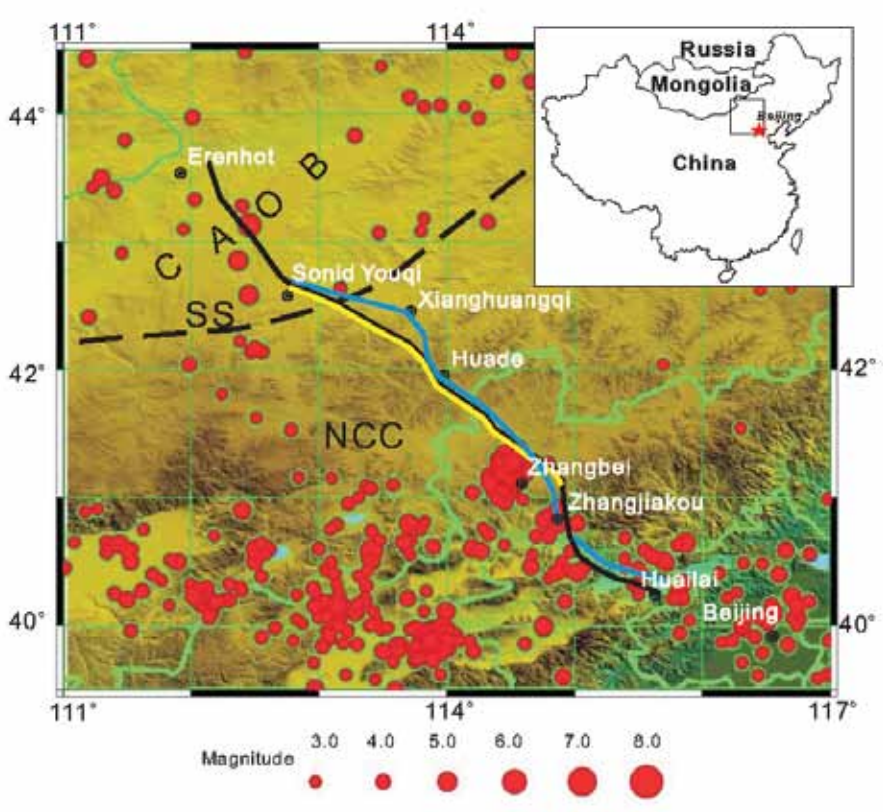

Index map of the Sinoprobe-2 reflection (black line) and refraction (yellow and blue lines) profiles. CAOB-Central Asian Orogenic Belt; SS-Solonker suture zone; NCC-North China Craton. Red circles are epicenters.

Radial Anisotropy in the Deep Crust beneath the Western US Caused by Extension

Morgan Moschetti *(US Geological Survey),* **Michael Ritzwoller** *(Univ. of Colorado),* **Fan-Chi Lin** *(Univ. of Colorado),* **Yingjie Yang** *(Univ. of Colorado)*

Although laboratory experiments have established that crustal rocks can be strongly anisotropic, the evidence for crustal anisotropy across large regions of the western US has not previously been documented. Surface waves can be used to identify crustal radial anisotropy (VSH != VSV), but the short period (< 20 s) surface wave dispersion measurements that are predominantly sensitive to crustal velocity structure are largely missing from distant earthquake signals because of scattering and attenuation. The development of noise interferometry methods now allows the measurement of surface wave dispersion at these shorter periods. Because Love and Rayleigh waves are predominantly sensitive to VSH and VSV, respectively, the simultaneous inversion of these measurements allows us to investigate the effects of crustal radial anisotropy. We invert Rayleigh and Love wave dispersion measurements from ambient noise and earthquake tomography for a radially anisotropic shear-velocity model of the crust and uppermost mantle beneath the western US (Moschetti et al., 2010a, 2010b). Where the Earth exhibits radially anisotropic properties, the effect of inverting for an isotropic model results in a characteristic data misfit termed the "Rayleigh-Love discrepancy" for which the predicted Rayleigh and Love wave speeds are faster and slower, respectively, than the observed surface wave speeds. An isotropic model results in large Rayleigh-Love discrepancies across most of the western US. We find that a model with an anisotropic uppermost mantle also results in a Rayleigh-Love discrepancy at periods that are mainly sensitive to crustal depths, but that the discrepancy is generally restricted to the Basin and Range (BR) and the Rocky Mountain BR (RMBR) provinces. The introduction of radial anisotropy in the deep crust resolves this discrepancy at all but a few, small regions in the western US. Within those geologic provinces that have experienced significant extension during the Cenozoic Era (~ 65 Ma), crustal anisotropy is often required to resolve the Rayleigh-Love discrepancy. Radial and azimuthal anisotropy in the upper mantle are generally ascribed to the alignment of olivine, and we similarly propose that the deep crustal anisotropy is caused by the alignment of anisotropic crustal minerals during crustal extension. This observation also supports the hypothesis that the response of the deep crust to crustal thinning is widespread within the extensional provinces.

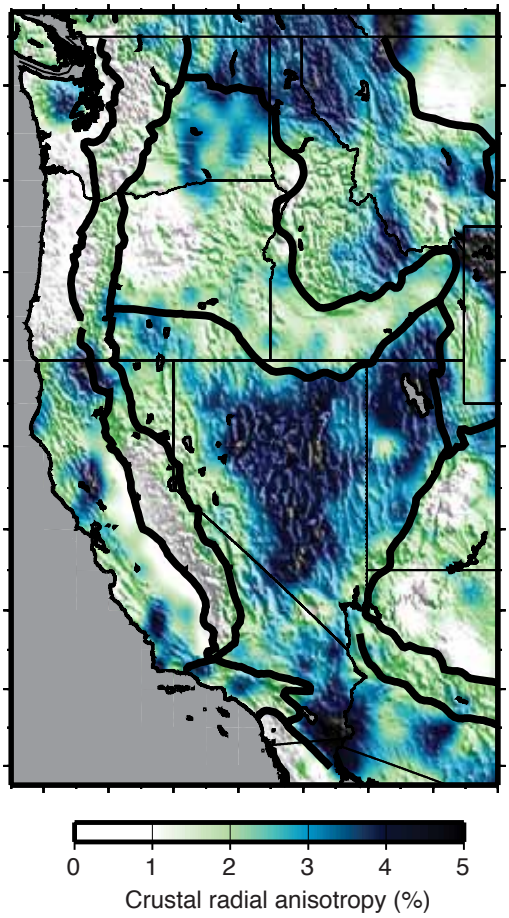

Amplitude of crustal radial anisotropy in the middle and lower crust. Strong anisotropy is mainly restricted to the predominant extensional provinces (Basin and Range, Rocky Mountain Basin and Range, and Omineca Extended Belt) of the western US.

References

Moschetti, M.P., M.H. Ritzwoller, F. Lin, Y. Yang (2010a) Seismic evidence for widespread western-US deep-crustal deformation caused by extension, *Nature, 464*, 885-889.

Moschetti, M.P., M.H. Ritzwoller, F. Lin, Y. Yang (2010b) Crustal shear-wave velocity structure of the western US inferred from ambient seismic noise and earthquake data, *J. Geophys. Res.* (In press)

Acknowledgements: Research support from the National Science Foundation (NSF) (EAR-0450082 and EAR-0711526) and an NDSEG Fellowship from the American Society for Engineering Education to M.P.M. are acknowledged. The facilities of the IRIS Data Management System, and specifically the IRIS Data Management Center, were used to access the waveform and metadata required in this study.

Structural Interpretations Based on a 3D Seismic Survey in Hawthorne, Nevada

Annie Kell-Hills *(Nevada Seismological Laboratory)*

Hawthorne, Nevada is located in the Walker Lake Domain of the Great Basin, a region in the western United States known for extensional tectonics and the high temperature gradients necessary for geothermal power production. Geothermal heat sources include magmatic and extensional types. The extensional type is more common for Nevada, where near-surface thermal gradients come from a thinned crust instead of from volcanism. Extensional systems often do not exhibit surface indicators such as springs or fumaroles; rather, the thermal fluids remain capped below the surface in "blind" systems requiring the need for geophysical exploration [*Coolbaugh et al., 2005*]. Heterogeneous structure and seismic velocities common to geothermal systems create particular seismic imaging difficulties because simplifying assumptions about velocity gradients cannot be made. A 3d seismic volume collected by the Navy Geothermal Programs Office on the Hawthorne Ammunition Depot represents a rare opportunity to examine the range of geologic interpretations that can exist on seismic data in the Great Basin. Strong reflection events within the volume project to a ~20 degree dip, allowing the possibility of a low angle normal fault; while bedding offsets could be interpreted as a series of steep basin-ward step faults. Synclines in vertical sections correspond to concentric circles in horizontal sections, not only raising questions about the possibility of migration processing artifacts, but also presenting similarities to sill intrusions as seen in North Sea 3d data. This data set reveals seismic evidence for a range of structural interpretations.

References

Coolbaugh, M. F., Arehart, G. B., Faulds, J. E., & Garside, L. J. (2005). Geothermal systems in the Great Basin, western United States: Modern analogues to the roles of magmatism, structure, and regional tectonics in the formation of gold deposits . Geological Society of Nevada Symposium, 1063, 1081.

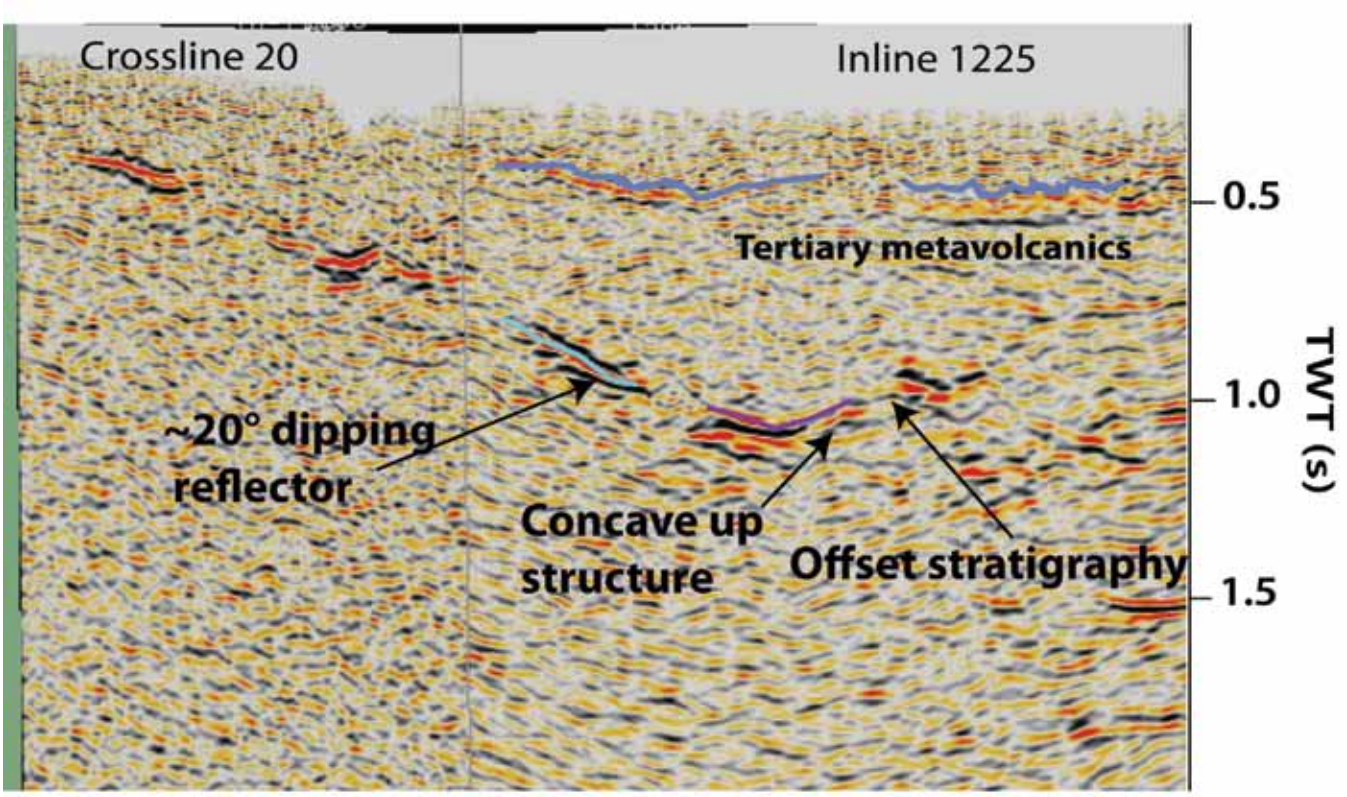

Inline and crossline sections showing strong reflections events indicating a range of structural interpretations. Inline sections clearly show 20° dipping reflectors, offset stratigraphy and synclinal events.

Assembling a Nevada 3D Velocity Model: Earthquake-Wave Propagation in the Basin & Range, and Seismic Shaking Predictions for Las Vegas

John N. Louie *(University of Nevada, Reno)*

The development of an open-source 3d modeling environment allows seismologists, explorationists, engineers, and students to predict wave propagation through geologically complex regions. The environment combines geologic and geotechnical data sets with gridding, modeling, and output specifications into portal packs for execution on standalone workstations, clusters, and supercomputing grids. A tutorial interface helps the user scale the grid to the facilities available, from small test runs to efforts requiring major resources. The ability to configure computations at a range of scales and model complexity is intended to promote wide use of advanced seismic modeling. Geologic models can include many basins in addition to the target urban basin, and detailed geotechnical information where available. To predict earthquake shaking in Nevada urban areas, the 3d model assembles several data sets at a wide variety of scales, from regional geologic maps to shallow shear-velocity measurements from microtremor transects having 0.3-km spacing (fig. 1). For Las Vegas the principal earthquake hazard is from the Furnace Creek fault system, capable of M7.5 events. Peak ground velocity (PGV) results from finite-difference wave modeling at 0.3 Hz show no obvious correlation between amplification and basin depth or dip of the basin floor. Animations of shaking show the expected strong trapping and long shaking durations within basins, as well as diffusion and scattering of energy between the many basins in the region. The two Furnace Creek scenarios tested, involving rupture away from and toward Las Vegas, produced unexpectedly different PGV in the city (fig. 2). Rupture directivity toward the city may amplify shaking by a factor of fifteen at some locations. Despite affecting only the very shallowest zone of models (<30 m), the Vs30 geotechnical shear-velocity shows clear correlation to 0.3-Hz PGV predictions in basins. Increasing basin thicknesses to 1.3 km correlate with increased PGV, but the basin effect at 0.3 Hz saturates for basin thicknesses greater than 1.3 km; deeper parts of the basin show variance and uncertainty of a factor of two in predicted PGV.

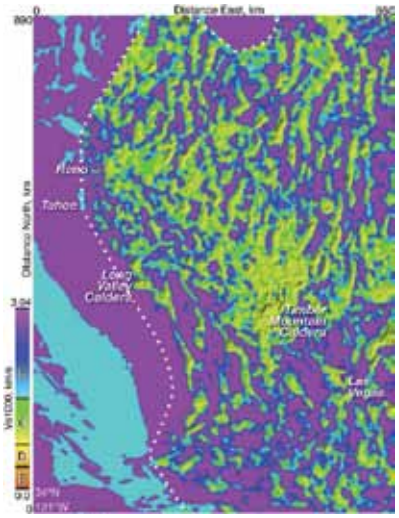

Figure 1: Map of average shear velocity from the surface to 1000 m depth assembled for the Nevada region, with part of California, on a shaded-relief basin-thickness map.

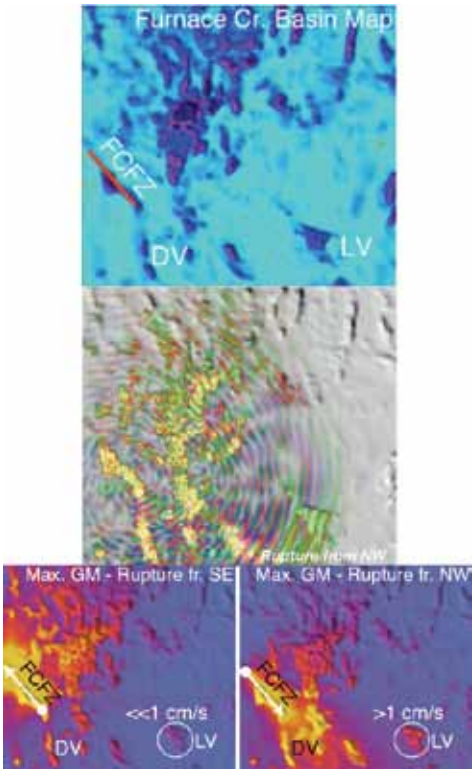

Figure 2: Maps comparing M7.5 Furnace Creek fault scenarios affecting Las Vegas. The upper image is a basin thickness map for the region of computation; middle is a snapshot map of E3D wave propagation at 0.3 Hz through the assembled model. Below are maximum ground-motion (PGV) maps, on the left for rupture away from Las Vegas, and on the right for rupture toward the city.

References

Louie, John N., 2008, Assembling a Nevada 3-d velocity model: earthquake-wave propagation in the Basin & Range, and seismic shaking predictions for Las Vegas: SEG Expanded Abstracts, 27, 2166-2170.

Acknowledgements: Research supported by the U.S. Geological Survey (USGS), Department of the Interior, under USGS award numbers 08HQGR0015 and 08HQGR0046; by Lawrence Livermore National Laboratory under LDRD Test Readiness funds; and by a Fulbright Senior Scholar award for work in New Zealand. The views and conclusions contained in this document are those of the authors and should not be interpreted as necessarily representing the official policies, either expressed or implied, of the U.S. Government. Instruments used in the field program were provided by the PASSCAL facility of the Incorporated Research Institutions for Seismology (IRIS) through the PASSCAL Instrument Center at New Mexico Tech. Data collected during this experiment will be available through the IRIS Data Management Center. The facilities of the IRIS Consortium are supported by the National Science Foundation under Cooperative Agreement EAR-0552316 and by the Department of Energy National Nuclear Security Administration.

Optimized Velocities and Prestack Depth Migration in the Reno-Area Basin

John N. Louie *(University of Nevada, Reno),* **Satish Pullammanappallil** *(Optim, Inc.),* **Annie Kell-Hills** *(University of Nevada, Reno)*

We collected seismic reflection profiles in the Reno, Nevada area basin in collaboration with the USGS and nees@UTexas during June 2009. Stratigraphic horizons and vertical offsets associated with faulting appear along a 6.72 km Truckee River profile while strong, horizontally propagating body waves are seen in shot gathers from the southern 3.84 km Manzanita Lane profile (fig. 1). Reno-area basin fill overlies Miocene andesitic volcanic rocks and consists of Neogene sedimentary rocks and Quaternary outwash deposits. Using the seismic shot records, we created optimized velocity models of the Reno basin using commercial SeisOpt®@2D™ software. The refracted P-wave arrivals provide inputs for a global velocity model over the length of the profiles and to a depth proportional to the source offset distances, expected to be 150-200 m. Within this basin most of the lateral velocity heterogeneity appears within 200 m of the surface. Comparing this velocity model to stacked sections produced by the USGS added confidence to the interpretations of strong reflection boundaries seen in the seismic sections (fig. 2). Boundaries in the velocity model coincide with prominent reflection boundaries as well as with known depths of volcanic fill and other deposits, constraining their depths and velocities. The tomographic velocity sections were then used as input with the shot records to a Kirchhoff pre-stack depth migration (PSDM) imaging steeply dipping structure and further constraining current interpretations and fault/basin geometry. The PSDM resolved the cause of the horizontally propagating waves seen along Manzanita Lane as sidewall reflections from a steeply dipping fault (fig. 3).

Acknowledgements: Research supported by the U.S. Geological Survey (USGS), Department of the Interior, under USGS award numbers G09AP00051, 08HQGR0015, and 08HQGR0046. The views and conclusions contained in this document are those of the authors and should not be interpreted as necessarily representing the official policies, either expressed or implied, of the U.S. Government.

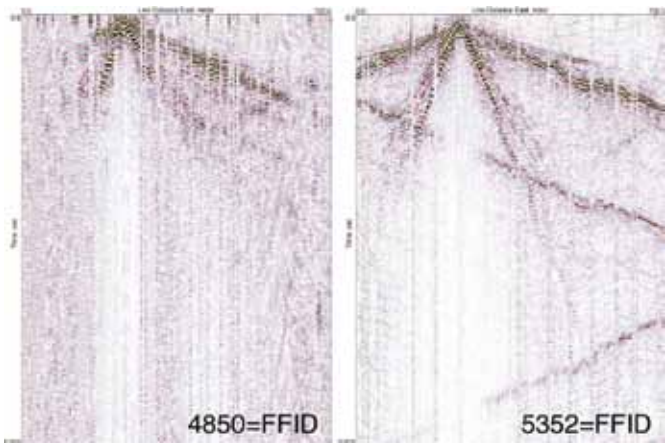

Figure 1: Two shot records from the Manzanita Lane survey, south Reno, showing strong horizontally-propagating body waves originating at surface fault traces.

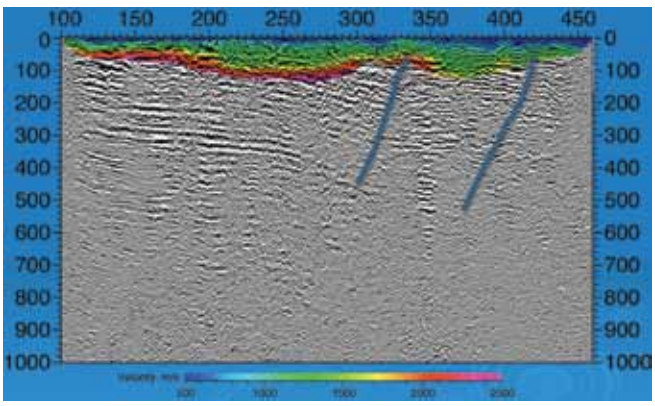

Figure 2: Depth section 2.3 km long extending to 1000 m depth, running west (left) to east (right) along the Truckee River through downtown Reno. No vertical exaggeration. Colors indicate velocities optimized from 1st-arrival picks, with Quaternary gravels (green) overlying Tertiary sands (red). The reflections are interpreted as showing two west-dipping normal faults (blue lines).

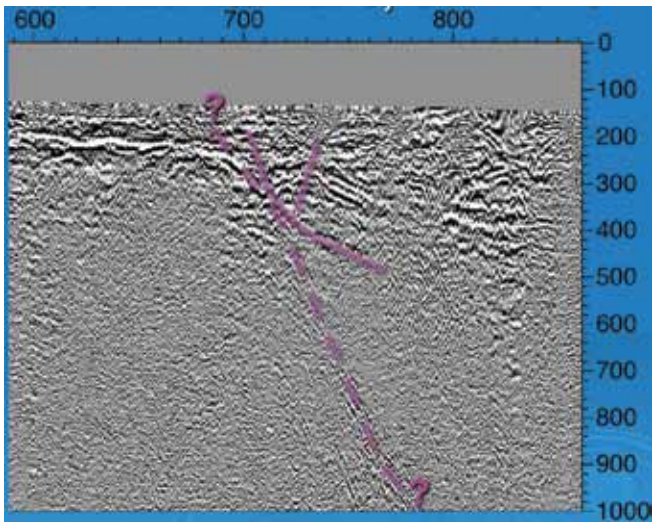

Figure 3: Portion of the depth section, 1.4 km long extending to 1000 m depth, running west (left) to east (right) along Manzanita Lane in south Reno. No vertical exaggeration- local ground surface is at 150 m depth on the vertical scale. The horizontally propagating waves image into a combination of a steeply dipping fault structure (dashed purple line) and a shallow-dipping structure (solid purple line).

Shallow Shear-Velocity Measurements and Prediction of Earthquake Shaking in the Wellington Metropolitan Area, New Zealand

John N. Louie *(University of Nevada, Reno)*

The city of Wellington, New Zealand's capital, sits astride the Australia-Pacific plate boundary at a transition from strike slip to subduction motion. The resulting high earthquake hazard and risk motivate multiple research efforts to better understand the potential for seismic shaking. Physics-based modeling of a Landers-type M7.2 rupture on the Wellington fault, which transects the city, by Benites and Olsen [2005] showed potential for peak ground velocities as high as 1.5 m/s. Such a high hazard demands a thorough understanding of the setting, and few measurements of ground-stiffness parameters such as the average shear velocity from the surface to 30 m depth (Vs30) existed in Wellington prior to 1996. That year Kaiser and Louie (2006 and not yet published) made refraction microtremor measurements of Vs30 at 46 sites in Wellington and Lower Hutt cities (fig. 1). Benites and Olsen's (2005) geotechnical model included velocities for "rock" sites that were a factor of two higher than the measurements, so we developed a revised model from the measurements. We then used the E3D physics-based modeling code of Larsen et al. [2001] to predict ground motions for a M3.2 event 8 km below the city that year, using both the original and revised models (fig. 2). The revised model is not quite as efficient at trapping wave energy in basins, as was the original model. Most of the Vs30 measurements were made at strong-motion recording stations, so the resulting seismometer data are now better calibrated for site conditions.

References

Benites, Rafael and Kim B. Olsen, 2005, Modeling strong ground motion in the Wellington metropolitan area, New Zealand: *Bull. Seismol. Soc. Amer., 95*, 2180–2196.

Kaiser, A. E., and J. N. Louie, 2006, Shear-wave velocities in Parkway basin, Wainuiomata, from refraction microtremor surface wave dispersion: GNS Science Report 2006/024, July, Lower Hutt, New Zealand, 16 pp.

Larsen, S., Wiley, R., Roberts, P., and House, L., 2001, Next-generation numerical modeling: incorporating elasticity, anisotropy and attenuation: Society of Exploration Geophysicists Annual International Meeting, Expanded Abstracts, 1218-1221.

Acknowledgements: Research supported by a 2006 Fulbright Senior Scholar award to Louie for work in New Zealand, and by GNS Science. Instruments used in the field program were provided courtesy of M. Savage of the Victoria University of Wellington, and S. Harder of the University of Texas El Paso.

Figure 1: Map of average shear velocity from the surface to 30 m depth assembled for the Wellington – Lower Hutt region of New Zealand, with the 1500 m/s velocity isosurface in shaded relief to show bedrock and basin-floor topography from Benites and Olsen (2005). Locations of 27 of 46 sites measured in 2006 for shallow shear velocity are marked with dashed circles, labeled with the measured Vs30 in m/s. Kaiser and Louie (2006) made an additional 19 measurements in one neighborhood in the lower center of the map, with only two results shown here. The measurements allowed a revision of the shallow velocity model, with Vs30 not exceeding 800 m/s. The basin-bounding Wellington fault runs along the northwest side of the basin.

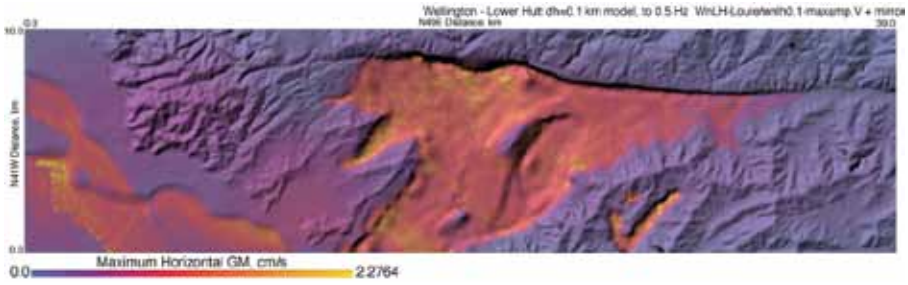

Figure 2: Map of peak ground velocity (PGV) computed for the Wellington – Lower Hutt region of New Zealand for a M3.2 event 8 km below the city, with the 1500 m/s velocity isosurface in shaded relief to show bedrock and basin-floor topography from Benites and Olsen (2005). The yellow color indicates PGV as high as 2.27 cm/s. 3D effects of complex basin geometry and soft soils are evident.

Crustal Structure beneath the High Lava Plains of Eastern Oregon and Surrounding Regions from Receiver Function Analysis

Kevin C. Eagar and Matthew J. Fouch *(Arizona State University),* **David E. James and Richard W. Carlson** *(Carnegie Institution of Washington)*

We analyze teleseismic P-to-S receiver functions to image crustal structure beneath the High Lava Plains (HLP) of eastern Oregon and surrounding regions. The coverage from 206 broadband seismic stations provides the first opportunity to resolve small scale variations in crustal composition, thickness, and heterogeneity. We utilize both Hκ stacking and a new Gaussian-weighted common conversion point stacking technique. We find crust that is ≥ 40 km thick beneath the Cascades, Idaho Batholith, and Owyhee Plateau, and thinner (~31 km) crust beneath the HLP and northern Great Basin. Low Poisson's ratios of ~0.250 characterize the granitic Idaho Batholith, while the Owyhee Plateau possesses values of ~0.270, typical of average continental crust. The Owyhee Plateau is a thick simple crustal block with distinct edges at depth. The western HLP exhibits high average values of 0.295, expected from widespread basaltic volcanism. Combined with other geological and geophysical observations, the areas of high Poisson's ratios (~0.320) and low velocity zones in the crust beneath north-central and southern Oregon are consistent with the presence of partial melt on either side of the HLP track, suggesting a central zone where crustal melts have drained to the surface, perhaps enabled by the Brothers Fault zone. Thicker crust and an anomalous N-S band of low Poisson's ratios (~0.252) skirting the Steens Mountain escarpment is consistent with residuum from a mid-crustal magma source of the massive flood basalts, supporting the view of extensive mafic under- and intraplating of the crust from Cenozoic volcanism.

References

Eagar, K.C., M.J. Fouch, D.E. James, R.W. Carlson, and the High Lava Plains Seismic Working Group, Crustal structure beneath the High Lava Plains of Eastern Oregon and surrounding regions from receiver function analysis, submitted to *J. Geophys. Res.,* June 2010.

Acknowledgements: This work would not have been possible without high quality seismic data provided through the hard work of the TA and the HLP Seismic Experiment teams (http://www.dtm.ciw.edu/research/HLP), and the services of the IRIS DMC. As always, the IRIS PASSCAL program provided world-class technical field support. A special thanks goes to Jenda Johnson, whose contributions to the project have been innumerable and immeasurable, and Steven Golden for providing field and data support. We would also like to acknowledge the work and productive discussions on the crustal evolution with the other PIs of the HLP project, including Anita Grunder, Bill Hart, Tim Grove, Randy Keller, Steve Harder, and Bob Duncan. This research was supported by National Science Foundation awards EAR-0548288 (MJF EarthScope CAREER grant), EAR-0507248 (MJF Continental Dynamics High Lava Plains grant) and EAR-0506914 (DEJ/RWC Continental Dynamics High Lava Plains grant).

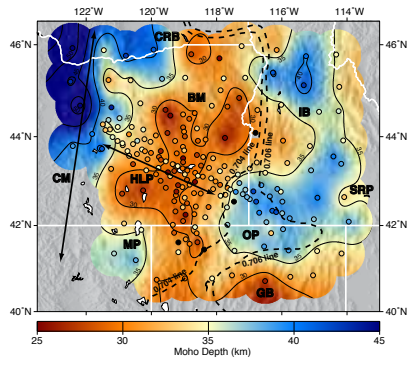

Figure 1: Map of Moho depth derived from H-k stacking analysis. Single station results (colored circles) are smoothed over a 10 x 10 km grid using splines under tension with a tension factor of 0.3 using the Generic Mapping Tools [Smith and Wessel, 1990]. Red colors denote shallower Moho; blue colors denote deeper Moho; gray regions represent areas of limited sampling in this study. Black solid lines denote 5 km contours. 87Sr/86Sr isopleths of 0.704 and 0.706 (".704" and ".706" lines) denoted by black dashed lines. Geologic provinces include Cascade volcanic arc (CM), Blue Mountains (BM), High Lava Plains (HLP), Columbia River basin (CRB), Snake River Plain (SRP), Idaho batholith (IB), Owyhee Plateau (OP), Modoc Plateau (MP), and Great Basin (GB).

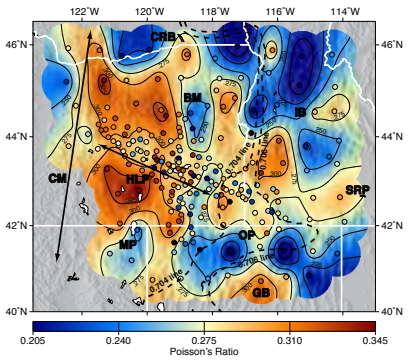

Figure 3: Map of Poisson's ratios derived from H-k stacking analysis. Smoothing parameters and geological/geochemical features are the same as in figure 1. Black solid lines denote 0.025 contours.

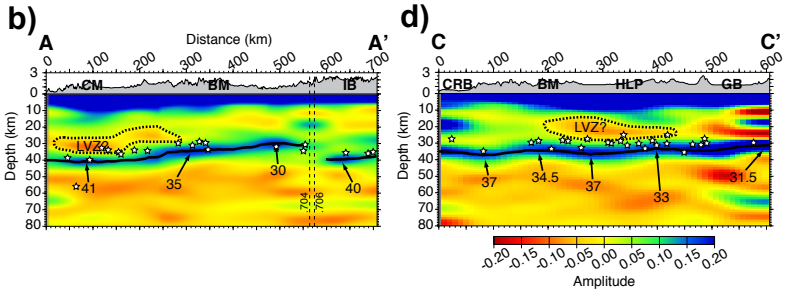

Figure 2: Cross-sections of Moho depths and crustal features. Geologic and geochemical provinces labeled as in the maps. Colored background is amplitudes from GCCP stacking. Solid line with depth labels is Moho valued picked from maximum amplitudes in GCCP stacks. Dotted black lines labeled LVZ are areas of strong negative amplitudes in the crust. White stars represent Hk Moho depths from the nearest stations along each profile. Profile A-A' is oriented east-west; profile C-C' is oriented north-south.

Imaging Radially Anisotropic Crustal Velocity Structure in NW Canada

Colleen A. Dalton *(Boston University),* **James B. Gaherty** *(LDEO, Columbia University),* **Anna M. Courtier** *(James Madison University)*

The tectonic evolution of Northwestern Canada spans several billion years of Earth history. As such, it presents an ideal environment for studying the processes of continental accretion and growth. We use ambient-noise cross-correlation to image anisotropic crustal seismic-velocity structure in NW Canada. Our focus area surrounds the CANOE (CAnadian NOrthwest Experiment) array, a 16-month IRIS PASSCAL deployment of 59 broadband seismic stations. We also include 42 broadband stations from the Canadian National Seismograph Network and the POLARIS network. We estimate the Green's function for each pair of stations by cross-correlating day-long time series of ambient noise in the time period July 2004 - June 2005. We observe fundamental-mode Rayleigh waves on cross-correlated vertical-component records and Love waves on the transverse components. We measure group velocities for the surface waves in the period range 5-30 s. Laterally, group velocities vary by as much as ±15% at the shortest periods and ±6% at longer periods, with the fastest velocities found within the Slave province and very slow velocities associated with thick sedimentary layers at short periods.

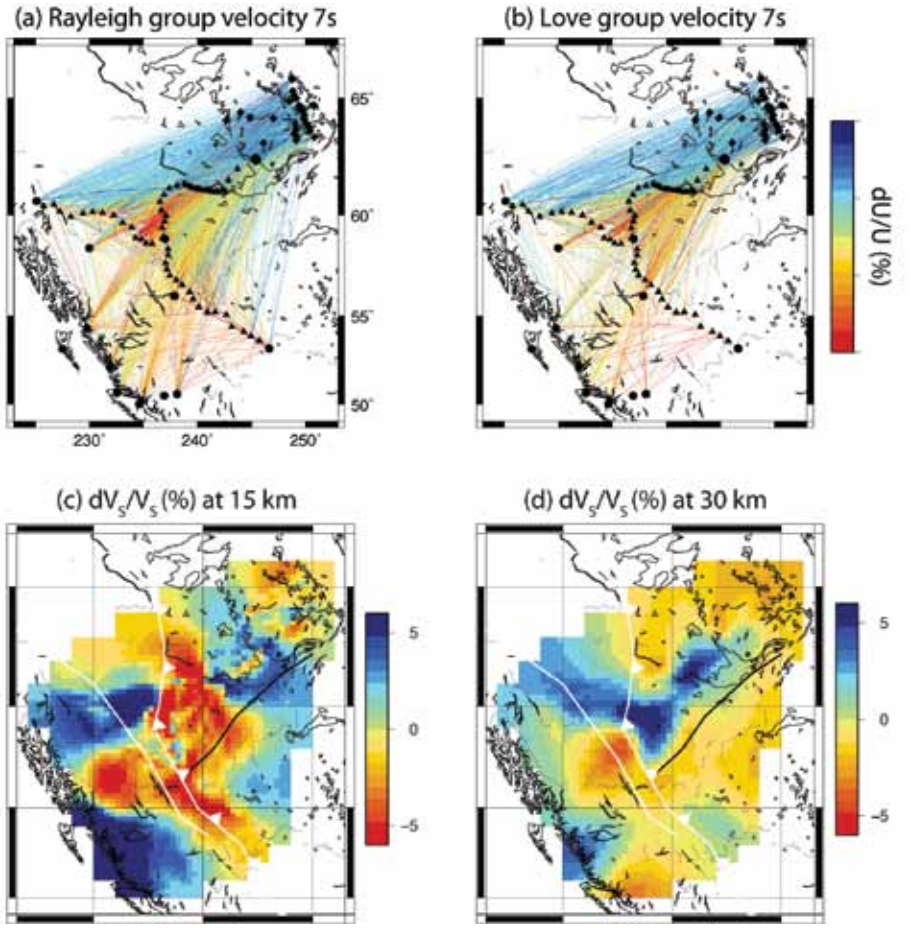

(a,b) Measurements of Rayleigh and Love wave group velocity, plotted as color-coded line segments along the great-circle path connecting each station pair. Color scale ranges from 2.75-3.25 km/s and 3.0-3.6 km/s for the Rayleigh and Love waves, respectively. (c,d) Isotropic velocity perturbation in the 3-D seismic model of the study area, shown here at 15- and 30-km depth. The white and black lines indicate the Tintina fault and Great Slave Lake Shear Zone, respectively. The white barbed line shows the eastern limit of Cordilleran deformation.

We investigate 3-D shear-velocity structure using two approaches. We use a Monte Carlo approach to test whether the data are consistent with isotropic velocity and find that the Love wave data require faster velocities in the middle--lower crust than the Rayleigh waves do; i.e., VSH>VSV. We also invert the group-velocity values (>2500 interstation paths) for 3-D radially anisotropic shear-wave velocity within the crust. Since the sensitivity kernels depend strongly on the assumed elastic structure, we use local kernels to account for the effects of laterally variable sedimentary structure. The resulting model correlates with several known geologic structures, including sedimentary basins at shallow depths and possibly the Cordillera-craton transition in the lower crust. The crustal model will also be useful for future studies of the upper mantle in this area.

Controlled-Source Seismic Investigation of the Generation and Collapse of a Batholith Complex, Coast Mountains, Western Canada

K. Wang *(Virginia Tech),* **J. A. Hole** *(Virginia Tech),* **A. L. Stephenson** *(University of Victoria), G. D. Spence (University of Victoria),* **K. C. Miller** *(Texas A&M University)*, **S. H. Harder** *(University of Texas, El Paso),* **R. M. Clowes** *(University of British Columbia)*

In 2009, the BATHOLITHS project acquired a 400-km long refraction and wide-angle reflection seismic survey across the Coast Mountains of British Columbia, Canada, a Jurassic to Eocene continental arc batholith complex.

Granitic batholiths created by magmatic differentiation in arcs above subduction zones make continental crust more felsic than the original materials derived from the mantle. However, differentiation from a mafic protolith results in a large volume of ultramafic residual that is petrologically part of the crust, not changing the bulk composition. This residue may reside hidden beneath the geophysical Moho, or it may have delaminated to sink into the mantle due to its relative density. Delamination may occur during subduction or during the collapse of the arc after subduction stops, and may coincide with a commonly observed late pulse of magmatism. As part of the BATHOLITHS multi-disciplinary investigation of these processes, traveltimes from the seismic survey are being used to build a 2-D P-wave velocity model of the crust.

East of the batholith complex, surface Mesozoic sedimentary and volcanic rocks are indicated by velocities of 4-5 km/s to 2-5 km depth. Beneath this basin, the Stikine terrane, an accreted late Paleozoic to early Mesozoic island arc, has felsic seismic velocities of 5.8-6.2 km/s to at least 15 km depth. A seismic reflector is observed at ~20 km depth beneath Stikinia but does not extend into the arc complex. Based on wide-angle reflections, the lower crust has a velocity of ~6.8 km/s under Stikinia, indicating mafic rocks. The Moho is at 35-38 km depth and the upper mantle has a fast velocity of ~8.1 km/s under Stikinia.

To the west in the continental arc complex, velocities of 5.6-6.2 km/s indicate granitic rocks in the upper crust to at least 15 km depth. A strong seismic reflector is observed at ~27 km depth only beneath the highest mountains and youngest batholiths in the eastern part of the batholith complex.

Wide-angle reflections indicate a velocity <6.6 km/s above the 27-km reflector and above the Moho in the western arc complex, indicating a felsic to intermediate composition. The Moho is at 30-33 km depth under the western Coast Mountains and dips eastward to maximum of 38-40 km beneath the highest mountains. The velocity between the 27-km reflector and the deepest Moho is >6.8 km/s, but the data are currently being analyzed to better constrain this number and search for magmatic residual. The upper mantle has a slow velocity of ~7.9 km/s under the arc complex.

Acknowledgements: The BATHOLITHS controlled-source seismic project is funded by an NSF grant from the Continental Dynamics Program and by a Canadian NSERC grant.

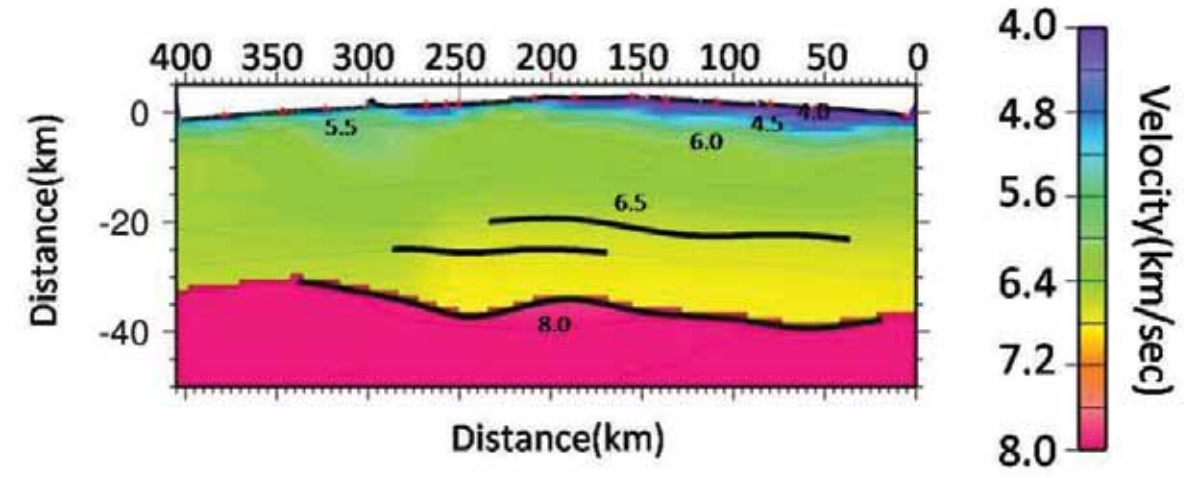

Preliminary seismic velocity model from the BATHOLITHS controlled-source seismic survey. Lower crust and Moho structure is still being modeled, and may change from this figure. The Stikine terrane to the east of the arc extends from model km 0 to 210. The Jurassic-Cretaceous arc lies west of the Coast Shear Zone at about model km 320. The youngest arc (Cretaceous-Eocene) and highest mountains are from model km 210 to 320. The curved surface of the model represents the spherical Earth.

SIMA/PICASSO: Seismic Investigations of the Moroccan Atlas/ program to Investigate Convective Alboran Sea System Overturn

R. Carbonell *(CSIC Earth Science Institute),* **J. Gallart** *(CSIC Earth Science Institute),* **M. Harnafi** *(Scientific Institute of Rabat, Rabat, Morocco),* **A. Levander** *(Rice University, Earth Science Department)*

In April 2010 we conducted a ~500 km long seismic refraction survey extending from the Sahara Desert to the Mediterranean Sea across Morocco. The refraction profile crossed the recently uplifted High Atlas, the Middle Atlas, and the western edge of the Rif Mountains. The project, Seismic Investigations of the Moroccan Atlas (SIMA), is affiliated with the PICASSO program in Spain and Morocco.

SIMA utilized 930 Reftek 125 Texan seismographs from the PASSCAL Instrument Center. Nominal instrument spacing was 350m from El Hajeb (central Morocco) south to the Sahara, and 500m to the north. The instruments recorded six 1000 kg shots located from El Hajeb south. An internationally diverse field crew of 75 faculty and students from more than a dozen institutions in Africa, Europe, and North America conducted the 2 week long experiment. Preliminary examination of the data shows quite complicated wide-angle reflections from several levels of the crust.

PICASSO is a project that includes land and sea magnetotelluric measurements, active and passive seismic experiments, geochemical sampling, structural geology, and geodynamic investigations of the western Mediterranean, and particularly of the Betics, the Gibraltar Arc, the Alboran Sea, the Rif, and the Atlas Mountains. PICASSO institutions include Rice, USC, Oregon, and WHOI in the USA, CSIC Earth Science Institute "Jaume Almera", Barcelona, the University of Barcelona, and the University of Salamanca in Spain, the Dublin Institute for Advanced Studies in Ireland, GEOMAR and the University of Muenster in Germany, and the Scientific Institute of Rabat, in Morocco.

Acknowledgements: SIMA was funded by a grant from the Spanish Science Foundation (FECYT), and was supported as part of PICASSO by grant EAR 0808939 from the NSF Continental Dynamics Program. We thank the Scientific Institute of Rabat, Rabat, Morocco, for generous assistance in the field, and Lloyd Carothers, Mike Fort, and Lisa Foley from the PASSCAL Instrument Center for outstanding field support.

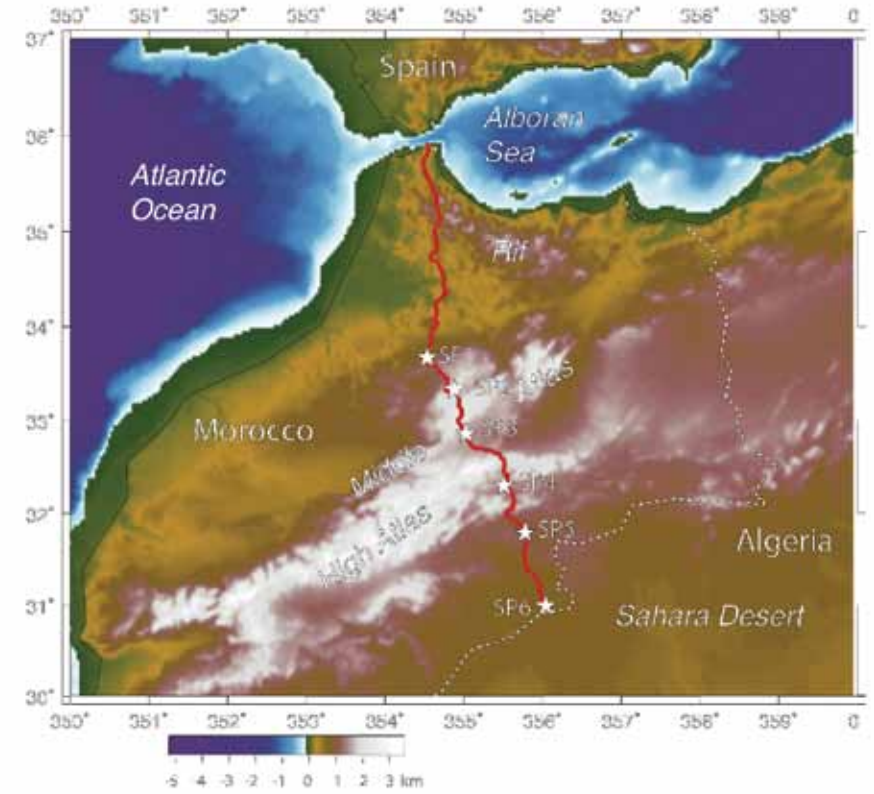

Map showing SIMA seismic refraction profile (stations are plotted in red), and shotpoints (black stars). SP1 is near El Hajeb, Morocco.

Northward Thinning of Tibetan Crust Revealed by Virtual Seismic Profiles

Tai-Lin Tseng *(University of Illinois, Urbana-Champaign),* **Wang-Ping Chen** *(University of Illinois, Urbana-Champaign),* **Robert L. Nowack** (*Purdue Univetrsity, W. Lafayette, IN)*

A new approach of constructing deep-penetrating seismic profiles reveals significant, regional variations in crustal thickness under near-constant elevation of Tibet. Over distances of hundreds of kilometers, the crust is as thick as 75 km in southern Tibet but shoals to just over 60 km under the Qiangtang terrane in central Tibet where the deviation from Airy isostasy is equivalent to a thickness of over 10 km in missing crust. Northward thinning of crust occurs gradually over a distance of about 200 km where mechanical deformation, instead of pervasive magmatism, also seems to have disrupted the crust-mantle interface.

References

Tseng, T.-L., W.-P. Chen and R. L. Nowack, Northward thinning of Tibetan crust revealed by virtual seismic profiles, *Geophys. Res. Lett., 36*, L24304 (with on-line supplements), doi:10.1029/2009GL040457, 2009.

Acknowledgements: The study was supported by U.S. National Science Foundation grants EAR99-09362 (Hi-CLIMB), EAR06-35419 and U.S. Air Force contract FA8718-08-C-002.

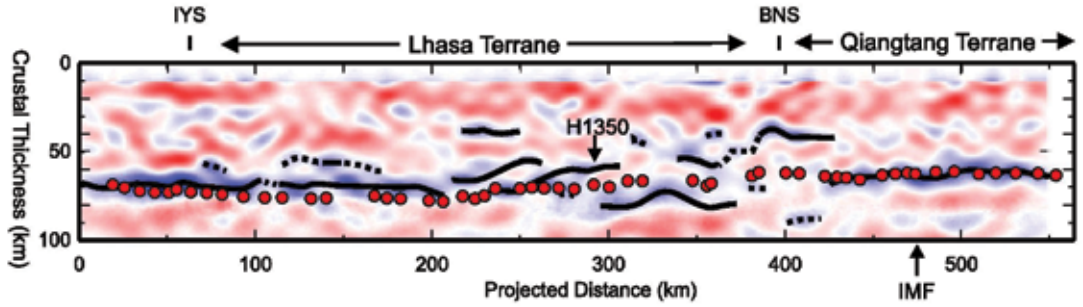

A comparison between crustal thickness estimated from wide-angle P-wave reflections (red dots) and an image of the Tibetan lithosphere obtained by Gaussian beam migration of direct P- to S-wave conversions [Nowack et al., 2010]. The convention is that a scatterer representing an increase in impedance with depth results in a blue pixel centered on the position of the scatterer. Black curves (dashed when uncertain), highlighting particularly strong impedance contrasts, show interpretations of the Moho transition zone in Nowack et al. [2009]. Notice near-constant crustal thickness over distances of hundreds of kilometers when the Moho is a simple interface near both ends of the profile. In the intervening zone of disrupted Moho, average crustal thickness decreases gradually northward by more than 10 km, from as much as 75 km to just over 60 km. Notice that the IMF is offset from the onset of shoaled Moho near the BNS. "H1350" marks the location of station whose observed waveform is discussed in detail by Tseng et al. [2009].

Quantification of Landscape Evolution Processes with Seismic Refraction Imaging, Boulder Creek Watershed, Colorado

Kevin M. Befus *(University of Colorado at Boulder),* **Anne F. Sheehan** *(University of Colorado at Boulder)*

We use minimally invasive shallow geophysical techniques to image the structure of the critical zone from surface to bedrock (0-25 m) throughout two small drainages within the Boulder Creek Critical Zone Observatory (BcCZO). Shallow seismic refraction (SSR) reveals the physical characteristics of the shallow subsurface. Results of the SSR surveys provide a pseudo-3D network of critical zone compressional wave velocity (Vp) structure within each catchment.

The evolution of each catchment within the BcCZO contain signals of both erosion and weathering dependent upon the large-scale geomorphic processes down to the microbial weathering of mineral grains. The geophysical approach describes the arena for the small-scale processes while also providing a quantitative description of the critical zone structure at an instant in time. This study encompasses two catchments, Betasso and Gordon Gulch, with connected recent and continuing geomorphic processes: fluvial rejuvenation and long-term quiescent erosion, respectively.

Geophysical results show crystalline bedrock Vp was greater than 3500 m/s, unconsolidated material Vp was generally less than 700 m/s and various gradients of weathered bedrock and consolidated material ranged from 700-3500 m/s if present. Fresh bedrock values in Betasso were imaged 12.1±2.8 m below the ground surface. Moderately weathered bedrock (Vp > 2000 m/s) was imaged at 6.0±2.4 m depth. Weathered rock and consolidated materials were imaged at 3.4±1.8 m depth. Unconsolidated materials were generally thinner than the sensitivity of our line setup at 0.9±0.8 m thick. In Gordon Gulch fresh bedrock values were imaged 11.7±3.1 m below the ground surface, moderately weathered bedrock at 5.8±2.7 m depth, and weathered rock and consolidated materials at 3.2±1.9 m depth. Again, unconsolidated materials were generally thinner than the sensitivity of our line setup at 0.9±0.7 m thick.

Significant topography and irregular bedrock surfaces contribute additional complexity to the critical zone architecture in each catchment. Aspect driven differences in the subsurface within each catchment overprints the broader geomorphic signals. SSR subsurface structure models will guide future investigations of critical zone processes from landscape to hydrologic modeling and assist in expanding point measurements of physical, chemical, and biological processes to the catchment scale.

Acknowledgements: I appreciate working as a research assistant as part of the Boulder Creek Critical Zone Observatory (BcCZO) funded by NSF grant NSF-EAR 0724960. I acknowledge the Mentorship Program of the University of Colorado's Department of Geological Sciences and the BcCZO in funding my field assistants. Also, I thank Austin Andrus for taking time out of working on his own related IRIS project to assist me with my fieldwork. I appreciate IRIS Passcal for loaning Geometrics Geode seismic equipment and field computers with important analysis software.

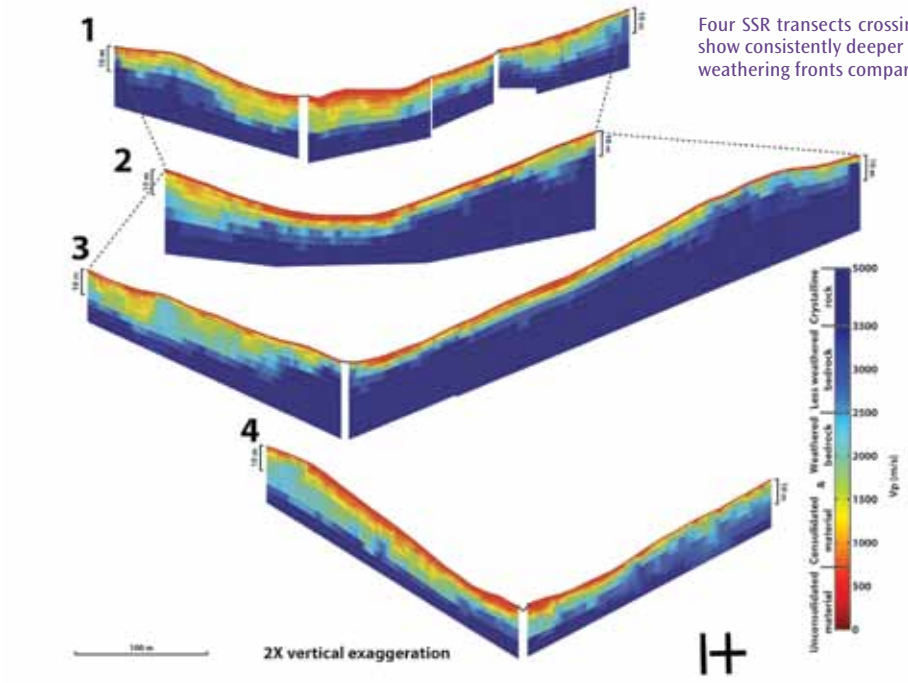

Four SSR transects crossing the Gordon Gulch catchment. North-facing slopes show consistently deeper low velocities (< 2500 m/s) and likely describe deeper weathering fronts compared to the profiles on the south-facing slope.

An Integrated Analysis of an Ancient Plate Boundary in the Rocky Mountains

Eva-Maria Rumpfhuber *(University of Oklahoma),* **Randy Keller** *(University of Oklahoma)*

Integration of multiple data sets to obtain better resolved, multiple parameter earth models has recently received new emphasis. We conducted an integrated analysis of the controlled-source seismic (CSS) and passive source seismic data from the CD-ROM (Continental Dynamics of the Rocky Mountains) experiment along with gravity and seismic reflection data. A specific goal of this study was establish a stronger tie between the CD-ROM and Deep Probe experiments that together form a profile that extends from northern New Mexico to Alberta, Canada. A major advantage of the CD-ROM seismic experiment dataset was the coincidence of the seismic profiles (Fig. 1), which facilitated a joint interpretation of our new results and the previous CD-ROM results. As the first step in this process, we created a new P-wave velocity and interface model from the CSS data based on an advanced picking strategy that produced a new and extended set of travel-time picks relative to those employed in previous studies. In addition, we were able to identify a substantial set of S-wave arrivals and establish an independent S-wave model. Thus, we were able to compare and jointly interpret crustal thicknesses the various techniques produced as well as vp/vs ratios from receiver functions and the CSS dataset. Furthermore, the comparisons provided insights about the strengths and uncertainties of each technique. Thanks to the integration of the controlled-source and receiver function results, we were able to construct a well-constrained structural model and tectonic interpretation that shows the structural framework of the transition from the Wyoming craton to the north across the suture Cheyenne belt suture zone into the Proterozoic terranes to the south (Fig. 2). The interpretation that crustal-scale crocodile structures are present provides an explanation for the south dip of the Cheyenne belt suture in the upper crust and the north-dipping slab in the mantle (Fig. 2). The very distinct crustal structures north and south of the suture zone are clearly shown in our model and document that the blocks that collided ~1.8 Ga to form the Cheyenne belt suture zone have retained their basic crustal and uppermost mantle structure since that time.

Acknowledgements: This work was supported by the National Science Foundation as part of the GEON project (EAR-0225670)

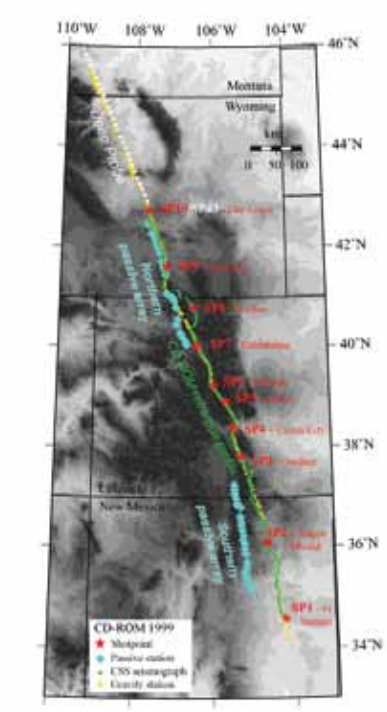

Figure 1: Index map of the CD-ROM seismic experiments. The controlled source seismic stations (green), their corresponding shotpoints (red stars), and the northern and southern passive arrays (light blue diamonds) are shown. Yellow dots indicate the locations of gravity stations. The Deep Probe experiment profile that also used the Day Loma shotpoint is shown as a white dashed line.

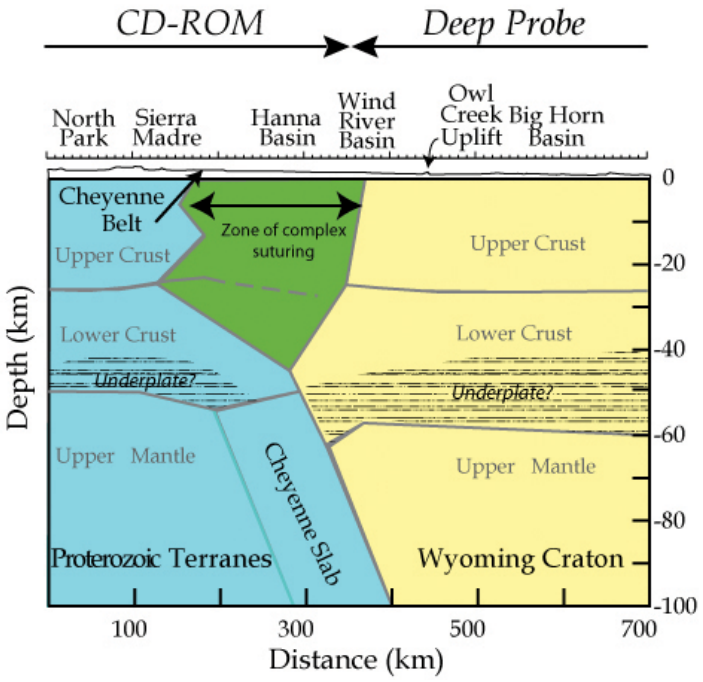

Figure 2: Tectonic synthesis based on the integration of the seismic data from the CD-ROM and Deep Probe experiments. The yellow color indicates the Wyoming Craton in the north, and the blue color represents the Proterozoic terranes to the south. An area of complex suturing (Crocodile structure) is indicated in green. The horizontal lined pattern in the lower crust indicates interpreted zones of underplated material based on xenolith data.

Full-Wave Ambient Noise Tomography of Northern Cascadia

Yang Shen *(University of Rhode Island),* **Wei Zhang** *(University of Rhode Island)*

We use empirical Green's functions derived ambient noise to iteratively improve a 3D velocity model of the crust and uppermost mantle beneath northern Cascadia. The data set includes up to 5 years (2005-2009) continuous records from 69 broadband seismic stations. Wave propagation is simulated using a finite-difference method with boundary conforming grids that account for the effects of topography and 3D heterogeneity. The initial reference model is CRUST 2.0. Travel time anomalies are measured by cross-correlating empirical and synthetic Green functions. Finite-frequency sensitivity kernels are computed using the scattering integral method. In the frequency and time window of interest, the empirical Green's function derived from cross-correlation of vertical-to-vertical component is dominated by Rayleigh waves, which are sensitive to not only shear but also compressional wave speeds. So the inverse problem is structured as a joint solution for Vp and Vs. The solution converges after 4 model iterations, with a total 96% variance reduction. Resolution tests show a Vp resolution in the shallow crust. The Vp structure is validated by a comparison with active-source experiments and well logs. A comparison of the observed and predicted earthquake waveforms shows a much-improved waveform fit, indicating that the new model could be used to refine seismic hazard assessment. The new model also reveals features that relate to geological observations, such as the sediment basins, the accretionary complex and the Siletz terrane.

References

Shen, Y., and W. Zhang (2010), Full-wave ambient noise tomography in Northern Cascadia, *Seismol. Res. Lett., 81* (2), SSA 2010 Abstract.

Acknowledgements: This research was supported by the National Science Foundation under grant 0727919 and the Air Force Research Laboratory under contract FA9453-10-C-0217. The IRIS DMC provided seismic waveforms.

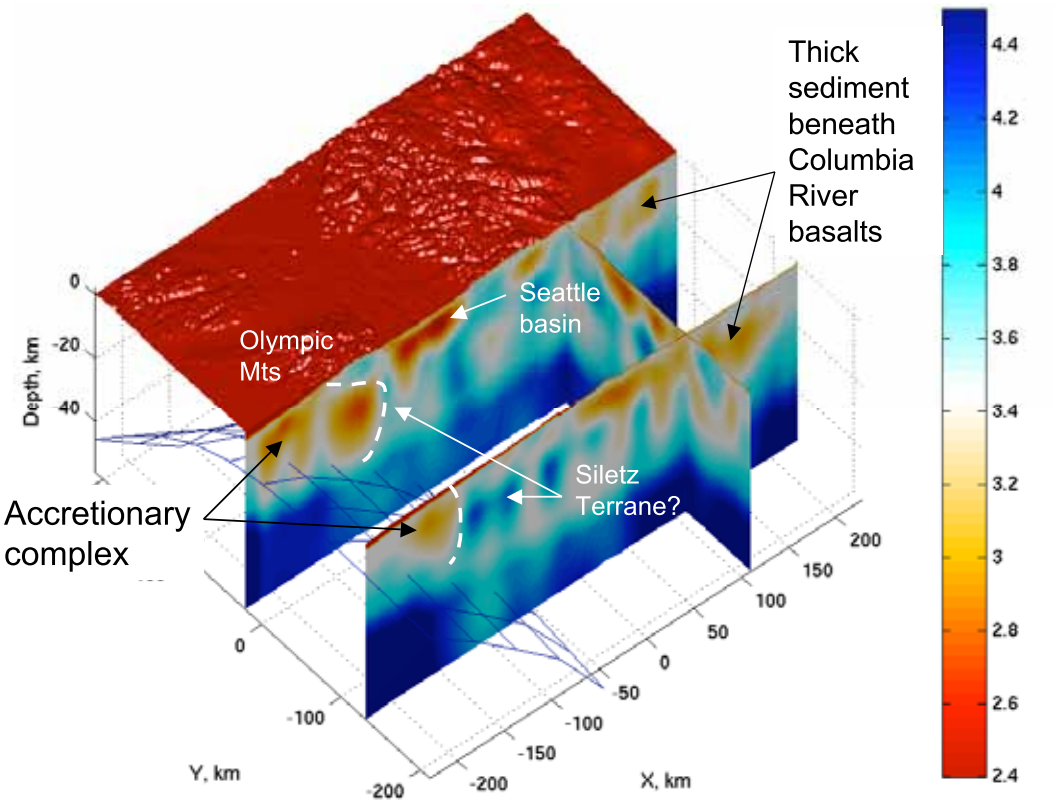

The 3D shear velocity model of northern Cascadia from full-wave ambient noise tomography. The mesh represents the upper surface of the subducted oceanic crust. Color indicates the wave speed in km/s. Several geological features are clearly imaged, such as the Seattle Basin, the accretionary complex, the Siletz Terrane and the sediment beneath Columbia River basalts.

Crustal Velocity Structure of Turkey from Ambient Noise Tomography

Linda M. Warren *(Saint Louis University),* **Susan L. Beck** *(University of Arizona),* **George Zandt** *(University of Arizona),* **C. Berk Biryol** *(University of Arizona),* **A. Arda Ozacar** *(Middle Eastern Technical University),* **Yingjie Yang** *(University of Colorado)*

In eastern Turkey, the ongoing convergence of the Arabian and African plates with Eurasia has resulted in the westward extrusion of the Anatolian plate. To better understand the current state and the tectonic history of this region, we image crust and uppermost mantle structure with ambient noise tomography. Our study area extends from longitudes of 32-44 degrees E. We use continuous data from two PASSCAL deployments, our 2006-2008 North Anatolian Fault Passive Seismic Experiment and the 1999-2001 Eastern Turkey Seismic Experiment, as well as from additional seismometers in the region. We compute daily cross-correlations of noise records between all station pairs and stack them over the entire time period for which they are available, as well as in seasonal subsets, to obtain interstation empirical Green's functions. After selecting interstation cross-correlations with high signal-to-noise ratios and measuring interstation phase velocities, we compute phase velocity maps at periods ranging from 8-40 s. At all periods, the phase velocity maps are similar for winter and summer subsets of the data, indicating that seasonal variations in noise sources do not bias our results. Across the study area, we invert the phase velocity estimates for shear velocity as a function of depth. The shear velocity model, which extends to 50 km depth, highlights tectonic features apparent at the surface: the Eastern Anatolian Volcanic Province is a prominent low-velocity anomaly whereas the Kirsehir Block has relatively fast velocities. In addition, in the southeastern part of our study area, we image a high velocity region below 20 km depth which may be the northern tip of the underthrusting Arabian plate. There are velocity jumps across the Central and East Anatolian Fault Zones. The North Anatolian Fault Zone appears as a fast anomaly in the upper crust.

Acknowledgements: This work was fund by the National Science Foundation through grant EAR-0309838 and Independent Research and Development time.

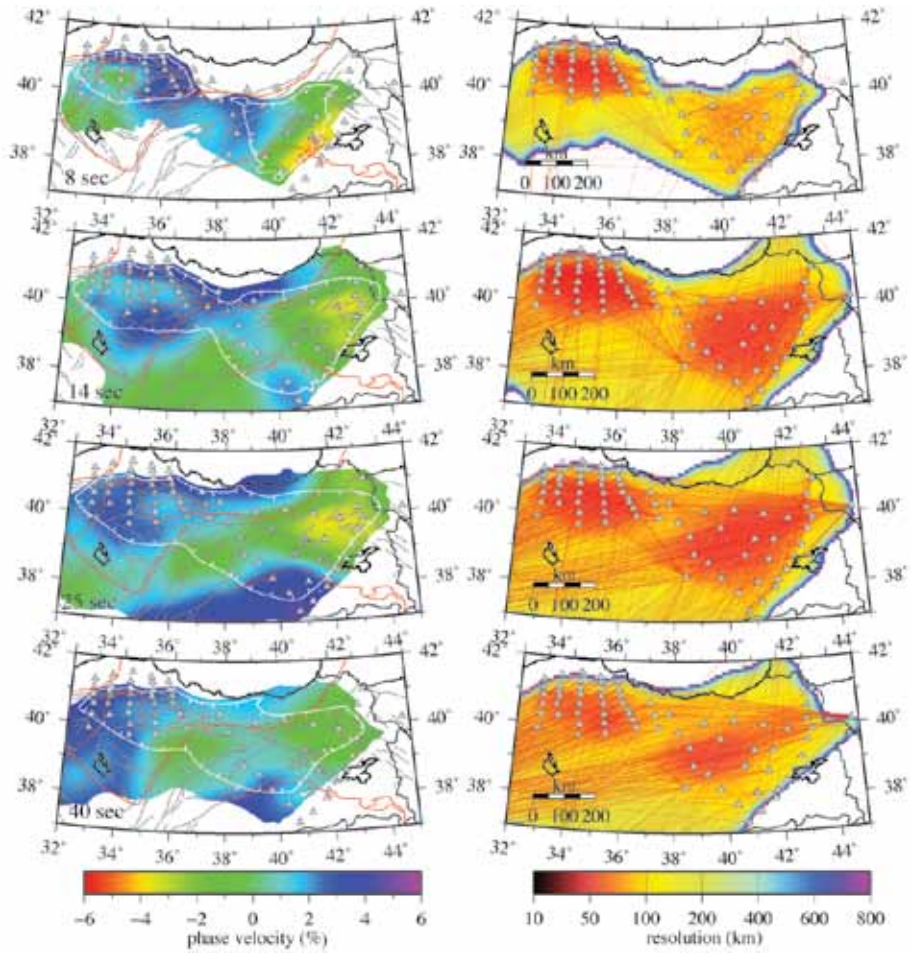

Phase velocity (left column) and horizontal resolution maps (right column) for periods of 8, 14, 25, and 40 s. Phase velocity maps, with period labeled in the lower left, show percent variations relative to the mean phase velocity. Phase velocities are plotted for regions with horizontal resolution <=150 km, with white contour lines showing regions with resolution <=100 km. Stations (gray triangles), faults (gray lines), and paleo-sutures (red lines) are also shown. The resolution maps in the right column show path coverage (red lines) and horizontal resolution.

Seismic Noise Tomography in the Chile Ridge Subduction Region

A. Gallego *(University of Florida),* **R. M. Russo** *(University of Florida),* **D. Comte** *(Universidad de Chile),* **V. I. Mocanu** *(University of Bucharest),* **R. E. Murdie** *(Goldfields Australia),* **J. C. Vandecar** *(DTM -Carnegie Institution of Washington)*

We used cross-correlation of ambient seismic noise recorded in the Chile Triple Junction (CTJ) region to estimate inter-station surface wave time-domain Green's functions, and then inverted travel times to obtain crustal surface wave velocity models. Inter-station distances within the Chile Ridge Subduction Project temporary seismic network ranged from 40 to ~100 km. We selected 365 days, and cross-correlated and stacked 24 hours of vertical component data at 38 stations pairs, resulting in nominally 703 travel-times along assumed-straight inter-station paths. Velocities in two-dimensional cells of 30 x 30 km were calculated using a linear least-squares inversion of the Rayleigh wave travel times. Furthermore we performed a Rayleigh wave dispersion analysis to estimate the sensitivity of different period waves at depth and to calculate a 3D model of the Patagonian crust. The process was applied to cross correlation pairs determined in two period bands, 5-10 sec, corresponding to shallow crustal velocities down to approximately 10 km depth, and 10-20 sec, for velocities down to around 20 km.Our results show that cell velocities correlate well with known geologic features: We find high crustal velocities where the Patagonian Batholith outcrops or is likely present at depth, and low velocities correlate with the active volcanic arc of the Southern Volcanic Zone and the subducted Chile ridge, where thermal activity is present. High velocities in the mountainous portions of the southeastern study area appear to correlate with outcropping older metamorphic units. Low velocity in the east correlate with sequences of volcaniclastic deposits.

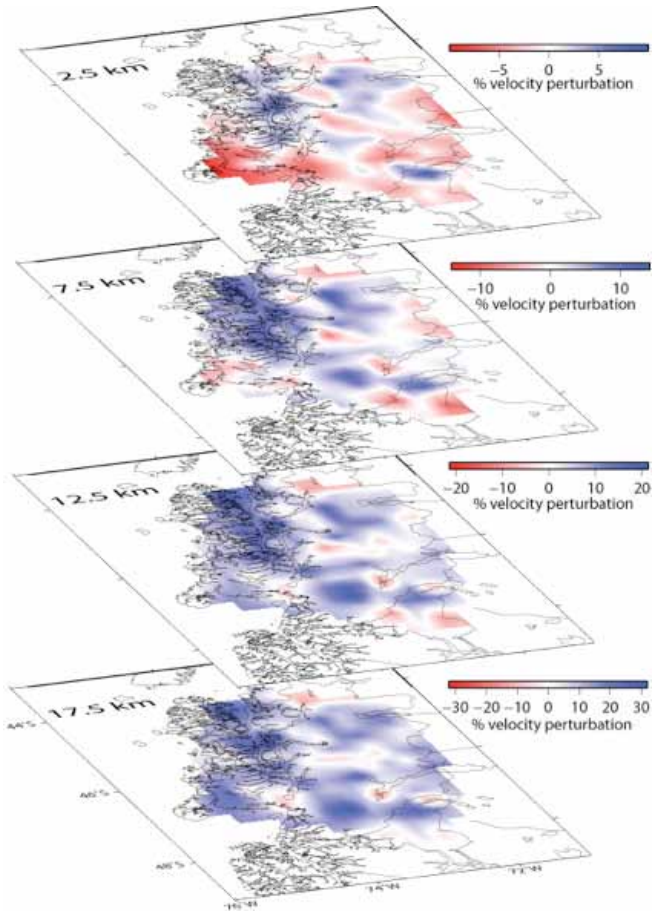

3-D inversion derived from dispersion analysis; the color bands correspond to the percentage variation with respect to the calculated 1-D model

References

Gallego, A., R. M. Russo, D. Comte, V. Mocanu, R. Murdie, and J. VanDecar, Seismic noise tomography in the Chile Ridge Subduction region, accepted for publication in *Geophysical Journal International*, 03 June 2010.

Acknowledgements: This work was supported by U.S. National Science Foundation grant EAR-0126244 and CONICYT-CHILE grant 1050367.

Ambient Noise Tomography of the Pampean Flat Slab Region

Ryan Porter *(University of Arizona),* **George Zandt** *(University of Arizona),* **Susan Beck** *(University of Arizona),* **Linda Warren** *(Earthscope Program, Division of Earth Sciences, NSF),* **Hersh Gilbert** *(Purdue University),* **Patricia Alvarado** *(Universidad Nacional de San Juan),* **Megan Anderson** *(Colorado College)*

Ambient noise tomography is a recently developed seismic analysis technique that uses background noise to approximate the seismic velocities with a region. We apply this technique to a study of the Pampean flat slab region (Fig. 1) to better understand crustal features related to the convergence of the Nazca and South American Plates. Flat slab subduction has led to a shutoff of arc magmatism and a migration of deformation inboard from the plate margin. The region's crust is composed of several terranes accreted on the Rio de la Plata craton with zones of thin-skinned deformation in the Precordillera and thick-skinned deformation in the Sierras Pampeanas. The purpose of this work is to use ambient noise to better understand the role these features play in the region's tectonic evolution. Ambient noise tomography is based on the principal that the cross-correlation of seismic noise recorded at two seismic stations can approximate the Green's function between the stations. This noise is generally associated with ocean waves colliding with the coast. We use the ambient noise to calculate Rayleigh wave dispersion curves and convert those measurements into shear wave velocities. A detailed description of the method is found in Benson et al. [*2007*]. Two advantages of ambient noise over traditional surface wave tomography are that it produces a higher quality signal at shorter periods and it does not require earthquakes at certain backazimuths and distances. Initial results from this work suggest that shear wave velocities in the upper crust are primarily controlled by the presence of (slow) basins and (fast) bedrock exposures and that these basins may extend as deep as ~10-12 km (Fig 2). Lower velocities are observed beneath the shutoff volcanic arc than in the Sierras Pampeanas suggesting that a) the presence of arc related rocks is retarding seismic velocities or b) that the differences in Moho depth is impacting the measured seismic velocities. We generally observe faster seismic velocities in areas of thick-skinned deformation than in thin-skinned areas. This is especially true beneath the Precodillera, which has accommodated 60–75% of the surface shortening since 10 Ma [*Allmendinger, 1990*], and exhibits relatively slow velocities down to 30 km, suggesting that deformation is preferentially focused in this low velocity region.

References

Allmendinger, R., D. Figueroa, D. Snyder, J. Beer, C. Mpodozis, and B. Isacks (1990), FORELAND SHORTENING AND CRUSTAL BALANCING IN THE ANDES AT 30°S LATITUDE, *Tectonics, 9*(4), 789-809.

Anderson, M.L., Alvarado, P., Zandt, G., Beck, S. (2007), Geometry and brittle deformation of the subducting Nazca Plate, Central Chile and Argentina. *Geophys. J. Int., 171*, 419-434.

Bensen, G.D., M.H. Ritzwoller, M.P. Barmin, A.L. Levshin, F. Lin, M.P. Moschetti, N.M. Shapiro, and Y. Yang (2007), Processing seismic ambient noise data to obtain reliable broad-band surface wave dispersion measurements, *Geophys. J. Int., 169*, 1239-1260.

Acknowledgements: This work was funded by NSF award #0510966.

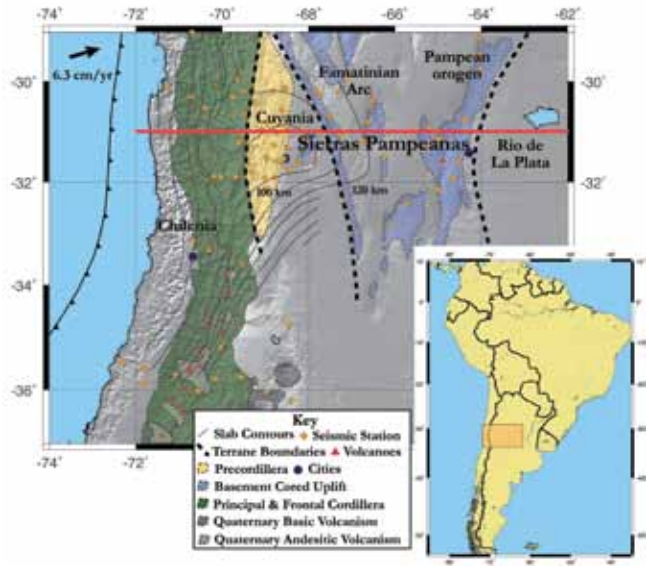

Figure 1. Location map of the study area. Red line shows location of cross section in Figure 2. Slab contours from Anderson (2007).

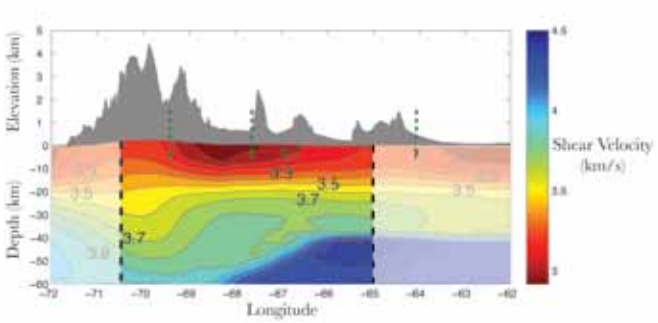

Figure 2. Cross-section of shear wave velocities at 31 degrees S. (Location shown in Figure 1). The low velocities observed above the Moho at -66 to -68 degrees are likely due to uncertainties in Moho depth. Measurements are corrected for topography and zones with less than 100 km resolution are shaded out. Green dashed lines show surface locations of terrane boundaries. Topography is exaggerated 10x.

Pacific Northwest Crust and Lithosphere Structure Imaged with Ambient Noise Tomography

Haiying Gao *(University of Oregon),* **Eugene Humphreys** *(University of Oregon),* **Huajian Yao** *(Mass. Inst. of Tech.),* **Robert van der Hilst** *(Mass. Inst. of Tech.)*

Rayleigh-wave ambient noise tomography from periods 6-40 seconds is used to study the Pacific Northwest crust and uppermost mantle structures with the methods of Yao et al. [*2006*]. We include a total of about 300 broadband stations recording from 2006-2009, including EarthScope US Transportable Array, the Wallowa flex-array, a portion of the High Lava Plains flex array, and seven permanent stations. The western U.S. model of Yang et al. [*2008*] is used for shear-wave velocity reference. We focus on three areas:

1) Cascades. In the Washington Cascades, where magmatic production diminishes northward to low values, the upper crust near magmatic centers usually is fast and the lower crust is slow. In Oregon, magmatic production rate is high and the crust and upper mantle are slow, whereas the old western Cascades upper crust is quite fast. These observations are consistent with the idea that magmatic intrusions make crust fast, but that high temperature can be dominant.

2) Pasco Basin. The upper crust is very slow, suggesting that this deep sedimentary basin (which is covered by Columbia River flood basalt flows) is larger than previously mapped.

3) Siletzia. The fast lower crust and upper mantle of eastern Washington and north-central Oregon is attributed to Siletzia, a fragment of ocean lithosphere that accreted ~ 50 Ma. The SE boundary of Siletzia (the Klamath-Blue Mountains gravity lineament; dashed line) is thought to represent a transform suture, and is well defined by the tomography. The NE suture is thought to be a subduction thrust system that trends NW to Vancouver Island (dotted line). We suggest that eastern Washington's low-lying (see dash-dot line), tectonically rigid and seismically faster lower crust and upper mantle is underthrust Siletzia lithosphere.

References

Yang, Y., Ritzwoller, M.H., Lin, F.-C., Moschetti, M.P., and Shapiro, N.M., Structure of the crust and uppermost mantle beneath the western United States revealed by ambient noise and earthquake tomography, *J. Geophys. Res., 113*, doi:10.1029/2008JB005833, 2008.

Yao, H., van der Hilst, R.D., and de Hoop, M.V., Surface-Wave array tomography in SE Tibet from ambient seismic noise and two-station analysis – I. Phase velocity maps, *Geophys. J. Int., 166*(2), 732-744, doi:10.1111/j.1365-246X.2006.03028.x., 2006.

Gao, H., E. D. Humphreys , H. Yao, and R. D. van der Hilst, Crustal and lithosphere structure of the Pacific Northwest with ambient noise tomography, in prep.

Acknowledgements: This research is supported by NSF award EAR-051000.

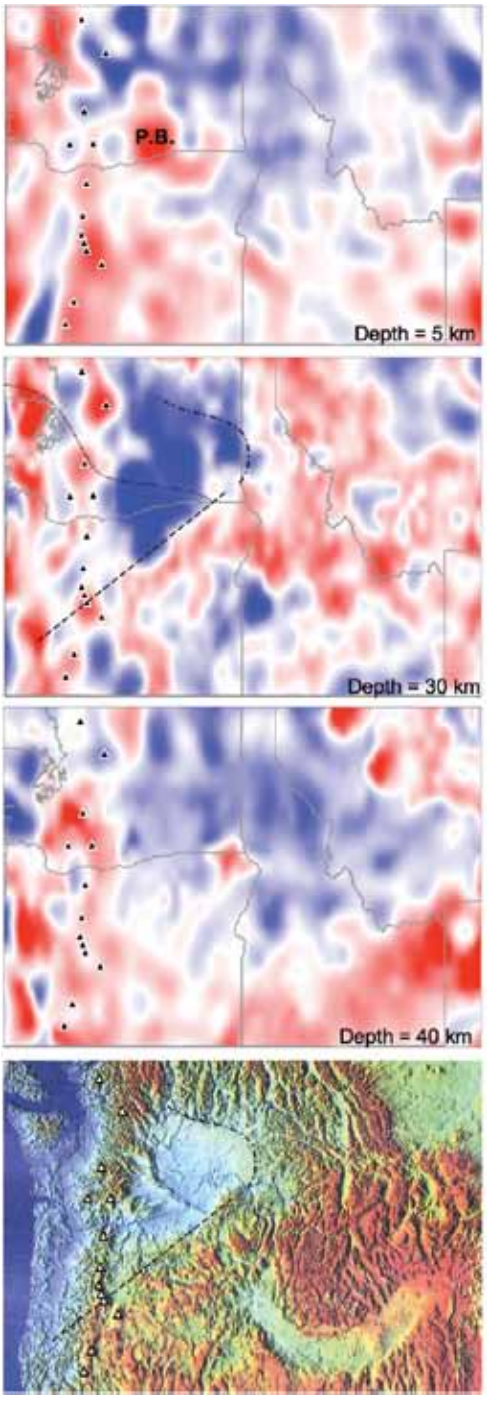

Tomography maps show the inverted isotropic shear-wave velocity structures (perturbations of ± 0.5 km/s relative to the average velocity; blue is fast). Triangles show the Quaternary volcanoes of the Cascade arc, and P.B. is the Pasco Basin.

Ambient Noise Monitoring of Seismic Speed

Michel Campillo *(Université Joseph Fourier and CNRS, Grenoble, France),* **Nikolai Shapiro** *(IPGP and CNRS, Paris, France),* **Florent Brenguier** *(Observatoire Volcanologique de la Réunion),* **Matthieu Landes** *(CEA, Bruyère-le-Chatel)*

With the availability of continuous recordings from numerous seismological networks, it is now possible to use the ambient seismic noise to monitor the temporal evolution of mechanical properties of the Earth's crust. As an example, we show the detection of co-seismic and post seismic change of seismic speeds associated with the 2004 Parkfield earthquake based on correlations of seismic noise recorded by stations of the High Resolution Seismic Network [*Brenguier et al., 2008*]. The velocity drops at the time of the earthquake, and recovers slowly during the next years. The similarity of the time evolution of the velocity anomaly with the strain measured by GPS suggests that the velocity change can be associated to both the well-documented response of shallow layers to strong motions, and the strain at depth. Changes of velocity are small and a high precision of measurement is required. Specifically, we must separate the effect of changes at depth and the apparent changes due to the temporal migration of the sources of noise. The latter can be also studies from the analysis of long continuous seismic recordings available at international data centers such as IRIS DMC [*e.g. Landes et al., 2010*].

References

Brenguier F., M. Campillo,C. Hadziioannou, N.M. Shapiro, R.M. Nadeau, E. Larose (2008), Postseismic relaxation along the San Andreas fault in the Parkfield area investigated with continuous seismological observations *SCIENCE, 321 (5895)*, 1478-1481.

Landes M, Hubans F, Shapiro NM, Paul A., and M. Campillo Origin of deep ocean microseisms by using teleseismic body waves *J. Geophysical Res. 115*: B05302,2010

Acknowledgements: This work is supported by the European Research Council Advanced Grant WHISPER

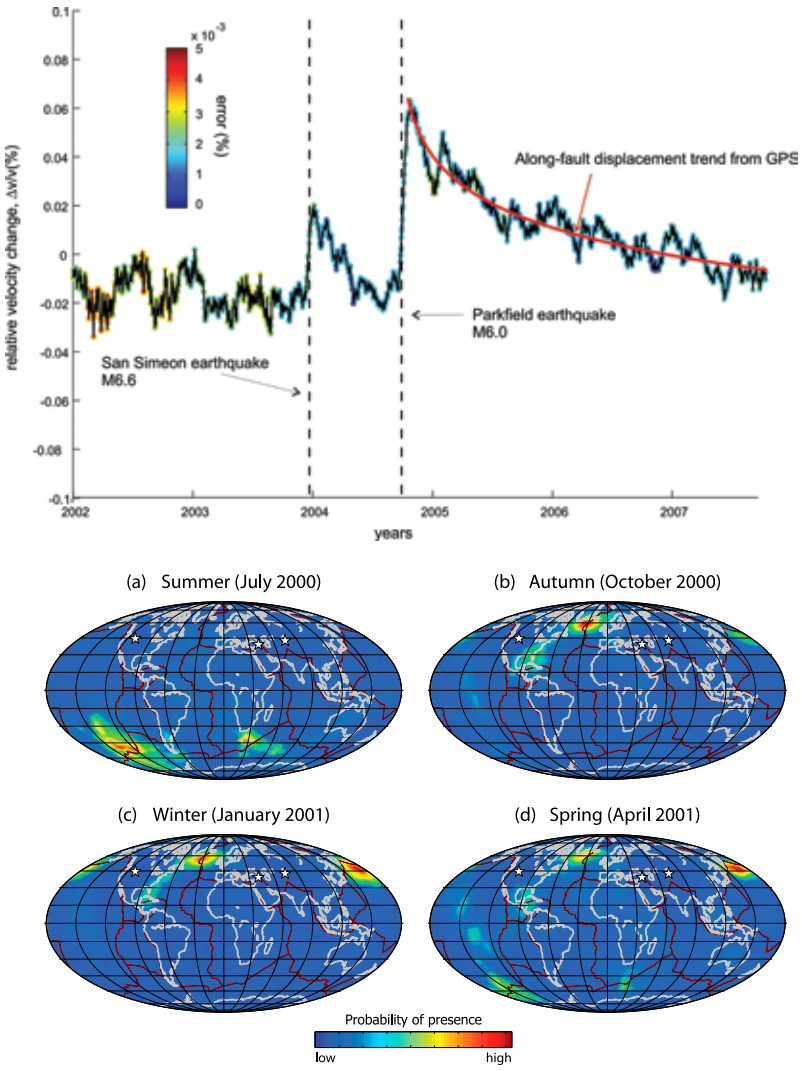

Top: Temporal evolution of the velocity in the region of Parkfield for the period 2002-2008 (see Brenguier et al. 2008 for details). Bottom: an example of the seasonal variation of the sources of secondary microseisms obtained from teleseismic body waves (see Landes et al. 2010 for details).

Vp Structure of Mount St. Helens Imaged with Local Earthquake Tomography

Gregory Waite *(Michigan Technological University),* **Seth Moran** *(USGS)*

We present a new P-wave velocity model for MSH using local earthquake data recorded by the Pacific Northwest Seismograph Stations and Cascades Volcano Observatory since the 18 May 1980 eruption. These data were augmented with records from a dense array of 19 temporary stations deployed during the second half of 2005. Between June 1980 and the September 2004, 19,379 earthquakes were located by the PNSN within a 50 km by 50 km area centered on MSH. An additional 6916 events were located in this area between October 2004 and the end of 2005, which represents a small fraction of the total number of events associated with the 2004-2008 eruption. The large number of earthquakes in the catalog permits a careful selection of data for only the best-quality 7798 events. Because the distribution of earthquakes in the study area is concentrated beneath the volcano and within two nearly linear trends, we used a graded inversion scheme to compute a coarse-grid model that focused on the regional structure, followed by a fine-grid inversion to improve spatial resolution directly beneath the volcanic edifice.

The well-resolved velocity anomalies below MSH are generally consistent with previous studies that have found two igneous intrusive bodies NE and NW of the edifice, and a structural boundary that parallels the SHZ. North of MSH, the SHZ is bounded by a low-velocity anomaly to the west and the Spirit Lake Pluton to the east. The coincidence of the velocity anomalies and the trend of earthquakes strengthens the argument that MSH sits along a significant NNW-trending structural anomaly [*e.g., Parsons et al., 1999*].

Small-scale features of the magmatic system were less well resolved, but a significant low-velocity zone from 1-3 km bsl may be due to a shallow magma-storage reservoir (Figure 1). A strong high-velocity anomaly, previously interpreted as a magma plug [*Lees, 1992*] was found to be east of the vertical zone of earthquakes directly beneath MSH instead of within the earthquake zone. This anomaly may be attributed to crystallized magma, but we do not interpret it as a plug within the conduit. The deeper low-velocity anomaly that we interpret as part of the magma storage system is poorly resolved due to the lack of deep earthquakes, but is consistent with earlier suggestions that the earthquake-free region is likely to be magma rich.

References

Lees, J.M. (1992), The magma system of Mount St. Helens; non-linear high-resolution P-wave tomography, *J. Volcanol. Geotherm. Res., 53*, 103-116.

Parsons, T., R.E. Wells, M.A. Fisher, E. Flueh, and U.S. ten Brink (1999), Three-dimensional velocity structure of Siletzia and other accreted terranes in the Cascadia forearc of Washington, *J. Geophys. Res., 104*(B8), 18,015-18,039.

Waite, G. P., and S. C. Moran (2009), VP Structure of Mount St. Helens, Washington, USA, Imaged with Local Earthquake Tomography, *J. Volcanol. Geotherm. Res., 182*(1-2), 113-122.

Acknowledgements: We thank the staff at the PNSN for their dedication to providing high-quality data and IRIS-PASSCAL Instrument Center for providing instruments and support for the temporary network. Data collected will be available through the IRIS Data Management Center. The facilities of the IRIS Consortium are supported by the National Science Foundation under Cooperative Agreement EAR-0552316, the NSF Office of Polar Programs and the DOE National Nuclear Security Administration.

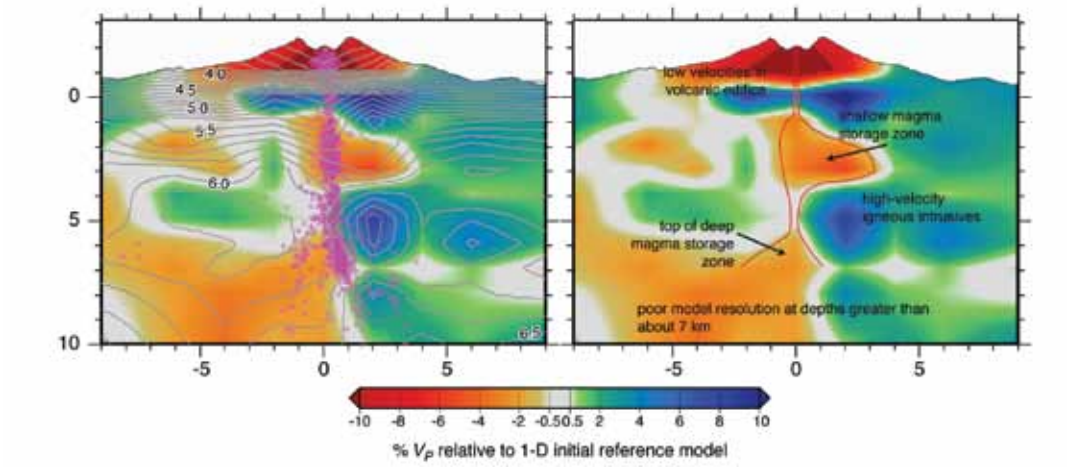

A west-east cross section through a single fine-grid model highlights the low velocity anomaly directly beneath the volcano. There is no vertical exaggeration.

Mushy Magma beneath Yellowstone

Risheng Chu *(California Institute of Technology),* **Don Helmberger** *(California Institute of Technology),* **Daoyuan Sun** *(California Institute of Technology),* **Jennifer M. Jackson** *(California Institute of Technology),* **Lupei Zhu** *(Saint Louis University)*

Recent GPS and InSAR studies show that the Yellowstone caldera is uplifting at a rate of 7 cm/year, which is apparently related to a magma recharge (Fig. A) [*Chang et al., 2007*]. Seismic tomographic studies, however, claim a high degree of crystallization of the underlying magma body based on velocities inferred from regional seismic data. In this research, we analyzed receiver functions recorded by EarthScope station H17A from 100 teleseismic earthquakes in 2008. Two P-to-SV converted phases that correspond to the top and bottom of a low velocity layer (LVL) are identified (Fig. B-C). After modeling these phases, we found the LVL at about 5 km depth beneath the caldera. P- and S-wave velocities are 2.3 km/sec and 1.1 km/sec, respectively. This shallow LVL beneath the Yellowstone Caldera is severe enough to cause difficulties with seismic tool applications. In particular, seismologists expect teleseismic P waves to arrive with motions up and away or down and back. Many of the observations recorded by the YISA PASSCAL array violate this assumption. Stations near the trailing edge have reversal radial-component motions, while stations near the leading edge do not (Fig. D). Synthetic wave propagation show that it is the edge of the LVL that are sharp enough for P wave to wrap around the ends to reach the receivers before the direct arrivals. If the velocity drop is not severe enough, radial and vertical components have the same polarities (Fig. D). The flipping of the radial component can be used to validate the low P velocity. We modeled the degree of magma melt by assuming a fluid-filled porous material consisting of granite and a mixture of rhyolite melt and supercritical water and CO2 at temperature of 800°C and pressure at 5 km. We found that this shallow magma body has a volume of over 4,300 km^3 and is at least 32% melt saturated with about 8% water plus CO2 by volume.

References

Chang, W. L., R. B. Smith, C. Wicks, J. M. Farrell, and C. M. Puskas, Accelerated uplift and magmatic intrusion of the Yellowstone Caldera, 2004 to 2006, *Science, 318*, 952-956, 2007.

Chu, R., D. V. Helmberger, D. Sun, J. M. Jackson, and L. Zhu, Mushy magma beneath Yellowstone, G*eophys. Res. Lett., 37*, L01306, 2010.

Acknowledgements: All waveform data used in this study were obtained from IRIS Data Management Center. This work is funded by the Tectonics Observatory at California Institute of Technology under Grant No. GPS.TO2-4.1-GRANT.MOORETO2. This is contribution 10035 of the Tectonics Observatory at Caltech.

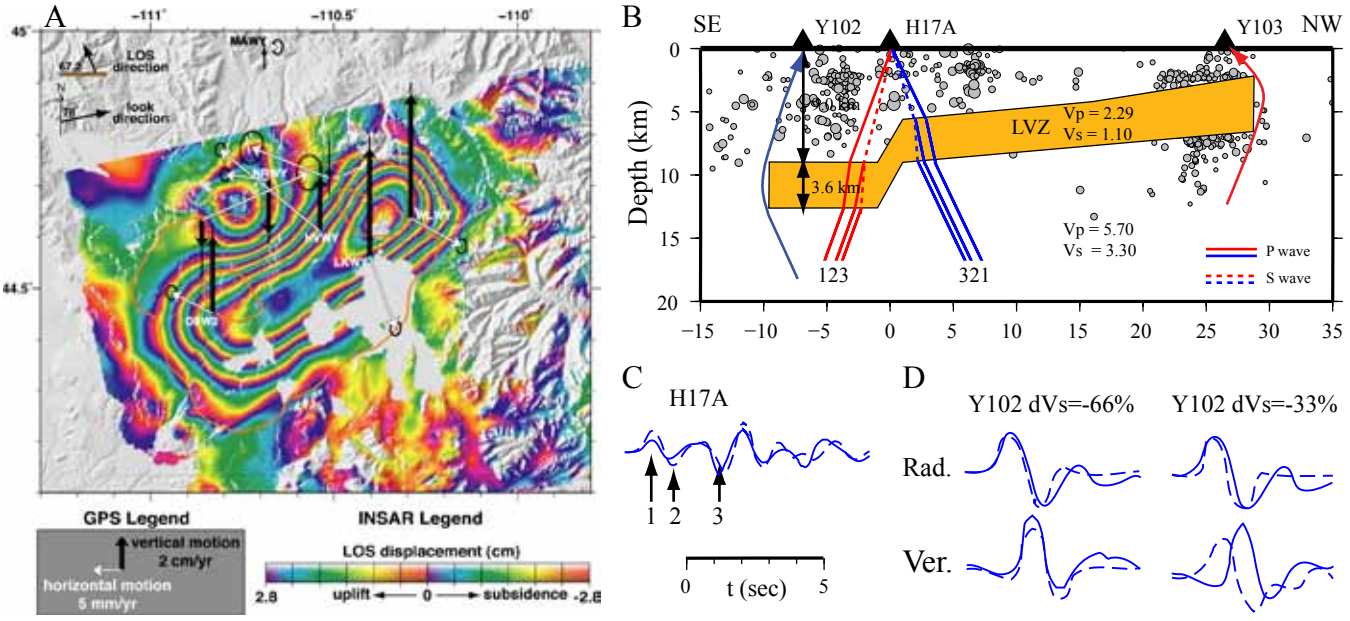

Recent GPS and InSAR studies show that the Yellowstone caldera is uplifting at a rate of 7 cm/year, which is apparently related to a magma recharge (Chang et al. 2007, Fig. A). In receiver functions recorded by EarthScope station H17A from 100 teleseismic earthquakes in 2008, two P-to-SV converted phases exist that are consistent with the top and bottom of a low velocity layer (LVL) at about 5 km depth beneath the Yellowstone caldera (Fig. B and C). Comparisons of synthetic waveforms and observed data for two velocity reductions are shown in Fig. D. Our preferred P- and S-wave velocities suggest at least 32% melt saturated with about 8% water plus CO2 by volume.

Structure of the Chesapeake Bay Impact Crater from Wide-Angle Seismic Waveform Tomography

W. Ryan Lester *(Virginia Tech; now at U. Texas Austin),* **John A. Hole** *(Virginia Tech),* **Rufus D. Catchings** *(U. S. Geological Survey, Menlo Park),* **Florian Bleibinhaus** *(University of Salzburg)*

The Chesapeake Bay impact structure is one of the largest and most well preserved impact structures on Earth. It has a unique morphology composed of an inner crater penetrating crystalline basement surrounded by a wider crater in the overlying sediments. In 2004, the U.S. Geological Survey conducted a seismic survey with the goals of constraining crater structure and in support of the drilling of a borehole into the deepest part of the crater [*Catchings et al., 2008*]. Waveform inversion was applied to these data to produce a higher-resolution velocity model of the crater. Northeast of the crystalline crater, undeformed, eastward-sloping crystalline basement is ~1.5 km deep. The edge of the inner crater is at ~15 km radius and slopes gradually down to a depth of 1.5–1.8 km. A central peak of 4-5 km radius rises to a depth of ~0.8 km. Basement velocity in the crystalline crater is much lower than undeformed basement, which suggests ~10% fracturing of the crater floor, and up to 20% fracturing of the central uplift. A basement uplift and a lateral change of basement velocity occur at a radius of ~11 km, and are interpreted as the edge of the transient crater. Assuming a 22-km diameter transient crater, scaling laws predict a ~30 km diameter crater and central peak diameter of 8-10 km, consistent with the seismic image. This indicates that post-impact collapse processes that created the ~30-km diameter crystalline crater were unaffected by the much weaker rheology of the overlying sediments.

References

Catchings, R. D., D. S. Powars, G. S. Gohn, J. W. Horton Jr., M. R. Goldman, and J. A. Hole (2008), Anatomy of the Chesapeake Bay impact structure revealed by seismic imaging, Delmarva Peninsula, Virginia, USA, *J. Geophys. Res., 113*, B08413.

Lester, W. R., (2006), Structure of the Chesapeake Bay Impact Crater from Wide-Angle Seismic Waveform Tomography, M.S. Thesis, Virginia Tech.

Acknowledgements: The data were acquired by the U.S. Geological Survey funded by the National Cooperative Geologic Mapping Program and used IRIS-PASSCAL seismometers.

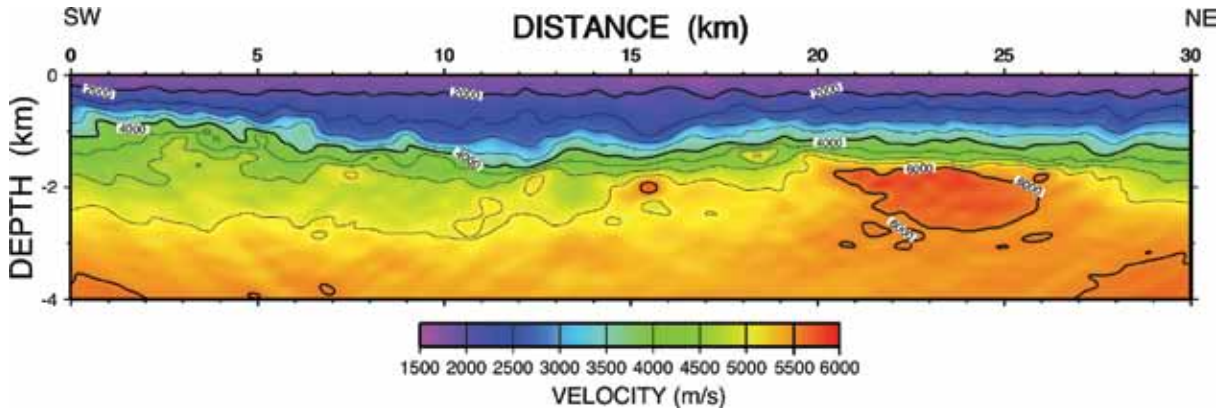

Seismic velocity model produced by waveform inversion of 3-16 Hz data.

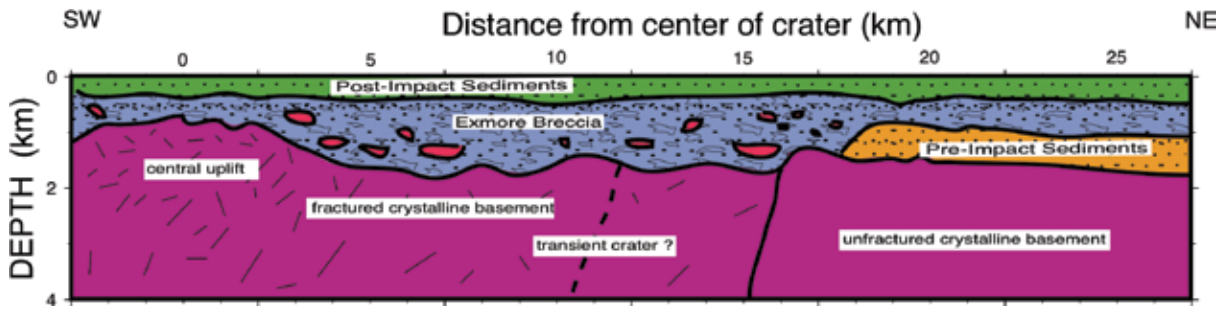

Model of the inner crystalline crater of the Chesapeake Bay impact structure as interpreted from the seismic model. The crater is defined at the base of the Exmore tsunami breccia.

Imaging the Seattle Basin to Improve Seismic Hazard Assessments

Andrew A Delorey *(University of Washington),* **John E Vidale** *(University of Washington)*

Much of Seattle lies atop a deep sedimentary basin. The Seattle Basin amplifies and distorts the seismic waves from nearby moderate and large earthquakes in ways that modulate the hazard from earthquakes. Seismic hazard assessments heavily depend upon upper crustal and near-surface S-wave velocity models, which have traditionally been constructed from P-wave models using an empirical relationship between P-wave and S-wave velocity or by interpolating across widely spaced observations of shallow geologic structures. Improving the accuracy and resolution of basin S-wave models is key to improving seismic hazard assessments and predictions for ground shaking. Tomography, with short-period Rayleigh waves extracted using noise interferometry, can refine S-wave velocity models in urban areas with dense arrays of short period and broadband instruments. We apply this technique to the Seattle area to develop a new shallow S-wave model for use in hazard assessment. Continuous data from the Seismic Hazards in Puget Sound (SHIPS) array as well as permanent stations from the Pacific Northwest Seismograph Network (PNSN) and Earthscope's Transportable Array (TA) have inter-station distances are as short as a few kilometers. This allows us to extract Rayleigh waves between 2 and 10 seconds period that are sensitive to shallow basin structure. Our results show that shear wave velocities are about 25% lower in some regions in the upper 3 km than previous estimates. Using the new velocity model we run earthquake simulations using a finite difference code to validate the model, and then to make predictions on the level of ground-shaking for various realistic earthquake scenarios at various locations around the urban area.

Acknowledgements: This study is funded by the National Earthquake Hazards Program (NEHRP).

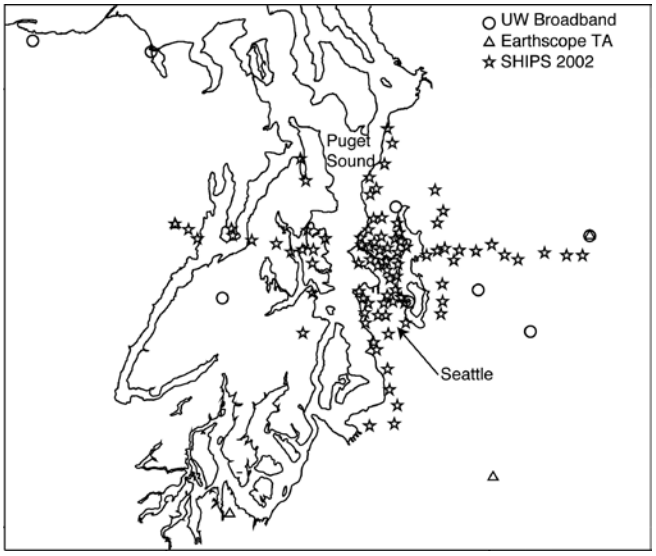

Shown are the stations used for this study. The black curves indicate the coastline of Puget Sound and Seattle is located where stations are clustered in the center of the figure. The UW Broadband (circles) and Earthscope Transportable Array stations (triangles) were used to get background velocity and the SHIPS stations (stars) were used to image the Seattle Basin.

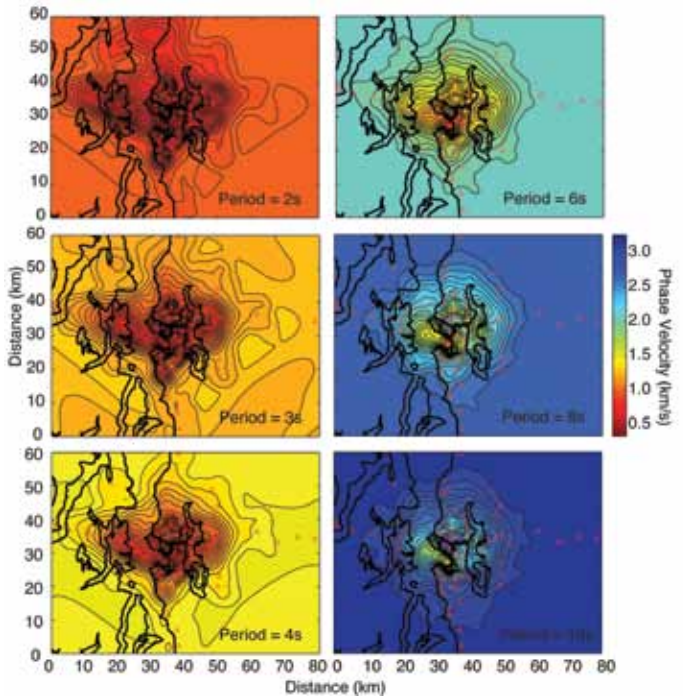

Shown are Rayleigh wave phase velocities for periods between 2 and 10 seconds.

Earthquake Hazard Class Mapping by Parcel in Las Vegas Valley

John N. Louie *(University of Nevada, Reno),* **Satish Pullammanappallil** *(Optim SDS),* **Aasha Pancha** *(Optim SDS),* **Travis West** *(Optim SDS),* **Werner Hellmer** *(Clark County Building Department)*

Clark County, Nevada is completing the Nation's very first effort to map earthquake hazard class systematically through an entire urban area. The resulting geotechnical shear-velocity map is a layer added to the County's existing soil-hazards map. The map already includes layers such as fault proximity, ground subsidence, and potential for swelling clay soils. The new earthquake-hazard map layer will be available on the County's web GIS interface. Geotechnical shear velocity is a basic building block in foundation design, and in predictions of potential for ground liquefaction, landslides, and seismic shaking, as a few examples. The map will be used in development and disaster response planning, in addition to its direct use for building code implementation and enforcement. Clark County contracted with the Nevada System of Higher Education to apply the refraction microtremor geophysical surveying technique, a State of Nevada-owned technology, to the hazard classification of about 500 square miles Las Vegas Valley.

The parcel map includes almost 9000 measurements that classify parcels on the NEHRP hazard scale, from NEHRP A at least hazardous to NEHRP E at the most. No site in Nevada has yet been measured to be less hazardous than NEHRP B or more hazardous than NEHRP D; and this represents the range of classifications found in unincorporated Clark County. The measured parcel map shows a clearly definable NEHRP B-C boundary on the west side of Las Vegas Valley, rarely more than 300 m wide. The NEHRP C-D boundary is on the other hand much more complex. Using the parcel map in computing shaking in the Valley for scenario earthquakes is crucial for obtaining realistic predictions of ground motions. For Las Vegas the principal earthquake hazard is from the Furnace Creek fault system, capable of M7.5 events. Animations of shaking show the expected strong trapping and long shaking durations within basins, as well as diffusion and scattering of energy between the many basins in the region. Despite affecting only the very shallowest zone of models (<30 m), the Vs30 geotechnical shear-velocity from the parcel map shows clear correlation to 0.3-Hz PGV predictions in basins. Increasing basin thicknesses from 0 to 1.3 km correlate with increased PGV, but the basin effect at 0.3 Hz saturates for basin thicknesses greater than 1.3 km; deeper parts of the basin show variance and uncertainty of a factor of two in predicted PGV.

Acknowledgements: Research supported primarily under contract to the Clark County Building Department; also partially by the U.S. Geological Survey (USGS), Department of the Interior, under USGS award number 08HQGR0015; and by a 2006 Fulbright Senior Scholar award to Louie for work in New Zealand. The views and conclusions contained in this document are those of the authors and should not be interpreted as necessarily representing the official policies, either expressed or implied, of the U.S. Government.

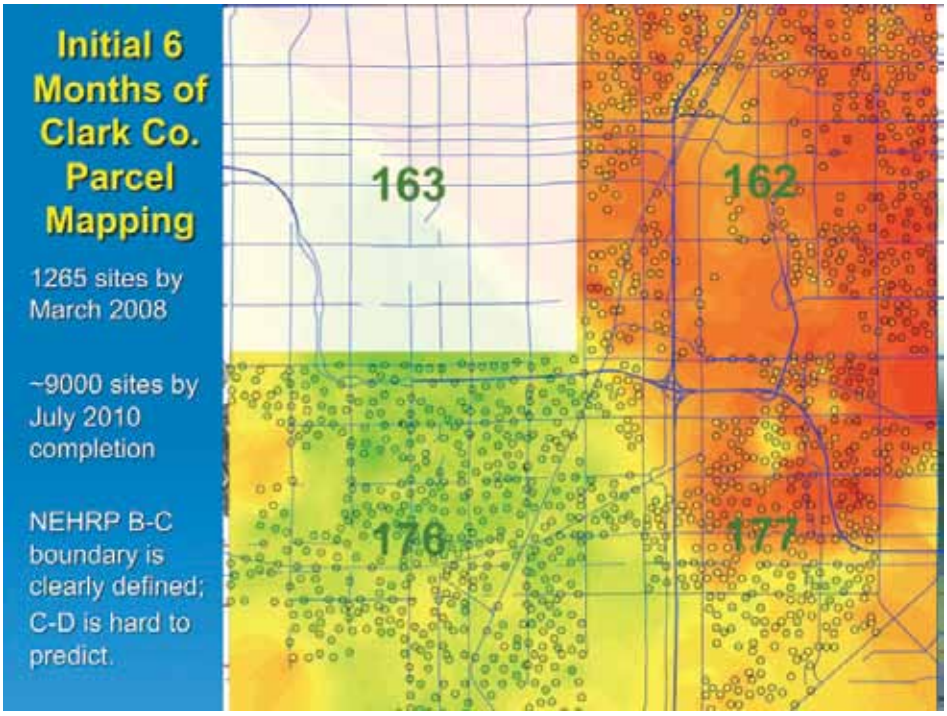

Preliminary hazard map of a portion of Las Vegas Valley, Nevada, prepared from measurements of 1265 sites as of March 2008. (Map book 163 – green numbers – was mapped later that year.) A sharp NEHRP B-C boundary (green to orange) is visible between map books 176 and 177; the NEHRP C-D boundary (orange to red in map book 162) is much more complicated, requiring dense measurements to locate accurately.

Developing a Database of ENA Ground Motions for NGA East

Chris Cramer *(CERI, University of Memphis)*

A five-year Next Generation Attenuation (NGA) East project to develop new ground motion prediction equations for stable continental regions (SCRs), including eastern North America (ENA), has begun at the Pacific Earthquake Engineering Research (PEER) Center funded by the Nuclear Regulatory Commission (NRC), the U.S. Geological Survey (USGS), the Electric Power Research Institute (EPRI), and the Department of Energy (DOE). As part of a pre-project effort, the NRC has funded the two-year initial development of an ENA database of ground motions similar to the NGA active-tectonic-regions strong-motion database. This initial effort focused on database design and collection of appropriate M>4 ENA broadband and accelerograph records to populate the database. Ongoing work under PEER funding will focus on adding records from smaller ENA earthquakes and from other SCRs such as Europe, Australia, and India. This effort to develop a database of ENA ground motions for the NGA East project has used waveform data from GSN and USArray stations.

Acknowledgements: This research was supported under USGS cooperative agreement 07CRAG0015 and is currently supported by a contract with PEER.

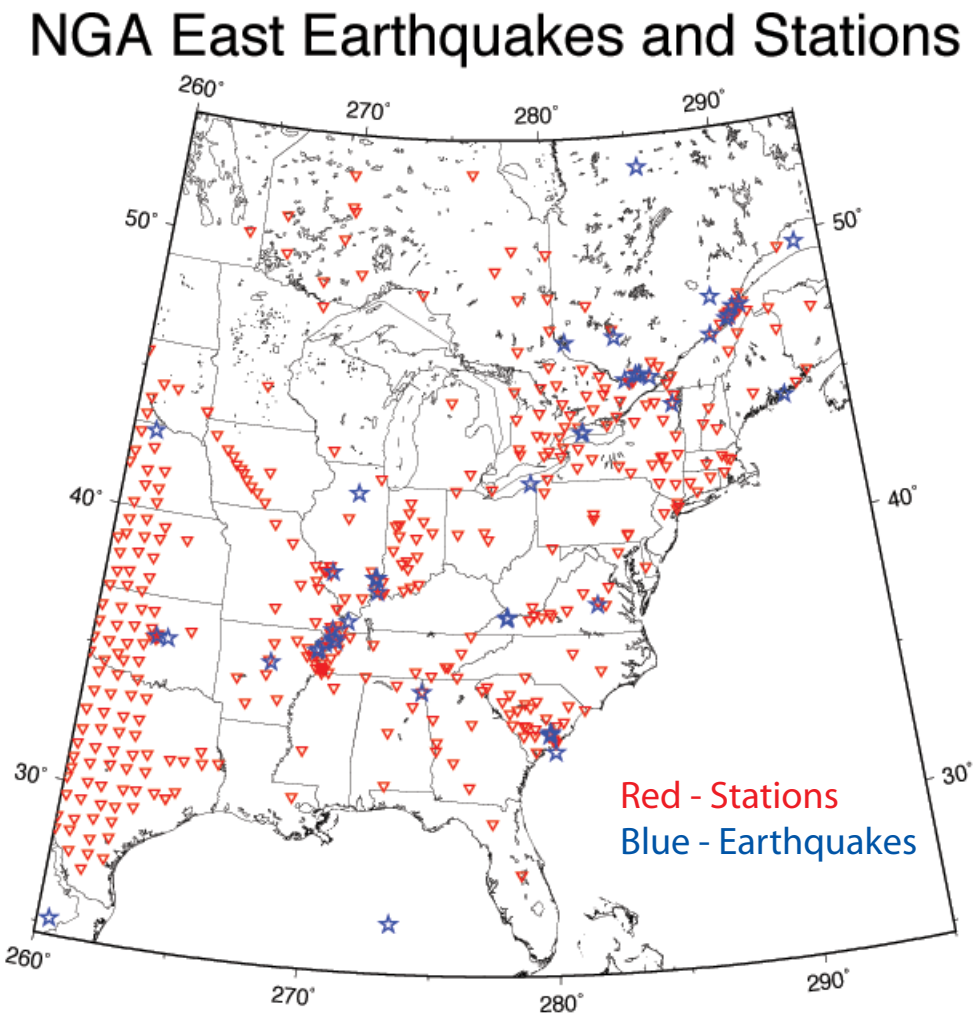

The stations and earthquakes used in the NGA East project so far.

Seismic Wave Gradiometry Using Multiwavelets: Documented Surface Wave Reflections

Christian Poppeliers *(Augusta State University, Dept. of Chem. and Physics)*

In the IRIS-produced document "Seismological Grand Challenges in Understanding Earth's Dynamic Systems", states several challenges to the seismological community. The work presented here addresses the second Challenge: 'How Does the Near Surface Environment Affect Natural Hazards and Resources'. Specifically, this work makes strides in quantifying highly complex scattering affects attributed to near-surface geologic conditions using a new seismic processing technique known as seismic wave gradiometry. The method is based on using displacement gradients as measured by a small scale array to estimate wave velocity, wave propagation direction, and spatial amplitude changes at all points on the seismogram [*e.g. Langston, 2007*]. Conventional seismic array processing is not ideally suited to resolve highly complex wave attributes as the wavelength of the wave is typically much smaller than the array aperture. Thus, small-scale time-dependant scattering affects may be missed. Conversely, an array designed as a gradiometer has an aperture of less than 10% of the smallest wavelength of the wavefield being analyzed. Thus a gradiometer is essentially a "point array", recording the wavefield within a fraction of a wavelength.

The work presented here shows an example of complex surface wave interactions as recorded at the edge of an artificially-created sedimentary basin [Poppeliers, 2010]. The study site consists of a former open-pit coal mine in which the pit has subsequently been backfilled with mine tailings [*Poppeliers and Pavlis, 2002*]. A series of artificial-source explosions provided the seismic source. Because the wave attributes are highly frequency dependant, we have incorporated multi-wavelets into existing wave gradiometery methodologies, which allows us to quantify frequency-dependent wave attributes as well as calculate formal uncertainty estimates; the result is that wave attributes, as well as their confidence intervals, can be estimated as a function of time and frequency. The figure shows that the estimated vector slowness of the vertical-component wavefield suggests a series of reflected surface waves that traverse the basin multiple times. The reflections of the surface waves likely occur at the vertical boundary between the unconsolidated mine tailings and the surrounding bedrock.

References

Poppeliers, C., 2010, Seismic Wave Gradiometry Using the Wavelet Transform: Application to the Analysis of Complex Surface Waves Recorded at the Glendora Array, Sullivan, Indiana, USA., *Bull. Seismol. Soc. Amer., 100*, 1211-1224.

Poppeliers, C., G.L. Pavlis, 2002, The Seismic Response of a Steep Slope: High-Resolution Observations with a Dense, Three-Component Seismic Array, *Bull. Seismol. Soc. Amer., 92*, 3102-3115.

Langston, C.A., Wave Gradiometry in Two Dimensions, *Bull. Seismol. Soc. Amer., 97*, 401-416.

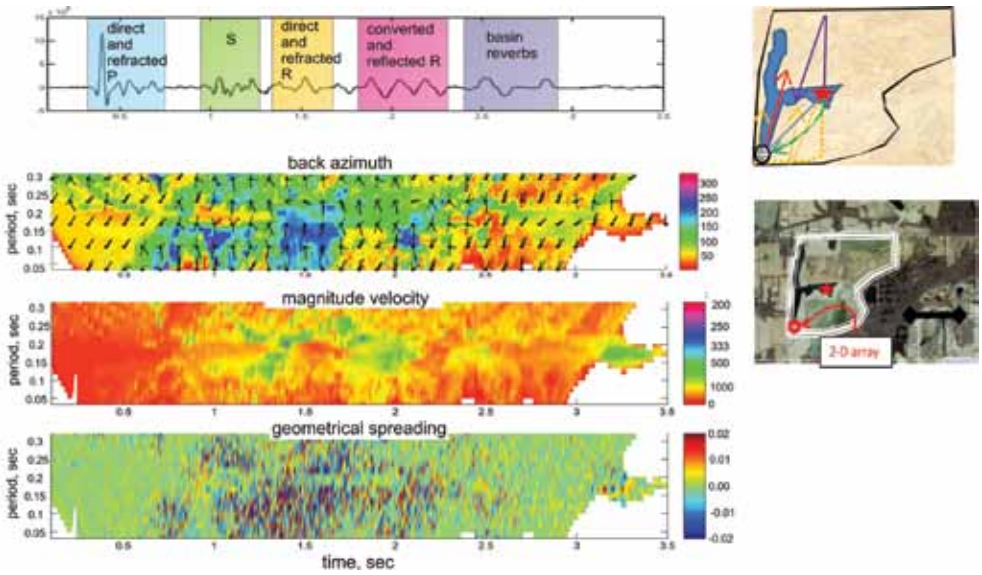

Multiwavelet seismic wave gradiometry applied to the active-source data collected by a portion of the Glendora array. The seismogram shows the vertical-component displacement. The colored boxes show the wave arrivals interpreted with the help of the resolved wave attributes. The panel showing the resolved back azimuth shows a colormap that corresponds to resolved back azimuth as well as "stick-and-ball" figures as a function of both time and frequency. The ball indicates a given time-frequency location, where the stick points back towards the resolved source. 95% confidence intervals of resolved back azimuth are also shown. The panel showing the magnitude velocity shows a prominent low-velocity arrival between 1.0 and 2.0 seconds which corresponds to various surface wave arrivals. For brevity, formal uncertainties are not shown for the magnitude velocity or geometrical spreading estimates.

Lithospheric Layering in the North American Craton

Huaiyu Yuan *(Berkeley Seismological Laboratory),* **Barbara Romanowicz** *(Berkeley Seismological Laboratory)*

Recent receiver function studies detect structural boundaries under continental cratons at depths too shallow to be consistent with the lithosphere-asthenosphere boundary (LAB) as inferred from seismic tomography and other geophysical studies. Using the new results from our regional surface wave tomographic inversion for the North American upper mantle shear wave structure, we show (Figure1) that changes in the direction of azimuthal anisotropy with depth reveal the presence of two distinct lithospheric layers throughout the stable part of the North American (NA) continent [*Yuan and Romanowicz*, 2010]. (Figure 1 here) The top layer is thick (~150 km) under the Archean core and tapers out on the Paleozoic borders. Its thickness variations follow those of a highly depleted layer inferred from thermo-barometric analysis of xenoliths [*Griffin et al.*, 2004]. The LAB is relatively flat (180-240km), in agreement with the presence of a thermal conductive root that subsequently formed around the depleted chemical layer [*Cooper et al.*, 2004]. Our findings tie together seismological, geochemical and geodynamical studies of the cratonic lithosphere in North America. They also suggest that the horizon detected in receiver function studies likely corresponds to the sharp mid-lithospheric boundary rather than to the more gradual LAB. The change of fast axis direction of azimuthal anisotropy with depth is a powerful tool for the detection of lithospheric layering under continents. Our study indicates that the "tectosphere" is no thicker than ~200-240km and that its chemically most depleted part reaches thicknesses of ~160-170 km (Figure 1). While the morphology of the North American craton may be exceptionally simple, the application of this tool to other continents should provide further insights on the assembly and evolution of cratons worldwide.

References

Cooper, C. M., A. Lenardic, and L. Moresi (2004), The thermal structure of stable continental lithosphere within a dynamic mantle, *Earth Planet. Sci. Lett., 222*(3-4), 807-817.

Griffin, W. L., S. Y. O'Reilly, B. J. Doyle, N. J. Pearson, H. Coopersmith, K. Kivi, V. Malkovets, and N. Pokhilenko (2004), Lithosphere mapping beneath the North American plate, *Lithos, 77*(1-4), 873-922.

Yuan, H., and B. Romanowicz (2010), Lithospheric layering in the North American Craton, *Nature*, DOI: 10.1038/nature09332, in press.

Acknowledgements: This study was supported by NSF EAR-0643060 grant to BR. We are grateful to the IRIS DMC and the Geological Survey of Canada for providing the waveforms, K. Liu, M. Fouch, R. Allen, A. Frederiksen and A. Courtier for sharing their SKS splitting measurements, and S. Whitmeyer and K. Karlstrom for providing their Proterozoic Laurentia structural map.

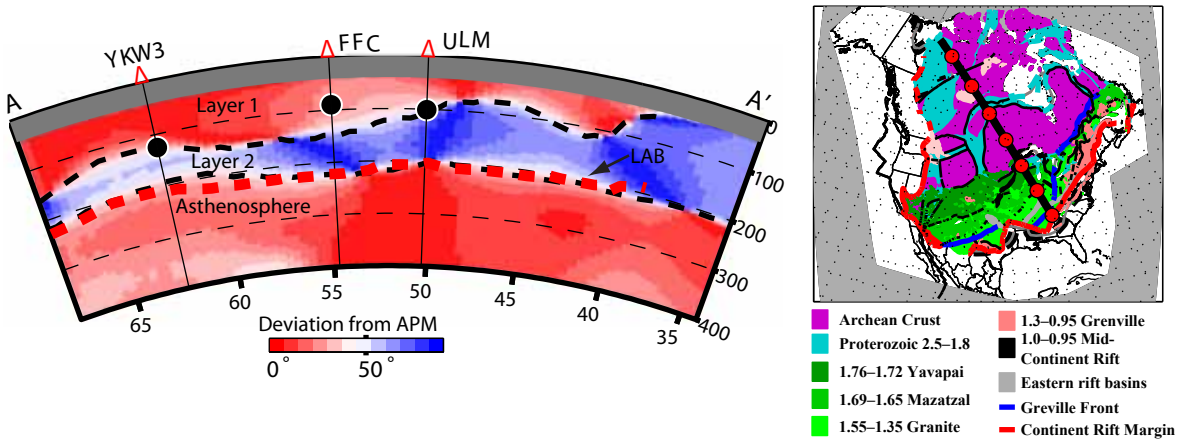

Upper mantle layering defined by changes in the direction of fast axis of azimuthal anisotropy. Left: deviation of the fast axis direction from the NA absolute plate motion direction, as a function of depth along a depth cross-section AA. Rapid changes of the fast axis directions mark the boundarie

Survival and Demise of Thick Continental Lithosphere under Highly Extended Crust

Vera Schulte-Pelkum *(University of Colorado at Boulder),* **Glenn Biasi** *(University of Nevada, Reno),* **Anne Sheehan** *(University of Colorado at Boulder),* **Craig Jones** *(University of Colorado at Boulder)*

We find an unusually thick lithosphere under a highly extended portion of the Basin and Range. We determined Moho depths using P-to-S receiver functions from the EarthScope Transportable Array and the Southern Great Basin Digital Seismic Network. As one would expect from isostasy, the crust is thicker under the high-elevation Northern Basin and Range and thinner in the low-lying Southern Basin and Range. However, we find an unexpected crustal keel under the highly extended Death Valley extensional area in between, underlying low surface elevations and putting the crust well outside of isostatic equilibrium. Dense crust is not found in this area in refraction results, but a lithospheric mantle keel fits the seismic observations as well as the observation of anomalous isotope ratios in basalts from this area that require an old, enriched lithospheric source [*Farmer et al., 1989*]. Unusually low εNd values indicating an old lithospheric mantle source were replaced by asthenospheric basalts in the Lake Mead extensional area, but persist during the entire history of basaltic magmatism (12-0 Ma) in the Death Valley extensional area, matching the geographical extent of dense mantle. If the anomaly is isostatic and a lithosphere-asthenosphere density contrast of 50 kg/m^3 (0.05 g/cm^3) is assumed, the lithosphere-asthenosphere boundary lies at a mean depth of 120 km within the anomaly, compared to a mean of 40 km outside the anomaly. We conclude that deformation was highly incoherent between the surface and the lower crust and mantle lithosphere, and that an island of Precambrian lithosphere has survived beneath the Death Valley extensional area and may currently be sinking.

References

Farmer, G.L., F.V. Perry, S. Semken, B. Crowe, D. Curtis, D.J. DePaolo, Isotopic evidence on the structure and origin of subcontinental lithospheric mantle in southern Nevada, *J. Geophys. Res. 94*, B6, 7885-7898, 1989

Acknowledgements: This research is funded by NSF grant EAR-0838509. Seismic data with the exception of those from the Southern Great Basin Digital Seismic Network were obtained from the IRIS DMC.

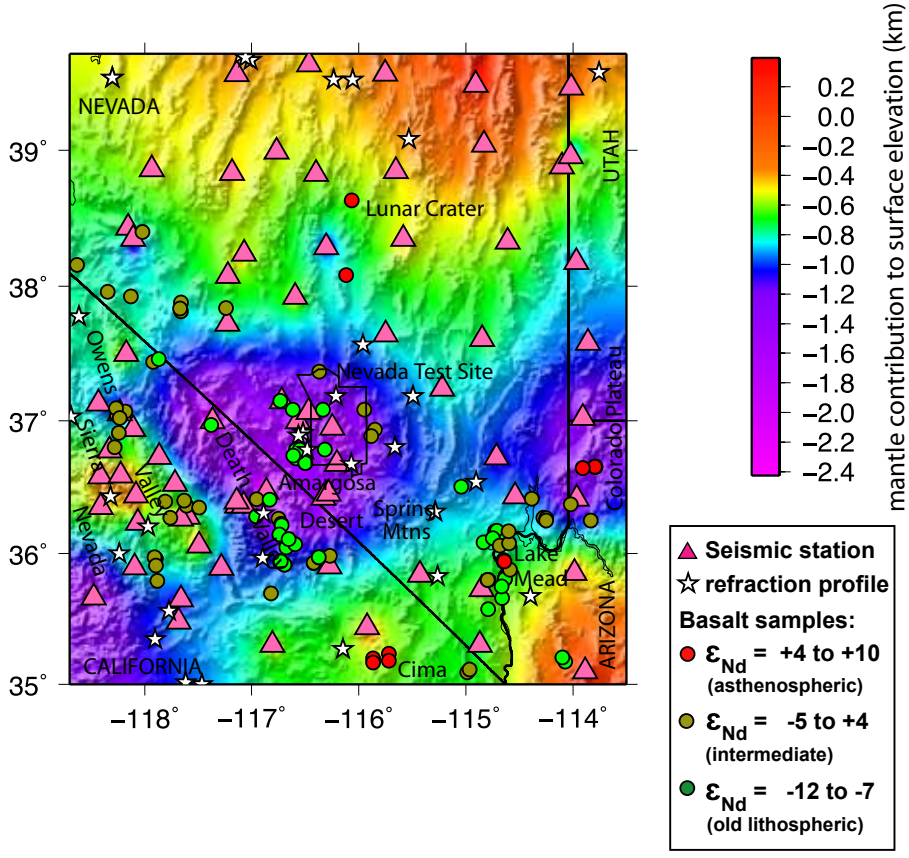

Mantle contribution to surface elevation (color), overlaid by topography (shading) for orientation. Pink triangles (seismic stations) are location where Moho depth was measured, white stars (refraction profile centers) mark crustal velocity and density values from refraction experiments used to convert receiver function Moho times to depth and to calculate isostatic contribution of the crust. Mantle buoyancy is well constrained in areas where both seismic stations and refraction data exist in the vicinity. Circles mark locations of basalts with measured Neodymium isotope ratios and are plotted so that younger samples overlay older ones.

The Lithospheric Structure of the Mendocino Triple Junction from Receiver Function Analysis

Yongbo Zhai *(Rice University),* **Alan Levander** *(Rice University)*

The Mendocino Triple Junction (MTJ), which occurs offshore from Cape Mendocino at ~ 40.50N in northern California, is the intersection of the Gorda plate, Pacific plate, and North American plate. It was formed ~28 Ma when the Pacific spreading ridge first contacted the western margin of the North American plate. In rigid plate frame, the northward migrating MTJ leaves in its wake a slab-free region filled by upwelling asthenospheric mantle just south of the Gorda plate, widely known as the "slab window" model.

To examine the lithospheric structure in the MTJ region, especially the structure of the "slab window", we generated a 3D PdS receiver function CCP image. We used 186 earthquakes recorded at 111 broadband stations of the Flexible Array Mendocino Experiment (FAME) together with the Berkeley Digital Seismic Network and USArray Transportable Array. The data were depth mapped and laterally migrated incorporating 3D traveltime corrections determined from 3D P-and S-tomography models.

The resulting image confirms the crustal structure of the Mendocino Triple Junction Seismic Experiment (MTJSE) and reveals detailed lithospheric structure. The top and bottom of the Gorda slab are identified by the Moho and Lithosphere-Asthenosphere Boundary (LAB) in the subduction regime, showing that the thickness of the Gorda slab is ~ 40 km, comparable with that predicted by half-space cooling model. The "slab window" in the transform regime has a complex structure, but its top can be traced continuously to the Gorda LAB, although the transition is more abrupt than that suggested by the refraction velocity model. The LAB is shallowest beneath Clear Lake volcano and Lake Pillsbury where high heat flow and basalt intrusions are observed respectively. Under the western part of northern Great Valley, the Moho signal is absent, likely due to the hydration and serpentinization of the upper mantle during the subduction of the Gorda slab ~2Ma. The Great Valley ophiolite is observed at the crustal depth instead.

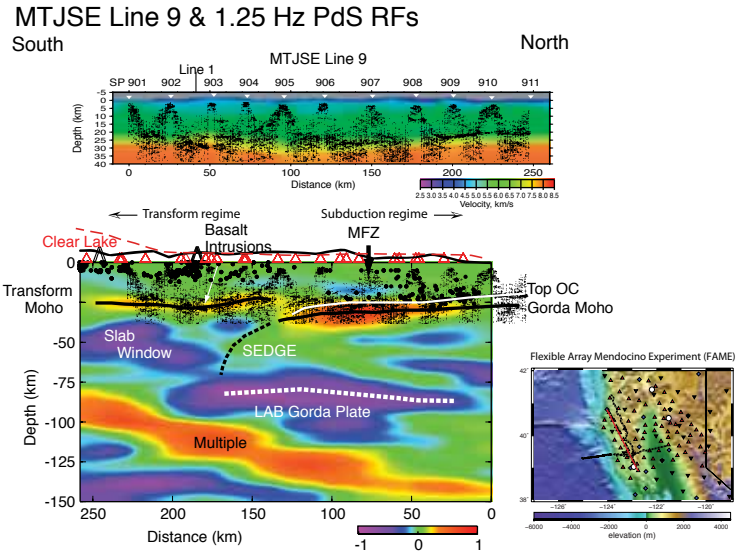

Figure 1. Coast-range-parallel receiver function cross-section. P-wave velocity model of MTJSE line 9 is shown in the upper panel, superimposed by the depth migrated single-fold section. The black solid line on top of the CCP image schematically shows the surface elevation along the cross-section, whereas the red dashed line schematically shows the heat flow. The red triangles denote projected stations, and the black dots denote the projected earthquake hypocenters since 1985 with M > 3.0. The three strong events in the CCP image in order of depth are the Moho, LAB, and first Moho multiple respectively. The black lines mark the Moho depth determined by the RF image, and white lines mark the top and bottom of the Gorda slab. The basalt intrusions near Lake Pillsbury are represented by strong reflections of the depth migrated section from the lower crust and Moho. Black dashed line illustrates the southern edge of the Gorda plate, which dips to the south.

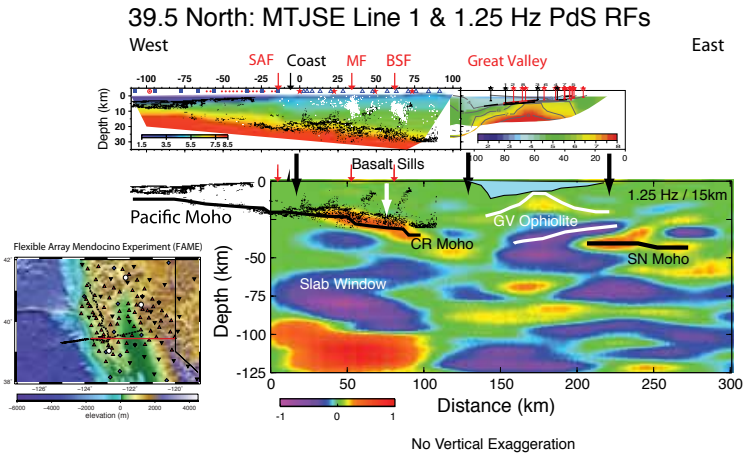

Figure 2. East-west receiver function cross-section at 39.50N. P-wave velocity model of the MTJSE line 1 is shown in the upper panel, superimposed by the depth migrated single-fold section. The white dots denote the projected earthquakes beneath the Maacama Fault and Bartlett Springs Fault. The black lines mark the Moho depth determined by the RF image. The basalt intrusions near Lake Pillsbury are represented by strong reflections from the lower crust and Moho. The Great Valley Ophiolite (GVO) is a high velocity body bounded by white lines between the Coast Ranges (CR) and Sierra Nevada (SN) Moho. Note that no clear Moho signal is observed beneath the northern Great Valley.

References

Zhai, Y., and A. Levander (2010), The Lithosphere-Asthenosphere Boundary and the Slab Window in the Mendocino Triple Junction Region, in preparation.

Acknowledgements: This project is supported by NSF grants EAR-0642474 and EAR-0746379.

Lithospheric Structure beneath the Western US Using USArray Data

Meghan S. Miller *(University of Southern California),* **Alan Levander** *(Rice University)*

Using a combination teleseismic data from the USArray Transportable Array, previous PASSCAL experiments, and the COARSE array in Arizona we have produced images of the lithospheric structure beneath the Western United States. We have made common conversion point (CCP) stacked Ps and Sp receiver function image volumes to determine, in more detail and higher resolution than previously obtained, the crustal thickness and the depth to the Moho and lithosphere-asthenosphere boundary (LAB) throughout the Western U.S. Individual receiver functions have been converted to depth and laterally "migrated" to their conversion point using 3D P- and S-wave tomography velocity models, with redundant signals stacked for signal enhancement. Both S and P receiver functions have imaged an unusually complex crust-mantle boundary region beneath the Colorado Plateau in comparison to most other parts of the western U.S., although we also see features that correlate with expressions of lithospheric drips in the southern Sierra Nevada and the Wallowa Mountains. The Moho shallows significantly from an average of ≥40 km to the southern Basin and Range, where the crust is ~30 km. These complications in the Moho are correlated with low upper mantle velocities observed in P and S body wave tomography and S-velocity structure determined from Rayleigh wave inversion. Throughout the model, the LAB is a negative amplitude feature that has significant topographic variation, and cannot be described as a single surface. We see a particularly strong correlation between calculated equilibration pressures of primitive basalt whole rock samples from across the western United States, extracted from the NAVDAT database (http://www.navdat.org/), and the LAB estimate from the Sp images beneath the southern Basin and Range, the Colorado Plateau, and the Sierra Nevada. The depth estimates from the geochemistry data and comparison with the PdS receiver function images for the same region allows us to interpret the lithosphere-asthenosphere boundary and its relation to the tectonic provinces in the western United States. We will present different geologic scenarios that can explain these structures.

Acknowledgements: We would like to thank Kaijian Liu, Yongbo Zhai, Yan Xu, and Meijuan Jiang for assisting with data processing. The Sp receiver function study began as an exercise at the 2008 CIDER (Cooperative Institute for Deep Earth Research) summer school. This research was funded by Earthscope grant EAR-0844741 and 0844760. AL gratefully acknowledges a Humboldt Research Prize from the Alexander von Humboldt Foundation. The Ps study was initiated by AL while on sabbatical at the GeoForschungsZentrum Potsdam, Germany.

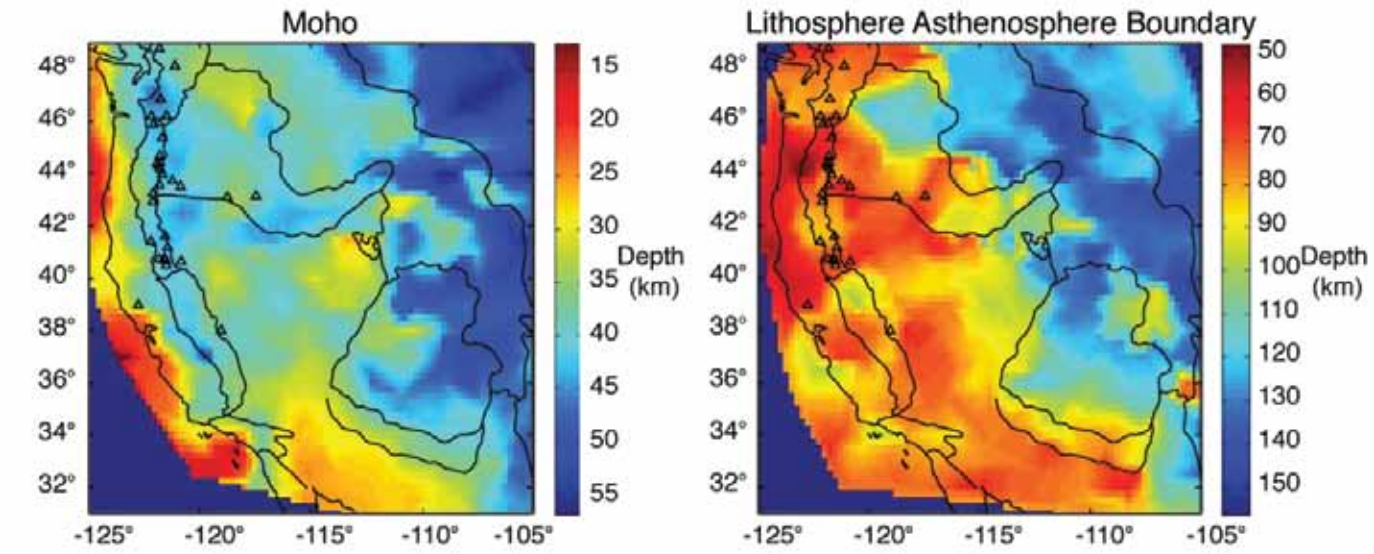

Maps of depth to (a) Moho and (b) LAB. The thick lines illustrate the physiographic boundaries in the western U.S. The LAB map is a smoothed estimate of the shallowest event we identified as the LAB in the Ps and Sp receiver functions.

The Lithosphere-Asthenosphere Boundary beneath North America and Australia

Heather A. Ford *(Brown University),* **David L. Abt** *(ExxonMobil Exploration Company),* **Karen M. Fischer** *(Brown University)*

The concept of a strong lithosphere that translates as a relatively coherent layer over a weak asthenosphere is fundamental to models of plate motions, tectonics, and mantle convection. However, much remains to be learned about the physical and chemical properties that create rheological differences between the lithosphere and asthenosphere. We have used Sp and Ps scattered waves to image mantle discontinuities beneath North America and Australia.

In the tectonically active western U.S., large portions of the Phanerozoic eastern U.S., Phanerozoic eastern Australia and the adjacent edge of the Australian craton, prominent Sp phases from a negative velocity contrast were found at depths of 50-130 km, consistent with the lithosphere-asthenosphere boundary depth range from surface wave tomography. These phases imply significant (4-10%) velocity drops over depth ranges of 30-40 km or less, and thus cannot be simply explained by a lithosphere-asthenosphere boundary that is governed purely by temperature. Rather, they imply that the asthenosphere is hydrated with respect to a drier, depleted lithosphere or contains a small amount of partial melt.

In contrast, no significant negative Sp phase was found at the base of the thick cratonic lithosphere in either continent, implying that the cratonic lithosphere-asthenosphere velocity gradient is distributed over more than 50-70 km in depth. This gradient may be purely thermal in origin, although gradational changes in composition or melt content cannot be ruled out. A negative discontinuity internal to the cratonic lithosphere was observed at depths of 50-115 km. The depth of this boundary is comparable to the thickness of oceanic and younger continental lithosphere. This discontinuity may date from the formation of the cratonic lithosphere, or it could reflect later alteration of the cratonic lithosphere by melting and metasomatism, perhaps as the top of a melt cumulate layer.

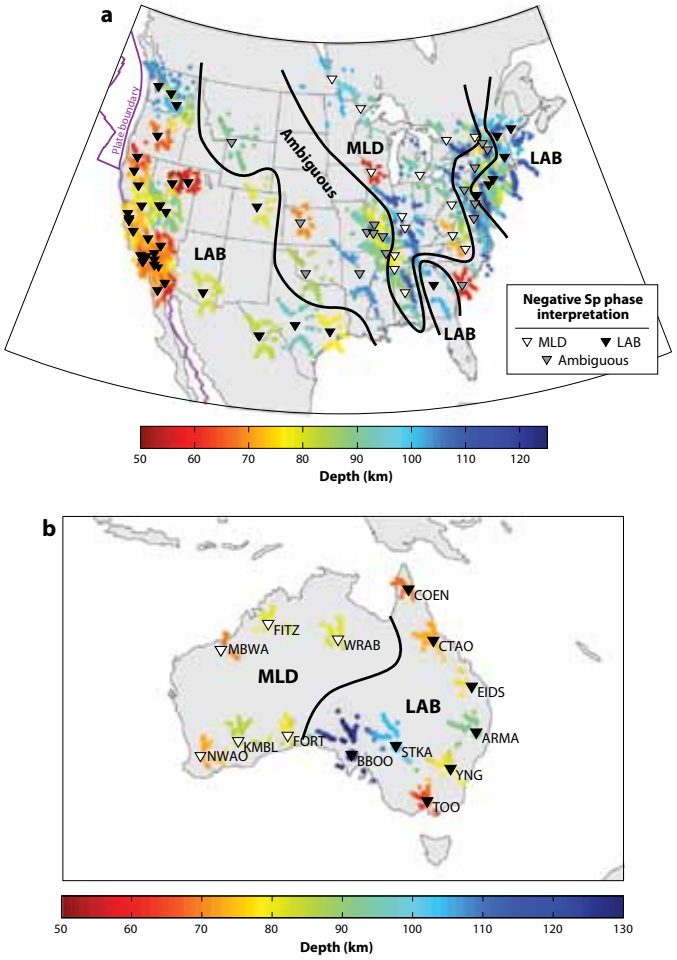

Mantle discontinuity depths estimated from Sp receiver functions in North America by Abt et al. (2010) (a) and in Australia by Ford et al. (2010) (b). The dots are colored for depth/amplitude and represent Sp piercing points that have been interpolated onto a fine grid and smoothed with a circular filter with a 30 km radius. (a) North America. Black inverted triangles indicate stations where the negative Sp phase is interpreted as the lithosphere-asthenosphere boundary (LAB), white inverted triangles are stations where the phase is interpreted as a mid-lithospheric discontinuity (MLD), and gray stations indicate ambiguity in the interpretation of the negative Sp phase. (b) Australia. Negative Sp phases at stations in Phanerozoic eastern Australia and just within the eastern margin of the Proterozoic craton (BBOO and stations to its east) are interpreted as the LAB. Negative Sp phases at most stations in the Proterozoic and Archean craton (station WRAB and the stations to its west

References

Ford, H. A., K. M. Fischer, D. L. Abt, Catherine A. Rychert, L. T. Elkins-Tanton (2010), The lithosphere-asthenosphere boundary and cratonic lithospheric layering beneath Australia from Sp wave imaging, *Earth Planet. Sci. Lett.*, submitted.

Abt, D. L., K. M. Fischer, S.W. French, H.A. Ford, H. Yuan, B. Romanowicz (2010), North American lithospheric discontinuity structure imaged by Ps and Sp receiver functions, *J. Geophys. Res.*, in press.

Fischer, K. M., H. A. Ford, D. L. Abt, C. A. Rychert (2010), The lithosphere-asthenosphere boundary, *Ann. Rev. Earth Planet. Sci., 38*, 551-575.

Acknowledgements: Data used in these studies were collected from the IRIS DMS. This work was supported by the National Science Foundation under awards EAR-0538155 (Geophysics) and EAR-0641772 (EarthScope).

Receiver Function Imaging of the Lithosphere-Asthenosphere Boundary

Catherine A. Rychert *(University of Bristol, U.K.),* **Peter M. Shearer** *(University of California, San Diego, U.S.A.)*

The lithosphere-asthenosphere boundary, or LAB, is often defined seismically as the top of the low velocity zone underlying the higher velocities of the lithospheric lid. Surface-wave studies have shown the global extent of upper-mantle low-velocity zones, but do not have the vertical resolution to constrain the details of LAB depth and sharpness. Better depth resolution, at least in the vicinity of seismic stations, is provided by receiver-function studies of converted phases, although care must be taken to distinguish LAB signals from noise and crustal reverberations. The continued operation of the global seismic networks, by IRIS and other agencies, has provided a sufficient volume of data that receiver-function imaging of the LAB is now possible on a global scale. We have analyzed 15 years of global seismic data using P-to-S (Ps) converted phases from over 150 stations and imaged an interface that correlates with tectonic environment, varying in average depth from 95 ± 4 km beneath Precambrian shields and platforms to 81 ± 2 km beneath tectonically altered regions and 70 ± 4 km at oceanic island stations. Because the polarity of the Ps arrivals indicates a shear-velocity drop with depth, this interface is likely the LAB in most regions, although it may constitute another boundary beneath the cratonic interiors of continents where the LAB is expected to be much deeper. The high frequencies observed in the Ps arrivals require a sharp discontinuity, implying a change in composition, melting, or anisotropy, not temperature alone.

References

Rychert, C. A., and P. M. Shearer, A global view of the lithosphere-asthenosphere boundary, *Science, 324*, 2009.

Rychert, C. A., P. M. Shearer and K. M. Fischer, Scattered wave imaging of the lithosphere-asthenosphere boundary, *Lithos, 2010*.

Jordan, T. H., Global Tectonic regionalization for seismological data analysis, *Bull. Seismol. Soc. Amer., 71*(4): 1131-1141, 1981.

Acknowledgements: This research was supported by National Science Foundation awards EAR-0229323 and EAR-0710881.

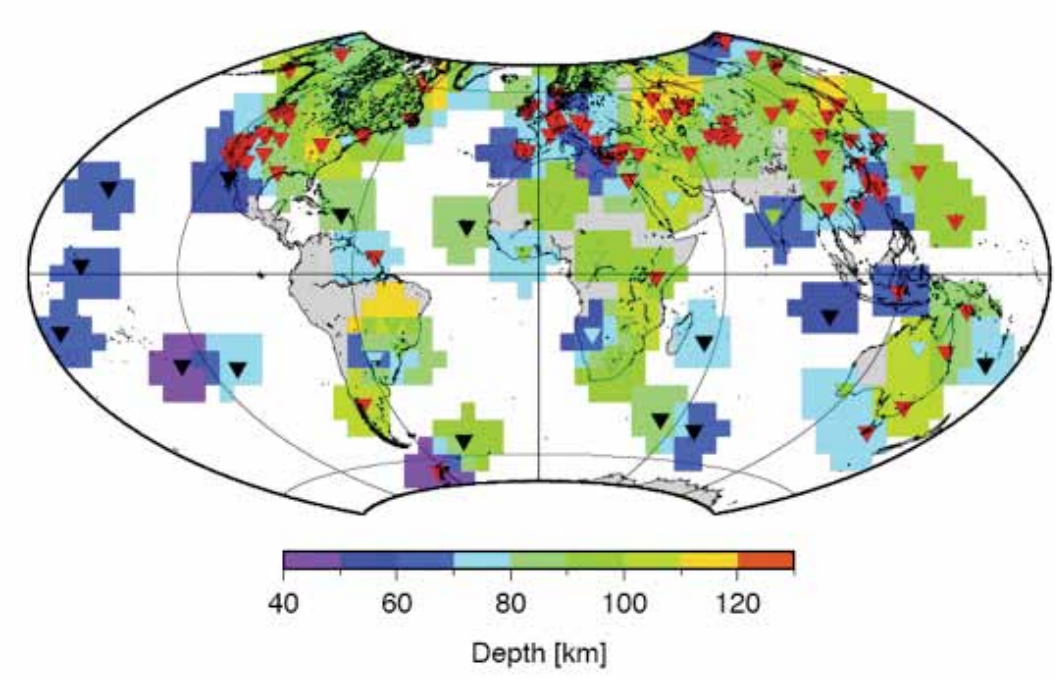

Global map of the depth to the lithosphere-asthenosphere boundary imaged using Ps receiver functions. Color indicates depth. Triangles show the 169 stations used in this study. Station color corresponds to tectonic regionalization, after Jordan (1981). Tectonic regions colored as follows: Oceanic – black, Phanerozoic orogenic zones and magmatic belts – red, Phanerozoic platforms – cyan, Precambrian shields and platforms – green. Although the work of Jordan (1981) divides oceanic environments into three age groupings, a single oceanic bin, encompassing all ages, is used here, since sampling of this region is sparse.

S-Velocity Structure of Cratons, from Broad-Band Surface-Wave Dispersion

Sergei Lebedev *(Dublin Institute for Advanced Studies),* **Jeannot Trampert** *(Utrecht University)*

Despite recent progress in mapping the lateral extent of cratonic roots worldwide [e.g. Lebedev & van der Hilst, 2008], profiles of seismic velocities within them remain uncertain. Here, a novel combination of waveform-analysis techniques was used to measure inter-station, Rayleigh- and Love-wave phase velocities in broad period ranges. The new measurements yield resolution from the upper crust to deep upper mantle beneath a selection of cratons from around the globe and provide new constraints on the thermal and compositional structure and evolution of Precambrian lithosphere.

Shear-wave speed Vs is consistently higher in the lithosphere of cratons than in the lithosphere of Proterozoic foldbelts. Because known effects of compositional variations in the lithosphere on Vs are too small to account for the difference, this confirms that temperature in the cratonic lithosphere is consistently lower. This is in spite of sub-lithospheric mantle beneath continents being thermally heterogeneous, with some cratons currently underlain by a substantially hotter asthenosphere compared to others.

An increase in Vs between the Moho and a 100-150 km depth is consistently preferred by the data and is likely to be due to phase transformations, in particular the transition from spinel peridotite to garnet peridotite, proposed previously to give rise to the "Hales discontinuity" within this depth interval. The depth and the width of the phase transformation depend on mantle composition; it is likely to occur deeper and over a broader depth interval beneath cratons than elsewhere because of the high Cr content in the depleted cratonic lithosphere, as evidenced by a number of xenolith studies. Seismic data available at present would be consistent with both a sharp and a gradual increase in Vs in the upper lithosphere (a Hales discontinuity or a "Hales gradient").

Radial anisotropy in the upper crust indicates vertically oriented anisotropic fabric (Vsh < Vsv); this may yield a clue on how cratons grew, lending support to the view that distributed crustal shortening with sub-vertical flow patterns occurred over large scales in hot ancient orogens. In the lower crust and upper lithospheric mantle, radial anisotropy reveals horizontal fabric (Vsh > Vsv), likely to be a record of horizontal ductile flow in the lower crust and lithospheric mantle at the time of the formation and stabilisation of the cratons.

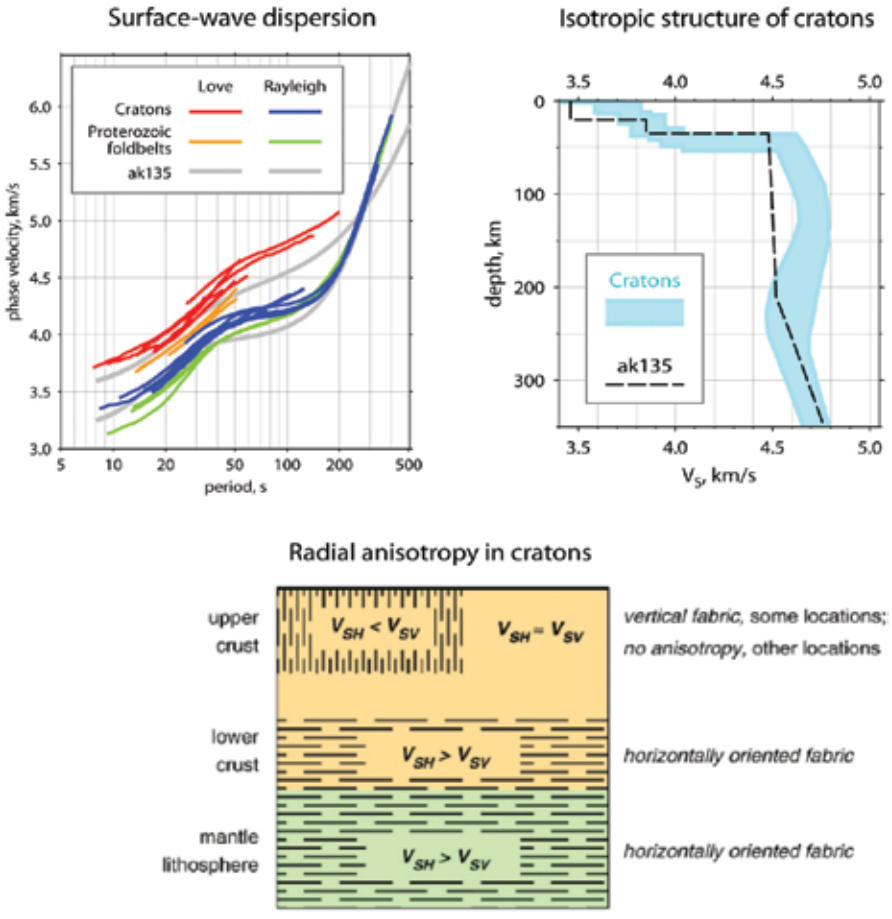

Top left: phase-velocity measurements sampling Precambrian continental lithosphere. Top right: summary profile of the isotropic-average shear speed beneath Archean cratons. The ranges of Vs values include the best-fitting profiles from all the cratonic locations sampled. Bottom: radial anisotropy within the upper Precambrian lithosphere. Anisotropy with horizontally polarised shear waves propagating faster than vertically polarised ones (Vsh > Vsv) is observed in the lower crust and mantle lithosphere and indicates horizontally oriented fabric. Anisotropy with Vsh < Vsv is observed in the upper crust beneath a number of locations and suggests the occurrence of vertically oriented fabric.

References

Lebedev, S., J. Boonen, J. Trampert, Seismic structure of Precambrian lithosphere: New constraints from broadband surface-wave dispersion, *Lithos*, Special Issue "Continental Lithospheric Mantle: the Petro-Geophysical Approach", 109, 96-111, 2009.

Lebedev, S., R. D. van der Hilst, Global upper-mantle tomography with the automated multimode inversion of surface and S-wave forms, *Geophys. J. Int., 173*, 505-518, 2008.

First Multi-Scale, Finite-Frequency Tomography Illuminates 3-D Anatomy of the Tibetan Plateau

Shu-Huei Hung *(National Taiwan University, Taiwan, R.O.C.),* **Wang-Ping Chen** *(University of Illinois, Urbana-Champaign),* **Ling-Yun Chiao** *(National Taiwan University, Taiwan, R.O.C.)*

With a new multi-scale parameterization, 3-D images from finite-frequency seismic tomography, including the very first images beneath central Tibet from S-waves, reveal that regions of low electric resistivity in the crust, previously observed along active rifts in southern Tibet, correlate well with regions of low P- and S-wave speeds (V). However, such regions are not interconnected, indicating that a prevailing south-directed, channel-like crustal flow seems inactive or this popular geodynamic model needs modification. In the upper mantle, there is no clear indication of regional down-welling between depths of 100 to 400 km. Instead, a strong, lateral boundary between high and low V extends up to 33°N, marking the northern limit of sub-horizontally advancing Indian lithospheric mantle.

References

Hung, S.-H., W.-P. Chen, L.-Y. Chiao and T.-L. Tseng, First multi-scale, finite-frequency tomography illuminates 3-D anatomy of the Tibetan plateau, *Geophys. Res. Lett., 37*, doi:10.1029/2009GL041875 (with on-line supplements), 2010.

Acknowledgements: We thank S.-L. Chung for helpful discussions, L. Zhao, an anonymous referee, and the Editor for their comments that help improve the manuscript. This work was supported by National Science Council of Taiwan grants 96-2119-M-002-016 and 97-2745-M-002-011 (S.-H.H.) and U.S. National Science Foundation grants EAR99-09362 ("Hi-CLIMB"), EAR05-51995, and EAR06-35419 (W.-P.C.)

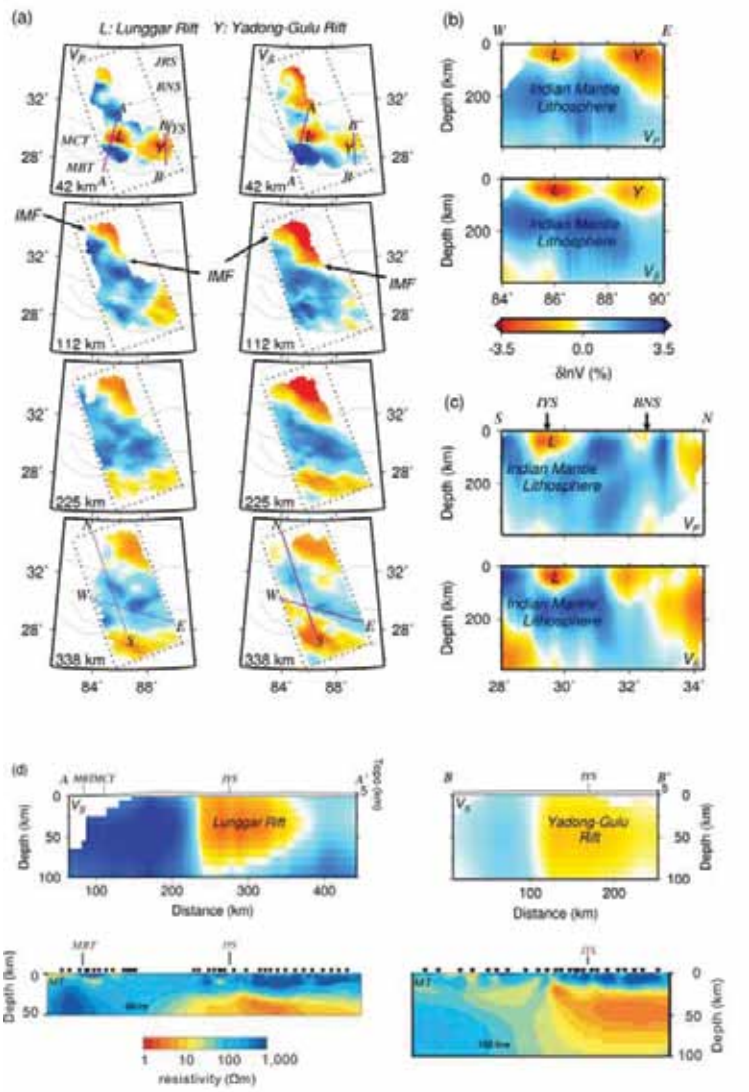

A map showing color-coded topography of the Himalayan-Tibetan collision zone. Finite-frequency travel-times recorded by 108 broadband stations (green triangles) are used to obtain multi-scaled, tomographic images for a large volume beneath western Tibet (box outlined by dashed lines). Blue solid lines indicate locations of profiles along which cross-sections of $\delta \ln V_P$ and $\delta \ln V_S$ are shown in Figure 3b and 3c. Blue dashed lines mark profiles across the Lunggar and the Yadong-Gulu rifts where profiles of electric resistivity are inferred from magnetotelluric (MT) measurements (at locations shown as purple open circles) and being directly compared with our results of $\delta \ln V_S$ in Figure 3d. For reference, positions of other temporary seismic stations, located to the east of our region of study and whose data were used to construct the tomographic profile of Tilmann et al. [2003], are also plotted (brown dashed line and orange inverted triangles). Other features not explained in the legend are: Young or active normal faults (red curves, Taylor and Yin [2009]); major geologic boundaries (solid curves), including (from north to south) JRS, the Jinsha River Suture; BNS, the Bangong-Nujiang Suture; IYS, the Indus-Yarlung Suture; STD, the South Tibet Detachment System; MCT, the Main Central Thrust; and MBT, the Main Boundary Thrust.

Seismic Structure of the Crust and the Upper Mantle beneath the Himalayas

Gaspar Monsalve (University of Colorado at Boulder), **Anne Sheehan** (University of Colorado at Boulder)

Seismic structure of the crust and the upper mantle beneath the Himalayas: Evidence for eclogitization of lower crustal rocks in the Indian Plate G. Monsalve, A. Sheehan, C. Rowe, and S. Rajaure Variations in the seismic velocity structure of the Himalayan collision zone include significant differences between its north and south portions, with transitions in physical properties across the Greater Himalaya. We combined P- and S-wave traveltimes from a temporary broadband seismic network in eastern Nepal and southern Tibet with arrival times at the permanent station network of the Department of Mines and Geology of Nepal to determine the seismic velocity structure across the Himalaya, using local earthquake tomography and traveltimes of regional earthquakes. The P-to-S velocity ratio (Vp/Vs) structure marks the difference between the Indian Plate and the overlying materials, with the Vp/Vs ratios being high for the former and low for the latter. We also found a significant increase in the uppermost mantle seismic velocities from south to north, reaching P-wave velocities (Vp) over 8.4 km/s north of the Greater Himalaya. These high Vp values do not seem to be the result of biases due to anisotropy in the upper mantle beneath the Greater and Tethyan Himalayas. Instead, we suggest that rocks in the lower crust of the underthrusting Indian Plate undergo metamorphism to eclogite as they plunge to greater depth beneath the mountain range, explaining the high seismic velocities.

References

Monsalve, G., A. Sheehan, C. Rowe, and S. Rajaure (2008), Seismic structure of the crust and the upper mantle beneath the Himalayas: Evidence for eclogitization of lower crustal rocks in the Indian Plate, *J. Geophys. Res., 113,* B08315, doi:10.1029/2007JB005424.

Acknowledgements: Broadband seismometers used in this experiment are from the IRIS PASSCAL program and data are archived at the IRIS DMC. We thank the staff of the Department of Mines and Geology of Nepal for their assistance with the experiment and for sharing their network seismic data with us. This work was supported by grants from the National Science Foundation and the Department of Energy.

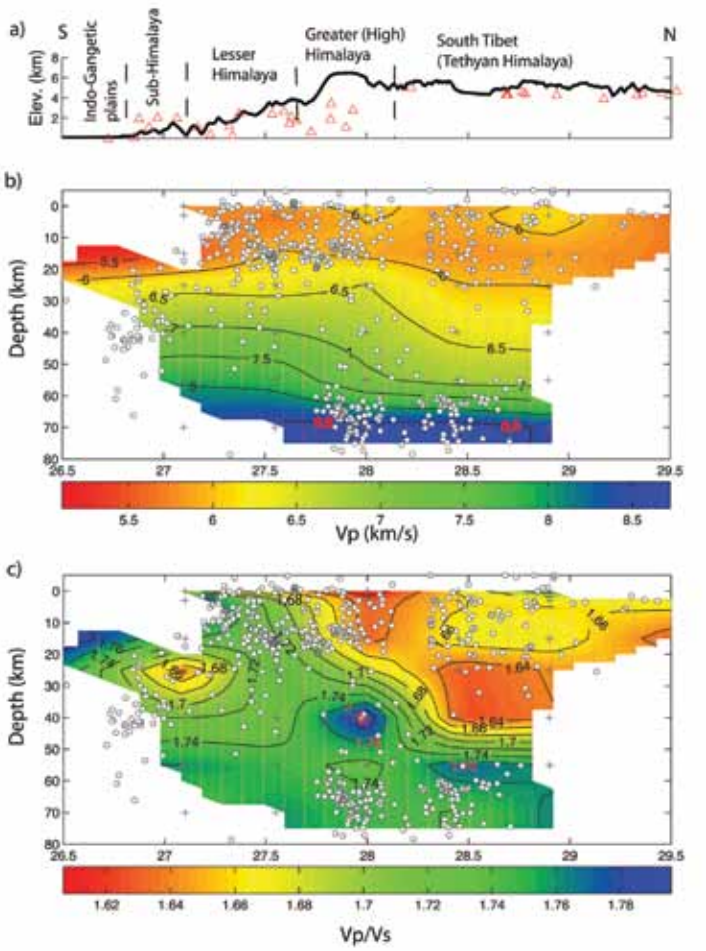

Two-dimensional north-south structure of Vp and Vp/Vs beneath eastern Nepal and the southern Tibetan Plateau. Earthquakes are projected onto an N-S cross-section. (a) North-south topographic cross-section at 86.5°E, red triangles denote projected station locations. (b) North-south Vp structure. Horizontal axis is latitude in degrees North. (c) North-south Vp/Vs structure.

Evolution of Caribbean – South American Plate Boundary from Surface Wave Tomography

Meghan S. Miller *(University of Southern California),* **Alan Levander** *(Rice University),* **Fenglin Niu** *(Rice University)*

We have measured shear wave velocity structure of the crust and upper mantle of the Caribbean – South American boundary region by analysis of fundamental mode Rayleigh waves in the 20-100s period band recorded at the BOLIVAR/GEODINOS stations from 2003 to 2005. The model shows lateral variations that primarily correspond to tectonic provinces and boundaries. A clear linear velocity change parallels the plate bounding dextral strike-slip fault system along the northern coast of Venezuela, illustrating the differences between the South American continental lithosphere, the Venezuelan archipelago, and the Caribbean oceanic lithosphere. At depths up to 120 kilometers beneath the Venezuelan Andes and the Maracaibo block there is evidence of underthrusting of the Caribbean plate, but there is no other evidence of subduction of the Caribbean plate beneath the South American plate. In eastern Venezuela linear crustal low velocities are associated with the fold and thrust belts whereas as higher crustal velocities are imaged in the Guayana shield lithosphere. The subducting oceanic part of the South American plate is imaged beneath the Antilles Arc. The surface wave images combined with seismicity data suggest shear tearing of the oceanic lithosphere away from the buoyant continental South American plate offshore of northeastern Venezuela. The continental lithosphere south of the slab tear is bent down towards the plate boundary in response to the propagating tear in the lithosphere. We interpret a nearly vertical low velocity "column" west of the tear centered beneath the Cariaco Basin, with three dimensional asthenospheric flow around the southern edge of the subducting oceanic lithosphere, with the asthenosphere escaping from beneath continental South America, and rising into the plate boundary zone. The complex plate boundary structure is best examined in three-dimensions. We discuss the new surface wave tomographic inversion in the context of results from other researchers including local seismicity, teleseismic shear wave splits, and interpretations from active source profiling.

Acknowledgements: BOLIVAR was funded by grants EAR0003572 and EAR0607801 from the NSF Continental Dynamics Program, and funding to our Venezuelan colleagues from CONICIT, the Venezuela Science Foundation, and PDVSA.

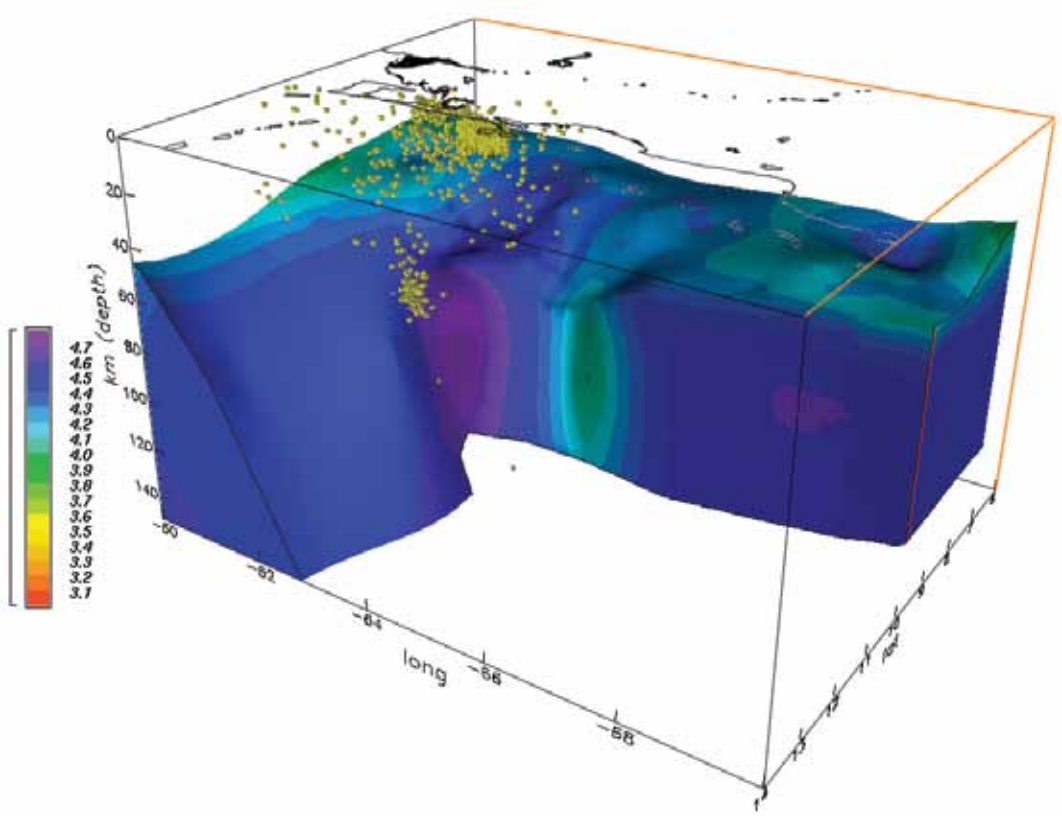

Surface wave tomography model illustrating the structure of the South American mantle lithosphere as viewed from the northwest. The yellow dots are relocated seismicity, which define the Paria cluster and the location of the subducted oceanic lithosphere beneath the Antilles arc tearing away from the continental lithosphere along the Caribbean-South American plate boundary.

Subducted Oceanic Asthenosphere and Upper Mantle Flow beneath the Juan de Fuca Slab

R. M. Russo *(University of Florida)*

Many studies have shown that typical oceanic lithosphere is underlain by a well developed asthenosphere characterized by slow seismic velocities from ~100-250 km depth. However, the fate of the oceanic asthenosphere at subduction zones is poorly understood. I show here using shear wave splitting of S waves emanating from earthquakes in the Juan de Fuca slab that upper mantle asthenospheric anisotropy beneath the slab is consistent with the presence of two distinct subducted asthenospheric layers, one with fast shear trends parallel to the subduction trench, and a second, deeper layer with fast upper mantle fabrics parallel to the motion of the Juan de Fuca plate with respect to the deeper mantle. The consistent orientation of unsubducted Pacific asthenospheric anisotropy in the direction of current plate motion implies that the trench-parallel sub-slab anisotropy develops when the lithosphere subducts.

References

Russo, R. M., Subducted oceanic asthenosphere and upper mantle flow beneath the Juan de Fuca slab, *Lithosphere, 1,* 195-205, 2009.

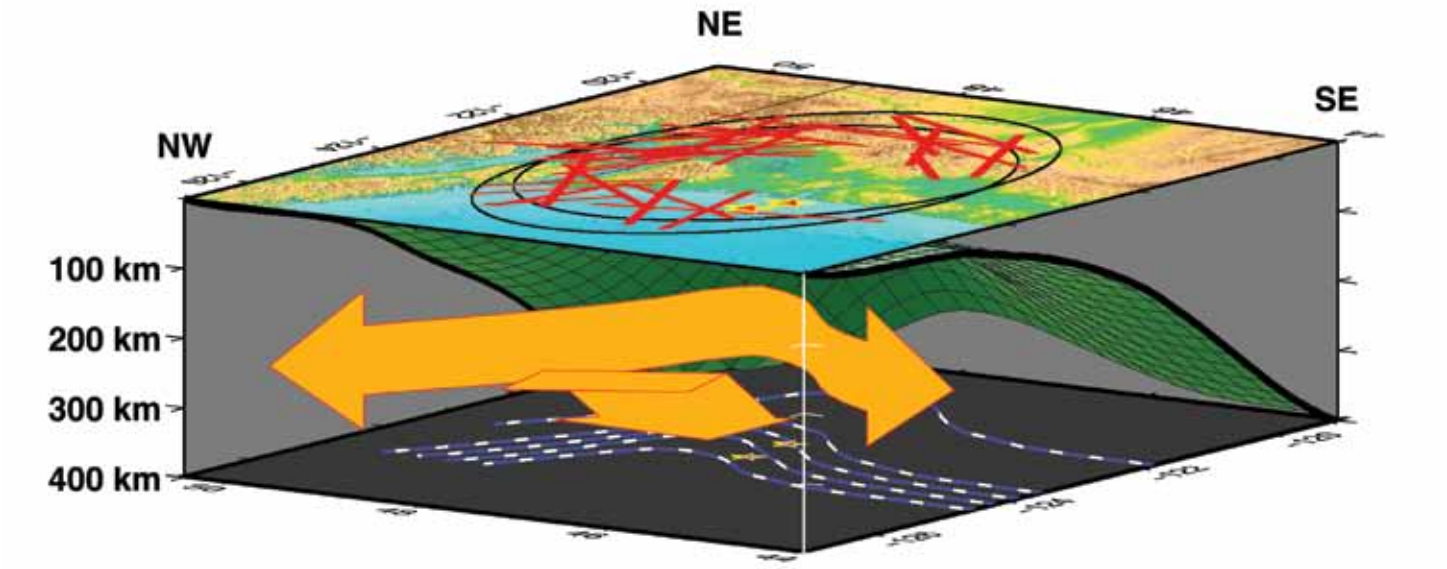

Block diagram showing Juan de Fuca slab geometry (green meshed surface), and top-of-slab depth contours (heavy blue dashed lines, bottom). Source side S splitting measurements are compatible with presence of two anisotropic layers beneath the Juan de Fuca slab: a layer immediately beneath the slab which is characterized by trench-parallel fast shear azimuths, and a deeper layer with fast shear trends parallel to the motion of the Juan de Fuca plate with respect to assumed fixed hotspots (Gripp and Gordon, 2003). Orange arrows schematically show the anisotropy and possibly upper mantle flow directions in these two layers.

Subduction of the Chile Ridge: Upper Mantle Structure and Flow

R. M. Russo *(University of Florida),* **J. C. VanDecar** *(DTM - Carnegie Inst. Washington),* **D. Comte** *(Universidad de Chile),* **V. I. Mocanu** *(University of Bucharest),* **A. Gallego** *(University of Florida),* **R. E. Murdie** *(Goldfields Australia)*

We deployed 39 broadband seismometers in southern Chile from Dec. 2004 to Feb. 2007 to determine lithosphere and upper mantle structure, including possible slab windows, in the vicinity of the subducting Chile Ridge. Body-wave travel-time tomography clearly shows the existence of a long-hypothesized slab window, a gap between the subducted Nazca and Antarctic lithospheres. P-wave velocities in the slab window are distinctly slow relative to surrounding asthenospheric mantle. Thus, the gap between slabs visible in the imaging appears to be filled by unusually warm asthenosphere, consistent with subduction of the Chile Ridge. Shear-wave splitting in the Chile Ridge subduction region is very strong (mean delay time nearly ~3 s) and highly variable. North of the slab window, splitting fast directions are mostly trench parallel, but, in the region of the slab gap, splitting fast trends appear to fan from NW-SE trends to the north, through ENE-WSW trends toward the middle of the slab window, to NE-SW trends south of the slab window. We interpret these results as

indicating flow of asthenospheric upper mantle into the slab window.

References

Russo, R. M., J.C. VanDecar, D. Comte, V.I. Mocanu, A. Gallego, and R.E. Murdie, Subduction of the Chile Ridge: Upper Mantle Structure and Flow, *GSA Today, 20* (9), 4-10, doi: 10.1130/GSATG61A.1, 2010.

Acknowledgements: Supported by U.S. National Science Foundation grant EAR-0126244 and CONICYT grant no. 1050367 from the government of Chile.

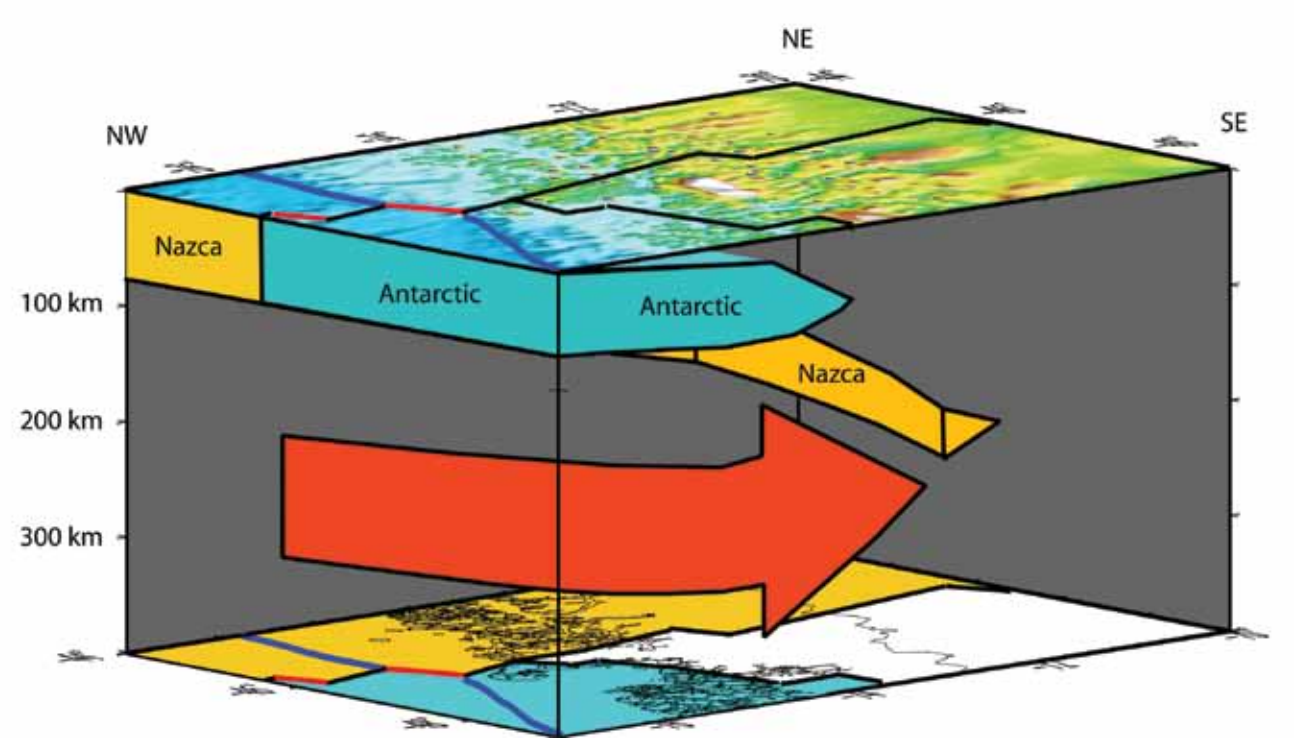

Schematic 3-d block diagram of upper mantle flow in the vicinity of the slab window delineated by the travel time inversions. Map on top of block shows relief and locations of Chile Ridge structures before subduction and after. Bottom of block shows coastline and Chile Ridge structures over color-coded slab plates: Nazca plate in dark yellow, Antarctic plate in blue-green. Same colors for portions of slab visible in the block diagram itself. Red arrow parallels shear wave splitting fast trends and upper mantle flow in the vicinity of the slab window opening. View from the SW, looking NE. Note the northern, shallower portion of the slab window is not visible from this viewpoint.

Detecting the Limit of Slab Break-off in Central Turkey: New High-resolution Pn Tomography Results

C.R. Gans *(University of Arizona),* **S.L. Beck** *(University of Arizona),* **G. Zandt** *(University of Arizona),* **C.B. Biryol** *(University of Arizona),* **A.A. Ozacar** *(Middle East Technical University)*

Inversion of Pn travel time residuals from a 39-station portable broadband array (instruments provided by IRIS PASSCAL) provides a high-resolution image of the velocity structure in the uppermost mantle beneath central Turkey. Individually picked Pn phase arrivals from events recorded by the North Anatolian Fault Passive Seismic Experiment and the Kandilli Observatory were combined with additional events associated with the Eastern Turkey Seismic Experiment. Tomography results show no change in Pn velocity across the North Anatolian Fault, although longitudinal variations are evident. A region of very low Pn velocities (< 7.8 km/s) is imaged east of the Central Anatolian Fault Zone (CAFZ), with a transition to faster velocities (> 8.1 km/s) west of the fault. The sharp transition along the CAFZ, which follows the paleotectonic Inner Tauride Suture, may represent the location of the edge of the slab window, created when the oceanic slab broke off along the Bitlis-Zagros Suture around 11 Ma, as the Arabian plate collided with the Eurasian plate.

References

Faccenna, C., Bellier, O., Martinod, J., Piromallo, C. and V. Regard (2006), Slab detachment beneath eastern Anatolia: A possible cause for the formation of the North Anatolian fault, *Earth Planet. Sci. Lett., 242*, 85-97.

Acknowledgements: National Science Foundation Grant EAR0309838

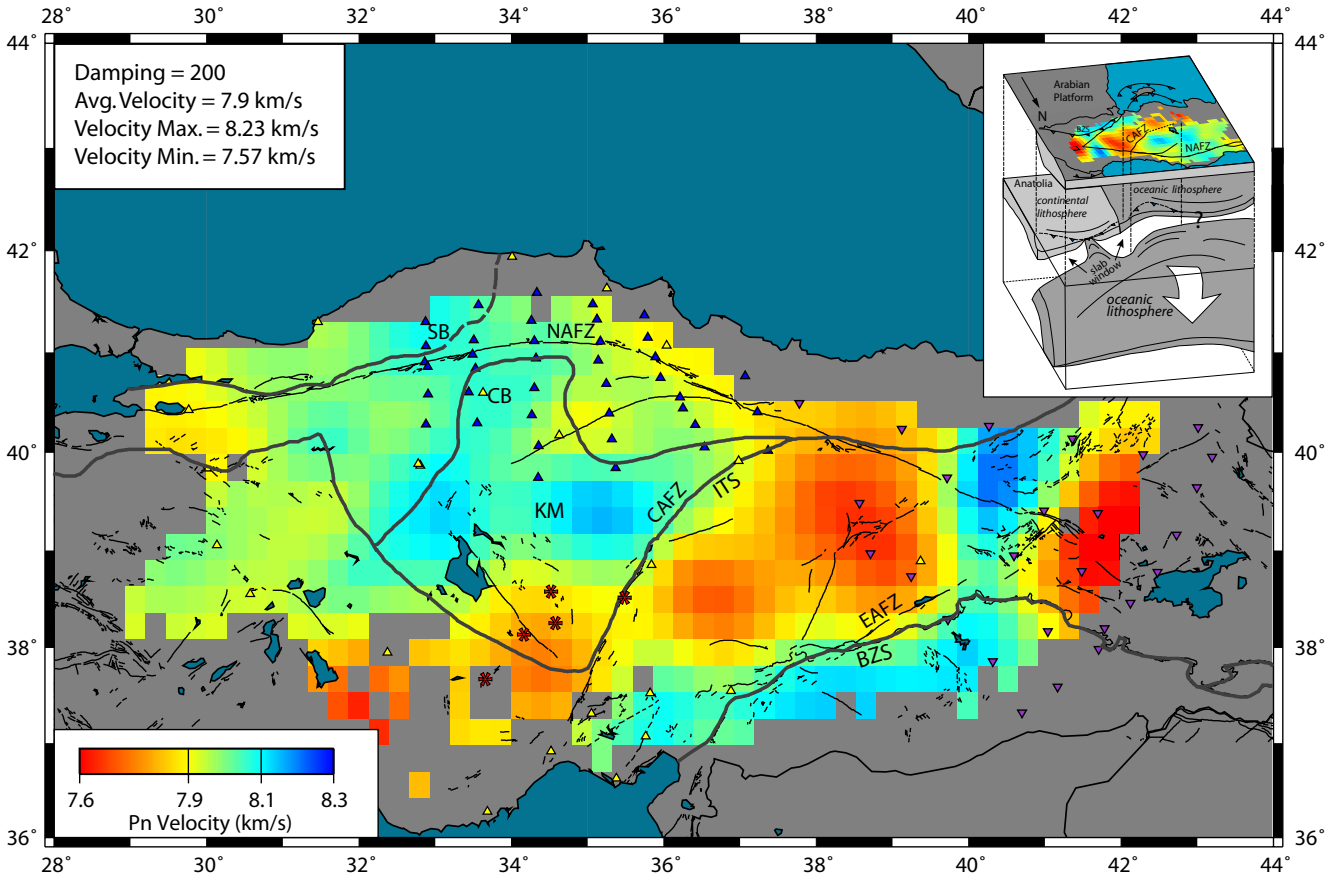

Figure 1. Pn tomography results for north-central Turkey. Stations shown by triangles, Holocene volcanoes by red asterisks. NAFZ - North Anatolian Fault Zone, CAFZ - Central Anatolian Fault Zone, EAFZ - East Anatolian Fault Zone, ITS - Inner Tauride Suture, KM - Kirsehir massif, SB - Safranbolu Basin, CB - Cankiri Basin, BZS - Bitlis Zagros Suture. Red asterisks are Holocene volcanoes. Inset: Cartoon showing hypothesized upper mantle slab detachment and resulting slab window consistent with Pn tomography results. The downdip edge of the slab window corresponds to the northern edge of the low Pn region that partially follows the CAFZ. The western extent of the tear is uncertain. Modified after Faccenna et al. [2006].

Imaging the Flat Slab Beneath the Sierras Pampeanas, Argentina, Using Receiver Functions: Evidence for Overthickened and Broken Subducted Oceanic Crust

C.R. Gans *(University of Arizona),* **S.L. Beck** *(University of Arizona),* **G. Zandt** *(University of Arizona),* **H. Gilbert** *(Purdue University),* **P. Alvarado** *(Universidad Nacional de San Juan, Argentina)*

The western margin of South America between 30° and 32° S is characterized by the flat slab subduction of the ~43 Ma oceanic Nazca plate beneath the continental South American plate. Several arrays of PASSCAL broadband seismic instruments have been deployed in Chile and western Argentina to study this phenomenon (e.g., CHARGE, 2000-2002; SIEMBRA, 2007-2009; ESP, 2008-2010). The low angle subduction has prevented magmatism in the area since the late Miocene, and spatially correlates with the formation of both thick-skinned (Sierras Pampeanas) basement cored uplifts and the thin-skinned (Andean Precordillera) fold and thrust belt within the region. In order to better constrain the crust and upper mantle structure in the transition region between flat slab and normal subduction to the south, we have calculated receiver functions (RFs) from teleseismic earthquakes. Using our dense SIEMBRA array, combined with the broader CHARGE and ESP arrays, we are able to image in detail the flat slab, which contains a distinct negative arrival (indicative of a low velocity zone) at the top of the flat slab, followed by a strong positive P-to-S conversion. While the exact causes of flat slab subduction continue to be debated, one overriding theme is the necessity of having an overthickened crust in order to increase the buoyancy of the subducting slab. In this region, the hotspot seamount chain of the Juan Fernandez Ridge (JFR) is thought to provide such a mechanism. Kopp et al. [2004], however, did not find overthickened crust in the offshore portion of the JFR, but rather only moderately thick oceanic crust. Preliminary results from our RFs, compared with synthetic RFs, indicate that the oceanic crust at the top of the slab (the low velocity zone) must be at least ~12-14 km thick. Our results support the idea of an overthickened crust in the subducted flat slab beneath western Argentina. Further, there are indications in the receiver functions that the subducted oceanic crust in the region directly along the path of the subducted ridge is broken by trench parallel faults. One explanation for this could be that these are older faults in the oceanic crust, created when the crust was first subducted. Alternatively, it is possible that new faults are forming due to stresses induced by increased coupling in the flat slab region.

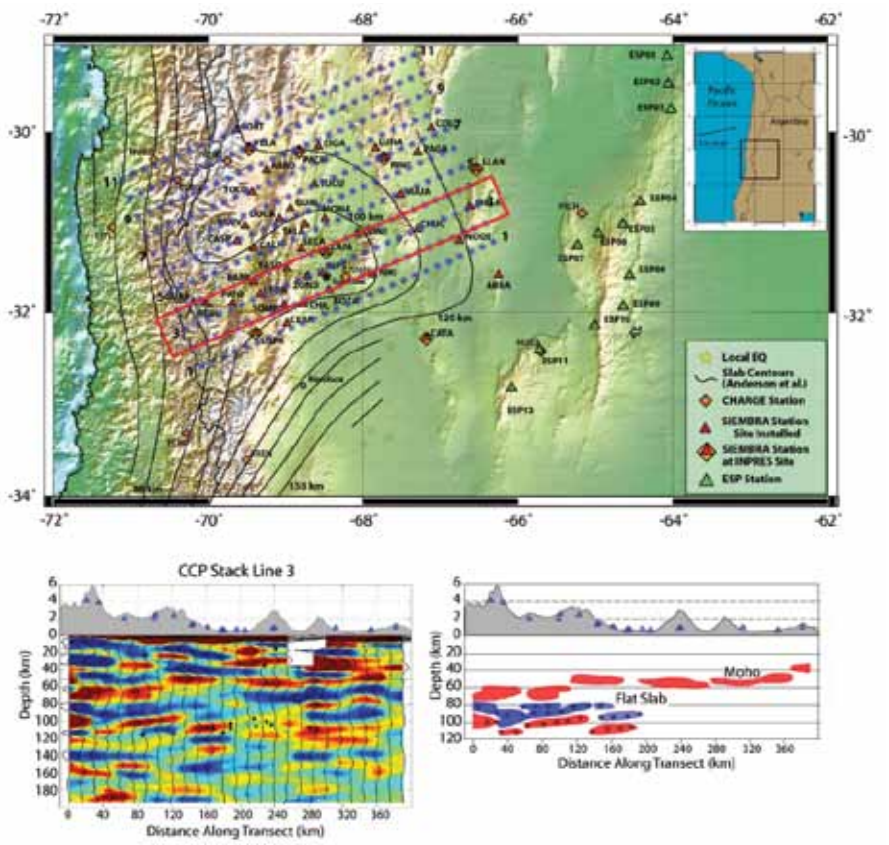

Top: Location map with PASSCAL stations and nodes for Common Conversion Point (CCP) mesh. Bottom: Line 3, along the direct line of the JFR. Note the complex and broken character of the oceanic crust. Blue triangles are seismic stations, black circles are slab earthquakes recorded during SIEMBRA.

References

Kopp, H., Flueh, E.R., Papenberg, C. and D. Klaeschen (2004), Seismic investigations of the O'Higgens Seamount Group and Juan Fernandez Ridge: Aseismic ridge emplacement and lithosphere hydration, *Tectonics, 23*

Acknowledgements: National Science Foundation Grant # EAR-0510966.

Pn Tomography of the Western United States using USArray

Janine Buehler *(SIO, University of California, San Diego),* **Peter Shearer** *(SIO, University of California, San Diego)*

In this study, we analyze Pn arrival times from the transportable stations of USArray to resolve crust and uppermost-mantle structure. Seismic tomography has the potential to provide detailed images of Earth structure, but is often limited by the coverage of the available seismic data. The USArray with its very dense and almost uniformly spaced stations has greatly improved tomographic resolution for much of the western United States. Because of the large contrast in seismic velocities between the lower crust and the upper mantle and the shallow velocity gradient in the upper mantle, Pn tomographic velocity perturbation images show results for a very confined depth in the uppermost mantle, complementing surface-wave or other body-wave tomographies that average anomalies over larger depth intervals.

Acknowledgements: We thank Luciana Astiz and the operators of the Array Network Facility for making their phase picks available. This research was funded by grant EAR-0710881 from the National Science Foundation.

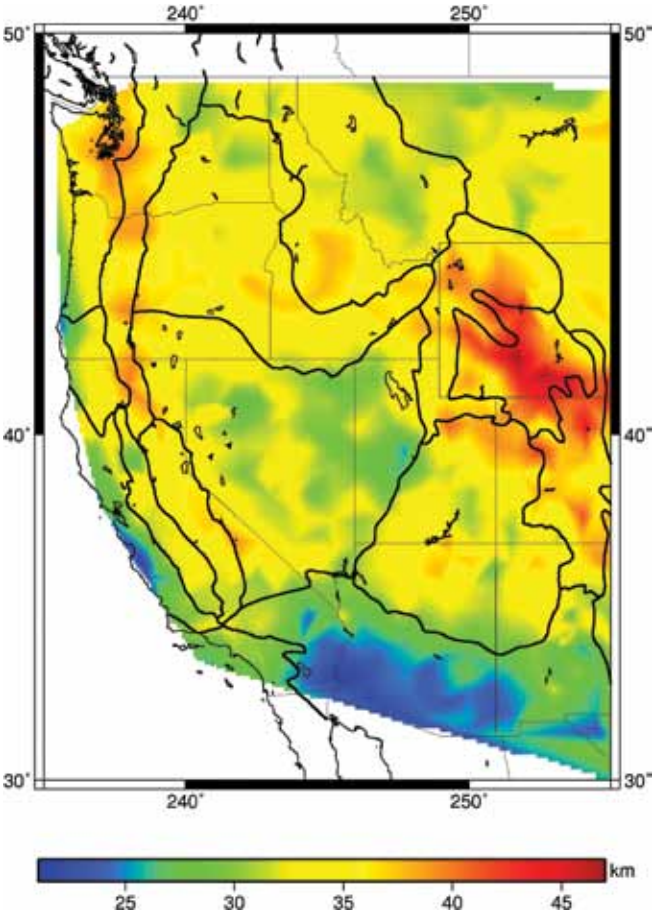

Crustal thickness estimates. Thicker crust is observed in the Sierra Nevada, the Cascade Range, and southern Wyoming. In the northern Basin and Range province crustal thickness is reduced as expected in an extensional tectonic regime. The thinner crust in the southern Basin and Range is very distinct, with thicker crust indicated to the north below the Colorado Plateau.

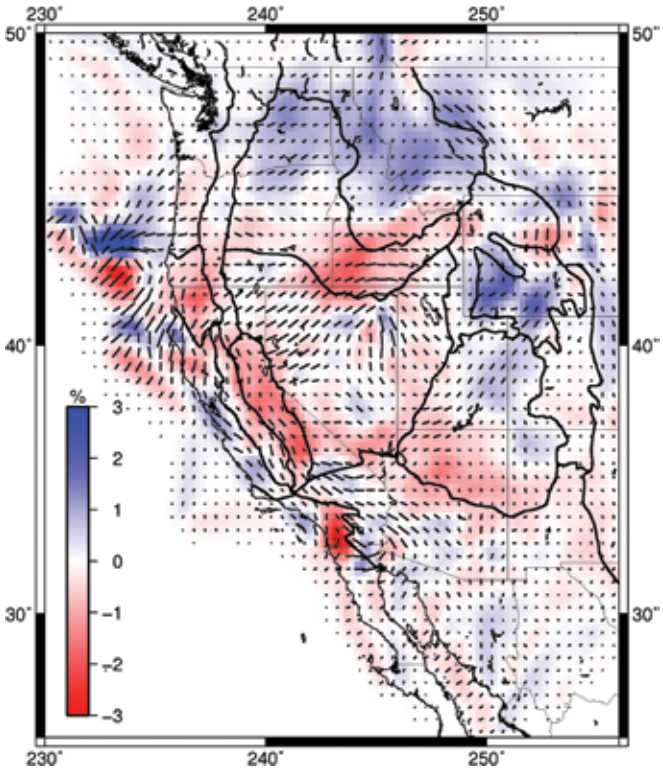

Isotropic velocity perturbations resulting from a combined iso-anisotropic inversion. Red colors indicate areas of lower velocities and blue colors regions with higher velocities. The locations of the major anomalies correlate well with known active processes, as for example the large low velocity anomalies in the Snake River Plain leading to the Yellowstone hotspot. The black lines indicate the Pn fast axis with the length of the line proportional to the strength of the anisotropy. We obtain large anisotropic anomalies in the Great Basin desert, off the coast of northern California, and in southern California/northern Mexico.

Geophysical Detection of Relict Metasomatism from an Archean (~3.5 Ga) Subduction Zone

Chin-Wu Chen (Carnegie Institution of Washington), **Stephane Rondenay** *(Massachusetts Institute of Technology),* **Rob. Evans** *(Woods Hole Oceanographic Institution),* **David Snyder** *(Geological Survey of Canada)*

The origin of Archean cratonic lithosphere is the subject of much debate. Geological and geochemical data are consistent with a plate tectonic origin involving assembly of predominantly oceanic terranes and micro continents into large stable cratons. Deep probing geophysical surveys of Archean cratons provide a means of understanding the processes responsible for the formation of these earliest continents, although the signals are complex and present-day cratons are only the surviving remnants of once larger entities. Here we present a unique geophysical view of structure within the Archean Slave craton, in northwestern Canada, that shows clear evidence for subduction processes frozen into Archean lithosphere. New seismic imaging results from the central Slave are synthesized with a coincident magnetotelluric model, and interpreted using petrological and geochemical constraints from mantle xenoliths. We find the most striking correlation between seismic and electrical structures ever observed in a continental setting in the form of a coincident seismic discontinuity and electrical conductor at ~100 km depth. The magnitude of both anomalies, in conjunction with the occurrence of phlogopite rich xenoliths originating at the same depth, point to a metasomatic origin. We believe that fluids were released from a subducting slab and altered the mantle directly below the base of a pre-cratonic lithosphere. Our model suggests that cratons are formed by subduction underplating and accretion of pre-existing fragments, and that these processes were active as early as 3.5 billion years ago.

References

Chen, C.-W., S. Rondenay, R. L. Evans, and D. B. Snyder, Geophysical detection of relict metasomatism from an Archean (~3.5 Ga) subduction zone, *Science, 326*, 1089-1091, 2009.

Jones, A.G., P. Lezaeta, I.J. Ferguson, A.D. Chave, R. L. Evans, X. Garcia and J. Spratt, The electrical structure of the Slave craton. *Lithos, 71*, 505-527, 2003.

Acknowledgements: This work is funded by the POLARIS consortium and NSF grant EAR-0409509 (S. R.).

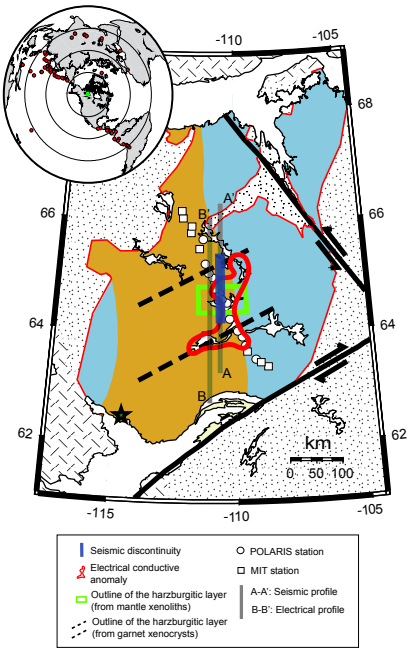

Map of the Slave craton (exposed craton outlined in red). Inset shows the craton in center (green square), with the 62 earthquakes (red circles) used for the analysis. Crustal topology and geochemical signatures broadly subdivide the Slave craton into two distinct regions: The older (4.03-2.83 Ga) Central Slave Basement Complex to the west (brown), and isotopically juvenile rocks (2.67-2.6 Ga) to the east (blue). The lateral extent of an ultra-depleted harzburgitic layer of the mantle lithosphere has been inferred from petrological analysis of mantle xenoliths (green outline) and geochemical analyses of garnet xenocrysts (between black dashed lines). The seismic stations are from POLARIS (circles) and MIT (squares). A-A' marks the location of the seismic profile shown in Fig. 2. The lateral extent of the seismic discontinuity is indicated by blue shading, and that of the conductive anomaly is outlined in red. B-B' is the nominal projected location of the MT array.

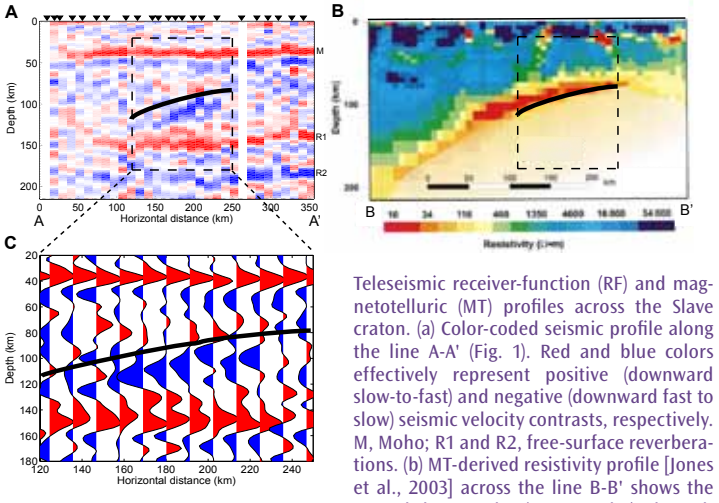

Teleseismic receiver-function (RF) and magnetotelluric (MT) profiles across the Slave craton. (a) Color-coded seismic profile along the line A-A' (Fig. 1). Red and blue colors effectively represent positive (downward slow-to-fast) and negative (downward fast to slow) seismic velocity contrasts, respectively. M, Moho; R1 and R2, free-surface reverberations. (b) MT-derived resistivity profile [Jones et al., 2003] across the line B-B' shows the central Slave conductive anomaly (red to yellow) at 80-120 depth. The solid black line highlights the base of the conductive anomaly within the region of interest (dashed black box), repeated to scale in RF profiles for comparison. (c) Close-up RF traces for bins in the region of interest.

3-D Isotropic Shear Velocity Model from Ambient Noise and Earthquake Tomography

Weisen Shen *(University of Colorado at Boulder),* **Yingjie Yang** *(University of Colorado at Boulder),* **Fan-Chi Lin** *(University of Colorado at Boulder),* **Michael H. Ritzwoller** *(University of Colorado at Boulder)*

Ambient Noise Tomography (ANT) is an efficient way to image the earth's crust since its inception in 2005. We use over 300,000 cross-correlations from ambient noise based on the past three years of EarthScope/USArray Transportable Array (TA) data. This data set provides empirical green's functions between each pair of stations and finally results in over 100,000 high SNR Rayleigh wave dispersion measurements from 8 and 40 sec period. Figure 1 shows the 12s Rayleigh wave velocity map with the Yellowstone hotspot and the principal sedimentary basins identified: CV (Central Valley), UB (Uinta Basin), GRB (Green River Basin), YS (Yellowstone), WB (Washakie Basin), PRB (Powder River Basin), DB (Denver Basin), AB (Albuquerque Basin), PB (Permian Basin), AB (Anadarko Basin). In addition, we perform surface wave tomography based on teleseismic earthquakes with the same station set using more than 200 earthquakes in two-plane-wave tomography (TPWT) to produce Rayleigh wave dispersion maps at from 25 to 144 sec. At In overlapping period band (25-40s) the two methods produce similar dispersion maps.

With these dispersion maps from 8 to 144 sec period, we apply Monte-Carlo inversion to construct a 3-D shear velocity model on the western US and the transition region to cratonic North America. Figure 2 shows a cross section of the 3model along 40oN in which geological provinces are shown: BR (Basin and Range), CP (Colorado Plateau), RM (Rocky Mountains), and GP (Great Plains). Low velocities are observed in the Great Plains and the northern Colorado plateau in the shallow crust, which coincides with sedimentary basins. In the mantle, low velocity anomalies are observed beneath the entire Basin and Range province extending from 113oW to 120oW. High velocity anomalies beneath the Colorado Plateau and the Great Basin extend to the depth of ~150km, indicating thickened lithosphere. The high horizontal velocity gradient along the Rocky Mountain front reveals the boundary between the tectonic western US and the cratonic eastern US. Future work will assimilate body wave information (receiver functions) and geothermal information to reduce the crustal thickness-velocity trade-off.

References

Yang, Y., M. H. Ritzwoller, F.-C. Lin, M. P. Moschetti, and N. M. Shapiro (2008), Structure of the crust and uppermost mantle beneath the western United States revealed by ambient noise and earthquake tomography, *J. Geophys. Res., 113*, B12310

Acknowledgements: All data used were obtained from the IRIS Data Management Center. The authors are grateful to Hersh Gilbert for providing the crustal thickness map.

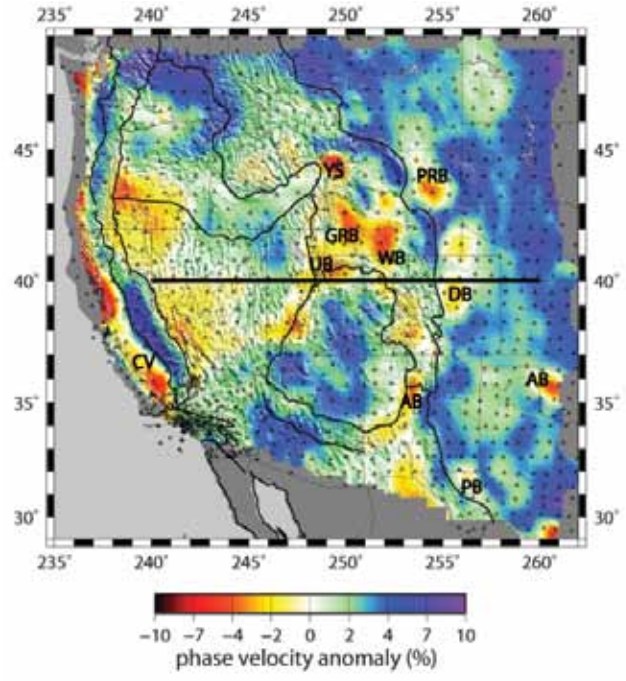

Figure1. Rayleigh wave phase velocity map derived from ANT at 12 s period where the main geological units are outlined with black contours and the principal sedimentary basins and hotspot are identified with abbreviations.

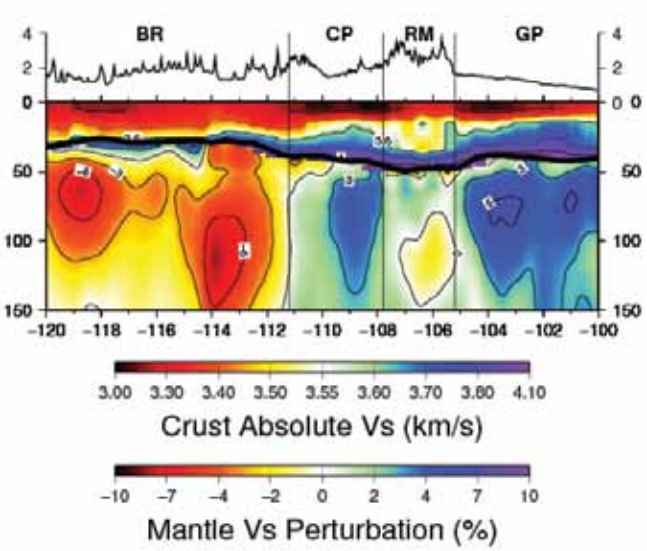

Figure2. Vertical cross section of shear wave velocity along 40°N delineated by the black line in Figure 1, where the crustal part is plotted as absolute shear velocity and the mantle is plotted as the shear velocity perturbation relative to the average velocity profile.

Shear-Wave Birefringence and Current Configuration of Converging Lithosphere under Tibet

Wang-Ping Chen *(University of Illinois, Urbana-Champaign),* **Michael Martin** *(University of Illinois, Urbana-Champaign)*

New data from west-central Tibet show that birefringence of S-waves has two pronounced increases in magnitude toward the hinterland. Null birefringence persists to about 75 km north of the Indus-Yarlung suture (IYS) between the Indian shield and the Lhasa terrane of southern Tibet. A second, rapid increase occurs about 100 km farther north of the Bangong-Nujiang sutures between the Lhasa terrane and the Qiangtang terrane in central Tibet. The latter feature is consistently observed along three long transects that collectively span a lateral (orogen-parallel) distance of about 600 km and is likely to mark the northern, leading edge of sub-horizontally advancing mantle lithosphere of the Indian shield (the "Greater India") – an interpretation consistent with the latest results of finite-frequency tomography using both P- and S-wave travel-times, previous results of modeling gravity anomalies, and a host of other seismic observations. Similarly, complementary constraints indicate that the sudden onset of significant birefringence north of the IYS is likely to be the southern termination of Eurasian mantle lithosphere. Curiously, the shortest of three transects showed null birefringence through much of the Lhasa terrane, a pattern inconsistent with those of He isotopes and gravity.

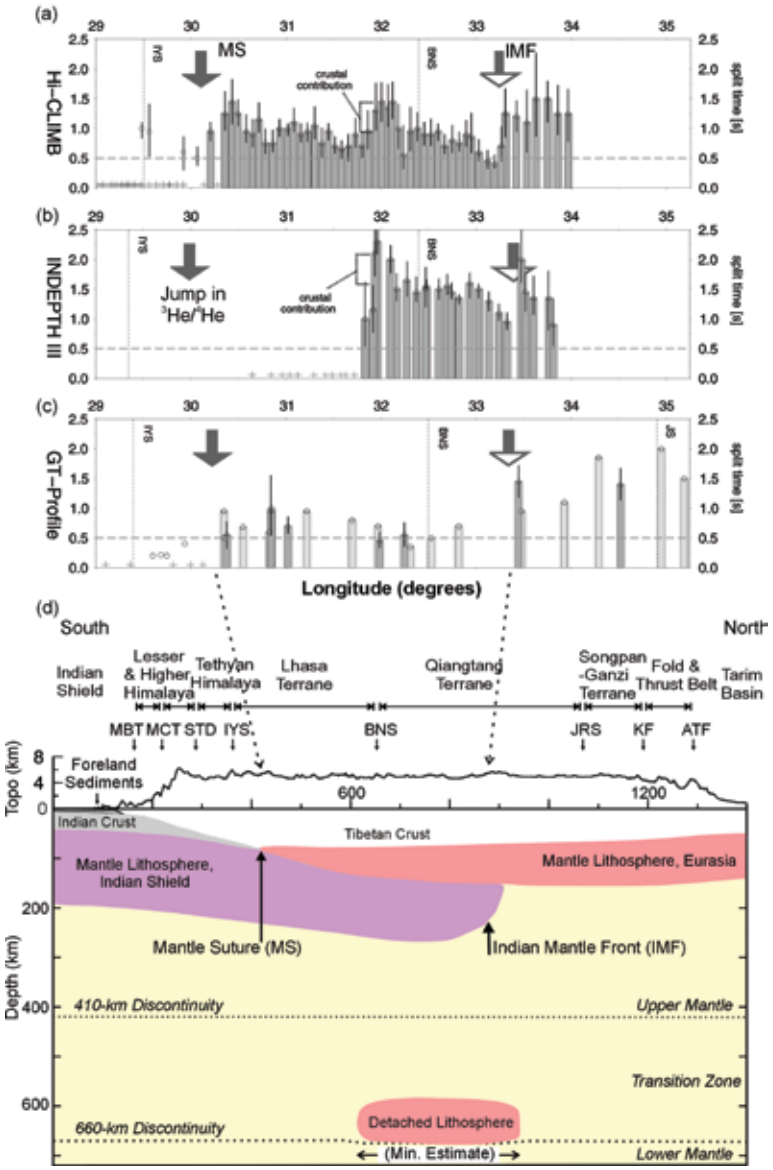

(a) to (c) Comparisons of three large-scale profiles of S-wave split time (*dt* in s) across Tibet. Open circles are isolated cases of birefringence south of the mantle suture. Measurements with error-bars (and shown in dark grey) are those analyzed by us; otherwise we plot values reported in the literature. The horizontal dotted-line represents the threshold for null birefringence. (d) A schematic cross-section showing the current configuration of the sub-continental lithospheric mantle, including a large-scale anomaly of high *P*-wave speed resting on top of the lower mantle and interpreted as the remnant of thickened (and subsequently detached due to Rayleigh-Taylor instability) lithospheric mantle (Chen and Tseng, 2007).

References

Chen, W.-P., M. Martin, T.-L. Tseng, R. L. Nowack, S.-H. Hung, and B.-S. Huang, Shear-wave birefringence and current configuration of converging lithosphere under Tibet, *Earth Planet. Sci. Lett., 295*(1-2), 297-304, doi:10.1016/j.epsl.2010.04.017, 2010

Chen, W.-P., and T.-L. Tseng, Small 660-km seismic discontinuity beneath Tibet implies resting ground for detached lithosphere, *J. Geophys. Res., 112*, B05309 (15 pp.), doi:10.1029/2006JB004607, 2007.

Acknowledgements: This work was supported by U.S. National Science Foundation grants EAR99-09362, EAR05-51995, EAR06-35419 (W.-P.C.), EAR EAR06-35611(R.L.N.), U.S. Air Force contract FA8718-08-C-002 (R.L.N. and W.-P.C.), National Science Council of Taiwan grants 96-2119-M-002-016 and 97-2745-M-002-011 (S.-H.H.), and Academia Sinica, Taiwan (B.-S.H.) which provided additional personnel (Wen-Tzong Liang, Chia-Lung Wu, John Lin, and Chun-Chi Liu). Seismic experiments were carried out jointly with Oregon State University (lead by John Nabelek), Chinese Academy of Geological Sciences (lead by Jiang Mei and Heping Su), Nepal Department of Mines and Geology (lead by Soma Sapkota and M. Pandey) and Peking University (lead by John Chen). We thank two anonymous reviewers for useful comments on the manuscript, F. Tilmann for discussions, and Zhaohui Yang (University of Illinois) for help with GIS databases.

Seismic Anisotropy Associated with Continental Lithosphere Accretion beneath the CANOE Array

Anna M. Courtier *(James Madison University),* **James B. Gaherty** *(Lamont-Doherty Earth Observatory),* **Justin Revenaugh** *(University of Minnesota),* **Michael G. Bostock** *(University of British Columbia),* **Edward J. Garnero** *(Arizona State University)*

The Canadian Northwest Experiment (CANOE) is an array of ~60 broadband seismometers located in northern Alberta and British Columbia and southern Yukon and Northwest Territories. The array spans nearly 4.0 Ga of geologic history, transitioning from the ancient craton in the east across the Canadian cordillera in the west. We examined anisotropy beneath the array using shear wave splitting of SKS, SKKS, and sSKS phases. Fast directions are roughly consistent with absolute plate motion across much of the array, suggesting that a coherent, asthenospheric fabric underlies the region. Variability in fast directions on smaller length scales (~50-200 km) generally correlates with surface structures and tectonic features, indicating a lithospheric contribution to the anisotropy. Within the craton, anomalous splitting is observed at an ancient suture zone and appears to stem from dipping fabric produced during continental assembly [*Mercier et al., 2008*]. The mantle signature of the craton-cordillera transition appears to coincide with the Rocky Mountain front, indicated by an abrupt change in fast directions. In the western cordillera, fast directions become parallel to the plate boundary, indicating that fabrics associated with the plate boundary deformation extend ~200 km into the continent. Splitting times average ~0.65 s across the array, though delay times are smaller across much of the cordillera. Smaller delay times indicate that anisotropy is weaker or less coherent across the cordillera relative to the craton.

References

Courtier, A.M., J.B. Gaherty, J. Revenaugh, M.G. Bostock, and E.J. Garnero (In Press). Seismic anisotropy associated with continental lithosphere accretion beneath the CANOE array, northwestern Canada, Geology.

Gripp, A.E., and R.G. Gordon (2002). Young tracks of hotspots and current plate velocities: *Geophys. J. Int., 150*, 321–361.

Mercier, J.-P., M.G. Bostock, P. Audet, J.B. Gaherty, E.J. Garnero, and J.S. Revenaugh (2008). The Teleseismic Signature of Fossil Subduction: Northwestern Canada, *J. Geophys. Res., 113*, B04308.

Acknowledgements: All data were obtained from the IRIS DMC; Data for CNSN stations were made available by the Geological Survey of Canada. Funding was provided by the National Science Foundation-Geophysics, the LITHOPROBE project, and a University of Minnesota Doctoral Dissertation Fellowship (AMC).

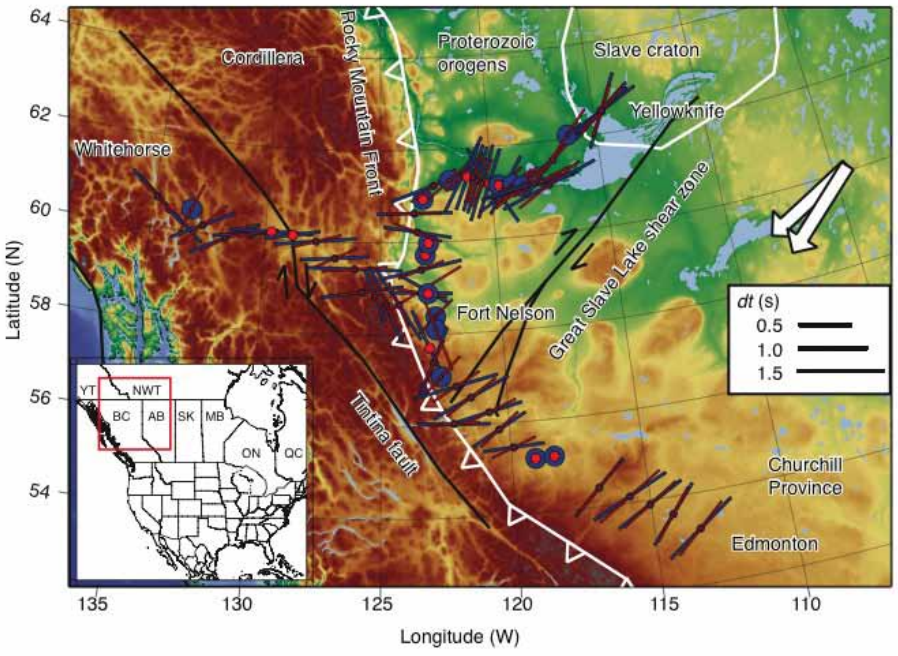

Regional geologic setting and multi-event station averages at CANOE and CNSN stations. Center of bar indicates station location; Length of bar indicates dt; Orientation of bars indicates fast direction (φ). Red = NE components, Blue = RT components. Uncertainty estimates are φ ±8° and dt ±0.2 s. Circles indicate null measurements; white arrows indicate plate motion from hot spot and no net rotation models (Gripp and Gordon, 2002).

Stratified Seismic Anisotropy beneath the East Central United States

Frédéric Deschamps (ETH Zurich), **Sergei Lebedev** *(DIAS Dublin),* **Thomas Meier** *(University Bochum),* **Jeannot Trampert** *(University Utrecht)*

A key problem in seismology is to resolve the radial distribution of azimuthal anisotropy beneath continents. Seismic anisotropy can be related to rock deformation that occurs during various geodynamical events, and can thus be used to better understand the deformation history of continental lithosphere. Array studies of azimuthal variations in surface-wave phase velocity are well suited to recover the radial distribution of anisotropy, provided that dispersion curves can be measured in a broad enough period range. Using about 20000 records from the IRIS database, we measured broadband inter-station dispersion curves of the Rayleigh-wave phase velocity and built an anisotropic Rayleigh-wave model that clearly resolves the radial distribution of azimuthal anisotropy beneath the East-central United States (31°-41° N and 82°-92° E) [Deschamps et al., 2008a]. We then estimated the amplitude of VS-anisotropy as a function of depth, from the lower crust to the upper asthenospheric mantle (≤400 km) [Deschamps et al., 2008b]. Beneath the orogenic terrains (south and east of the Grenville front), distinct patterns can be identified in three period ranges (Figure 1), suggesting that anisotropy is radially distributed within three distinct layers. At 20-35s (sampling the upper lithosphere), anisotropy is strong (~ 1% of the regional average isotropic velocity), with a direction of fast propagation sub-parallel to orogenic fronts. At 45-60s (sampling the lower lithosphere), anisotropy is moderate (~ 0.5%), and the direction of fast propagation is parallel to the reconstructed motion of the North-American plate 160-125 Ma ago. Finally, around 140s (sampling the upper asthenosphere), anisotropy is strong again (> 1%), and the direction of fast propagation is in good agreement with SKS splitting and with the absolute plate motion of North America. Beneath the cratonic terrains (north and west of the Grenville front), only the anisotropy at 140s, likely related to the current motion of the North American plate, is clearly visible. This distribution suggests the following scenario: ca 270 My ago, the upper lithosphere deformed during the final stages of the Appalachian orogeny (for instance, due to lateral extrusion), leading to fabrics that are now frozen and seen by Rayleigh wave azimuthal anisotropy at 20-35s. After the orogen, the hotter, softer, lower lithosphere recorded the motion of the North-America plate during a brief laps of time (160-125 Ma), resulting in fabrics that are now observed at 45-60s. Finally, at present time, the asthenospheric flow induces deformations at the top of the asthenosphere, which are mapped around140s.

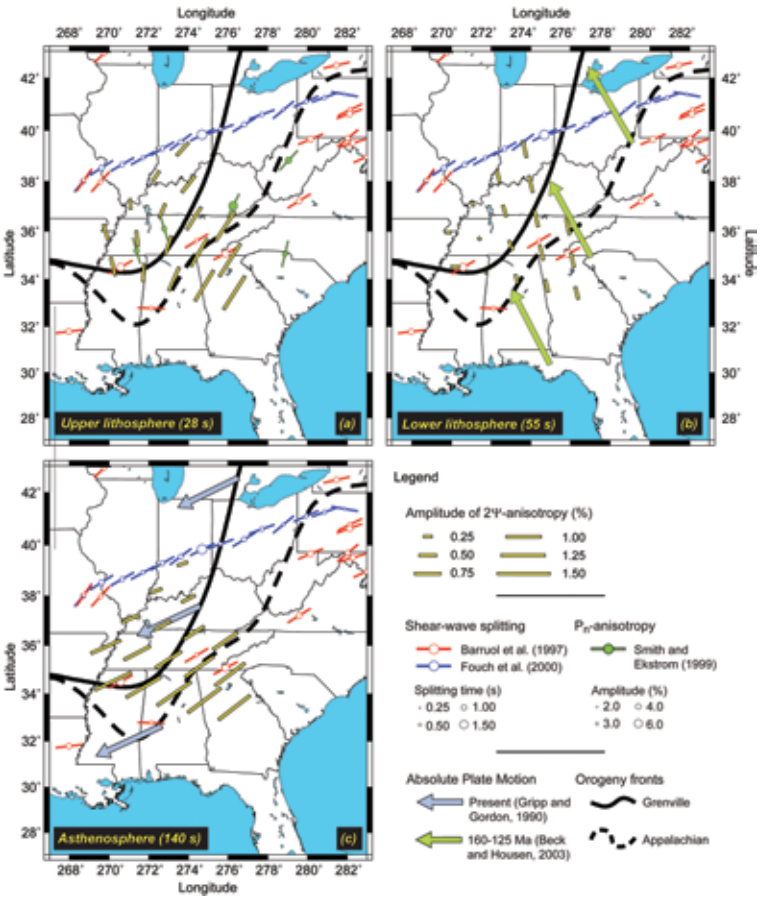

Rayleigh wave azimuthal anisotropy (yellow bars) at 28, 55, and 140 s. The orientation and size of the bar show the direction of fastest propagation of Rayleigh waves at the period and the amplitude of the anisotropy, respectively. Also plotted are main tectonic boundaries, past and present absolute plate motion, and previous anisotropy measurements. (a) At 28 s, the Rayleigh-wave fast-propagation direction beneath orogenic provinces is roughly parallel to the Grenville and Appalachian fronts, as well as to Pn fast-propagation direction. (b) At 55 s, the fast-propagation azimuth is close to the direction of the NNW drift of the North American plate during the Mesozoic. (c) At 140 s, the fast-propagation direction is parallel to the current absolute plate motion, as well as to most fast-propagation directions inferred from shear-wave splitting observations in the area.

References

Deschamps, F., S. Lebedev, T. Meier, et J. Trampert, 2008a. Azimuthal anisotropy of Rayleigh-wave phase velocities in the east-central United States, *Geophys. J. Int., 173*, 827-843, DOI:10.1111/j.1365-246X.2008.03751.x.

Deschamps, F., S. Lebedev, T. Meier, et J. Trampert, 2008b. Stratified seismic anisotropy reveals past and present deformation beneath the east-central United States, *Earth Planet. Sci. Lett., 274*, 489-498, doi:10.1016/j.epsl.2008.07.058.

Anisotropy in the Great Basin from Rayleigh Wave Phase Velocity Maps

Caroline Beghein *(University of California at Los Angeles),* **J. Arthur Snoke** *(Virginia Polytechnic Institute and State University),* **Matthew J. Fouch** *(Arizona State University)*

The Great Basin region, Nevada, is characterized by a semi-circular shear-wave splitting pattern around a weak azimuthal anisotropy zone. A variety of explanations have been proposed to explain this signal, including an upwelling, toroidal mantle flow around a slab, lithospheric drip, and a megadetachment, but no consensus has been reached.

In order to obtain better constraints on the origin of this intriguing anisotropy pattern, we performed fundamental mode Rayleigh-wave dispersion measurements using data from the USArray Transportable Array. We then inverted these measurements to obtain azimuthally anisotropic phase velocity maps at periods between 16 s and 102 s.

At periods of 16 s and 18 s, which mostly sample the crust, we found a region of low anisotropy in central Nevada coinciding with locally reduced phase velocities, and surrounded by a semi-circular pattern of fast seismic directions. Combined with recent crustal receiver function results, these short period phase velocity maps are consistent with the presence of a semi-circular anisotropy signal in the lithosphere in the vicinity of a locally thick crust. We calculated that our short period phase velocity anisotropy can only explain ~30% of the SKS splitting times, which implies that the origin of the regional shear-wave splitting signal is complex and must have both lithospheric and sublithospheric origins.

At periods between 28 and 102 s, which sample the uppermost mantle, we detected a significant reduction in isotropic phase velocities across the study region, and found more uniform fast directions with a E-W fast axis. We attributed the transition in phase velocities and anisotropy to the lithosphere-asthenosphere boundary at depths of ~60 km. We interpreted the longer periods fast seismic directions in terms of present-day asthenospheric deformation, possibly related to a combination of Juan de Fuca slab rollback and eastward-driven mantle flow from the Pacific asthenosphere.

References

Beghein, C., Snoke, J.A., and Fouch, M.J., Depth Constraints on Azimuthal Anisotropy in the Great Basin from Rayleigh Wave Phase Velocity Maps, *Earth Planet. Sci. Lett., 289*, 467-478, 2010.

Acknowledgements: This research was partially funded by NSF grants EAR-0548288 (MJF EarthScope CAREER grant).

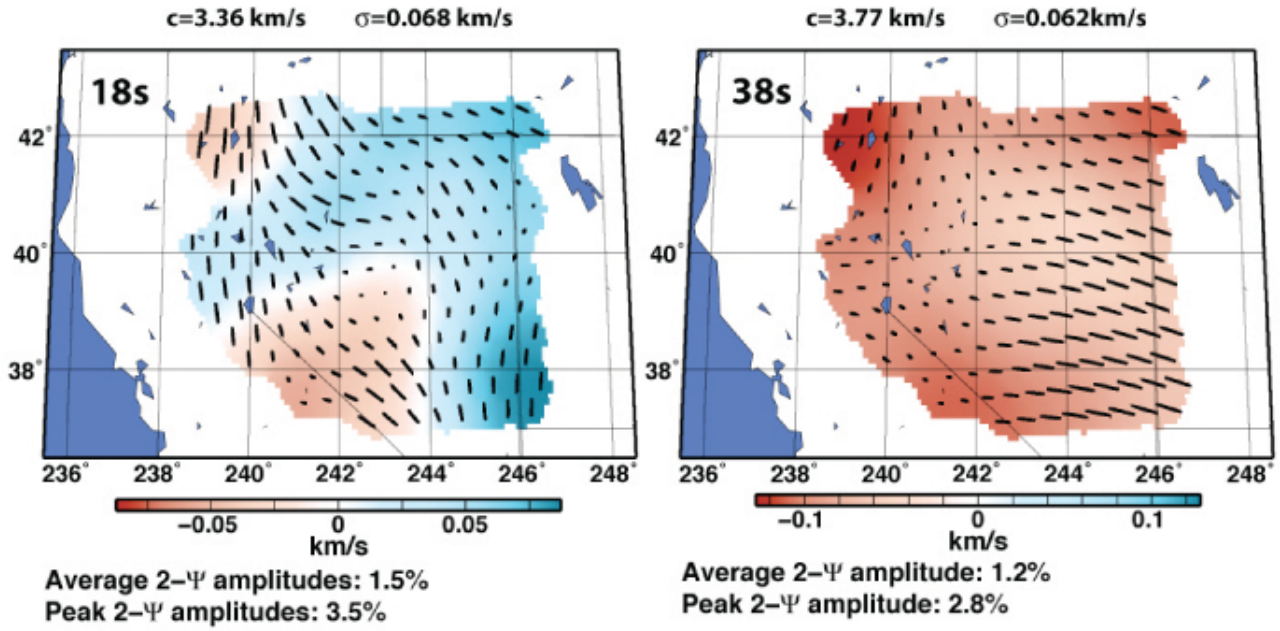

Azimuthally anisotropic phase velocity maps at 16 s and 38 s period. The background colors represent the isotropic phase velocity anomalies. The black lines show the fast direction of propagation for Rayleigh waves (2Ψ anisotropy). The reference phase velocity, calculated using the reference mTNA model defined by Beghein et al. (2010), and the average measurement uncertainty are given on top of each each map.

Source-Side Shear Wave Splitting and Upper Mantle Flow in the Romanian Carpathians and Surroundings

R. M. Russo *(University of Florida),* **V. I. Mocanu** *(University of Bucharest)*

We present shear wave splitting measurements from 5 earthquakes that occurred in the Vrancea seismic zone of the Carpathian Arc. S waves from these events, all with magnitudes > 5.4 Mw and deeper than 88 km, were recorded at broadband stations of the Global Seismic Network, and the Geoscope and Geofon Networks, and used by us to measure shear wave splitting corrected for substation splitting and anisotropy. In order to carry out these corrections we used published shear wave splitting parameters, thus isolating contributions to observed splitting from the Vrancea source region and upper mantle surrounding the Carpathian Arc. The resulting 32 good observations of source-side shear wave splitting, along with 54 null splitting observations (which yield two potential splitting directions) clearly show that upper mantle anisotropy is strongly variable in the region of the tightly curved Carpathian Arc: shear waves taking off from Vrancea along paths that sample the East and Southern Carpathians have fast anisotropy axes parallel to these ranges, whereas those leaving the source region to traverse the upper mantle beneath the Transylvanian Basin (i.e., mantle wedge side) trend NE-SW. Shear waves sampling the East European and Scythian Platforms are separable into two groups, one characterized by fast shear trends to the NE-SW, and a second, deeper group, with trends to NW-SE; also, the majority of null splits occur along paths leaving Vrancea in these NE-E azimuths. We interpret these results to indicate the presence of at least three distinct upper mantle volumes in the Carpathians region: the upper mantle beneath the Carpathian Arc is strongly anisotropic with fabrics parallel to the local arc strike; the Transylvanian Basin upper mantle fabrics trend NE-SW; and the anisotropy beneath the westernmost East European Platform may be characterized by a shallow NW-SE trending fabric concentrated in the cratonic lithosphere of the East European Platform, and a second, deeper fabric with E-W trend marking asthenospheric flow beneath the craton's base. This more complex anisotropy beneath the western edge of the East European Platform would account for both the variability of observed splitting of waves that sample this volume, and also the strong prevalence of nulls observed along eastward-departing azimuths.

References

Russo, R. M., and V. I. Mocanu, Source-Side Shear Wave Splitting and Upper Mantle Flow in the Romanian Carpathians and Surroundings, *Earth and Planet. Sci. Lett. 287*, 205-216, doi: 10.1016/j/epsl.2009.08.028, 2009.

Acknowledgements: An early version of this work was supported by National Science Foundation grant EAR-0230336.

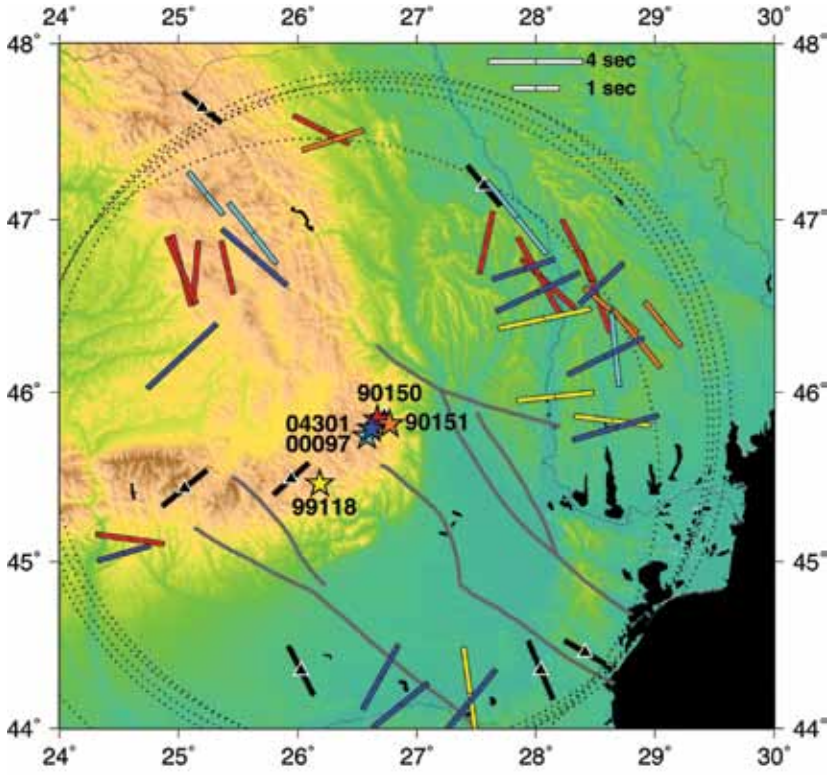

Source-side shear wave splitting results from all 5 study earthquakes, event locations (stars) and splits (bars) color coded to match. Gray circles are surface projections of 2 ÌŠ radius source lower focal hemispheres for reference. Splits plotted at surface projections of 200 km depth piercing points along event-station path to show geometry of sampling for individual event-station pairs. Splitting delay times as per key, upper right.Black bars with white bordered triangles are splitting from SK(K)S phases at stations in the study region (Ivan et al., 2008).

Source-Side Shear Wave Splitting and Upper Mantle Flow in the Chile Ridge Subduction Region

R. M. Russo *(University of Florida),* **A. Gallego** *(University of Florida),* **D. Comte** *(Universidad de Chile),* **V. I. Mocanu** *(University of Bucharest),* **R. E. Murdie** *(Goldfields Australia),* **J. C. Vandecar** *(DTM -Carnegie Institution of Washington)*

The actively spreading Chile Ridge has been subducting beneath Patagonian Chile since the Middle Miocene. After subduction, continued separation of the faster Nazca plate from the slow Antarctic plate has opened up a gapâ€"a slab windowâ€"between the subducted oceanic lithospheres beneath South America. We examined the form of the asthenospheric mantle flow in the vicinity of this slab window using S waves from six isolated, unusual 2007 earthquakes that occurred in the generally low-seismicity region just north of the ridge subduction region. The S waves from these earthquakes were recorded at distant seismic stations, but were split into fast and slow orthogonally polarized waves at upper mantle depths during their passage through the slab window and environs. We isolated the directions of fast split shear waves near the slab window by correcting for upper mantle seismic anisotropy at the distant stations. The results show that the generally trench-parallel upper mantle flow beneath the Nazca plate rotates to an ENE trend in the neighborhood of the slab gap, consistent with upper mantle flow from west to east through the slab window.

References

Russo, R. M., A. Gallego, D. Comte, V. Mocanu, R.E. Murdie, and J.C. VanDecar, Source-side shear wave splitting and upper mantle flow in the Chile Ridge subduction region, *Geology*, 38, 707-710, doi: 10.1130/GE30920.1, 2010.

Acknowledgements: This work was supported by U.S. National Science Foundation grant EAR-0126244 and CONICYT-CHILE grant 1050367.

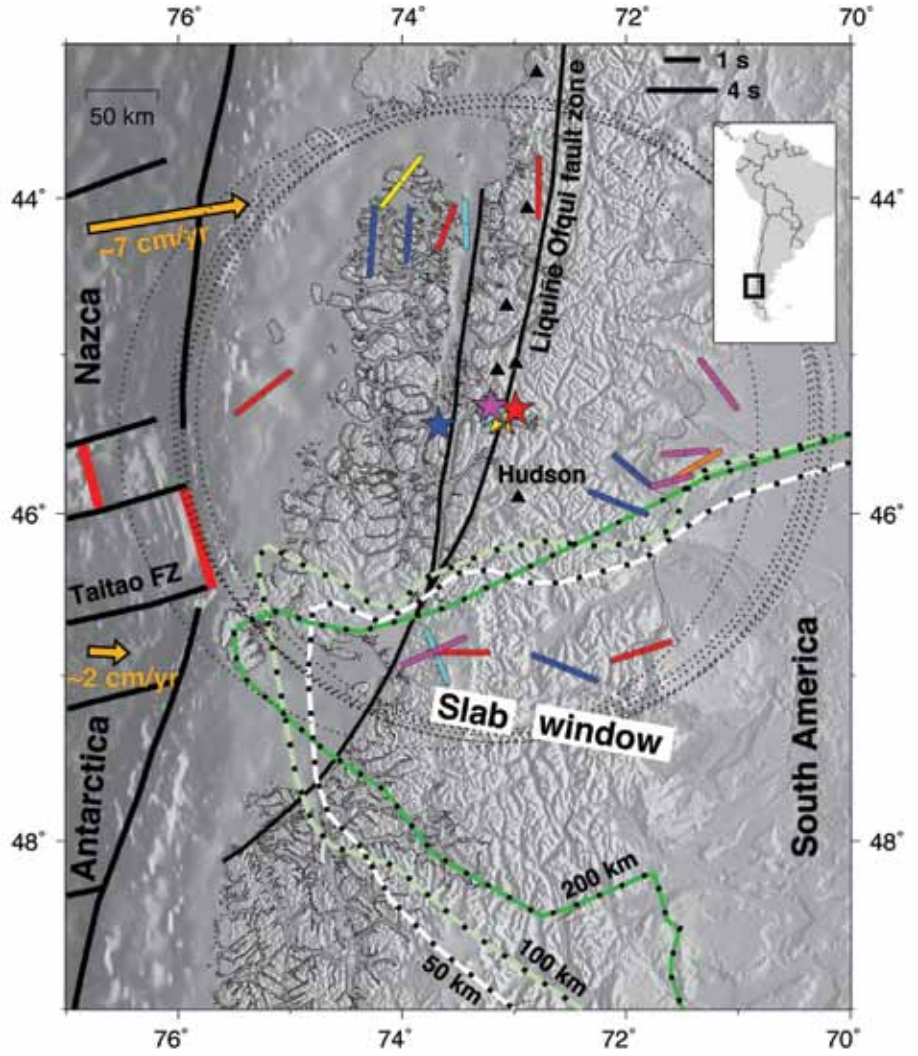

Tectonic and relief map of study region. Chile Ridge spreading centers (red) and transform-fracture zones (black) shown. Black triangles=volcanoes; FZ=fault zone. Stars mark epicenters of six study earthquakes, relocated by Russo et al. (2010) colored same as source-side splitting measurements (bars; see delay time scale, upper right). Dotted circles are 200 km radius about source events; splits plotted in azimuth of takeoff. Dashed lines mark the boundary of the slab window, defined as the "0.5% velocity perturbation con- tour at 50, 100, and 200 km depths from the tomography of VanDecar et al. (2007). Note that the northern slab window boundary is well resolved; the southern boundary is not.

An Earthscope Magnetotelluric Transect of the Southern Cascadia Subduction System, Washington

Philip E. Wannamaker *(University of Utah/EGI),* **Robert L. Evans** *(Woods Hole Oceanographic Institution)*

The first slow-slip earthquake events were observed over the Southern Cascadia Subduction system and exhibit a remarkably uniform 14 month periodicity. We collected 60 wideband magnetotelluric soundings in an east-west profile to examine state of deep crustal and upper mantle fluidization as it pertains to subduction zone locking and slow-slip nucleation. The responses of this profile are being compared to those of the earlier EMSLAB project across northwestern Oregon to the south, which is undergoing reanalysis. These results are new and not yet subject to formal non-linear inversion, but visual inspection reveals both similarities and important differences. A diagnostic high anomaly in the TM mode phase seen near the coast in Oregon is not visible in the Washington data and this tentatively is correlated with reduce fluid/subducted sediment content and greater observed plate locking for the latter area. Further inland, this phase develops more fully for both transects and is interpreted to reflect increased slab hydrate breakdown and fluid release. The inland results at lower frequencies are expected to yield geometry and physical properties of arc and back-arc melt zones of the deeper lithosphere and upper asthenosphere.

References

R. S. McGary; R.L. Evans; S. Rondenay; G. A. Abers; K. C. Creager; P. E. Wannamaker (2009), Joint magnetotelluric and seismic investigation of the Cascadia subduction zone structure: Preliminary results and outlook, EOS Trans AGU.

Acknowledgements: This project is being supported under NSF/Earthscope grants EAR08-44041 and EAR08-43725.

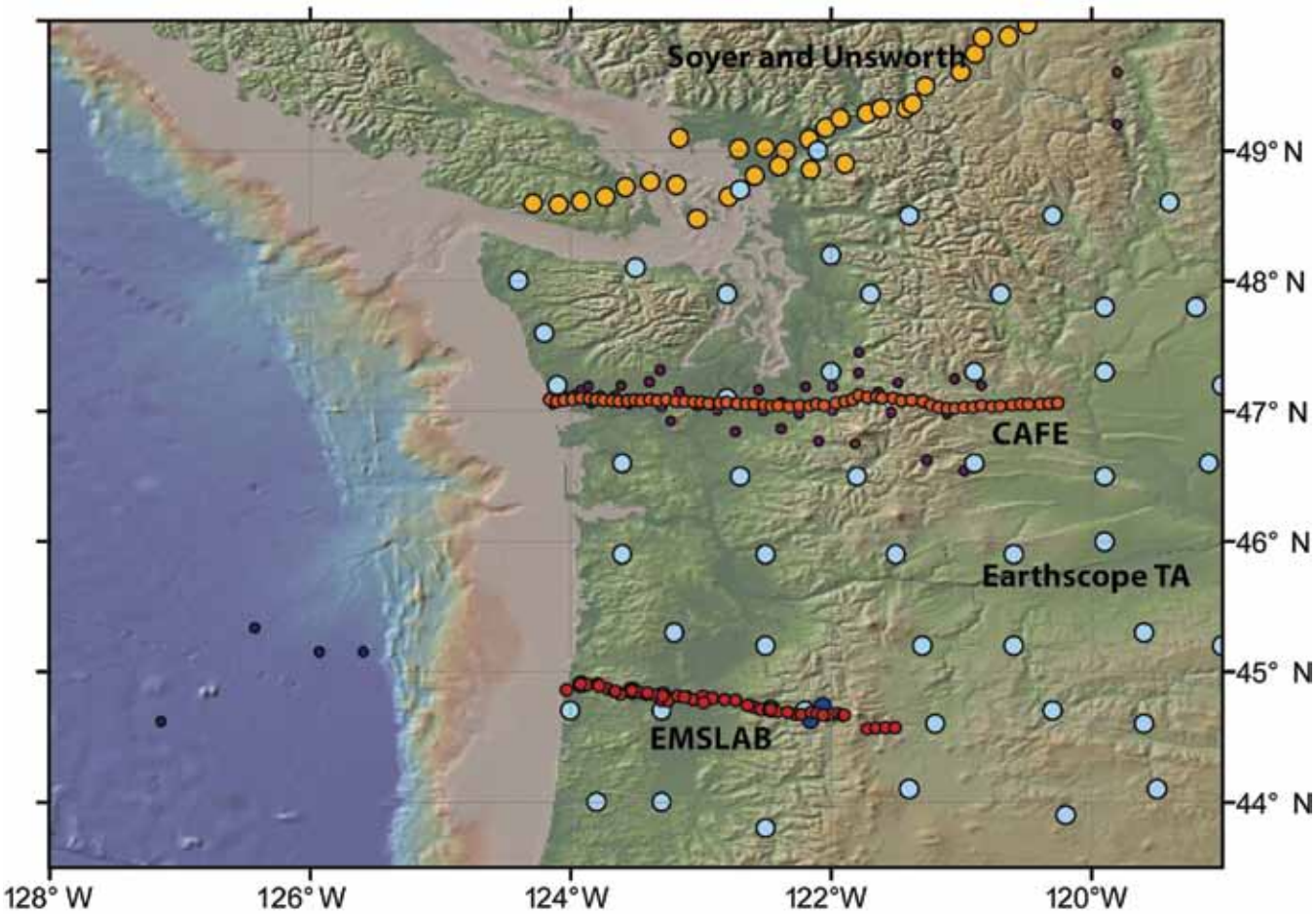

Figure 1. MT transect site distribution for the EMSLAB Lincoln Line (south) and the new Café-MT transect to the north. EMSLAB line contains 40 land sites plus seven sea-floor soundings (5 MT, 2 tipper only; see Wannamaker et al., 1989, JGR). Café line contains 60 wideband site; long-period sites are to be collected summer-fall of 2010.

S-Velocity Structure of the Upper Mantle

Sergei Lebedev *(Dublin Institute for Advanced Studies),* **Rob D. van der Hilst** *(MIT)*

Sv-velocity structure of the upper mantle (crust–660 km) is constrained by the Automated Multimode Inversion of surface and S-wave forms [*Lebedev et al., 2005*], applied to a large global data set retreived from IRIS facilities [*Lebedev and van der Hilst, 2008*]. Structure of the mantle and crust is constrained by waveform information from both the fundamental mode Rayleigh waves (periods from 20 to 400 s) and S and multiple S waves (higher modes). The reference model used in the waveform inversions and the tomographic linear inversion incorporates 3-D crustal structure. The tomographic model includes isotropic variations in S- and P-wave velocities and also S-wave azimuthal anisotropy. The lateral resolution of the imaging is a few hundred kilometres, varying with data sampling.

The technique has been benchmarked with a 'spectral-element' resolution test: inverting published global synthetic data sets computed with the spectral-element method for laterally heterogeneous mantle models, Lebedev and van der Hilst [2008] have been able to reconstruct the synthetic models accurately.

The tomographic model displays low-Sv-velocity anomalies beneath mid-ocean ridges and back-arc basins that extend down to ~100 km depth only. In the seismic lithosphere beneath cratons, strong high velocity anomalies extend to ~200 km. Pronounced low-velocity zones beneath cratonic lithosphere are rare; where present (South America; Tanzania) they are often neighboured by volcanic areas near cratonic boundaries. The images of these low-velocity zones may indicate hot material possibly of mantle-plume origin—trapped or spreading beneath the thick cratonic lithosphere [*Lebedev and van der Hilst, 2008*].

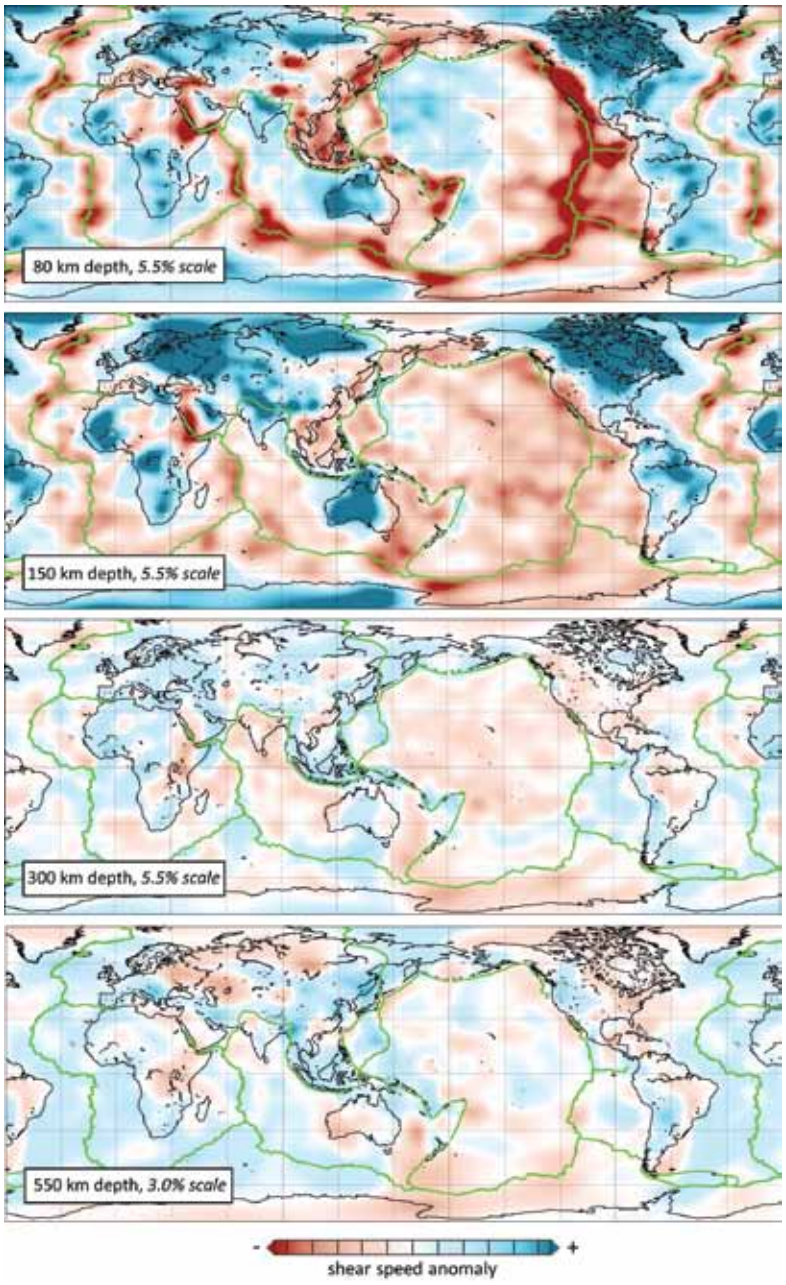

Cross-section depths and color-scale limits are specified within each frame. The reference Sv-wave velocity values are, for increasing depths: 4.38, 4.39, 4.69, 5.27 km/s—all at a reference period of 50 s.

References

Lebedev, S., G. Nolet, T. Meier, R. D. van der Hilst, Automated multimode inversion of surface and S waveforms, *Geophys. J. Int. 162*, 951-964, 2005.

Lebedev, S., R. D. van der Hilst, Global upper-mantle tomography with the automated multimode inversion of surface and S-wave forms, *Geophys. J. Int., 173*, 505-518, 2008.

P and S Body-Wave Tomography of the Western US Upper Mantle

Brandon Schmandt *(University of Oregon),* **Eugene Humphreys** *(University of Oregon)*

We invert teleseismic travel-time residuals from the EarthScope Transportable Array and more than 1700 additional temporary and permanent stations for 3-D velocity perturbations to a depth of 1000 km. The inversion uses recent advances in western U.S. crust models to better isolate the mantle component of travel-time residuals, and frequency-dependent 3-D sensitivity kernels to map travel-time residuals, measured in multiple frequency bands, into velocity structure. In addition to separate Vp and Vs models, we jointly invert the two datasets for Vp/Vs perturbations by imposing a smoothness constraint on the dlnVs/dlnVp field. The joint inversion helps us identify regions where partial melt is probable. The amplitude of Vp, Vs, and Vp/Vs variations is greatest in the upper 200 km of the mantle and the form of velocity anomalies suggests a provincially heterogeneous lithosphere and the occurrence of widespread small-scale convection. Partially molten mantle is inferred beneath Yellowstone and the eastern Snake River Plain (SRP), the Salton Trough, and the Clear Lake volcanic field. The inferred depth extent of partial melt is consistent with a generally hydrated upper mantle and elevated temperatures beneath the eastern SRP and Yellowstone. Despite more than 100 My of continuous subduction, the distribution of sub-lithospheric high-velocity anomalies is dissected (similar to other recent studies). Based on our new tomography models, western U.S. geologic history, and plate-tectonic reconstructions, we infer patchy and incomplete removal of the flat-subducting Laramide slab and slab tearing associated with Eocene accretion in the northwestern U.S.

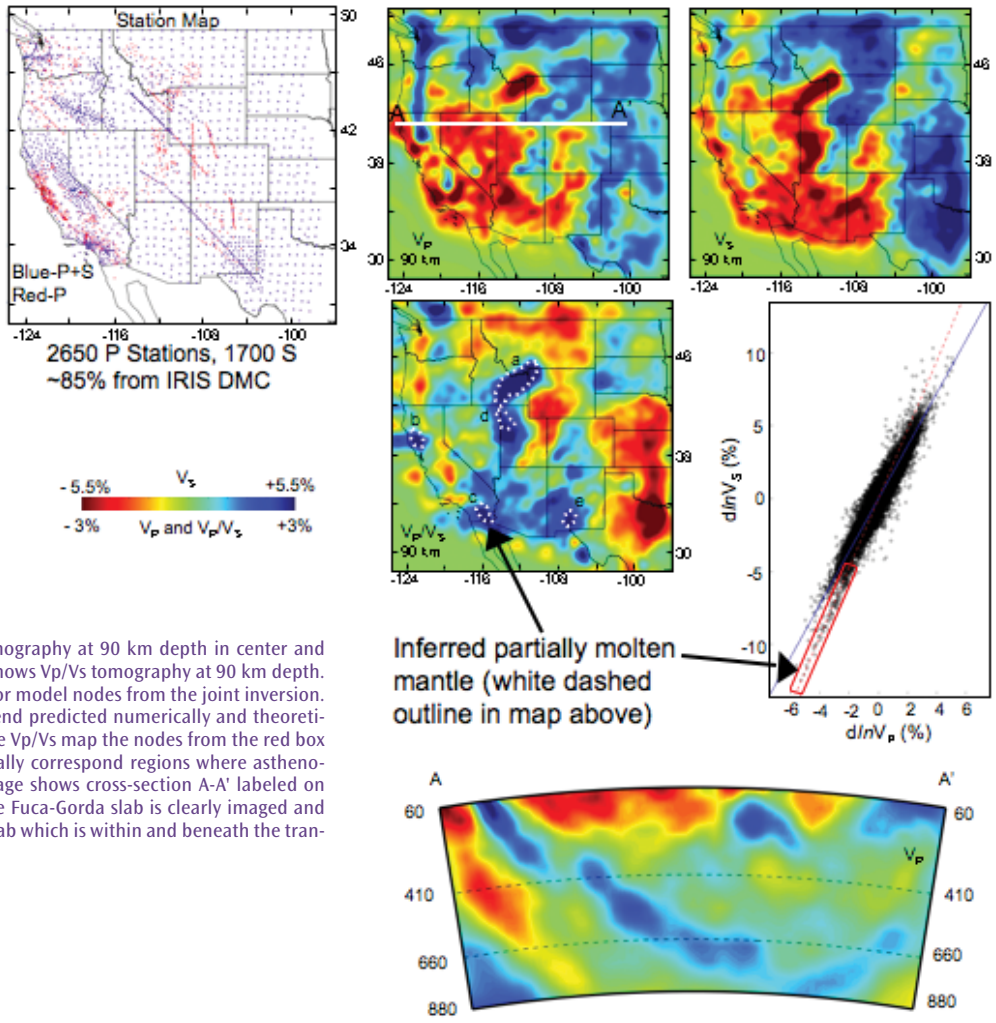

Station map in upper left. P and S tomography at 90 km depth in center and right panels in upper row. Middle left shows Vp/Vs tomography at 90 km depth. Middle right panel shows dlnVs/dlnVp for model nodes from the joint inversion. The nodes in the red box follow the trend predicted numerically and theoretically for partially molten mantle. On the Vp/Vs map the nodes from the red box are outlined (white dashed) and generally correspond regions where asthenospheric ascent is expected. Bottom image shows cross-section A-A' labeled on the Vp map in the top row. The Juan de Fuca-Gorda slab is clearly imaged and disconnected from the older Farallon slab which is within and beneath the transition zone.

Velocity Structure of the Western US from Surface Wave Phase Velocity Measurements

Anna Foster *(LDEO, Columbia University),* **Göran Ekström** *(LDEO, Columbia University),* **Vala Hjörleifsdóttir** *(Instituto Geofísica, UNAM)*

Knowledge of the velocity structure of the crust and upper mantle can improve source studies and aid investigations into mantle dynamics. Using an initial data set of single-station phase measurements of surface waves recorded on the USArray Transportable Array, we investigate the phase-velocity structure of the western United States at discrete periods between 25-100 s using two different methods. First, we estimate the local phase velocity at a station by subdividing the array into a set of mini-arrays, defined to include all stations within 2° radius of the station of interest. This is done for each event. We perform a grid search over back azimuth, and for each trial location, a phase velocity is determined in the least-squares sense that best predicts the observed phase measurements at all stations within the mini-array. The optimal local phase velocity corresponds to the back azimuth yielding the smallest misfit to the observed phase. This back azimuth also provides an estimate of the arrival angle of the energy at the mini-array. Local phase-velocity results from all events for a single station are averaged to produce the map shown in figure 1a. Our second method is based on the difference in phase anomaly between two stations that record the same event and lie roughly along the same great-circle path. The resulting phase anomaly is assigned to the inter-station path. This is done for all events, and data comprised of the median measurement for each path are inverted to obtain a velocity map at a given period. These results can be further improved by correcting for the estimated arrival angle of the wave energy, since off-great-circle arrivals bias the two-station method to higher velocities. We calculate the arrival angle using the previously described method. The arrival angle is used to correct the inter-station distance to which the two-station phase anomaly is assigned prior to inversion, resulting in a small change in the final velocity (up to 2%). This correction has been done for the inversion results shown in figure 1b. Most anomalies observed in both models correspond with well-known geologic features. The strong similarities between these two maps indicate that the methods are robust, and provide encouragement for the ongoing investigation into earth structure.

Acknowledgements: This work is funded by NSF award EAR-0952285 under the EarthScope program.

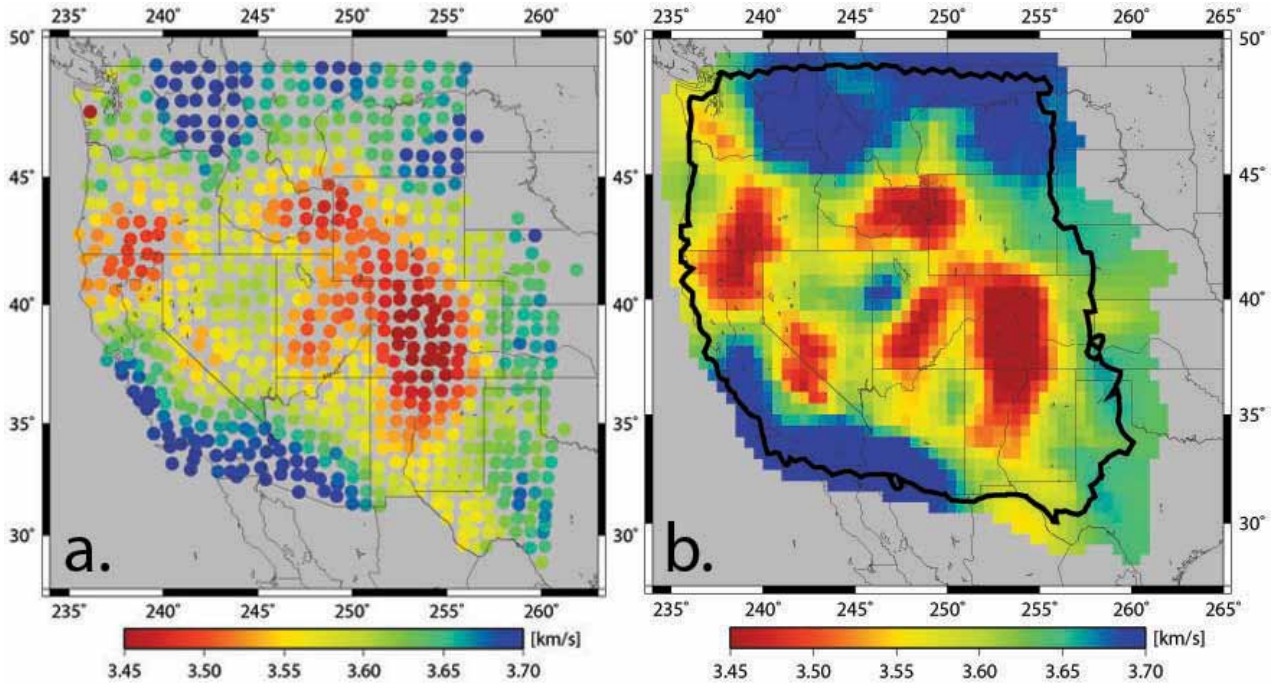

Figure 1: Phase velocity maps for Rayleigh waves at 25 s period. a) Averaged local phase velocity estimates from the mini-array method. b) Results of the inversion of two-station phase anomaly measurements that were corrected for the wave's arrival angle.

Imaging and Interpreting the Pacific Northwest

Eugene Humphreys *(University of Oregon),* **Brandon Schmandt** *(University of Oregon)*

Improved tomographic resolution of Pacific Northwest (PNW) upper mantle distinguishes two high velocity features in addition to subducted Juan de Fuca (JdF) ocean lithosphere:

50 m.y. old slab (Siletzia "curtain"). The large volume of this nearly vertical high-velocity "curtain" can only be attributed to subducted slab, and it lies where the Farallon ocean lithosphere subducted prior to Siletzia accretion at ~53 Ma (see figure). Flat-slab subduction probably occurred prior to accretion (55 Ma), during the amagmatic and compressive Laramide orogeny. We infer that the imaged curtain is Farallon slab that rolled back following accretion, leading to early ignimbrite flareup magmatism (the Challis trend) and core-complex extension that were active at 50 Ma.

Post-flood basalt drip (Wallowa "drip"). A spherical-shaped high-velocity body about 100 km across and centered at 250 km depth is imaged directly beneath the source area for the Columbia River flood basalts (CRB) and the resulting topographic bull's eye (see topography map). This feature could be downwelling North American lithosphere or basalt-depleted asthenosphere. Note that the CRB event occurred adjacent to the Siletzia curtain.

References

Schmandt, B. and Humphreys, E. 2010. Complex subduction and small-scale convection revealed by body-wave tomography of the western U.S. upper mantle. *Earth Planet. Sci. Lett.*, accepted.

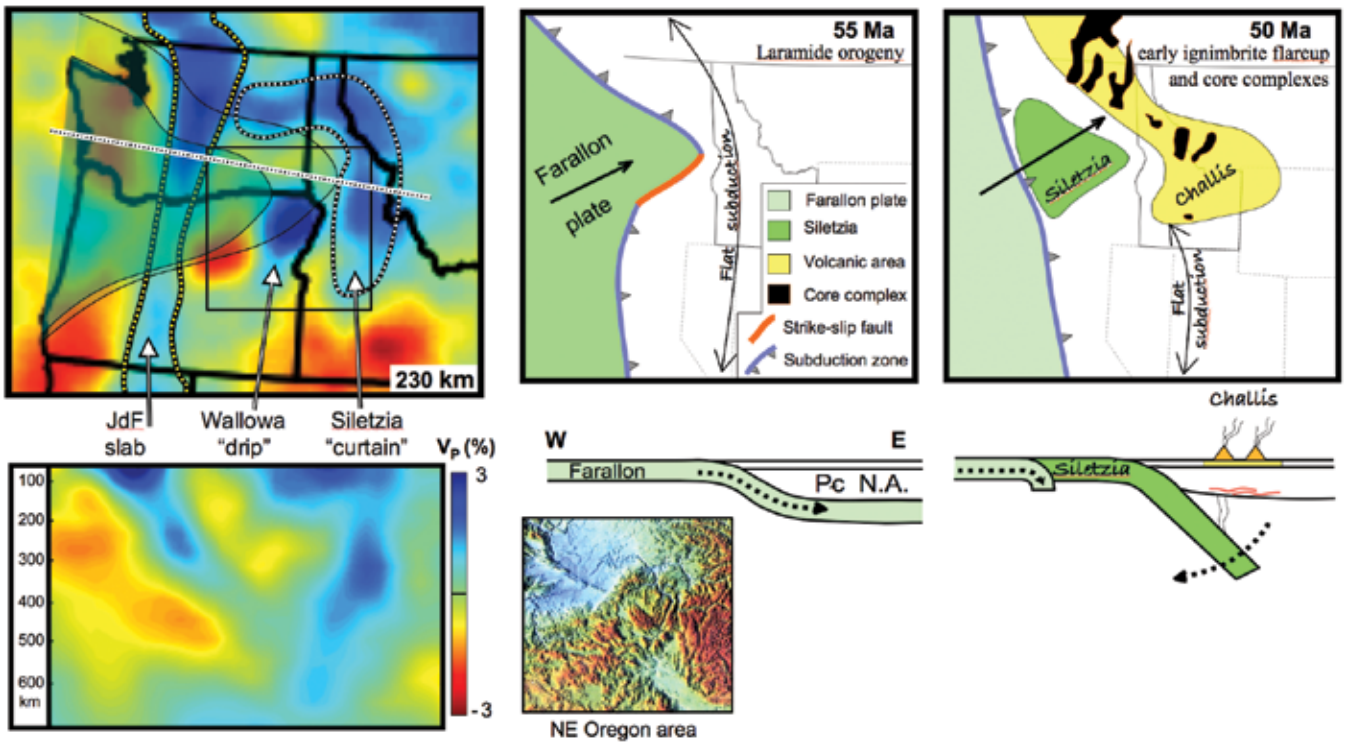

Upper and lower left panels show P tomography in map and cross-section, respectively. Center and right columns shows tectonic cartoons in map (upper) and cross-section (lower) of the PNW just before and just after Siletzia accretion. Dark gray = Siletzia. Light gray = Siletzia forearc. Bottom center panel shows a topographic map of CRB source area, with the high-standing Wallowa Mountains in the center of a topographic bull's eye.

Segmented African Lithosphere beneath Anatolia Imaged by Teleseismic P-wave Tomography

C. Berk Biryol *(University of Arizona),* **Susan L. Beck** *(University of Arizona),* **George Zandt** *(University of Arizona),* **A. Arda Ozacar** *(Middle East Technical University)*

Anatolia, a part of the Alpine-Himalayan orogenic belt, is shaped by a variety of complex tectonic processes that define the major tectonic provinces across which different deformation regimes exist. In order to study the deeper lithosphere and mantle structure beneath Anatolia, we used teleseismic P-wave tomography and data from several temporary and permanent seismic networks deployed in the region. A major part of the data comes from the North Anatolian Fault passive seismic experiment (NAF) that consists of 39 broadband seismic stations operated at the north central part of Anatolia between 2005 and 2008. The instruments for this experiment are provided by the IRIS-PASSCAL consortium. We also used data collected from permanent seismic stations of the National Earthquake Monitoring Center (NEMC) and stations from the Eastern Turkey Seismic Experiment (ETSE). Approximately 34,000 P-wave travel time residuals, measured in multiple frequency bands, are inverted using approximate finite-frequency sensitivity kernels. Our tomograms reveal a fast anomaly that corresponds to the subducted portion of the African lithosphere along the Cyprean Arc (Figure 1a). This fast anomaly dips northward beneath central Anatolia with an angle of approximately 45 degrees. However, the anomaly disappears rather sharply to the east beneath the western margin of the EAP and to the west beneath the Isparta Angle (IA). The western segment of the subducted African lithosphere appears as a continuous fast anomaly beneath the Aegean Sea (Figure 1b) separated from the eastern segment by a sub-vertical tear (Figure 1c). The tear between these segments is occupied by slow velocity anomalies that underlie the Kula Volcanic field in western Anatolia (Figure 1c). We conclude that the current segmented configuration of the subducted African lithosphere controls the geological configuration of Anatolia.

References

Acknowledgements: This research was supported by NSF grant EAR0309838.

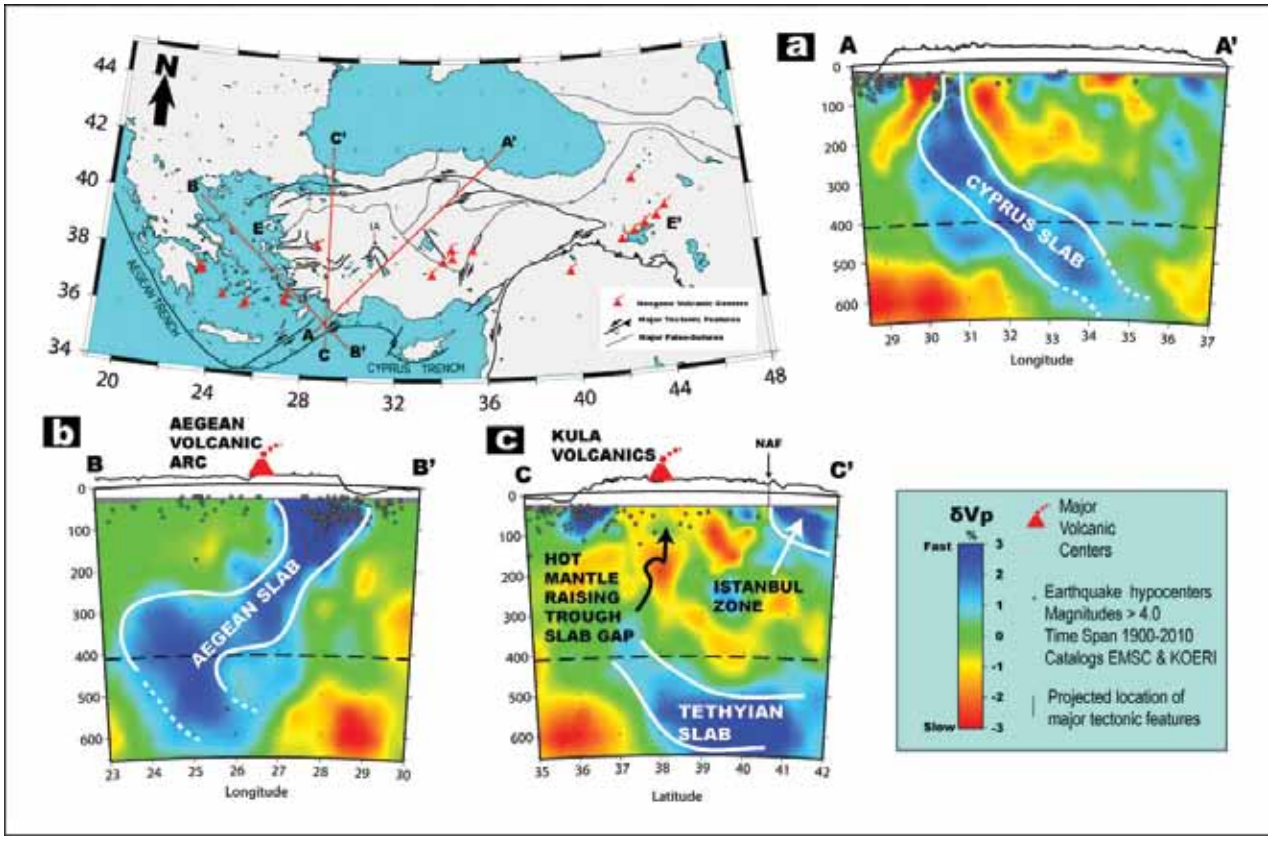

Vertical sections from our tomographic model. IA: Isparta Angle. a. The Cyprus slab and b. the Aegean slab dipping beneath Anatolia. c. The slab tear between the Cyprus and the Aegean slabs, occupied by raising hot mantle. Note that the slow velocity perturbations underlies the Kula volcanics.

High-resolution Images of Mantle-wedge Structure along the Western Hellenic Subduction Zone Using Scattered Teleseismic Waves

F. D. Pearce *(MIT),* **S. Rondenay** *(MIT),* **Maria Sachpazi** *(National Observatory of Athens),* **M. Charalampakis** *(National Observatory of Athens),* **A. Hosa** *(University of Edinburgh),* **J. Suckale (MIT), L. H. Royden** *(MIT)*

The Hellenic subduction zone is located in the east-central Mediterranean region and exhibits large variations in convergence rate along its western edge [McClusky et al., 2000]. Differences in the lithosphere entering the subduction zone are believed to drive the different rates of convergence. While recent work has shown evidence for subducted oceanic crust beneath southern Greece [Suckale et al., 2009], no detailed images of the mantle-wedge structure beneath northern Greece have been available to test this hypothesis. Here, we use high-resolution seismic images across northern and southern Greece to investigate differences in the subducted crust along the strike of the western Hellenic subduction zone. We deployed 40 broadband seismometers from the IRIS Passcal pool across Greece in a northern line (NL) and southern line (SL), each roughly perpendicular to the trench axis as shown in Figure 1a. We recorded over 50 high-quality teleseismic events with good azimuthal coverage from each line and processed them using a 2D migration algorithm based on the generalized radon transform. High-resolution images of perturbations in S-wave velocity reveal NE dipping low-velocity layers beneath both NL and SL as shown in Figure 1b. We interpret the ~10 km thick low-velocity layer beneath SL as subducted oceanic crust and the ~20 km thick low-velocity layer beneath NL as subducted continental crust. The two imaged subducted crusts connect smoothly with images from marine seismic surveys [Finetti, 2005] and show a progressive deepening of the oceanic crust of SL relative to the continental crust of NL (Figure 1c). We conclude that along strike changes in slab buoyancy cause differential rollback between the two segments, which helps drive the large difference in convergence rates along the western Hellenic subduction zone.

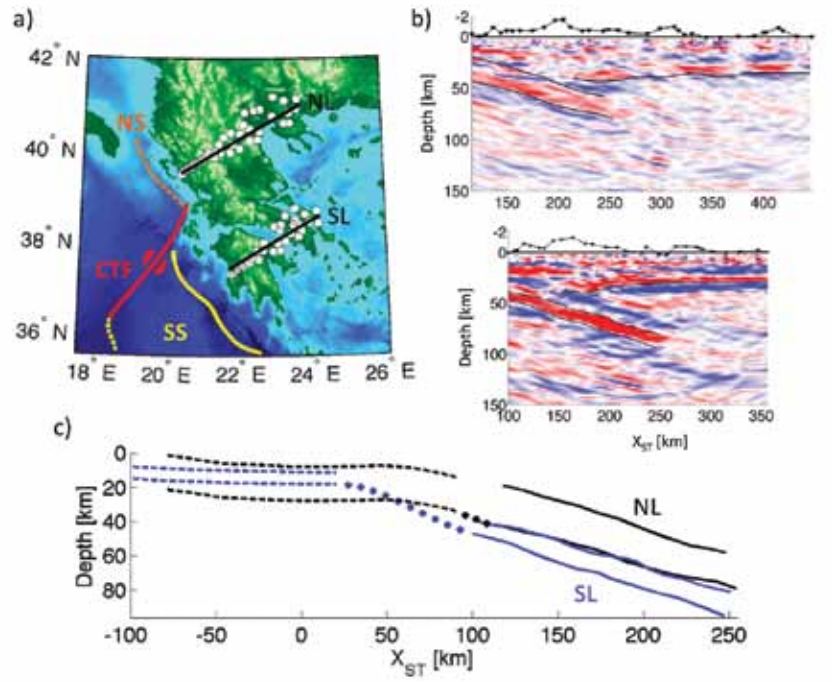

Figure 1: a) Map of study area showing location of southern segment (SS) and northern segment of western Hellenic subduction zone separated by the Cephalonia transform fault (CTF). White circles denote station locations for NL and SL deployments. b) Images of perturbation in S-wave velocity for SL (top) and NL (bottom) at -5% to +%5 (red to blue). Solid lines delineate top and bottom of low-velocity layer, and the Moho of overriding plate. X-axis is horizontal distance perpendicular to strike measured from the intersection of SL with the trench of southern segment (solid yellow line in a)). c) Comparison of subducted crusts imaged from marine seismics (dashed) and this study (solid) for NL (black) and SL (blue), with dots showing smooth interpolation.

References

Finetti, I. R. (2005), Depth contour map of the Moho discontinuity in the central Mediterranean region from new CROP seismic data, in CROP PROJECT: Deep seismic exploration of the central Mediterranean and Italy, edited by I. R. Finetti, pp. 597-606, Elsevier B.V., Amsterdam, The Netherlands.

McClusky, S. et al. (2000), Global Positioning System constraints on plate kinematics and dynamics in the eastern Mediterranean and Caucasus, *J. Geophys. Res., 105*(B3), 5695-5719.

Suckale J., S. Rondenay, M. Sachpazi, M. Charalampakis, A. Hosa, L. H. Royden (2009) High-resolution seismic imaging of the western Hellenic subduction zone using teleseismic scattered waves, *Geophys. J. Int., 178*(2), 775-791.

Acknowledgements: This project was carried out as part of project MEDUSA, funded by the NSF Continental Dynamics Program, grant EAR-0409373.

Imaging the Mantle Wedge in the Central America Subduction Zone: The TUCAN Broadband Seismic Experiment

Geoffrey Abers *(Lamont-Doherty Earth Observatory of Columbia University),* **Karen Fischer** *(Brown University),* **Ellen Syracuse** *(University of Wisconsin),* **Catherine Rychert** *(University of Bristol),* **Laura MacKenzie** *(Schlumberger Data and Consulting Services)*

Central America was selected as a MARGINS Focus Site for the Subduction Factory initiative. In order to understand how the Subduction Factory processes trench inputs into volcanic arc outputs, we make direct observations of mantle structure. The TUCAN (Tomography and other observations Under Costa Rica And Nicaragua) experiment deployed 48 broadband seismographs in the Central America Focus Site in 2004-6. This One-Pager shows results from three kinds of imaging in Nicaragua, where arc output features globally significant geochemical signatures of subduction. The migrated receiver function image (A) shows a strong P-S conversion from what appears to be the top of the subducting plate to 200 km depth, the first time a steep slab has been imaged with these kinds of signals. The velocity contrast at the top of the plate is sharp and below the seismicity shallower than 80 km depth, probably Moho of the subducting crust. Deeper, the mode conversion is broad, consistent with the 15-30 km gradient expected for the thermal boundary layer. Seismic attenuation (B), a proxy for temperature, indicates a typically hot wedge beneath arc and backarc, quantitatively consistent with temperatures and water contents inferred from primitive lavas and melt inclusions [*Plank et al., 2007*]. The updip limit of hot mantle is inferred to be where the slab reaches 80 km depth. These two images show that the subducting crust passes from beneath cold to hot mantle and rapidly metamorphoses to eclogite. The ratio of P to S velocities, Vp/Vs (C), shows a somewhat different pattern, near-normal values for much of the wedge but a narrow, high-Vp/Vs column ascending nearly vertically from the slab to the volcanic arc. Since this pattern differs from that of 1/Qs or 1/Vp alone, this anomaly cannot be purely due to temperature. The presence of partial melt could produce such an effect, and given the relationship between 1/Qs, Vp/Vs and the location of the arc. Thus, we are imaging separately but in one place the wedge geometry, temperature structure and melt distribution across the subduction factory, one of the major goals of MARGINS.

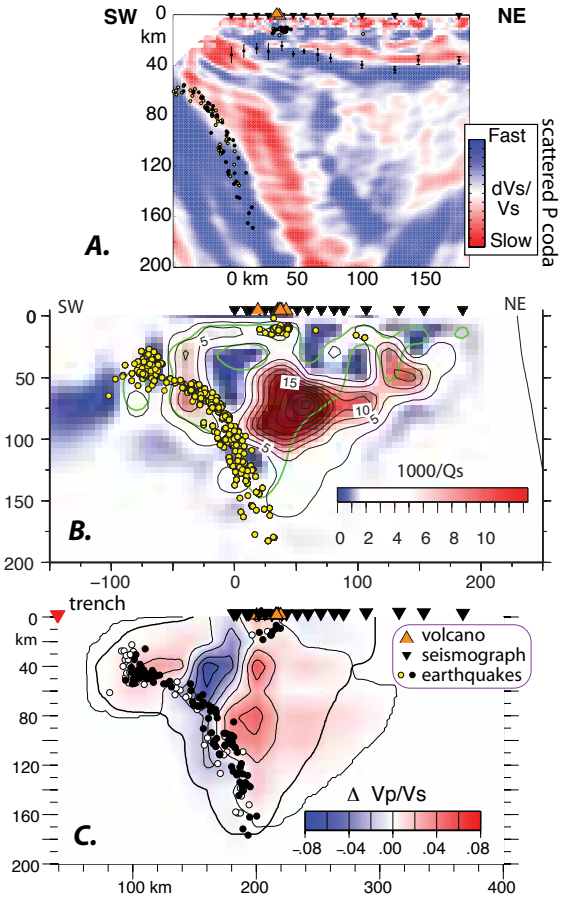

Three seismic images of the Nicaragua Subduction Factory. (A) 2D receiver function migration (MacKenzie et al., 2008, 2010). Image shows S-wave velocity variations needed to generate scattered wavetrain, such as Moho and top of subducting plate. (B) S-wave attenuation as 1000/Qs, from tomographic inversion (Rychert et al., 2008), at 1 Hz. 1/Qs responds to temperature and indicates high-temperature region beneath and behind arc. (C) Vp/Vs anomalies from regional travel-time tomography (Syracuse et al., 2008). In regions of high temperature, high Vp/Vs may indicate presence of melt, perhaps showing a vertical melt column beneath volcanic arc.

References

MacKenzie, L.M., G.A. Abers, S. Rondenay and K.M. Fischer, Imaging a steeply dipping subducting slab in southern Central America, *Earth Planet. Sci. Lett.*, in press, 2010.

MacKenzie, L.S., G.A. Abers, K.M. Fischer, E.M. Syracuse, J.M. Protti, V. Gonzalez, and W. Strauch, Crustal structure along the southern Central American volcanic front, Geochem. *Geophys. Geosyst., 9*, Q08S09, 2008. doi:10.1029/2008GC001991

Rychert, C.A., K.M. Fischer, G.A. Abers, T. Plank, E.M. Syracuse, J.M. Protti, V. Gonzalez, and W. Strauch, Strong along-arc variations in attenuation in the mantle wedge beneath Costa Rica and Nicaragua, *Geochem. Geophys. Geosyst., 9*, Q10S10, 2008. DOI: 10.1029/2008GC002040

Syracuse, E.M., Abers, G.A., K.M. Fischer, McKenzie, L., C. Rychert, J. M. Protti, V. Gonzalez, and W. Strauch, Seismic tomography and earthquake locations in the Nicaraguan and Costa Rican upper mantle, *Geochem. Geophys. Geosyst., 9*, Q07S08, 2008. doi:10.1029/2008GC001963

Acknowledgements: The TUCAN project was carried out in close collaboration with M. Protti and V. Gonzalez of OVSICORI/UNA in Costa Rica, and W. Strauch and colleagues of INETER in Nicaragua. This work funded by the National Science Foundations's MARGINS program, under awards OCE-0203650 (Boston Univ.) and OCE-0203607 (Brown).

Systematic Variation in Anisotropy beneath the Mantle Wedge in the Java-Sumatra Subduction System from Shear-Wave Splitting

J.O.S. Hammond *(University of Bristol, UK),* **J. Wookey** *(University of Bristol, UK),* **S. Kaneshima** *(Kyushu University, Japan),* **H. Inoue** *(Klimatologi dan Geofisika, Indonesia),* **T. Yamashina** *(Klimatologi dan Geofisika, Indonesia),* **P. Harjadi** *(Klimatologi dan Geofisika, Indonesia)*

The tectonic context of south-east Asia is dominated by subduction. One such major convergent boundary is the Java-Sunda trench, where the Australian-Indian plates are being subducted beneath the Eurasian plate. We measure shear-wave splitting in local and teleseismic data from 12 broadband stations across Sumatra and Java to study the anisotropic characteristics of this subduction system. Splitting in S-waves from local earthquakes between 75-300km deep show roughly trench parallel fast directions, and with time-lags 0.1-1.3s (92% less that 0.6s). Splitting from deeper local events and SKS, however, shows larger time-lags (0.8-2.0s) and significant variation in fast direction. To model deformation in the subduction zone we ray-trace through an isotropic subduction zone velocity model, obtaining event to station raypaths in the upper mantle. We then apply appropriately rotated olivine elastic constants to various parts of the subduction zone, and predict the shear-wave splitting accrued along the raypath. Finally, we perform grid searches for orientation of deformation, and attempt to minimise the misfit between predicted and observed shear-wave splitting. Splitting from the shallow local events is best explained by anisotropy confined to a 40km over-riding plate with horizontal, trench parallel deformation. However, in order to explain the larger lag times from SKS and deeper events, we must consider an additional region of seismic anisotropy in or around the slab. The slab geometry in the model is constrained by seismicity and regional tomography models, and many SKS raypaths travel large distances within the slab. Models placing anisotropy in the slab produce smaller misfits than those with anisotropy outside for most stations. There is a strong indication that inferred flow directions are different for sub-Sumatran stations than for sub-Javanese, with >60 degrees change over ~375km. The former appear aligned with the subduction plate motion, whereas the latter are closer to perpendicular, parallel to the trench direction. There are significant differences between the slab being subducted beneath Sumatra, and that beneath Java: age of seafloor, maximum depth of seismicity, relative strength of the bulk sound and shear-wave velocity anomaly and location of volcanic front all vary along the trench. We speculate, therefore, that the anisotropy may be a fossilised signature rather than due to contemporary dynamics.

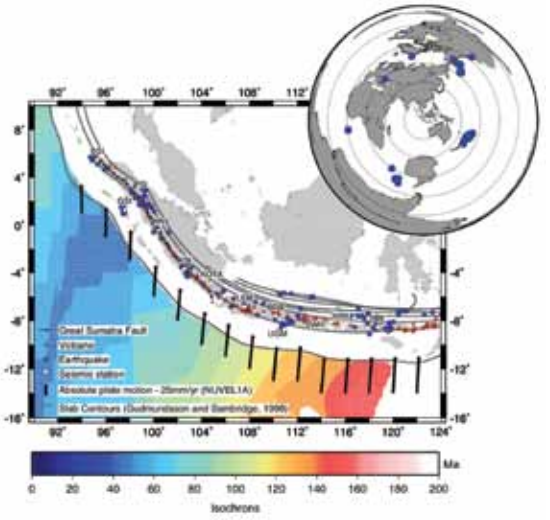

Map showing stations and events used in this study. White inverted triangles mark stations, blue circles show earthquakes (local events on main map, teleseismic events on top right map). Also shown are quaternary volcanos (red triangle), absolute plate motions (Gripp and Gordon (1990), black arrows), slab contours at 100 km depth intervals (Gudmundsson and Sambridge, 1998), the Great Sumatra Fault, and Isochrons (Müller et al., 1997).

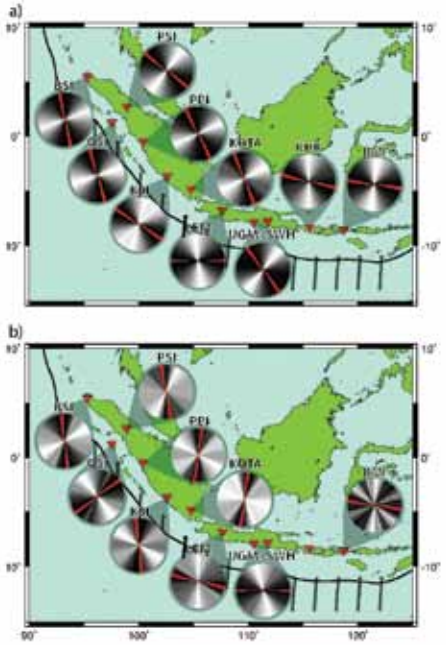

Density rotorgrams for models of subduction zone anisotropy showing the best fitting orientations obtained from forward modelling. (a) Olivine orientations best fitting the splitting results (red bars) obtained from local events <300 km deep; these are predominantly trench parallel. (b) Olivine orientations best fitting splitting results from local events >300 km deep and SKS/SKKS-wave splitting results (red bars). Note the rotation from north-south orientations beneath Sumatra (GSI is an exception), and the east west anisotropy orientations beneath Java. The complicated pattern at BMI reflects the scatter observed in the data. We speculate that this is due to complications arising from the slab bending beneath this station.

References

Hammond, J. O. S., Wookey, J., Kaneshima, S., Inoue, H., Yamashina, T., Harjadi, P. (2010). Systematic variation in anisotropy beneath the mantle wedge in the Java-Sumatra subduction system from shear-wave splitting. *Phys. Earth Planet. Int., 178*, 189-201.

Acknowledgements: Data used in this paper was provided by the Japan Indonesian Seismic Network (JISNET), IRIS, GEOFON and the Ocean Hemisphere Network Project, courtesy of the Earthquake Research Institute, University of Tokyo. This research was funded by a Japan Society for the Promotion of Science (JSPS) postdoctoral fellowship (short term), JSPS/FF1/367

A Slab Remnant beneath the Gulf of California

Hanneke Paulssen *(Utrecht University),* **Xiaomei Zhang** *(Utrecht University),* **Jeannot Trampert** *(Utrecht University),* **Robert Clayton** *(California Institute of Technology)*

Active extension in the Gulf of California is characterized by the transition from continental rifting to seafloor spreading. Puzzling variations in the patterns of both tectonics and magmatism are observed along the length of the gulf and are likely to be related to mantle heterogeneity. Regional-scale mantle structure, however, has been difficult to constrain due to the lack of broadband seismic stations in the region. In this study we utilized data from the deployment of the NARS-Baja array and other networks, and computed a three-dimensional shear-speed model of the upper mantle beneath the region. Applying a combination of cross-correlation analysis and multimode waveform inversion, we measured interstation Rayleigh wave dispersion for 450 pairs of stations in a broad period range of 9–250 s. We computed phase velocity maps and then inverted the phase-velocity data for shear-speed structure. Our results suggest that the location of the transition from seafloor spreading (South) to continental rifting (North) in the Gulf of California, as well as differences in volcanism across Baja California and the gulf, can be explained by heterogeneity in the upper mantle, in particular by the presence of a slab remnant beneath the south-central part and an absence of such a slab remnant beneath the northern part of the gulf.

References

Trampert J., H. Paulssen H, A. van Wettum, J. Ritsema, R. Clayton, R. Castro, C. Rebollar, and A. Perez-Vertti (2003) New array monitors seismic activity near Gulf of California, Mexico, Eos, 84, 4, pp 29,32.

Zhang X., H. Paulssen, S. Lebedev, and T. Meier (2007) Surface wave tomography of the Gulf of California, *Geophys. Res. Lett., 34*, L15305, doi:10.1029/2007GL030631.

Zhang X., H. Paulssen, S. Lebedev, and T. Meier (2009) 3D shear velocity structure beneath the Gulf of California from Rayleigh wave dispersion, *Earth Planet. Sci. Lett., 279*, 255-262.

Acknowledgements: Funding for this project was provided by the U.S. National Science Foundation (Grant number EAR-0111650 of the MARGINS program) and the Dutch National Science Foundation (Grant number NWO-GOA-750.396.01).

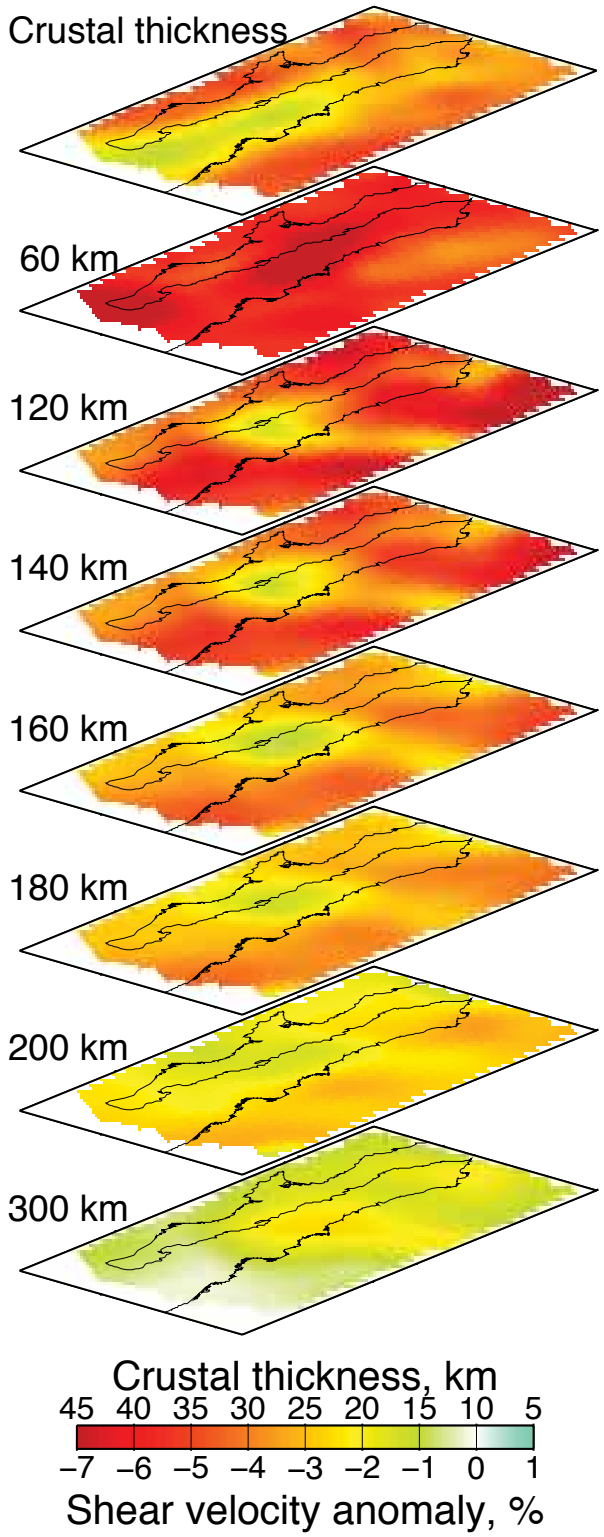

Maps of the crustal thickness (upper panel), and the shear velocity anomalies relative to the global reference model AK135 (Kennett et al., 1995) at depths of 60, 100, 120, 160, 200, and 300 km. The slab remnant is imaged as the relatively high velocity anomaly beneath the south-central part of the Gulf of California at depths between roughly 120 and 160 km.

Three-Dimensional Geometry of the Juan de Fuca/farallon Slab

Gary Pavlis *(Department of Geological Sciences, Indiana University, Bloomington)*

New understanding on the three-dimensional geometry of the western US subduction system is emerging by viewing multiple imaging results in a fully three-dimensional framework. The process is comparable to interpreting 3D seismic reflection data, but is complicated in USArray by the scale, which makes spherical geometry important. The figure shown is a first attempt at a joint interpretation of P tomography models by Burdick et al. [2009], Sigloch et al. [2008], and recently produced scattered wave images of Pavlis [submitted]. The scattered wave images show dipping features above the 410 km discontinuity I have interpreted as defining a shear zone at the boundary layer between the subducting slab and the overriding North American plate. The model shown in this figure is a kinematic model showing flow lines and constant time lines based on the current relative motion of the Juan de Fuca and North American plates. The surface is interpreted from data, but the time lines assume no longitudinal strain in the descending slab. The visualization shows the predicted edge of the slab window from the San Andreas based on the no longitudinal strain approximation and using the current trace of the San Andreas as an anchor point. The new scattered wave images and the reasonable geometry of this slab model provide strong support for the model of the Farallon slab described by Sigloch et al. [2008].

References

Burdick, S., C. Li, V. Martynov, T. Cox, J. Eakins, T. Mulder, L. Astiz, F. L. Vernon, G. L. Pavlis, and R. D. van der Hilst, 2009, Model update December 2008; upper mantle heterogeneity beneath North America from P-wave travel time tomography with global and USArray transportable array data, *Seismol. Res. Lett., 80*(4), 384-392, doi: 10.1785/gssrl.80.4.638.

Pavlis, G. L., submitted, Three-dimensional Wavefield Imaging of Data from the USArray: New Constraints on the Geometry of the Farallon Slab, *Geosphere*, in review.

Sigloch, K., N. McQuarrie, and G. Nolet, 2008, Two-stage subduction history under North America inferred from multiple-frequency tomography, *Nature Geosci., 1*, 458-462, doi:10.1038/ngeo231.

Acknowledgements: This work was supported by the National Science Foundation under CMG-0327827. It also benefited from advanced computing resources provided by the National Science Foundations TeraGrid program at Indiana University.

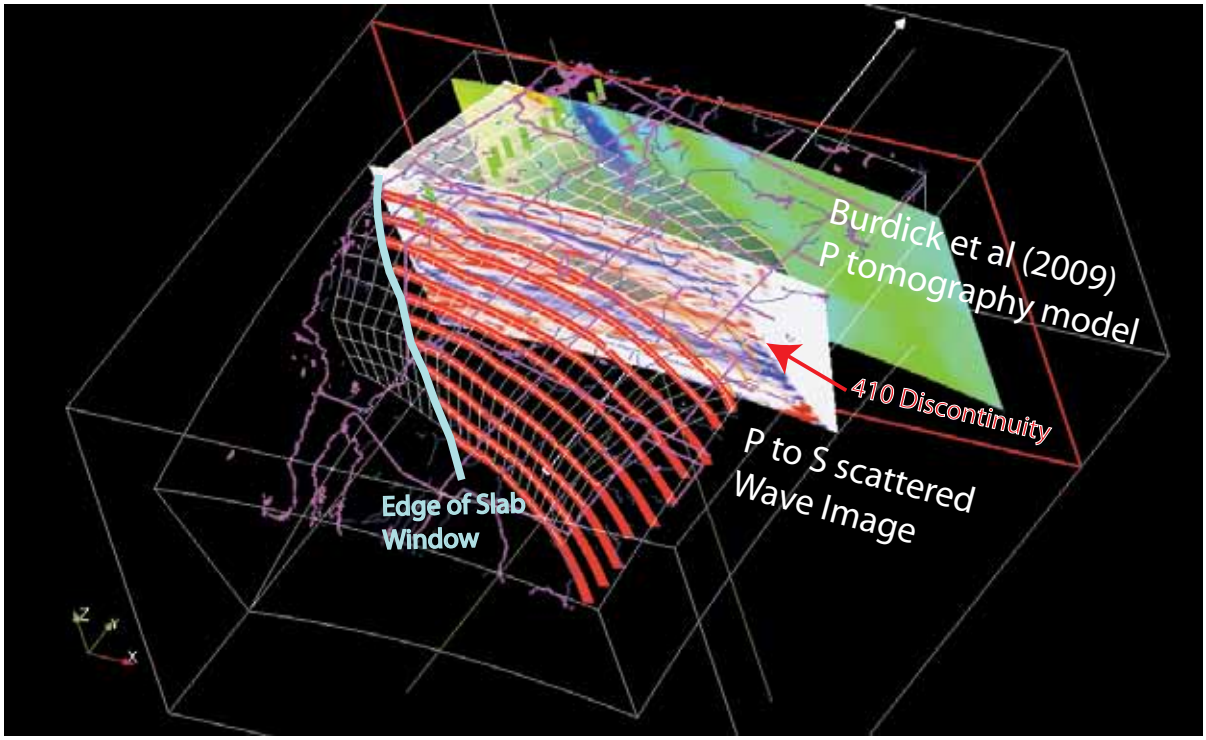

Juan de Fuca/Farallon lab model in 3D visualization framework. This is a still image from a 3D visualization scene used to overlay tomography models and results of a recently developed full 3D, scattered wave imaging method. Coastlines and state boundaries in magenta and rivers shown in blue provide a geographic reference. A section through the Burdick et al. (2009) P model and a section through the scattered wave image are shown to illustrate data that went into the interpretation. The slab model shows flow lines and constant time surface based on the NUVEL1 model of relative plate motion. The time ticks are based on a no strain approximation. The surface is constrained to daylight at the trench and pass through points 100 km below all active volcanoes in the Pacific Northwest. A estimate of the western edge of the slab window based on the no strain approximation is shown as the blue line passing through California and Arizona.

Imaging the Southern Alaska Subduction Zone

Josh A. Calkins *(Lamont-Doherty Earth Observatory),* **Geoffrey A. Abers** *(Lamont-Doherty Earth Observatory),* **Douglas Christensen** *(University of Alaska Fairbanks),* **Stéphane Rondenay** *(Massachusetts Institute of Technology),* **Jeffrey T. Freymueller** *(University of Alaska Fairbanks)*

The southern Alaska subduction zone, where the Pacific plate and the thick Yakutat block subduct beneath the accreted terranes that make up the margin of the North American plate, produced one of the largest ever instrumentally recorded earthquakes: the Mw 9.2 Good Friday earthquake of 1964. Between 1999 and 2009, two PASSCAL arrays were deployed between the coast and 400 km inland, with the aim of imaging the source region of the 1964 earthquake. Using data from the southern array (the "Multidisciplinary Observations of Onshore Subduction" or MOOS array), we produced 2-D scattered wavefield migration images of the upper 80 km of the subduction zone (top center panel in the figure). The cross sections show results of inverting forward and back-scattered S waves for perturbations in Vs, and highlight sharp changes or gradients in seismic velocities.

Our results reveal a shallowly north-dipping low velocity zone that is contiguous on its downdip end with previously obtained images of the subducting plate further north [*Rondenay et al., 2008*], and suggest that both the dip angle and the thickness of the subducting low velocity zone change along strike, across a roughly NNW-SSE striking line drawn through the eastern Kenai Peninsula. Previous geodetic studies [*Suito and Freymueller, 2009*] indicate a distinct change in locking at the subduction interface along the same NNW-SSE boundary. On the west end of the Kenai Peninsula, where seismically imaged downgoing crust appears oceanic, the geodetic signal mainly reflects postseismic deformation from the 1964 earthquake as evinced by southeast trending displacement vectors. While postseismic relaxation also continues on the eastern Kenai Peninsula, NNW-directed elastic deformation due to locking at the plate boundary dominates the geodetic signal, and imaging reveals thickened Yakutat crust is subducting. The collocation of sharp changes in both deep structure and surface deformation suggests that the nature of the plate interface changes drastically across the western edge of the Yakutat block and that variations in downgoing plate structure control the strain field in the overriding plate.

References

Brocher, T. M., G. S. Fuis, M. A. Fisher, G. Plafker, M. J. Moses, J. J. Taber, and N. I. Christensen (1994), Mapping the Megathrust beneath the Northern Gulf of Alaska Using Wide-Angle Seismic Data, *J. Geophys. Res., 99*(B6), 11663-11685.

Rondenay, S., G. A. Abers, and P. E. Van Keken (2008), Seismic imaging of subduction zone metamorphism, *Geology, 36*(4), 275-278.

Suito, H. and J.T. Freymueller (2009). A viscoelastic and afterslip postseismic deformation model for the 1964 Alaska earthquake, *J. Geophys. Res., 114* B11404.

Acknowledgements: This work was supported by NSF grant EAR-0814235.

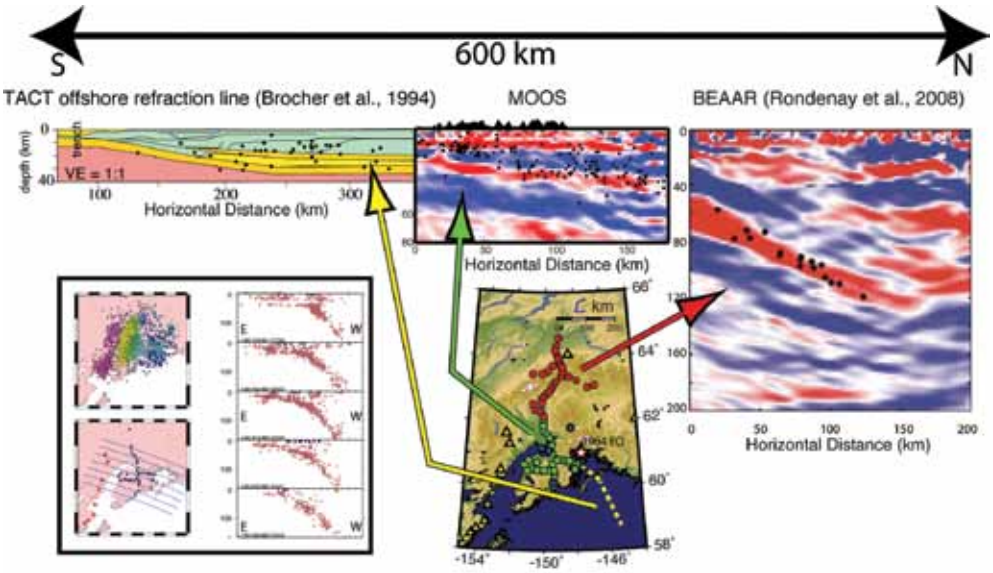

Seismicity and migration imaging results from the BEAAR (Rondenay et al, 2008) and MOOS broadband arrays. Upper (center and right) panels show results of scattered wavefield migration and clearly image the subducting oceanic crust as a prominent N- dipping low velocity (red) structure. Black circles mark the locations of earthquakes located using the two arrays. Joint migration of the two broadband data sets is a work in progress, and when combined with results from the TACT experiment (top left, Brocher et al., 1994)), these data will illuminate the structure along a 600 km cross-strike pro¬file of the southern Alaska subduction zone. The map (bottom center) shows the location of the arrays, and the inset in lower left shows the locations of earthquakes as determined by the MOOS array.

S-Velocity Mantle Structure at the Subducting Chile Ridge

Simon Lloyd *(Northwestern University),* **Suzan van der Lee** *(Northwestern University),* **Raymond M Russo** *(University of Florida),* **Diana Comte** *(University of Chile),* **Victor I Mocanu** *(Bucharest University),* **Alejandro Gallego** *(University of Florida),* **Ruth Elaine Murdie** *(Gold Fields Australia, St Ives Gold Mine),* **John C VanDecar** *(Carnegie Institution of Washington)*

At the triple junction between the Nazca, Antarctica and South American plate an actively spreading ridge is currently being subducted. The ridge continues to spread as it gets subducted beneath South America. However, no new lithosphere is formed in the process. As a result slab windows likeley exist beneath the overiding plate. These gaps allow asthenospheric mantle to flow through the slab, effecting mantle chemistry and thermal regime, seismic velocities and anisotropy as well as surface geology (*e.g.* gaps in arc volcanism).

Slab windows have sucessfully been imaged using P wave tomography [*Russo et al., 2009*]. In this study we analyze Rayleigh waves as they traverse the Chile Ridge Subduction Project (CRSP) array, in order to determine if additional constraints may be obtained from surface wave analysis.

We easily cross-correlated waveforms from an event at different stations to determine the relative arrival times, which allowed us to image the wavefront as it passes through the array. Typical for many events recorded at the CRSP array are wavepaths following the boundary between the Nazca and South American plates. For these events the incoming wavefront is not perpendicular to the great circle paths connecting the source and the receivers.

In order to get a first order estimate of the Rayleigh wave phase velocities we split the array into four regions defined by the 73°W meridian and 46°S parallel. We then invert relative arrival times for the average phase velocity within the defined regions. We repeat the inversion for several events, and combine the results. We conclude that

- Imaging Rayleigh wavefronts as they traverse the array region shows that particularly at shorter periods (*e.g.* 30 s) they are not perpendicular to the great circle path connecting the earthquake source and the seismometers.
- This needs to be taken into consideration when determining the phase velocities.
- A strong velocity contrast between the E (slow) and the W (fast) is derived from the delay times.
- Possibly a similar distinction can be made between the N (fast) and the S (slow).

References:

Russo, R.M., VanDecar, J.C., Comte, D., Mocanu, V.I., Gallego, A. Murdie, R.E., 2010. Subduction of the Chile Ridge: upper mantle structure and flow, *GSA Today*, in press.

Acknowledgements: This work was supported by National Science Foundation grant EAR 0538267.

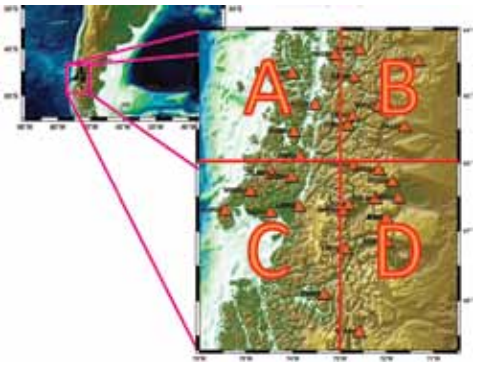

We deployed 39 broadband seismic stations from PASSCAL in southern Chile, aiming to investitgate the possible existance and effects of slab windows.

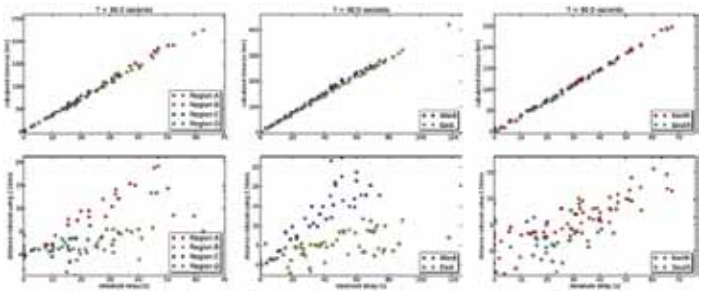

(left) The average Rayleigh wave phase velocity in region A is distinctly higher than in the other regions. (middle) Velocites in the west of the array are clearly higher than in the east. (right) The north-south contrast is not as strong, but the south appears be slightly slower than the north.

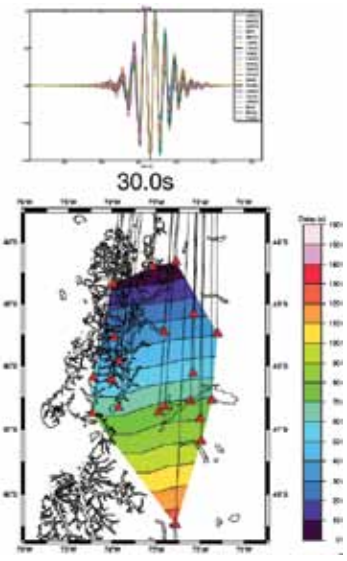

Owing to the small station spacing, the recorded waveforms are very similar at all stations. (below) For wavepaths following the boundary between the Nazca and South American plates, the incoming wavefront is not perpendicular to the great circle paths.

Opposing Slabs under Northern South America

M.J. Bezada *(Rice University, Earth Science Department),* **Alan Levander** *(Rice University, Earth Science Department),* **B. Schmandt** *(University of Oregon, Department of Geological Sciences),* **Fenglin Niu** *(Rice University, Earth Science Department),* **M. Schmitz** *(FUNVISIS, Caracas, Venezuela)*

The eastern boundary of the Caribbean plate is marked by subduction of the Atlantic under the Caribbean plate forming the Lesser Antilles volcanic arc. The southeastern plate boundary is a strike-slip margin while different configurations of subduction of the southwestern Caribbean under South America have been proposed. Using data from the BOLIVAR/GEODINOS experiment [*Levander*, 2006] we investigated the slab geometry in the upper mantle using finite-frequency, teleseismic P-wave tomography. Waveforms from P and PKIKP phases from 285 (Mb > 5.0) events occurring at epicentral distances from 30o to 90o and greater than 150o were bandpass filtered and cross-correlated to obtain up to three sets of delay times for each event. The delay times were inverted using first Fresnel zone approximate finite-frequency kernels. Our results show the subducting Atlantic slab, as well as a second slab in the west of the study area that we interpret as a subducting fragment of the Caribbean plate. Both slabs have steep dips where imaged and can be traced to depths greater than 600 km (Bottom figure). These results are consistent with transition zone boundary topography as determined by receiver function analysis (Juang et al, 2009. Top and middle figures). The Atlantic slab extends continentward south of the South America-Caribbean plate bounding strike-slip margin. We interpret part of this extension south of the faults as continental margin lithospheric mantle that is detaching from beneath South America and subducting along with the oceanic Atlantic slab. The steep subduction of the Caribbean occurs ~600 km landward from the trench, implying an initial stage of shallow subduction as far to the east as the Merida Andes-Maracaibo region, as has been inferred from intermediate depth seismicity. (Submitted to J. Geophys. Res.)

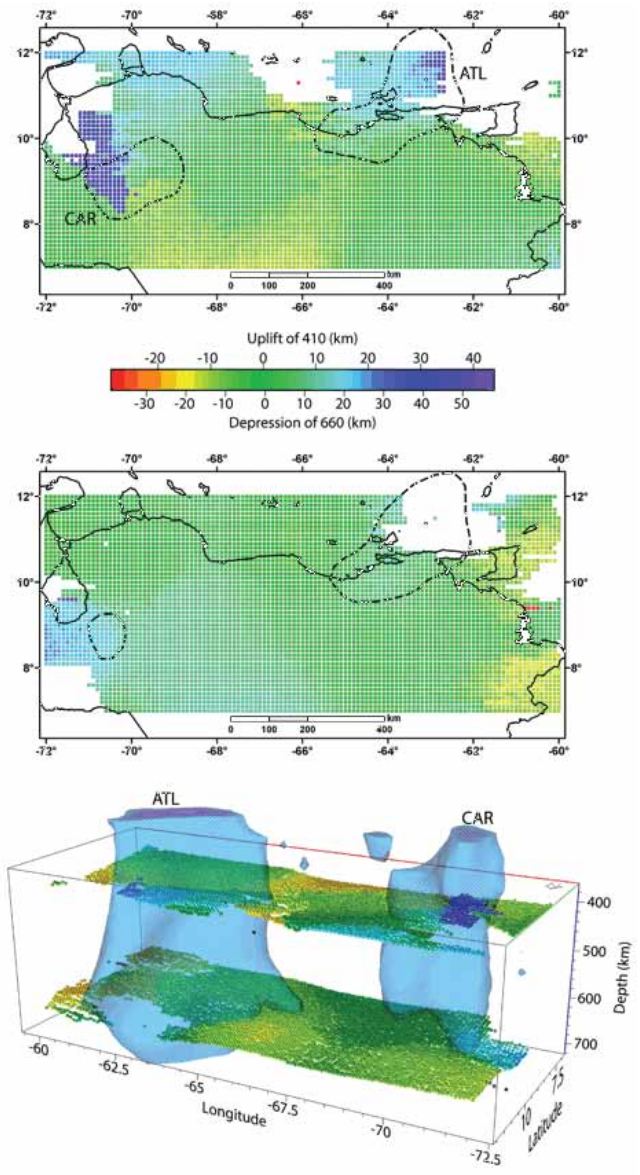

Subducting plate structure under northern South America and the southern Caribbean. ATL is the Atlantic (oceanic South American) plate, CAR is the Caribbean plate. Top: Depth of the 410 discontinuity showing elevated boundary where the slabs intersect the 410. Middle: Depth of the 660 discontinuity showing depressed boundary where the slabs intersect the 660. Bottom: 3D structure viewed from the northwest. The isosurface is the +1.5% anomaly. ATL subducts westward beneath CAR and northern South America. CAR subducts eastward beneath northern CA.

References

J.P. Huang, E. Vanacore, F. Niu, and A. Levander, 2009, Mantle transition zone beneath the Caribbean-South American plate boundary and its tectonic implications, *Earth Planet. Sci. Lett., 289*, 105-111

Levander, A., and 10 others, 2006, Evolution of the Southern Caribbean Plate Boundary, EOS, Trans. AGU, 87, Cover story, 97 and 100-101.

Acknowledgements: We would like to thank our colleagues at FUNVISIS, Caracas, Venezuela, the personnel at the PASSCAL Instrument Center and at OBSIP, and Gary Pavlis and Frank Vernon for outstanding data collection. BOLIVAR was funded by NSF Continental Dynamics Program grants EAR0003572 and EAR0607801, as well as by CONICIT and PDVSA. The 3D graphics were generated using EarthVision¨ software from Dynamic Graphics, Inc.

Arc-Parallel Flow beneath the TUCAN Broadband Seismic Experiment in Central America

David L. Abt *(ExxonMobil Exploration Company),* **Karen M. Fischer** *(Brown University),* **Geoffrey A. Abers** *(Lamont-Doherty Earth Observatory, Columbia University)*

Resolving the geometry of flow in subduction zones is essential in understanding mantle wedge thermal structure, slab dehydration, melting and melt transport in the wedge, and subduction zone dynamics. The TUCAN Broadband Seismic Experiment deployed 48 broadband IRIS/PASSCAL seismometers in Nicaragua and Costa Rica from 2004-2006. In three-dimensional models of anisotropy obtained by tomographically inverting shear-wave splitting measurements from local events recorded by the TUCAN array, olivine a-axes are predominantly arc-parallel in the mantle wedge beneath the arc and back-arc at depths of 50 to 150 km (except in northern Nicaragua). The arc-parallel a-axes extend into mantle wedge well beyond the cold, shallow wedge corner where B-type olivine fabric may occur. The observed anisotropy cannot be explained by simple two-dimensional arc-normal corner flow, and instead suggests significant arc-parallel flow. This hypothesis is confirmed by the trend of a distinct Pb and Nd isotopic signature in arc lavas associated with subducting seamounts offshore of Costa Rica. The anomalous signature systematically decreases for nearly 400 km from a maximum in central Costa Rica, directly inboard of the seamounts, down to background levels in northwestern Nicaragua. As the timing of the initial input of the isotopic signature beneath Costa Rica can be constrained and its transport distance is known, northwestward flow rates can be estimated (~63–190 mm/y) and are comparable to the magnitude of subducting Cocos plate motion (~85 mm/y). These results indicate flow in the mantle wedge can be significantly three-dimensional. Shear-wave splitting in SK(K)S phases recorded by the TUCAN array shows arc-parallel fast directions but significantly larger splitting times than seen in local S phases, indicating significant anisotropy consistent with arc-parallel flow below the slab.

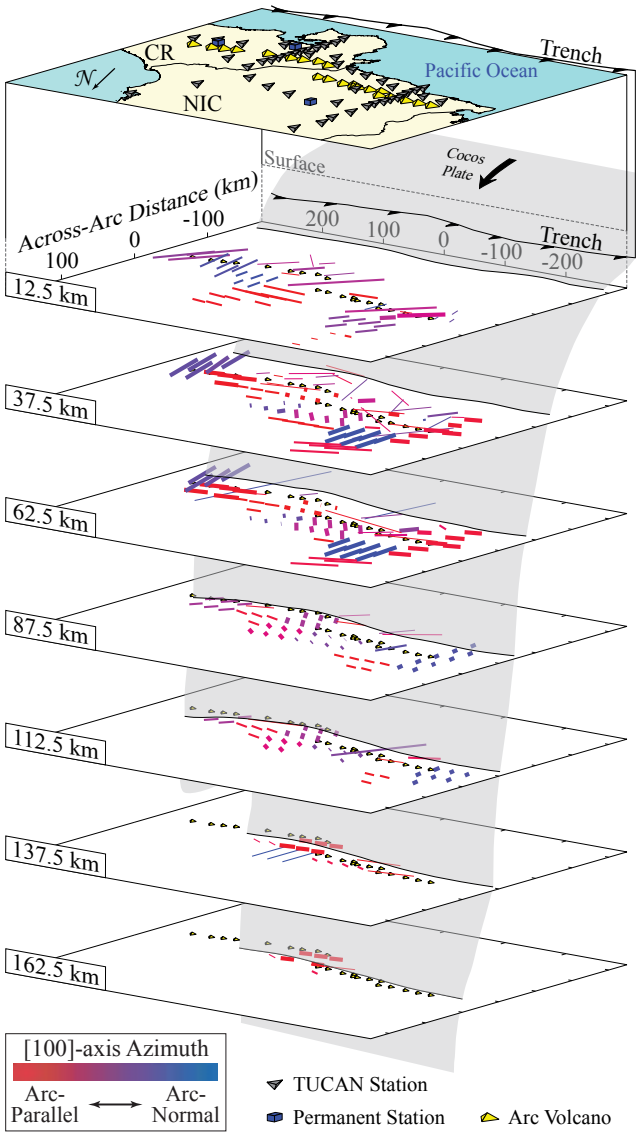

Model of anisotropy in the Nicaragua-Costa Rica subduction zone. Vectors represent well-resolved olivine a-axes in an olivine-orthopyroxene model. Vector orientation and color indicate horizontal azimuth, length corresponds to the strength of anisotropy relative to single-crystal values, and thickness corresponds to model parameter resolution. The TUCAN seismic array and volcanic arc are shown at the surface, and the volcanic arc position is plotted on each slice through the model. The slab–wedge interface is shown by grey shading. The mantle wedge is located in front of the slab in the layers spanning 50–175 km depth. Roughly arc-parallel a-axes dominate well-resolved wedge regions beneath the arc and the rear- and back-arc at depths of 50–150 km.

References

Abt, D. L., K. M. Fischer, G. A. Abers, J. M. Protti, V. González, and W. Strauch (2010), Constraints on upper mantle anisotropy surrounding the Cocos Slab from SK(K)S splitting, *J. Geophys. Res., 115*, B06316.

Abt, D. L., K. M. Fischer, G. A. Abers, W. Strauch, J. M. Protti, and V. González (2009), Shear wave anisotropy beneath Nicaragua and Costa Rica: Implications for flow in the mantle wedge, *Geochem. Geophys. Geosyst., 10*, Q05S15.

Hoernle K., D.L. Abt, K.M. Fischer, H. Nichols, F. Hauff, G. Abers, P. van den Bogaard, G. Alvarado, M. Protti, W. Strauch (2008), Geochemical and geophysical evidence for arc-parallel flow in the mantle wedge beneath Costa Rica and Nicaragua, *Nature, 451*, 1094-1098.

Acknowledgements: This research was supported by the NSF MARGINS program under awards OCE-0203650 (Boston University), and OCE-0203607 and EAR-0742282 (Brown University).

Effect of Prior Petrological Constraints on Global Upper Mantle Models of Radial Anisotropy

Caroline Beghein (University of California at Los Angeles)

Despite efforts from multiple research groups, large discrepancies remain among global models of seismic anisotropy. Besides the inherent non-uniqueness of inverse tomographic problems, one source of uncertainties can originate from the prior information introduced in the inversion. In the case of inversion of global surface wave phase velocity maps to obtain models of radial anisotropy, prior relationships are often imposed between the different elastic parameters. Inversions are then performed for the best-resolved parameters only, i.e. shear-wave velocity and anisotropy.

We tested the robustness of uppermost mantle radial anisotropy models with respect to these prior constraints [*Beghein, 2010*]. We applied a forward modeling technique [*Sambridge, 1999*] to fundamental mode Rayleigh and Love wave global phase velocity maps up to spherical harmonic degree 8. This forward modeling approach enabled us to obtain reliable model uncertainties, and to determine which model features are constrained by the data and which are dominated by the prior.

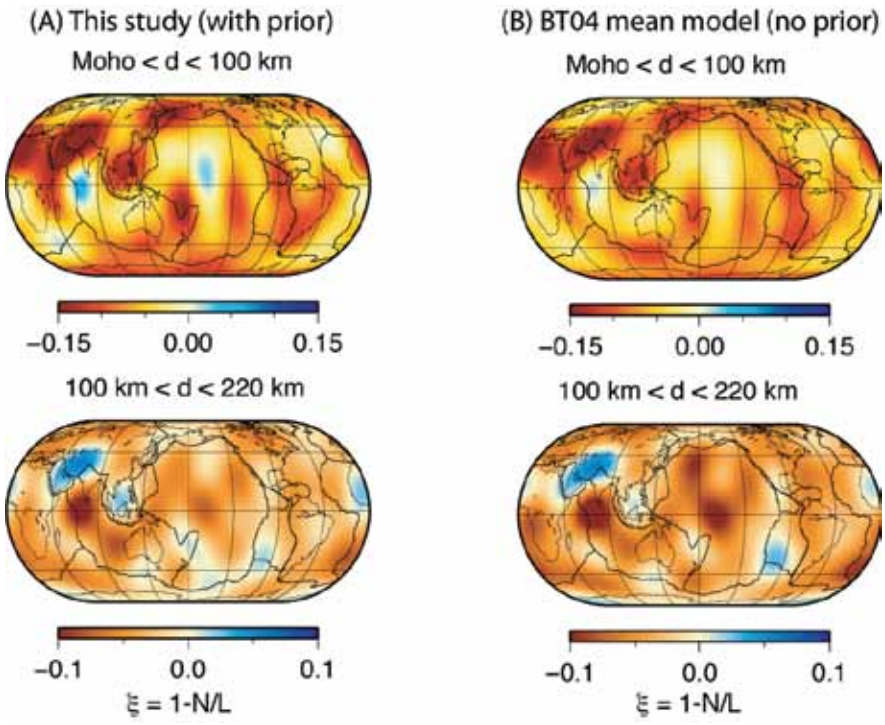

3-D models of S-wave radial anisotropy (ξ) in the uppermost mantle obtained with (A)andwithout(B)prior petrological constraints. In this convention, a negative ξ corresponds to fast horizontally propagating shear-waves. These models correspond to the mean of the model distributions obtained.

We compared the most likely and mean models obtained with and without prior constraints, and found that the most likely models obtained in both cases are highly correlated. This demonstrates that for the best data-fitting solution, the geometry of uppermost mantle radial anisotropy is not strongly affected by prior petrological constraints. We found, however, significant changes in the amplitude of the anomalies, with stronger amplitudes in the best data-fitting model obtained without petrological constraints. This could become an issue when quantitatively interpreting seismic anisotropy models, and thus emphasizes the importance of accurately accounting for parameter uncertainties and trade-offs, and of understanding whether the seismic data or the prior constraints the model.

In addition, we showed that model distributions are not necessarily Gaussian a priori, but that imposing petrological constraints can force the models to follow a Gaussian-like posterior distribution in addition to reducing posterior model uncertainties, in agreement with inverse theory. Finally, we demonstrated that the dependence of seismic wave velocities with the age of the ocean floor is robust and independent of prior constraints. A similar age signal exists for anisotropy, but with larger uncertainties without prior constraints.

References

Beghein, C., Radial Anisotropy and Prior Petrological Constraints: a Comparative Study, *J. Geophys. Res., 115*, 2010.

Sambridge, M., Geophysical inversion with a Neighbourhood Algorithm - I. searching a parameter space, G*eophys. J. Int., 138* (2), 479–494, 1999

Shear Wave Splits, Plate Motions and the Mérida Andes, Western Venezuela

Jeniffer Masy *(Rice University),* **Fenglin Niu** *(Rice University),* **Alan Levander** *(Rice University),* **Michael Schmitz** *(Fundacion Venezolana de Investigaciones Sismologicas-FUNVISIS)*

We measured shear wave splitting from SKS data recorded by the national seismic network of Venezuela and a linear broadband PASSCAL/Rice seismic array across the Merida Andes installed as part of the second phase of the BOLIVAR project. We modified the stacking method of Wolfe and Silver [1998] and applied it to a total of 22 stations. At each station, SKS waveforms from 2 to 36 earthquakes, mostly from the Tonga subduction zone, were stacked to yield a single measurement of the polarization direction and the splitting time. The measured parameters indicate that region can be divided into 3 zones, all congruent with surface motion observed by GPS. The first zone is located north of part of the strike-slip plate boundary prior to 7Ma. Here we observe the largest splitting times (1.6-2.5s), and the fast S-wave directions are orientated roughly in the EW direction, results consistent with previous studies and also with observations made in eastern Venezuela along the active strike slip plate boundary. An interpretation for these observations was proposed by Russo and Silver [1994]. The rollback of the Nazca plate induced a trench-parallel NS flow that passes around the northwest corner of the South America continent and forms an eastward flow beneath the Caribbean plate.

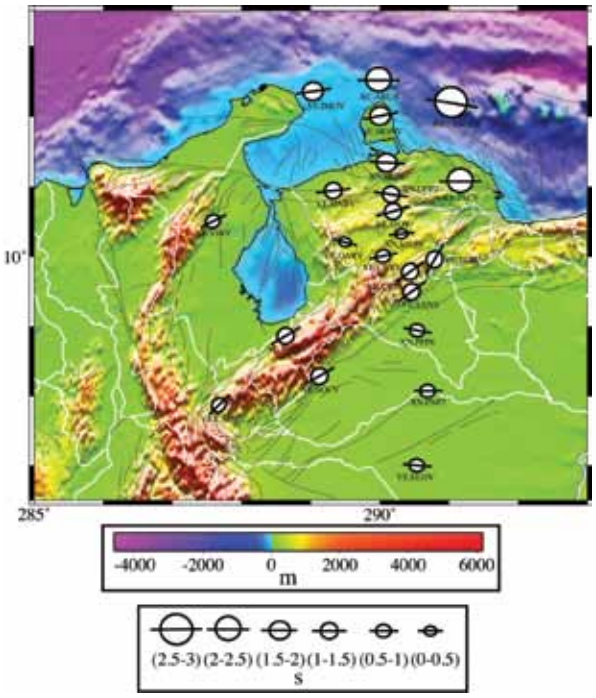

Measured splitting parameters are shown together with the topography of the study region. The orientation of the black solid lines indicates the orientation of the fastest direction. In general the study area can be divided in 3 different zones. The first one is north of the Oca-Ancon dextral strike slip fault, where splitting times are the largest (1.6 - 2.5 s) with an east-west orientation. The second zone is inside Barinas Apure Basin. The smallest split times are present in this region (0.6 - 1 s) also with an east-west orientation. The third zone, southeast of Maracaibo Block, shows a splitting direction N45E, parallel to Bocono Fault and Mérida Andes.

Zone two is located on the SA continent, east of the right lateral Bocono fault, where the measured split times are the smallest (0.6-1.0s) and have EW fastest direction. The observed fast direction and splitting times are consistent with those observed at the Guarico Basin, Maturin Basin and the Guayana shield in the east [Growdon et al., 2009], and are probably related to the westward drift of the South America continent.

Zone three is the Maracaibo block, which is bounded on the southeast by the Bocono fault, and on northwest by the Santa Marta Fault. Split orientations along the Bocono fault are N45°E, suggesting that the observed seismic anisotropy is likely caused by lithospheric deformation parallel to the fault. Split times in this zone range from 1s to 1.5s, requiring a vertically coherent zone of deformation extending to at least 200 km, suggesting a deep origin for the Venezuelan Andes. A recent tomography study [Bezada et al., 2010] suggests that beneath the Merida Andes the top of the flat slab is located at 200 km depth.

References

Russo, R., and P. G. Silver (1994), Trench-Parallel Flow Beneath the Nazca Plate from Seismic Anisotropy, *Science, 263*(5150), 1105-1111.

Growdon, M. A., G. L. Pavlis, F. Niu, F. L. Vernon, and H. Rendon (2009), Constraints on mantle flow at the Caribbean–South American plate boundary inferred from shear wave splitting, *J. Geophys. Res., 114*(B2), 1-7.

Wolfe, C., and P. Silver (1998), Seismic anisotropy of oceanic upper mantle: shear wave splitting methodologies and observations, *J. Geophys. Res.*-Solid Earth, 103(B1), 749-771.

Bezada, M.J., A. Levander, and B. Schmandt, 2010, Subduction in the Southern Caribbean: Images from finite-frequency P-wave tomography, submitted to *J. Geophys. Res.*, May 2010.

Acknowledgements: We would like to acknowledge IRIS-PASSCAL and FUNVISIS for providing the data and the temporal stations used in this study, and also for all the support they gave us during the deployment of the seismic stations. This research was supported by NSF grant EAR-0607801.

Global Azimuthal Seismic Anisotropy and the Unique Plate-Motion Deformation of Australia

Eric Debayle *(Institut de Physique du Globe de Strasbourg, Ecole et Observatoire des Sciences de la Terre, Centre National de la Recherche Scientifique and Universit ´e Louis Pasteur, 61084 Strasbourg, Cedex),* **Brian Kennett** *(Research School of Earth Sciences, The Australian National University, Canberra ACT 0200, Australia),* **Keith Priestley** *(Bullard Laboratories, University of Cambridge, Cambridge)*

Differences in the thickness of the high-velocity lid underlying continents as imaged by seismic tomography, have fuelled a long debate on the origin of the 'roots' of continents. Some of these differences may be reconciled by observations of radial anisotropy between 250 and 300 km depth, with horizontally polarized shear waves travelling faster than vertically polarized ones. This azimuthally averaged anisotropy could arise from present-day deformation at the base of the plate, as has been found for shallower depths beneath ocean basins. Such deformation would also produce significant azimuthal variation, owing to the preferred alignment of highly anisotropic minerals. Here we report global observations of surface-wave azimuthal anisotropy, which indicate that only the continental portion of the Australian plate displays significant azimuthal anisotropy and strong correlation with present-day plate motion in the depth range 175–300 km. Beneath other continents, azimuthal anisotropy is only weakly correlated with plate motion and its depth location is similar to that found beneath oceans. We infer that the fast-moving Australian plate contains the only continental region with a sufficiently large deformation at its base to be transformed into azimuthal anisotropy. Simple shear leading to anisotropy with a plunging axis of symmetry may explain the smaller azimuthal anisotropy beneath other continents.

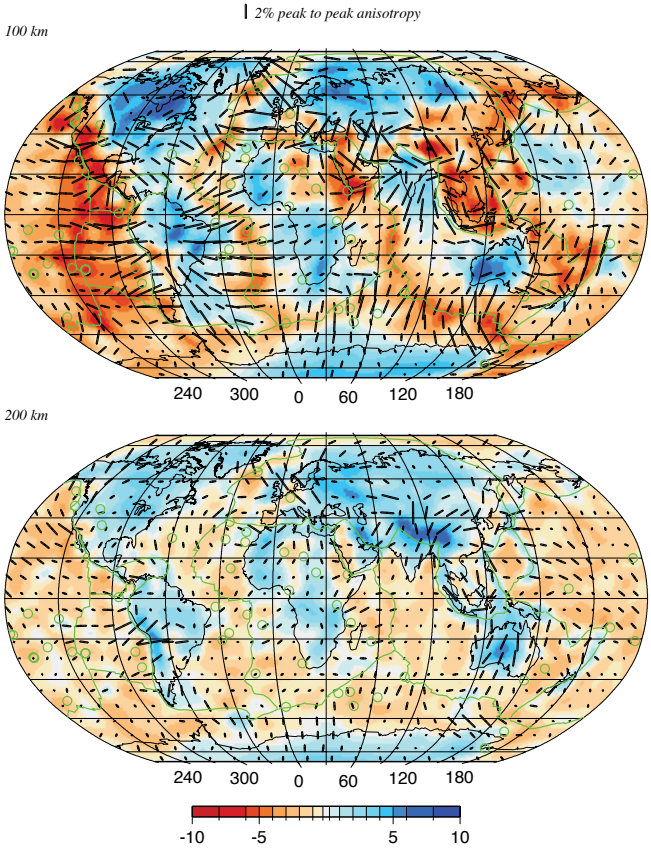

SV-wave heterogeneity and azimuthal anisotropy (black bars oriented along the axis of fast propagation) at 100 and 200 km depth obtained from the inversion of 100,779 Rayleigh waveforms. Hotspot locations are indicated by green circles. The length of theblack bars is proportional to the maximum amplitude of azimuthal anisotropy (bar length for 2% peak to peak anisotropy shown at top). SV-wave perturbations (in per cent relative to PREM) are represented with the colour scale.

References

E. Debayle, B. Kennett and K. Priestley, Global azimuthal seismic anisotropy and the unique plate-motion deformation of Australia, *Nature, 433*, 509-512, doi:10.1038/nature03247, 2005.

Acknowledgements: This work was supported by programme DyETI conducted by the French Institut National des Sciences de l'Univers (INSU). The data used in this work were obtained from the GEOSCOPE, GDSN, IDA, MEDNET and GTSN permanent seismograph networks, and completed with data collected after the PASSCAL broadband experiments, the SKIPPY and subsequent broadband deployments in Australia, and the INSU deployments in the Horn of Africa and the Pacific (PLUME experiment). Supercomputer facilities were provided by the IDRIS and CINES national centres in France. Special thanks to J. M. Brendle at EOST for technical support, S. Fishwick for providing broadband data from the Western Australian craton field deployment, the staff of the Research School of Earth Science who collected the SKIPPY data in the field, and A. Maggi for suggestions that improved the manuscript.

Depth Dependent Azimuthal Anisotropy in the Western US Upper Mantle

Huaiyu Yuan *(Berkeley Seismological Laboratory, University of California-Berkeley),* **Barbara Romanowicz** *(Berkeley Seismological Laboratory, University of California-Berkeley)*

We present the results of a joint inversion [Yuan and Romanowicz, 2010] of long period seismic waveforms and SKS splitting measurements for 3D lateral variations of anisotropy in the upper mantle beneath the western US, incorporating recent datasets generated by the USArray deployment as well as other temporary stations in the region. We find that shallow azimuthal anisotropy (Figure 1) closely reflects plate motion generated shear in the asthenosphere in the shallow upper mantle (70-150 km depth), whereas at depths greater than 150 km, it is dominated by northward and upward flow associated with the extension of the East-Pacific Rise under the continent, constrained to the east by the western edge of the north-American craton, and to the north, by the presence of the East-West trending subduction zone. (Figure 1 here) The strong lateral and vertical variations throughout the western US revealed by our azimuthal anisotropy model reflect complex past and present tectonic processes. In particular, the depth integrated effects of this anisotropy (Figure 2) explain the apparent circular pattern of SKS splitting measurements observed in Nevada without the need to invoke any local anomalous structures (e.g. ascending plumes or sinking lithospheric instabilities [Savage and Sheehan, 2000; West et al., 2009]): the circular pattern results from the depth-integrated effects of the lithosphere-asthenosphere coupling to the NA, Pacific and JdF plates at shallow depths, and in the depth range 200-400 km, northward flow from the EPR channeled along the craton edge and deflected by the JdF slab, and more generally slab related anisotropy. With the accumulating high quality TA data, surface wave azimuthal anisotropy makes it possible to resolve complex depth dependent anisotropic domains in the North American upper mantle. (Figure 2 here)

References

Savage, M. K., and A. F. Sheehan (2000), Seismic anisotropy and mantle flow from the Great Basin to the Great Plains, western United States, *J. Geophys. Res., 105*(6), 13,715-713,734.

West, J. D., M. J. Fouch, J. B. Roth, and L. T. Elkins-Tanton (2009), Vertical mantle flow associated with a lithospheric drip beneath the Great Basin, *Nature Geosci., 2*(6), 439-444.

Yuan, H., and B. Romanowicz (2010), Depth Dependent Azimuthal anisotropy in the western US upper mantle, *Earth Planet. Sci. Lett.*, in revision.

Acknowledgements: We thank the IRIS DMC and the Geological Survey of Canada for providing the waveforms used in this study and K. Liu, M. Fouch, R. Allen, A. Frederiksen and A. Courtier for sharing their SKS splitting measurements with us. This study was supported by NSF grant EAR-0643060. This is BSL contribution #10-05.

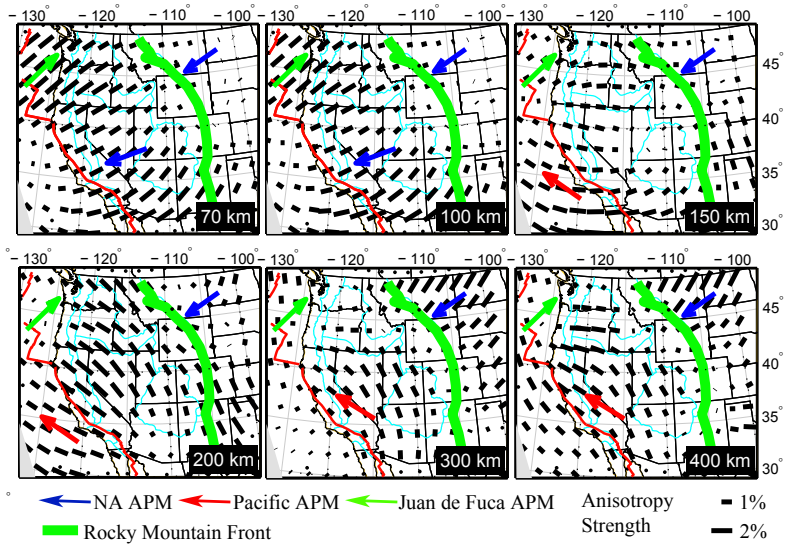

Figure 1. Azimuthal anisotropy variations with depth. Black bars indicate the fast axis direction and the bar length is proportional to the anisotropy strength. Blue, green and red arrows show the absolute plate motion (APM) directions of the North American, JdF, and the Pacific plates respectively, computed at each location using the HS3-NUVEL 1A model.

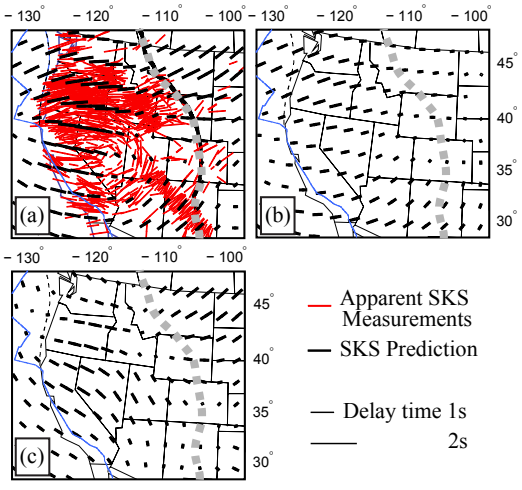

Figure 2. Comparison of observed and predicted station averaged SKS splitting direction and time. Red bars indicate observations and are shown in the left panels only, for clarity. Black bars indicate the model predictions. Predicted splitting is shown for integration of the models over, (a) the full depth range of the azimuthal anisotropy models, (b) the top 150 km of the models, and (c) the portion of the model between 150 and 500 km, respectively.

The Stratification of Seismic Azimuthal Anisotropy in the Western US

Fan-Chi Lin *(University of Colorado at Boulder),* **Michael H. Ritzwoller** *(University of Colorado at Boulder),* **Yingjie Yang** *(University of Colorado at Boulder),* **Morgan P. Moschetti** *(University of Colorado at Boulder),* **Matthew J. Fouch** *(Arizona State University)*

Knowledge of the stratification of seismic anisotropy in the crust and upper mantle would aid understanding of strain partitioning and dynamic coupling in the crust, lithospheric mantle, and athenospheric mantle. It has been difficult, however, to obtain an integrated, self-consistent 3D azimuthally anisotropic model for the crust and upper mantle based on both SKS splitting and surface wave measurements due to the rather different sensitivities of the two wave types. We applied surface wave tomography, including ambient noise tomography (ANT) and eikonal tomography, to data from the Transportable Array (TA) component of EarthScope/USArray to estimate the 3D anisotropic structure of the crust and uppermost mantle. These results were combined with SKS splitting measurements to investigate the deeper anisotropic structures. Figure 1 shows the anisotropic properties of the (a) middle-to-lower crust, (b) uppermost mantle, and (c) asthenosphere in our final model, where the fast propagation direction and anisotropic amplitude are represented by the orientation and length of the yellow/red bars on a 0.6° spatial grid. Isotropic shear wave speeds at depths of 15 and 50 km are color coded in the background of (a)-(b), and the fast direction is shown in the background in (c). The comparison of observations of SKS splitting (blue, red, or black) and predictions (yellow) from the 3D model of anisotropy model shown in (a)-(c) are also shown in (d), where the fast direction and splitting times are summarized by the orientation and length of the bars. The blue, red, and black colors of the observed measurements identify differences with the model predictions of the fast axis directions: Blue: 0°-30°, Red: 30°-60°, Black: 60°-90°. The inferred stratification of anisotropy demonstrates complex and highly variable crust-mantle mechanical coupling. Regional-scale azimuthal anisotropy is dominated by relatively shallow tectonic processes confined to the crust and uppermost mantle, although the patterns of anisotropy in the crust and mantle are uncorrelated. The more homogeneous asthenospheric anisotropy broadly reflects a mantle flow field controlled by a combination of North American plate motion and the subduction of the Juan de Fuca and Farallon slab systems. These results would not have been possible without the TA, and future work will involve applying the method to new TA stations to the east.

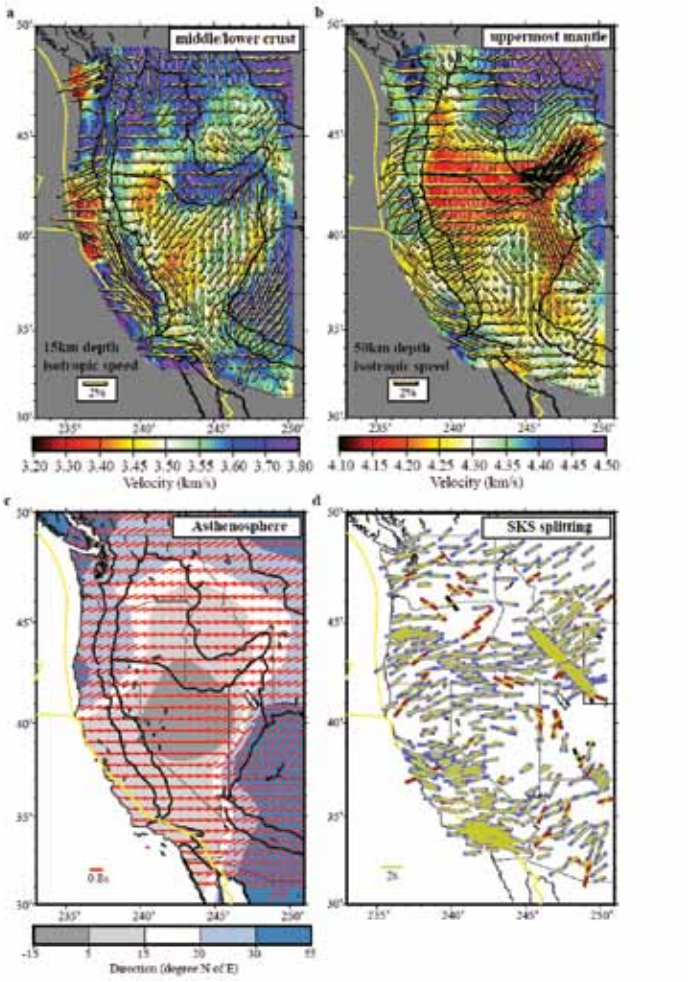

Azimuthal anisotropy in the crust, uppermost mantle, and asthenosphere and the comparison between predicted and observed SKS splitting.

References

Lin, F., Ritzwoller, M. H. & Snieder, R. Eikonal tomography: surface wave tomography by phase front tracking across a regional broad-band seismic array. *Geophys. J. Int. 177*, 1091-1110 (2009).

Lin, F., Ritzwoller, M. H., Yang, Y., Moschetti, M. P., & Fouch, M. J. The stratification of seismic azimuthal anisotropy in the western US. Submitted to *Nature Geosci.*.

Acknowledgements: Data used in this study were made available through EarthScope and the facilities of the IRIS Data Management Center. This work has been supported by NSF grants EAR-0711526 and EAR-0844097.

Rayleigh Wave Phase Velocities, Small-Scale Convection and Azimuthal Anisotropy beneath Southern California

Donald W. Forsyth *(Brown University),* **Yingjie Yang** *(University of Colorado)*

We use Rayleigh waves to invert for shear velocities in the upper mantle beneath southern California [*Yang and Forsyth, 2006*]. A one-dimensional shear velocity model reveals a pronounced low- velocity zone (LVZ) from 90 to 210 km. The pattern of velocity anomalies indicates that there is active small-scale convection in the asthenosphere and that the dominant form of convection is three-dimensional (3-D) lithospheric drips and asthenospheric upwellings, rather than 2-D sheets or slabs. Several of the features that we observe have been previously detected by body wave tomography: these anomalies have been interpreted as delaminated lithosphere and consequent upwelling of the asthenosphere beneath the eastern edge of the southern Sierra Nevada and Walker Lane region; sinking lithosphere beneath the southern Central Valley; upwelling beneath the Salton Trough; and downwelling beneath the Transverse Ranges. Our new observations provide better constraints on the lateral and vertical extent of these anomalies. In addition, we detect two previously undetected features: a high-velocity anomaly beneath the northern Peninsular Range and a low-velocity anomaly beneath the northeastern Mojave block. We also estimate the azimuthal anisotropy from Rayleigh wave data. The strength is 1.7% at periods shorter than 100 s and decreases to below 1% at longer periods. The fast direction is nearly E-W. The anisotropic layer is more than 300 km thick. The E-W fast directions in the lithosphere and sublithosphere mantle may be caused by distinct deformation mechanisms: pure shear in the lithosphere due to N-S tectonic shortening and simple shear in sublithosphere mantle due to mantle flow.

References

Yang, Y. and D.W. Forsyth, Rayleigh wave phase velocities, small-scale convection and azimuthal anisotropy beneath southern California, *J. Geophys. Res., 111*, B07306,2006

Acknowledgements: This work was supported by National Science Foundation grants OCE-9911729 and EAR-0510621.

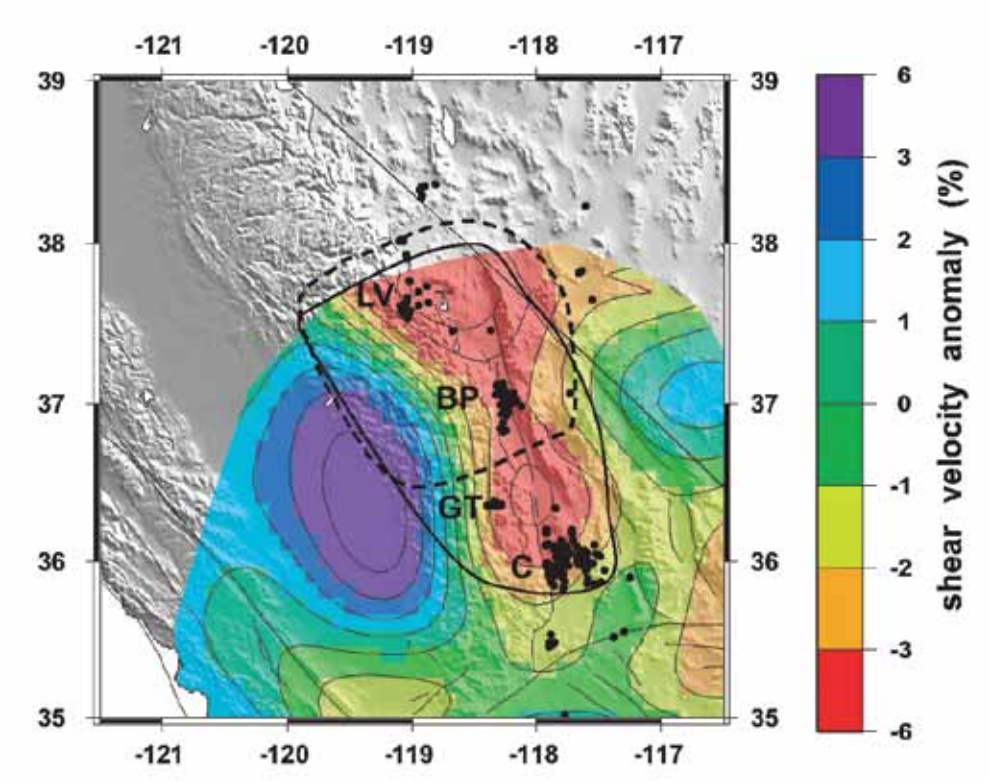

Distribution of volcanism (black dots) in southern Sierra Nevada during the Quaternary (1.5-0 Ma) period. Bold solid line outlines area with which Pliocene (chiefly 4-3 Ma) volcanism was prevalent; note that Quaternary volcanic fields (LV-Long Valley, BP-Big Pine, GT-Golden Trout, C-Coso) are all within area of Pliocene event. Dashed line outlines the area of Pliocene potassic volcanism 4-3 Ma. Colors show shear-wave velocity anomalies at depths of 70-90 km. Note that the Quaternary volcanism coincides with the region of lowest velocities.

Upper Mantle Anisotropy beneath the High Lava Plains, Oregon, USA: Linking Mantle Dynamics to Surface Tectonomagmatism

Maureen Long *(Yale University),* **Lara Wagner** *(University of North Carolina at Chapel Hill),* **Matthew Fouch** *(Arizona State University),* **David James** *(Carnegie Institution of Washington)*

The High Lava Plains (HLP) of southeastern and central Oregon represent a young (< 15 Ma), bimodal volcanic province that exhibits an age progression in silicic volcanism towards the northwest, along with widespread basaltic volcanic activity. A variety of models have been proposed to explain the recent volcanic history of the region, including the Steens and Columbia River flood basalt episodes and the subsequent evolution of the HLP. These models variously invoke the rollback and steepening of the Cascadia slab, interaction between the subduction-induced flow field and the inferred Yellowstone plume, the influence of basal lithospheric "topography," significant lithospheric extension, or a combination of these processes. Measurements of the seismic anisotropy that results from active mantle flow beneath the region can provide a crucial test of such models. To constrain this anisotropy, we measured SKS splitting at approximately 200 broadband seismic stations in eastern Oregon and the surrounding region, including ~100 stations of the temporary High Lava Plains seismic deployment [*Long et al., 2009*]. Stations in the region exhibit strong SKS splitting, with average delay times at single stations ranging from ~ 1.0 sec to ~ 2.7 sec. Nearly all observed fast directions are approximately E-W, which argues for well-organized contemporary mantle flow in an E-W direction beneath the HLP. Mantle flow beneath the HLP appears to be controlled by the rollback of the Juan de Fuca slab; the observed E-W fast directions are not consistent with a model in which mantle flow is driven along the strike of the HLP by Yellowstone plume material. We observe significant lateral variations in average delay times, with a region of particularly large dt that delineate a region in the heart of the HLP province and another region of large delay times just to the north of Newberry Volcano. There is a notable spatial correlation among stations that exhibit large delay times, the location of Holocene volcanic activity, and slow isotropic uppermost mantle wavespeeds from a surface wave velocity model [*Wagner et al., in review*]. Possible explanations for the pronounced lateral variations in splitting delay times include variations in the partial melt fraction or degree of alignment, variations in the strength or fabric type of olivine LPO, or variations in uppermost mantle mineralogy.

References

Long, M. D., H. Gao, A. Klaus, L. S. Wagner, M. J. Fouch, D. E. James, and E. Humphreys (2009), Shear wave splitting and the pattern of mantle flow beneath eastern Oregon, *Earth Planet. Sci. Lett., 288*, 359-369.

Wagner, L., D. Forsyth, M. Fouch, and D. James (2010), Detailed three dimensional shear wave velocity structure of the northwestern United States from surface wave two-plane-wave analyses. *Earth Planet. Sci. Lett.*, in review.

Acknowledgements: The High Lava Plains seismic deployment was funded through NSF awards EAR-0507248 (MF) and EAR-0506914 (DJ).

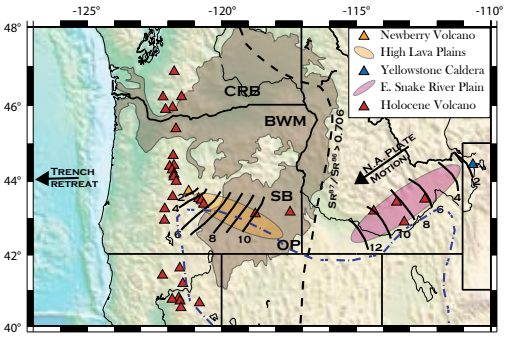

Geologic map of eastern Oregon and the surrounding region. Black contours indicate the age progression (in Ma) of silicic volcanism along both the High Lava Plains (yellow), and the Snake River Plain (pink). The black dashed line shows the location of the Sr87/Sr86=0.706 line, commonly interpreted to mark the boundary between cratonic North America to the east and the accreted arc terranes to the west. The blue dashed line shows the northern limits of Basin and Range extension. The brown highlighted area indicates the region covered by Miocene flood basalts including the Columbia River basalts (CRB) to the north and the Steens basalts (SB) farther to the south. Red triangles indicate locations of Holocene volcanism. The geographical locations of the Owyhee Plateau (OP) and the Blue and Wallowa mountains (BWM) are also shown, along with Newberry Volcano (orange triangle) and Yellowstone Caldera (blue triangle). The arrow at the Cascadia trench indicates its direction of motion.

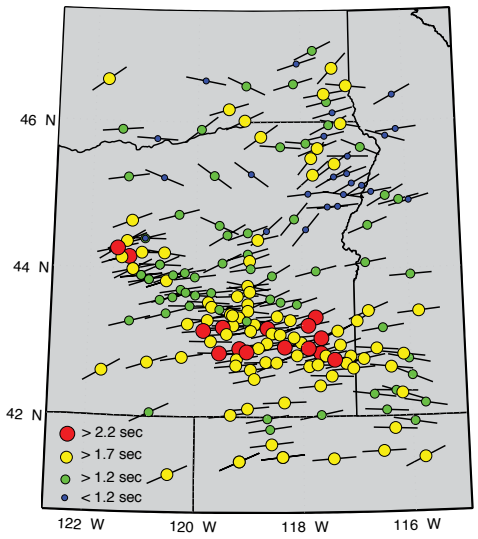

Map of average shear wave splitting parameters in the High Lava Plains and surrounding regions. Estimates were obtained by a simple average of the highest-quality measurements at each station. The symbols are color-coded by the magnitude of the delay time, as indicated by the legend at bottom left.

Mantle Flow in Subduction Systems from the Global Pattern of Shear Wave Splitting above and below Subducting Slabs

Maureen Long *(Yale University),* **Paul Silver** *(Carnegie Institution of Washington)*

The character of the mantle flow field in subduction zone regions remains poorly understood, despite its importance for our understanding of subduction dynamics. Observations of seismic anisotropy, which manifests itself in shear wave splitting, can shed light on the geometry of mantle flow in subduction zones, but placing constraints on anisotropy in various parts of the subduction system (including the overriding plate, the mantle wedge, the subducting slab, and the sub-slab mantle) remains challenging from an observational point of view. In order to identify dynamic processes that make first-order contributions to the pattern of mantle flow in subduction zones, we analyze a global compilation of shear wave splitting measurements for a variety of ray paths, including SK(K)S and teleseismic S phases as well as local S and source-side splitting from slab earthquakes. We have compiled shear wave splitting measurements from subduction zones globally to produce estimates of average shear wave splitting parameters – and their spatial variation – for the mantle wedge and the sub-wedge region for individual subduction segments [*Long and Silver, 2008*]. These estimates are then compared to other parameters that describe subduction. The sub-wedge splitting signal is relatively simple and is dominated by trench-parallel fast directions in most subduction zones worldwide (with a few notable exceptions). Average sub-wedge delay times correlate with the absolute value of trench migration velocities in a Pacific hotspot reference frame, which supports a model in which sub-slab flow is usually trench-parallel and is controlled by trench migration *[Long and Silver, 2009*]. Shear wave splitting patterns in the mantle wedge are substantially more complicated, with large variations in local S delay times and complicated spatial patterns that often feature sharp transitions between trench-parallel and trench-perpendicular fast directions. We find a relationship between average wedge delay times and the ratio of the trench migration velocity and the convergence velocity. This supports a model in which a trench-parallel flow field (induced by trench migration) interacts with a 2-D corner flow field (induced by downdip motion of the slab) in the mantle wedge, with the relative influence of these flows being governed by the relative magnitude of convergence velocity and trench migration velocity in a Pacific hotspot reference frame.

References

Long, M. D., and T. W. Becker (2010), Mantle dynamics and seismic anisotropy, *Earth Planet. Sci. Lett.*, in press.

Long, M. D., and P. G. Silver (2008), The subduction zone flow field from seismic anisotropy: A global view. *Science, 319*, 315-318.

Long, M. D., and P. G. Silver (2009), Mantle flow in subduction systems: The sub-slab flow field and implications for mantle dynamics. *J. Geophys. Res., 114*, B10312.

Acknowledgements: This work was supported by the Carnegie Institution of Washington and by NSF grant EAR-0911286.

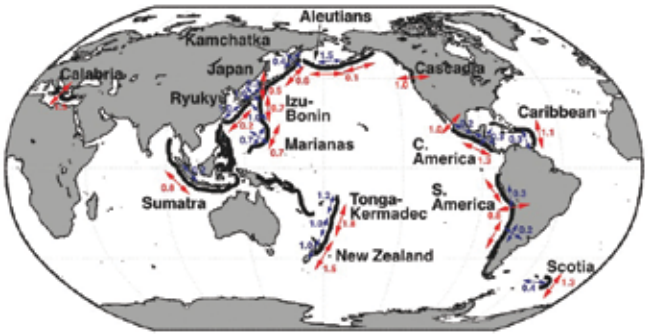

Sketch of constraints on subduction zone anisotropy from shear wave splitting measurements (figure from Long and Becker, 2010, after the compilation of Long and Silver, 2008, 2009). The anisotropic signals of the wedge and sub-slab regions are shown separately. Red arrows indicate average fast directions for the sub-slab splitting signal from SKS, local S, and source-side teleseismic S splitting measurements. The associated average sub-slab delay times are shown in red. Blue arrows indicate average fast directions for wedge anisotropy from local S splitting. In regions where multiple fast directions are shown, splitting patterns exhibit a mix of trench-parallel, trench-perpendicular, and oblique fast directions.

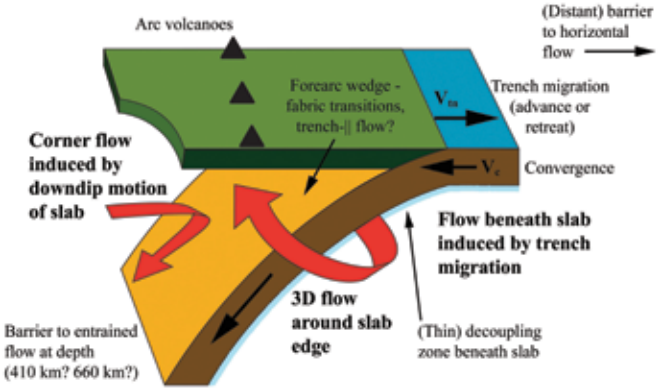

Sketch of the model proposed by Long and Silver (2008) for mantle flow in subduction zones controlled by trench migration.

The Teleseismic Signature of Fossil Subduction: Northwestern Canada

M. G. Bostock *(The University of British Columbia),* **J.-P. Mercier** *(The University of British Columbia),* **P. Audet** *(University of California, Berkeley),* **J.B. Gaherty** *(LDEO, Columbia University),* **E. J. Garnero** *(Arizona State University),* **J. Revenaugh** *(University of Minnesota)*

Between June 2003 and September 2005, 20 broadband, three-component seismometers were deployed along the MacKenzie-Liard Highway in Canada's Northwest Territories as part of the joint IRIS-Lithoprobe Canada Northwest Experiment (CANOE) [*Mercier et al., 2008*]. These stations traverse a paleo-Proterozoic suture and subduction zone that has been previously documented to mantle depths using seismic reflection profiling [Cook et al., 1999]. Teleseismic receiver functions computed from some 250 earthquakes clearly reveal the response of the ancient subduction zone. On the radial component, the suture is evident as a direct conversion from the Moho, the depth of which increases from ~30 km to ~50 km over a horizontal distance of some 70 km before its signature disappears. The structure is still better defined on the transverse component where the Moho appears as the upper boundary of a 10 km thick layer of anisotropy that can be traced from 30 km to at least 90 km depth. The seismic response of this layer is characterized by a frequency dependence that can be modeled by upper and lower boundaries that are discontinuous in material properties and their gradients, respectively. Anisotropy is characterized by a +/-5% variation in shear velocity and hexagonal symmetry with a fast axis that plunges at an oblique angle to the subduction plane. The identification of this structure provides an unambiguous connection between fossil subduction and fine-scale, anisotropic mantle layering. Previous documentation of similar layering below the adjacent Slave province and from a range of Precambrian terranes across the globe provides strong support for the thesis that early cratonic blocks were stabilized through processes of shallow subduction.

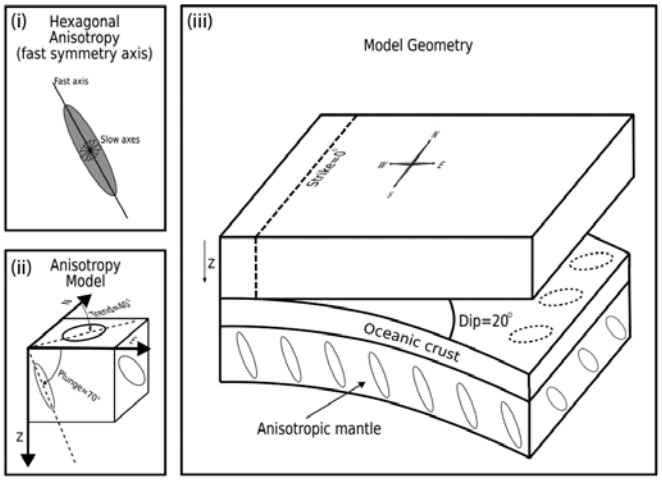

Cartoon showing structural elements of interpretation, including (i) definition of hexagonal anisotropy with fast symmetry axis, (ii) orientation of anisotropy, and (iii) tectonic configuration.

References

Cook, F.A, A.J. van der Velden, K.W. Hall, and B.J. Roberts (1999), Frozen subduction in Canada's Northwest Territories: Lithoprobe deep lithospheric reflection profiling of the western Canada shield, *Tectonics, 18*, 1-24.

Mercier, J.-P., M.G. Bostock, P. Audet, J.B. Gaherty, E.J. Garnero, and J. Revenaugh (2008), The teleseismic signature of fossil subduction: Northwestern Canada, *J. Geophys. Res., 113* B04308.

Acknowledgements: We gratefully acknowledge financial support from the National Science Foundation (grants NSF EAR-0453747 to JG, NSF EAR-0711401 to EG, NSF EAR-0003745-004 to JR) and the Natural Sciences and Engineering Research Council of Canada (NSERC-Lithoprobe supporting geoscience grant CSP0006963 to MB).

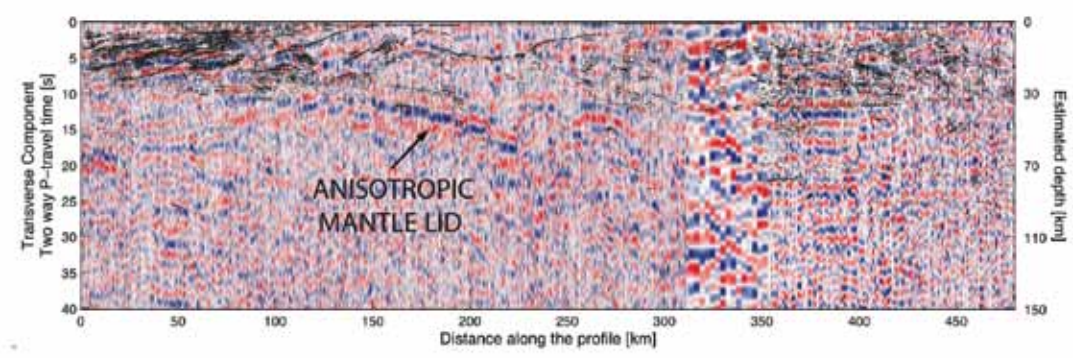

Superposition of line-drawing reflection section of Cook et al (1999) upon transverse component receiver function. Note teleseismic signature of anisotropic mantle lid that parallels reflections from subducted crust.

Seismic Anisotropy beneath Cascadia and the Mendocino Triple Junction: Interaction of the Subducting Slab with Mantle Flow

Caroline Eakin *(Imperial College London),* **Mathias Obrebski** *(UC Berkeley),* **Richard Allen** *(UC Berkeley),* **Devin Boyarko** *(Miami University),* **Michael Brudzinski** *(Miami University),* **Robert Porritt** *(UC Berkeley)*

Mantle flow associated with the Cascadia subduction zone and the Mendocino Triple Junction is poorly characterized due to a lack of shear wave splitting studies compared to other subduction zones. To fill this gap data was obtained from the Mendocino and FACES seismic networks that cover the region with dense station spacing. Over a period of 11-18 months, 50 suitable events were identified from which shear wave splitting parameters were calculated. Here we present stacked splitting results at 63 of the stations. The splitting pattern is uniform trench normal (N67°E) throughout Cascadia with an average delay time of 1.25 seconds. This is consistent with subduction and our preferred interpretation is entrained mantle flow beneath the slab. The observed pattern and interpretation have implications for mantle dynamics that are unique to Cascadia compared to other subduction zones worldwide. The uniform splitting pattern seen throughout Cascadia ends at the triple junction where the fast directions rotate almost 90°. Immediately south of the triple junction the fast direction rotates from NW-SE near the coast to NE-SW in northeastern California. This rotation beneath northern California is consistent with flow around the southern edge of the subducting Gorda slab.

References

Eakin, C.M., M. Obrebski, R.M. Allen, D.C. Boyarko, M.R. Brudzinski, R. Porritt, Seismic Anisotropy beneath Cascadia and the Mendocino Triple Junction: Interaction of the subducting slab with mantle flow, in review.

Acknowledgements: This work was funded by NSF EAR-0745934 and EAR-0643077. The work was facilitated by the IRIS-PASSCAL program through the loan of seismic equipment, USArray for providing data and the IRIS-DMS for delivering it.

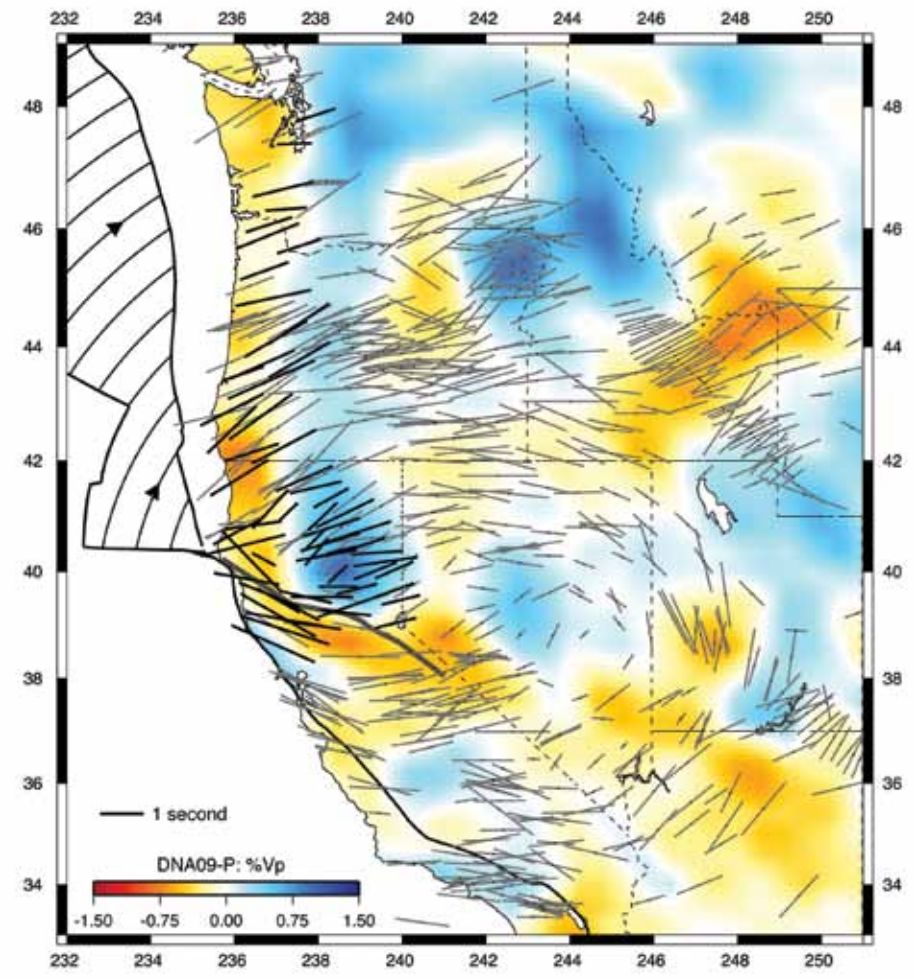

Figure. Regional splitting pattern overlain on the vertically averaged upper mantle velocity anomaly. Our splitting results are shown in black and those of previous studies are in grey (Long et al., 2009; Wang et al., 2008; West et al., 2009; Zandt and Humphreys, 2008 and references therein). The splitting pattern is shown to be uniform trench-normal throughout Cascadia. The velocity anomaly shown is a vertical average of the velocity anomaly from the DNA09 P-wave model over the 100-400km depth range (Obrebski et al., 2010). The slab is imaged as the north-south high velocity feature. The splitting measurements rotate around the southern end of the slab. Curved black lines on the G-JdF plate represent the direction of its absolute plate motion.

Seismic Anisotropy under Central Alaska from SKS Splitting Observations

Douglas Christensen *(Geophysical Institute, University of Alaska Fairbanks),* **Geoffrey Abers** *(Lamont Doherty Earth Observatory of Columbia University)*

Seismic anisotropy under central Alaska is studied using shear wave splitting observations of SKS waves recorded on the Broadband Experiment Across the Alaska Range (BEAAR), 1999-2001. Splitting results can be divided into two distinct regions separated by the 70 km contour of the subducting Pacific plate. Waves that travel through the thicker mantle wedge show fast directions that are parallel to the strike of the slab. These slab-parallel directions appear to indicate along-strike flow in the mantle wedge, and splitting delay times increase with path length in the mantle wedge suggesting anisotropy of 7.9 ± 0.9 percent. The region of along-strike flow corresponds to high seismic attenuation and hence high temperatures. Along-strike flow here may be driven by secular shallowing of the slab driven by subduction of buoyant Yakutat-terrane crust, or by torroidal flow around the east end of the Aleutian slab. Waves traveling southeast of the 70 km contour sample the Pacific plate and the nose of the mantle wedge; they show fast directions that parallel the direction of plate motion. These fast directions are most likely due to flow under the subducting Pacific plate and/or anisotropy within the subducting Pacific lithosphere. The high splitting delay times (0.8-1.7 sec) associated with these convergence-parallel directions cannot be produced in the mantle wedge, which is 10-30 km thick here. Thus, anisotropy shows a sharp 90° change in fabric associated with the onset of high-temperature wedge flow. Results have been published in Christensen and Abers [*2010*].

References

Christensen, D.H., G.A. Abers (2010). Seismic anisotropy under Alaska from SKS splitting observations, *J. Geophys. Res., 115*, B04315, doi:10.1029/2009JB006712.

Acknowledgements: The BEAAR deployment benefited from contributions by many people, including contributions from the Alaska Earthquake Information Center, the IRIS-PASSCAL Instrument Center, and a large number of students who helped with the deployment and its analysis. This work supported by National Science Foundation grant EAR-9725168.

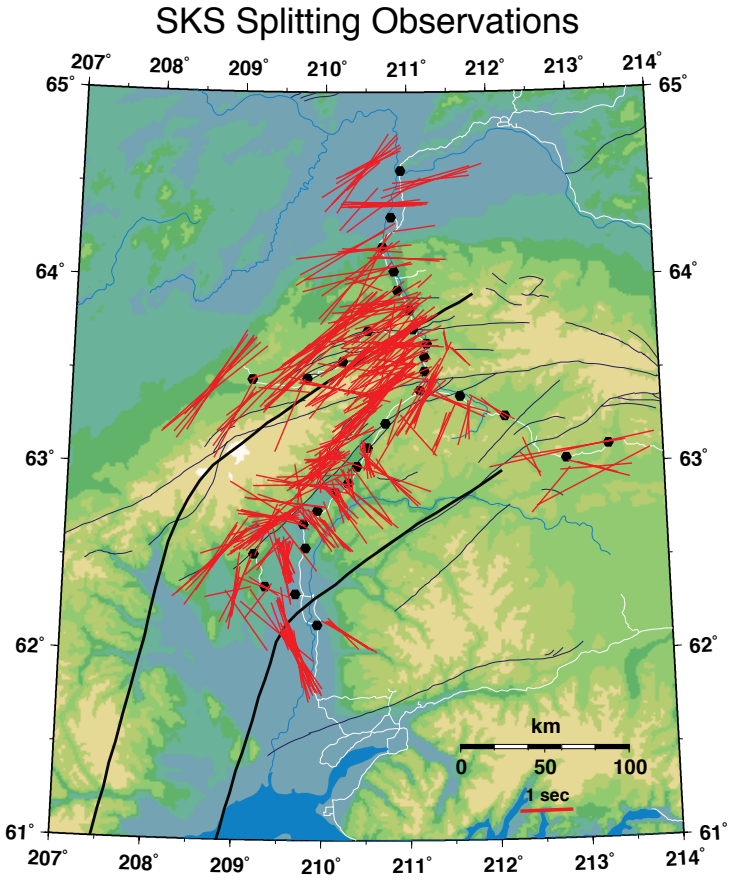

Figure. Compilation of SKS splitting results. Each measurement is plotted as a red line parallel to the fast direction, with length proportional to the delay time. The observations are plotted at the 100 km depth projection of the ray, in order to demonstrate the back- azimuthal pattern. Locations of seismic stations from the BEAAR experiment are shown by the black dots. Thick black lines show contours to slab seismicity (50 and 100 km). Thin dark lines show active faults, and white lines show roads.

Attenuation and Anisotropy in the Northern Apennines, Italy

J. Park *(Yale University),* **D. Piccinini** *(INGV),* **I. Bianchi** *(INGV),* **M. Di Bona** *(INGV),* **F. P. Lucente** *(INGV),* **N. Piana Agostinetti** *(INGV),* **V. Levin** *(Rutgers University)*

The Northern Apennines of Italy is marked by continental convergence and a downgoing slab derived from the Adriatic microplate. Seismicity is sparse, shallow, and lacks historical M>7.5 shallow thrust events. Has subduction ceased? Geodesy indicates near-zero present-day convergence, and fission-track thermochronology suggests that vertical uplift has superseded fold-and-thrust tectonics since 5-10 Ma in a large segment of the orogen. The RETREAT project (REtreating-TRench Extension and Accretion Tectonics) explored this region with broadband seismometers from the IRIS PASSCAL program, the Czech Academy of Sciences and the Istituto Nazionale de Geofisica e Vulcanologia (INGV).

Attenuation estimates from both S and P waves reveal high attenuation on the "back-arc" side of the Apennines orogen (Figure 1), near coastal geothermal areas but extending inland. Pleistocene volcanism is found here, but there is no present-day subduction-arc activity. A crude inversion of t-star (Δt^*) suggests comparable Q values (<100) for both S and P waves in the mantle wedge, suggesting either abundant partial melt or strongly hydrated rocks. Contemporary volcanism is scarce, so we favor hydration derived from the Apennines slab.

Receiver functions (RFs) projected onto a cross-orogen transect highlight how much Apennines subduction differs from typical subduction of oceanic lithosphere. The top of the Apennines slab is a double interface that dips from 40-km depth beneath the orogen crest to 80-km depth near the Tyrrhenian coast of Tuscany (Figure 2). Using constant and harmonic RF stacks with back azimuth, we conclude that a strongly anisotropic layer (~10-km thickness) lies atop the Apennines slab. Evidence for a velocity inversion is lacking, consistent with an eclogitic composition or the "ultra-high-pressure" (UHP) lithologies that are exhumed in the nearby (older) Alpine orogen. Because the top of the slab does not extend upward from 40-km depth, and strong anisotropy occurs deeper than typical for Japan or Cascadia, we hypothesize that Apennines "subduction" has entrained and sheared the lower continental crust of the Adriatic microplate.

If mantle-wedge attenuation suggests water or partial melt, where do these come from? Subducted lower continental crust should contain less water than oceanic crust, but need not be totally dry. Weaker crustal hydration might help explain weaker Tuscan volcanism. Some clues fit together, but our story still has gaps!

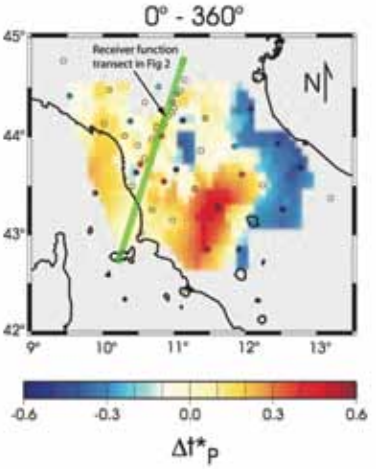

Figure 1. Spatial distribution of Δt^*, an estimate for seismic attenuation based on the high-frequency rolloff of P body-wave spectra recorded in Central Italy by the RETREAT deployment. The map interpolates the average Δt^* estimates at each station. The average Δt^* values at stations are shown as colored circles. The green line locates the receiver-function transect of Figure 2.

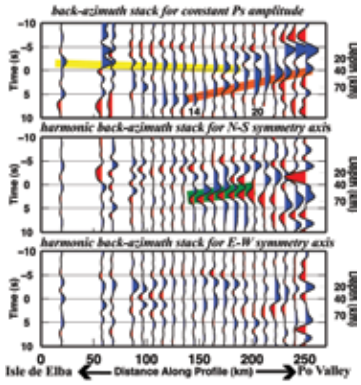

Figure 2. RF data-set along cross-Apennines transect, stacked with constant, $\cos\phi$ (N-S) and $\sin\phi$ (E-W) back-azimuth weighting. Blue and red pulses indicate positive and negative Ps converted-wave amplitudes, respectively. Colored stripes highlight the main features: yellow for the Tyrrhenian Moho, orange for Adriatic Moho and green for the layer atop the Apennines slab. The Y-axis shows RF delay time (depth), in s (km) referenced to a stacking-migration target at 40-km depth, so that pulses at negative delay time correspond to interfaces shallower than 40 km.

References

Piccinini, D., M. Di Bona, F. P. Lucente, V. Levin and J. Park, Seismic Attenuation and mantle wedge temperature in the Northern Apennines subduction zone (Italy) from teleseismic body waves, accepted by *J. Geophys. Res., 2010.*

Bianchi, I., J. Park, N. Piana Agostinetti,V. Levin, Mapping seismic anisotropy using harmonic decomposition of receiver functions: an application to Northern Apennines, Italy, submitted to *J. Geophys. Res., 2010.*

Thomson, S. N., M. T. Brandon, P. W. Reiners, M. Zattin, P. J. Isaacson, and M. L. Balestrieri, Thermochronologic evidence for orogen-parallel variability in wedge kinematics during extending convergent orogenesis of the northern Apennines, italy, *GSA Bulletin, 122* (7/8), 11601179, 2010.

Acknowledgements: JP and VL were supported by NSF grant EAR-0208652. IB is supported by DPC-S1 UR02.02. NPA was supported by project Airplane (funded by the Italian Ministry of Research, Project RBPR05B2ZJ 003). Other researchers supported by INGV

Stress-Induced Upper Crustal Anisotropy in Southern California

Zhaohui Yang *(University of Colorado at Boulder),* **Anne Sheehan** *(University of Colorado at Boulder)*

We use an automated method to analyze shear-wave splitting from local earthquakes recorded by the Southern California Seismic Network (SCSN) between 2000 and 2005. The observed fast directions of upper-crustal anisotropy are mostly consistent with the direction of maximum horizontal compression σHmax, suggesting that anisotropy in the top 20 km of crust under southern California is stress-induced anisotropy. At some stations, fast directions are aligned with the trends of regional faulting and local alignment of anisotropic bedrock. Delay times range widely from 0.02 s to 0.15 s. These upper-crustal anisotropy observations, together with previous studies of SKS shear-wave splitting and receiver functions, show different mechanisms of anisotropy at different depths under southern California. Anisotropy in the upper crust and upper mantle appears to be in response to the current horizontal maximum compression σHmax, whereas lower crustal anisotropy may be caused by the anisotropic schist accreted during the subduction of Farallon plate, which is frozen in the lower crust. We also explore possible temporal variations in upper-crustal anisotropy associated with pre-earthquake stress changes or stress changes excited by surface waves of great earthquakes. However, we do not observe any clear temporal variations in fast directions or time delays.

References

Yang, Z., A. F. Sheehan, and P. Shearer, Stress-Induced Upper Crustal Anisotropy in Southern California, submitted to *J. Geophys. Res.*, 2010.

Gripp, A.E., and R.G. Gordon (1990), Current Plate Velocities Relative to the Hotspots Incorporating the NUVEL-1 Global Plate Motion Model, *Geophysical Research Letters, 17*(8), 1109-1112.

McQuarrie, N., and B.P. Wernicke (2005), An animated tectonic reconstruction of southwestern North America since 36 Ma, *Geosphere, 1*(3), 147-172.

Porter, R., G. Zandt, and N. McQuarrie (2010), Pervasive lower crustal seismic anisotropy in southenr California: Evidence for underplated schists, Submitted.

Acknowledgements: The data used in this study were made available by the Southern California Seismic Network, and we are grateful to E. Hauksson for his assistance in creating a waveform database. We thank J. Polet for providing a digital table of his Southern California SKS measurements, R. Porter for sharing a preprint of his Southern California receiver function work, and M. Savage for her comments. The figures were made using GMT software by P. Wessel and W. Smith. AFS gratefully acknowledges a Green Foundation Fellowship that supported her sabbatical at IGPP/SIO. This work is supported by SCEC project 08129 and NSF EAR grant 0409835, and by U.S. Geological Survey award number G09AP00052.

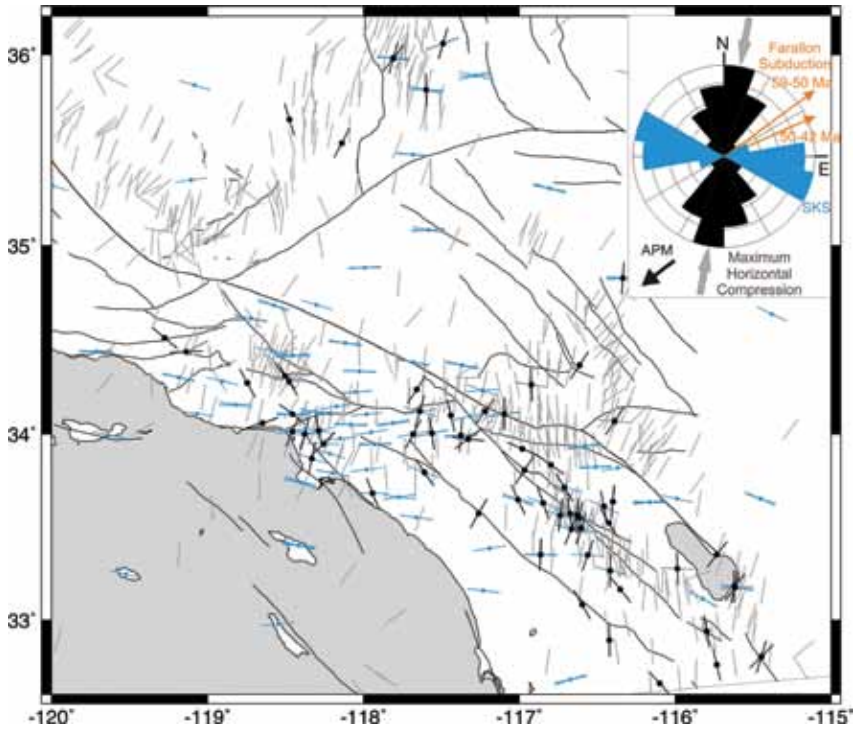

Map showing average fast directions of upper-crustal anisotropy (solid bars), SKS shear-wave splitting anisotropy (blue bars), and stress vectors (gray bars). The inset rose diagram summarizes the trends of anisotropies from three different depths in the area of the map: Top 20 km of crust (black), the fast directions are consistent with the direction of current maximum horizontal compression (gray arrows); and upper mantle, SKS shear-wave splitting show a preferred fast direction orienting E-W (blue bars). The orange arrows are Farallon plate subduction directions during 59-42 Ma [McQuarrie and Wernicke, 2005]. The trends of anisotropy in the lower crust (below 20 km), after rotation back to 36 Ma [Porter et al., 2010], are consistent with the Farallon subduction directions during 59-42 Ma. The black arrow indicates the absolute plate motion (APM) of the North American plate [Gripp and Gordon, 1990].

USArray Observations of Quasi-Love Surface-Wave Scattering: Orienting Anisotropy in the Cascadia Plate Boundary

Duayne M. Rieger *(Yale University),* **Jeffrey Park** *(Yale University)*

Love surface waves scatter to elliptically-polarized Rayleigh waves when they encounter regional concentrations of anisotropy. These scattered waves, called Quasi-Love, or QL waves, are useful for detecting shear near plate boundaries, where the strong lithosphere deforms mantle asthenosphere surrounding the plates as lithosphere sinks at oceanic trenches, spreads at rift zones, or crumples where continents collide. QL waves can be observed on individual seismograms, and complement other analyses of seismic data.

We found QL scattering in and around the Cascadia subduction zone in seismic data from the land-based USArray, a component of Earthscope. The dense sampling and broadband response of the USArray transportable array allows us to detect and correlate the scattering of 100-sec surface waves at closely-spaced locations. We demonstrate that a pattern of Love-to-Rayleigh scattering seen across the western USA (Figure 1) can be related to an anisotropic gradient that scatters energy from a location offshore the Juan de Fuca trench. The azimuthal variation of scattering (Figure 2) indicates an alignment of the anisotropic symmetry axis with present-day plate motion. We reject slab rollback as the causative process and suggest the entrainment of asthenosphere with the overriding Juan de Fuca and Gorda plates.

The strong coherence of scattered waveforms between neighboring stations in USArray suggests that such long-period surface wave motion can detect lateral gradients of anisotropy beneath Cascadia and, potentially, the rest of the western USA. Detailed reconstruction of anisotropy could be tried by grouping great-circle paths that intersect at a distribution of possible scattering points throughout the subduction system in an effort to further constrain its mantle dynamics.

References

Rieger, D. M., and J. Park, USArray observations of quasi-Love surface wave scattering: Orienting anisotropy in the Cascadia plate boundary, *J. Geophys. Res., 115*, B05306, doi:10.1029/2009JB006754, 2010.

Acknowledgements: This work was supported by NSF Grant EAR-0208652.

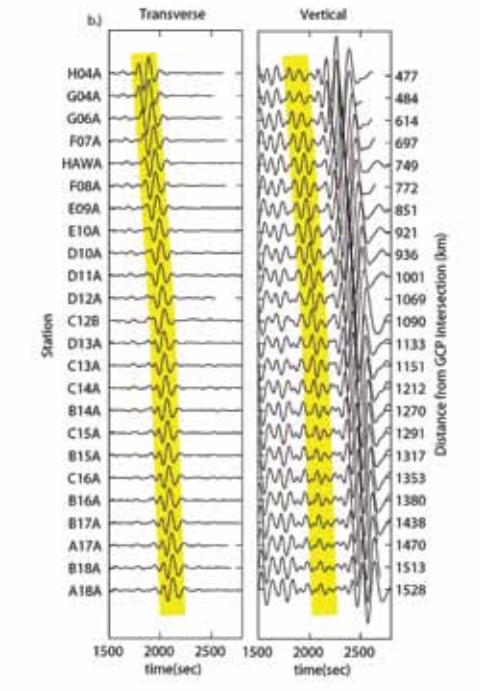

Figure 1. USArray record sweeps along the great-circle path for the Loyalty Islands 4/9/2008 (Ms=7.3) earthquake. The Love wave on the transverse components and the QL wave on the vertical-components are highlighted. The station each record was recorded at is along the left Y-axis and the distance from the great-circle path intersection at 42.5°N 127.5°W is along the right Y-axis. The variation in amplitude of the QL wave with distance appears to be accompanied by the gradual modulation of the waveform. This can be characteristic of an interference pattern that would suggest a more complex anisotropic structure than a single point scatterer with a horizontal axis of symmetry.

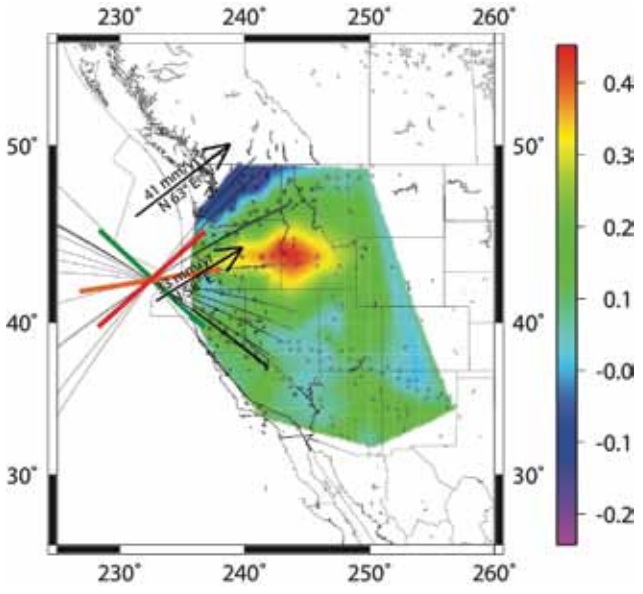

Figure 2. Spatial plot of the QL/Love amplitude ratio at 100s-lowpass, normalized by the Love-wave amplitude along each great-circle path. The black circles are station locations. The red line is the zero-scattering azimuth, parallel to our proposed anisotropic axis of symmetry. This orientation correlates well with the hotspot referenced Juan de Fuca plate motion, illustrated by the black arrows, and regional shear-wave splitting measurements. The orange line represents an oblique orientation to the anisotropic axis of symmetry suggested by the data. The largest QL/Love amplitude ratios are measured close to this orientation which is encouraging. The green line is the azimuth normal to the zero-scattering azimuth.

Tau-p Depropagation of Five Regional Earthquakes Recorded by the Earthscope Usarray to Constrain the 410-km Discontinuity Velocity Gradient

Josh Stachnik *(Univ. Wyoming),* **Ken Dueker** *(Univ. Wyoming)*

Seismic recordings by the EarthScope USArray from three Queen Charlotte region earthquakes and two southern Baja Mexico earthquakes are transformed to the Tau-P domain and the post-critical P-wave branches are picked. Five one dimensional velocity models are formed via depropagation of the picked Tau-P curves. All five models are in good agreement with the ak135 reference model velocity gradients both above and below the 410 km discontinuity and the observed 410 P-wave velocity step is within 10% of ak135. The 410 velocity gradients for three of the models are sharp (<5 km) and for two of the models are gradational (25-30 km). The maximum 410 velocity gradient is found at depths of 392-443 km. From this small sample set, no correlation between the 410 widths and depths is observed. All five models have 2-4% higher velocities in the 50-100 km depth interval above the 660 km discontinuity which may manifest stagnated slabs. The two models with a large 410 gradient can be explained by up to 500 ppm by mass hydration levels.

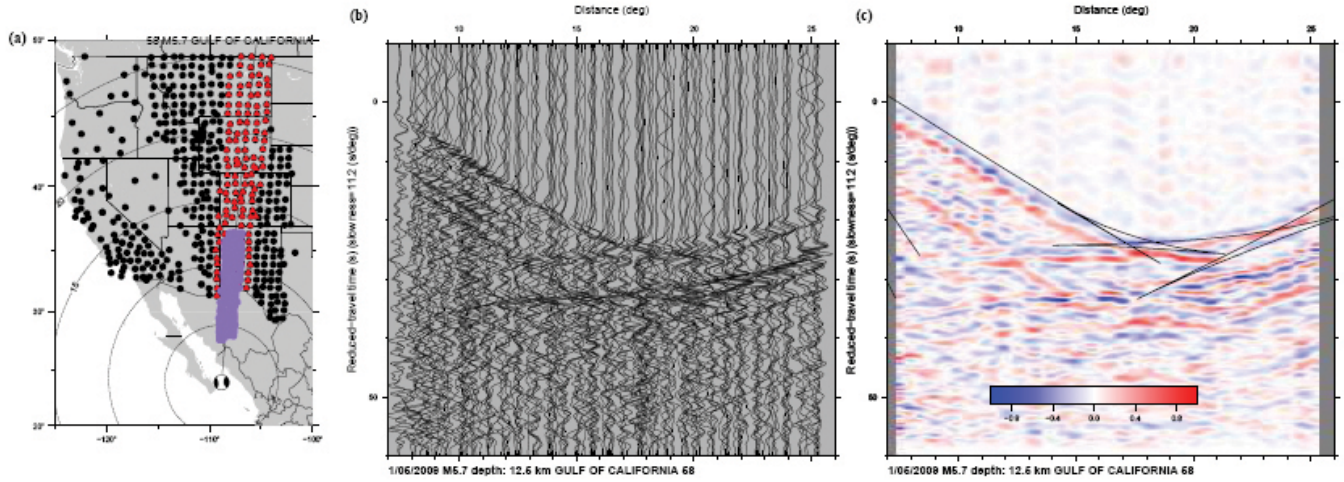

Baja California earthquake P-wave recorded by the Transportable array.

Steep Reflections from the Earth's Core Reveal Small-Scale Heterogeneity in the Upper Mantle

Hrvoje Tkalčić *(The Australian National University),* **Vernon F. Cormier** *(University of Connecticut),* **Brian L. N. Kennett** *(The Australian National University),* **Kuang He** *(University of Connecticut)*

We investigate arrivals of seismic phases reflected from the core-mantle boundary (PcP waves) and those reflected from the inner-core boundary (PKiKP waves) at subcritical angles, with the goal of measuring their amplitude ratios [Tkalčić et al., 2010]. This adds invaluable data points required to study the density jump across the inner-core boundary (ICB). One nuclear explosion and one earthquake, both with favourable focal mechanisms are identified as sources that produce an excellent and abundant record of arrivals of both PcP and PKiKP waves at multiple stations. There is only a limited number of detections of both types of waves on the same seismogram, while more frequently, either one or another of the two phases is detected. Thus, for those cases where at least one phase is above a detectable level, we observe a highly significant negative correlation (anti-correlation) of phase appearances on seismograms, where PcP and PKiKP phase-detections are treated as dichotomous, categorical random variables that can take values detected or undetected. The fact that similar anti-correlation is observed for both explosive and tectonic sources makes less likely the possibility that source effects or a specific near source structure is responsible for this phenomenon. Although laterally varying structure near the core-mantle boundary (CMB) can account for the magnitude of observed fluctuations in the amplitude ratio of PKiKP to PcP, the Fresnel volumes surrounding their ray paths are well separated at the CMB at the frequencies of interest. This separation excludes the possibility that complex structure at or near the CMB is the dominant effect responsible for the observed anti-correlation. We demonstrate that the interaction of the wave-field with near-receiver heterogeneities is an important additional source of amplitude fluctuations across arrays of stations, and the likely cause of the anti-correlation pattern. The combined effects of heterogeneities near the surface and the CMB have a profound impact on the estimates of the PKiKP/PcP amplitude ratios and the subsequent estimates of the density jump at the ICB.

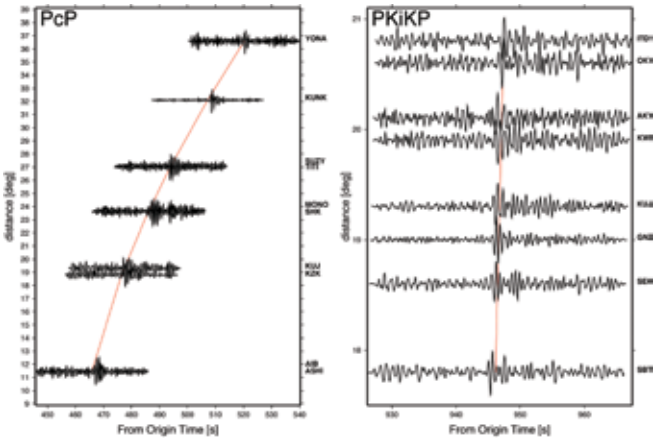

Selected PcP (left) and PKiKP (right) observations for the mb=5.7 earthquake located northwest of Kuril Islands and dated 02/07/2001. The broadband velocigrams are band-pass filtered between 1 and 3 Hz. The theoretical travel time prediction of PcP and PKiKP from the ak135 model is shown by solid line. The scales for PcP and PKiKP records are different to account for the space and changing slowness across the range of selected stations.

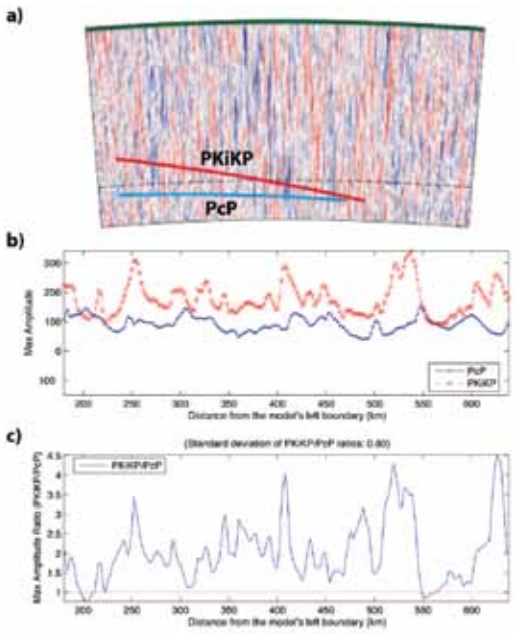

(a) Wavefronts of PcP (blue) and PKiKP (red) in the range 16 to 25 degrees incident on an earth model perturbed by statistically described heterogeneity in the crust and upper mantle beneath a receiver array. A 5 per cent RMS perturbation in P velocity is assumed with an exponential autocorrelation. (b) Predicted amplitude fluctuations of PKiKP and PcP at an array of surface receivers measured from bandpassed seismograms of particle velocity synthesized by a numerical pseudospectral method in anisotropic distribution of scale lengths with a vertical cutoff at 100 km and horizontal cutoff at 2 km. (c) The PKiKP/PcP ratio (includes only the effects of heterogeneity beneath the receiver array).

References

Tkalčić H., V.F. Cormier, B.L.N. Kennett and K. He (2010). Steep reflections from the Earth's core reveal small-scale heterogeneity in the upper mantle, *Phys. Earth Planet. Int., 178*, 80-91, DOI:10.1016/j.pepi.2009.08.004.

Acknowledgements: We would like to thank IRIS DMC for efficiently archiving and distributing continuous waveform data. V.F. Cormier's participation was supported by a grant from the Vice Chancellor of the Australian National University funding travel as a Visiting Fellow, and by the National Science Foundation under grant EAR 07-38492.

Mapping the Upper Mantle with the Spectral Element Method

Ved Lekic *(Berkeley Seismological Laboratory),* **Barbara Romanowicz** *(Berkeley Seismological Laboratory)*

Over the past quarter century, ray- and perturbation-theoretical techniques have enabled tomographers to map the large scale structure of the Earth's mantle. However, the approximations underpinning these techniques prevent them from accurately predicting the effects of sharp or strong heterogeneities [e.g. Wang and Dahlen, 1995], as well as those arising from crustal structures [e.g. Lekic et al., 2010]. As a result, the images obtained are incomplete and contaminated, and amplitudes of observed anomalies are poorly constrained. Yet, it is precisely the amplitude and sharpness of seismic anomalies that are needed to decipher the temperature and composition (T/C) variations that underlie them. Mapping T/C variations in the mantle is crucial for understanding how these control mantle convection, and is one of the grand challenges facing Earth Science.

We have replaced traditional forward modeling approximations by full waveforms computed using the coupled Spectral Element Method [CSEM: Capdeville et al. 2003], and have developed a new model of upper mantle 3D shear velocity and radial anisotropy variations. CSEM is a fully numerical technique that makes possible very accurate simulations of wave propagation through complex 3D Earth structures. Our model – SEMum – confirms the long wavelength structures imaged by previous efforts, but is characterized by stronger amplitudes, which implicate composition in explaining the observed heterogeneities. Furthermore, SEMum reveals structures not clearly imaged by earlier global studies. Perhaps the most intriguing of these is the pattern of low velocities beneath the Pacific Ocean, which might be indicative of ongoing small-scale convection.

Regional comparisons demonstrate that SEMum can match the resolution of smaller-scale studies, and replicate these throughout the globe. This is due to both the improved modeling technique and the wealth of information contained in – and successfully extracted from – high-fidelity recordings of complete seismic waveforms provided by the Global Seismographic Network (GSN), its international partners and regional broadband networks.

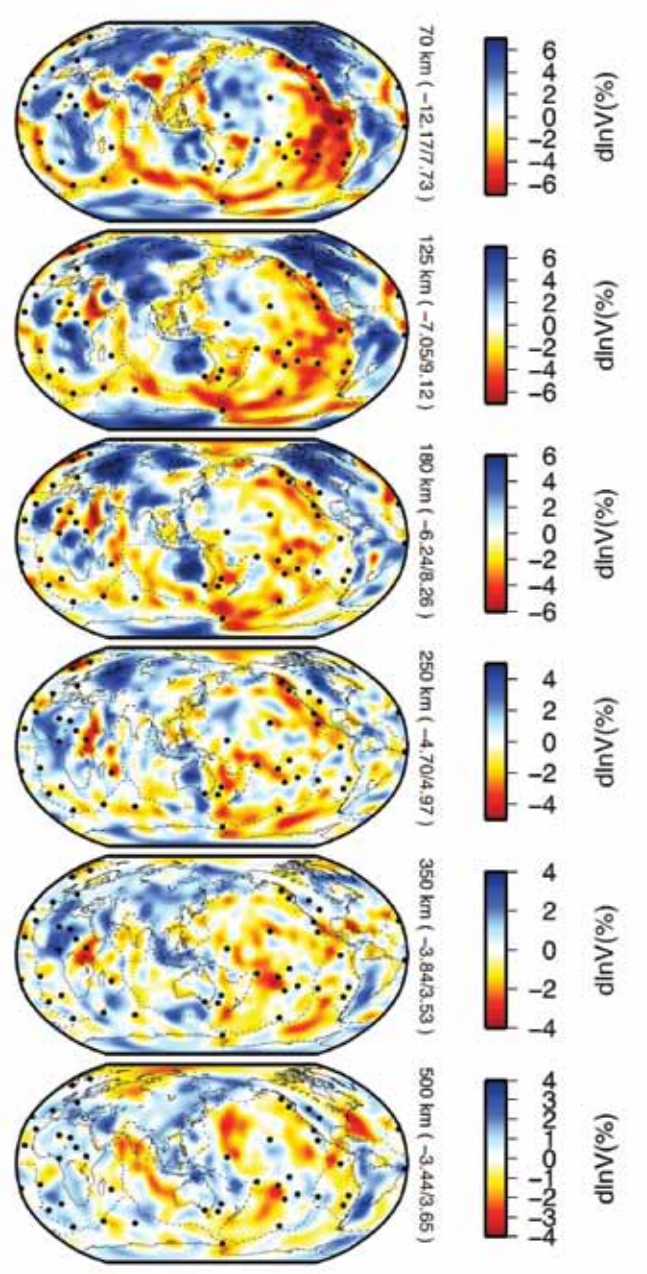

Maps of the Voigt average shear wave-speed variations with respect to the average velocity at each depth. Note that the limits of color scales change with depth and that the colors saturate in certain regions. Black circles indicate locations of hotspots.

References

Capdeville, Y., Chaljub, E., Vilotte, J. P., & Montagner, J. P., 2003. Coupling the spectral element method with a modal solution for elastic wave propagation in global earth models, *Geophys. J. Int., 152*, 34–67.

Lekic, V., Panning, M. & B. Romanowicz, 2010. A simple method for improving crustal corrections in waveform tomography, *Geophys. J. Int.*,

Wang, Z. & Dahlen, F., 1995. Validity of surface-wave ray theory on a laterally heterogeneous earth, *Geophys. J. Int., 123*(3), 757–773.

Acknowledgements: This study was supported by NSF EAR-0738284 to BR and an NSF Graduate Research Fellowship to VL.

Adjoint Tomography for the Middle East

Daniel Peter *(Princeton University),* **Brian Savage** *(University of Rhode Island),* **Arthur Rodgers** *(Lawrence Livermore National Laboratory),* **Jeroen Tromp** *(Princeton University)*

We evaluate 3D models of the Middle East by computing full waveforms for a set of regional earthquakes [Savage et al., 2009]. We measure traveltime shifts between observed broadband data obtained from IRIS and synthetic seismograms for distinct seismic phases within selected time windows using a recently developed, automated measurement algorithm [Maggi et al., 2009]. Based on the measurements for our study region, we selected a best model to feature as the starting seismic model for a fully numerical 3D seismic tomography approach.

In order to improve the initial 3D seismic model, the sensitivity to seismic structure of the traveltime measurements for all available, regional network recordings is computed. As this represents a computationally very intensive task, we take advantage of an adjoint method combined with spectral-element simulations [Tromp et al., 2005]. We calculate such sensitivity kernels for all seismic events and regional records and use them in a conjugate-gradient approach to iteratively update the 3D seismic model. This will lead to various improvements of the initial seismic structure in order to better explain regional seismic waveforms in the Middle East for nuclear monitoring.

References

Maggi, A., C. Tape, M. Chen, D. Chao and J. Tromp, 2009. An Automated time-window selection algorithm for seismic tomography, *Geophys. J. Int., 178*, 257–281.

Savage, B., D. Peter, B. Covellone, A. Rodgers and J. Tromp, 2009. Progress towards next generation, waveform based three-dimensional models and metrics to improve nuclear explosion monitoring in the Middle East, Proceedings of the 31th Monitoring Research Review of Ground-Based Nuclear Explosion Monitoring Technologies, LLNL-PROC-414451, 9 pages.

Tromp, J., C. Tape and Q. Y. Liu, 2005. Seismic tomography, adjoint methods, time reversal and banana-doughnut kernels, *Geophys. J. Int., 160*, 195–216.

Acknowledgements: This research is sponsored by Air Force Research Laboratory and by National Nuclear Security Administration, Contract No. FA8718-08-C-0009.

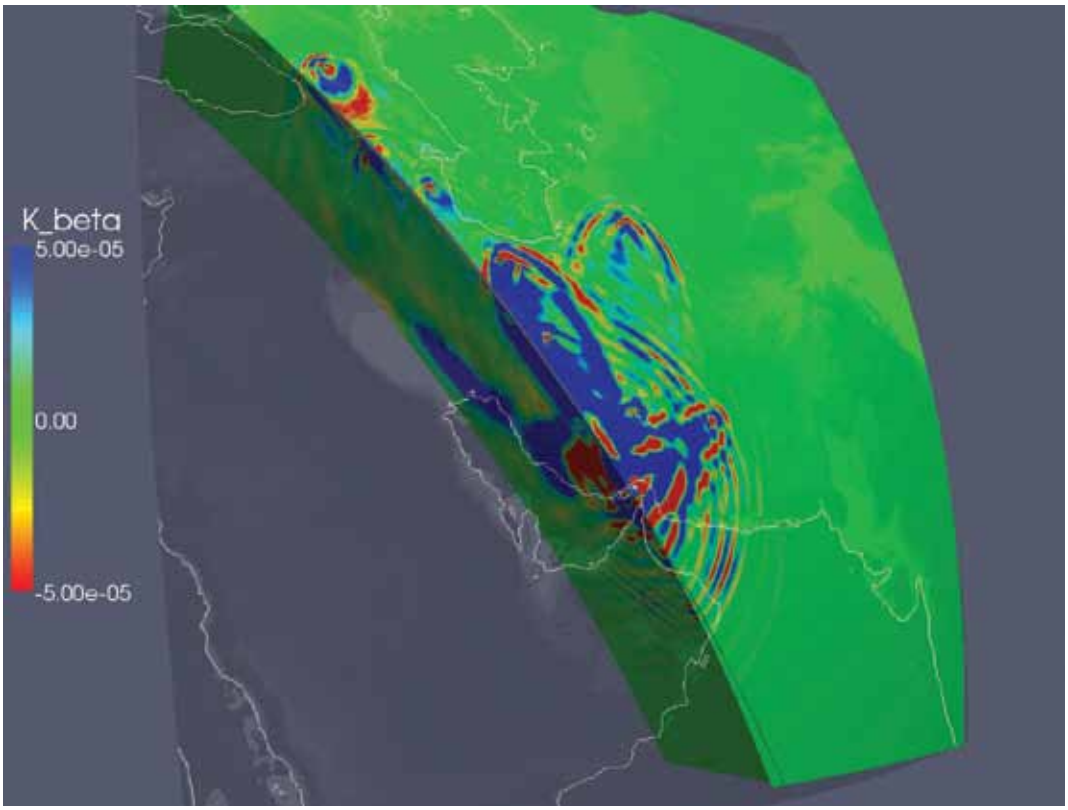

Shear-velocity event kernel for an earthquake in the strait of Hormuz recorded 2005 by several regional stations. Sensitivities are shown on a horizontal cross-section at 5 km depth and a vertical cross-section through the source and a station location down to a depth of 670 km.

Upper Mantle Structure of Southern Africa from Rayleigh Wave Tomography with 2-D Sensitivity Kernels

Aibing Li *(University of Houston)*

A 3-D shear wave model in southern Africa has been developed from fundamental mode Rayleigh wave phase velocities, which are computed at the period range of 20 to 167 s using a two-plane-wave tomography method. 2-D sensitivity kernels are applied in the phase velocity inversion to account for finite-frequency effects, which are significant at periods greater than 100 s. The new model (Figure 1 and 2) confirms the first-order observations found by Li and Burke [2006], a fast mantle lid extending to ~180 km depth and being underlain by a low velocity zone. One new feature in the model is the vertical alignment of a shallow low velocity anomaly with a deep high velocity anomaly at the western Bushveld province. The alignment makes more sense for interpreting the slow as the result of high iron content from the Bushveld intrusion and the fast as a more depleted residual mantle. A low velocity channel at the depths of 220-310 km from the southern end of the Kheiss belt to the northwest of the Kaapvaal craton is also imaged for the first time. It suggests that the hot asthenosphere outside the craton could migrate into the craton area through a weak channel and thermally erode the cratonic lithosphere from below. In addition, low velocity anomalies from 100 to 180 km agree well with the localities of kimberlites erupted at 65-104 Ma in the Kaapvaal craton, providing additional evidence for the depth extent of mantle xenoliths.

References

Li, A., and K. Burke (2006), Upper mantle structure of southern Africa from Rayleigh wave tomography, *J. Geophys. Res., 111*, B10303, doi:10.1029/2006JB004321.

Jelsma, H. A., M. J. De Wit, C. Thiart, P. H. Dirks, G. Viola, I. J. Basson, and E. Anckar (2004), Preferential distribution along transcontinental corridors of kimberlites and related rocks of Southern Africa, *S. Afr. J. Geol., 107,* 301-324.

Yang, Y., and D.W. Forsyth (2006), Regional tomographic inversion of amplitude and phase of Rayleigh waves with 2-D sensitivity kernels, *Geophys. J. Int., 166*, 1148-1160.

Acknowledgements: Data used in this study are from the IRIS DMC. Yingjie Yang kindly provided the inversion codes with 2-D sensitivity kernels. This research is supported by NSF grant EAR-0645503.

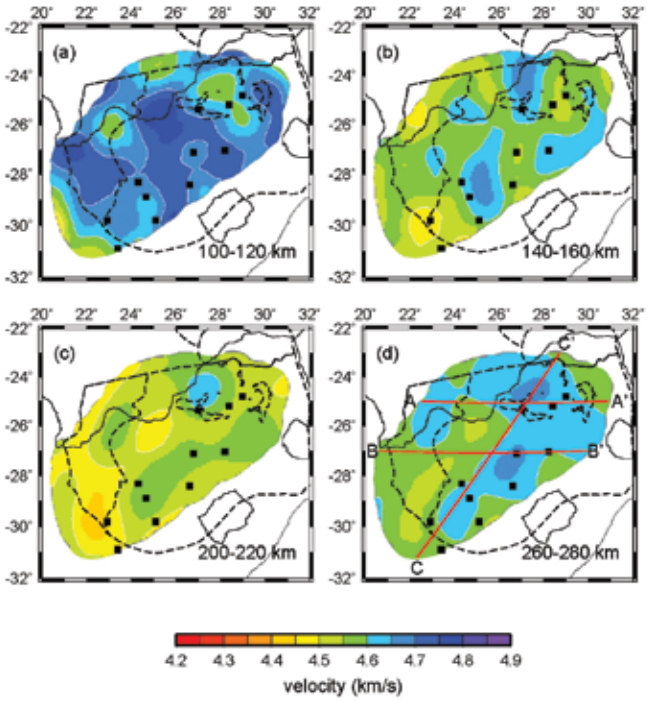

Figure 1. Shear-wave velocity variations at 4 depth ranges. Black squares delineate the sites of kimberlites at 104 to 65 Ma based on Fig. 7c in Jelsma et al. (2004), which show a better correlation with slow regions in shallow upper mantle (a and b). Red lines show the locations of profiles in Figure. 2. Dashed lines are tectonic boundaries.

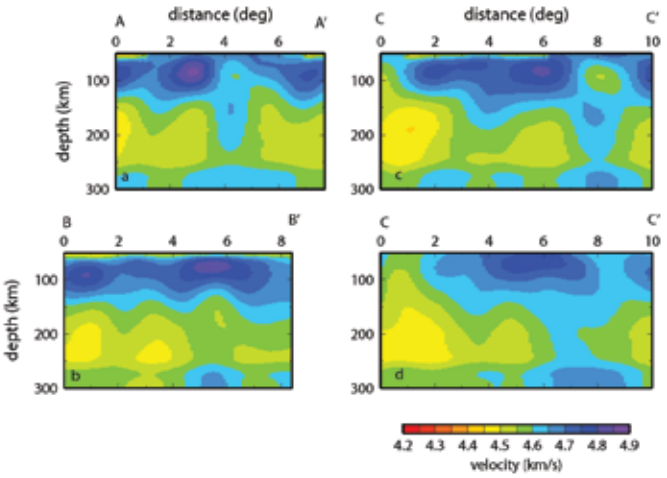

Figure 2. Shear-wave velocity profiles at the depths of 50-300 km. A relative low velocity zone appears on all profiles at roughly 160-260 km depths. (a-c) Velocity profiles of AA', BB' and CC' from this study. (d) Shear-wave velocity profile along CC' from the study of Li & Burke (2006). Note the good alignment of the shallow, slow anomaly and the deep, fast anomaly at the distance of 8 degree in (c), which is not well imaged in (d).

A Low Velocity Zone Atop the Transition Zone in Northwestern Canada

Andrew J. Schaeffer *(The University of British Columbia, now at Dublin Institute for Advanced Studies),* **Michael G. Bostock** *(University of British Columbia)*

Seismic studies over the past decade have identified a S-wave low-velocity zone (LVZ) above the transition zone at various locations around the globe. This layer is hypothesized to be a lens of dense, hydrous silicate melt ponding atop the 410 km discontinuity, beneath the silicate melt-density crossover theorized to exist within the upper mantle [*Bercovici and Karato, 2003*]. We have assembled a P- and S-receiver function (PRF and SRF, respectively) dataset from the CNSN Yellowknife Array (YKA), the CANOE array (obtained from the IRIS DMC), and the POLARIS-Slave array, in order to quantify the physical properties and geographical extent of the layer in Northwestern Canada.

In order to compute the Poisson's ratio, an important discriminant of possible composition and/or fluid content, we generated a suite of 1-D velocity models based on IASP91, but with varying thicknesses and velocity ratios for a hypothetical layer above the 410 km discontinuity. Through utilization of differential times of forward- and back-scattered arrivals from the LVZ bounding interfaces, the Poisson's ratio and thickness is isolated indepedently from the overlying column of material [*Audet et al, 2009*]. From these models, we computed moveout curves over the range of slowness for the main scattering modes (Pds and Ppds) observed in the YKA data. A grid search was performed over the model space of interval thickness and Poisson's ratio to obtain an estimate of the model that best accounts for the moveouts represented in the data. In addition, we performed a linearized inversion of transmission coefficient amplitudes to estimate the shear velocity contrast at the bounding interfaces of the LVZ. Results indicate a LVZ of thickness ~36 km with a Poisson's ratio of 0.42, and shear velocity contrasts of minus and plus 7.5% into and out of the LVZ, respectively. Bootstrap resampling error estimates for thickness and Poisson's ratio are ±3km and ±0.011. In combination, our results require an increase in compressional velocity associated with the shear velocity drop into the LVZ. The Poisson's ratio lies well above the IASP91 average of ~0.29-0.3 for this depth range and favours the presence of high melt or fluid fractions.

Geographic profiles of PRFs and SRFs 1-D migrated to depth from CANOE and POLARIS-Slave arrays reveal 410 km and 660 km discontinuities at nominal depths with little variation in transition zone thickness. PRF results from the Slave craton indicate a potential LVZ beneath many stations at an average nominal depth of ~340 km, highlighted by events from the northwest. The CANOE array SRF profile images an emergent LVZ beginning at ~280 km depth dipping eastwards to 310 km approaching YKA.

Reference

Audet, P., Bostock, M., Christensen, N. I., and Peacock, S. M. (2009). Seismic evidence for over-pressured subducted oceanic crust and megathrust fault sealing. *Nature, 457*, 76-78.

Bercovici, D. and Karato, S. (2003). Whole-mantle convection and the transition-zone water filter. *Nature, 425*(6953), 39-44.

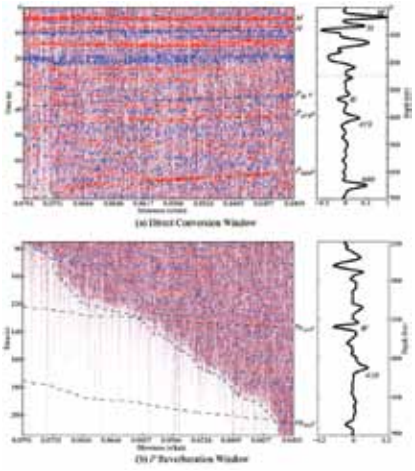

Figure 1: Radial PRFs for the Northwest corridor (274 - 313) YKA dataset. Top panel is windowed for direct conversions converting between the transition zone and the surface, whereas bottom panel is windowed for back-scattered reverberations. The relevant features are indicated in 1D mantle reectivity pro les on the right hand side. The phases utilized include Pds and Ppds.

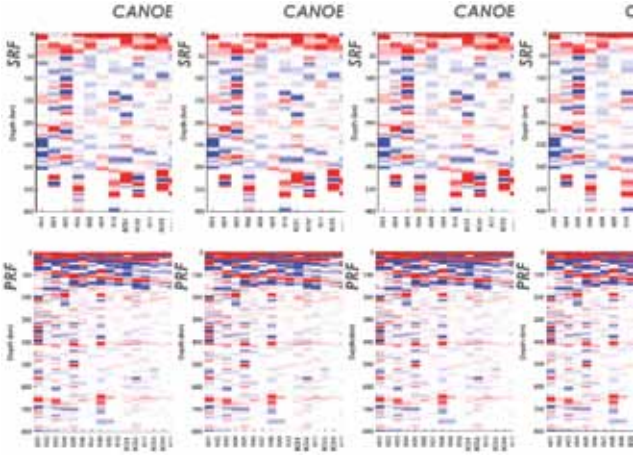

Figure 2: P and SRF pro les for the CANOE and POLARIS-Slave array datasets computing using analogous techniques to that of YKA. Top panels are SRFS and bottom panels are PRFs for CANOE (left) and POLARIS-Slave (right). The LVZ can be seen clearly in the CANOE SRFs at approximately 280 km depth beginning at station A11 and dipping gently eastwards. The Slave PRF image also clearly illustrates a potential LVZ at 330km depth in the Northern stations, and potentially dipping southwards from station MLON.

The Africa-Europe Plate Boundary in Central Italy, Marked by the Seismic Structure of the Crust and Upper Mantle

Vadim Levin *(Rutgers University),* **Jeffrey Park** *(Yale University),* **Nicola Piana Agostinetti** *(INGV, Italy),* **Simone Salimbeni** *(INGV, Italy),* **Jaroslava Plomerova** *(Geophysical Institute, Czech Republic),* **Lucia Margheritti** *(INGV, Italy),* **Silvia Pondrelli** *(INGV, Italy)*

We examined crustal properties in central Italy using receiver-function analysis, and probed mantle texture using observations of splitting in core-refracted shear waves. Our results reveal profound differences between the "Tyrrhenian" and the "Adriatic" sides of the convergence zone that is responsible for the formation of the Apennines.

In the Tyrrhenian domain the crust is apparently thin, and bound by a relatively sharp impedance contrast at a depth of approximately 20-25 km. In the Adriatic domain the definition of the crust–mantle boundary is problematic, suggesting a gradual and/or complicated transition from the crust to the mantle. Receiver function analysis is of less help here, as near-surface structure obscures signals at a number of sites. Where we can resolve it, the crustal thickness is larger (~35 km). We identify the transition between these two crustal thickness regimes, and find it to coincide with the high crest of the Apennines.

The high Apennines also mark the transition in the observations of shear-wave splitting. We see fairly uniform NW-SE fast polarizations beneath Tyrrhenian Sea and Tuscany, while on the Adriatic side we find nearly N-S alignment of fast polarization, as well as evidence for layering of seismic anisotropy.

We posit that the high Apennines mark the easternmost reach of both the "Tyrrhenian" crust and the "Tyrrhenian" upper mantle, and hence define the eastern edge of the Eurasian plate in central Italy.

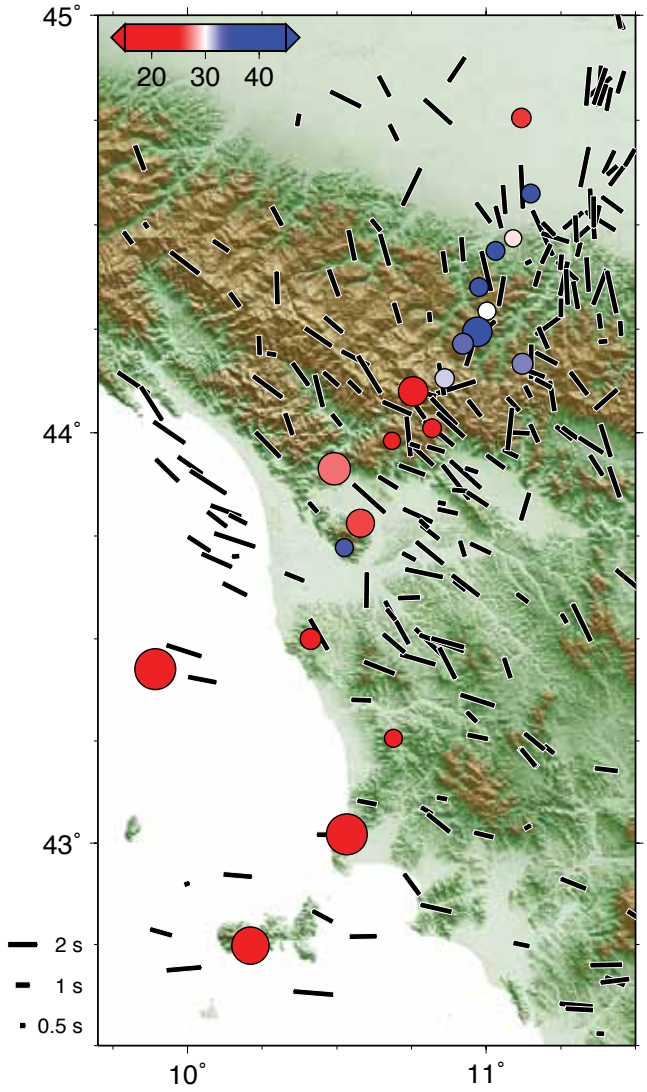

A topographic map illustrates a spatial coincidence of changes in inferred crustal thickness values (circles with depth-scaled color) and observed fast polarization directions of split shear waves (black bars). Circle size is proportional to confidence in the result (largest are most certain). Splitting observations are scaled with delay and aligned with the fast polarization. Both types of observations change dramatically across the highest part of the Apennines.

References

Piana Agostinetti, N., V. Levin and J. Park, Crustal structure above a retreating trench: Receiver function study of the northern Apennines orogen, *Earth Planet. Sci. Lett., 2008.*

Salimbeni, S., S. Pondrelli, L. Margheriti, V. Levin, J. Park, J. Plomerova and V. Babuska, Abrupt change in mantle fabric across northern Apennines detected using seismic anisotropy, *Geophys. Res. Lett., 34*, L07308, 2007

Plomerova, J., L. Margheriti, J. Park, V. Babuska, S. Pondrelli, L. Vecsey, D. Piccinini, V. Levin, P. Baccheschi, and S. Salimbeni, Seismic anisotropy beneath the Northern Apennines (Italy): Mantle flow or lithosphere fabric *Earth Planet. Sci. Lett.., 247*, pp. 157- 170, 2006.

Acknowledgements: Research reported here resulted from the PASSCAL deployment in Italy (http://www.iris.edu/mda/YI?timewindow=2003-2006) that was a part of the RETREAT project funded by the NSF Continental Dynamics program. Field operations and subsequent work on data were supported by Istituto Nazionale di Geofisica e Vulcanologia (INGV) and the Geophysical Institute of Prague.

Imaging Lithospheric Foundering beneath the Central Sierra Nevada with Receiver Functions, Teleseismic Surface Waves, and Earthquake Locations

Andy Frassetto *(University of Copenhagen),* **Hersh Gilbert** *(Purdue University),* **Owen Hurd** *(Stanford University),* **George Zandt** *(University of Arizona),* **Thomas J. Owens** *(University of South Carolina),* **Craig H. Jones** *(University of Colorado)*

The southern Sierra Nevada represents a fundamental example of a Cordilleran batholith which has recently lost its eclogitized, mafic-ultramafic lower crust and lithospheric mantle. From May 2005 through September 2007, the Sierra Nevada EarthScope Project (SNEP) targeted the central and northern Sierra Nevada with an array of broadband seismometers to characterize how lithospheric foundering relates to the Isabella and Redding deep seismic anomalies, the modern relief of the Sierra, and ongoing deformation and volcanism in eastern California. Selected key findings from our current study show evidence for ongoing foundering beneath the west-central Sierra Nevada, just southwest of Yosemite National Park.

Conversions from the Moho in stacked receiver functions change from high amplitude and shallow (30-35 km depth) along the High Sierra and Walker Lane to low amplitude and deep (50-55 km) beneath the west-central foothills (Figure 1). Strong negative conversions beneath the Walker Lane, including Long Valley Caldera, are consistent with low wavespeed layering associated with partial melt. Coincidently, surface wave phase velocities show an extensive region of fast material beneath the central Sierra foothills within the lower crust and upper mantle (Figure 2). This fast anomaly merges with the Isabella Anomaly at deeper levels beneath the south-western Great Valley. Beneath the eastern portion of the Sierra, a broad slow anomaly underlies much of the Walker Lane and regions of recent volcanism, indicating the presence of asthenospheric mantle encroaching beneath the High Sierra. Earthquakes located by SNEP show two distinct trends localized along the west-central foothills and batholith. A scattered zone of seismicity lies above the region encompassing diffuse Moho. A more confined trend of earthquakes occurs near where the conversions from the Moho diminish and deepen. This seismicity includes long-period events which occasionally occur at the Moho, likely signaling magma intrusion into the lower crust.

Incorporating observations from geophysical studies and xenoliths sampling the crust and upper mantle, we interpret the region of diffuse Moho and fast lower crust and upper mantle as the remaining gravitationally unstable, actively foundering root of the central Sierra Nevada batholith. The region of slow upper mantle phase velocities and sharp Moho demarcates the region where the batholithic root has been removed.

References

Zandt, G., Gilbert, H., Owens, T.J., Ducea, M., Saleeby, J., and Jones, C.H., 2004, Active foundering of a continental arc root beneath the southern Sierra Nevada in California, *Nature,* ***431***, 41–46.

Acknowledgements: This work was supported by the National Science Foundation's EarthScope grants EAR-0454554, EAR-0454524, and EAR-0454535 to the Universities of Arizona, Colorado, and South Carolina. This work was also made possible by funding from the National Science Foundation through the Graduate Research Fellowship Program.

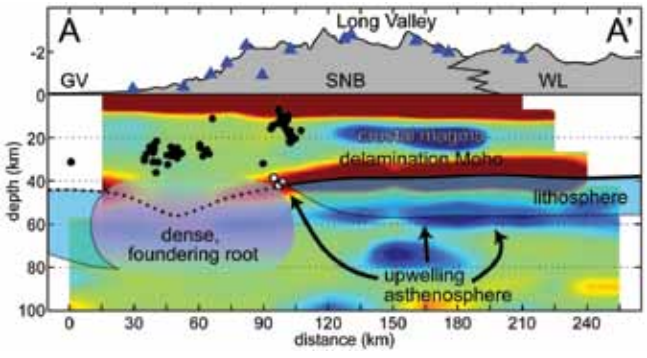

Figure 1: Interpreted common-conversion-point stack of receiver functions from broadband stations (blue) deployed across the central Sierra Nevada. Red represents strong conversions off the up-going P-wave from high-to-low steps in wavespeed; blue represents low-to-high steps. Locations of nearby earthquakes are projected onto the profile. White circles denote long period earthquakes. GV = Great Valley, SNB = Sierra Nevada batholith, WL = Walker Lane. The transect is shown in map view in Figure 2.

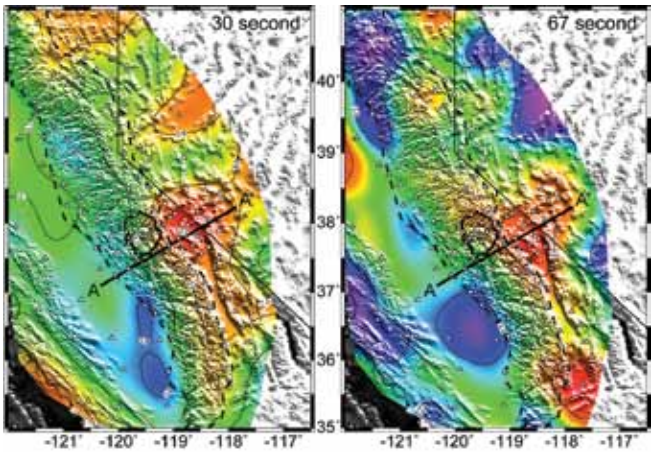

Figure 2: Phase velocities for 30 second (left) and 67 second (right) period teleseismic surface waves. Shading ranges from pink (>4.2 km/s) to red (<3.3 km/s). White triangles denote stations used, including the more densely spaced SNEP array. Locations of receiver function transect (A-A') and Yosemite National Park (north of profile) are shown.

The Isabella Anomaly Imaged by Earthquake and Ambient Noise Rayleigh Wave Dispersion Data: A Composite Anomaly of Sierra Nevada Batholith Root Foundering and Pacific Plate Slab-Flap Translation?

Josh Stachnik *(Univ. Wyoming),* **Ken Dueker** *(Univ. of Wyoming),* **Hersh Gilbert** *(Purdue Univ.),* **George Zandt** *(Univ. of Arizona)*

Sierra Nevada Earthscope Project (SNEP) and Earthscope Transportable Array (TA) Rayleigh wave dispersion data are inverted to construct a shear velocity model of the Sierra Nevada and San Joaquin valley. The Rayleigh wave dispersion dataset was measured using the two-plane wave method with earthquake records and the parametric Bessel-zeros method [*Ekstrom et al.*, 2009] with correlated ambient noise records. Two starting velocity models have been tested: a uniform (4.4 km/s) starting model and a starting model with the Moho mapped by Pn station time terms [*Buehler and Shearer*, in review].

With respect to previous body and surface wave tomograms, the Isabella anomaly is imaged as more geometrically rich. This observation leads us to consider a composite explanation of the anomaly as a Pacific plate slab-flap (Monterey microplate) and the foundering roots of the southern Sierra Nevada batholith. The slab flap is identified as a 4.4-4.6 km/s NW-SE striking 140 km wide planar anomaly imaged at 60-110 km depth beneath the San Joaquin valley. The foundering southern Sierra batholithic root is identified as an N-S trending 4.4-4.5 km/s high velocity region beneath the southern Sierran foothills. This anomaly is bowed down beneath the high standing southern Sierra block to form a wedge filled with 4.2 km/s mantle which is interpreted as in-flowed asthenosphere. The pros and cons of this composite interpretation will be discussed.

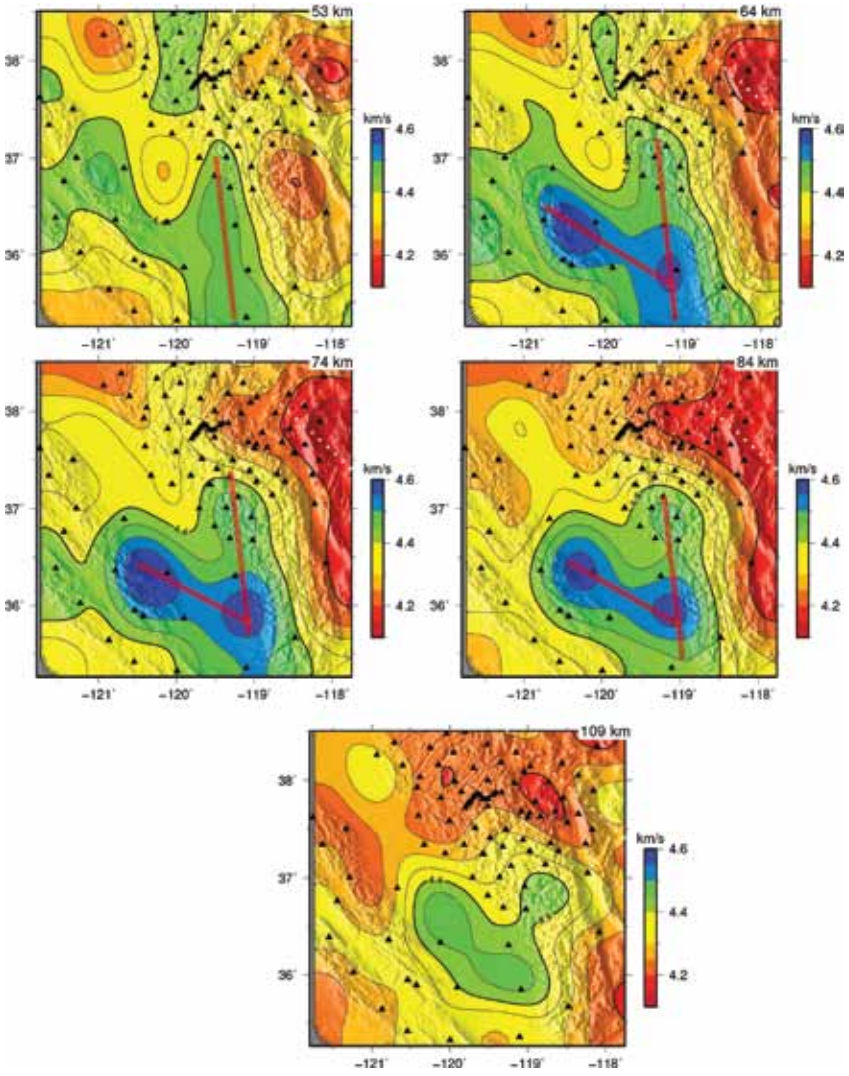

Shear velocity image from inversio of ambient and earthquake Rayleigh wave dispersion measurements using SNEP and Transportable array data.

Comparison of our velocity model with the only other joint ambient/earthquake surface wave model [*Moschetti et al.*, in review] finds that the two models are well correlated. Comparison of our velocity model with teleseismic body wave tomograms reveals substantial differences in the geometry and depth extent of the Isabella anomaly related to differences in the resolution of surface and body waves.

References

Ekström, G., G. A. Abers,and S. C. Webb, Determination of surface-wave phase velocities across USArray from noise and Aki's spectra formulation, *Geophys. Res. Lett., 36*, L18301, 2009.

Detection of a Lithospheric Drip beneath the Great Basin

John D. West *(Arizona State University),* **Matthew J. Fouch** *(Arizona State University),* **Jeffrey B. Roth** *(Arizona State University/ExxonMobile),* **Linda T. Elkins-Tanton** *(Massachusetts Institute of Technology)*

Using a combination of shear-wave splitting and seismic P-wave delay time tomography, we investigated a region of greatly diminished shear-wave splitting times, collocated with a sub-vertical cylinder of increased seismic velocity in the upper mantle beneath the Great Basin in the western United States. The localized reduction of splitting times is consistent with a rotation in flow direction from predominantly horizontal to sub-vertical, and the high velocity cylinder is characteristic of cooler lithospheric mantle. We suggest that the reduced splitting times and higher than average seismic velocities are the result of a cold mantle downwelling (a lithospheric drip). The cylinder of higher seismic velocities is approximately 100 km in diameter, extends near-vertically from ~75 km depth to at least 500 km, and plunges to the northeast. Near 500 km depth, the cylinder merges with a separate zone of high-velocity material, making resolution of a distinct cylinder difficult below this depth.

We generated geodynamic numerical models of Rayleigh-Taylor instabilities originating in the mantle lithosphere, using structural constraints appropriate to conditions in the central Great Basin. These models predict downwelling lithospheric mantle in the form of a strong, focused lithospheric drip developing over time periods of <1 to ~25 Myr, triggered from local density anomalies as small as 1% and initial temperature increases of ~10%.

Lithospheric drips are often inferred based on surface expressions of rapid uplift, subsidence, or voluminous magmatic activity, but have remained challenging to detect directly due to their relatively small size and transient nature. The Great Basin drip was detected by purely geophysical means and does not exhibit significant recognizable surface topography modifications, consistent with our numerical models.

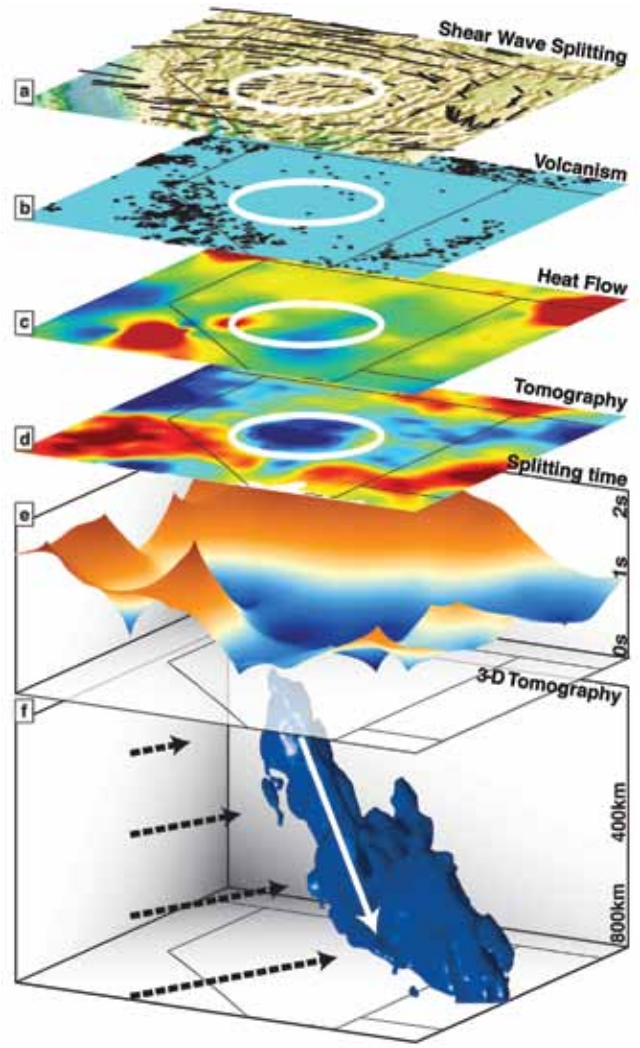

Summary of geological and geophysical constraints for the central Great Basin. a, Shear-wave splitting with the topography background for reference. b, Post-10-Myr volcanism (black circles) shows a regional dearth of volcanic activity. c, Heat flow showing reduced values (~50mWm, blue) in the regional high (>100mWm; yellow and red). d, Seismic tomography horizontal slice at 200 km depth. e, Shear-wave splitting times surface showing the strong drop in the central Great Basin. f, Isosurface at +0:95% velocity perturbation for NWUS08-P2 showing the morphology of the drip, which merges with a larger structure at ~500 km depth. The black arrows denote the inferred mantle flow direction; the white arrow denotes the flow direction of the Great Basin drip.

The interpretation of a lithospheric drip beneath the Great Basin is consistent with geophysical and geological characteristics of the region, including a distinct paucity of post-12 Ma volcanic activity and a heat flow low. Lithospheric material feeding horizontally into the drip would be expected to generate contractional forces if significant mantle/crust coupling exists, and surface contraction centered near the drip has been observed. The northeast plunge of the drip provides a unique indicator of northeast-directed regional mantle flow relative to the North American plate.

References

West, J.D., M.J. Fouch, J.B. Roth, and L.T. Elkins-Tanton, (2009), Vertical mantle flow associated with a lithospheric drip beneath the Great Basin, *Nature Geosci., 2*, 439-444

Holt, W., M.J. Fouch, E. Klein, and J.D. West, (2010), GPS measured contraction in Nevada above the Great Basin mantle drip, in preparation.

Acknowledgements: Thanks to the USArray Transportable Array team for the instrumentation which made this study possible, and to the IRIS Data Management Center for providing access to the data. Partial support for this project came from US National Science Foundation grants EAR-0548288 (MJF EarthScope CAREER grant) and EAR-0507248 (MJF Continental Dynamics High Lava Plains grant).

Tomographic Image of the Crust and Upper Mantle Beneath the Western Tien Shan from the MANAS Broadband Deployment: Possible Evidence for Lithospheric Delamination

Steven Roecker *(Rensselaer Polytech. Inst.),* **Li Zhiwei** *(Rensselaer Polytech. Inst)*

We combined teleseismic P arrival times from the MANAS deployment of broad band sensors with P and S arrival times from local events recorded by the GENGHIS deployment and analogue observations from the Kyrgyz Institute of Seismology to generate a high resolution (~20 km) image of elastic wavespeeds in the crust and upper mantle beneath the western Tien Shan. The total data set consists of 29,006 P and 21,491 S arrivals from 2176 local events recorded at 144 stations along with 5202 P arrivals from 263 teleseismic events recorded at 40 stations. The most significant feature in our image of the mantle beneath the Tien Shan is a pair of large, elongated high wavespeed regions dipping in opposite directions from the near surface to depths of at least 400 km. These regions appear to be continuous and extend upwards to bounding range fronts where the Tarim Basin is being overthrust by the Kokshal range on the south side, and the Kazach shield underthrusts the Kyrgyz range on the north side. While it is tempting to interpret these high wavespeed anomalies as evidence for contemporary subduction of continental lithosphere, such a scenario is difficult to reconcile with both 2the timing of the orogen and the size of the wavespeed anomaly. We suggest instead that they represent downwelling side-limbs of a lithospheric delamination beneath the central part of the Tien Shan, possibly by siphoning of the bordering continental lithosphere as the central part descends.

Acknowledgements: All of the broad band seismic equipment used in the MANAS and GHENGIS projects was provided by the IRIS PASSCAL program. This work was supported by the NSF Continental Dynamics Program (EAR-0309927).

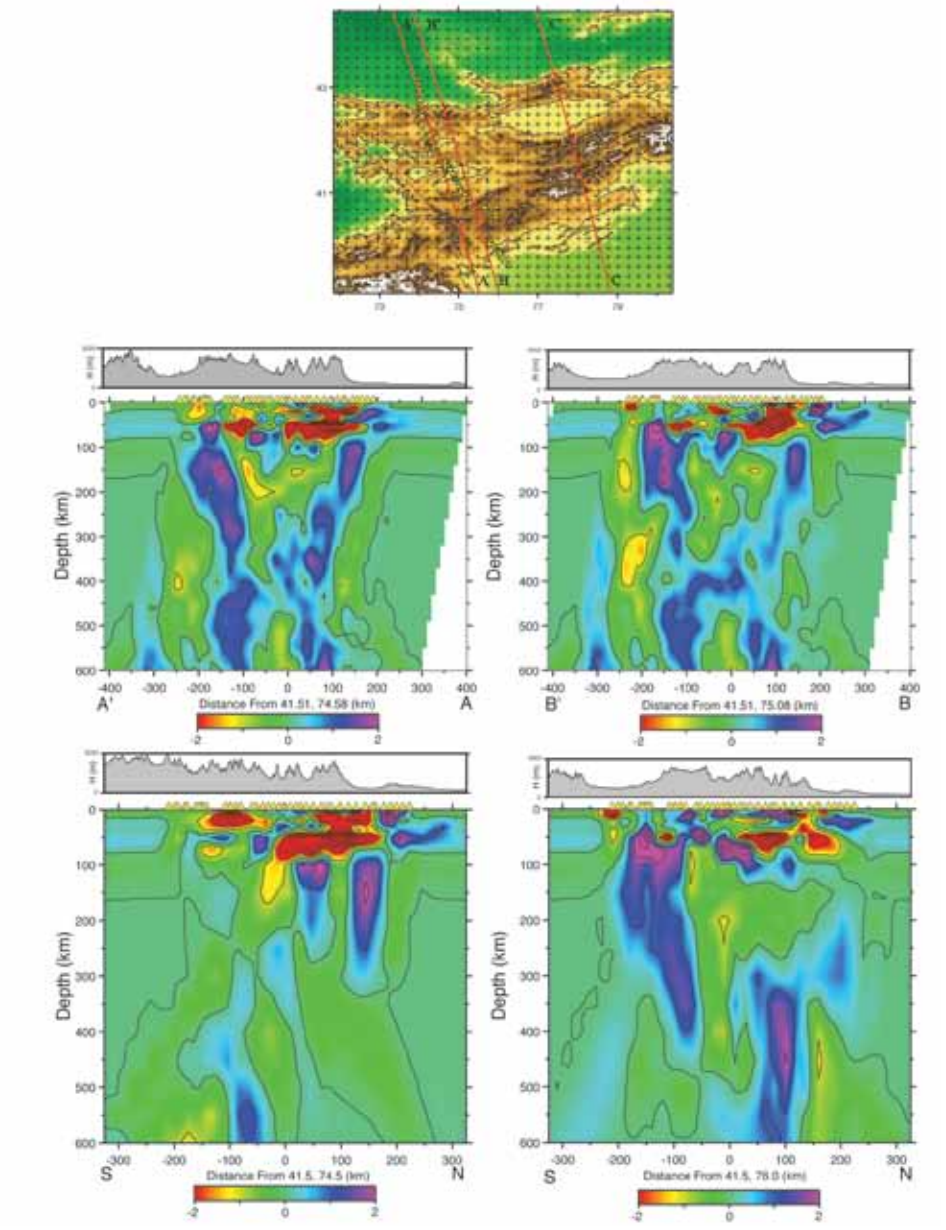

Perturbations to P wavespeed (dVp/Vp) from an average 1D background model determined by inversion of the teleseismic travel time residuals. The locations of the slanted cross sections are shown at the top of the figure: the maximum resolution projection onto a plane extending from AA' to CC' is shown on the upper left. A slightly displaced plane from BB' to CC' is shown on the upper right. The vertical axis in these sections is true depth in km (as opposed to downdip length). The lower two plots are NS sections taken at 74.5o (left) and 76.0 o (right) longitude. The 74.5 o section has better resolution at shallow depths in the north, while the 76.0 o section has better resolution at shallow depth in the south. Perturbations relative to the 1D average background wavespeeds are in percent as indicated in the palettes below each section. Locations of the MANAS stations are shown as yellow triangles at the surface. Topography along each section is shown in the box above each section.

Global Variations of Temperature and Water Content in the Mantle Transition Zone from Higher Mode Surface Waves

Jeannot Trampert *(Utrecht University),* **Ueli Meier** *(IDSIA Lugano),* **Andrew Curtis** *(University of Edinburgh)*

We estimated lateral variations of temperature and water content in Earth's mantle transition zone from models of transition zone thickness and S-wave velocity (Meier et al., 2009). The latter were obtained by a fully nonlinear inversion of surface wave overtone phase velocities using neural networks. Globally we observe a broader than previously reported transition zone and explain this by a broad olivine to wadsleyite transition at around 400 km depth where the minerals co-exist with water induced melt. Within the transition zone we observe relatively cold subduction zones as well as relatively warm regions beneath continents and hot spots. We find that the transition zone is wettest away from subduction zones.

References

Meier U., Trampert J., Curtis A., 2009. Global variations of temperature and water content in the mantle transition zone from higher mode surface waves, *Earth Planet. Sci. Lett., 282*, 91-101.

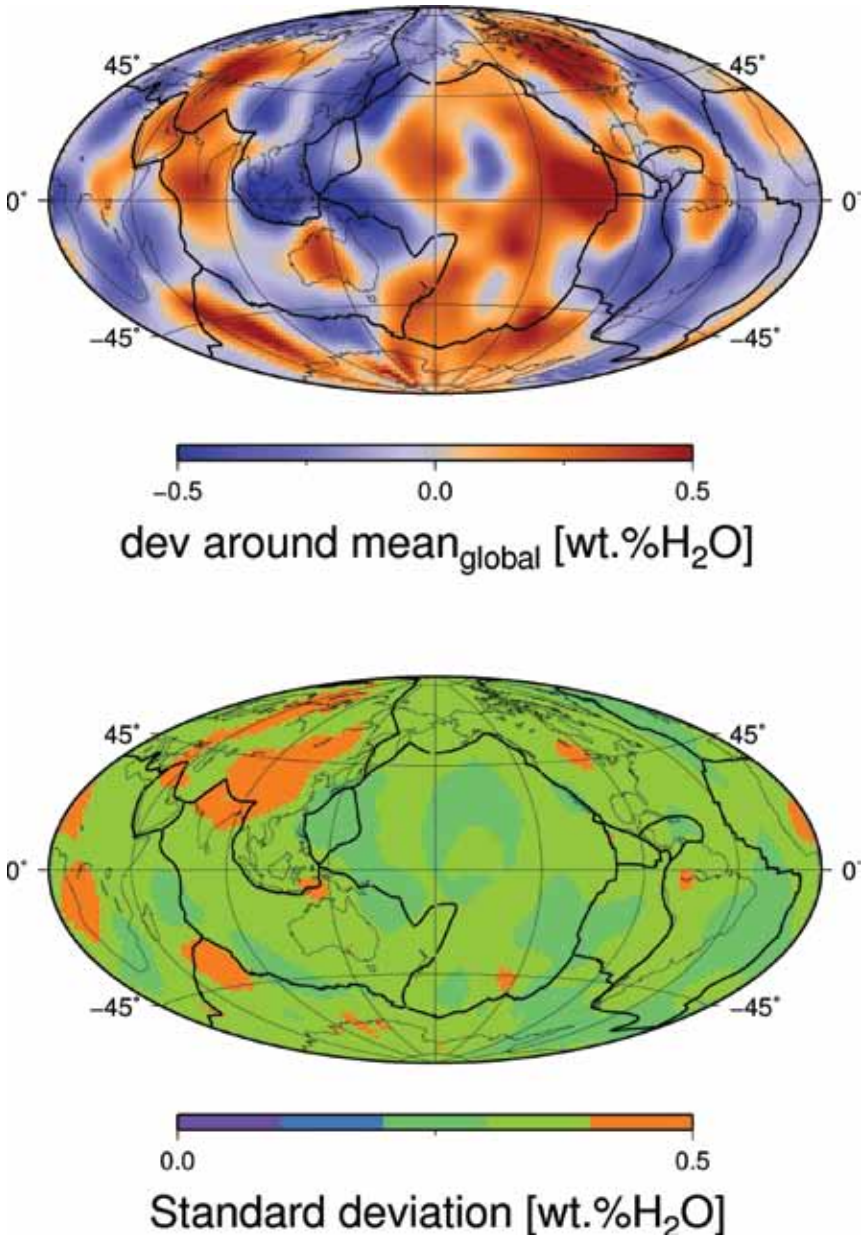

Mean water content variation from the unknown global mean in the mantle transition zone (top) together with the corresponding standard deviations (bottom).

Small-Scale Mantle Heterogeneity and Dynamics beneath the Colorado Rocky Mountains Revealed by CREST

Jonathan MacCarthy *(New Mexico Institute of Mining and Technology),* **Rick Aster** *(New Mexico Institute of Mining and Technology),* **Ken Dueker** *(University of Wyoming),* **Steven Hansen** *(University of Wyoming),* **Karl Karlstrom** *(University of New Mexico)*

Recent crustal thickness and shear wave velocity estimates from the CREST (Colorado Rockies Experiment and Seismic Transects, NSF Continental Dynamics) experiment indicate that the highest elevations of the Colorado Rocky Mountains (> 2.5 km) are not primarily supported in the crust. Mantle buoyancy and dynamics are therefore of fundamental importance. We present results of teleseismic body wave tomography of the upper mantle beneath western Colorado interpreted in consort with ongoing CREST results. Using a network of over 160 CREST and USArray stations with a minimum spacing of ~24 km, we invert approximately 20,000 P arrivals and nearly 10,000 S arrivals for regularized 3-D models of upper mantle Vp and Vs structure. We find Vp perturbations relative to AK135 of >6% and Vs variations of >8%, with structure being largely confined to the upper 300 km of the mantle. The previously noted "Aspen Anomaly" of low mantle velocities in this region is revealed to be fragmented, with the lowest Vp and Vs velocities beneath the San Juan mountains being clearly distinct from low velocities associated with the northern Rio Grande Rift. The San Juan anomaly probably represents thermal and/or chemical heterogeneity in the uppermost mantle related to voluminous Cenozoic magmatism and possible subsequent piecewise lithospheric dripping and/or crustal delamination. CREST thermochronology and Colorado River incision constraints additionally point to significant Neogene uplift and denudation in the southwestern and central Colorado Rockies associated with mantle forcing. A northeast-southeast grain in shallow Vs domains parallel to the Colorado Mineral Belt may be influenced by Proterozoic accretionary lithospheric architecture. We find that the low velocity anomalies beneath southwest Colorado in particular may provide significant support for enigmatic high elevations. These high-resolution tomography results CREST illuminate a remarkably high-degree of spatial heterogeneity in the region of transition between tectonic and stable North America that may reflect vigorous small-scale convection and related processes linking the lithosphere and mantle transition zones, with characteristic length scales of just 10s of km.

Acknowledgements: The CREST project is supported by the National Science Foundation Continental Dynamics Program, award #0607837, with instrument and field support from the IRIS PASSCAL Instrument Center.

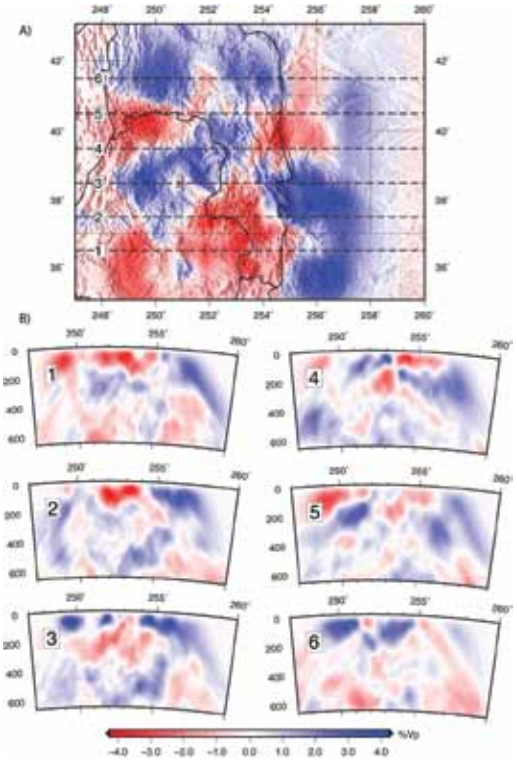

Figure 1 – (A) Depth slices through ΔVp model at 90 km, showing outlines of the Colorado Plateau and southern Rocky Mountains. Cross-section lines 1-6 are shown in (B).

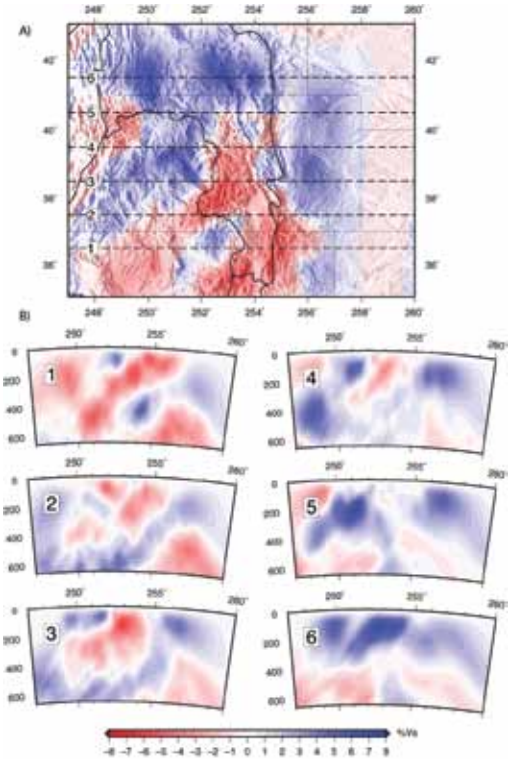

Figure 2 – (A) Depth slices through ΔVs model at 90km, showing outlines of the Colorado Plateau and southern Rocky Mountains. Cross-section lines 1-6 are shown in (B).

The Effect of S-Velocity Heterogeneity in the North American Crust and Mantle on Waveforms of Regional Surface Waves from the February 2008 Nevada Earthquake

Sung-Joon Chang *(Northwestern University),* **Suzan van der Lee** *(Northwestern University)*

We compare observed waveforms recorded at the USArray Transportable Array stations from the 02/21/08 Nevada earthquake (Mw 6.0) with synthetics through three-dimensional (3D) velocity models such as S20RTS [*Ritsema et al., 1999*] and NA04 [*Van der Lee and Frederiksen, 2005*]. A crustal model CRUST2.0 is incorporated into the mantle velocity model S20RTS. We calculate synthetics down to 17 s through: 1) mode summation for a 1D model obtained by averaging velocity variations in the 3D model between the epicenter and the station (path-average method), and 2) the Spectral Element Method [*Komatitsch and Tromp, 1999*]. Because the Nevada earthquake occurred almost at the center of the Transportable Array stations at that time, distances between the epicenter and stations are typically less than 1000 km. In general, the 3D models predict the observed waveforms better than a reference 1D model, but some waveform fits need to be significantly improved by better 3D models of velocity heterogeneity and discontinuity depth. We find the spectral element method and path-averaging method produce similar waveforms for inland, while a little different synthetics are generated with the two methods for ocean-continent boundary.

References

Komatitsch, D. and J. Tromp (1999), Introduction to the spectral-element method for 3-D seismic wave propagation, *Geophys. J. Int., 139,* 806-822.

Ritsema, J., H. J. van Heijst, and J. H. Woodhouse (1999), Complex shear wave velocity structure imaged beneath Africa and Iceland, *Science, 286*, 1925-1928.

Van der Lee, S. and A. Frederiksen (2005), Surface wave tomography applied to the North American upper mantle, in Seismic Earth: Array analysis of broadband seismograms, pp. 67-80, eds. A. Levander and G. Nolet, Geophys. Mono. 157, AGU, Washington, DC.

Acknowledgements: We thank the IRIS DMC for providing waveform data used in this research. This study was supported by NSF EAR-0645752.

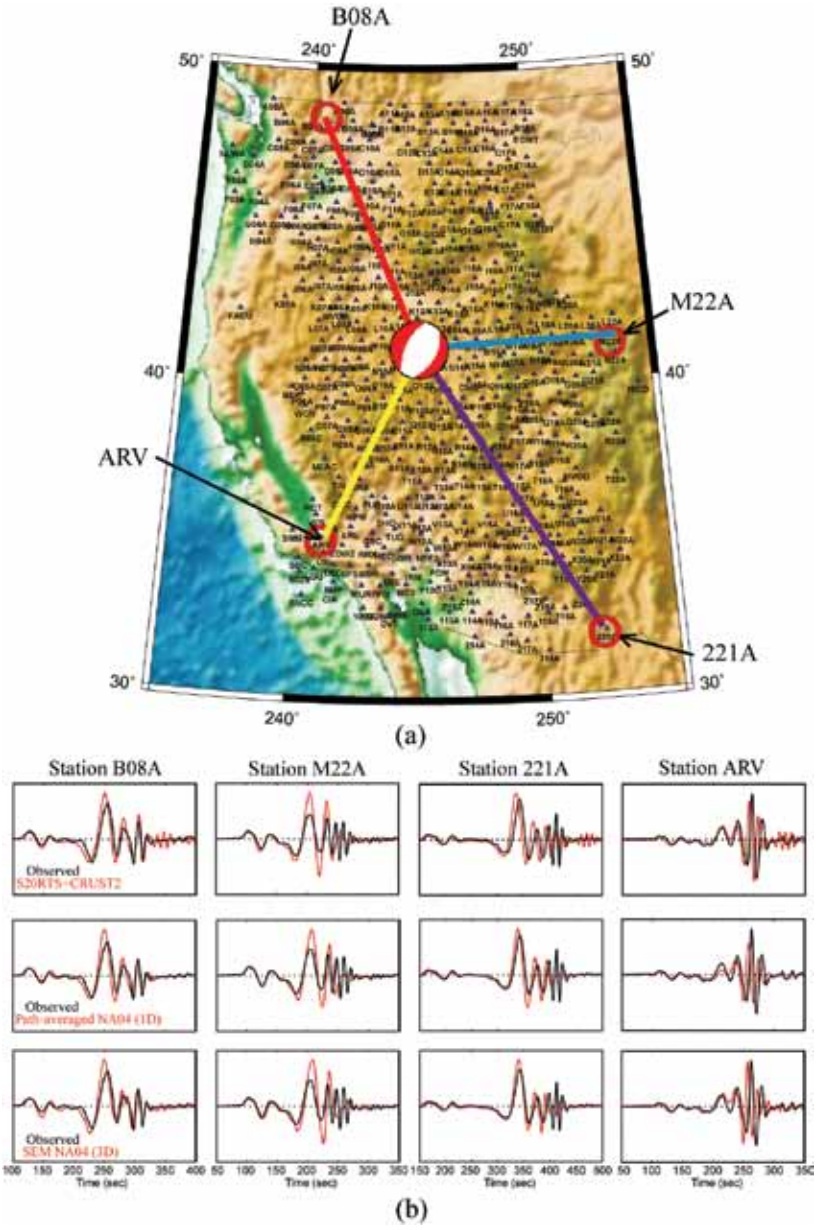

(a) The Nevada Earthquake (Mw 6.0) indicated as a star was recorded at over 400 broadband stations in USArray indicated as triangles. Some stations are surrounded by red circles where observed waveforms are obtained to be compared with synthetics. (b) Comparison between observed waveforms and several synthetics at stations surrounded by red circles in (a).

Mantle Heterogeneity West and East of the Rocky Mountains

Xiaoting Lou *(Northwestern University),* **Suzan van der Lee** *(Northwestern University)*

Separated by the Rocky Mountains, North America is divided into a tectonically active western part and a tectonically stable eastern part. We have measured teleseismic P and S relative delay times using waveforms from IRIS PASSCAL seismic arrays and EarthScopes Transportable Array sampling both western and eastern North America. Relative delay times were corrected for ellipticity, topography, Moho depth and sediments using the Crust 2.0 Model [Bassin et al., 2000]. To investigate the delay time differences between tectonically active and stable North America, seismic stations are divided into two groups: (1) TA stations west of the Rocky Mountains; (2) TA stations east of the Rocky Mountains and stations of MOMA, ABBA, FLED and Abitibi. Delay times within each group of stations are shifted relative to other groups using predicted average delay times by tracing 1D raypath through 3D model NA04 [Van der Lee and Frederiksen, 2005]. The range of relative delay times from seismic stations east of the Rocky Mountains is comparable to that for stations west of the Rocky Mountains, which holds for both station average delay times (Figure 1) and all individual measurements (Figure 2). This suggests that the mantle heterogeneity in the east is comparable to that in the west, despite there being relatively little surface or tectonic expression of this heterogeneity in the east. For both groups of stations, the measured S and P delay times have a significant linear correlation, with S delays at approximately 3 times the P delays, which confirms the dominant effect of mantle temperature on mantle velocity structure.

References

Bassin, C., G. Laske, and G. Masters (2000), The current limits of resolution for surface wave tomography in North America, Eos Trans AGU, 81, F897.

Van der Lee, S., and A. Frederiksen (2005), Surface wave tomography applied to the North American upper mantle, in Seismic Earth: Array Analysis of Broadband Seismograms, Geophys. Monogr. Ser., vol. 157, edited by A. Levander and G. Nolet, pp. 67–80, AGU, Washington, D. C.

Acknowledgements: This study is supported by NSF EAR-0645752 grant to Suzan van der Lee. The authors are grateful to the IRIS DMC for providing seismic waveform data.

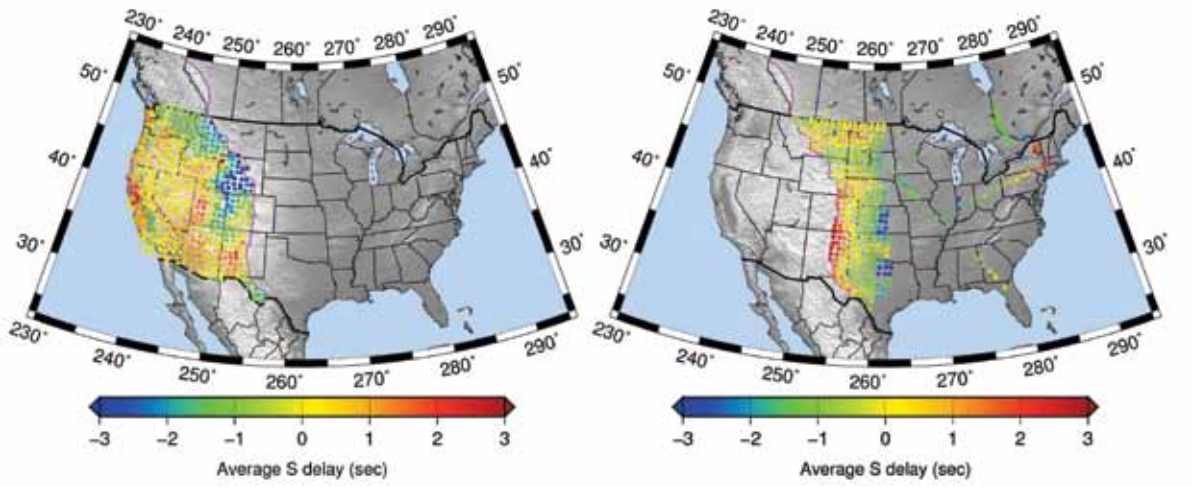

Figure 1: Station average S relative delay times for the two groups of stations west and east of the Rocky Mountains, respectively.

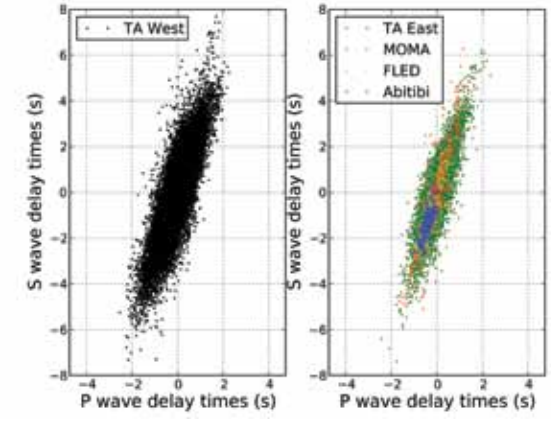

Figure 2: Measured individual relative S delays plotted against P delays for the two groups of stations west and east of the Rocky Mountains, respectively.

Receiver Function Imaging of Upper Mantle Complexity beneath the Pacific Northwest, United States

Kevin C. Eagar *(School of Earth and Space Exploration, Arizona State University),* **Matthew J. Fouch** *(School of Earth and Space Exploration, Arizona State University),* **David E. James** *(Department of Terrestrial Magnetism, Carnegie Institution of Washington)*

Small-scale topographic variations on the upper mantle seismic discontinuities provide important constraints on the thermal influences of upwellings and downwellings in geodynamically complex regions. Subduction of the Juan de Fuca plate and other tectonic processes dominating the Pacific Northwest, United States in the Cenozoic involve massive thermal flux that likely result in an upper mantle that has strong 3-D temperature variations. We address the interaction of such processes in the region using receiver functions to image the upper mantle seismic discontinuities at 410 and 660 km. We utilized over 15,000 high quality receiver functions gathered from 294 teleseismic earthquakes recorded at 277 regional broadband seismic stations, primarily those of the Earthscope/USArray Transportable Array. We find the average depths of the discontinuities to be 412 km and 658 km, respectively, with no obvious 520 km discontinuity detected. The peak-to-peak range is greater on the '410' than the '660', suggesting the possibility of more significant regional dynamic processes at upper mantle depths. Our results are not consistent with a mantle plume below central Oregon in the High Lava Plains region. Our observation of a thinner transition zone beneath the western Snake River Plain region, however, is consistent with a regional increase in mantle temperatures, perhaps due to either asthenospheric flow from beneath and around the southern edge of the Juan de Fuca plate, or to vertical flow in the form of regional mantle upwelling related to the Snake River Plain / Yellowstone hotspot track. Further, our results are not consistent with a simple subducting Juan de Fuca slab morphology, but rather suggest similar levels of significant complexity in slab structure found by recent regional tomographic studies. We find evidence for a thickened and therefore cooler mantle transition zone beneath the Wallowa / Idaho Batholith region, consistent with tomographic models which suggest broad scale increased seismic velocities to transition zone depths. We speculate that this region may be the location of mantle downwelling at larger scales than previously proposed.

References

Eagar, K.C., M.J. Fouch, and D.E. James, Receiver function imaging of upper mantle complexity beneath the Pacific Northwest, United States, in press, *Earth Planet. Sci. Lett., 2010.*

Acknowledgements: This work would not have been possible without high quality seismic data provided through the hard work of the TA and the HLP Seismic Experiment teams (http://www.dtm.ciw.edu/research/HLP), and the services of the IRIS DMC. As always, the IRIS PASSCAL program provided world-class technical field support. A special thanks goes to Jenda Johnson, whose contributions to the project have been innumerable and immeasurable, and Steven Golden for providing field and data support. We would also like to acknowledge the work and productive discussions on the crustal evolution with the other PIs of the HLP project, including Anita Grunder, Bill Hart, Tim Grove, Randy Keller, Steve Harder, and Bob Duncan. This research was supported by National Science Foundation awards EAR-0548288 (MJF EarthScope CAREER grant), EAR-0507248 (MJF Continental Dynamics High Lava Plains grant) and EAR-0506914 (DEJ Continental Dynamics High Lava Plains grant).

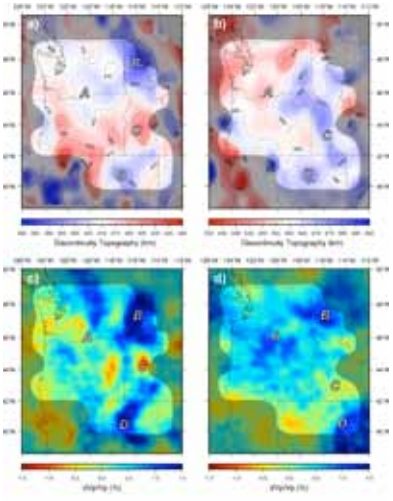

Upper mantle discontinuity topography and regional P wave tomography beneath the Pacific Northwest.

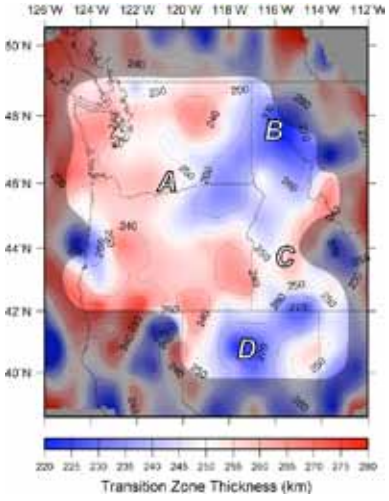

Transition zone thickness beneath the Pacific Northwest.

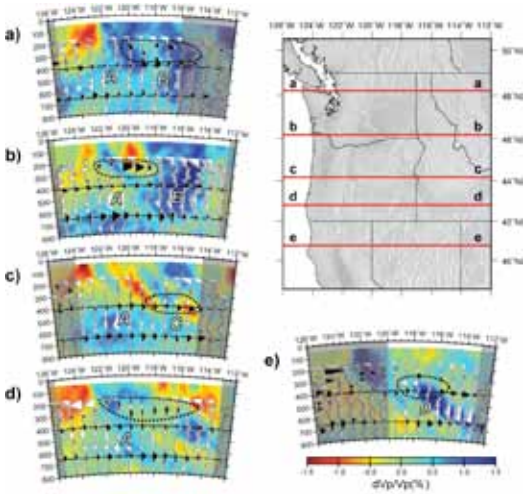

Cross-sections of CCP stacked receiver functions.

New Geophysical Insight into the Origin of the Denali Volcanic Gap

Stéphane Rondenay *(MIT)*, **Laurent Montési** *(University of Maryland)*, **Geoffrey Abers** *(Lamont-Doherty Earth Observatory)*

Volcanic gaps are segments of subduction zones that lack the volcanic activity usually found at these convergent margins. They are regions where the necessary conditions to produce melt may appear favourable, but where volcanoes are surprisingly absent from the surface. In this study, we present a new model that can explain the occurrence of such volcanic gaps. It is based on seismic imaging and geodynamic modelling of the Denali volcanic gap, a ~400 km-wide region at the eastern end of the Alaska-Aleutian subduction zone. Here, the thick crust of the Pacific plate and Yakutat terrane subduct at shallow angle beneath North America. A high-resolution seismic profile across the IRIS-PASSCAL BEAAR array [*Ferris et al., 2003*] clearly images the subducting crust undergoing progressive dehydration between 50-120 km depth, and a negative sub-horizontal velocity contrast at 60 km depth in the overlying mantle wedge. We interpret this 60 km discontinuity as marking the top of a layer of partial melt that pools at the base of the overriding plate. In steady-state subduction models, melt accumulates at the apex of a vaulted mantle wedge, the `pinch zone', from where it may break through the overlying lithosphere to the surface. Beneath the Denali volcanic gap, the pinch zone is absent (or greatly reduced) because shallow subduction of the Yakutat terrane progressively cools the system, and causes the slab to advance and replace the hot core of the mantle wedge. This regime can be seen as the opposite of subduction roll-back. It prevents the formation of a pinch zone, reduces the length of the melting column and causes melt to pool at the base of the overriding plate, thus inhibiting magma generation and extraction.

References

Ferris, A., G.A. Abers, D.H. Christensen, and E. Veenstra, High resolution image of the subducted Pacific (?) plate beneath central Alaska, 50–150 km depth, *Earth Planet. Sci. Lett., 214*, 575–588, 2003.

Rondenay, S., L.G.J. Montési, and G.A. Abers, New geophysical insight into the origin of the Denali volcanic gap, *Geophys. J. Int.*, in press, 2010.

Acknowledgements: This work was supported by National Science Foundation grants EAR-0544996 (SR), EAR-0911151 (LM) and EAR-9996451 (GA).

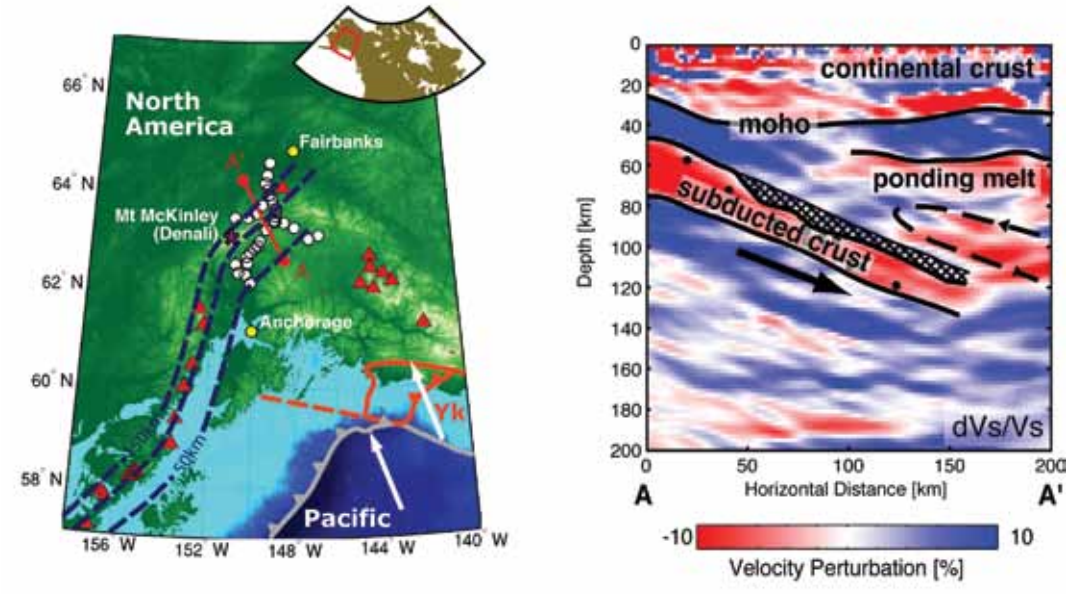

Left panel: Location map. Right panel: Vs perturbation profile across line A-A'. Discontinuities appear as rapid changes in perturbation polarity, where an increase (decrease) in velocity with depth is referred to as a positive (negative) gradient in the text.

Anomalous Seismic Structure beneath the Klyuchevskoy Group, Kamchatka, as Indicated by Receiver Function Analysis

Alex Nikulin *(Rutgers University),* **Vadim Levin** *(Rutgers University),* **Ashley Shuler** *(LDEO, Columbia University),* **Michael West** *(AVO, University of Alaska - Fairbanks)*

The Klyuchevskoy Group (KG) of volcanoes in Kamchatka, Russia is among the largest volcanic features on the planet, yet its position within the Kamchatka subduction zone is hard to explain with a simple tectonic mechanism. Geochemical evidence (Ishikawa et al., 2010) indicates that lavas of the KG are typical products of subduction-induced flux melting, yet the depth to the subducting Pacific plate beneath this volcanic center is much larger than the average depth of subduction associated with arc volcanism (Syracuse and Abers, 2006). We present new seismological constraints on the upper mantle structure beneath the KG, based on receiver function analysis of data collected by the PIRE project (Nikulin et al., 2010). We identify a sharply bounded zone of anomalous velocities in the mantle wedge beneath the KG (Figure 1), which we refer to as the Klyuchevskoy Upper Mantle Anomaly (KUMA). The presence of a sharp velocity deviation in the mantle wedge does not conform to our understanding of the standard subduction model, where a homogeneous velocity profile is expected in the mantle wedge. We contend that the observed anomaly is essential for understanding the location and the exceptional nature of the volcanic activity at the KG. Located at the typical depth of volatile release within the mantle wedge, this feature is a likely source of melts erupting at the KG. Presence of this heterogeneity in the upper mantle beneath the KG may explain the elevated level of volcanic activity of the KG and its position relative to the subducting Pacific Plate.

References

Ishikawa T., F Tera, and T. Nakazawa (2001), Boron Isotope and trace element systematics of the three volcanic zones in the Kamchatka arc. *Geoch. Cosm. A., 65*, 4523-4537

Nikulin, A., V. Levin, A. Shuler, and M. West (2010), Anomalous seismic structure beneath the Klyuchevskoy Group, Kamchatka, *Geophys. Res. Lett.*, in press.

Syracuse, E. M., and. G.A. Abers (2006), Global compilation of variations in slab depth beneath arc volcanoes and implications, *Geochem. Geophys. Geosyst., 7*, Q05017

Acknowledgements: The authors would like to aknowledge the support of the Partnership In Research and Education (PIRE) project, funded by the National Science foundation and the support of the Graduate School of Rutgers University, New Brunswick.

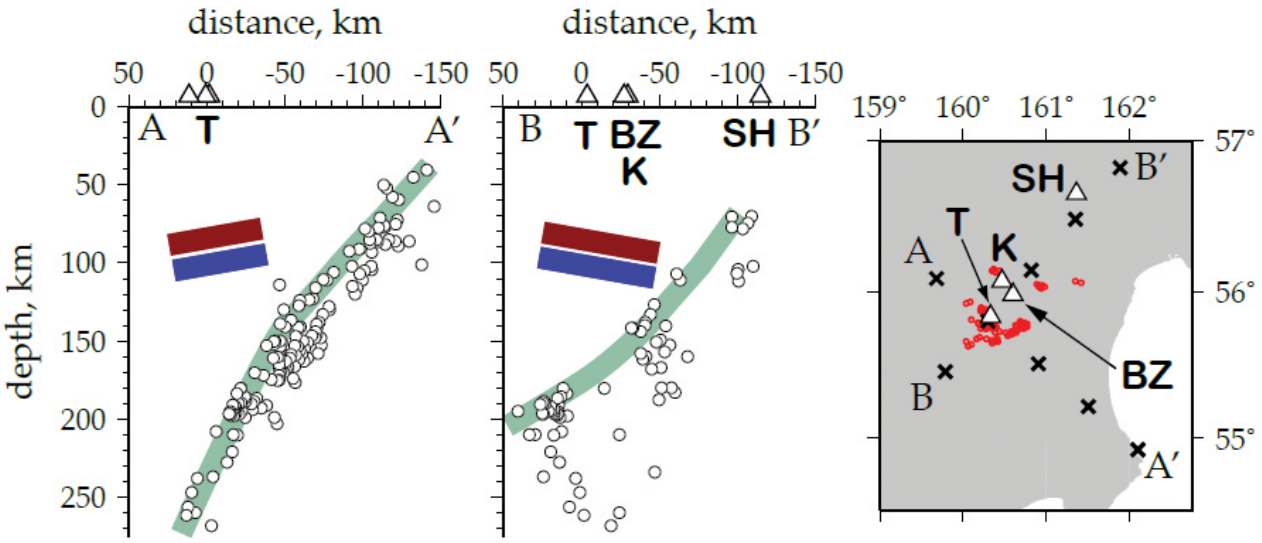

Position of the KUMA (red-blue bar) with respect to the subducting Pacific plate outlined by seismicity and the CKD volcanoes. Vertical cross-sections show earthquakes (circles) located over 10 years (2000-2009) by the Kamchatka Branch of the Geophysical Service of Russian Academy of Sciences. The online catalog (www.emsd.ru) includes events with M=3.5 and larger. Cross-sections are centered on the Tolbachik volcano, aligned along A-A' and normal B-B to the Pacific plate motion direction, and include events within 25 km of the profile. Crosses on the map correspond to 50 km tick marks on the distance axes of cross-sections, red circles denote 100 km depth pierce points of 166 individual rays from earthquakes used to construct RF gather in Figure 2. CKD volcanoes marked by triangles: BZ – Bezymianny, K – Klyuchevskoy, T – Tolbachik, SHShiveluch.

The Plume-slab Interaction beneath Yellowstone Revealed by Multiple-frequency Tomography

Yue Tian *(Princeton University (now at Chevron), USA),* **Ying Zhou** *(Virginia Tech, USA),* **Karin Sigloch** *(Ludwig-Maximilians-Universität, Germany),* **Guust Nolet** *(Université de Nice/Antipolis, France),* **Gabi Laske** *(University of California, San Diego, USA)*

S-velocity structure under the Yellowstone region is obtained from multiple-frequency tomography of a mixed data set of shear waves and Love waves. In this study, we used a total of 211440 data measurements measured from 36344 seismic waveforms, and over 95% of the waveforms are from IRIS. A strong slow anomaly (Y0) with large velocity gradient is observed under the Yellowstone Caldera (Figures 1-2), reaching ~200 km depth. Y0 connects to a slow anomaly (Y1) in the transition zone, which is centered at ~1° north of Y0 (Figure 2AA'). To the southwest, Y0 abuts a belt of strong slow anomalies (SR0) under the eastern Snake River Plain. Down in the lower mantle, a plume-shaped conduit (Y2) is observed with its top directly under Y1. The plume comes from south, tilting ~40° from vertical, reaches as deep as 1500 km, but spreads out at 700–1100 km depth. The spreading of SR2 can be explained either if the 660-km discontinuity acts as a barrier, or if the slab fragment S1 [*Sigloch et al., 2008; Tian et al., 2009*] acts as a barrier for the uprising Y2 (Figure 1b). Y2 might have distorted in two ways in response to the barrier. Part of Y2 might have navigated its path around S1 and found its way up through the slab gap, and the other part of Y2 might have smeared southwestward along the base of S1 and formed SR2. Though much of this explanation is speculative, it is clear that we witness a complex interaction between upwellings and downwellings in this part of the mantle. The very high resolution we obtained under the Yellowstone region would not be possible without the USArray, one of the densest networks in the world. The eastward movement of the USArray will make it possible to image detailed structure under the central and eastern US with similar resolution.

References

Sigloch, K., N. McQuarrie, and G. Nolet (2008), Two-stage subduction history under North America inferred from finite-frequency tomography, *Nature Geoscience, 1*, 458–462.

Tian, Y., K. Sigloch, and G. Nolet (2009), Multiple-frequency SH-wave tomography of the western U.S. upper mantle, *Geophys. J. Int., 178*, 1384–1402.

Acknowledgements: NSF grants EAR-0309298, EAR-0105387, and EAR-0809464.

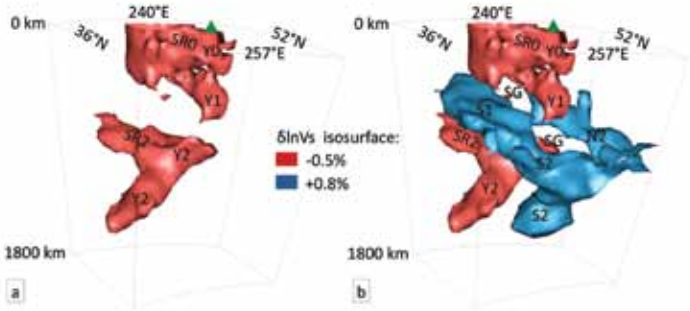

Figure 1. Three-dimensional view of the plume-slab interaction system under the Yellowstone and the eastern Snake River Plain, looking from the southwest. The green triangle represents the location of the Yellowstone Caldera. a: Slow anomalies only. b: Superimposing the fast anomalies on top of the slow anomalies. Labels S1, N1, S2, N2, SG identify the same subduction structure as in Sigloch et al. [2008] and Tian et al. [2009].

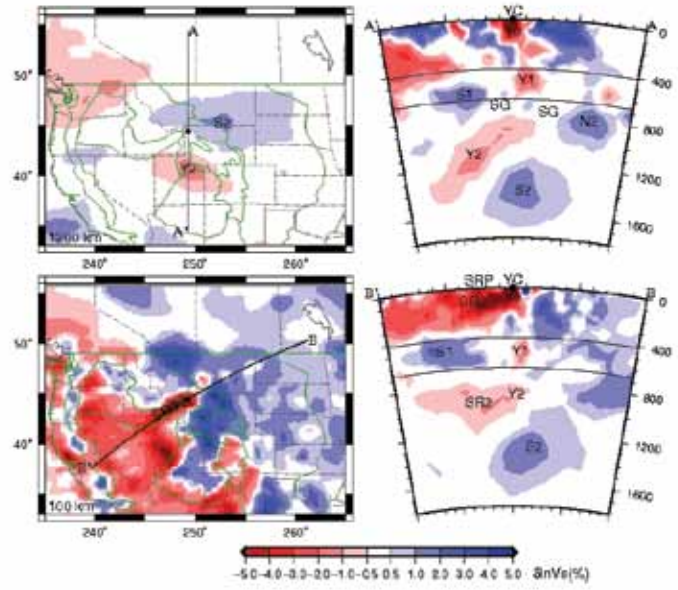

Figure 2. Great-circle cross sections of the velocity structure under the Yellowstone Caldera (YC) and the eastern Snake River Plain (SRP). The black dot and 0° represent the location of the Yellowstone Caldera and the mid-point of the great circle arc. In the cross-section views, each grid along the arc represents 1°. Labels S1, S2, N2, SG identify the same subduction structure as in Sigloch et al. [2008] and Tian et al. [2009].

Yellowstone Hotspot: Insights from Magnetotelluric Data

Anna Kelbert *(College of Oceanic and Atmospheric Sciences, Oregon State University, Corvallis, OR, USA),* **Gary D. Egbert** *(College of Oceanic and Atmospheric Sciences, Oregon State University, Corvallis, OR, USA),* **Catherine deGroot-Hedlin** *(Scripps Institution of Oceanography, University of California, San Diego, La Jolla, CA, USA)*

We have performed a set of three dimensional inversions of magnetotelluric (MT) data in the Snake River Plain and Yellowstone areas. We used a total of 73 sites from USArray MT Transportable Array (Idaho, Montana and Wyoming areas) and a subset of 19 sites from an earlier long-period MT survey in the Snake River Plain (SRP). The images reveal extensive areas of high conductivity in the upper mantle and lower crust beneath Yellowstone and the SRP. A highly conductive (~ 1 S/m) shallow anomaly directly beneath the Yellowstone caldera extends to no more than 20 km depth (Figure 2a), but connects to a deeper (40-100 km) conductive feature in the mantle that extends at least 200 km southwest (Figure 1a) roughly parallel to the direction of North America absolute motion. In several locations beneath the Eastern SRP very high conductivities (a few S/m) are imaged at or near the base of the lower crust (Figures 2b, c).

The lateral spatial extent of the mantle conductive anomalies correlates well with low velocity anomalies in the upper mantle imaged teleseismically [*e.g., Humphreys et al, 2000; Smith et al, 2009*], and with surface wave tomography [*Schutt et al., 2008*]. We see little evidence for a deep narrow plume extending directly beneath Yellowstone, although conductivities remain elevated to depths of at least 200 km over a broad area in the vicinity of the putative hotspot. Plausibly the seismically imaged thermal anomaly is present, but poorly resolved by the MT data, which is much more strongly impacted by partial melt and fluids present at shallower depths. Overall our images are quite consistent with interpretations that emphasize the role of local convection and lithospheric interaction to explain patterns of progressive magmatism along the Yellowstone "hot spot" track [*e.g., Humphreys et al, 2000*]. High conductivites imaged at the base of the crust beneath the Eastern SRP are probably due to a combination of partial melt, and highly saline fluids exsolved during magmatic underplating.

References

Humphreys, E.; Dueker, K.; Schutt, D. & Smith, R. (2000), 'Beneath Yellowstone: evaluating plume and nonplume models using teleseismic images of the upper mantle', *GSA Today, 10*, 1-7.

Smith, R.B.; Jordan, M.; Steinberger, B.; Puskas, C.M.; Farrell, J.; Waite, G.P.; Husen, S.; Chang, W. & O'Connell, R. (2009), 'Geodynamics of the Yellowstone hotspot and mantle plume: Seismic and GPS imaging, kinematics, and mantle flow', *J. Volcanol. Geoth. Res. 188*(1-3), 26 - 56.

Schutt, D.; Dueker, K. & Yuan, H. (2008), 'Crust and upper mantle velocity structure of the Yellowstone hot spot and surroundings', *J. Geophys. Res.* (Solid Earth), 113, 3310-.

Acknowledgements: Support from the US DOE under grant DE-FG02-06ER15819 for development of the 3D inversion code is acknowledged.

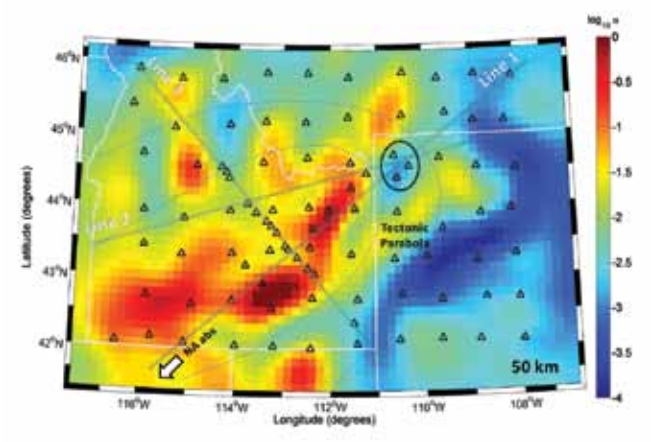

Electrical conductivity model at 50 km depth beneath Snake River Plain. Data locations are indicated by black triangles. The direction of absolute motion of North American plate is marked with a white arrow. Also schematically indicated are the "tectonic parabola" around the Eastern Snake River Plain, and the Yellowstone National Park (black oval). The grey lines are the transects shown in detail in Figure 2.

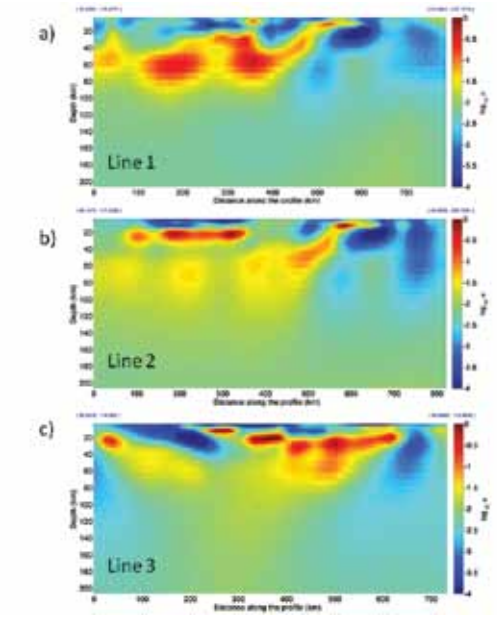

Electrical conductivity transects across the Snake River Plain (see Figure 1).

Imaging the Shear Wave Velocity "Plumbing" beneath the Northwestern United States with Rayleigh Wave Tomography: The High Lava Plains vs Yellowstone

Lara Wagner *(University of North Carolina at Chapel Hill),* **Donald Forsyth** *(Brown University),* **Matthew Fouch** *(Arizona State University),* **David James** *(Carnegie Institution of Washington)*

Since the mid-Miocene, the northwestern United States has experienced extensive flood basalt volcanism, followed by the formation of two time-progressive tracks of silicic volcanism: the Yellowstone/Snake River Plains (YSRP) and the High Lava Plains (HLP). The YSRP track progresses towards the northeast, parallel to North American plate motion, and has therefore often been attributed to a deep mantle plume source. However, the HLP track progresses to the northwest over the same time frame in a direction not consistent with any regional plate motion. The causes of the mid-Miocene flood basalts and the tracks of the YSRP and HLP are a matter of ongoing debate. We performed Rayleigh wave phase velocity inversions and inversions for 3-D shear wave velocity structure of the northwestern United States using data collected from the High Lava Plains Deployment and the EarthScope USArray Transportable Array (TA). The large number of stations used in these inversions allows us to show an unprecedented level of detail in the seismic velocity structures of this tectonically complex area. Our velocity images indicate that low S-wave velocities in the uppermost mantle do not well match the track of HLP volcanism. While at the surface the Newberry caldera appears to anchor the NW end of the HLP hotspot track, the seismic results show that it lies in a separate, north-south trending low velocity band just east of the Cascades that is distinct from the main HLP trace. The eastern edge of this low velocity band also correlates with a change in the magnitude of shear wave splitting delay times, possibly indicating changes in amount of partial melt present [Long et al., 2009]. In contrast, the ultra-low S-wave velocities beneath the YSRP track extend locally to at least 175 km depth and are by far the most prominent seismic anomalies in the region. Along axis, the YSRP hotspot track is characterized by a discrete low velocity channel in the upper mantle that shallows, narrows and intensifies to the northeast, but then deepens rapidly to the north beneath Yellowstone. Because Rayleigh wave tomography loses resolution below ~200 km, we cannot determine whether or not this anomaly is caused by a deep mantle plume source. However, the shallowing of the low velocity anomaly to the northeast is consistent with a moving heat source coming from below 200 km depth.

Geologic map of the northwestern United States with -3% low velocity surface contour shown in 3-D below the map: Shown are the locations of the Blue Mountain Province (BMP), Steens Mountain (SM), and the Owyhee Plateau (OP). Red triangles show Holocene arc volcanism. The black dashed line is the 87Sr/86Sr = 0.706, usually taken to represent the edge of cratonic North America. The boundaries of Basin and Range extension are shown with a purple dashed line. Black contours indicate the age progression for rhyolites in the High Lava Plains and the Snake River Plains. The yellow and blue contours in the HLP track show our <5 Ma and > 7 Ma contours for High Lava Plains rhyolites.

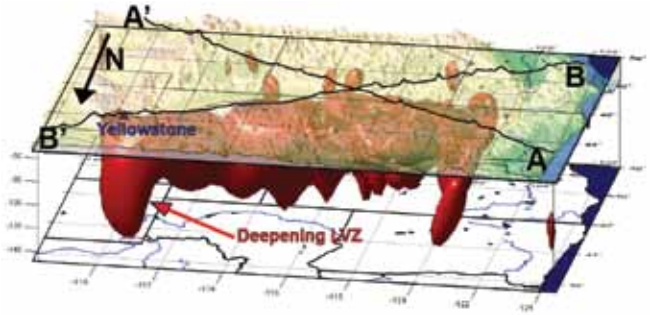

Yellowstone/Snake River Plains low velocity zone: shown is the -3% surface contour in perspective, looking from the north down towards the southeast. Shown is the location of Yellowstone Caldera (blue triangle).

References

Wagner, L., D. Forsyth, M. Fouch, and D. James (2010), Detailed three dimensional shear wave velocity structure of the northwestern United States from Rayleigh wave tomography. *Earth Planet. Sci. Lett.*, in review.

Long, M. D., H. Gao, A. Klaus, L. S. Wagner, M. J. Fouch, D. E. James, and E. Humphreys (2009), Shear wave splitting and the pattern of mantle flow beneath eastern Oregon, *Earth Planet. Sci. Lett., 288*, 359-369.

Acknowledgements: The High Lava Plains deployment was funded through NSF award EAR-0507248 (MJF) and EAR-0506914 (DEJ). LW's participation was supported by NSF award EAR-0809192 and DWF was supported by NSF award EAR-0745972.

Temperature of the Yellowstone Hotspot

Derek L Schutt *(Colorado State University)*, **Ken Dueker** *(University of Wyoming)*

Recent studies show that the Yellowstone hotspot is associated with a plume-like low velocity pipe that ascends from at least the transition zone to the lithosphere-asthenosphere boundary, where the plume is sheared to the southwest by North American plate motion. Rayleigh wave tomography shows this plate-sheared plume layer has an extremely low S wave velocity of 3.8 ± 0.1 km/s at 80 km depth, ~0.15–0.3 km/s lower than the velocity observed beneath normal mid-ocean ridges.

To constrain the temperature of the plume layer, a grid search with respect to grain size and temperature is performed to fit the observed Rayleigh wave phase velocities. Using a variety of velocity-temperature scalings--including testing the effects of grain-size sensitivity--and varying such poorly constrain parameters as activation volume, we find that an excess temperature is needed to explain the upper mantle low velocity trend associated with Yellowstone. At 95% confidence, we find the plume layer is >55–80°C hotter than ambient mantle, strongly implying this is a weak thermal upwelling that nucleated off a deeper thermal boundary layer: i.e. confirming that Yellowstone is a plume.

References

Schutt, D. L. and K. Dueker (2008), Temperature of the plume layer beneath the Yellowstone Hotspot, *Geology, 36*(8), 4.

Acknowledgements: We thank the National Science Foundation (NSF) for support in the form of time to work on the project and for publication costs, as well as for Geophysics/Geochemistry NSF grant EAR-0409538. This work was built on data collected during a 2000 PASSCAL experiment supported by Continental Dynamics Programs Grant EAR-CD-9725431.

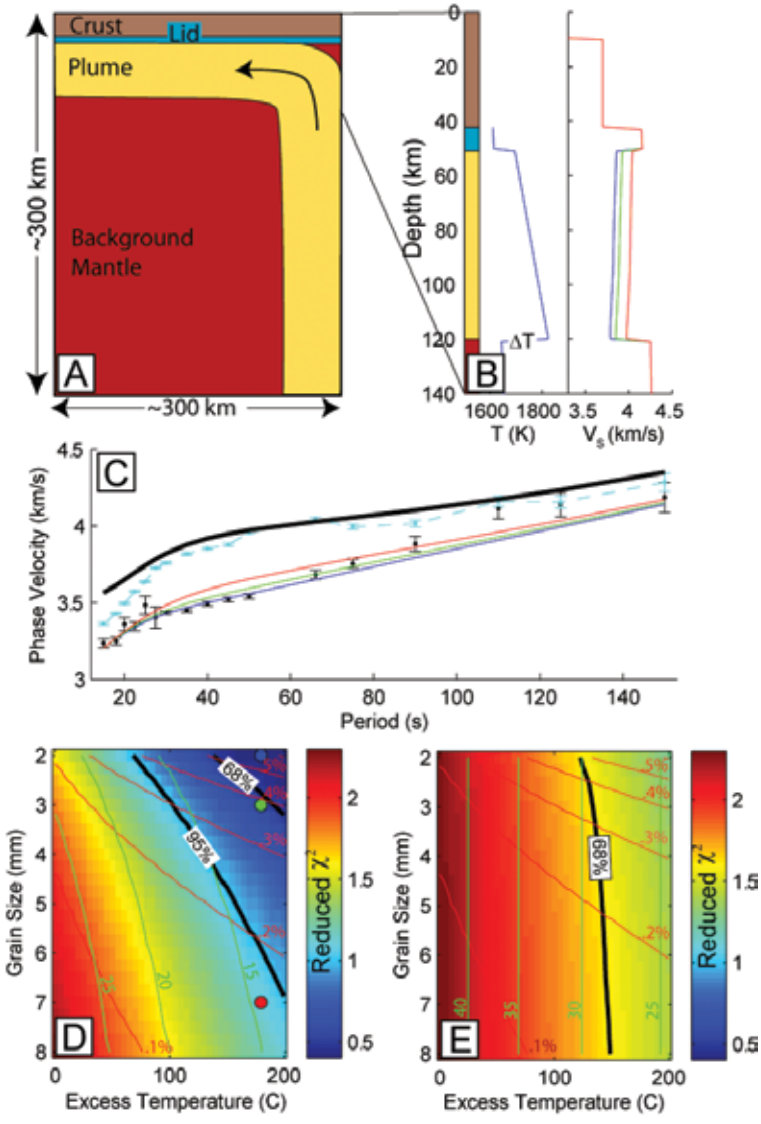

Yellowstone plume layer temperature, melt porosity, and shear wave attenuation. A: Cross section along Yellowstone hotspot track from surface wave tomography. B: Hotspot structure is approximated by four layers: crust, mantle lid, plate-sheared plume layer, and underlying mantle. Example thermal profile is shown for 180°C excess temperature (T). Temperature decreases within plume layer are due to latent heat of melting. Colored lines in plume layer are example VS profiles calculated for this temperature structure using grain-size–sensitive anelastic velocity scaling for grain sizes of 2 mm (blue), 3 mm (green), and 7 mm (red). C: Predicted phase velocities for the three example Vs models shown in B and observations with their one standard error bars. Cyan dashed line and black solid lines are for Wyoming craton and PREM (Dziewonski and Anderson, 1981) velocity models. D&E: Reduced chi-squared error surface for grain-size–sensitive (D) and non-grain-size sensitive anelastic (E) models.

Slab Fragmentation and Edge Flow: Implications for the Origin of the Yellowstone Hotspot Track

D.E. James *(Carnegie Institution/DTM),* **M.J. Fouch** *(School of Earth and Space Exploration, Arizona State University),* **J.B. Roth** *(Exxon/Mobil),* **R.W. Carlson** *(Carnegie Institution/DTM)*

The Snake River Plain/Yellowstone (SRP/Y) volcanic complex is widely considered a classic example of a plume generated continental hotspot (e.g. Smith et al., 2009). By that model, the plume head appeared ca 17 Ma near the Oregon-Idaho-Nevada border with the outpouring of the Steens and Columbia River flood basalts. The SRP/Y hotspot is taken to be the product of plume tail upwelling over the past 12 Ma. Our recent S-wave and P-wave tomographic images, however, instead suggest a subduction-related process by which volcanism along the SRP/Y hotspot track results from slab fragmentation, trench retreat, and mantle upwelling at the leading edge of the descending plate and around its truncated edges (Faccenna et al., 2010; K. Druken and C. Kincaid, pers. comm.). Seismic images of the deeper upper mantle show that the subducted oceanic plate extends locally eastward well into stable North America. The break-up and along-strike fragmentation of the descending plate is related in both time and space to the onset of flood volcanism and the formation of the SRP/Y hotspot. A sub-horizontal branch of subducting oceanic plate, orphaned from the descending plate by the northward migration of the Mendocino triple junction, resides in the mantle transition zone (400-600 km) directly beneath the SRP/Y track (Figure 1a). Its truncated northern edge is parallel to the northwestern margin of the hotspot track itself and marks the southern edge of a slab gap (Figure 1b). Numerical and physical tank modeling show that a rapidly retreating and severely fragmented downgoing plate drives mantle flow around both the tip and the edges of the descending slab. Our seismic results show that the morphology of the subducting slab is appropriate for generating large-scale poloidal flow (flood volcanism) in the upper mantle during the re-initiation phase of slab descent ca 20 Ma and for generating smaller-scale toroidal and poloidal upwellings (hotspot volcanism) around both the leading tip and northern edge of the slab as it descends into the deeper upper mantle. Plate reconstructions are consistent with the timing and position of both flood and hotspot volcanism.

Acknowledgements: This work is part of the High Lava Plains (HLP) Project, supported by Continental Dynamics NSF grants EAR-0507248 (MJF) and EAR-0506914 (DEJ and RWC), as well as EAR-0548288 (MJF EarthScope CAREER grant). We thank the USArray team for a remarkable effort and the superb efforts of the PIC staff and the HLP seismic team in the deployment and operation of the HLP seismic array. Data were provided through the IRIS Data Management Center. We thank ranchers throughout the HLP region who hosted seismic stations. The Eastern Oregon Agricultural Research Center provided critical logistical assistance for the High Lava Plains seismic team during this project.

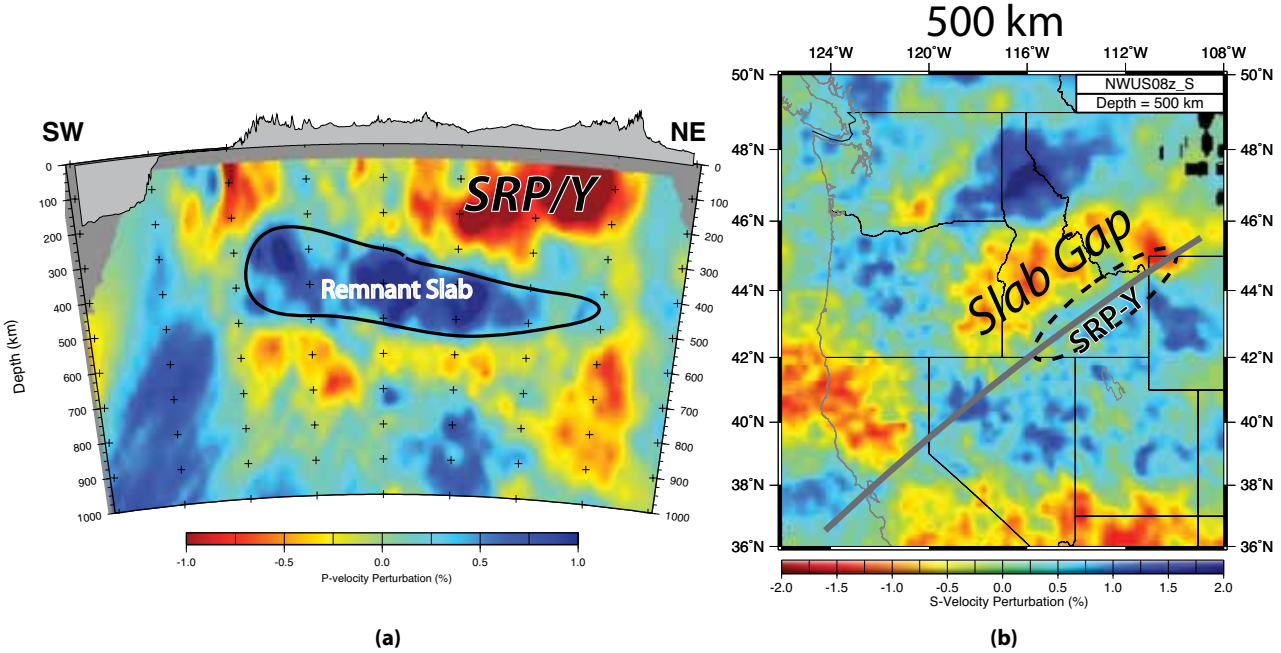

Figure 1. (a) P-velocity vertical cross-section parallel to plate convergence on axis of SRP/Y showing a sub-horizontal remnant of the Farallon slab adrift in the mantle transition zone beneath the SRP/Y hotspot track, its leading edge just beneath Yellowstone; (b) S-velocity perturbations at 500 km depth a "slab gap" just north of and parallel to the SRP/Y track itself. The slab gap extends from north of Yellowstone into eastern Oregon, its southern margin coinciding with the northern boundary of the remnant slab in (a).

Plume-Slab Interaction beneath Western US

Mathias Obrebski *(UC Berkeley),* **Richard Allen** *(UC Berkeley),* **Mei Xue** *(Tongji University),* **Shu-Huei Hung** *(National Taiwan University)*

Using the Earthscope Transportable Array, Flexible Arrays in Cascadia, and regional seismic networks, we have constructed 3D P- and S-velocity models for the mantle structure beneath the western US. The DNA09-P and –S models use teleseismic body-wave traveltime measurements that have been cross-correlated at a range of frequencies for relative arrival times and them inverted for velocity structure using finite-frequency sensitivity kernels. The independent P- and S-velocity models show good agreement in the structures imaged. The figure illustrates some of the more interesting features in the region. Panel (a) maps the structures at 200 km depth and clearly shows the subducting Juan de Fuca slab high velocity anomaly (JdF) and the Yellowstone-Snake River Plain low-velocity anomaly (YS). The three west-to-east cross-sections illustrate the variable nature of the subducting slab. At its southern end (C-C') the slab anomaly is strong, but at the latitude of Oregon it becomes weaker and shallower. Further east a strong low-velocity anomaly is imaged beneath Yellowstone that can be tracked from the Caldera to the base of model resolution at ~1000km depth. This is interpreted as the Yellowstone plume responsible for the hotspot rack at the surface. Panel (e) shows a 3D view of the subducting slab (JdF) and the low-velocity Yellowstone anomaly. The DNA models are available at http://dna.berkeley.edu.

References

Obrebski, M., R.M. Allen, M. Xue, S.-H. Hung, Slab-plume interaction beneath the Pacific Northwest, *Geophys. Res. Lett., 37*, doi:10.1029/2010GL043489, 2010.

Acknowledgements: This work was funded by NSF EAR-0745934 and EAR-0643077. The work was facilitated by the IRIS-PASSCAL program through the loan of seismic equipment, USArray for providing data and the IRIS-DMS for delivering it.

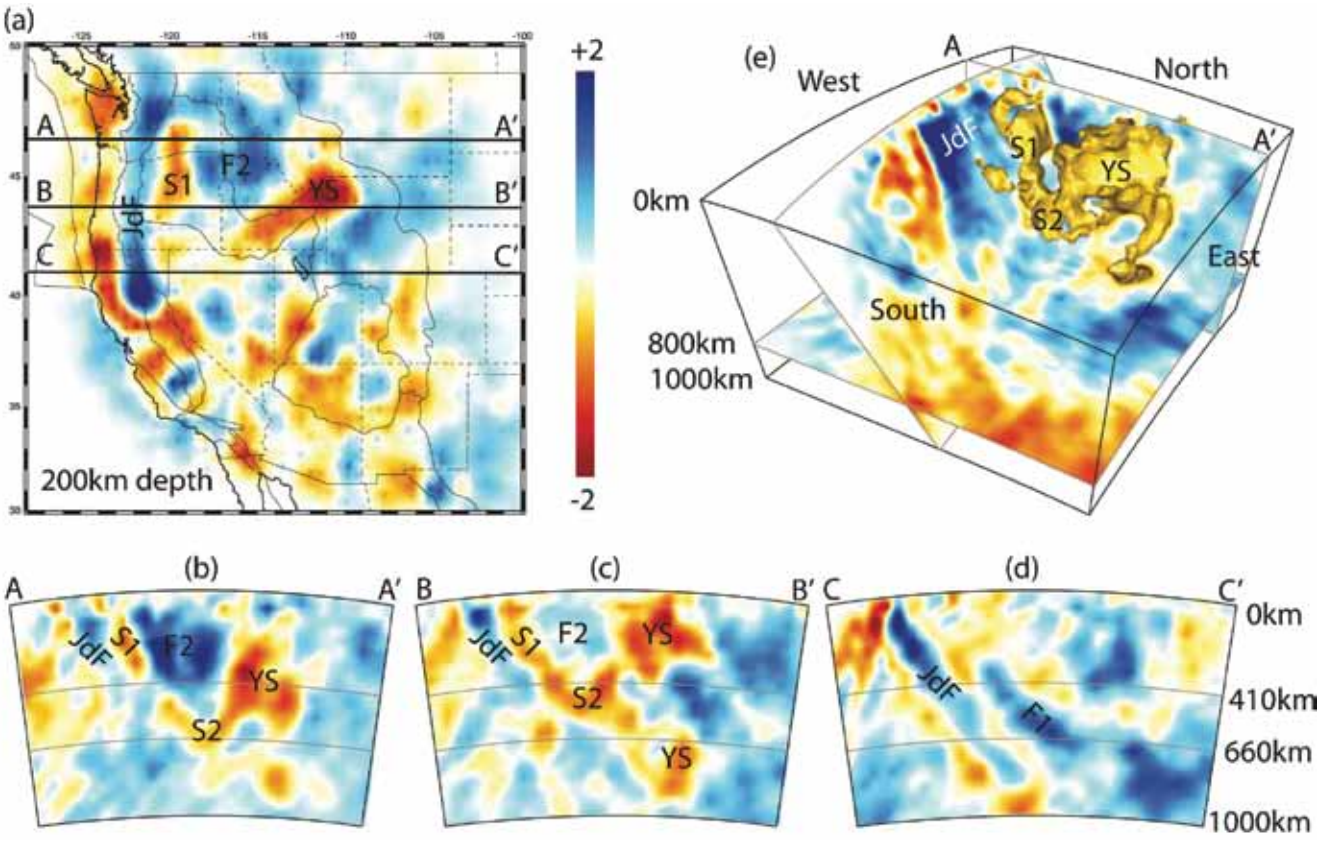

Figure. Slices through the DNA09-P velocity model. See text for description.

Mantle Shear-Wave Velocity Structure beneath the Hawaiian Hotspot

Cecily Wolfe *(University of Hawaii at Manoa),* **Sean Solomon** *(Carnegie Institution of Washington),* **Gavi Laske** *(Scripps Institution of Oceanography),* **Robert S. Detrick** *(Woods Hole Oceanographic Institution),* **John A. Orcutt** *(Scripps Institution of Oceanography),* **David Bercovici** *(Yale University),* **Erik H. Hauri** *(Carnegie Institution of Washington)*

Hawaii is the archetypal hotspot and has been suggested to be the surface expression of a mantle plume, a localized upwelling of hot buoyant material from Earth's deep mantle, although such an origin has been debated. One of the most straightforward indications of whether a hotspot is the result of a plume is the presence of a narrow, vertically continuous zone of low seismic velocities in the underlying mantle, indicative of higher-than-normal temperatures, anomalous mantle composition, or partial melt. Defining the mantle structure that lies beneath hotspots such as Hawaii is thus important for revealing the origin of such features. The Hawaiian Plume-Lithosphere Undersea Melt Experiment (PLUME) was a multidisciplinary program whose centerpiece was a large network of four-component broadband ocean-bottom seismometers and three-component portable broadband land stations [*Laske et al., 2009*]. Data from IRIS Global Seismic Network stations KIP and POHA were used in this study, and all of the collected data were archived at the IRIS Data Management Center.

Three-dimensional images of shear-wave velocity beneath the Hawaiian Islands obtained from the PLUME records show an upper-mantle low-velocity anomaly that is elongated in the direction of the island chain and surrounded by a high-velocity anomaly that is parabola-shaped in map view [*Wolfe et al., 2009*]. Low velocities continue downward to the mantle transition zone between 410 and 660 kilometers depth, a result that is in agreement with prior observations of transition-zone thinning at this location. The inclusion of SKS observations extends the imaging resolution downward to a depth of 1500 kilometers and reveals a several-hundred-kilometer-wide region of low velocities beneath and southeast of Hawaii. These images support the hypothesis that the Hawaiian hotspot is the result of an upwelling high-temperature plume from the lower mantle.

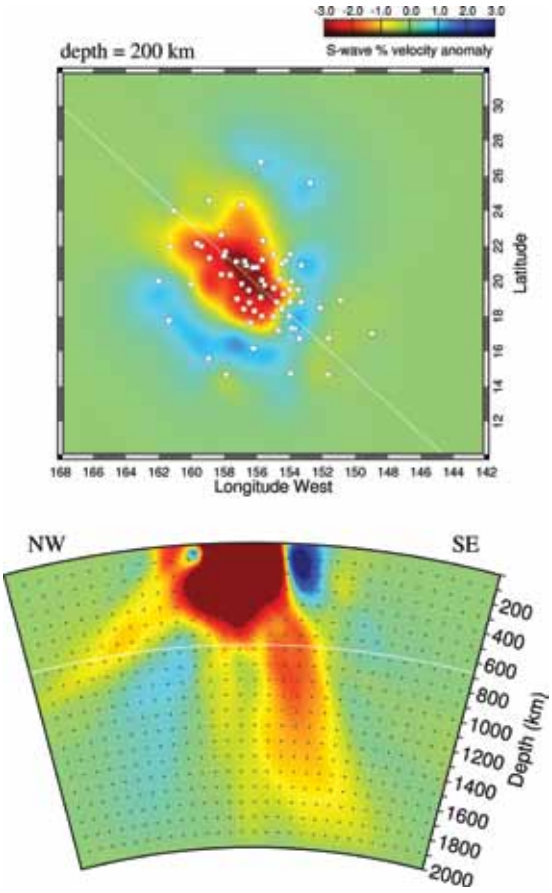

Top plot: Upper mantle shear-wave velocity heterogeneity at 200 km depth. Station locations are indicated by squares. The scale is given at the upper right and ranges ±3%. Bottom plot: Vertical cross section. The scale ranges over ±1%.

References

Laske, G., J. A. Collins, C. J. Wolfe, S. C. Solomon, R. S. Detrick, J. A. Orcutt, D. Bercovici, and E. H. Hauri, Probing the Hawaiian hotspot with new broadband ocean bottom instruments, Eos Trans. AGU, 90, 362-363, 2009.

Wolfe, C. J., S. C. Solomon, G. Laske, J. A. Collins, R. S. Detrick, J. A. Orcutt, D. Bercovici, and E. H. Hauri, Mantle shear-wave velocity structure beneath the Hawaiian hotspot, *Science, 326*, 1388-1390, 2009.

Acknowledgements: This project was supported by the U.S. National Science Foundation. We also acknowledge the crews of the research vessels Melville, Ka'imikai-O-Kanaloa, and Kilo Moana, the Jason remotely operated vehicle team, the Ocean Bottom Seismograph Instrument Pool, the Carnegie Institution's portable seismology laboratory, IRIS, and the hosts of temporary stations on the Hawaiian Islands.

Rayleigh Waves Observed During the Hawaiian Plume Deployment Trace Anomalously Low Shear Velocities in the Lithosphere and Asthenosphere

G. Laske *(UC San Diego),* **J.A. Orcutt** *(UC San Diego),* **J.A. Collins** *(Woods Hole Oceanographic Institution),* **C.J. Wolfe** *(University of Hawaii at Manoa),* **S.C. Solomon** *(Carnegie Institution of Washington),* **R.S. Detrick** *(Woods Hole Oceanographic Institution),* **D. Bercovici** *(Yale University)*

Hawaii has long been viewed as the textbook example of a plume-fed hotspot although other models such as a progressively cracking lithospheric plate have been considered to explain Hawaii's island chain. The plume model has been heavily contested by some as it has been difficult to obtain comprehensive and unambiguous geophysical observational constraints. One major problem that seismology has faced has been its complete reliance on land stations. During two field campaigns from 2005 to 2007, the Plume-Lithosphere-Undersea-Mantle Experiment (PLUME) occupied 83 sites to provide continuous year-long seismic records [*Laske et al., 2009*]. Nearly 70 of these sites were occupied by ocean bottom seismometers (OBSs), most of which featured a broadband seismometer (a Guralp CMG-3T or a Nanometrics Trillium 240). To date, we have compiled two-station Rayleigh wave phase velocity curves for over 600 paths across the 1000-km-wide network, and we have use these curves in inversions for 3-dimensional (3-D) shear velocity structure. Our 3-D images in the lithosphere and asthenosphere reveal a pronounced low velocity anomaly to the west of the island of Hawaii at depths of 80 km and greater. Toward shallower depths, the anomaly appears to diminish in size and magnitude and is centered between the islands of Hawaii and Maui. We interpret this anomaly as the likely source of melt that feeds Hawaii's extensive volcanism.

References

Laske, G., J. A. Collins, C. J. Wolfe, S. C. Solomon, R. S. Detrick, J. A. Orcutt, D. Bercovici, and E.H. Hauri (2009), Probing the Hawaiian hotspot with new broadband ocean bottom instruments, Eos Trans. AGU, 90, 362-363.

Nishimura, C.E. and D.W. Forsyth, (1989), The anisotropic structure of the upper mantle in the Pacfic. *Geophys. J., 96*, 203-229.

Acknowledgements: The waveforms from this experiment are available at the IRIS-DMC. This research was financed by the National Science Foundation under grants OCE-00-02470 and OCE-00-02819.

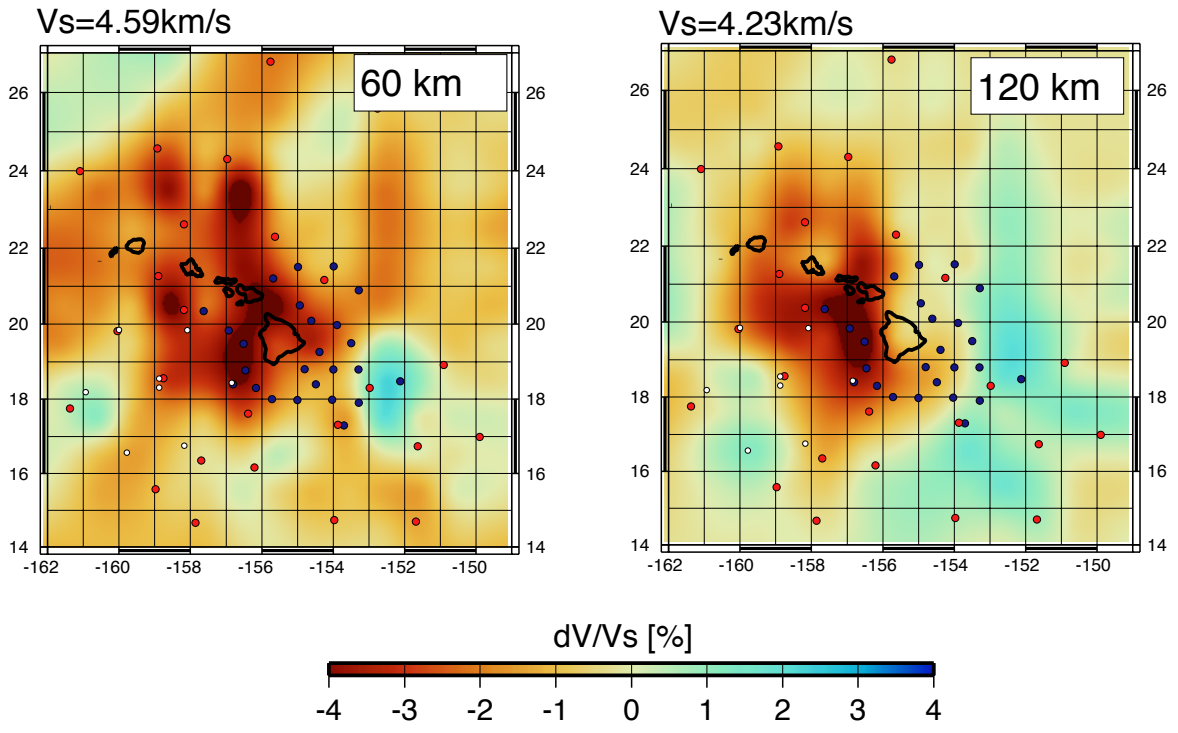

Model of shear velocity anomalies obtained from inverting Rayleigh wave phase velocity curves. The maps show percentage perturbations to reference velocities for 52-100 Ma old oceanic lithosphere (Nishimura and Forsyth, 1989).

Discordant Contrasts of P- and S-Wave Speeds Across the 660-km Discontinuity beneath Tibet: A Case for Hydrous Remnant of Sub-Continental Lithosphere

Tai-Lin Tseng *(University of Illinois, Urbana-Champaign),* **Wang-Ping Chen** *(University of Illinois, Urbana-Champaign)*

Using high-resolution, triplicate shear-waveforms recorded by broadband seismic arrays, we show that a corresponding anomaly of high S-wave speed (VS) is absent where an anomaly of high P-wave speed (VP) was recently recognized in the transition zone of the mantle (TZ) beneath central Tibet. A likely cause of the discrepancy between anomalies in VP and VS is a minor amount of water in nominally anhydrous polymorphs of olivine. Prior to thickening by continent-continent collision, the Tibetan mantle was part of a mantle wedge which has been hydrated during past episodes of subduction. Hydration of the sub-continental lithospheric mantle (SCLM) provides a natural mechanism to facilitate ductile deformation, so rapid thickening of the SCLM, which would have been hindered by advection of cold materials, can take place. Convective instability would then lead to removal and sinking of thickened, cold SCLM, leaving a remnant in the TZ detectable only in VP. This interpretation not only is consistent with previous reconstruction of the SCLM in Tibet based on several types of independent data, but also provides a new pathway for water to enter and be stored in the TZ.

References

Chen, W.-P., and T.-L. Tseng, Small 660-km seismic discontinuity beneath Tibet implies resting ground for detached lithosphere, *J. Geophys. Res.*, ***112***, B05309, doi:10.1029/2006JB004607, 2007.

Tseng, T.-L., and W.-P. Chen, Discordant contrasts of P- and S-wave speeds across the 660-km discontinuity beneath Tibet: A case for hydrous remnant of sub-continental lithosphere, *Earth Planet. Sci. Lett. , 268*, 450-462, 2008.

Chen, W.-P., M. Martin, T.-L. Tseng, R. L. Nowack, S.-H. Hung, and B.-S. Huang, Shear-wave birefringence and current configuration of converging lithosphere under Tibet, *Earth Planet. Sci. Lett., 295*(1-2), 297-304, doi:10.1016/j.epsl.2010.04.017, 2010.

Acknowledgements: Data centers of the IRIS (USA), the Institute of Earth Sciences, Academia Sinica (Taiwan, R. O. C.), and GEOSCOPE (France) kindly provided seismograms to us. We benefited from discussions with C.-T. Lee, P. Kapp, S.-L. Chung, J. Wang, J. Bass, J. Smyth, and S. Jacobsen; and an anonymous reviewer provided insightful comments. This work is supported by the U. S. National Science Foundation Grants EAR9909362 (Project Hi-CLIMB: An Integrated Study of the Himalayan-Tibetan Continental Lithosphere during Mountain Building, contribution I07) and EAR0551995. Any opinions, findings and conclusions or recommendations expressed in this material are those of the authors and do not necessarily reflect those of the NSF.

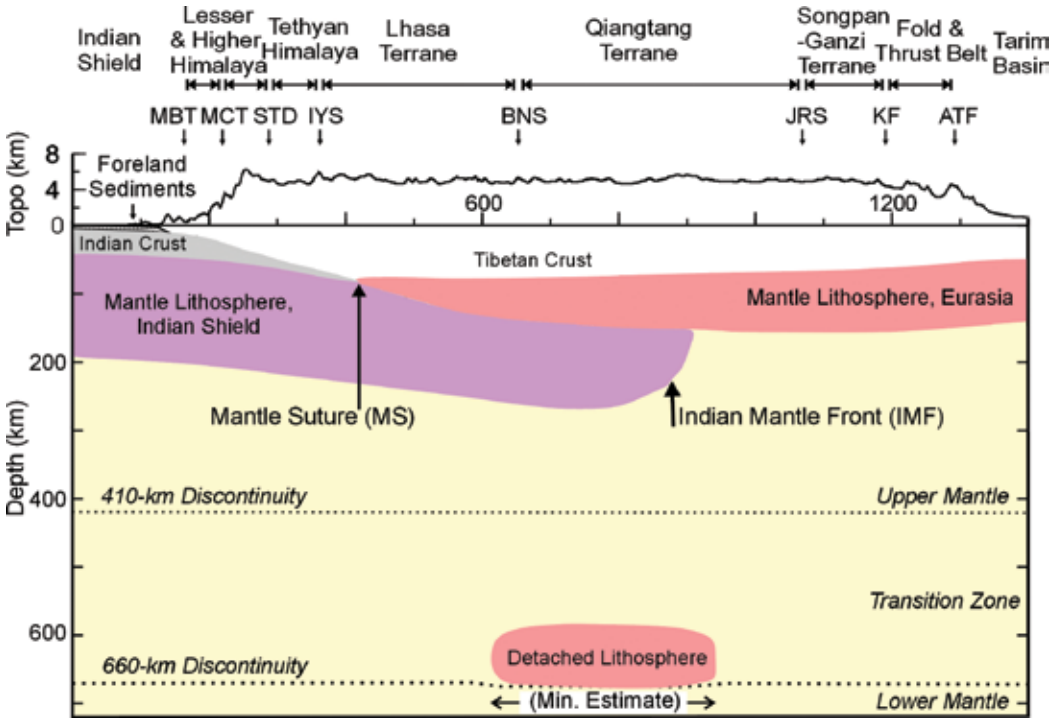

A schematic cross-section (Chen et al., 2010) showing the current configuration of the sub-continental lithospheric mantle, including a large-scale anomaly of high P-wave speed resting on top of the lower mantle and interpreted as the remnant of thickened (and subsequently detached due to Rayleigh-Taylor instability) lithospheric mantle (Chen and Tseng, 2007). This anomaly is invisible to S-waves, indicating the presence of water deep beneath an active zone of continental collision. The dimension of the detached lithosphere shown is a minimal estimate, limited by current coverage of seismic arrays around Tibet. For reference, we also show key geologic units/boundaries and topography at the present (vertically exaggerated by a factor of 13.15).

Deep Mantle Plumes and Convective Upwelling beneath the Pacific Ocean

Nicholas Schmerr *(Carnegie Institution of Washington),* **Edward Garnero** *(Arizona State University),* **Allen McNamara** *(Arizona State University)*

The 410 and 660 km discontinuities arise from solid-to-solid phase changes in the mineral olivine, and lateral variations in temperature and composition incurred by dynamical processes in the mantle produce topography on each boundary. To query discontinuity structure in the presence of mantle downwellings and upwellings, we use underside reflections of shear waves, a technique that requires the stacking of hundreds to thousands of seismograms. This method has flourished from the deployment of global and regional seismic arrays, whose data are freely available from the IRIS DMC. We collected a dataset of over 130,000 broadband seismograms that sample beneath the Pacific Ocean. In our study, we resolve the discontinuities to be relatively flat beneath most of the Pacific, except under subduction zones and volcanic hotspots. We find the phase boundaries are closer together beneath the Hawaiian hotspot, and also in a larger region of the south Pacific that is flanked by a number of volcanic hotspots. This region overlies the southern part of the large-scale low shear velocity province in the lowermost mantle, indicative of a large plume head or cluster of several plumes originating in the lowermost mantle and impinging upon the south Pacific 660 km discontinuity. This feature may be related to large volume volcanic eruptions, such as the Cretaceous Ontong Java Plateau flood basalts, which have been proposed to originate in the south Pacific.

References

Schmerr, N., et al. (2010), Deep mantle plumes and convective upwelling beneath the Pacific Ocean, *Earth Planet. Sci. Lett., 294*, 143-151.

Acknowledgements: NSF Grants EAR-0711401, EAR-0453944, EAR-0510383, EAR-0456356

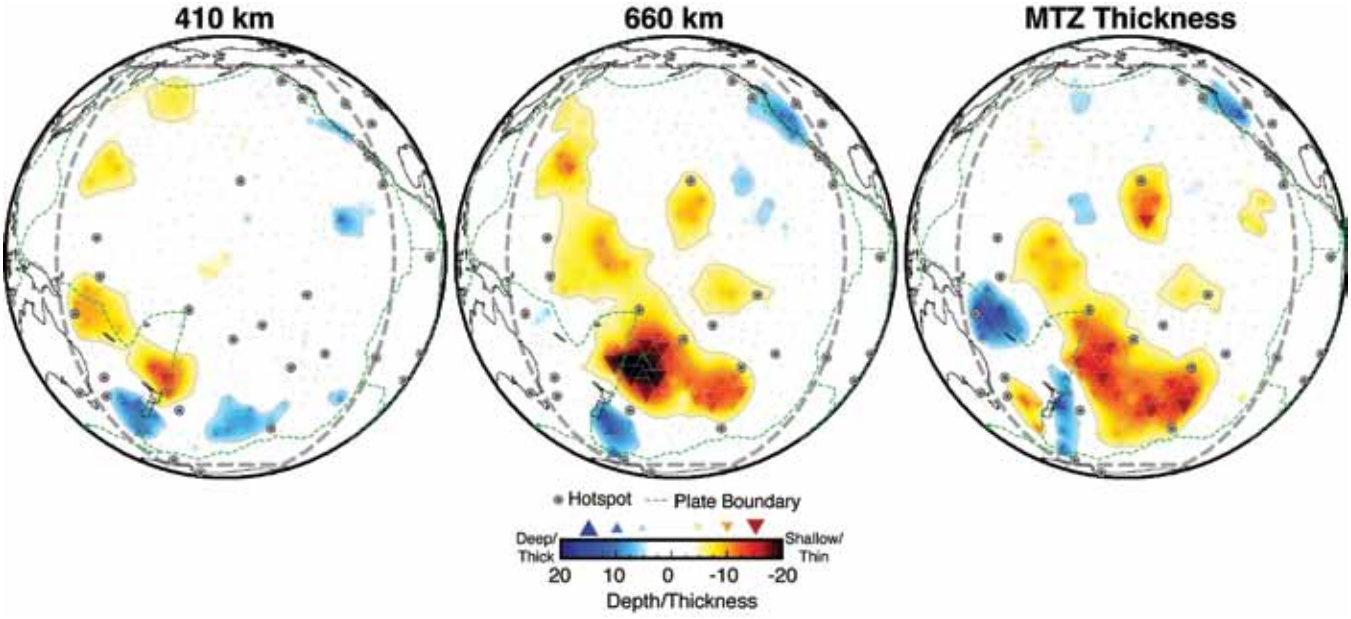

Topography maps for discontinuity depths and transition zone thickness in our Pacific study region. The depths are plotted relative to average values of 418 km, 656 km, and an average transiton zone thickness of 242 km.

Upper Mantle Discontinuity Topography from Thermal and Chemical Heterogeneity

Nicholas Schmerr *(Carnegie Institution of Washington),* **Edward Garnero** *(Arizona State University)*

Utilizing high resolution stacks of precursors to the seismic phase SS, we investigated seismic discontinuities associated with mineralogical phase changes at approximately 410 and 660 kilometers deep within the Earth beneath South America and the surrounding oceans. We utilized a dataset of over 17,000 broadband seismograms collected from the IRIS DMC and EarthScope. Our maps of phase boundary topography revealed deep 410- and 660-km discontinuities in the down-dip direction of subduction, inconsistent with cold material at 410-km depth. We explored several mechanisms invoking chemical heterogeneity within the mantle transition zone to explain this feature. In some regions, we detected multiple reflections from the discontinuities, consistent with partial melt near 410-km depth and/or additional phase changes near 660-km depth. Thus, the origin of upper mantle heterogeneity has both chemical and thermal contributions, and is associated with deeply rooted tectonic processes.

References

Schmerr, N., and E. Garnero (2007), Upper mantle discontinuity topography from thermal and chemical heterogeneity, *Science, 318*(5850), 623-626.

Acknowledgements: NSF Awards EAR-0453944 and EAR-0711401

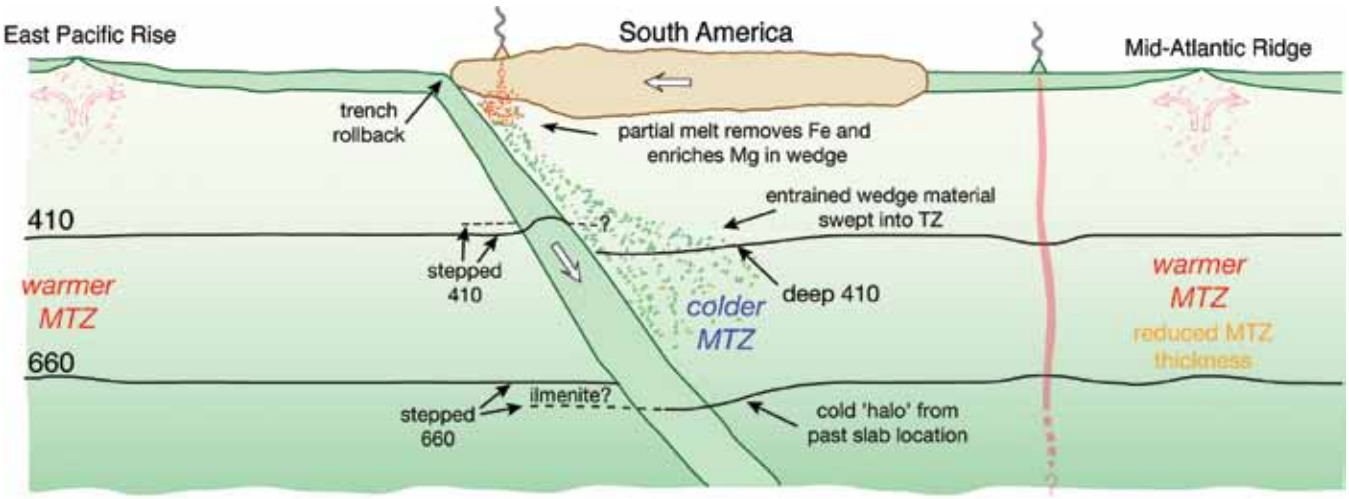

A cross section explaining our results, whereby iron is removed by melting in the mantle wedge and the Mg-enriched residue is swept into the transition zone along with the subducting lithosphere. This increases the pressure at which olivine transforms into wadsleyite, deepening the 410 km boundary.

Mantle Dynamics beneath North Central Anatolia

C. Berk Biryol *(University of Arizona),* **George Zandt** *(University of Arizona),* **Susan L. Beck** *(University of Arizona),* **A. Arda Ozacar** *(Middle East Technical University),* **Hande E. Adiyaman** *(University of Arizona),* **Christine R. Gans** *(University of Arizona)*

The North Anatolian Fault Zone (NAFZ) is a transform structure that constitutes the boundary between the Anatolian Plate to the south and the Eurasia Plate to the north. In this study we used shear-wave splitting analysis to study the upper mantle dynamics beneath Anatolia region and the the northward convex part of the NAFZ. The seismic data for our analysis comes from 39 broadband seismometers of the North Anatolian Fault passive seismic experiment (NAF) deployed at the central north Anatolia between 2005 and 2008 (Figure 1). The instruments for this experiment are provided by the IRIS-PASSCAL consortium. Our results reveal fairly uniform NE-SW trending anisotropy directions with decreasing delay times from west to east (Figure 1). The existence of significant and uniform anisotropy across major tectonic boundaries and plate margins in the study area argues for an asthenospheric source for the anisotropy rather than a lithospheric source. Our analysis also show that the lag times of the measured anisotropy varies with short spatial wavelengths beneath central Anatolia and the eastern section of the region is associated with lower lag times. We suggest the slab roll-back taking place along the Aegean trench and the different amounts of trench retreat for the Aegean and Cyprean trenches contributes significantly to the upper mantle dynamics of the region and induces a SW-directed astheonospheric flow with differential strengths from east to west (Figure 1). The similar patterns of variation for both crustal strain filed and observed fast polarization directions also support the idea of SW asthenospheric flow under the effects of Aegean and Cyprean slab roll-back processes.

References

Hatzfeld, D., Karagianni, E., Kassaras, I., Kiratzi, A., Louvari, E., Lyon-Caen, H., Makropoulos, K., Papadimitriou, P., Bock, G., & Priestley, K., 2001. Shear wave anisotropy in the upper-mantle beneath the Aegean related to internal deformation, *J. Geophys. Res., 106*, 737-753.

McClusky, S., Reilinger, R., Mahmoud, S., Ben Sari, D. & Tealeb, A., 2003. GPS constraints on Africa (Nubia) and Arabia plate motions, *Geophys. J. Int., 155*, 126–138.

Sandvol, E., Turkelli, N., Zor, E., Gok, R., Bekler, T., Gurbuz, C., Seber, D. & Barazangi, M., 2003. Shear wave splitting in a young continent-continent collision: An example from Eastern Turkey, *Geophys. Res. Lett.,30*(24), 8041.

Acknowledgements: This research was supported by NSF grant EAR0309838.

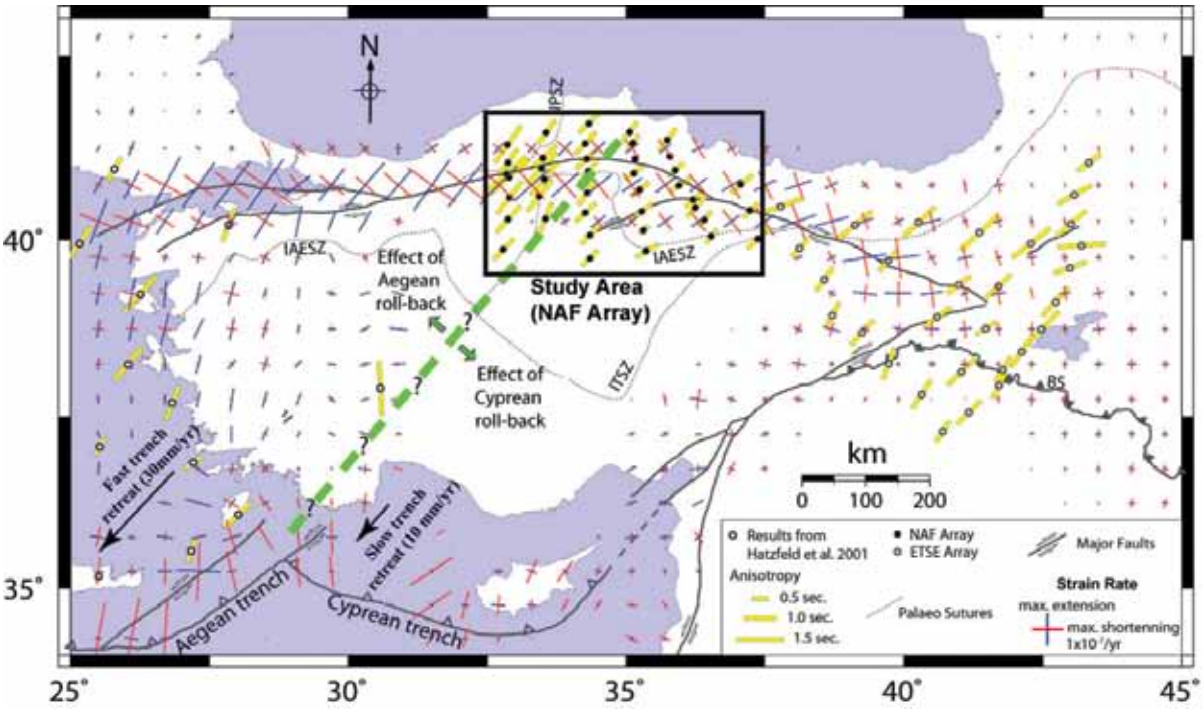

Results of splitting analysis from ETSE (Sandvol et al., 2003), NAF and Hatzfeld et al. (2001). BS: Bitlis Suture, IASZ: Izmir-Ankara-Erzincan Suture Zone, ITSZ: Inner Tauride Suture Zone, IPSZ: Inner Pontide Suture Zone.The trench retreat rates (black arrows) are from McClusky et al. (2003).

Edge-Driven Convection beneath the Rio Grande Rift

Jay Pulliam *(Baylor University),* **Stephen P. Grand** *(University of Texas at Austin),* **Tia Barrington** *(Baylor University),* **Yu Xia** *(University of Texas at Austin),* **Carrie Rockett** *(Baylor University)*

The Rio Grande Rift is a series of north-south trending faulted basins extending for more than 1000 km from Colorado to Chihuahua, Mexico and the Big Bend region of Texas. The rift is a Cenozoic feature with a mid-Oligocene (~30 Ma) early rifting stage, possibly related to foundering of the flat-subducting Farallon plate, and a recent late Miocene (~10 Ma) phase, which continues today.

There is no clear cause for the resurgence in magmatism and extension. However, the rift location at the edge of the stable, thick lithosphere Great Plains suggests that edge-driven convection along the eastern border of the Southern Rockies may play an important role in the current tectonics of the Rio Grande Rift. In particular, edge-driven convection may erode the lithosphere beneath the Rift and Great Plains, cause the lower crust to flow, and produce magma.

In 2008, a group of university scientists and high school teachers deployed 71 broadband seismographs interspersed between the EarthScope Transportable Array stations (Figure 1). The dense SIEDCAR (Seismic Investigation of Edge Driven Convection Associated with the Rio Grande Rift) network increases resolution of tomographic and receiver function images and shear wave splitting measurements, and allows construction of a detailed 3-D model of the eastern edge of the Rio Grande Rift structure.

Initial results of SKS splitting measurements to constrain patterns of mantle anisotropy (Figure 1), receiver functions to show crustal thickness (Figure 2), and body-wave and surface-wave tomography to determine P and S wave velocities show patterns consistent with edge-driven convection. Tomographic images indicate that the fast upper mantle anomaly beneath the eastern flank of the Rio Grande Rift is clearly separated from the Great Plains craton and that it extends southward to at least the Big Bend region of Texas. SKS splitting measurements show a marked decrease in splitting times above the fast "downwelling" anomaly in the mantle and generally larger splits on the rift flank proper. Receiver function images suggest a thickening of the crust to the east, which might indicate lower crustal flow induced by the edge convection or even delamination of lithosphere

Edge-driven convection may explain why, after a long period of quiescence, the Rio Grande Rift again became active. The SIEDCAR project seeks to understand how this process continues to modify the sub-continental lithosphere long after the formation of the rift.

Acknowledgements: The SIEDCAR project is supported by NSF grant #0746321 (EAR Division, EarthScope Program).

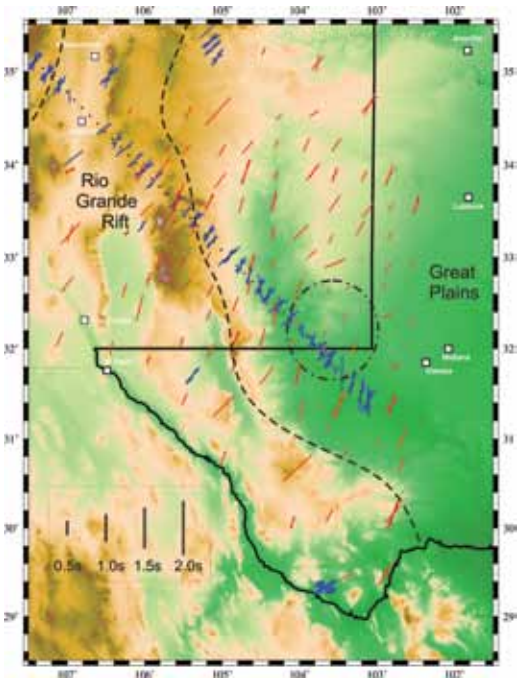

SKS splitting parameters for SIEDCAR (red) and TA (green) stations deployed 2008-2010 in the study area. Previous splitting measurements (La Ristra linear array and others) are shown in blue. Dash-dot circle indicates area where the SKS delay-times decrease; this area coincides with the "downwelling" fast anomaly in the mantle. The NW-SE-oriented La Ristra line is indicated by a dotted line.

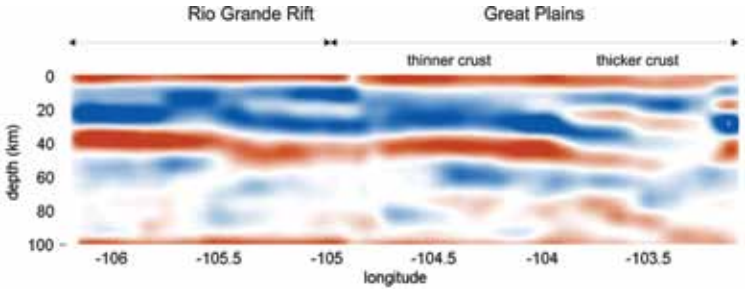

Receiver function image of crust and uppermost mantle beneath the eastern flank of the Rio Grande Rift from SIEDCAR and TA data for the NW-SE oriented La Ristra transect (dotted line in Figure 1). Thickened crust beneath the Great Plains extends both to the north and to the south, but, south of this cross-section, the transition from thick to thin crust moves to the southwest.

The Mantle Flow Field beneath Western North America

Matthew J. Fouch *(School of Earth and Space Exploration, Arizona State University),* **John D. West** *(School of Earth and Space Exploration, Arizona State University)*

The goal of this study is to image the mantle flow field beneath western North America. We utilize broadband data from regional and portable seismic arrays, with an emphasis on stations from EarthScope's USArray Transportable Array, to image seismic anisotropy and constrain deformation in the lithosphere and asthenosphere across the region.

Regional shear wave splitting parameters show clear variations with geologic terrane. In the Pacific NW, splitting times are large and fast directions are ~E-W with limited variability. Away from the Pacific-North American plate boundary, and sandwiched between broad regions of simple and strong splitting, stations within the Great Basin (GB) exhibit significant complexity. Fast directions show a clear rotation from E-W in the northern GB, to N-S in the eastern GB, to NE-SW in the southeastern GB. Splitting times reduce dramatically, approaching zero within the central GB.

While lithospheric fabric likely contributes to the shear wave splitting signal at many of the stations in this study, the broad-scale trends in both fast directions and delay times argue for a substantial asthenospheric source to the anisotropy. The regional mantle flow field therefore appears to be strongly controlled by significant and recent changes in plate boundary geometry. Assuming a North American plate reference frame, mantle flow appears to be controlled by absolute plate motion away from tectonic North America; conversely, rapid westward slab rollback of the Juan de Fuca plate dominates the Pacific NW U.S. flow field. To fill this gap in asthenospheric material, mantle flows strongly eastward S of the Juan de Fuca plate. Beneath the Great Basin, the paucity of shear wave splitting, combined with tomographic images and a range of geochemical and geologic evidence, supports a model of downward mantle flow due to a lithospheric drip.

Acknowledgements: This work would not have been possible without high quality seismic data provided through the hard work of the USArray Transportable Array team, the USArray Array Network Facility, and the IRIS Data Management Center. This research was supported by National Science Foundation awards EAR-0548288 (MJF EarthScope CAREER grant) and EAR-0507248 (MJF Continental Dynamics High Lava Plains grant).

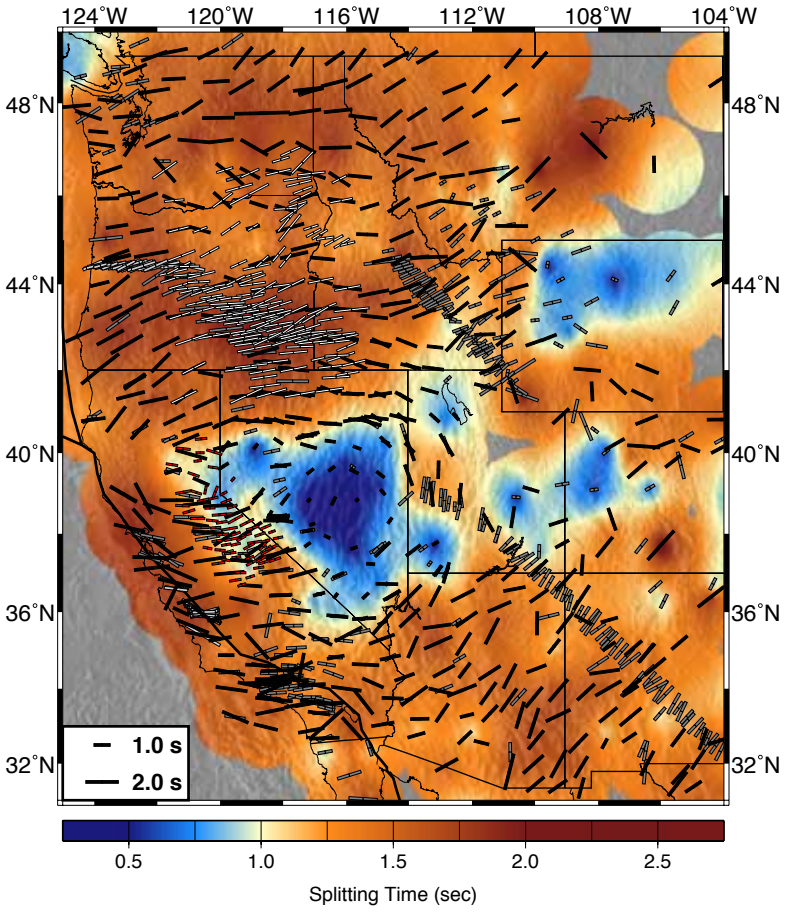

Station-averaged shear wave splitting beneath the western United States. Fast polarization directions denoted by azimuth of bar; splitting times denoted by length of bar. Background is smoothed, contoured splitting time magnitude. Black symbols represent new measurements from this study; red symbols represent splitting measurements from the SNEP experiment (courtesy Ian Bastow); white symbols represent measurements from Long et al. [2009]; gray symbols from other previous published studies. Clear, broad-scale regional similarities exist over hundreds of km, with significant complexity over shorter spatial scales in some regions. Large splitting times dominate most of region with the exception of very small splitting times beneath Great Basin.

Imaging Attenuation in the Upper Mantle with the GSN

Colleen A. Dalton *(Boston University),* **Goran Ekstrom** *(LDEO, Columbia University),* **Adam M. Dziewonski** *(Harvard University)*

Seismic-wave attenuation (1/Q) is thought to be highly sensitive to variations in temperature, and joint interpretation of attenuation and velocity models should aid in distinguishing between thermal and chemical heterogeneity in the mantle. However, imaging attenuation remains a challenging problem, because factors other than attenuation influence wave amplitude. Principally, amplitudes are affected by focusing due to lateral velocity variations, but uncertainties in the calculation of source excitation as well as inaccuracies associated with the instrument response can also obscure the attenuation signal in the data. We have developed a method to remove these extraneous effects and isolate the signal due to attenuation. We invert a large data set of fundamental-mode Rayleigh wave amplitudes, measured from waveforms recorded by the IRIS GSN and other global networks, in the period range 50--250 seconds simultaneously for a 3-D model of upper-mantle shear attenuation, maps of phase velocity, and amplitude correction factors for each source and receiver in the data set. The new three-dimensional attenuation model (QRFSI12) contains large lateral variations in upper-mantle attenuation, 60% to 100%, and exhibits strong agreement with surface tectonic features at depths shallower than 200 km. At greater depth,QRFSI12 is dominated by high attenuation in the southeastern Pacific and eastern Africa and low attenuation along many subduction zones in the western Pacific. QRFSI12 is found to be strongly anti-correlated with global velocity models throughout the upper mantle, and individual tectonic regions are each characterized by a distinct range of attenuation and velocity values in the shallow upper mantle. By comparing with laboratory experiments, we have found that lateral temperature variations can explain much of the observed variability in velocity and attenuation, although oceanic and cratonic regions appear to be characterized by different major-element composition or volatile content for depths < 225 km.

References

Dalton, C.A., G. Ekstrom, and A.M. Dziewonski. The global attenuation structure of the upper mantle, *J. Geophys. Res., 113*, doi:10.1029/2007JB005429, 2008.

Kustowski, B., G. Ekstrom, and A.M. Dziewonski. Anisotropic shear-wave velocity structure of the Earth's mantle: A global model, *J. Geophys. Res., 113*, doi:10.1029/2007JB005169, 2008.

Faul, U.H., and I. Jackson. The seismological signature of temperature and grain size variations in the upper mantle, *Earth Planet. Sci. Lett., 234*, 119-134, 2005.

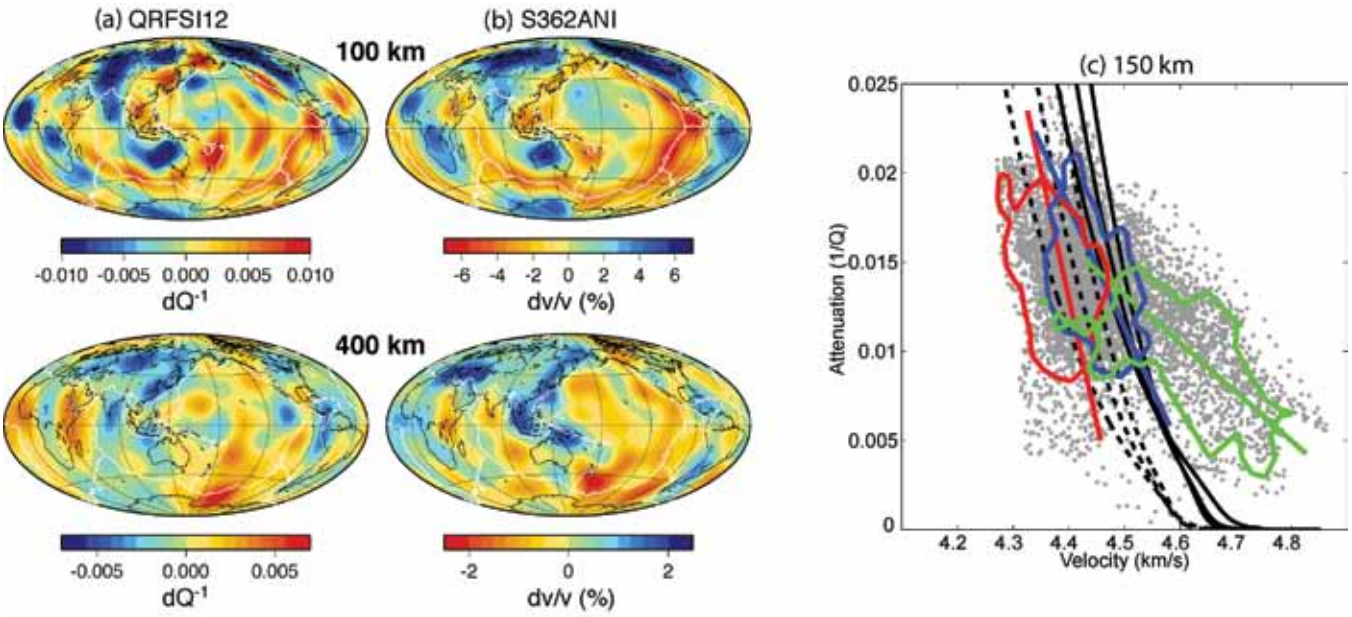

Comparison of global shear-attenuation (a) and shear-velocity (b) models at 100-km and 400-km depth. The attenuation model is from Dalton et al. (2008) and the velocity model is from Kustowski et al. (2008). (c) Grey points show seismologically observed shear velocity (S362ANI) and attenuation (QRFSI12) models sampled at 5762 points at 150-km depth. Colored contours enclose 75% of points from oceanic regions of age < 70 Myr (red) and > 70 Myr (blue) and from old-continental regions (green). Black lines show the predicted relationship between shear velocity and attenuation using the experiment-derived model of Faul and Jackson (2005).

S-Wave Velocity Structure beneath the High Lava Plains, Oregon, from Rayleigh-Wave Dispersion Inversion

Linda M. Warren *(Saint Louis University),* **J. Arthur Snoke** *(Virginia Tech),* **David E. James** *(Carnegie Institution of Washington)*

The High Lava Plains (HLP) "hotspot" track is a prominent volcanic lineament that extends from the southeast corner of Oregon in the northern Great Basin to Newberry volcano in the eastern Cascades. With the age of silicic volcanism decreasing along track to the northwest, the HLP and Newberry volcano are a rough mirror image to the Eastern Snake River Plain and Yellowstone but, in the case of the HLP, at an orientation strongly oblique to North American plate motion. Since this orientation is incompatible with plate motion over a fixed hotspot, other proposed origins for the HLP, such as asthenospheric inflow around a steepening slab, residual effects of a Columbia River/Steens plume, backarc spreading, and Basin and Range extension, relate it to various tectonic features of the Pacific Northwest. To begin distinguishing between these hypotheses, we image upper-mantle structure beneath the HLP and adjacent tectonic provinces with fundamental-mode Rayleigh-waves recorded by stations of the USArray Transportable Array, the recently-initiated HLP seismic experiment, the United States National Seismograph Network, and the Berkeley seismic network [*Warren et al., 2008*]. We estimate phase velocities along nearly 300 two-station propagation paths that lie within and adjacent to the HLP and cross the region along two azimuths, parallel to and perpendicular to the HLP track. The dispersion curves, which typically give robust results over the period range 16-171 seconds, are grouped by tectonic region, and the composite curves are inverted for S-wave velocity as a function of depth. The resulting variations in upper-mantle structure correlate with variations in surface volcanism and tectonics. The lowest velocities (~4.1 km/s) occur at ~50 km depth in the SE corner of Oregon, where there has been extensive basaltic volcanism in the past 2-5 Kyr, and suggest uppermost mantle temperatures sufficient to produce basaltic partial melting. While the seismic velocities of the uppermost mantle beneath the volcanic High Lava Plains are low relative to the standard Tectonic North America (TNA) model [*Grand and Helmberger, 1984*], they are only slightly lower than those found for the adjacent northern Great Basin and they appear to be significantly higher than upper mantle velocities beneath the Eastern Snake River Plain. Our results provide no evidence for a residual plume signature beneath the HLP region, leaving open questions as to the origin of the HLP volcanic track itself.

References

Warren, L.M., J.A. Snoke, and D.E. James, S-wave velocity structure beneath the High Lava Plains, Oregon, from Rayleigh-wave dispersion inversion, *Earth Planet. Sci. Lett., 274*, 121-131, 2008.

Grand, S.P., and D.V. Helmberger, Upper mantle shear structure of North America, *Geophys. J. R. Astron. Soc., 76*, 399-438, 1984.

Acknowledgements: This work was supported by the National Science Foundation through grant EAR-0506914 and by the Carnegie Institution of Washington.

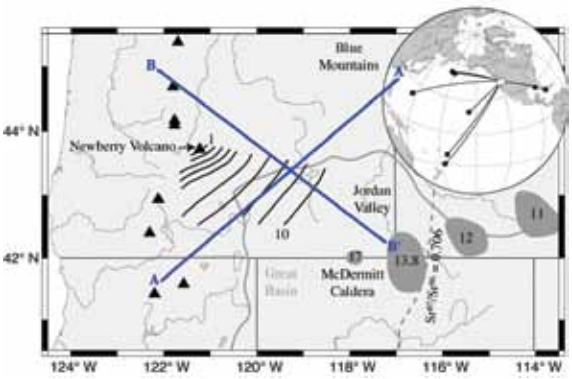

The tectonic setting of the High Lava Plains. Black triangles mark locations of Cascade volcanoes. Black lines beginning at Newberry Volcano and extending to southeast show increasing age of rhyolitic volcanism [Jordan et al., 2004]. McDermitt Caldera indicates onset of volcanism 16.1 Ma. Colored gray regions show rhyolite calderas along the Snake River Plain [Priest and Morgan, 1992]. Gray line outlines the Great Basin [Wernicke, 1992]. The dashed Sr87/Sr86 = 0.706 line approximates the western boundary of Proterozoic North America [Ernst, 1988]. Lower Sr87/Sr86 values lie to the west. The blue lines labeled A-A' and B-B' indicate the locations of the cross-sections in Figure 2. The inset shows the geographic setting of the study area and the great circle paths to that area from the nine analyzed earthquakes (black circles).

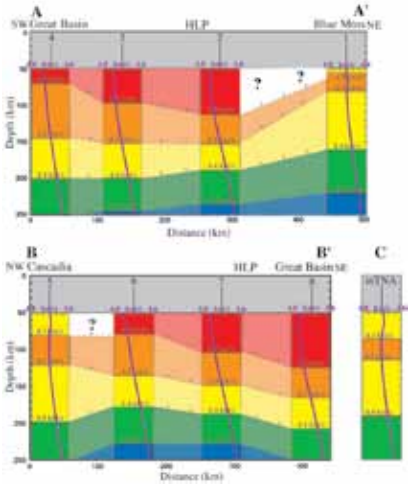

Cross-Sections interpreting S-wave velocity with depth along lines A-A' and B-B' of Figure 1. Velocity profiles for the eight regionalized paths are plotted at the center of the appropriate region and dashed lines with question marks interpolate structure between the regions. The large question marks in two of the transition regions indicate possible discontinuities in structure for which we have no constraints. S-wave velocity structure shallower than 50 km is not interpreted because it trades off with crustal thickness. (c) The velocity-depth profile for the modified TNA model is shown for comparison.

Three-Dimensional Electrical Conductivity Structure of the Pacific Northwest

Gary D. Egbert *(Oregon State University),* **Prasanta K. Patro** *(NGRI, Hyderabad, India)*

In conjunction with the USArray component of EarthScope, long period magnetotelluric (MT) data are being acquired in a series of arrays across the continental US. Initial deployments in 2006 and 2007 acquired data at 110 sites covering the US Pacific Northwest. The MT sites, distributed with the same nominal spacing as the USArray seismic transportable array (~70 km), produced data in the period range 10-10,000s of very good (2007) to excellent (2006) quality. Three-dimensional inversion of this dataset (Patro and Egbert, 2008) reveals extensive areas of high conductivity in the lower crust beneath the Northwest Basin and Range (C1), and beneath the Cascade Mountains (C2-C3), contrasting with very resistive crust in Siletzia (R1), the accreted thick ocean crust which forms the basement rocks in the Cascadia forearc and the Columbia Embayment). The conductive lower crust beneath the southeastern part of the array is inferred to result from fluids (including possibly partial melt at depth) associated with magmatic underplating. Beneath the Cascades high conductivities probably result from fluids released by the subducting Juan de Fuca slab. Resistive Siletzia represents a stronger crustal block, accommodating deformation in the surrounding crust by rigid rotation. Significant variations in upper mantle conductivity are also revealed by the inversions, with the most conductive mantle beneath the Northeastern part of the array, and the most resistive corresponding to subducting oceanic mantle beneath the Pacific plate (R2).

References

Patro P. K., G. D. Egbert, 2008. Regional conductivity structure of Cascadia: Preliminary results from 3D inversion of USArray transportable array magnetotelluric data, *Geophys. Res. Lett., 35*, L20311.

Acknowledgements: This work was partially supported by grants from the National Science Foundation (NSF-EAR0345438) and the U.S. Department of Energy 212 (DE-FG02-06ER15819).

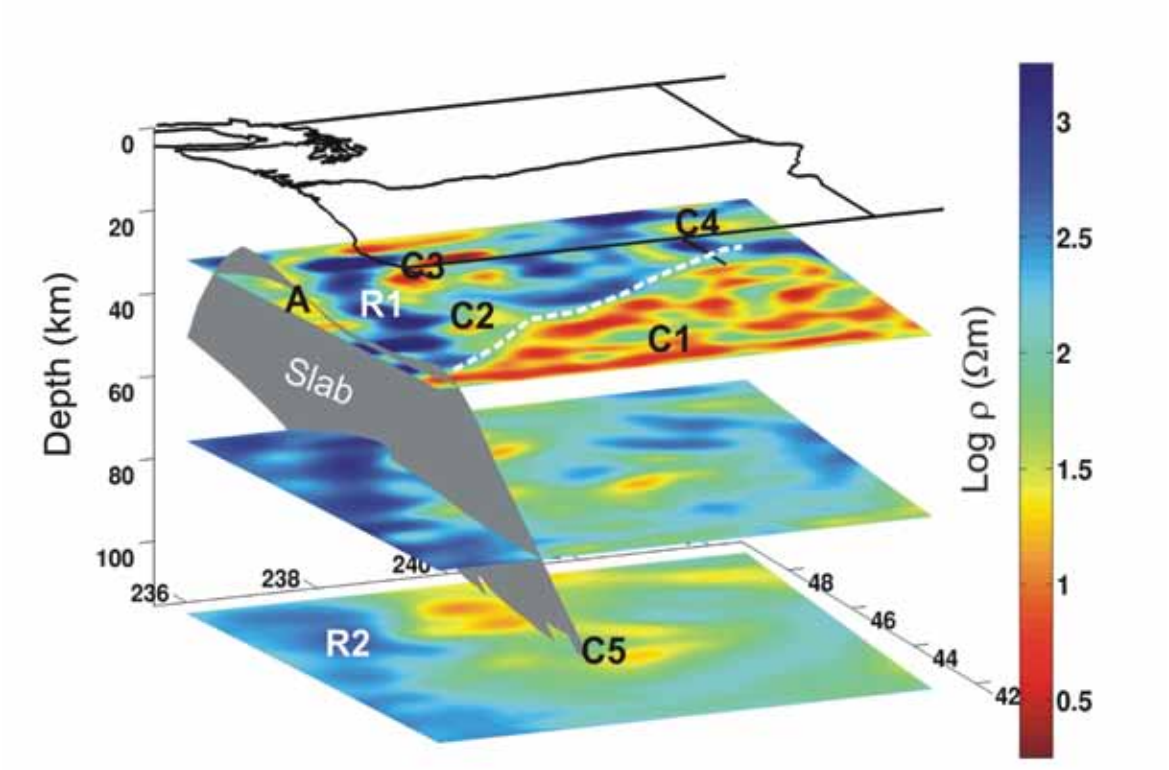

3D resistivity image of Pacific Northwest derived from the 3D inversion A: conductive zones in the forearc; C1: conductive lower crust in the Basin and Range, High lave plains and Blue Mountains; C2-C3: conductive features beneath the Cascades; R1: resistive Siletz terrane; R2: resistive oceanic mantle. Dashed white line marks contact interpreted as the southern boundary of Siletzia.

Observation of a Mid-Mantle Discontinuity beneath Northeast China from S to P Converted Waves Recorded by the USArray Stations

Fenglin Niu *(Department of Earth Science, Rice University)*

Strong and localized seismic discontinuity and reflectors have been observed in the lower mantle at various depths beneath western Pacific subduction zones [Niu and Kawakatsu, 1997; Kaneshima and Helffrich, 1999; Castle and Creager, 1999; Niu et al., 2003]. The lateral extension of these anomalous structures, however, is not well constrained. The information may hold the key to the understanding of the nature of these seismic structures as well as the related mantle processes. The USArray opens a new window for "viewing" and mapping these seismic anomalies. We found a clear later phase ~35-42 s after the direct P wave at most of the USArray recordings of two deep earthquakes that occurred near the border between east Russia and northeast China. The measured incident angle and arriving direction of this arrival suggest that it is an S to P wave converted at ~1000 km below Earth's surface. The mid-mantle discontinuity has a lateral dimension of greater than 200 km and 50 km along the EW and NS direction, respectively. It dips toward the east by ~12 degrees. The discontinuity is located in a region with a slightly higher P- and S-wave velocity, suggesting that the discontinuity is likely related to the subducted Pacific slab. One possible explanation is the breakdown of hydrous magnesium silicate phases, which is observed to be stable in cold environment at uppermost lower mantle pressure condition.

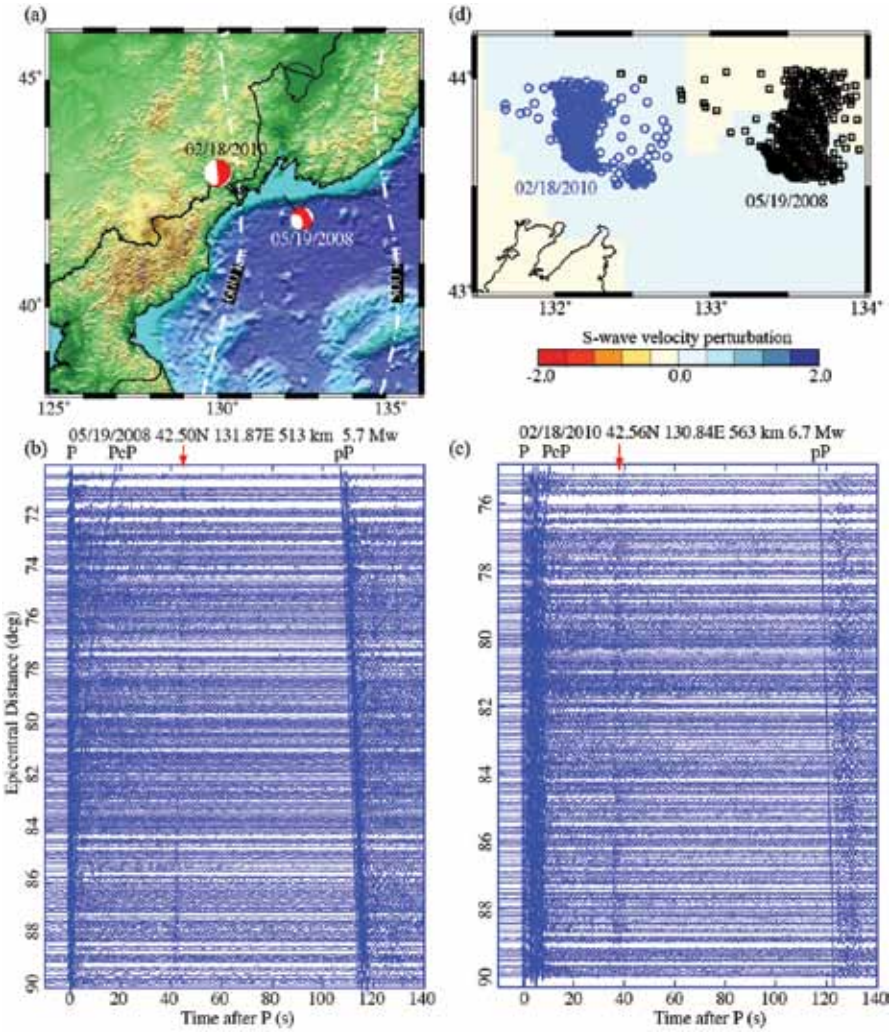

(a) Geographic locations of the two deep earthquakes near the border of China, Russia, and North Korea. White dashed lines indicate the Wadati-Benioff zone. (b) A portion of the USArray records of the 05/19/2008 deep earthquake. Theoretical travel times of the iasp91 model for the major expected body wave arrivals are indicated by straight lines. Note a clear phase between 40 and 45 s after the direct P arrival (indicated by red arrows) can be seen in most of the individual seismograms. The phase has a slightly negative slowness compared to the P wave. (c) same as (b) for the 02/18/2010 event. Not that in this case the unknown phase arrives at 35-40s after the direct P arrival, a few seconds earlier than those observed from the 05/19/2008 event. (d) Geographic distribution of the S to P conversion points from the 05/19/2008 (black squares) and the 02/18/2010 (blue circles). S-wave velocity perturbations at ~1000 km depth from Grand (2002) is also shown.

References

Castle, J. C., and K. C. Creager (1999), A steeply dipping discontinuity in the lower mantle beneath Izu-Bonin, *J. Geophys. Res., 104*, 7279 – 7292.

Kaneshima, S., and G. Helffrich (1999), Dipping lower-velocity layer in the mid-lower mantle: Evidence for geochemical heterogeneity, *Science, 283*, 1888–1891, 1999.

Niu, F., and H. Kawakatsu (1997), Depth variation of the mid-mantle seismic discontinuity, *Geophys. Res. Lett., 24*, 429– 432.

Niu, F., H. Kawakatsu, and Y. Fukao (2003), Seismic evidence for a chemical heterogeneity in the mid-mantle: A strong and slightly dipping seismic reflector beneath the Mariana subduction zone, *J. Geophys. Res., 108*(B9), 2419, doi:10.1029/2002JB002384,

Acknowledgements: Acknowledgments. We thank the EarthScope and IRIS for supplying the USArray data. This work is supported by NSF and the Department of Earth Science, Rice University

Core-Mantle Boundary Heat Flow

Thorne Lay *(Department of Earth and Planetary Sciences, Univ. California Santa Cruz),* **John Hernlund** *(Department of Earth and Planetary Sciences, Univ. California Berkeley),* **Bruce A. Buffett** *(Department of Earth and Planetary Sciences, Univ. California Berkeley)*

The current total heat flow at Earth's surface, 46 ± 3 TW (10**12 J/s), involves contributions from secular cooling, radiogenic heating from decay of U, Th and K, heat entering the mantle from the core, and various minor processes such as tidal deformation, chemical segregation and thermal contraction. Over the past decade, estimates of the heat flow across the core-mantle boundary (CMB), or across a chemical boundary layer above the CMB, have generally increased by a factor of 2 to 3, yielding values in the range 5-15 TW from independent considerations of core temperature, geodynamo energetics, buoyancy flux of lower mantle thermal plumes, and direct temperature determinations in the lowermost mantle enabled by relating seismic velocity discontinuities to a laboratory-calibrated phase change in magnesium-silicate perovskite (MgSiO3) (*Lay et al., 2008*). Relative to earlier ideas, the increased estimates of deep mantle heat flow indicate a more prominent role for thermal plumes in mantle dynamics, more extensive partial melting of the lowermost mantle in the past, and a more rapidly growing and younger inner core and/or presence of significant radiogenic material in the outer core or lowermost mantle.

References

Lay, T., J. Hernlund, and B. A. Buffett (2008). Core-mantle boundary heat flow, *Nature Geosci., 1*, 25-32.

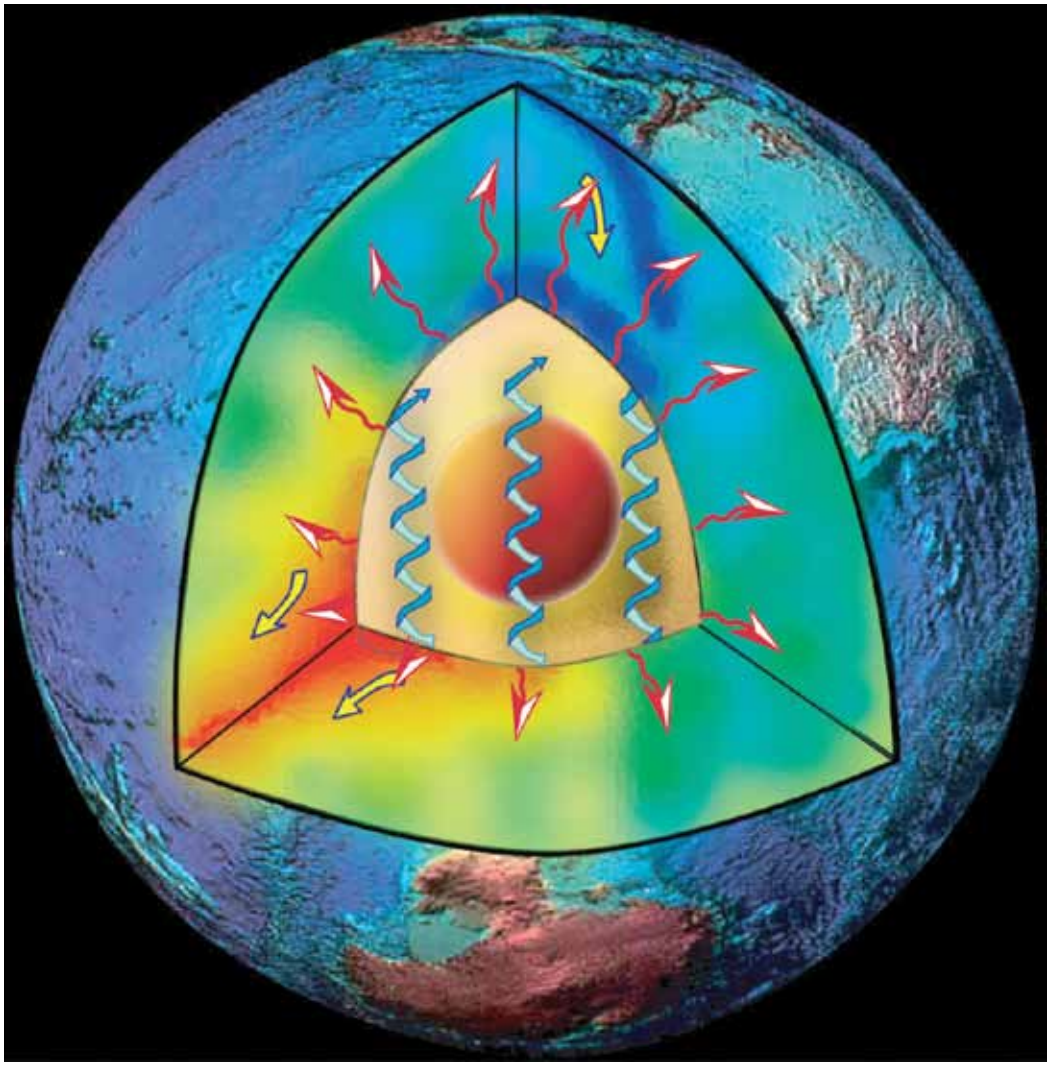

Cut-away Earth schematic indicating dynamic regimes in the mantle and core, along with variation in heat flux through the core-mantle boundary. Heat flux from the core into the mantle (represented by red arrows) is highest in areas cooled by downwellings, and lowest in hot upwelling regions.

Localized Seismic Scatterers Near the Core-Mantle Boundary beneath the Caribbean Sea: Evidence from PKP Precursors

Meghan S. Miller *(University of Southern California),* **Fenglin Niu** *(Rice University)*

The nature of the core-mantle boundary (CMB) region, the D", has been a focus of research for decades because it is a crucial part in understanding the evolution of geodynamics and whole earth structure. The D" region is very heterogeneous and has complicated seismic structures that require involvements of both chemical and thermal processes. One representative and well studied area is Central America and Caribbean, where the D" region is featured by a well defined seismic discontinuity underlain by anisotropic and higher velocity materials. Here we used seismic phase arrivals from earthquakes in the Western Pacific recorded by broadband seismic stations in northern South America and the Caribbean to investigate the core-mantle boundary and the D" region beneath the central Caribbean plate. We identified precursors to the PKP phases in 14 events, which can be explained by a region of heterogeneous scattering located above the CMB beneath the central Caribbean plate. The seismic scatterers are localized to the vicinity between approximately 5°N to 20°N and -80°W to -65°W. Other similar distance events that display no precursors, interpreted to have traversed non-scattering regions on the core-mantle boundary, lie to the south and southwest of the identified cluster of seismic scatterers. We found that the small-scale seismic scatterers are not uniformly distributed, are concentrated, and are surrounded by relatively fast shear velocity perturbations in the lower mantle imaged with global seismic tomography. The fast velocity perturbations may be residual slab from the subducted Farallon plate and the scatterers to the east-northeast of the high velocity material could be remnants of heterogeneous material, perhaps former basaltic crust, that has been transported ahead or on top of the subducted slab material as it impacts and bends at the core-mantle boundary.

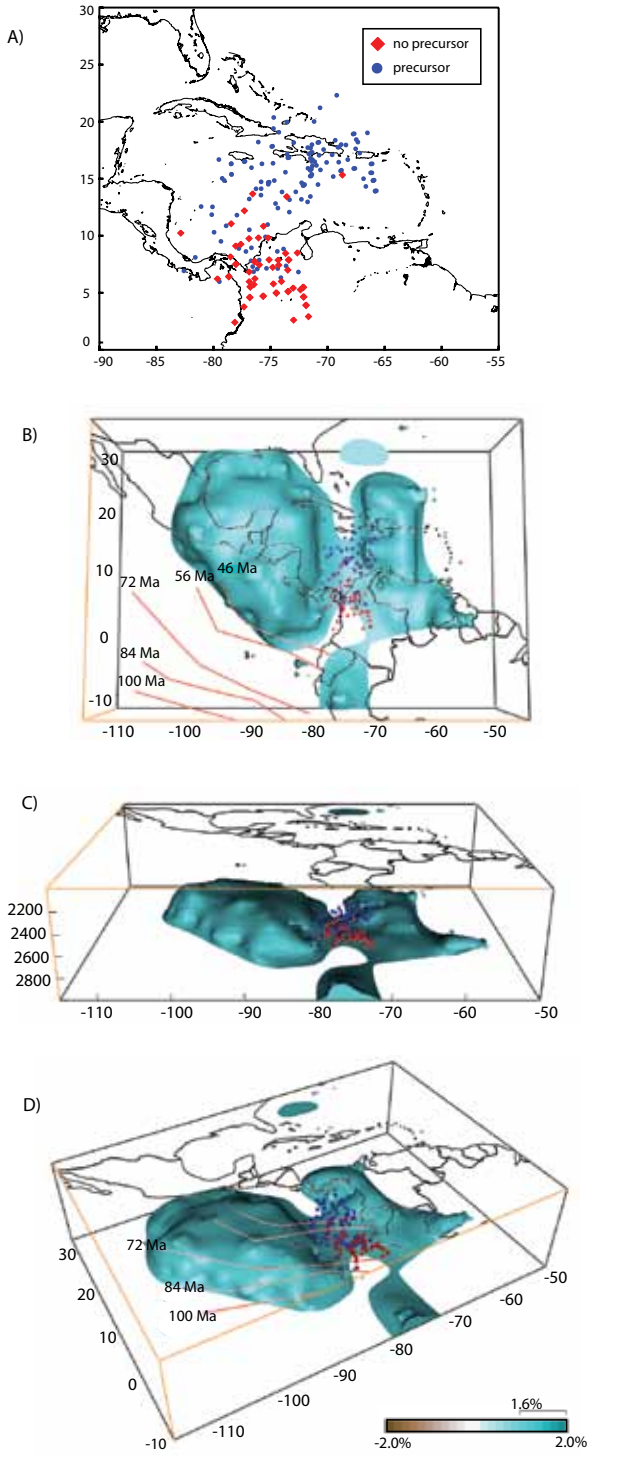

A) Map of the Caribbean region showing the calculated points of ray paths exiting the core and entering the mantle. Blue circles indicate the events with precursors, with a good (> 5) signal to noise ratio and red diamonds indicate the events with no evident precursor, which also have a good (> 5) signal to noise ratio. B-D) Tomographic images of the lower mantle (Grand, 2002) with isosurfaces of 1.6% shear velocity perturbation and greater. The exit points are also plotted with the images showing the localization of the scatterers and their relationship to the surrounding high velocities. The red lines (and ages) are the estimated Farallon plate boundaries from plate and kinematic reconstructions between 100 and 46 Ma (Pindell et al., 2005).

References

Grand, S.P., 2002. Mantle shear-wave tomography and the fate of subducted slabs. *Phil. Trans. R. Soc. Lond. A, 360*(1800): 2475-2491.

Pindell, J. *et al.*, 2005. Plate-kinematics and crustal dynamics of circum-Caribbean arc-continent interactions: Tectonic controls on basin development in Proto-Caribbean margins. In: H.G. Lallemant and V.B. Sisson (Editors), Caribbean-South American Plate Interactions, Venezuela. Geological Society of America, Boulder CO, pp. 7-52.

Acknowledgements: The BOLIVAR project is funded by the National Science Foundation EAR0003572 and EAR0607801 and MSM was funded by a NSERC postdoctoral fellowship.

Constraints on Lowermost Mantle Anisotropy beneath the Eastern Pacific from SKS-SKKS Splitting Discrepancies

Maureen Long *(Yale University)*

Measurements of the birefringence of SKS and SKKS phases are commonly used to infer seismic anisotropy and flow in the upper mantle beneath a seismic station. Comparisons of SKS and SKKS splitting for stations around the globe have demonstrated that in 95% of cases, SKS and SKKS phases for the same event/station pair yield the same splitting parameters [Niu and Perez, 2004] In an important minority of cases, however, these measurements diverge, and in this case the difference in splitting must be attributed to anisotropic structure in the lower mantle far away from the receiver side. Strongly discrepant SKS-SKKS splitting has been observed at broadband stations in western Mexico and California [Long, 2009]. In particular, strong SKKS splitting with fast polarization directions near ~60° and delay times of up to ~ 3 sec is observed for a group of raypaths that sample the lowermost mantle beneath the eastern Pacific Ocean. The region most likely to cause the observed discrepancies is the deepest mantle, as this is the least similar portion of the SKS/SKKS path. Because there is considerable seismological evidence for anisotropy in the D" layer, and because there is laboratory and seismological evidence that the bulk of the lower mantle is seismically isotropic, my preferred interpretation of the anomalous SKKS splitting observed in western North America is that it is due to complex anisotropy in the D" region at the base of the mantle. The anomalous SKKS splitting appears to delineate a region of fairly uniform azimuthal anisotropy in the D" layer beneath the eastern Pacific; this anisotropy coincides geographically with a sharp lateral gradient in isotropic S wavespeed structure at the base of the mantle. One possible model to explain the observations invokes a broad region of high-strain deformation associated with the impingement of the Farallon slab upon the CMB beneath North America, inducing the LPO of lowermost mantle minerals to produce a region of anomalous D" anisotropy at its edge.

References

Houser, C., G. Masters, P. Shearer, and G. Laske (2008), Shear and compressional velocity models of the mantle from cluster analysis of long-period waveforms, *Geophys. J. Int., 174*, 195-212.

Niu, F., and A. M. Perez (2004), Seismic anisotropy in the lower mantle: A comparison of waveform splitting of SKS and SKKS, *Geophys. Res. Lett., 31*, L24612.

Long, M. D. (2009), Complex anisotropy in D" beneath the eastern Pacific from SKS-SKKS splitting discrepancies, *Earth Planet. Sci. Lett., 283*, 181-189.

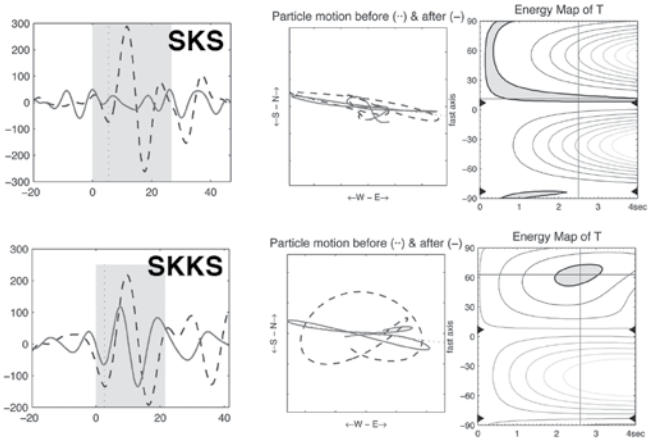

An example of an anomalous SKS-SKKS splitting measurement at station UNM. Columns show the radial (dashed) and transverse (solid) components of the phase (left panel), the initial (dashed) and corrected (solid) particle motion (center panels), and the energy map of the transverse component (right panels). The SKS phase (top row) exhibits null or near-null splitting, while the SKKS phase (bottom row) exhibits well-constrained splitting parameters of φ = 63°, δt = 2.6 sec.

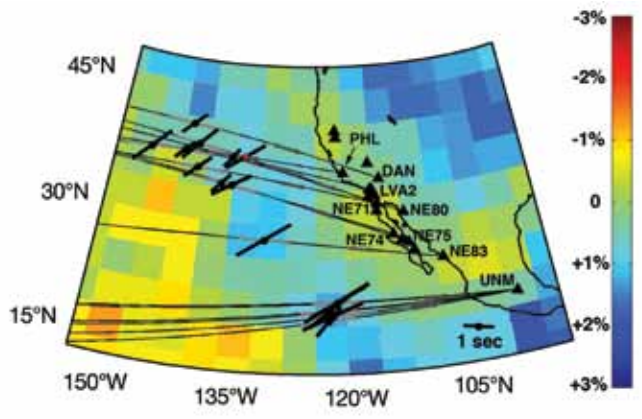

Shear wave splitting parameters (black bars) attributed to D" anisotropy for anomalous SKKS phases are plotted at the midpoint of their D" paths. The colors indicate isotropic S wavespeeds at the base of the mantle from the model of Houser et al. [2008] as a % deviation from the reference model.

Constraints on Lowermost Mantle Mineralogy and Fabric beneath Siberia from Seismic Anisotropy

James Wookey *(University of Bristol, UK),* **J-Michael Kendall** *(University of Bristol, UK)*

Seismic anisotropy is an important tool for studying the nature, origin and dynamics of the lowermost mantle (D"). Here we present analysis of the seismic anisotropy beneath Siberia from shear-wave splitting measured in ScS phases. Data come from two near-perpendicular raypaths (Hindu-Kush to Northern Canada and the Kuril Arc to Germany; both at ~80 degrees epicentral distance) with close ScS reflection points on the Core-Mantle boundary (CMB). We apply differential S-ScS splitting to minimise contamination from the source and receiver side upper mantle. The two raypaths show different ScS splitting times and fast shear-wave orientations, incompatible with the VTI style of anisotropy inferred for much of the lowermost mantle. The availability of data at two azimuths give us an opportunity to better understand D" anisotropy than in previous studies. For example, the results provide the first accurate measurement of the dip of the symmetry plane. Several mechanisms have been suggested to explain lowermost mantle anisotropy, including the lattice-preferred orientation of lower mantle minerals such as perovskite or post-perovskite, or the shape-preferred orientation of inclusions of melt. In order to infer the flow regime implied by these mechanisms we use elasticities from published deformation experiments to forward model shear-wave splitting. Tomography of the region suggests a north-south trend in the geodynamics, and a model incorporating post-perovskite with a [100](010) slip system or aligned melt inclusions are most naturally compatible with such a trend. This may suggest a connection with remnant slab material from past subduction in the north Pacific.

References

Wookey, J., Kendall, J-M. (2008) Constraints on Lowermost Mantle Mineralogy and Fabric beneath Siberia from Seismic Anisotropy, *Earth Planet. Sci. Lett., 275,* 32-42

Acknowledgements: Data came from the CNSN and SZGRF datacentres. JW was supported by a NERC fellowship grant.

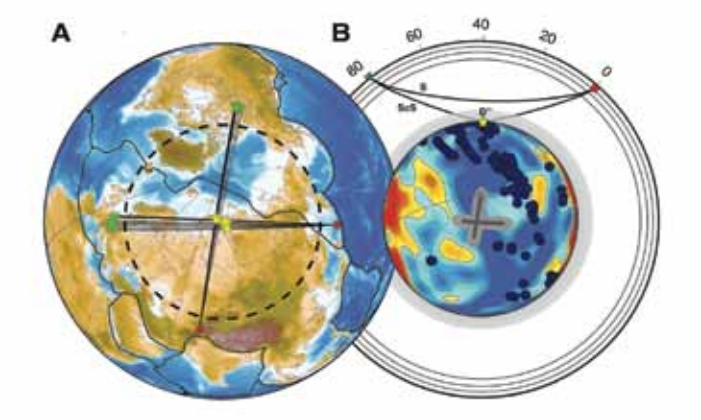

Raypaths and bouncepoints for data used in the study. Panel A shows the great-circle paths for the phases studied, from Hindu-Kush and Kuril Arc events (circles) to POLARIS and GRSN stations (triangles). Stars mark the reflection point of ScS: for both paths these are very close. Panel B shows the variation of shear-wave speed at the CMB from Masters et al (2000) (blue colours are faster than average) and the predicted location of paleosubducted slab material from Lithgow-Bertelloni and Richards (1998) (blue cirles). The grey region shows the approximate Fresnel zone of the ScS phases in the lowermost mantle. Also shown are the S and ScS raypaths; S turns above D$''$ whilst ScS samples it.

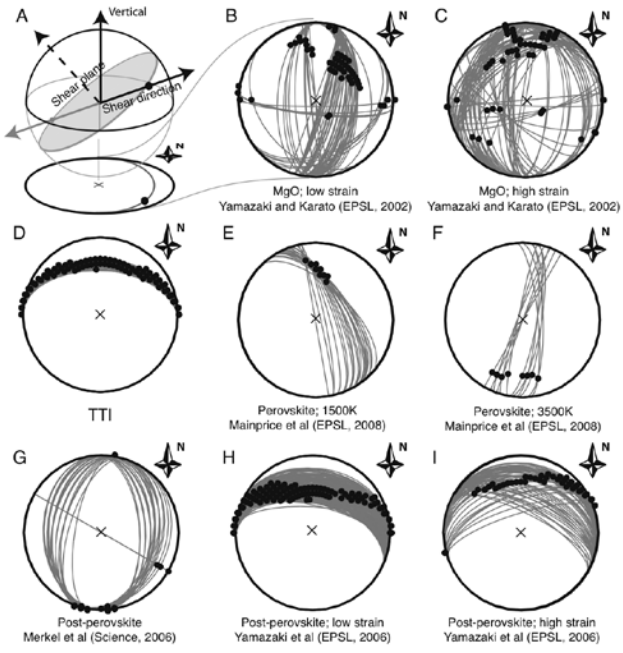

Orientations of candidate elastic models which fit the shear-wave splitting observed beneath Siberia. Panel A is a cartoon showing how to interpret the other panels. Plots are upper hemispheric projections of the shear plane (grey arcs) and direction (black circles) predicted by matching orientations of different elastic tensors to the polarisations observed in the data. North is up the page, as indicated, and normal to the page is vertical (i.e., radially in the Earth). The elastic tensors tested are: B and C, an LPO of MgO; D, an ideal TTI medium; E and F, MgSiO3 perovskite at 1500K and 3500K; G, post-perovskite LPO using MgGeO3; H and I, post-perovskite LPO using CaTiO3.

Localized Double-Array Stacking Analysis of PcP: D'' and ULVZ Structure beneath the Cocos Plate, Mexico, Central Pacific, and North Pacific

Thorne Lay *(University of California Santa Cruz),* **Alexander R. Hutko** *(U. S. Geological Survey, NEIC),* **Justin Revenaugh** *(University of Minnesota)*

A large, high quality P-wave data set comprising short-period and broadband signals sampling four separate regions in the lowermost mantle beneath the Cocos plate, Mexico, the central Pacific, and the north Pacific is analyzed using regional one-dimensional double-array stacking and modelling with reflectivity synthetics. A data-screening criterion retains only events with stable PcP energy in the final data stacks used for modelling and interpretation. This significantly improves the signal stacks relative to including unscreened observations, allows confident alignment on the PcP arrival and allows tight bounds to be placed on P-wave velocity structure above the core-mantle boundary (CMB). The PcP reflections under the Cocos plate are well-modelled without any ultra-low velocity zone from 5 - 20° N. At latitudes from 15 – 20° N, we find evidence for two P-wave velocity discontinuities in the D" region. The first is ~182 km above the CMB with a δlnVp of +1.5%, near the same depth as a weaker discontinuity (<+0.5%) observed from 5 - 15° N in prior work. The other reflector is ~454 km above the CMB, with a δlnVp of +0.4%; this appears to be a shallower continuation of the joint P- and S-wave discontinuity previously detected south of 15° N, which is presumed to be the perovskite to post-perovskite phase transition. The data stacks for paths bottoming below Mexico have PcP images that are well-matched with the simple IASP91 structure, contradicting previous inferences of ULVZ presence in this region. These particular data are not very sensitive to any D" discontinuities, and simply bound them to be <~2%, if present. Data sampling the lowermost mantle beneath the central Pacific confirm the presence of a ~15-km thick ultra-low velocity zone (ULVZ) just above the CMB, with δlnVp and δlnVs of around -3 to -4% and -4 to -8%, respectively. The ULVZ models predict previous S-wave data stacks well. The data for this region indicate laterally varying Vp discontinuities in D", with one subregion having a δlnVp of 0.5% 140 km above the CMB. Beneath the north Pacific, the PcP arrivals are compatible with only weak ULVZ (δlnVp ~ 0 to -3%), and there is a weak D'' reflector with δlnVp = 0.5%, near 314 km above the CMB. These results indicate localized occurrence of detectable ULVZ structures rather than ubiquitous ULVZ structure and emphasize the distinctiveness between the large low shear velocity province under the central Pacific and circum-Pacific regions.

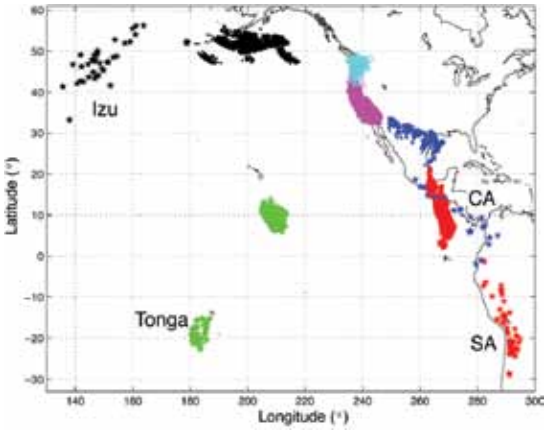

Map of PcP data stacking configurations; earthquake epicenters (stars), recording stations in western North America (triangles), and PcP midpoints (small dots). The red, blue, green, and black colour earthquakes and midpoints are the South America (SA), Central America (CA), Tonga, and Izu data sets, respectively. The CA events were recorded by University of Washington short period-stations (cyan triangles), all other data sets incorporate broadband and short-period data from the TriNet, SCSN and NCSN networks (magenta triangles). All data shown have been screened to ensure a stable PcP detection in individual event stacks. About a third (half) of the Tonga (Izu) data are a screened subset of the data used by Revenaugh and Meyer (1997).

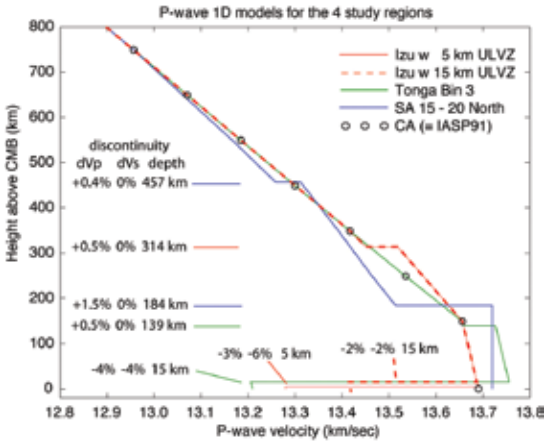

Summary of P-wave velocity structures for the four study regions. The discrepancy in depth between the observed and synthetic PcP stack (when using the direct P-wave as the reference phase) was matched for each region. We do not model the absolute travel times of the P-waves, so the absolute velocities are not constrained. Perturbations from the reference 1D model are so small that relative depths of discontinuities are well constrained. This is not the case when modelling S-wave data. Our modelling has little sensitivity to density contrasts or the sign or magnitude of dVp/dZ, however for some source-receiver geometries, there is some sensitivity to abrupt changes in dVp/dZ (Hutko et al. 2008). All discontinuities were modelled as sharp discontinuities. Distributing the velocity changes at the discontinuities across some depth can reduce the effective reflection coefficient by varying degrees, depending on the source-receiver geometry.

References

Hutko, A. R., T. Lay, and J. Revenaugh (2009). Localized double-array stacking analysis of PcP beneath the Cocos Plate, Mexico, central Pacific and north Pacific, *Phys. Earth Planet. Int.*r., 173, 6-74.

Acknowledgements: This work was supported in part by the U.S. National Science Foundation under grants EAR-0453884, and EAR-0635570.

Anti-Correlated Seismic Velocity Anomalies from Post-Perovskite in the Lowermost Mantle

Thorne Lay *(University of California Santa Cruz),* **Alexander R. Hutko** *(University of California, Santa Cruz),* **Justin Revenaugh** *(University of Minnesota),* **Edward J. Garnero** *(Arizona State University)*

Earth's lowermost mantle has thermal, chemical, and mineralogical complexities that require precise seismological characterization. Stacking, migration, and modeling of over 10,000 P- and S-waves that traverse the deep mantle under the Cocos plate resolves structures above the core-mantle boundary (CMB). A small -0.07 ± 0.15% decrease of P-wave velocity (Vp) is accompanied by a 1.5 ± 0.5% increase in S-wave velocity (Vs) near a depth of 2570-km. Bulk-sound velocity (Vb = [Vp^2–4/3Vs^2]**½) decreases by −1.0 ± 0.5% at this depth. Transition of the primary lower mantle mineral, (Mg1-x-y FexAly)(Si,Al)O3 perovskite, to denser post-perovskite is expected to have negligible effect on the bulk modulus while increasing the shear modulus by ~6%, resulting in local anti-correlation of Vb and Vs anomalies; this explains the data well.

References

Hutko, A. R., T. Lay, J. Revenaugh, E. J. Garnero (2008). Anti-correlated seismic velocity anomalies from post-perovskite in the lowermost mantle, *Science, 320*, 1070-1074.

Acknowledgements: This work was supported in part by the U.S. National Science Foundation under grants EAR-0453884, and EAR-0453944.

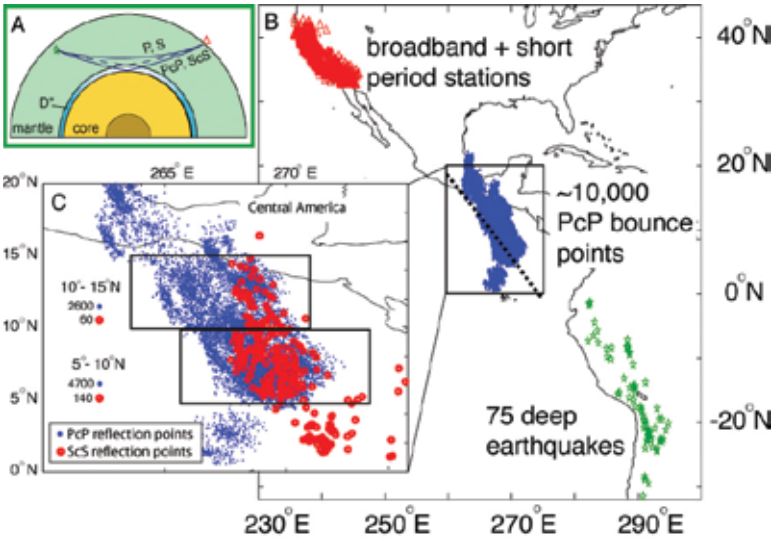

(A) Earth cross-section with representative raypaths for direct (P/S) and CMB reflected (PcP/ScS) phases, and any reflections from deep mantle discontinuities (dashed). The D" region structure in the lowermost mantle is the focus of this study. (B) Map indicating the study configuration, involving 75 earthquake epicenters (green stars), seismic stations (red triangles) and surface projections of PcP core-mantle boundary (CMB) reflection points (blue dots). The dashed line shows the surface trace of a cross-section made through the migration image volume in the lower mantle (Fig. 3). The inset map (C) shows both PcP and ScS CMB reflection points and two data bins where these overlap, used in waveform stacking analysis.

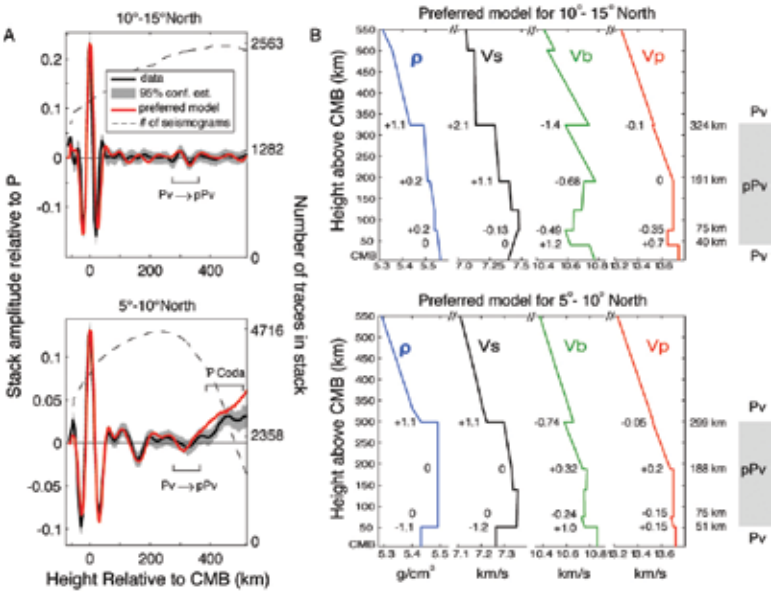

(A) P-wave double array stacking results for two 5° latitudinal bins beneath the Cocos Plate. The solid black line shows the data stack amplitude relative to the direct *P* amplitude. The grey shaded region is the 95% confidence interval of the stack from bootstrap re-sampling, and the dashed line is the number of seismograms contributing to the data stack at a particular depth (right scales). Above 400 km the stack for 5-10°N is contaminated by *P* coda. The red lines are stacks of synthetic seismograms generated from our preferred models. The synthetics were sampled to match the source-receiver geometry and had the same processing as the data. (B) Elasticity models obtained by modeling the data: ρ is density (gm/cm^3), V_s is S-wave velocity (km/s), V_b is bulk-sound velocity (km/s) and V_p is P-wave velocity (km/s). Percent changes in these parameters are shown at first-order discontinuities at the indicated depths. The depth range likely to contain post-perovskite (pPv) is indicated on the right.

Waveform Modeling of D" Discontinuity Structure

Michael S. Thorne (University of Utah), **Edward J. Garnero** *(Arizona State University),* **Thorne Lay** *(University of California, Santa Cruz),* **Gunnar Jahnke** *(Ludwig Maximilians University, Munich, Germany),* **Heiner Igel** *(Ludwig Maximilians University, Munich, Germany)*

The 3-D velocity structure of the deep mantle has been inferred from imaging procedures such as migration, tomography, stacking, and waveform modeling, all which utilize localized 1-D reference structures. As these methods often have limiting assumptions it is essential to assess to what extent 3-D solution models are self-consistent with the imaging procedures from which they were produced; this is possible through synthesizing waveforms in laterally varying media. We use a 3-D axi-symmetric finite difference algorithm (SHaxi) to model SH-wave propagation through cross-sections of recent 2- and 3-D lower mantle models along a north-south corridor roughly 700 km in length beneath the Cocos Plate. Synthetic seismograms with dominant periods up to 3 sec are computed to assess fit of 3-D model predictions to data. Model predictions show strong waveform variability not observed in 1-D model predictions. It is challenging to predict 3-D structure based on localized 1-D models when lateral structural variations are on the order of a few wavelengths of the energy used. Iterative approaches of computing synthetic seismograms and adjusting model characteristics by considering path integral effects are necessary to accurately model fine-scale D" structure.

References

Thorne, M.S., Lay, T., Garnero, E.J., Jahnke, G., Igel, H., Seismic imaging of the laterally varying D" region beneath the Cocos Plate, *Geophys. J. Int.* (170), pp. 635-648, doi: 10.1111/j.1365-246X.2006.03279.x, 2007.

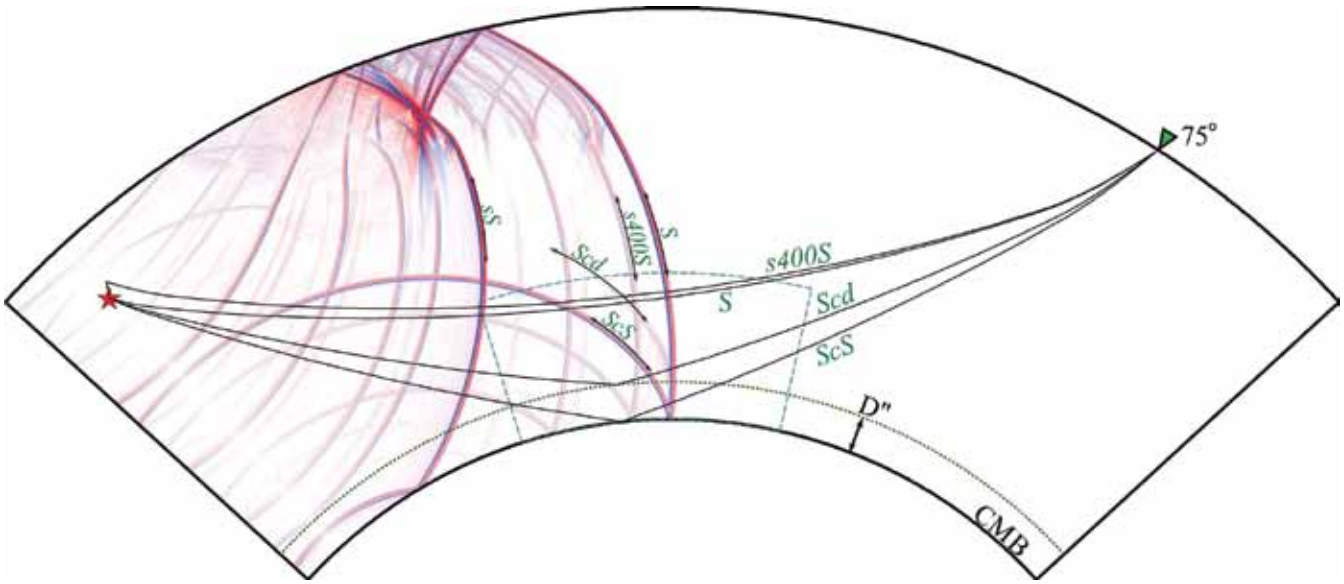

The SH- velocity wave field is shown at propagation time of 600 sec for a 500 km deep event with dominant source period of 6 sec. Selected wave fronts are labeled with black double-sided arrows. Ray paths are drawn in black for an epicentral distance of 75°. The calculation is done for the D" discontinuity (indicated with a dashed green line) model of Fig. 1. Non-linear scaling was applied to the wave field amplitudes to magnify lower amplitude phases.

A Narrow, Mid-Mantle Plume below Southern Africa

Daoyuan Sun *(Carnegie Institution of Washington),* **Don Helmberger** *(California Institute of Technology),* **Michael Gurnis** *(California Institute of Technology)*

Current tomographic models of the Earth display perturbations to a radial stratified reference model. However, if these are chemically dense structures with low Rayleigh numbers, they can develop enormous relief, perhaps with boundaries closer to vertical than radial. Here, we develop a new tool for processing array data based on such a decomposition referred to as a multi-path detector which can be used to distinguish between horizontal structure (in-plane multi-pathing) vs. vertical (out-of-plane multi-pathing) directly from processing array waveforms. We demonstrate the usefulness of this approach by processing samples of both P and S data from the Kaapvaal Array in South Africa. The result displays a narrow plume-like feature emitting from the top of the large African low-velocity structure in the lower mantle. A detailed SKS wavefield is assembled for a segment along the structure's southern edge by combining multiple events recorded by a seismic array in the Kaapvaal region of southern Africa. With a new processing technique that emphases multi-pathing, we locate a relatively jagged, sloping wall 1000 km high with low velocities near it's basal edge. Forward modeling indicates that the plume's diameter is less than 150 km and consistent with an iso-chemical, low-viscosity plume conduit.

References

Sun, D., D. Helmberger, and M. Gurnis (2010), A narrow, mid-mantle plume below southern Africa, *Geophys. Res. Lett., 37*, L09302, doi:10.1029/2009GL042339.

Acknowledgements: The waveform data were obtained from IRIS. This work was supported by NSF grant MCG.00021-NSF.CSEDIFINE.

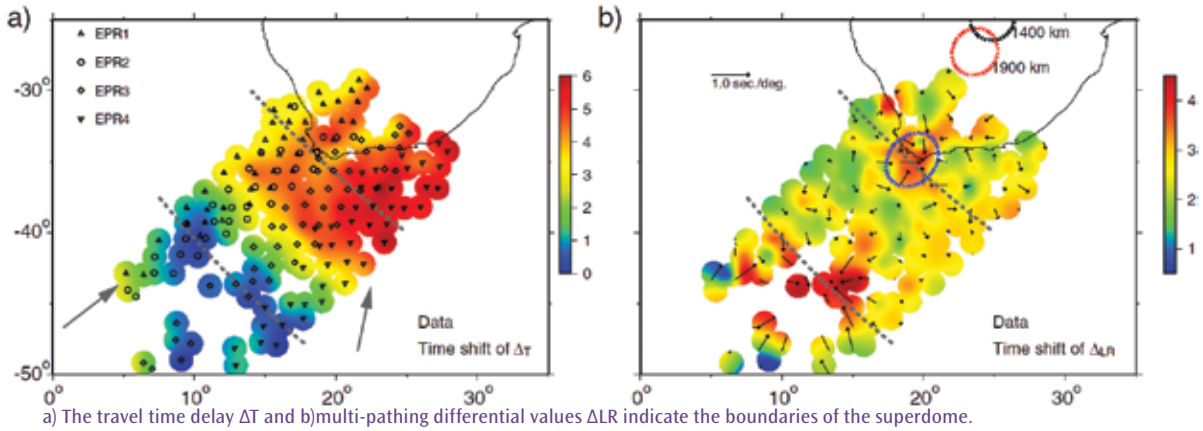

a) The travel time delay ΔT and b)multi-pathing differential values ΔLR indicate the boundaries of the superdome.

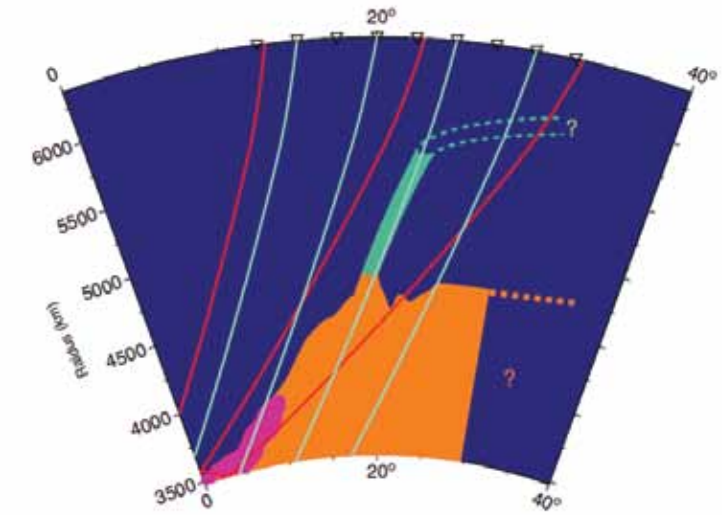

With a new processing technique that emphases multi-pathing, we find that the plume's diameter is less than 150 km and consistent with an iso-chemical, low-viscosity plume conduit (green). A 2D cross-section sampling the plume is displayed idealized with a uniform reduction of 3% inside the superdome (yellow).

Absence of Ultra-Low Velocity Zones at the CMB

Sebastian Rost *(School of Earth and Environment, University of Leeds, Leeds, UK),* **Edward J. Garnero** *(School of Earth and Space Exploration, Arizona State University, Tempe, AZ, USA),* **Michael S. Thorne** *(Dept. of Geology & Geophysics, University of Utah)*

Seismological studies of Earth's core mantle boundary (CMB) show evidence for heterogeneities and structures on many scales. Among the most enigmatic structures detected at the CMB are ultra-low velocity zones (ULVZs). ULVZs are thin layers of strongly reduced seismic velocities that have been detected at the CMB in several locations. Typical ULVZ thicknesses are on the order of 5 to 40 km with velocity reductions of up to 10 and 30% relative to 1D velocity models for P- and S-waves, respectively. Some studies also indicate strongly increased ULVZ density relative to the surrounding mantle. Several models for ULVZ have been proposed including partial melting of mantle material and iron enrichment of perovskite and/or post-perovskite. The knowledge of the global distribution of ULVZs on Earth is essential for distinguishing between different ULVZ hypotheses. Unfortunately, only a limited number of regions covering roughly half of the CMB area have been probed to date.

Here we use an aftershock of the relatively large Hawaiian earthquake on October 15, 2006 (moment magnitude, Mw ~ 6.7) that was recorded by roughly 1100 stations from several networks in the western United States and Canada. Using core reflected P-waves (PcP) allows the study of a previously unprobed region just north of the large low shear velocity province (LLSVP) beneath the Pacific Ocean. The large amount of high quality stations sampling this patch of CMB allows unprecedented waveform quality to sample the fine scale structure of the CMB.

Stacked seismograms show PcP amplitudes clearly out of the background noise level, but no evidence for a PcP precursor that would indicate ULVZ existence. Synthetic modelling of a large parameter space of ULVZ properties indicates that this region of the CMB is likely devoid of ULVZ, although ULVZs with thicknesses below the vertical resolution level (~5 km) of PcP might exist.

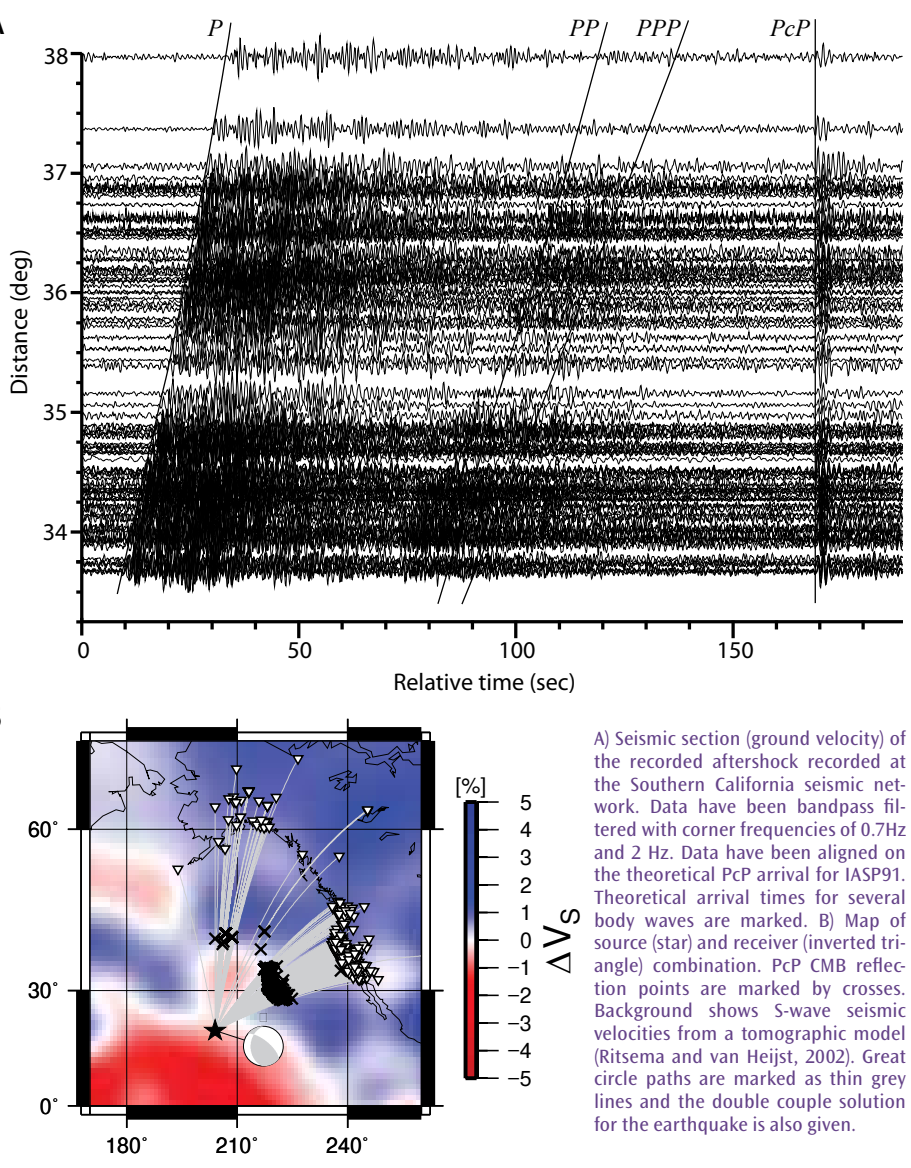

A) Seismic section (ground velocity) of the recorded aftershock recorded at the Southern California seismic network. Data have been bandpass filtered with corner frequencies of 0.7Hz and 2 Hz. Data have been aligned on the theoretical PcP arrival for IASP91. Theoretical arrival times for several body waves are marked. B) Map of source (star) and receiver (inverted triangle) combination. PcP CMB reflection points are marked by crosses. Background shows S-wave seismic velocities from a tomographic model (Ritsema and van Heijst, 2002). Great circle paths are marked as thin grey lines and the double couple solution for the earthquake is also given.

References

Rost, S., Garnero, E., Thorne, M., Hutko, A., (2010). On the absence of an ultralow-velocity zone in the North Pacific. *J. Geophys. Res., 115*, doi:10.1029/2009JB006420.

Acknowledgements: This work was supported by CSEDI grant EAR-0456356 (SR) and NERC New Investigator grant NE/F000898/1 (SR), and grant NSF EAR-0453944 (EJG).

Chemical Heterogeneity in the Mantle: Inferences from Seismology, Mineral Physics and Geodynamics

Jeannot Trampert *(Utrecht University),* **Frederic Deschamps** *(ETH Zurich),* **Paul Tackley** *(ETH Zurich)*

Probabilistic Tomography allows us to infer robust probability density functions (pdfs) for long wavelength models of bulk-sound and shear wave speed, density and boundary topography in the mantle. Using appropriate depth-dependent sensitivities, these pdfs can be converted into likelihoods of variations in temperature, perovskite and iron content throughout the mantle (Trampert et al., 2004). The sensitivities are calculated using full uncertainties in mineral physics data and, more importantly, in the thermo-chemical reference state of the mantle. We find that bulk-sound speed (density) variations are an excellent proxy for perovskite (iron) variations, and that shear-wave speed is not highly correlated to temperature as is often assumed. Compositional variations are essential to explain the seismic, gravity and mineral physics data. In particular, the regions of low shear-wave velocity in the deep mantle (> 2000 km) beneath Africa and the Pacific, usually referred to as superplumes, are mainly due to an enrichment in iron, which makes them denser than the surrounding mantle. We performed statistical comparisons between these contributions and some chosen models of thermo-chemical convection. We find that a stable and ubiquitous layer of dense material is unlikely to be present at the bottom of the mantle. Models containing piles explain the observation significantly better (Deschamps et al. 2007).

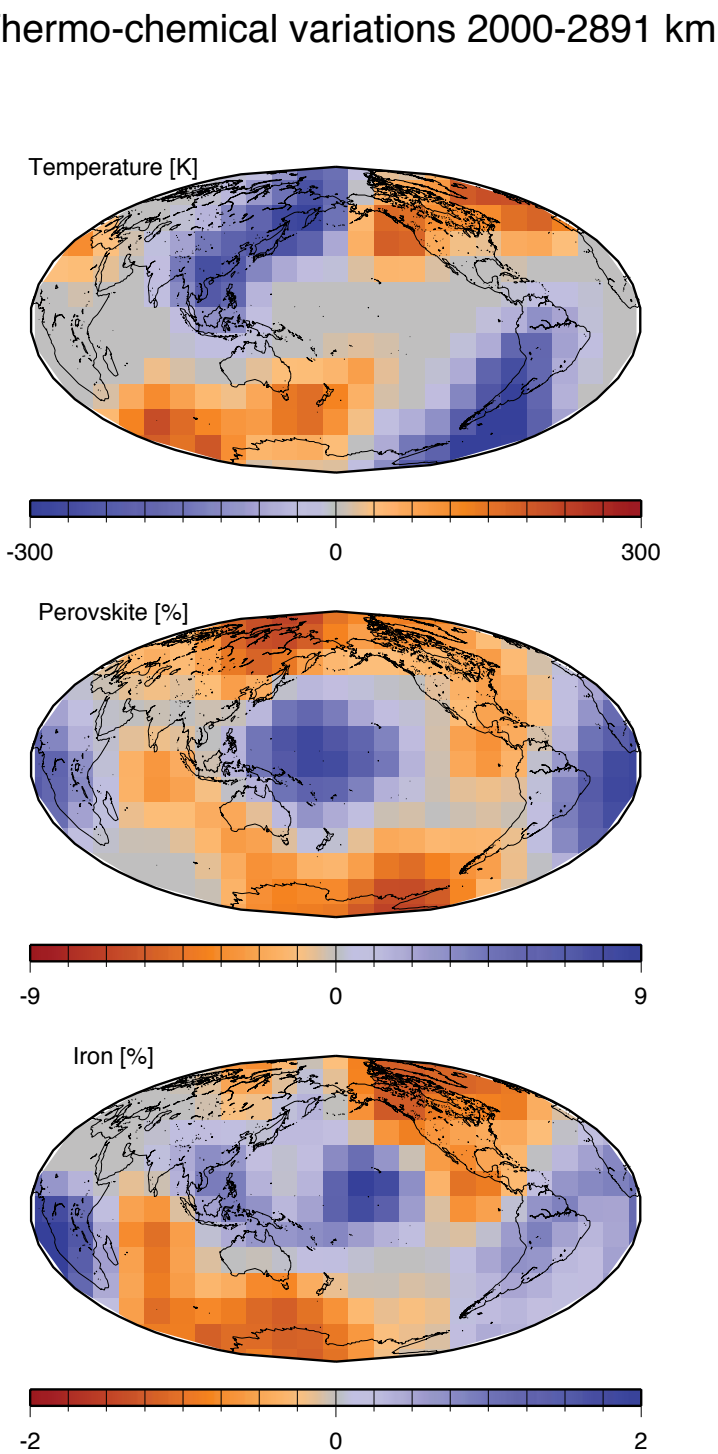

Mean anomalies of temperature, perovskite and iron in the lowermost mantle. Grey areas represent anomalies which are smaller than one standard deviation and therefore not robust.

References

Trampert J., Deschamps F., Resovsky J., Yuen D., 2004. Probabilistic tomography maps chemical heterogeneities throughout the lower mantle, *Science, 306*, 853-856.

Deschamps F., Trampert J., Tackley P.J., 2007. Thermo-chemical structure of the lower mantle: seismological evidence and consequences for geodynamics, in Superplume: beyond plate tectonics', edited by D.A. Yuen, S. Maruyama, S.I. Karato, and B.F. Windley, Springer, p. 293-320.

Acknowledgements: This research was funded by Netherlands Research Center for Integrated Solid Earth Sciences (ISES).

Moving Seismic Tomography Beyond Fast and Slow to Thermo-Chemical/Mineralogical Modeling

Christine Houser *(University of California Santa Cruz)*

The current reach and extent the Global Seismic Network (GSN) provides the seismic data needed to determine the seismic structure of the entire mantle. In fact, with the large amount of data available through the GSN, there is now enough confidence in the imaged seismic structure that we can begin to interpret seismically slow and fast regions in terms of temperature, chemistry, and mineralogy. The shear velocity (Vs) and compressional velocity (Vp) as well as normal modes are combined with their respective sensitivities to temperature and composition to map out variations in temperature (T), the mole fraction of iron (XFe), and the mole fraction of perovskite (XPv) near the core-mantle boundary (Houser et al., 2008). Since the phase transformation of perovskite to post-perovskite is temperature dependent, the temperature maps are used to determine where post-perovskite may exist at the bottom of the mantle [*Houser 2007*]. Thus, global seismic tomography is moving beyond slow and fast to a thermo-chemical understanding of the mantle in order to address Grand Challenge #9 "How do temperature and composition variations control mantle and core convection?".

References

Houser, C., Masters, G., Shearer, P., Laske, G. (2008) Shear and compressional velocity models of the mantle from cluster analysis of long-period waveforms, *Geophys. J. Int., 174* (1), 195-212.

Houser, C. (2007) Constraints on the presence or absence of post-perovskite in the lowermost mantle from long-period seismology,Post-Perovskite: The Last Mantle Phase Transition, Geophysical Monograph Series 174, K. Hirose, J. Brodholt, T. Lay, D. Yuen editors, American Geophysical Union.

Acknowledgements: This research was funded by the National Science Foundation grants EAR01-12289, EAR05-38238, and EAR06-52985 and was made possible by through the Instrumentation and Facilities Program (NSF EAR-0004370) funding of the IRIS Data Management Center.

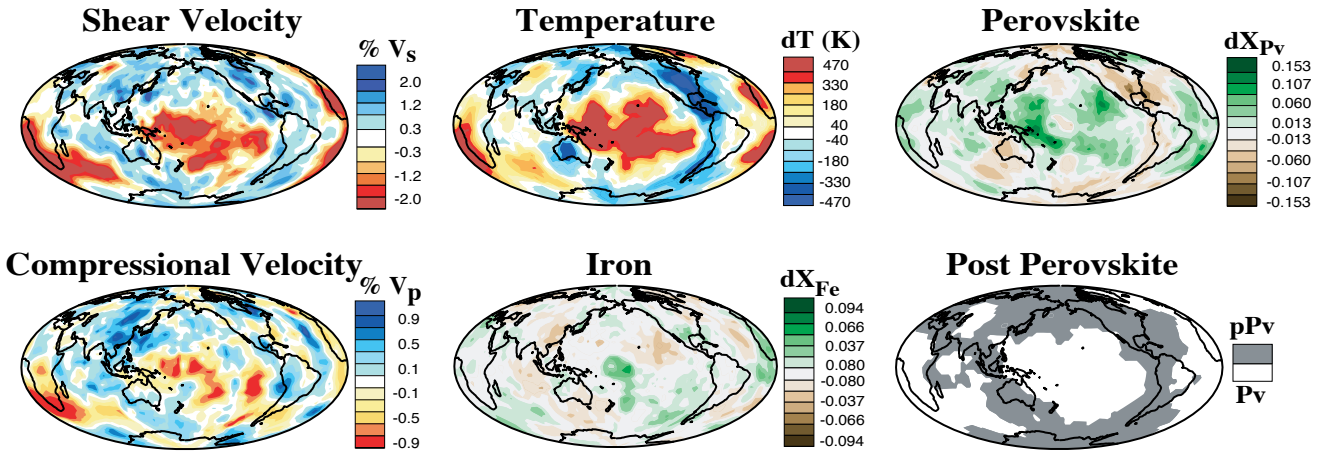

Shear and compressional velocity maps from the layer extending 200 km above the core-mantle boundary from the seismic tomography models HMSL-S and HMSL-P (Houser et al., 2008). Temperature and chemistry heterogeneity are shown using a scale such that the maximum/minimum translates to a -2%/+2% shear velocity anomaly. The temperature map is used to predict which regions may be cold enough to support the perovskite (Pv) to post perovskite (pPv) phase transition (Houser 2007).

Mantle Heterogeneity and Flow from Seismic and Geodynamic Constraints

Nathan Simmons *(Lawrence Livermore National Laboratory),* **Alessandro Forte** *(Universite de Quebec),* **Stephen Grand** *(University of Texas at Austin)*

Images of mantle heterogeneity are most commonly in the form of seismic velocity since seismic waves are the most direct mantle probe. Although these static images provide general patterns of heterogeneity in the mantle, it is difficult to directly translate them to mantle flow for a variety of reasons. Some reasons include the inherent non-uniqueness of tomographic inversion and the uncertainties in the mineral physics parameters linking seismic velocity to density perturbations which are the driving force behind mantle flow. In attempts to overcome these obstacles, we have developed tomographic images of the mantle through simultaneous inversion of shear-wave constraints and a suite of convection-related observations including the global free-air gravity field, tectonic plate divergences, dynamic surface topography and the excess ellipticity of the core-mantle boundary. The convection-related observations are interpreted via viscous-flow response functions and density perturbations are internally linked to velocity heterogeneity with mineral physics constraints. This joint inversion procedure has allowed us to directly investigate many hypotheses regarding the style of mantle flow as well as the sources of mantle heterogeneity since the process effectively removes biases inherent to pure seismically-derived models. We conclude that temperature variations likely dominate shear-wave and density heterogeneity in the non-cratonic mantle. However, notable compositional anomalies are detected, most strongly within the African superplume structures [*Simmons et al. 2006, 2007, 2009*]. Time-dependent flow calculations from the jointly-derived density models provide evidence that the (usually) minor compositional anomalies play an important dynamic role, particularly beneath the African plate. The static density models have also been used in dynamic flow calculations that predict anomalous flow patterns that coincide with known tectonic features including the New Madrid Seismic Zone [*Forte et al., 2007*], the Colorado Plateau [*Moucha et al., 2008*], and several features within the African plate [*Forte et al., 2010*]. Collectively, these observations lend support to the validity of jointly-derived images of mantle heterogeneity.

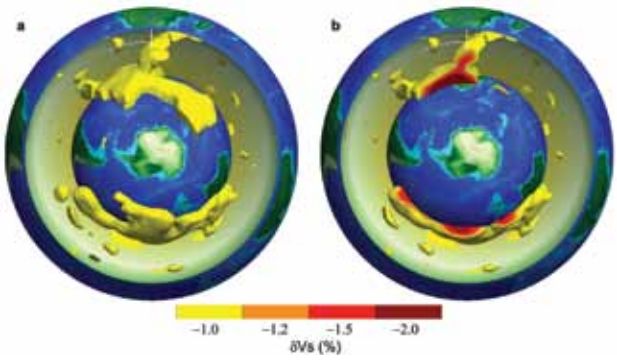

Model showing contoured slow shear velocity anomalies with corresponding density and thermal anomalies(Simmons et al., 2007). The density anomalies here are inferred assuming heterogeneity is due solely to temperature anomalies.

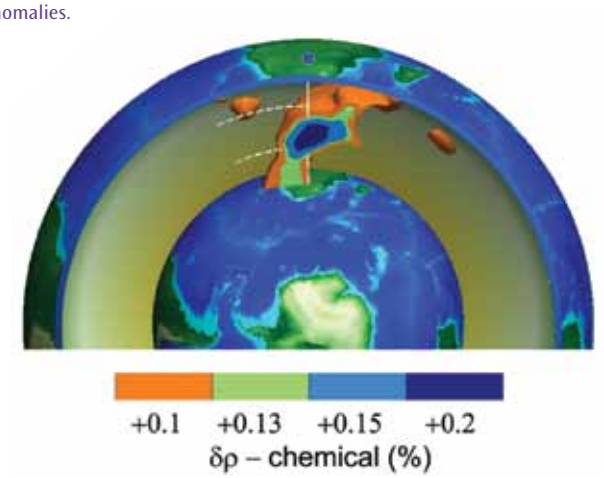

To fit geodynamic data with the thermal model shown in figure 1 additional density anomalies are needed as shown here. The "Africa Superplume" is unique in the required high chemical density anomaly needed to fit the geodynamic data.

References

Forte, A. M., N. A. Simmons, R. Moucha, S. P. Grand, and J. X. Mitrovica, 2007, Descent of the ancient Farallon slab drives localized mantle flow below the New Madrid seismic zone, *Geophys. Res. Lett., 34*, doi: 10.1029/2006GL027895.

Moucha, R., A. M. Forte, D. B. Rowley, J. X. Mitrovica, N. A. Simmons, and S. P. Grand, 2008. Mantle convection and the recent evolution of the Colorado Plateau and the Rio Grande Rift valley, *Geology, 36*, 439-442, doi:10.1130/G24577A.1.

Simmons, N., A. Forte, and S. P. Grand, 2006. Constraining mantle flow with seismic and geodynamic data: A joint approach, *Earth Planet. Sci. Lett., 246*, 109-124, doi:10.1016/j.epsl.2006.04.003.

Simmons, N., A. Forte, and S. P. Grand, 2007, Thermochemical structure and components of the African superplume, *Geophys. Res. Lett., 34*, doi:10.1029/2006GL028009

Simmons, N., A. Forte, and S. P. Grand, 2009, Joint seismic, geodynamic and mineral physical constraints on three-dimensional mantle heterogeneity: Implications for the relative importance of thermal versus compositional heterogeneity, *Geophys. J. Int., 177*, 1284-1304, doi:10.1111/j.1365-246X.2009.04133.x

Acknowledgements: This work was supported by NSF grant EAR0309189.

A Three-Dimensional Radially Anisotropic Model of Shear Velocity in the Whole Mantle

Mark Panning *(University of Florida),* **Barbara Romanowicz** *(University of California, Berkeley)*

We present a 3-D radially anisotropic S velocity model of the whole mantle (SAW642AN), obtained using a large three component surface and body waveform data set primarily recorded on IRIS GSN stations. An iterative inversion for structure and source parameters was performed based on Non-linear Asymptotic Coupling Theory (NACT). The model is parametrized in level 4 spherical splines, which have a spacing of ~8°. The model is parameterized with isotropic shear velocity and the radial anisotropic parameter ξ (VSH^2/VSV^2). The model shows a link between mantle flow and anisotropy in a variety of depth ranges. In the uppermost mantle, we confirm observations of regions with VSH > VSV starting at ~80 km under oceanic regions and ~200 km under stable continental lithosphere, suggesting horizontal flow beneath the lithosphere. We also observe a VSV > VSH signature at ~150–300 km depth beneath major ridge systems with amplitude correlated with spreading rate for fast-spreading segments. In the transition zone (400–700 km depth), regions of subducted slab material are associated with VSV > VSH , while the ridge signal decreases. While the mid-mantle has lower amplitude anisotropy (<1 per cent), we also confirm the observation of radially symmetric VSH > VSV in the lowermost 300 km, which appears to be a robust conclusion, despite an error in our previous paper which has been corrected here. The 3-D deviations from this signature are associated with the large-scale low-velocity superplumes under the central Pacific and Africa, suggesting that VSH > VSV is generated in the predominant horizontal flow of a mechanical boundary layer, with a change in signature related to transition to upwelling at the superplumes. The included figure shows the isotropic and anisotropic signature in the core-mantle boundary region, showing the strong blue (VSH > VSV) signature in most regions with deviations generally associated with the low velocity superplumes. This work was originally published in Geophysical Journal International [*Panning and Romanowicz, 2006*].

References

Panning, M., and B. Romanowicz (2006), A three-dimensional radially anisotropic model of shear velocity in the whole mantle, *Geophys. J. Int., 167*, 361–379.

Acknowledgements: This research was supported by NSF grant EAR-0308750.

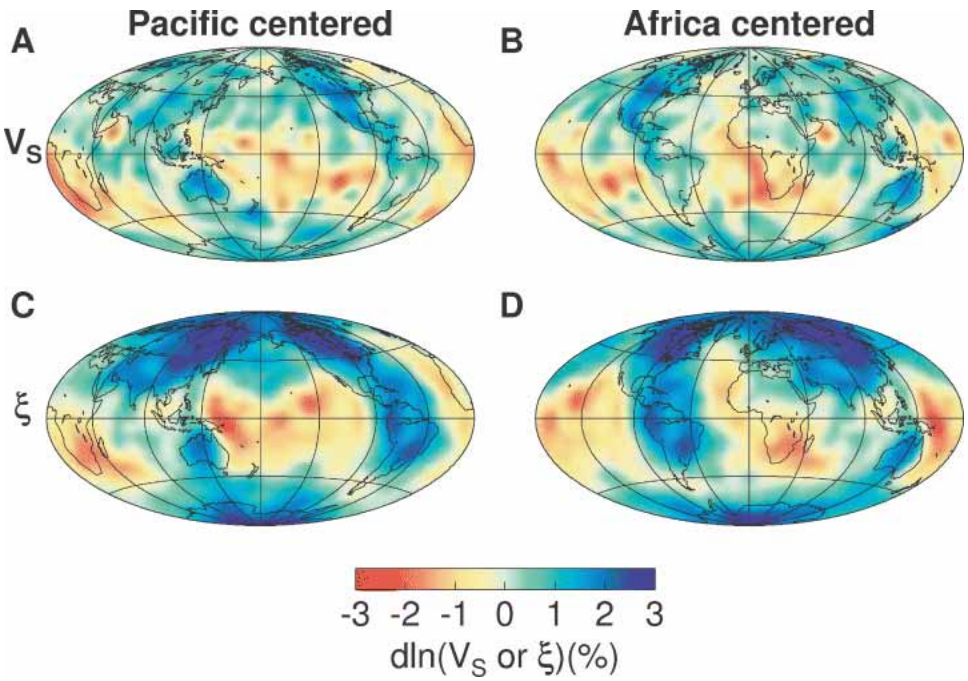

VS (A, B) and ξ structure (C, D) at a depth of 2800 km centered under the central Pacific (A, C) and Africa (B, D).

Global Mantle Anisotropy and the Coupling of Free Oscillations

Caroline Beghein *(University of California at Los Angeles),* **Joseph Resovsky** *(Roosevelt Academy, The Netherlands),* **Robert D. van der Hilst** *(Massachusetts Institute of Technology)*

Seismic anisotropy can be generated by large-scale deformation, and therefore provide us with a unique way of constraining mantle dynamics. However, because its detection below ~300 km depth remains challenging, it is unclear whether and what kind of seismic anisotropy is present in the deep upper mantle and transition zone. Due to their sensitivity to structure throughout the entire mantle, the Earth's free oscillations, or normal modes, constitute a unique source of data to constrain large-scale mantle seismic anisotropy. While isolated mode multiplets have been widely used in the literature to constrain Earth's large-scale structure, little attention has been given to mode coupling, which can occur due to Earth's rotation, ellipticity, and three-dimensional (3-D) isotropic and anisotropic structure.

Mode coupling measurements require high quality long-period seismic data. Few such measurements have been made so far, but we were able to take advantage of an existing small data set composed of 0Tl-0Sl+1 coupled mode multiplets [Beghein et al., 2008]. They had been measured by Resovsky and Ritzwoller [1995] for spherical harmonic degrees 2 and 4, and corrected for the effect of rotation and ellipticity. These multiplets have high sensitivity to shear-wave radial anisotropy and to six elastic parameters describing azimuthal anisotropy in the deep upper mantle and transition zone. They constitute therefore a potential new source of data to constrain anisotropy at these depths.

We first attempted to fit the degree two measurements using existing isotropic and transversely isotropic mantle models. However, the signal could not be explained by any of these models. After correction for the effect of crustal structure and mantle radial anisotropy, we tested whether the remaining signal could be explained by azimuthal anisotropy. We explored the model space with a forward modeling approach to identify the most likely azimuthal anisotropy models and associated model uncertainties. We determined that, although the variance was large, a robust azimuthal anisotropy signal could be extracted from the data. In addition, we showed that the data tend to slightly favor the presence of azimuthal anisotropy below 400 km depth.

While the depth extent and distribution of the anisotropy were not well constrained due to parameter tradeoffs and a limited coupled mode data set, it is clear that mode coupling measurements constitute a promising tool to study deep mantle anisotropy. In addition, because some of the elastic parameters that can lead to mode coupling do not affect surface wave phase velocities, coupled free oscillations complement surface wave data, and have the potential to provide new and unique constraints on other elastic parameters, yielding a more complete description of Earth's elastic structure. In the future more coupled mode measurements could help us discriminate between different compositional models of the mantle [Montagner and Anderson, 1989].

References

Beghein, C., Resovsky, J., and van der Hilst, R.D., The signal of mantle anisotropy in the coupling of normal modes, *Geophys. J. Int., 175*, 1209-1234, 2008.

Montagner, J.P., and Anderson, D.L., Petrological constraints on seismic anisotropy, *Phys. Earth Planet. Int., 54*, 82-105, 1989.

Resovsky, J., and Ritzwoller, M., Constraining odd-degree Earth structure with coupled free-oscillations, *Geophys. Res. Lett., 22*, 2301-2304, 2005.

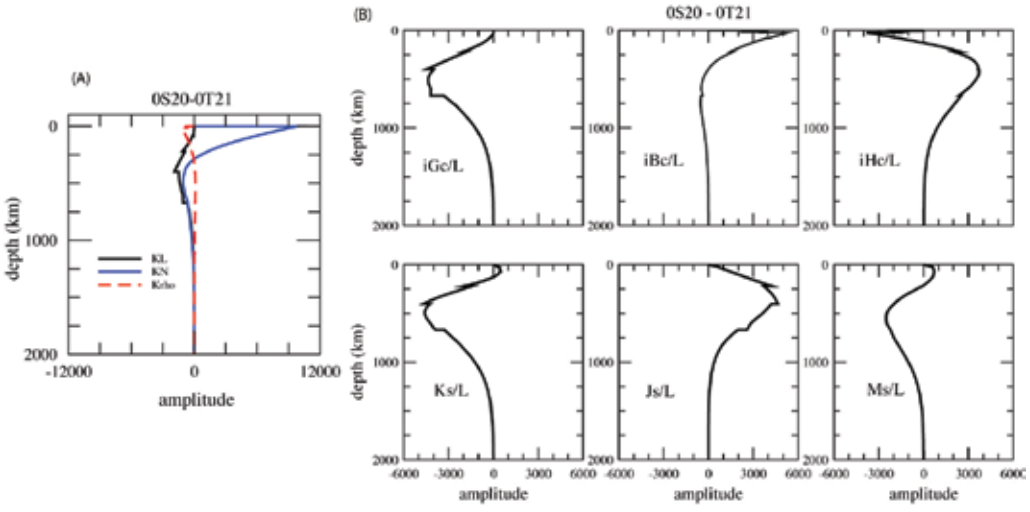

Sensitivity kernels of coupled modes 0S20-0T21 for (A) elastic parameters related to S-wave radial anisotropy and (B) elastic parameters describing azimuthal anisotropy.

The Importance of Crustal Corrections in the Development of a New Global Model of Radial Anisotropy

Mark Panning *(University of Florida),* **Vedran Lekic** *(Brown University),* **Barbara Romanowicz** *(University of California, Berkeley)*

Accurately inferring the radially anisotropic structure of the mantle using seismic waveforms requires correcting for the effects of crustal structure on waveforms. Recent studies have quantified the importance of accurate crustal corrections when mapping upper mantle structure using surface waves and overtones. Here, we explore the effects of crustal corrections on the retrieval of deep mantle velocity and radial anisotropy structure. We apply a new method of non-linear crustal corrections to a 3 component surface and body waveform dataset derived primarily from IRIS GSN data, and invert for a suite of models of radially anisotropic shear velocity. We then compare the retrieved models against each other and a model derived from an identical dataset, but using a different non-linear crustal correction scheme. While retrieval of isotropic structure in the deep mantle appears to be robust with respect to changes in crustal corrections, we find large differences in anisotropic structure that result from the use of different crustal corrections, particularly at transition zone and greater depths. Furthermore, anisotropic structure in the lower mantle, including the depth-averaged signature in the core-mantle boundary region, appears to be quite sensitive to choices of crustal correction. Our new preferred model, SAW642ANb, shows improvement in data fit and reduction in apparent crustal artifacts. We argue that the accuracy of crustal corrections may currently be a limiting factor for improved resolution and agreement between models of mantle anisotropy. The included figure shows the correlation for the anisotropic portion of a suite models developed with the new crustal corrections with that of SAW642AN, which was developed with the same dataset but a different implementation of non-linear crustal corrections. The new model, SAW642ANb is freely available through the website http://www.clas.ufl.edu/users/mpanning/SAW642ANb.html. This work is currently in revision for publication in the Journal of Geophysical Research [*Panning et al., 2010*].

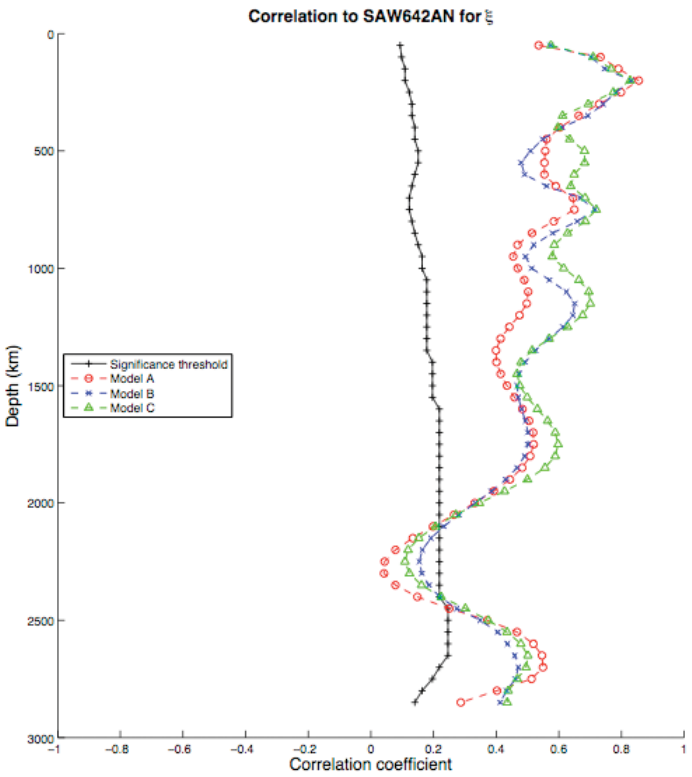

Correlation of the ξ models A, B, and C (red, blue, and green dashed lines, respectively) to SAW642AN (derived from the same dataset with different crustal corrections) up to spherical harmonic degree 24. The black line shows the 95% confidence threshold for significant correlation. Correlations for ξ throughout the mantle are lower than those for isotropic shear velocity which generally are 0.8 or above throughout the mantle.

References

Panning, M.P., V. Lekic, and B.A. Romanowicz (2010), The importance of crustal corrections in the development of a new global model of radial anisotropy, *J. Geophys. Res.*, in revision.

Acknowledgements: This work was supported through NSF grant EAR-0911414.

Analysis of the Mantle's Small Scale-Length Heterogeneity

Michael S. Thorne *(University of Utah),* **Sebastian Rost** *(University of Leeds)*

The scattering of seismic waves from small spatial variations of material properties (e.g., density and seismic wave velocity) affects all seismic observables including amplitudes and travel-times and also gives rise to seismic coda waves. A large amount of the seismic energy observed at high frequencies is contained in these coda waves, and is especially evident in the P-wavefield. Analysis of seismic scattering has provided a means to quantify small-scale seismic properties that cannot be determined through travel-time analysis or ray theoretical approaches. Numerical wave propagation techniques, such as Finite Difference (FD) techniques, have been utilized in analyzing the full waveform effects of the scattered wave field, although application of these techniques has been focused on studies in regional distance ranges.

We examine the seismic coda of the phases P, Pdiff, PP, and PKiKP for events occurring globally recorded at the short period arrays: Yellowknife (YKA) located in northwestern Canada, Eilson (ILAR) located in Alaska, and Gräfenberg (GRF) located in Germany. We model the envelope of the coda wave train using the axi-symmetric finite difference approach PSVaxi. Although, we do not model full 3D scatterer geometries, the 2.5D axi-symmetric approach allows us to reach dominant seismic periods on the order of 2 sec. The result of using 2.5D scatterer geometries is that our scattering strength is smaller than suggested by full 3D geometries, thus producing a conservative estimate to the scattering strength. Using this numerical approach is the first attempt at actually synthesizing waveforms for seismic scattering at the global scale.

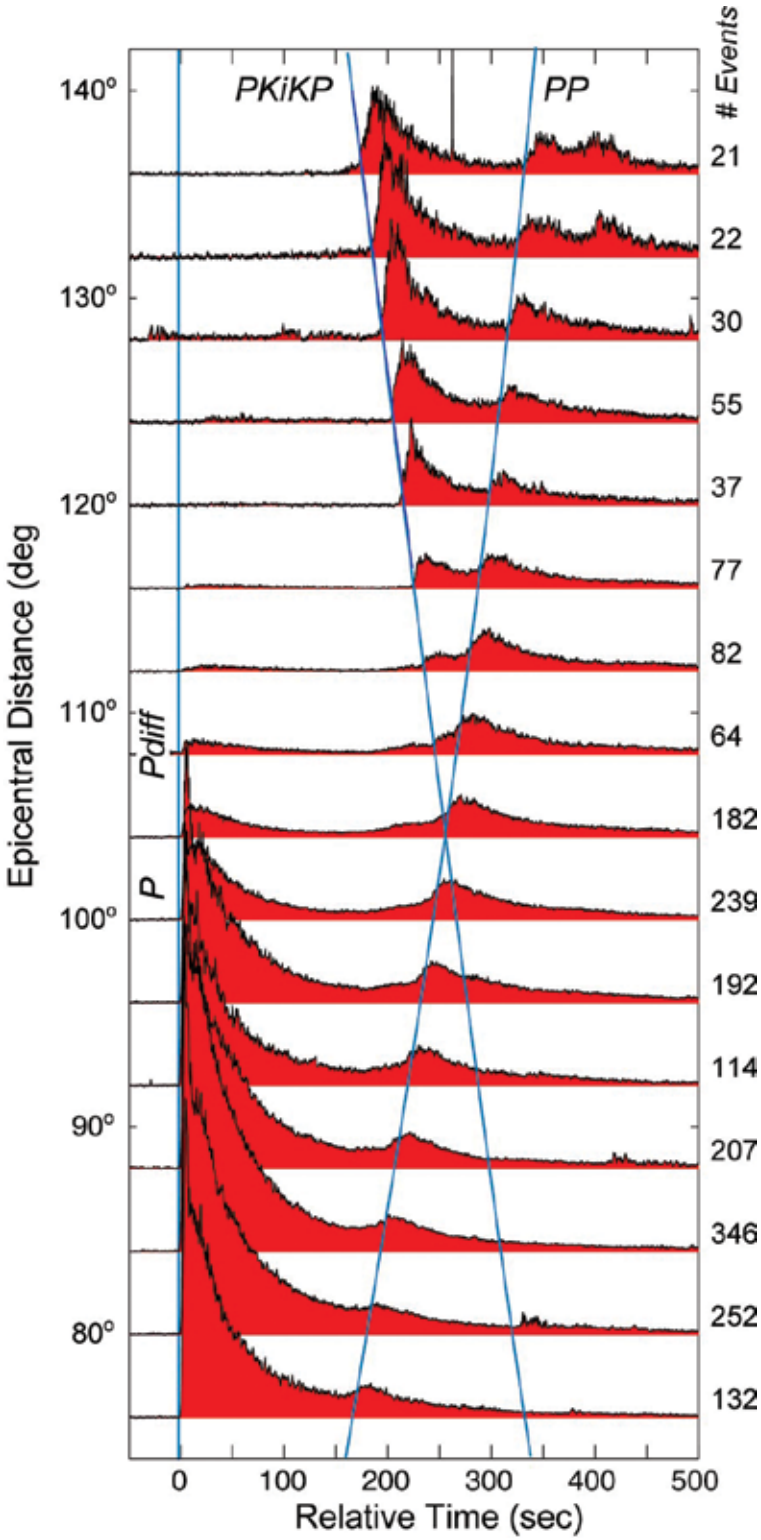

Envelope stacks of 2169 events. The data are grouped into 4° epicentral distance bins with the number of events going into each bin listed to the right of the plot window. Data are aligned in time on the P or Pdiff arrival and normalized to unity on the PP arrival. Data are SP, vertical component seismograms, beam formed on the PP slowness.

Slabs Do Not Go Gentle

Karin Sigloch *(Ludwig-Maximilians-University Munich, Germany),* **Guust Nolet** *(Geosciences Azur Nice, France & Princeton University),* **Yue Tian** *(Chevron Exploration and Production, San Ramon, CA)*

One of the big surprises from the EarthScope experiment is the extent to which the ancient Farallon plate has fractured into pieces during its 150+ years of subduction history under North America. A first multi-frequency P-wave inversion of USArray data by *Sigloch et al.* [2008] brought sharp contrast to the picture of the North American mantle, through unambiguous resolution of the narrow tears and breaks that separate different episodes of subduction. This was confirmed last year by the S-wave tomography of *Tian et al.* [2009].

The gain in image resolution results from two significant improvements, both accomplished through NSF-funded projects: the dense station deployment of USArray, and the development of finite-frequency tomography. Initially conceived as a theoretical improvement on classical ray theory, finite-frequency tomography has proved its worth in practice. Its advantage over ray tomography increases with station density, making it an ideal tool to exploit the array data. Modeling the frequency dependence of traveltime and amplitudes that is due to wave scattering yields superior resolution, especially in the lower mantle and in very heterogeneous regions.

We have been able to link some of the observed slab breaks to tectonic episodes inferred from surface geology. The origin or surface manifestations of others remain to be understood. These finding may well trigger a change in our thinking about the dynamics of convergent margins. *Nolet* [2009] has observed that in all three regions where station density allows for high-resolution tomography, *i.e.* the western U.S., Italy, and Japan, slabs show effects of tearing and detachment.

References

K. Sigloch, N. McQuarrie, and G. Nolet. Two-stage subduction history under North America inferred from multiple-frequency tomography. *Nature Geosci., 1*, 458-462, 2008.

Y. Tian, K. Sigloch, and G. Nolet. Multiple-frequency SH-wave tomography of the western US upper mantle. *Geophys. J. Int., 178*, 1384-1402, 2009.

G. Nolet. Slabs do not go gently. *Science, 324*, 1152-1153, 2009.

Acknowledgements: The graduate research of Sigloch and Tian at Princeton University was supported by the NSF with Nolet as PI (most recently under contracts EAR0345996 and EAR 0309298).

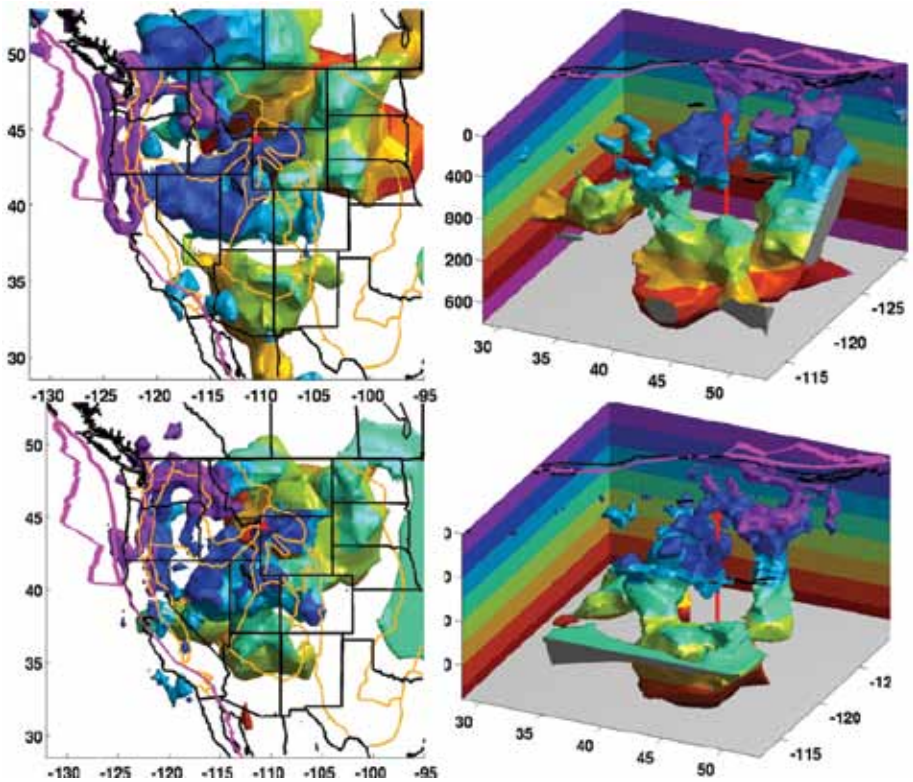

Subducted slab fragments (seismically fast anomalies) in the upper and lower mantle beneath western North America. Contoured 3-D iso-surfaces of the Cascadia subduction system down to 1800 km depth. Color codes for depth and changes every 200 km. Top row shows the P-wave model by Sigloch (2008), bottom row the S-wave model by Tian (2009). Left column shows map views, right column bird's-eye views from north-east. Lithospheric structure is not rendered except close to the trench. The red arrow marks the vertical downward projection of the Yellowstone hotspot. The models show good agreement on details such as a major vertical plate tear that runs from Oregon to Saskatchewan, just north of and parallel to the hotspot track.

A Glassy Lowermost Outer Core

Vernon F. Cormier *(University of Connecticut)*

New theories for the viscosity of metallic melts at core pressures and temperatures, together with observations of translational modes of oscillation of Earth's solid inner core, suggest a rapid increase in the dynamic viscosity near the bottom of the liquid outer core. If the viscosity of the lowermost outer core (F region) is sufficiently high, it may be in a glassy state, characterized by a frequency dependent shear modulus and increased viscoelastic attenuation. In testing this hypothesis, the amplitudes of high frequency PKiKP waves are found to be consistent with an upper bound to shear velocity in the lowermost outer core of 0.5 km/sec at 1Hz. The fit of a Maxwell rheology to the frequency dependent shear modulus constrained by seismic observations at both low and high frequency favors a model of the F region as a 400 km thick chemical boundary layer. This layer has both a higher density and higher viscosity than the bulk of the outer core, with a peak viscosity on the order of 10^9 Pa-sec or higher near the inner core boundary. If lateral variations in the F region are confirmed to correlate with lateral variations observed in the structure of the uppermost inner core, they may be used to map differences in the solidification process of the inner core and flow in the lowermost outer core.

References

Cormier, V.F., (2009) A glassy lowermost outer core, *Geophys. J. Int., 179*, 374-380.

Acknowledgements: This research was supported by grant EAR 07-38492 from the National Science Foundation. The author appreciates discussions with David Gubbins and the ICB group of the 2008 CIDER workshop, as well as reprints from and discussions with Douglas Smylie.

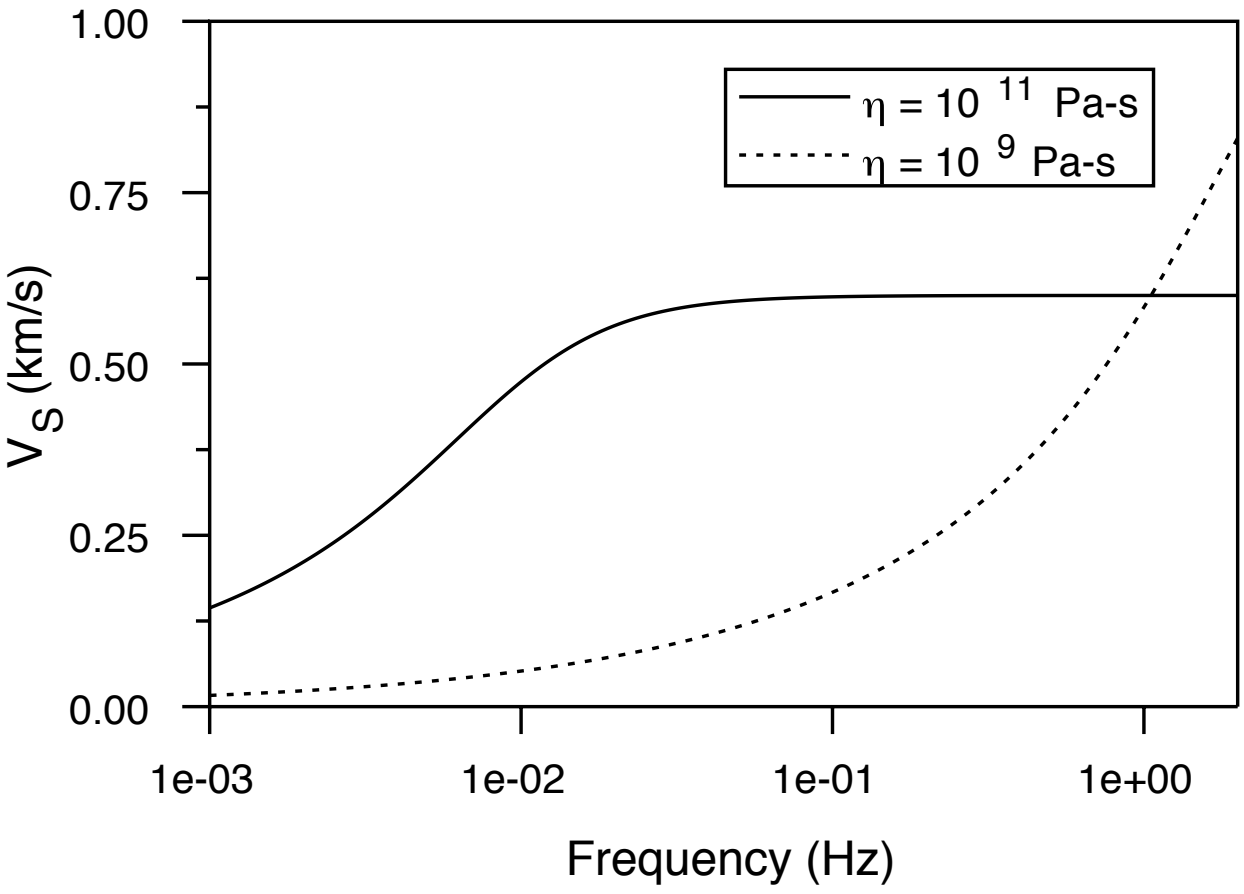

Shear velocity as a function of frequency for two different models of viscosity and in the lowermost outer core.

Localized Temporal Change of the Earth's Inner Core Surface

Lianxing Wen *(State University of New York at Stony Brook)*

The accumulation of seismic data recorded in the Global Seismographic Network (GSN) makes it possible for many discoveries to be made related to the Earth's inner core. One of these discoveries in recent years is the localized temporal change of the Earth's inner core surface. The discovery is made by comparing the seismic signals of an earthquake doublet, defined as earthquakes that occurred at different times but in almost exactly same location, recorded by the GSN stations.

Seismic phases used are the compressional waves reflected off the inner core surface (PKiKP) and propagating through the inner core (PKIKP) for an earthquake doublet occurring in South Sandwich on 12/01/1993 and 09/06/2003. Temporal changes of PKiKP travel time and waveform are observed at three GSN stations, ARU, AAK and OBN (Fig. 1), while no discernable temporal change at other seismic stations. The PKiKP and PKIKP phases recorded at station ARU arrives 0.11 s earlier and the PKIKP phase about 0.04 s earlier in event 2003 than in event 1993 (Fig. 1b). Moreover, the PKiKP-PKIKP differential travel time is about 0.07 s smaller in event 2003 than in event 1993 (Fig. 1c). The later portion of the AAK waveforms, with the energy primarily associated with the PKiKP phases, arrives about 0.07 s earlier in event 2003 than in event 1993, while the earlier portion of energy appears arriving at about the same time (Fig. 1d). The PKiKP waveforms observed at station OBN exhibit two characteristics: 1) the PKiKP main phase in event 2003 arrives about 0.07 s earlier than in event 1993; and 2) the PKiKP coda waves show waveform dissimilarities between the two events (Fig. 1e). These observations indicate a localized enlarged inner core radius by 0.98 to 1.75 km beneath middle Africa between the occurring times of the doublet.

The discovered localized temporal change of the inner core surface will have many implications to our understanding of the growth of the inner core, thermodynamic processes near the inner core boundary, convection in the outer core and driving forces for geodynamo. The GSN contributes uniquely to the discovery with its anchoring stations providing continuous open-access data, making it possible 1) to discover and locate many earthquake doublets, and 2) to confidently identify the subtle signals related to the temporal change of Earth's inner core surface between the doublets.

References

Wen, L., Localized temporal change of the Earth's inner core boundary, *Science, 314*. no. 5801, pp. 967 - 970, DOI: 10.1126/science.1131692, 2006.

Acknowledgements: I acknowledge the Global Seismographic Network for providing seismic data. This work is supported by the National Science Foundation, under grant #EAR 0609717.

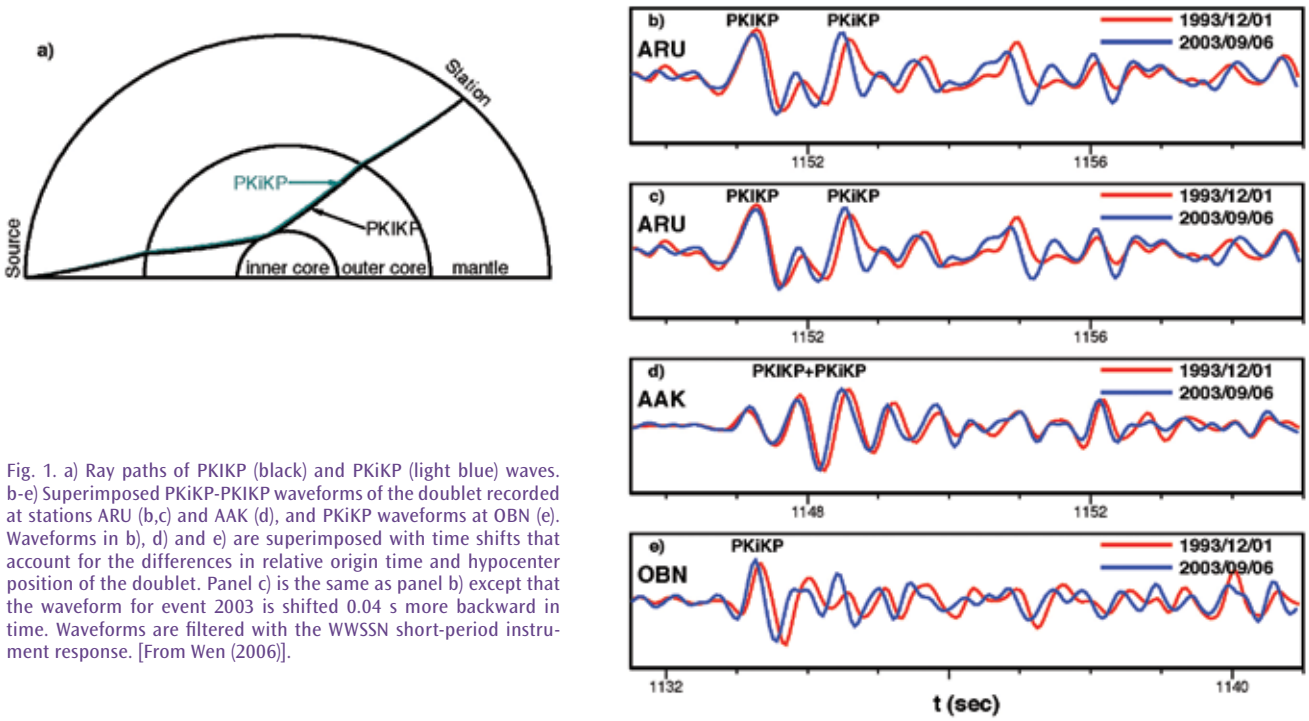

Fig. 1. a) Ray paths of PKIKP (black) and PKiKP (light blue) waves. b-e) Superimposed PKiKP-PKIKP waveforms of the doublet recorded at stations ARU (b,c) and AAK (d), and PKiKP waveforms at OBN (e). Waveforms in b), d) and e) are superimposed with time shifts that account for the differences in relative origin time and hypocenter position of the doublet. Panel c) is the same as panel b) except that the waveform for event 2003 is shifted 0.04 s more backward in time. Waveforms are filtered with the WWSSN short-period instrument response. [From Wen (2006)].

On the Inner-Outer Core Density Contrast from PKiKP/PcP Amplitude Ratios and Uncertainties Caused by Seismic Noise

Hrvoje Tkalčić *(The Australian National University),* **Brian L. N. Kennett** *(The Australian National University),* **Vernon F. Cormier** *(University of Connecticut)*

The inner core boundary of the earth is characterised by a discontinuous change in elastic properties between the liquid outer and solid inner core. In the ray theory approximation, a measure of the density contrast at the inner core boundary is given by the amplitude ratio of P waves reflected from the core-mantle boundary (PcP waves) and the inner core boundary (PKiKP waves), since that ratio conveniently appears in an explicit form in the transmission/reflection coefficient equations. The results for inner-outer core density contrast derived from direct amplitude picks of these waves in the time domain have varied significantly among different authors.

The transmission/reflection coefficients on the liquid-solid and solid-liquid boundaries derived from ground displacements enable a direct comparison between the amplitude measurements on displacement seismograms in the time domain and theoretical values. A new approach is proposed and applied to integrate effects of microseismic and signal-generated noise with the amplitude measurements, thus providing a direct maximal uncertainty measure [*Tkalčić et al., 2009*]. To suppress the effects of varying radiation pattern and distinctively different ray-paths at longer epicentral distances, this new method was applied to high-quality arrivals of PcP and PKiKP waves from a nuclear explosion observed at epicentral distances 10° to 20° from recording stations. The resulting uncertainties are high precluding precise estimates of the inner core boundary density contrast, but provide a robust estimate of an upper bound from body waves of about 1100 kg/m^3. Median values of two amplitude ratios observed around 17° epicentral distance indicate a small density contrast of 200-300 kg/m^3 and suggest the existence of zones of suppressed density contrast between the inner and the outer core, a density contrast stronger than 5000 kg/m^3 at the core-mantle boundary, or a combination of both.

References

Tkalčić H., B.L.N. Kennett and V.F. Cormier (2009). On the inner-outer core density contrast from PKiKP/PcP amplitude ratios and uncertainties caused by seismic noise, *Geophys. J. Int.*, DOI:10.1111/j.1365-246X.2009.04294.x

Acknowledgements: We are grateful to IRIS DMC for efficiently archiving and distributing continuous waveform data.

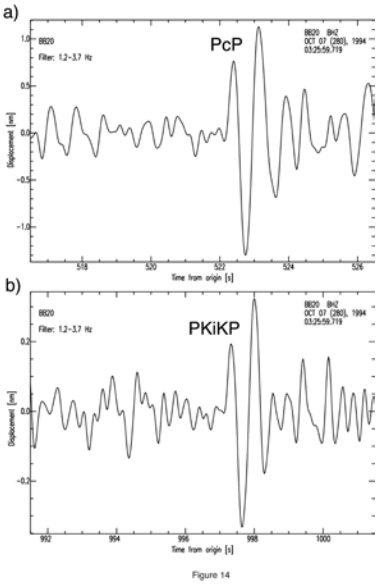

Bandpass-filtered ground displacements recorded at station BB20 using an optimal filter of 1.2-3.7 Hz for a nuclear event in China. Clear observations with similar waveforms of the PcP and PKiKP waves are visible.

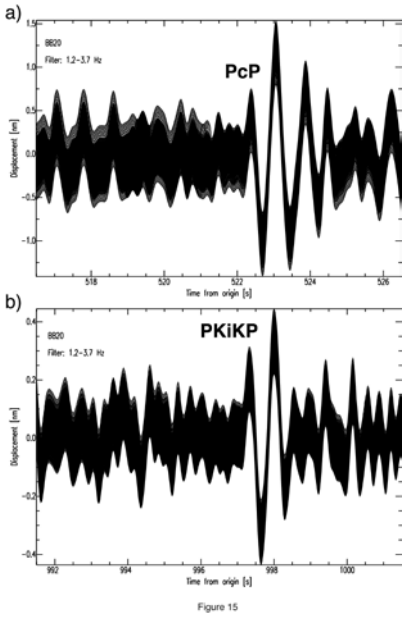

The subtraction of bandpass-filtered (1.2-3.7 Hz) seismic noise preceding the PKiKP waves from the PKiKP-wave signal recorded at station BB20 for the same event. 500 consecutive, 14 second long sliding windows of noise time series are calculated by shifting the time series by 1 sample toward earlier time and are then subtracted from the bandpass-filtered PKiKP-wave signal. Only 10 seconds of the time series are shown for clarity. Compare with Figure 1.

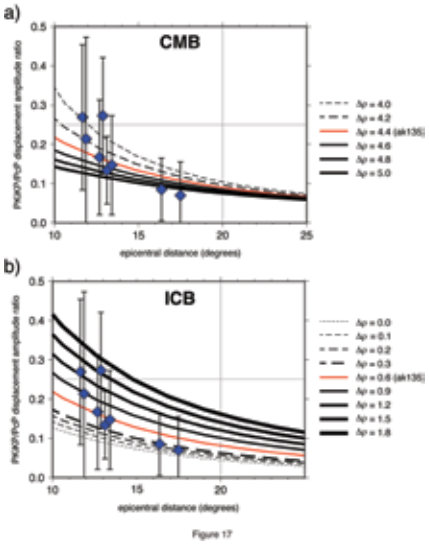

PKiKP/PcP amplitude measurements and their uncertainties (the median values are shown by diamonds, and the uncertainties are shown by error bars) plotted as a function of epicentral distance for: a varying density contrast at the ICB (top) and the CMB (bottom). Theoretical values (from ray theory) for different density contrast at the boundaries are shown with lines.

Core Structure Reexamined Using New Teleseismic Data Recorded in Antarctica: Evidence For, at Most, Weak Cylindrical Seismic Anisotropy in the Inner Core

Hrvoje Tkalčić *(The Australian National University),* **Daniel Leykam** *(The Australian National University),* **Anya M. Reading** *(University of Tasmania)*

We present a significant addition to the dataset of travel times of seismic PKP waves that sample the Earth's lowermost mantle and core along the Earth's rotation axis [*Leykam et al., 2010*]. Recorded at permanent Global Seismic Network (GSN) and temporary SSCUA deployment broadband seismographic stations in Antarctica, the new data improve the previously poor and biased coverage that underlies the seismic constraints on recent models of inner core structure and anisotropy. New differential PKP travel time measurements improve the sampling of predominantly the eastern inner core hemisphere. PKPab-df and PKPbc-df differential travel time residuals, with respect to the spherically symmetric model ak135, are consistently smaller than two seconds along the north-south paths sampled. Axially symmetric models of inner core seismic anisotropy with fast axis parallel to the Earth's rotation axis require only (0.4±0.1)% anisotropy to be consistent with our PKPbc-df observations. If only PKPbc-df observations from the top 200km of the quasi-eastern hemisphere are considered, this is reduced to (0.1±0.2)%, consistent with an isotropic layer. The dataset also increases constraints on D" structure beneath the South Pole. In contrast to previous inferences based on data from northern stations, we find no evidence of a velocity heterogeneity in the outer core near the inner core boundary associated with the cylinder tangent to the inner core in the southern hemisphere. Coverage of the quasi-western hemisphere along polar paths with differential travel times still needs improvement and may be biased by large anomalies in the mantle along the South Atlantic to Alaska path, as the new differential time residuals for polar paths from this study are consistently smaller than 2s.

References

Leykam, D., H. Tkalčić, and A.M. Reading (2010). Core structure reexamined using new teleseismic data recorded in Antarctica: Evidence for, at most, weak cylindrical seismic anisotropy in the inner core, *Geophys. J. Int.*, DOI:10.1111/j.1365-246X.2010.04488.x.

Tkalčić H., B. Romanowicz, and N. Houy (2002). Constraints on D" structure using PKP(AB-DF), PKP(BC-DF) and PcP-P travel time data from broadband records, *Geophys. J. Int. 149*(3), 599-616.

Acknowledgements: Field logistic support of the temporary SSCUA stations was provided by the Australian Antarctic Division. The facilities of the IRIS Data Management System, and specifically the IRIS Data Management Center, were used for access to waveform and metadata required in this study. IRIS provided data from the permanent Antarctic stations SNAA, QSPA, SPA, SYO, MAW and VNDA. We acknowledge the Bachelor of Philosophy Program of The Australian National University.

Locations of receiving stations in Antarctica. SSCUA stations are shown with black triangles.

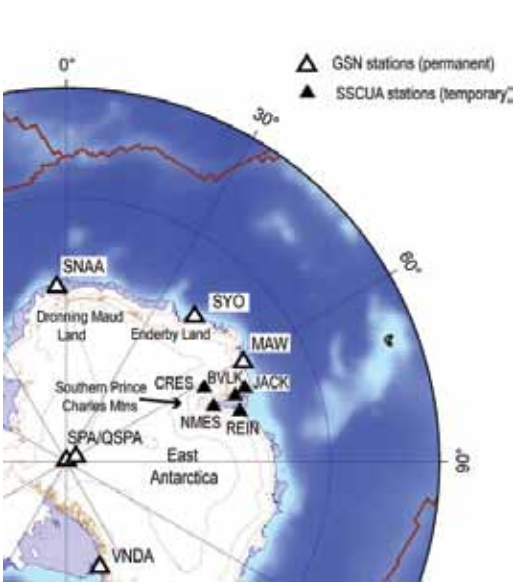

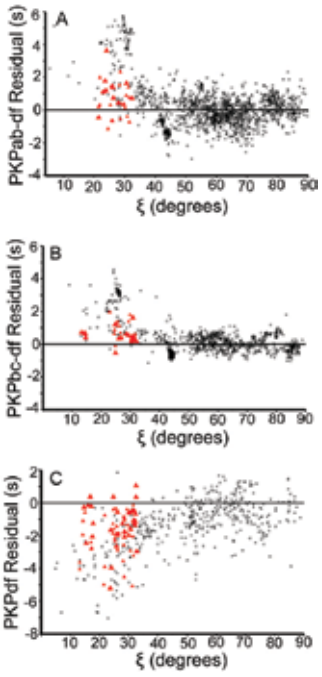

Travel time residuals with respect to the model ak135 plotted against angle between PKPdf in the inner core and Earth's rotation axis, ξ. A) Differential travel time residuals PKPab-df; B) Differential travel time residuals PKPbc-df; C) Absolute travel time residuals PKPdf. New data are in red triangles. Smaller triangles indicate lower quality data. Data from **Tkalčić** et al. [2002] are plotted with open circles.

On Iris Contribution to Deep Earth Studies

Satoru Tanaka *(IFREE, JAMSTEC)*

I have thankfully utilized the IRIS data for my deep Earth studies. This is a summary of my studies in recent 5 years.

A global data set consisting of 1211 SmKS (m≥2) waveforms collecting from IRIS database has been analyzed to investigate the radial seismic velocity structure around the core–mantle boundary (CMB). Although the thin low S-wave velocity at the base of the mantle is not conclusive, the possibility of a low P-wave velocity layer in the outermost core is remained because the waveform fitness for the part of S4KS is improved by the combination of the ULVZ and a 140 km thick layer with a 0.8% P-wave velocity reduction at the core top [*Tanaka, 2007*].

Combination of IRIS permanent observation and temporary seismic experiments reveals the mantle structure beneath South Pacific. Three-dimensional P- and S-wave velocity structures of the mantle beneath the South Pacific Superswell are determined through passive broadband seismic experiments on the ocean floor and islands between 2003 and 2005. First, we collect approximately 1500 relative times of long-period teleseismic P-waves. We analyze this data set with relative time tomography to depths of 2000 km. Our new tomographic images reveal that the large low velocity region rooted in the deep lower mantle is split into two sheets at 1200km depth and these terminate at approximately 800km depth [*Tanaka et al., 2009a*]. Second, we collect only approximately 800 long-period teleseismic SH-waves. We conduct relative time tomography to obtain a 3D structure to depths of 1600 km. The most prominent features are a large doughnut-shaped low-velocity region at 800 km depth, and an elongated large low-velocity region beneath the Society to Pitcairn hotspots at 1200 km depth. [*Tanaka et al., 2009b*].

P4KP-PcP differential travel times are examined to infer the core-mantle boundary (CMB) topography. A total of 362 P4KP-PcP times mainly collected from IRIS data are obtained. The resultant features indicate that the maximum amplitude of the CMB topography does not exceed }2 km, with an uncertainty of less than 0.5 km. A numerical test confirms that the pattern of degree 4 is more reliable with less amplitude recovery. The obtained degree 4 pattern shows an amplitude of less than }1 km and indicates the presence of depressions under the circum-Pacific, the central Pacific, and South Africa [*Tanaka, 2010*].

References

Tanaka, S. Possibility of a low P-wave velocity layer in the outermost core from global SmKS waveforms, E*arth Planet. Sci. Lett., 259*, 486-499, 2007.

Tanaka, S., M. Obayashi, D. Suetsugu, H. Shiobara, H. Sugioka, J. Yoshimitsu, T. Kanazawa, Y. Fukao, and G. Barruol, P-wave tomography of the mantle beneath the South Pacific Superswell revealed by joint ocean floor and islands broadband seismic experiments, *Phys. Earth Planet. Int., 172*, 268-277, 2009a.

Tanaka, S., D. Suetsugu, H. Shiobara, H. Sugioka, T. Kanazawa, Y. Fukao, and G. Barruol, D. Reymond, On the vertical extent of the large low shear velocity province beneath the South Pacific Superswell, *Geophys. Res. Lett.,* L07305, doi:10.1029/2009GL037160, 2009b.

Tanaka, S., Constraints on the core-mantle boundary topography from P4KP–PcP differential travel times, *J. Geophys. Res.*, B04310, doi10.1029/2009JB006563, 2010.

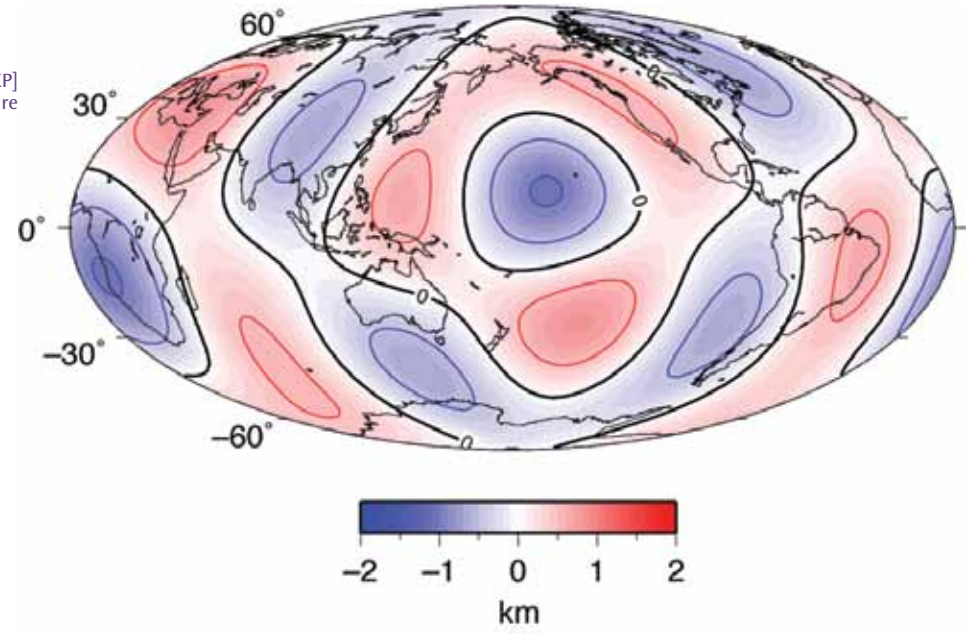

Map of the CMB topography derived from P4KP] PcP travel times. Components of degrees 4 are used. The contour interval is 0.5 km.

Large Variations in Travel Times of Mantle-Sensitive Seismic Waves from the South Sandwich Islands: Is the Earth's Inner Core a Conglomerate of Anisotropic Domains?

Hrvoje Tkalčić *(The Australian National University)*

Cylindrical anisotropy in Earth's inner core has been invoked to account for travel times of PKP core-sensitive seismic waves, such as from the South Sandwich Islands (SSI) earthquakes observed in Alaska, which depart from predictions. Newly collected travel-time residuals from seismic waves from the SSI region that sample only Earth's mantle (PcP and P waves) have a comparable range to the PKP differential travel-time residuals, yet they are insensitive to core structure [*Tkalčić, 2010*]. This observation suggests that mantle structure affects PKP travel time residuals more than previously acknowledged and challenges the existing conceptual framework of a uniform inner core anisotropy.

The small average value of 0.7% that is recently derived for anisotropy from a number of new PKP travel-time data observed in Antarctica, but without the inclusion of the SSI data [*Leykam et al., 2010*] (for rays sampling deeper than 100 km below the ICB) shows that elastically anisotropic fabric in the IC does not on average preserve the direction of fast axis of anisotropy over the entire IC volume. The inner core could be a conglomerate of anisotropic domains, and the PKP travel times are most likely influenced by the geometry of inner core sampling and inhomogeneous mantle structure. Thus, only for certain geometries of sampling, the accumulated travel time anomaly will be strong enough to be detected at the surface. Contrary, if elastic anisotropy in the inner core is weak or cancels out in the domains sampled by body waves, then some very anomalous travel times with respect to spherically symmetric models of Earth for those ray paths are likely to be a result of inhomogeneous or anisotropic structure outside the inner core.

Normal modes observed at the Earth's surface integrate contributions over the entire depth range, and are less sensitive to local variations. Hence, if the inner core is a conglomerate of anisotropic domains with variable strength, but with a net predominance in the direction of fast anisotropic axis, this will still produce an effect needed to explain anomalous splitting of free oscillations. The patchiness of anisotropic domains in the inner core reconciles observed complexities in travel times while preserving a net inner core anisotropy that is required by observations of Earth's free oscillations.

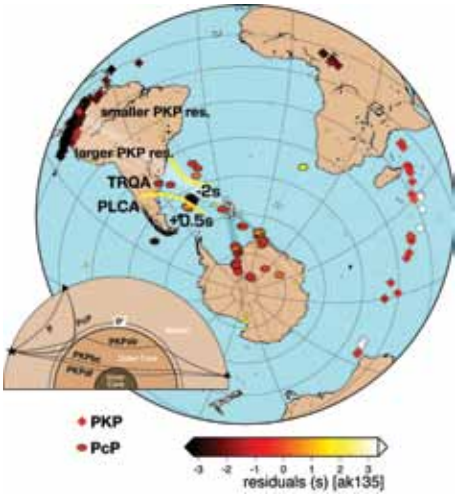

Map of locations of the SSI earthquakes used in this and in the previous study of PKP travel times (stars). Reflection points of PcP waves at the core-mantle boundary are projected to the surface (ellipses) in different colors corresponding to the observed PcP-P differential travel-time residuals. Piercing points of PKPdf and PKPbc waves in the IC are projected to the surface (small and large diamonds) with the corresponding PKPdf-PKPbc differential travel-time residuals using the same color scheme. Travel-time residuals are relative to the model ak135. PKP and PcP ray-paths projected to the surface are shown in white and black lines. GSN stations PLCA and TRQA are highlighted. Yellow lines indicate a corridor in which some of the largest departures from theoretical predictions in PKPdf-PKPbc and PcP-P travel times are observed. A schematic representation of Earth's cross-section and ray-paths of seismic phases PKP, PcP and P waves used in the study is shown in the inset.

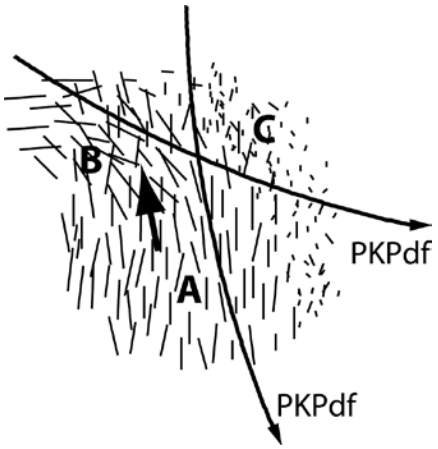

A schematic representation of three distinct anisotropic domains in the IC where the strength and orientation of fast crystallographic axes are shown as straight lines. Two different PKPdf ray paths are shown sampling different domains. "A" represents a semi-constant anisotropy domain with a predominant alignment of fast anisotropic axes; "B" is a transitional domain with a mixed orientation of fast anisotropic axes, and "C" is an isotropic or a weakly anisotropic domain. The arrow in the middle represents the net direction of the fast axis of anisotropy.

References

Tkalčić H. (2010). Large variations in travel times of mantle-sensitive seismic waves from the South Sandwich Islands: Is the Earth's inner core a conglomerate of anisotropic domains, *Geophys. Res. Lett*., in press.

Leykam, D., H. Tkalčić, and A. M. Reading (2010), Core structure reexamined using new teleseismic data recorded in Antarctica: Evidence for, at most, weak cylindrical seismic anisotropy in the inner core, *Geophys. J. Int.*, DOI:10.1111/j.1365-246X.2010.04488.x.

Acknowledgements: IRIS DMC is acknowledged for its efficient archiving and distributing of continuous waveform data and metadata required in this study. Thanks to Y. Fang for her dedication and help with the PcP-P data collection, and to S. Tanaka, V. Cormier and B.L.N. Kennett for productive discussions.

Three-Dimensional Anisotropic Structure of the Earth's Inner Core

Xinlei Sun *(University of Illinois at Urbana-Champaign),* **Xiaodong Song** *(University of Illinois at Urbana-Champaign)*

Seismological studies have generally suggested that the Earth's inner core is strongly anisotropic and the anisotropy changes significantly both laterally and with depth. To image the complex structure, we have recently performed a non-linear tomographic inversion of the inner core anisotropy using three-dimensional (3D) ray tracing and a large collection of PKP differential travel times [*Sun and Song, 2008a,b*]. The data are mainly from IRIS global and regional networks up to 2006, and other local and regional networks around all over the world. The data are from various sources, including waveforms of global (WWSN, GSN, GEOSCOPE) and regional stations from various data centers (IRIS DMC, ORFEUS, GEOFON, NARS, and China Earthquake Network Center). Our 3D anisotropy model has the following major features. (1) The model has strong hemispherical and depth variation in both isotropic velocity in the topmost inner core and anisotropic velocity at deeper depth to about 600-700 km below the inner core boundary (ICB). (2) The anisotropy form changes sharply (over a depth range of about 150 km) at the radius of about 600 km, slightly less than half of the inner core radius, forming a distinct inner inner core (IIC). (3) Despite large variation of the anisotropy, the isotropic velocity (Voigt average) throughout the inner core is nearly uniform. The results suggest that the outer inner core (OIC) is likely composed of single iron phase with different degrees of preferred alignment, but the IIC may be composed of a different type of crystal alignment, a different iron phase, or a different chemical composition.

References

Sun, X.L., and X.D. Song (2008), Tomographic inversion for three-dimensional anisotropy of Earth's inner core, *Phys. Earth. Planet. Inter., 167*, 53-70.

Sun, X.L., and X.D. Song (2008), The inner inner core of the Earth: Texturing of iron crystals from three-dimensional seismic anisotropy, *Earth Planet. Sci. Lett., 56*-65.

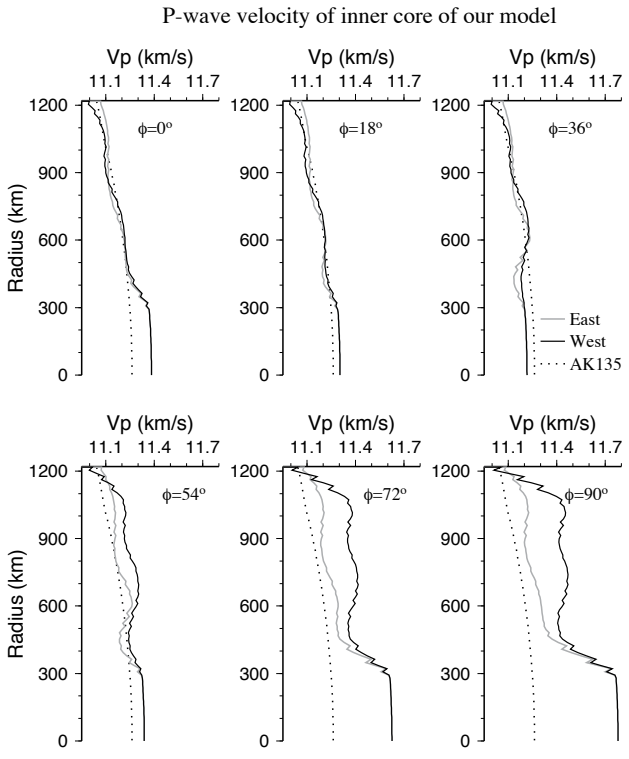

Averaged P-wave velocity of inner core for quasi-eastern hemisphere (gray) and quasi-western hemisphere (black) at different ray angle.

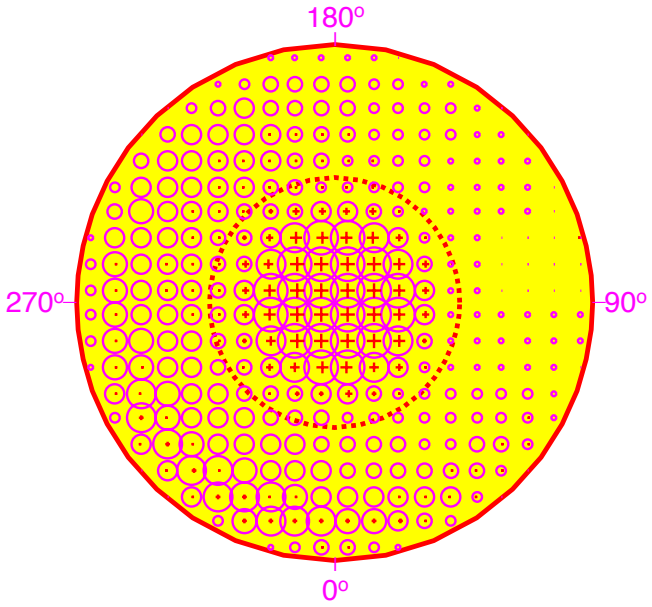

A model of inner core texturing derived from 3D inner core anisotropy, viewing from the North Pole (a) and along Meridians 40 and 220 degree (b), 100 and 280 degree (c), and 160 and 340 degree (d). The outer circle and the inner core circle (dotted) indicate the ICB and the radius of 590 km, respectively. The dashed line in the western hemisphere of topmost inner core marks the region where anisotropy increases sharply with depth. Note that the IIC part could also compose of different iron phase or different chemistry. (a) The circles and pluses indicate the fractions of polar alignment and equatorial alignment of the iron crystal's fast axis, respectively. The symbol size is proportional to the fraction. (b–d) The line segments indicate the fractions of polar and equatorial alignments.

Observations of Antipodal PKIIKP Waves: Seismic Evidence for a Distinctly Anisotropic Innermost Inner Core

Fenglin Niu *(Department of Earth Science, Rice University),* **Qi-Fu Chen** *(Institute of Earthquake Science, China Earthquake Administration)*

Studies of the seismic structure of the inner core using body waves that propagate through the inner core, such as PKIKP, are always hindered by contamination from mantle heterogeneities. A common approach in eliminating mantle anomalies is to use differential travel time or relative amplitude between PKIKP and a reference phase, which travels along a very close ray path to PKIKP in the mantle. Waves reflected at or refracted above the inner-core boundary (ICB), PKiKP and PKPbc, have been frequently employed to study the top ~400 km of the inner core [*e.g., Niu and Wen, 2001; Creager, 1992*]. On the other hand, no such reference phase has been identified as suitable for modelling the deeper part of the inner core [Breger et al., 2000]. As the result the seismic structure of the deeper ~800 km of the inner core is less constrained compared to the top ~400 km of the inner core. We found that PKIIKP is an ideal reference phase to PKIKP for deciphering seismic structure at the centre of the earth, as the two have very similar ray paths in the mantle (Figure 1a).

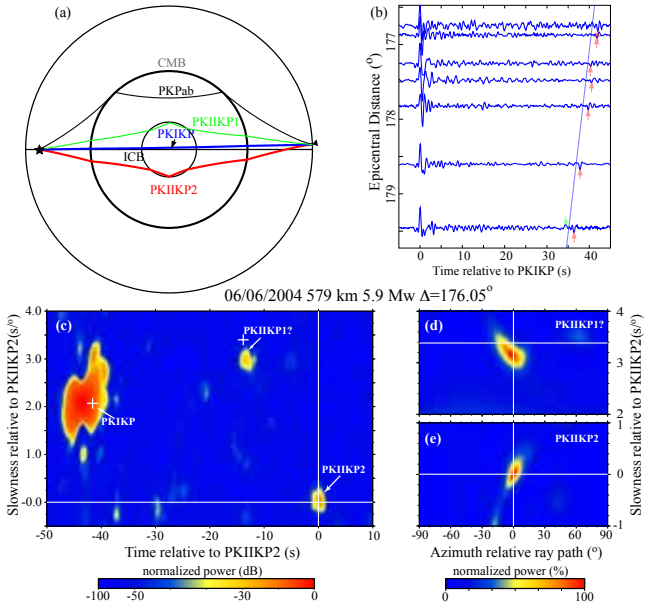

Figure 1. (a) Ray paths of the core phases: PKIKP (blue), PKPab (black), PKIIKP1 (green) and PKIIKP2 (red) at an epicentral distance of 178°. (b) Examples of seismograms recorded by the BOLIVAR array. (c) Color contour map of the vespagram stacked from the BOLIVAR data. Beam power showing the arrival direction and incident angle of the PKIIKP1 (c) and PKIIKP2 (e) phases.

We found clear PKIIKP arrivals from two deep-focus earthquakes that occurred in Indonesia and Argentina, respectively. The Indonesia event was recorded by 61 stations of a temporary PASSCAL deployment in northern South America and the southern Caribbean known as the BOLIVAR array (Figure 1b), while the Argentina earthquake was recorded by 40 short-period and broadband mixed stations that belong to the China Digital Seismic Network (CDSN). We performed stacking (Figure 1d) and beam forming analysis (Figure 1e) with the array data. Both PKIIKP phases are clearly identifiable in the vespagrams of the two events with a positive and a negative slowness relative to PKIKP, respectively. We found that the Indonesia-Venezuela path exhibits a ~1.8 s positive differential travel-time residual while the Argentina-China path shows no significant anomaly with respect to PREM. As the Indonesia-Venezuela and Argentina-China paths are in the directions of ~8° and 28° from the equatorial plane, respectively, our observation suggests that the slowest direction of wave propagation is no longer in the east-west direction for the innermost inner core [*Ishii and Dziewonski, 2002*]. The Earth's centre has a distinct seismic anisotropy relative to the rest part of the inner core.

References

Breger, L., H. Tkalcic, and B. Romanowicz (2000), The effects of D" on PKP (AB-DF) travel time residuals and implications for inner core structure. *Earth Planet. Sci. Lett., 175*, 133– 143.

Creager, K. C. (1992), Anisotropy of the inner core from differential travel times of the phases PKP and PKIKP, *Nature 356*, 309–314.

Ishii, M., and A. M. Dziewonski (2002), The innermost inner core of the earth: evidence for a change in anisotropic behaviour at the radius of about 300 km, *Proc. Natl. Acad. Sci. 99*, 14,026-14,030 .

Niu, F., and L. Wen (2001), Hemispherical variations in seismic velocity at the top of the Earth's inner-core. N*ature 410*, 1081–1084.

Acknowledgements: We thank the BOLIVAR team, FUNVISIS (Venezuelan Foundation for Seismological Research) and the Chinese Earthquake Administration for providing the data. This work is supported by the Rice University and the BOLIVAR project was supported by NSF.

Inner-Core Shear-Wave Anisotropy and Texture from an Observation of PKJKP

James Wookey *(University of Bristol, UK),* **George Helffrich** *(University of Bristol, UK)*

Since the discovery of the Earth's core a century ago, and the subsequent discovery of a solid inner core (postulated to have formed by the freezing of iron) seismologists have striven to understand this most remote part of the deep Earth. The most direct evidence for a solid inner core is the observation of shear-mode body waves which traverse it, but these phases — for example, PKJKP — are extremely hard to observe. Two reported observations in short period data have proved controversial. Arguably more successful have been two studies in longer period data but such data somewhat limits the usefulness of the waveform beyond reported sightings. We present two observations of this phase at higher frequencies in stacked data from the Japanese High-Sensitivity Array, Hi-Net. From an analysis of timing, amplitude and waveform of PKJKP we derive constraints on inner core VP and shear attenuation at ~0.3 Hz which differ from standard isotropic core models. We can explain waveform features and can partially reconcile the otherwise large differences between core wavespeed and attenuation models that our observations apparently suggest if we invoke inner core shear-wave anisotropy. A simple model of an inner core composed of hcp-structured iron with its c-axis aligned perpendicular to the rotation axis yields anisotropy which is compatible with both the shear-wave anisotropy that we observe and the well-established 3% P-wave anisotropy.

References

Wookey, J., Helffrich, G. (2008) Inner-core shear-wave anisotropy and texture from an observation of PKJKP. *Nature, 454*, 873-876

Acknowledgements: Data were provided by Hinet (National Research Institute for Earth Science and Disaster Prevention, Tsukuba, Japan). JW was supported by a NERC postdoctoral fellowship grant.

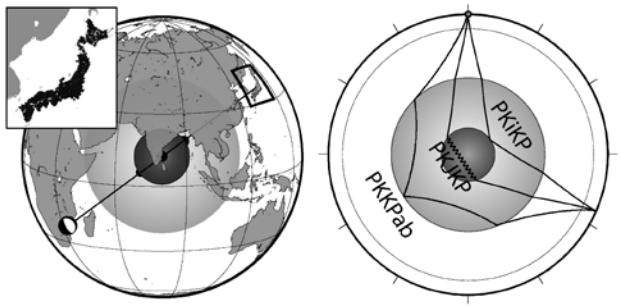

Source, raypath and receiver geometry. We search for evidence of PKJKP in records of the Mw=7.0 shallow (depth approx. 14 km) 22nd February 2006 event in Mozambique at the Japanese Hi-net array (inset). The epicentral distance to the centre of the array is 113.7 degrees. The right panel shows the raypaths for PKKPab, PKiKP and PKJKP at this distance (straight lines are P-wave segments, wiggly are S-wave).

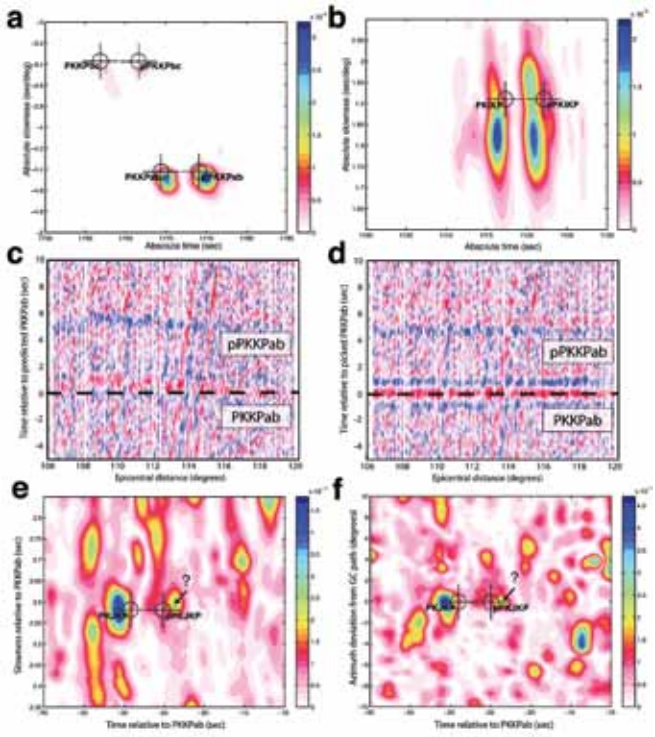

Seismic data. Panels a & b show vespagrams for the PKKPab and PKiKP time-slowness windows respectively. These vespagrams are computed using a phase-weighted slant-stack. Crosshairs denote predicted times and slownesses from ak135 for various core phases. Clear maxima associated with PKKPab, pPKKPab, PKiKP and pPKiKP arrivals are visible, with weaker maxima for PKKPbc and pPKKPbc. c, time window for PKKPab in the unstacked data. Since PKKPab is clearly visible we use it as reference phase to calculate a receiver side static time correction, and d shows this correction applied to PKKPab. e, time-slowness window (relative to the PKKPab reference phase) where PKJKP is predicted to arrive. A clear maximum can be seen 1.5 s before the prediction, at the correct slowness to within the resolution of the array (approx. 0.05 sec/deg). There is also energy near the time predicted for pPKJKP, though this is low amplitude (near the noise level) and poorly constrained in slowness. f, azimutha

Regional Variation of Inner Core Anisotropy from Seismic Normal Mode Observations

Arwen Deuss *(Bullard Labs, University of Cambridge, United Kingdom),* **Jessica Irving** *(Bullard Labs, University of Cambridge, United Kingdom),* **John H. Woodhouse** *(Oxford University, United Kingdom)*

The Earth's core, consisting of an iron alloy, makes up one third of our planet's total mass. As the Earth cools, the inner core grows by solidification of the fluid outer core. Solidification results in the release of light elements and latent heat, which drive the geodynamo generating the Earth's magnetic field. We studied inner core structure using long period normal mode splitting functions and made observations of regional variations in inner core anisotropy which are consistent with short period compressional body waves.

Previous seismic studies using compressional body waves had suggested hemispherical variation in the isotropic and anisotropic structure of the inner core. However, because of the limited distribution of earthquakes and receivers, the global extent of the hemispherical variations was poorly constrained. Normal mode observations have the potential to provide robust evidence, but so far had been elusive due to lack of theory and suitable data. Previous studies investigated isolated modes, which are only sensitive to even-degree structure, and showed strong evidence for inner core anisotropy. To investigate hemispherical variations, which is odd-degree structure, we take cross-coupling between pairs of modes into account.

To improve data coverage, we made a new long period data set for all large earthquakes from 1975 to 2009, including the 2004 Sumatra event and the 2008 Wenchuan China event. We measured splitting functions of odd-degree structure for pairs of coupled modes sensitive to the inner core in comparison with body wave observations. The observed odd-degree structure suggests more complicated regional variations than a simple Eastern versus Western hemispherical pattern. Our results open up possibilities for directly linking regional variations in inner core structure to the strength of the magnetic field and thermal evolution of the Earth's core. The similarity of the observed seismic pattern with Earth's magnetic field suggests freezing-in of crystal alignment during solidification or texturing by Maxwell stress as origins of the anisotropy. These observations also limit the amount of inner core super rotation, but would be consistent with oscillation.

References

Deuss, A., Irving, J. C. E. and J. H. Woodhouse, 2010. Regional variation of inner core anisotropy from seismic normal mode observations. Originally published in Science Express on 15 April 2010. *Science, 328* (5981), 1018-1020

Acknowledgements: The research was funded by the European Research Council (ERC) under the European Community's Seventh Framework Programme (FP7/2007-2013)/ERC grant agreement number 204995.

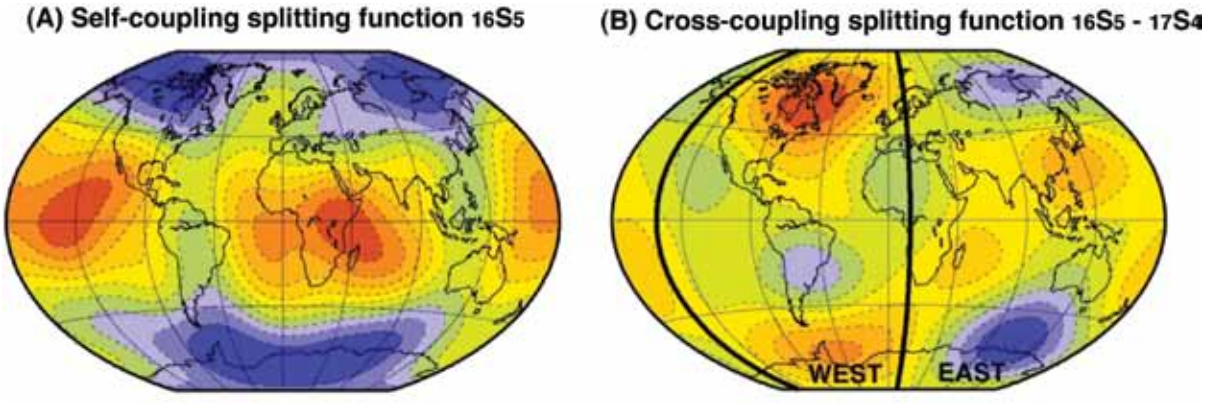

Observed and predicted splitting functions for the mode pair 16S5 and 17S4. (A) Observed splitting function using self-coupling only for 16S5 showing zonal splitting typical of inner core anisotropy. (B) Observed cross-coupled splitting function showing anti-symmetric splitting, which is characteristic of hemispherical variation (i.e. East versus West) in inner core anisotropy.

Inner Core Rotation and Its Variability from Non-Parametric Modeling

Daniela Lindner *(Department of Geology, University of Illinois at Urbana-Champaign),* **Xiaodong Song** *(Department of Geology, University of Illinois at Urbana-Champaign),* **Ping Ma** *(Department of Statistics, University of Illinois at Urbana-Champaign),* **Doug H. Christensen** *(Geophysical Institute, University of Alaska, Fairbanks)*

We present a new approach to gain insight into the inner core rotation by separating the underlying inner core structure from its time evolution without any a priori constraints. This is achieved by fitting existing seismic travel time residual data with a smoothing spline analysis of variance model [*Gu, 2002*]. Our data are PKP BC-DF differential travel time measurements from South Sandwich Islands (SSI) earthquakes that were recorded at Alaskan stations (Fig. 1) dating back to as far as 1951 in case of the longtime College, Alaska station. We add our newly acquired seismic data from the recent PASSCAL experiment ARCTIC in northern Alaska, which increases our time resolution as well as lateral coverage of the inner core structure. Our method allows us not only to separate the time independent mantle contribution from the time dependent core contribution without any a priori constraints but also to estimate the error of the fit. In addition we are able to determine the average rotation rate of the inner core over a given period, assuming a rigid body motion. Synthetic tests support the applicability of our approach and when it is applied to the actual data enables us [*Lindner et al., 2010*] to:

- Unveil a clear spatial gradient of the inner core structure which and is non-linear.
- Determine the average rotation rate of the inner core to 0.39° per year to the East in agreement with previous studies.
- Rule out westward and no rotation.

References

Lindner, D., X. Song, P. Ma, and D. H. Christensen (2010), Inner core rotation and its variability from nonparametric modeling, *J. Geophys. Res., 115*, B04307.

Gu, C. (2002), Smoothing Spline ANOVA Models, Springer-Verlag, New York, New York.

Song, X. D. (2000), Joint inversion for inner core rotation, inner core anisotropy, and mantle heterogeneity, *J. Geophys. Res., 105* (B4), 7931-7943

Acknowledgements: Historical data were acquired with the help of many people [Song, 2000]. We thank constructive comments from two anonymous reviewers. The research was supported by NSF EAR-0330749 (XDS) and NSF DMS-0723759 (PM)and utilized National Center for Supercomputing Applications machines Tungsten and Cobalt.

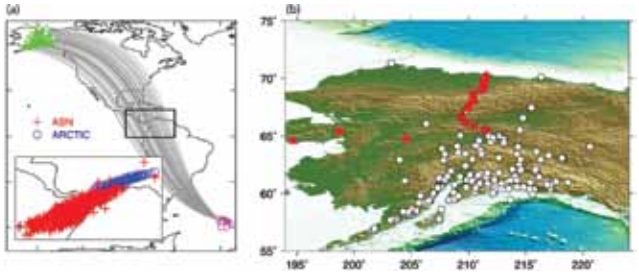

(a) Map of pathways from South Sandwich Islands (SSI) earthquakes to Alaska Seismic Network (ASN) and ARCTIC stations. The inset is an enlarged view of the PKP-DF ray turning points in the inner core beneath the Central America. The ARCTIC stations extend the inner core samples further to east. (b) Locations of stations used in this study, including ASN stations (circles) and ARCTIC stations (triangles) along the NS line. The ARCTIC stations along the EW direction are not used in this study.

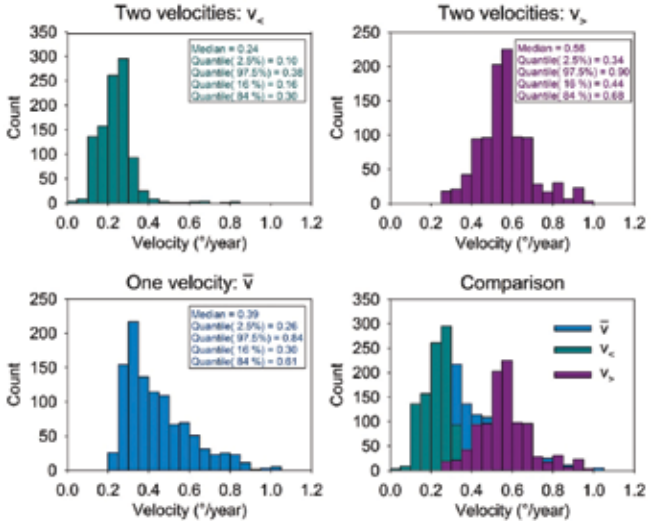

Figure 2. Histograms of inner-core rotation rates obtained in this study. Best average velocities v_{<}=v(t<1990) (Top left), v_{>}=v(t>1990) (Top right) \bar{v} (Bottom left) over the whole study period from 1951 to 2007 (Bottom left). (Bottom right) Comparison between \bar{v}, v_{<} and v_{>}.

Wide-Scale Detection of Earthquake Doublets and Further Evidence for Inner Core Super-Rotation

Paul G. Richards *(Lamont-Doherty Earth Observatory of Columbia University),* **Jian Zhang** *(Scripps Institution of Oceanography),* **David P. Schaff** *(Lamont-Doherty Earth Observatory of Columbia University)*

The best evidence for a super-rotation of the Earth's inner core is provided by comparing the signals of earthquakes occurring years apart but in almost exactly the same location (doublets). The method was developed in the context of high-quality doublets by Li and Richards and has been used by many subsequent authors. *Zhang et al.* [2008] report on more than 100 earthquake waveform doublets in five subduction zones, including an earthquake nest in Bucaramanga, Colombia. Each doublet is presumed to be a pair of earthquakes that repeat at essentially the same location. These doublets are important for studying earthquake physics, as well as temporal changes of the inner core. In particular we have data for six different paths. They partition into three paths for which the travel time of PKIKP changes significantly and measurably (on the order of 0.01 s per year), and three paths that show little or no change (no more than 0.005 s per year, if any) of inner core travel-times. In the former set of three paths, there is a high angle between the ray path within the inner core, and the equatorial plane. In the latter set of ray paths, the path in the inner core is nearly parallel to the equatorial plane. Such a pattern of observations showing both presence and apparent absence of inner-core travel-time change can be explained by the geometry and relative directions of ray path, lateral velocity gradient and inner-core particle motion due to an eastward super-rotation of a few tenths of a degree per year.

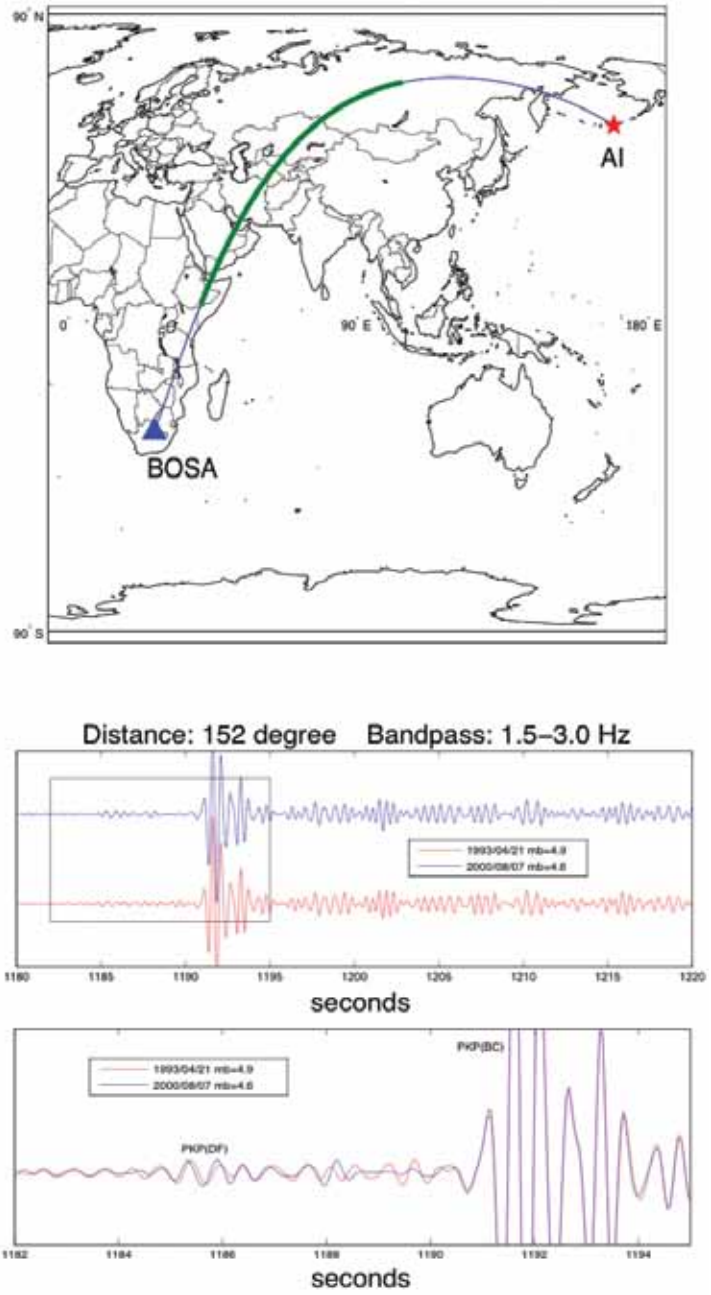

An apparent temporal change (about 0.1 s) of inner core travel-times observed from an Aleutian Islands doublet (about 7 yr apart in time) recorded at station BOSA. Top: Map view of the ray path projected on the Earth's surface. Star represents the doublet location. Triangle represents station BOSA. Blue curve represents the ray path projected on the Earth's surface. The green part of the curve represents the projected part of the ray path within the inner core. Bottom: Comparison of the highly similar waveforms of an Aleutian Islands doublet recorded at BOSA. PKP signals within the box in the upper panel are superimposed and enlarged in the lower panel, showing an apparent change of both inner core travel-times and PKP(DF) coda.

References

Paul G. Richards and Anyi Li, Inner core rotation, in Encyclopedia of Geomagnetism and Paleomagnetism, ed. David Gubbins and Emilio Herrero-Bervera, Encyclopedia of Earth Sciences Series, general editors Rhodes Fairbridge and Michael Rampino, pages 423-425, Springer: Dordrecht, The Netherlands, 2007.

Jian Zhang, Paul G. Richards, and David Schaff, Wide-scale detection of earthquake waveform doublets and further evidence for inner core super-rotation, *Geophys. J. Int., 174*, 993-1006, September 2008.

Acknowledgements: Our research was largely funded by two grants from NSF/EAR.


IRIS